

Philips Technical Review

DEALING WITH TECHNICAL PROBLEMS
RELATING TO THE PRODUCTS, PROCESSES AND INVESTIGATIONS OF
THE PHILIPS INDUSTRIES

COMBINATIONS OF VALVES AND TRANSISTORS IN A STABILIZED 2000 V POWER SUPPLY

by G. KLEIN *) and J. J. ZAALBERG van ZELST *)

621.314.671:621.382.3

The article below — the third in a series on electronic circuits for special measuring equipment — describes a highly stabilized 2000 V DC power supply. A special feature is that in some parts of the circuit valves and transistors are used in combination. In this way results are obtained that can be achieved only with great difficulty using valves or transistors alone. An example given is a cascode consisting of an EL 34 pentode and an OC 139 transistor: the effective amplification factor of this cascode is greater than 10^5 .

Thermionic valves and transistors are elements that do not at first sight seem likely partners in one and the same circuit. Closer examination shows, however, that it is possible to combine them to form circuits possessing unusual properties, enabling elegant solutions to be found for certain problems of circuitry.

Some years ago, for example, the need arose for a stabilized HT power supply to provide a variable DC voltage for the operation of scintillation counters. The photomultiplier, which is a major component of

*) Philips Research Laboratories, Eindhoven.

such counters, is extremely sensitive to fluctuations in the DC supply voltage. This voltage therefore had to be very highly stabilized.

The power-supply apparatus, delivering a current of 0 to 5 mA, had to meet the following specifications:

- 1) DC voltage variable in small steps from 400 to 2000 V.
- 2) Optional earthing of either the positive or the negative terminal.
- 3) A 10% change in the mains voltage should cause no more than 0.01% change in the DC output voltage.



Fig. 1. The stabilized DC voltage source for 400-2000 V in a version that meets the same requirements as the apparatus described in this article, but which can supply a higher current, up to 10 mA.

- 4) A 10% change in the current drain should cause no more than 0.01% change in the DC output voltage.
- 5) The peak value of the sum of hum and ripple voltages should not exceed 10^{-5} times the chosen value of the DC voltage¹⁾.
- 6) In prolonged operation the chosen value of the DC voltage should remain constant to within 0.1%.
- 7) Short-circuiting of the DC terminals should have no adverse consequences.

Fig. 1 shows a later developed variant which meets the above specifications at currents from 0 to 10 mA.

Principle

Fig. 2 illustrates the principle of stabilized power supplies. A control system ensures that the instantaneous value of the output voltage U_o depends very little on the fluctuations present in the "uncontrolled" voltage U_i — irrespective of their cause — and on the changes in the load. The system consists of a valve T_1 (triode or pentode) which is in series with the load and is driven by an amplifier that amplifies the difference between a certain fraction k of the output voltage U_o and a fixed reference voltage U_{ref} .

To a good approximation the change ΔU_o in the output voltage produced by changes ΔU_i in the uncontrolled voltage and changes ΔI_o in the load current is given by:

¹⁾ The disturbing voltages denoted as hum enter along stray paths, e.g. via the stray capacitance between the transformer coils. In the present case, screening in the transformer and appropriate assembly reduce the hum sufficiently for it to be disregarded in the following considerations.

$$\Delta U_o = \frac{1}{kA\mu} \Delta U_i - \frac{1}{kAS} \Delta I_o.$$

Here A is the gain of the control amplifier, while μ and S are respectively the amplification factor and the transconductance of the series valve T_1 . The

$$P = kA\mu \text{ and } R_i = \frac{1}{kAS} \dots (1)$$

quantities will be called the stabilization and the internal resistance of the stabilized power supply, respectively.

Where the power is small and the requirements are not too rigorous as regards the constancy of the DC voltage, a convenient solution can sometimes be an RF oscillator whose output voltage is stepped up, rectified and stabilized. In the case under consideration, however, the power (10 W at the output) is on the high side for such a system, and would make it difficult to satisfy the stability and internal-resistance requirements.

In the case of stabilized power packs for low voltages the various capacitors can be generously dimensioned; this is particularly important as regards the buffer capacitor C_2 (fig. 2) across the output. In the case of high voltages, on the other hand, the volume, weight and price of the capacitors should not be unduly large compared with those of the other components. As will be shown, however, limiting the values of these capacitors can have far-reaching adverse consequences. For the capacitors C_1 and C_2 (fig. 2) a compromise value of 0.2 μ F was chosen. From a simple calculation it follows that, using a smoothing capacitor of 0.2 μ F and under full load, the ripple voltage of C_1 has an amplitude of 125 V.

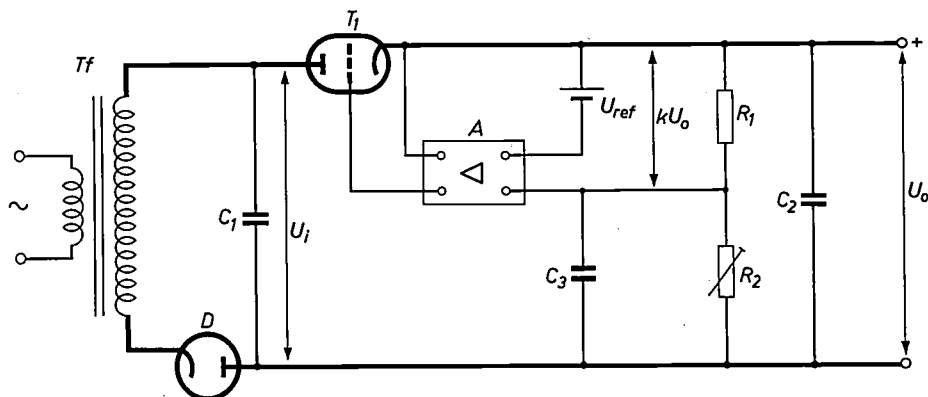


Fig. 2. Basic diagram of a stabilized power supply. T_f power transformer. D rectifying valve. C_1 smoothing capacitor across which the unregulated voltage U_i appears. T_1 series valve driven by the control amplifier A . The input voltage of A is the difference between the part kU_o of the DC output voltage U_o and a reference voltage U_{ref} ; the fraction k is determined by the voltage divider R_1 - R_2 . Buffer capacitor C_2 is needed for the stability of the control system. C_3 bypasses R_2 , so that the full ripple voltage of U_o is present at the input of A ; in this way the ripple is minimized.

The only type of valve suitable for use as T_1 , while still belonging to the class of "receiving valves", is the EL 34 pentode. Since we preferred to avoid the use of tap switches on the HT winding of the transformer, a high voltage appears across T_1 in the case of a low output voltage: in the situation with the nominal mains voltage, the lowest output voltage (400 V) and full load, the series valve must take about 2500 V. At this voltage the anode dissipation (15 W) remains far below the permitted maximum, but the voltage itself exceeds the officially permitted maximum value, which is 2000 V for a cut-off valve. In the tests subsequently carried out on a number of EL 34 pentodes we did not, however, encounter any difficulties. Fig. 3 gives a plot of the

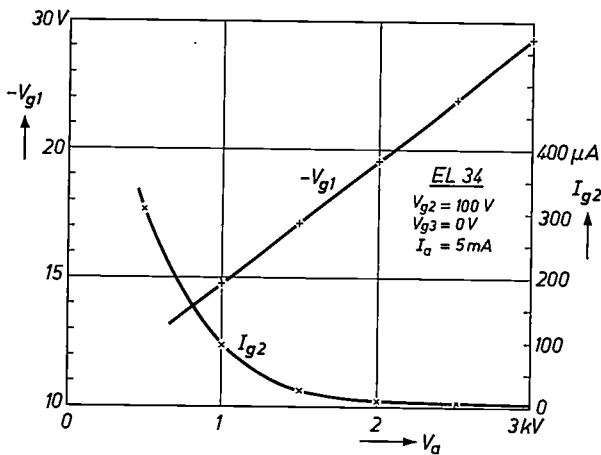


Fig. 3. Control-grid voltage V_{g1} and screen-grid current I_{g2} of the EL 34 pentode as a function of the anode voltage V_a , at constant anode current ($I_a = 5 \text{ mA}$) and constant screen-grid voltage ($V_{g2} = 100 \text{ V}$). The form of both curves indicates that the valve still behaves quite normally at anode voltages of 2 to 3 kV.

control-grid voltage V_{g1} and the screen-grid current I_{g2} versus the anode voltage V_a for constant anode current (5 mA) and constant screen-grid voltage (100 V). Both curves show that the valve still behaves quite normally at the exceptionally high anode voltages. We therefore preferred to accept the minor risk of the high tension rather than to adopt the alternative solutions of transformer tap switches, two EL 34 valves in series, or a transmitting valve (which would be much more expensive).

A screen-grid voltage of about 70 V is found to be sufficient for the EL 34 in our circuit. The slope of $V_{g1} = f(V_a)$ in fig. 3 corresponds to an amplification factor μ of 225. At 5 mA anode current the transconductance ranges from about 2.5 to 3.0 mA/V. We shall need these data presently.

Calculations relating to the gain

The specifications (3) and (5) above relate to the stabilization (of the mains-voltage fluctuations and

the reduction of ripple resp.) and specification (4) concerns the regulation. In the following we shall calculate what the magnitude of the gain A of the control amplifier (denoted by A in fig. 2) should be to meet these specifications, taking the EL 34 as the series valve. We shall then consider what the permissible gain is, having regard to the transient response of the control system.

Stabilization against mains-voltage fluctuations

For slow changes the factor k in (1) is equal to $R_1/(R_1 + R_2)$; see fig. 2. Since the control system endeavours to keep kU_o identical with U_{ref} , we can also write: $k = U_{ref}/U_o$.

At the nominal mains voltage and a current drain of $I_o = 5 \text{ mA}$, the value of U_i is about 2500 V. At a 10% deviation of the mains voltage, U_i therefore changes by approximately 250 V. According to the stabilization requirement, this should cause a change in U_o not exceeding $10^{-4} U_o$. The stabilization should therefore be at least $250/10^{-4} U_o$:

$$\frac{\mu A U_{ref}}{U_o} \geq \frac{250}{10^{-4} U_o}$$

Given $\mu = 225$ and $U_{ref} = 83 \text{ V}$, it follows that:

$$A \geq 135. \dots \dots (2)$$

Smoothing of ripple

The ripple in the output voltage is P times smaller than the ripple in the uncontrolled voltage, provided that the factor k occurring in P (see eq. 1) can easily be made almost equal to unity for the frequencies of the ripple. For this purpose all that is needed is to bypass the resistor R_2 (fig. 2) with a capacitor C_3 of sufficiently high capacitance: almost the entire output ripple then appears at the input of the control amplifier A instead of only the fraction $R_1/(R_1 + R_2)$.

As mentioned above, under full load the amplitude of the ripple over C_1 is 125 V, the peak-to-peak value thus being 250 V. According to specification (5) the output ripple should be no more than $10^{-5} U_o$. This specification is most severe when U_o is set to the lowest value (400 V). One then finds:

$$\frac{250}{\mu A} \leq 10^{-5} \times 400,$$

from which, given $\mu = 225$, it follows that:

$$A \geq 270. \dots \dots (3)$$

Regulation

According to eq. (1) the internal resistance R_i of a stabilized power supply is: $R_i = 1/kAS$. The regulation specification (4) states that a 10% change in the

current I_o should cause a change of no more than $10^{-4} U_o$ in the output voltage. Hence:

$$\frac{1}{kAS} \leq \frac{10^{-4} U_o}{0.1 I_o}$$

In this expression the maximum value (5 mA) should be substituted for I_o and the minimum value (2.5 mA/V) for S . We then find, with $k = U_{ref}/U_o$ and $U_{ref} = 83$ V:

$$A \geq \text{approx. } 25 \dots (4)$$

From (2), (3) and (4) it follows that all three specifications are only met where $A = 270$.

Transient response

Control systems can respond to a step-function disturbance in various ways. In general, reactions with an oscillatory character are undesired: in other words, *the transient response should show little or no overshoot*. If this requirement is fulfilled, the *stability* of the control system will be assured, even with the conventional tolerance in the values of the components. The question is now whether, in the present case, a gain A of 270 is compatible with a transient response without overshoot.

For simple linear control systems with two time constants, τ_1 and $\tau_2 < \tau_1$, it is easily deduced that the condition for the required form of the transient response is: loop gain $kA \leq \frac{1}{4} \tau_1/\tau_2$, hence:

$$A \leq \frac{\tau_1}{4k\tau_2} \dots (5)$$

For simple linear control systems with two time constants (fig. 4) the following differential equation holds:

$$\left[\tau_1 \tau_2 \frac{d^2}{dt^2} + (\tau_1 + \tau_2) \frac{d}{dt} + kA + 1 \right] v = Av_i$$

For the transient response to be free from oscillations (including

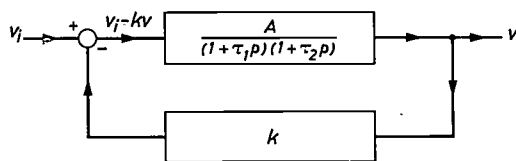


Fig.4. Schematic representation of a linear control system with two time constants, τ_1 and τ_2 . The letter p denotes the differential operator d/dt , v the output voltage, and k the gain (< 1) in the feedback path.

damped ones) the discriminant of the form between square brackets must be positive:

$$(\tau_1 + \tau_2)^2 - 4 \tau_1 \tau_2 (kA + 1) > 0.$$

This condition may also be written as follows:

$$\frac{\tau_1}{\tau_2} + \frac{\tau_2}{\tau_1} > 4kA + 2.$$

If $\tau_1 \gg \tau_2$ and $kA \gg 1$, this reduces in good approximation to

$$\frac{\tau_1}{\tau_2} > 4kA,$$

from which (5) directly follows.

In our case there are indeed only two principal time constants involved. One is the time constant of the control amplifier, the minimum value of which is determined by a resistance and a stray capacitance. If the gain A is to be of the order of 100, a time constant of at least about 5 microseconds should be taken into account. The other time constant is equal to the product of the differential resistance of the series valve ($= 1/S$) and the buffer capacitance C_2 . Either of the two time constants can be made the larger one by adding capacitance.

Which of the two should we now choose as the larger and which as the smaller time constant? In DC voltage supply apparatus it is favourable to shunt a buffer capacitance C_2 across the output; this capacitance smooths the effect of sudden changes in the load, and does so more effectively the larger it is. This apart, it remains of course desirable that the amplifier should respond as quickly as possible, i.e. that it should have the lowest possible time constant. Here, then, the obvious course is to make the latter time constant the smaller one: $\tau_2 = \text{approx. } 5 \mu\text{s}$, and C_2/S the larger one. In the other case a sudden change in the load current would produce a jump in the output voltage which would only slowly be compensated by the amplifier: the power supply has a "recovery time". With many HT apparatus this is of the order of some tenths of a second. Given $k = U_{ref}/U_o$, eq. (5) now becomes:

$$A \leq \frac{U_o}{4U_{ref}} \frac{C_2}{S\tau_2} \dots (6)$$

Substituting in this expression the minimum value (400 V) for U_o and the maximum (3 mA/V) for S , and taking $U_{ref} = 83$ V, $C_2 = 0.2 \mu\text{F}$ and $\tau_2 = 5 \mu\text{s}$, we find as condition for the transient response without overshoot:

$$A \leq \text{approx. } 15.$$

The maximum permissible value $A = 15$ is thus far below the value 270 which, according to the foregoing considerations, is the minimum necessary to satisfy the requirements in regard to stabilization and regulation.

If it were a stabilized power supply for low voltage, one could easily get out of the impasse by choosing a larger capacitance for C_2 : time constant τ_1 then increases, so that the gain A can be increased without the transient response showing overshoot. As remarked above, however, the voltage in the present

case is so high that C_2 should preferably not be larger than $0.2 \mu\text{F}$.

Cascode consisting of a pentode and a transistor

The conflict would disappear if the series valve had an amplification factor and a transconductance substantially greater than 225 and 3 mA/V respectively, for as appears from (1), the stabilization is proportional to μ and the regulation to S .

A high amplification factor might be obtained by combining the EL 34 with a second valve to form a *cascode*, the effective μ of a cascode being roughly equal to the product of the amplification factors of each of the valves ²⁾. If we make the EL 34 the "upper" valve in the cascode and the second valve the "lower" one, then the effective transconductance of the cascode is more or less identical with the transconductance of the second valve ²⁾. As regards transconductance, the cascode would thus be more favourable than the EL 34 if one could have a second valve possessing a transconductance substantially larger than 3 mA/V . No valves exist, however, with a transconductance of this order at currents from 1 to 5 mA.

By now using a *transistor* in lieu of the second valve, a solution is found which is satisfactory both as regards amplification factor and transconductance. Moreover, the power supply is simpler than with a cascode consisting of two valves. Because of the current direction, an *N-P-N* transistor is needed, e.g. an OC 139.

The circuit is shown in *fig. 5*. The control amplifier *A* drives the transistor between base and emitter, and the voltage between collector and emitter is used for driving the pentode (for the moment we shall disregard the resistance R_3). Since the latter voltage is -4 and -16V in the extreme cases, the voltage between collector and emitter never rises above 20V ³⁾, a value which must not be exceeded. A maximum of 0.1 W is dissipated in the transistor, which is far below the permissible maximum.

The effective amplification factor μ_{tr} of transistors (this quantity is explained in the text in small print below) can easily attain a value of more than 500, so that the *effective amplification factor* μ_{casc} of the cascode is greater than 10^5 . The transconductance of transistors (defined similarly to that of valves) is also appreciably higher than the transconductance of valves at the same current, viz about $40 I_e \text{ mA/V}$, where I_e is the emitter current in mA ⁴⁾. This

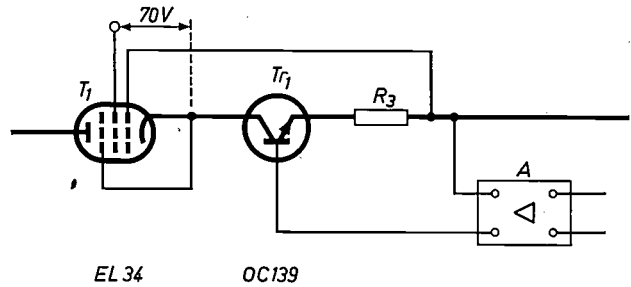


Fig. 5. Cascode formed by a valve T_1 (EL 34 pentode) and a transistor Tr_1 (*N-P-N* type OC 139). This cascode has an effective amplification factor of more than 10^5 and a high transconductance; it can therefore replace the valve T_1 in *fig. 2* with advantage.

A control amplifier. R_3 (e.g. 68 ohms) limits the effective transconductance of the cascode (equal to the transconductance of the transistor, hence proportional to the emitter current); under full load the transconductance would otherwise become so high that the control system would show overshoot or even become unstable.

may be put in another way: whereas in valves the ratio I_a/S is of the order of 1 V at anode currents of a few mA, the corresponding ratio in transistors is of the order of 0.1 V , and even about 25 mV at very low collector currents.

The effective amplification factor of a transistor circuit

Fig. 6 shows the simplified circuit containing the transistor Tr_1 of *fig. 5*. The resistances through which the emitter and base currents flow are denoted by r_e and r_b respectively, the amplified driving voltage $A(kU_o - U_{ref})$ by v_b , and the current and voltage changes by i and v respectively; the subscripts e, b and c refer to the emitter, the base and the collector.

The changes of the collector and base currents are given by the following equations:

$$i_c = S(v_b - v_e) + \frac{S}{\mu}(v_e - v_e), \dots (7)$$

$$i_b = \frac{S}{\alpha'}(v_b - v_e) - \frac{S}{\alpha'\mu}(v_e - v_e) \dots (8)$$

Eq. (7) is completely analogous with the equation for a triode, the cathode of which corresponds to the emitter, the grid to the base and the anode to the collector, and with a transconductance S and an amplification factor μ . In (8) α' is the amplification factor of the transistor in common-emitter circuits ⁵⁾, and μ' is a

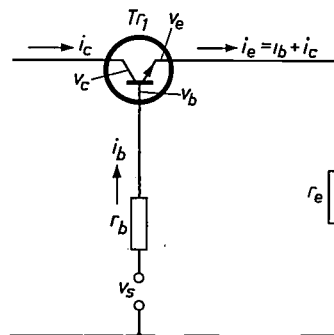


Fig. 6. For deriving the effective amplification factor μ_{tr} of the transistor Tr_1 in *fig. 5*.

²⁾ See e.g. Philips tech. Rev. 23, 145, 1961/62.
³⁾ Except when the DC terminals are short-circuited. We shall return to this point later.
⁴⁾ F.H. Stieltjes and L.J. Tummars, Philips tech. Rev. 17, 244, 1955/56.

⁵⁾ See page 242 of the article under reference ⁴⁾.

factor that differs relatively little from μ . In addition the following relations hold:

$$v_c = (i_c + i_b)r_c \dots \dots \dots (9)$$

and

$$v_s = v_b + i_b r_b \dots \dots \dots (10)$$

By adding (7) and (8) we find an equation from which, using (9), we can eliminate $i_b + i_c$. The result is:

$$\frac{1}{S} \frac{v_c}{r_c} = \left(1 + \frac{1}{a'}\right) (v_b - v_c) + \left(\frac{1}{\mu} - \frac{1}{a'\mu'}\right) (v_c - v_e) \dots (11)$$

Elimination of i_b and v_b from (8), (10) and (11) leads to an equation for v_c in which v_s and v_e occur with the following coefficients:

$$\frac{1 + \frac{1}{a'}}{1 + \frac{S r_b}{a'}} \text{ and } \left(\frac{1}{\mu} - \frac{1}{a'\mu'} + \frac{S r_b}{1 + \frac{S r_b}{a'}}\right), \text{ respectively.}$$

The first coefficient is a measure of the influence of v_s on v_c , the second is a measure of the influence of v_e on v_c . In the circuit of fig.5 they are therefore a measure of the respective influences of the driving voltage and the collector voltage (= cathode voltage of the EL 34) on the output voltage. The ratio of these coefficients may be called the *effective amplification factor* μ_{tr} of the transistor. Since in practice a' is much greater than unity and μ' is of the same order of magnitude as μ , we can write to a good approximation:

$$\mu_{tr} = \frac{1}{\frac{1}{\mu} + \left(\frac{1}{\mu} + \frac{1}{\mu'}\right) \frac{S r_b}{a'}} \dots \dots \dots (12)$$

If $r_b \leq a'/S$ (of the order of 1 k Ω) and given $\mu' \approx \mu$, it follows from (12) that

$$\mu_{tr} > \frac{1}{3}\mu.$$

In most types of transistor μ is 1500 or more, so that μ_{tr} is greater than 500.

The quantity $(\mu^{-1} + \mu'^{-1})S$ which occurs in (12), and likewise $(\mu^{-1} + \mu'^{-1})$, are easily derived from the published characteristics of the transistors. Evidently, given a constant base current ($i_b = 0$), eq. (8) becomes:

$$v_b - v_e = \frac{1}{\mu'} (v_c - v_e).$$

From (7) we therefore find:

$$i_c = \left(\frac{1}{\mu} + \frac{1}{\mu'}\right) S (v_c - v_e),$$

hence

$$\left(\frac{1}{\mu} + \frac{1}{\mu'}\right) S = \frac{i_c}{v_c - v_e} \dots \dots \dots (13)$$

The last fraction corresponds to the slope of the characteristics which give the collector current as a function of $v_c - v_e$ at a constant base current.

Plainly, using a cascode with such an exceptionally high effective amplification factor, we can accept a very low gain A (about 10). This can easily be obtained with a single stage. The number of time constants is thus kept to a minimum, aiding the simplicity and stability of the control system.

At 5 mA load the transconductance of the transistor (and hence of the cascode too) rises to about 100 mA/V. The time constant $\tau_1 = C_2/S$ therefore decreases to about 2 μ s, which is of the same order

as τ_2 . To maintain the stability a resistor R_3 is therefore put in series with the emitter (fig.5). This makes $\tau_1 = C_2(R_3 + S^{-1})$, so that it is less dependent on S , in other words less dependent on the load. A resistance $R_3 = 68$ ohms is found to be large enough; the regulation requirement is for this value to remain amply fulfilled.

Other components

Reference-voltage source

The source of the reference voltage is a type 83 A 1 voltage stabilizer tube. The glow discharge in this tube has a sustaining voltage of about 83 V. Since the latter depends slightly on the current through the tube, the current is drawn from an auxiliary stabilized voltage source (-150 V with respect to the positive terminal). The temperature coefficient of the reference voltage is -3.5 mV/ $^{\circ}$ C, i.e. roughly $-4 \times 10^{-5} U_{ref}$ per $^{\circ}$ C.

Control amplifier

The circuit diagram of the control amplifier is shown in fig. 7. It consists of a double triode T_2 - T_3 (type E 80 CC) in push-pull, in which the voltage kU_0 is compared with the reference voltage. In this circuit the E 80 CC triode allows the use of an unstabilized heater voltage: a 10% change in this voltage has the same effect as a disturbing voltage at the input of no more than about 8 mV, i.e. $10^{-4} \times U_{ref}$. In most other types of tubes that might be used for this purpose the equivalent disturbing voltage is at least 3 times greater.

Since Tr_1 works single-ended, no anode resistor is needed for one half (T_2) of the E 80 CC triode. This half is fed from the -150 V auxiliary voltage source just mentioned. An auxiliary voltage of about +80 V is needed for the half with the anode resistor (T_3). These auxiliary voltage sources, which are both stabilized, will be discussed under the next heading.

The transistor Tr_1 must be driven by a source having a low impedance. In principle one might therefore insert a cathode follower between T_3 and Tr_1 . Here, however, a valve has the drawback that a 10% change in the heater voltage causes the driving voltage to vary by 0.15 to 0.20 V, which corresponds to a disturbing voltage of 15 to 20 mV at the input of the control amplifier. For this reason, instead of a cathode follower a transistor (Tr_2) is used, which is circuited as an emitter follower, i.e. the emitter of Tr_2 (connected to the base of Tr_1) follows the voltage changes of the base of Tr_2 , which is connected to the anode of T_3 . The transistor Tr_2 , like Tr_1 , is a type OC 139.

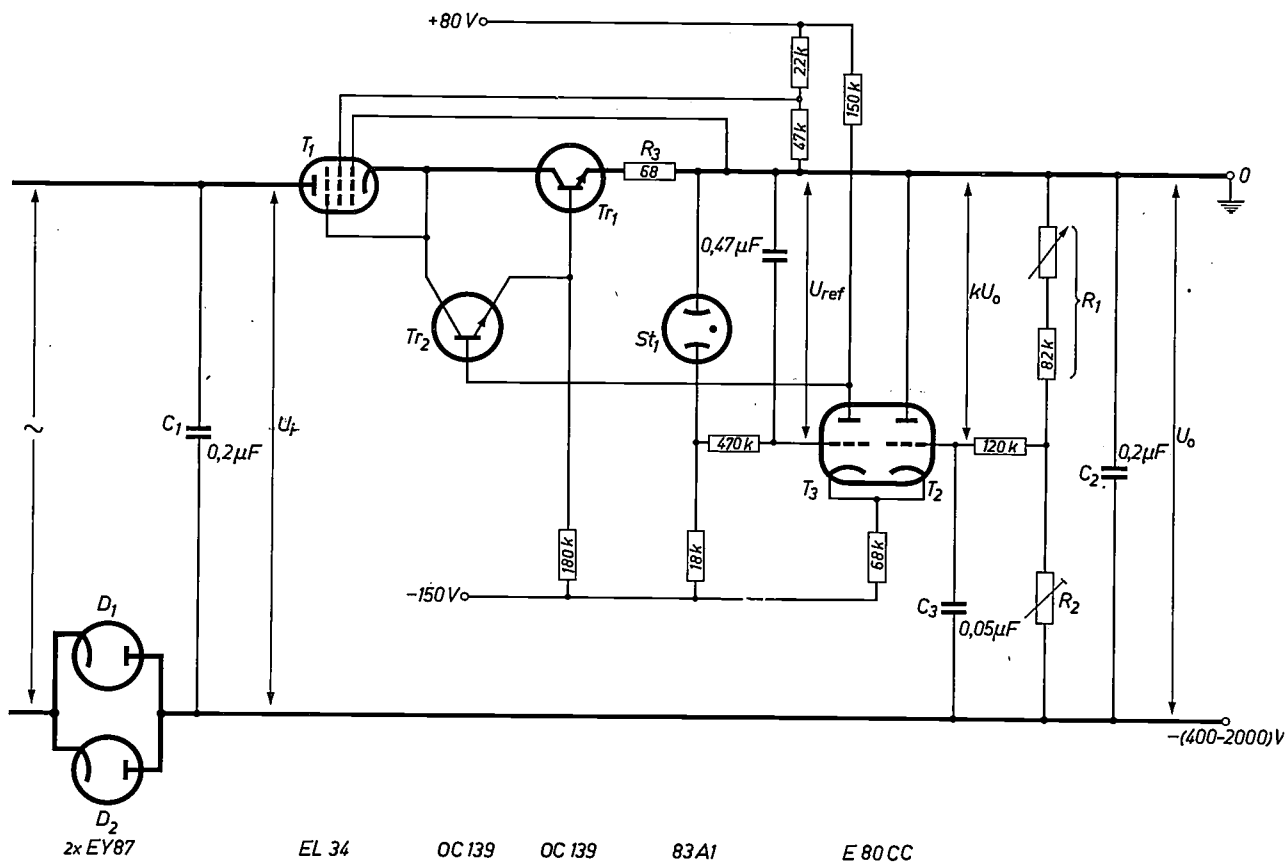


Fig. 7. The principal part of the circuit of the stabilized DC voltage source of 400-2000 V, maximum 5 mA, using the cascode T_1 - Tr_1 of fig. 5. D_1 , D_2 are two EY 87 rectifying valves in parallel. C_1 , C_2 , C_3 , R_1 and R_2 have the same meanings as in fig. 2.

The control amplifier (A in fig. 2) contains a double triode T_2 - T_3 in push-pull, with a common cathode resistor. Here the voltage kU_o is compared with the reference voltage U_{ref} supplied by the voltage stabilizer tube St_1 . The anode of T_3 drives the base of Tr_1 via a transistor Tr_2 (emitter follower).

T_2 , T_3 and Tr_2 and the screen grid of T_1 are fed from stabilized auxiliary voltage sources of +80 and -150 V with respect to the positive terminal (here shown earthed).

Auxiliary voltage sources

As we have seen, two auxiliary stabilized voltage sources are needed, one of which delivers -150 V and the other +80 V with respect to the positive terminal. Both voltages are drawn from one auxiliary stabilized power supply. Here, too, a combination of a valve and a transistor is used to good advantage.

The circuit is shown in fig. 8. One half (T_4) of an ECC 82 double triode is used as the series valve of the auxiliary stabilized power supply, a stabilizer tube St_2 (type 150 A1) serves as the reference voltage source, and the other half of the ECC 82 (T_5) serves as the control amplifier. To obtain sufficient gain it is necessary to give T_5 a fairly high anode resistance. An ordinary resistor, however, would call for a high supply voltage. As such only the unregulated DC voltage is available, but if this were used it would considerably reduce the stabilization.

This difficulty is circumvented by employing a transistor (Tr_3) as the anode resistor. This can be done

because a transistor with a fixed base voltage and a resistor in series with the emitter (fig. 8) has a very high differential resistance in the collector circuit. The DC resistance of the transistor is low, however, so that the stabilized DC voltage can be used (+80 V terminal) for feeding the valve T_5 and the transistor together. The only condition here is that the cathode of the series valve T_4 should be more than 3 V positive with respect to the grid, which is easily fulfilled.

Differential resistance of the transistor in fig. 8

The circuit containing the transistor Tr_3 of fig. 8 is shown in fig. 9a. Using equations (7), (8) and (9) and the relation $v_b = -i_b r_b$, we find for the changes in the collector and base currents the following expressions:

$$\left\{ 1 + \left(1 + \frac{1}{\mu} \right) S r_e \right\} i_c + \left\{ S r_b + \left(1 + \frac{1}{\mu} \right) S r_e \right\} i_b = \frac{S}{\mu} v_e,$$

$$\left(1 - \frac{1}{\mu} \right) S r_e i_c + \left\{ a' + S r_b + \left(1 - \frac{1}{\mu} \right) S r_e \right\} i_b = -\frac{S}{\mu} v_e.$$

From this we can solve v_e/i_c , which is equal to the required

diffusion technique ("p.o.b." transistors)⁶, such as type OC 171, this influence is much less than in other transistors, e.g. type OC 71. With an OC 171 transistor, therefore, exceptionally high differential resistances can be obtained.

If r_c is infinitely large and r_b is finite, R_d according to (15) attains its maximum value, which is equal to $\alpha' \rho$. For the OC 171 this limiting value is about 10 M Ω , for the OC 71 about 0.5 M Ω . As already noted, in the present case a much lower value of R_d suffices.

Voltage divider

The DC output voltage can be varied by varying the resistance R_2 of the voltage divider (fig.7). In a particular case it was required that the voltage should be variable in steps of 200 V from 2000 V to 400 V, and moreover that there should be ten steps of 20 V and ten steps of 2 V available. For this purpose R_2 was built up from seven resistors of 180 k Ω , ten of 18 k Ω and ten of 1.8 k Ω ; R_1 consisted of a fixed resistor of 82 k Ω in series with a continuously variable correction resistor of 0 to 15 k Ω . All these resistors are metallic and their temperature coefficient is lower than 5×10^{-5} per $^{\circ}\text{C}$.

When varying R_2 measures are needed to guard against switching transients that could endanger the transistors. This is done by the circuit described below, which offers protection against the consequences of short-circuiting the output.

The transistors could also be damaged if the high tension came on too quickly after switching on the apparatus. For this reason a thermistor (Th in fig.8), which at room temperature has a 70 times greater resistance than at the working temperature, is connected in series with the heaters of the rectifying valves (2 EY 87 rectifiers in parallel). This thermistor delays the heating of the cathodes to such an extent that the high tension does not come on until the control amplifier is already in operation.

Protection against the consequences of short-circuiting of the output

It is particularly useful for power-supply apparatus — especially if intended for experimental purposes — to be proof against short-circuiting. It proved possible to give this property to the DC voltage source described here by the addition of only one transistor, one diode and a few resistors.

A short-circuited output presents two dangers:

- 1) During a short-circuit the voltage between the cathode and control grid of the EL 34 can rise above 20 V, thereby exceeding the permissible value for the transistor Tr_1 .

- 2) The direct current becomes so high that various components are overloaded.

Both dangers are averted by using the $P-N-P$ transistor Tr_4 (type OC 71) in combination with the resistor R_4 in the circuit of fig. 10. The emitter of Tr_4 carries with respect to the positive terminal a fixed voltage of +5 V, taken from a voltage divider across

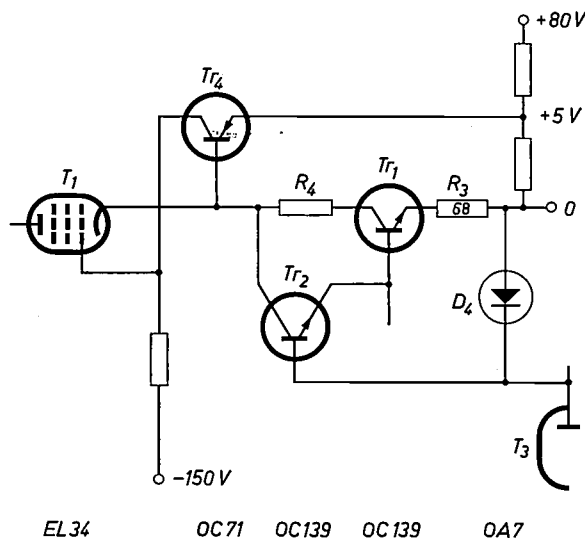


Fig.10. Circuit for safeguarding the apparatus against the consequences of short-circuiting.

Tr_1 , Tr_2 , R_3 and Tr_4 have the same meanings as in fig. 7. Since the control grid of Tr_1 is now at a point of lower potential than before, there is no longer any danger that Tr_1 will have to carry more than 20 V under exceptional conditions. Transistor Tr_4 can be regarded as a control amplifier which tends to keep the cathode of Tr_1 at a fixed potential with respect to the positive terminal, equal to the reference voltage of 5 V. A voltage of about 5 V is therefore across $R_4 + Tr_1 + R_3$, so that the current has an upper limit of $5 \text{ V} / (R_3 + R_4)$ ohms. The short-circuit current is limited to approx. 7 mA by making $R_4 = 650$ ohms.

Germanium diode D_4 — normally non-conducting — prevents a high negative voltage surge being applied to the base of Tr_2 upon the removal of a short-circuit.

the stabilized auxiliary voltage source of +80 V; the collector of Tr_4 is fed via a resistor from the point carrying the stabilized voltage of -150 V. Tr_1 can be regarded as the series valve and Tr_4 as the control amplifier of a primitive stabilized power supply having a reference voltage of 5 V, which tries to keep the cathode of Tr_1 at a potential of 5 V with respect to the positive terminal. Since the control grid of Tr_1 is no longer connected to the emitter of Tr_2 , but to a point of lower potential (the collector of Tr_4), the voltage between control grid and cathode can safely exceed 20 V without endangering Tr_1 . Tr_4 is a transistor that can take a collector voltage of 30 V.

Since Tr_4 keeps the cathode of Tr_1 at a voltage of about 5 V, this voltage is also across the series arrangement of R_4 , Tr_1 and R_3 . The current through this configuration cannot therefore go higher than $5 \text{ V} / (R_4 + R_3)$, though it may well be lower, de-

⁶ P.J.W. Jochems, The alloy-diffusion technique for manufacturing high-frequency transistors, Philips tech. Rev. 24, 231-239, 1962/63 (No. 8).

pending on the drive for Tr_1 . By the choice of $R_4 = 650$ ohms, the current concerned is limited to $5\text{ V}/(650 + 68)$ ohms = approx. 7mA and the short-circuit current cannot therefore exceed this harmless value. The short-circuit current can be adjusted by making R_4 variable.

The foregoing considerations apply to the *stationary* short-circuited state. The occurrence and the removal of the short-circuit give rise to transients that could be dangerous to certain transistors. The removal of the short-circuit endangers transistor Tr_2 . This can easily be avoided by inserting between the base of Tr_2 and the positive terminal a diode D_4 (type OA 7 germanium diode); see fig. 10. In the normal state diode D_4 passes no current, but upon removal of a short-circuit it becomes momentarily conductive, thereby preventing the voltage at the base of Tr_2 from going too negative.

The tendency of Tr_4 to keep the cathode of T_1 at a fixed potential (5V) also contributes to the stabilization, which is thus an incidental advantage of the circuit.

Results

Measurements have been carried out under the following load conditions:

2000 V - 0 mA,	2000 V - 5 mA,
400 V - 0 mA,	400 V - 5 mA.

Stabilization against mains-voltage fluctuations. Tests on various E 80 CC double triodes (T_2 - T_3) at the above settings showed that a 10% increase or decrease of the mains voltage caused a change in the output voltage ranging from 0.008 to 0.002%. The mutual disparities are attributable to the difference in the effect of changes in the heater voltage in the E 80 CC. Stabilization of the heater voltage can reduce these figures to about 0.001%. If even

better stabilization of the auxiliary voltages (+80 and -150 V) were applied, the output variations would ultimately be caused only via the still unstabilized high tension; in that case the variations are smaller than 1 in 10^6 .

Regulation. A change of 0.5 mA in the current drain caused a change of 0.005% in the output voltage.

Hum and ripple. At all settings, both with earthed positive and earthed negative terminals, the hum plus ripple was found to be lower than 2 mV peak-to-peak (0.0005% of the output voltage when this was 400 V).

Long-term drift. After the apparatus had been switched on for one hour, the drift in the output voltage during many hours of operation was less than 0.01%, in an ambient temperature which remained constant within a few °C. When the apparatus, after having been switched off, was again switched on, the output voltage returned after some time to within 0.01% of the original value. The magnitude of this deviation is principally determined by the quality of the E 80 CC valve and of the resistors in the voltage divider R_1 - R_2 . A limit of 0.1% can certainly be guaranteed.

Summary. Description of a DC voltage source for 400-2000V and 0-5 mA which meets very high demands: a 10% fluctuation in the mains voltage or in the current drain causes a maximum of 0.01% change in the DC voltage; hum + ripple (peak-to-peak) is no more than 10^{-5} times the output voltage; voltage drift maximum 0.1%. If an EL 34 pentode is chosen as the series tube, more gain is needed to meet the requirement than is compatible with the specified absence of overshoot in the control system. A favourable solution was found by combining the EL 34 with an OC 139 N-P-N transistor to form a cascode, the effective amplification factor of which is greater than 10^5 . The control amplifier drives this transistor via a second transistor OC 139. In an auxiliary stabilized power supply, delivering two stabilized DC voltages, the anode resistor is a third transistor (OC 171), which has a high differential resistance and a low DC resistance. A fourth transistor (OC 71) safeguards the apparatus against short-circuits.

A PRECISION GRINDING MACHINE FOR TRACER DIFFUSION STUDIES

621.925

To investigate the diffusion of a particular element in a solid the following procedure is one often used. The element is deposited on a slice of the relevant solid — the specimen — which is then annealed for a suitable time at a controlled temperature in a furnace. To indicate the order of magnitude of the various quantities involved, we shall take as an example the results of an experiment on the diffusion of manganese in gallium arsenide, where the diffusion took place during 18 hours at 900 °C. At the end of the experiment the curve of the manganese concentration c_{Mn} versus penetration depth x was as shown in *fig. 1*. The method of deriving from this the diffusion constant and other required quantities does not concern us here ¹⁾.

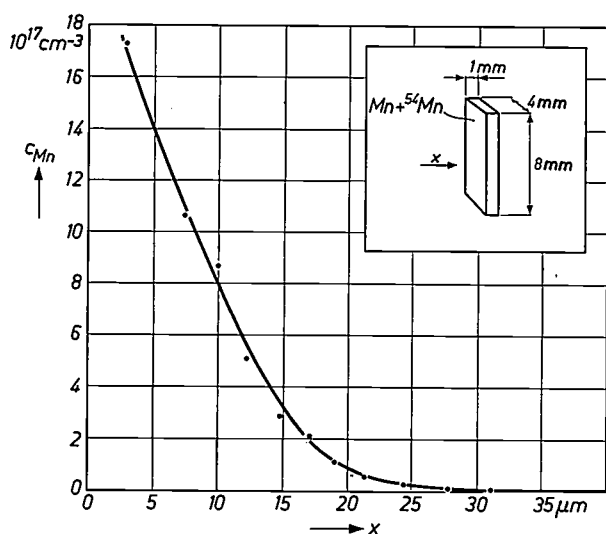


Fig. 1. Diffusion of manganese in gallium arsenide. The curve gives the manganese concentration c_{Mn} (in atoms per cm^3) as a function of the penetration depth x . The sketch gives the dimensions of the specimen, the arrow indicating the direction of diffusion. The manganese, which contains a small fraction (about 0.1%) of the radioactive isotope ^{54}Mn , is applied to the specimen by moistening a side face with a solution of Mn^*Cl_2 and letting the solvent evaporate. (Mn^* means a mixture of normal and radioactive Mn.)

The problem is how to determine the concentration curve. For this purpose thin layers can be removed from the specimen by etching, grinding or turning, and the concentrations of the diffusing element in each successive layer determined. Chemical determination of these concentrations is time-consuming and moreover not always accurate enough,

¹⁾ See e.g. P. G. Shewmon, *Diffusion in solids*, McGraw-Hill, New York 1963.

while for self-diffusion studies the method cannot be applied. Therefore use is made of a tracer diffusion method, employing a radioactive isotope of the element — provided a suitable one exists. The concentration curve can be established in two ways, either by measuring the radioactivity of the specimen after each layer is removed or by measuring the radioactivity of the removed layers. The latter method is the more accurate, and in the case of metals easy to apply. The layers are machined off on a precision lathe and the turnings collected. Where the materials are hard and brittle, however, grinding is necessary, and special steps are then required to ensure that all the removed material is collected. In such cases the measurements are often done on the specimen itself to save trouble, but at the expense of reduced accuracy.

The radioactivity involved in such experiments is always weak and no safety measures, such as lead shielding, are necessary.

In the literature descriptions have been given of several precision grinding machines specially designed for diffusion studies and allowing the complete collection of the material ground from the specimen ²⁾. We too have built a grinding machine of this kind (*fig. 2*), which serves its purpose very satisfactorily.

From the sketch (*fig. 3*) it can be seen that the machine has a horizontal grinding table G . The specimen S rests on a piece of brass foil F , 0.1 mm thick, which is held by suction to the surface of the table. To this end the table top contains concentric grooves which are connected by radial grooves to a central hole. *Fig. 3* shows how the latter ultimately communicates with a vacuum line V_1 . The shaft A_G about which the table rotates is mounted 30 mm off centre in the intermediate plate E , which rotates about the shaft A_E . When E rotates — driven by the pinion P — the grinding table rolls around the inside of the housing I and describes a planetary motion. To this effect the grinding table and housing are provided with gear teeth, the housing of course internally. The resultant rolling motion of the table ensures uni-

²⁾ W. C. Dunlap, Jr., *Diffusion of impurities in germanium*, *Phys. Rev.* **94**, 1531-1540, 1954, in particular pages 1534 and 1536. H. Letaw, Jr., L. M. Slifkin and W. M. Portnoy, *A precision grinding machine for diffusion studies*, *Rev. sci. Instr.* **25**, 865-868, 1954. B. Goldstein, *Precision lapping device*, *Rev. sci. Instr.* **28**, 289-290, 1957. H. W. Schamp, Jr., D. A. Oakes and N. M. Reed, *Grinder for sectioning solid diffusion specimens*, *Rev. sci. Instr.* **30**, 1028-1031, 1959.

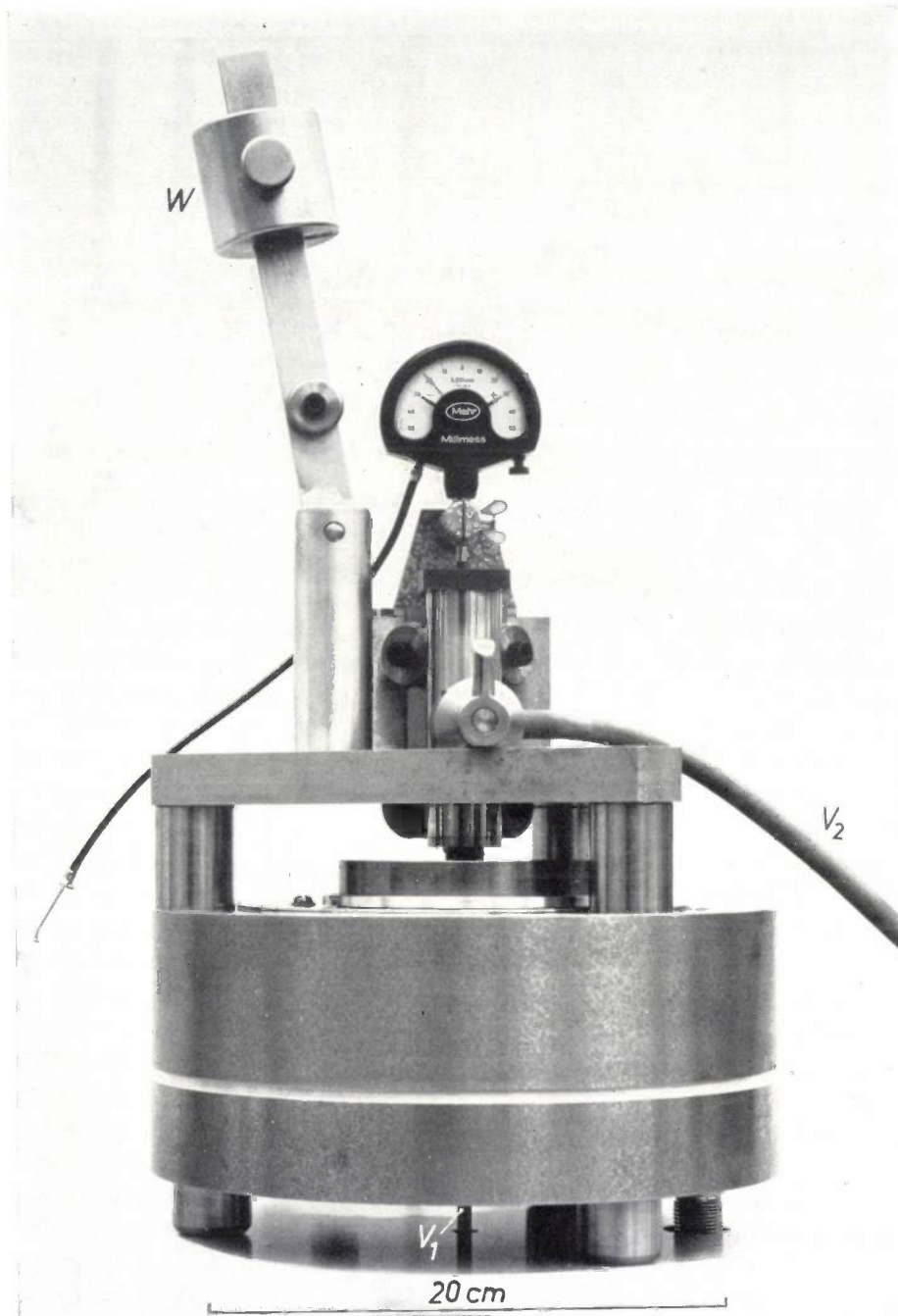


Fig. 2. The precision grinding machine for studying diffusion in solids.

form grinding. The ratio of the pitch circles of the teeth of table and housing is 5 : 8, so that *E* makes five and *G* eight revolutions before the table returns to exactly the same position. The components *U*, *I*, *E* and *G* are of pearlitic cast iron.

The specimen is fixed to the bottom of a carrier disc *D* by means of wax, the disc being held by suction to the vertical holder *H*. Both *D* and *H* are made of stainless chromium steel. The vacuum line *V*₂ can be seen in fig.2. The holder is pressed against the ball bearings *K* (a total of four) by the spring *V*

and a fifth ball bearing *K'*. The holder is therefore able to move in the vertical direction without much friction, and can also readily be removed as a whole from the machine by pulling the bearing *K'* outwards against the action of spring *V*. The dead weight of the holder (approx. 600 g) is usually sufficient to press the specimen against the grinding table. The pressure can be increased by a sliding weight *W* on an arm (fig.2), which can be laid on the holder with a roller. So far, however, this has not proved necessary. The arm is not drawn in fig. 3.

Before grinding begins, the grinding plate is provided with a new brass foil *F*, to which the abrasive and a few drops of kerosene are applied. During grinding the abrasive distributes itself over a ring-shaped path on the foil (*fig.4*). The ground particles remain behind here, except for a fraction that adheres to the specimen and which is collected in the wadding used to clean the specimen. The wadding and the foil together thus contain all the material ground from the specimen. The abrasive used is diamond powder with grain sizes of 2-4, 4-7, 10-15 or 20-40 μm ; the thicker the layer to be removed the coarser the abrasive.

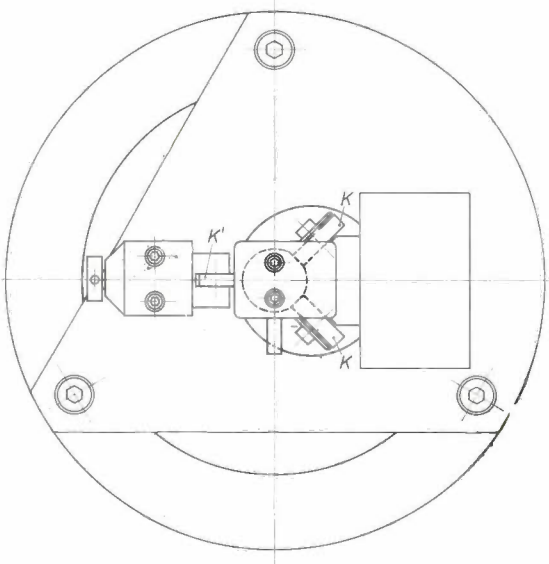
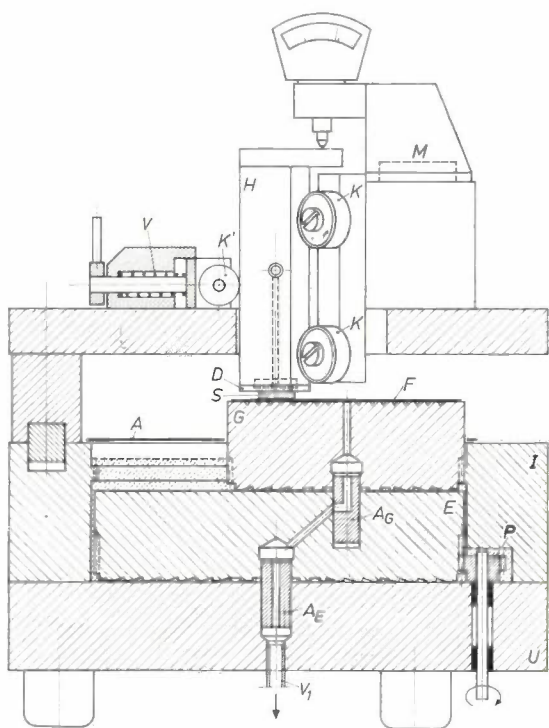


Fig. 3. Sketch of the grinding machine in fig. 2.

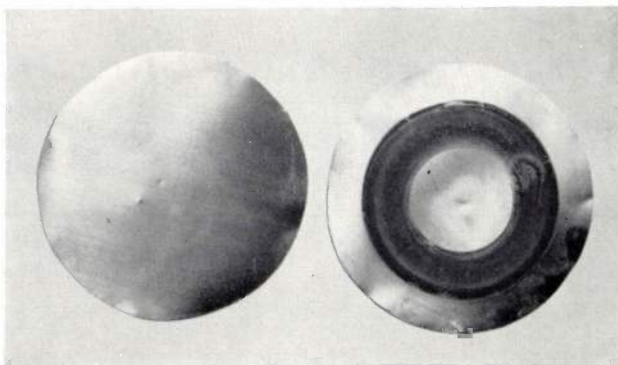


Fig. 4. Brass foils 0.1 mm thick, which are held by suction to the grinding table. Left, a new foil; right, a used one. It can clearly be seen on the latter where the specimen was last in contact with it.

During the grinding process the reduction of specimen thickness can be followed roughly on a dial gauge mounted on the holder *H* (figs. 2 and 3). For easy removal, which is necessary if the holder *H* has to be lifted out of the machine, the dial gauge is attached by means of a permanent magnet *M* (fig.3).

The exact thickness of the removed layer is determined by weighing together the specimen and the carrier disc *D* before and after a grinding run, or by measuring the thickness of specimen and disc together on a dial gauge before and after grinding. The fact that the specimen does not have to be detached from *D* for every measurement is a great advantage in connection with the successive grinding of numerous layers. The disc *D* weighs about 20 g, the specimen roughly 1 g or less. The combined weight of disc and specimen is therefore not too great for it to be determined with a precision balance. If the area of the specimen to be ground is very small (less than about 0.5 cm²), the thickness measurement is more exact.

The concentration of the diffusing element in the removed material is easiest to determine by a gamma-radiation measurement. In most unstable atomic nuclei the radioactive decay is accompanied by the emission of gamma rays, so that this method can usually be adopted. For the measurement the brass foil is folded up — with the radioactive particles inside — and placed, together with the wadding used to clean the specimen, in a glass vial of e.g. 16 mm diameter and 50 mm length (*fig.5*). The gamma radiation is measured with a well-type scintillation crystal of NaI(Tl) (sodium iodide with 0.1% thallium); see *fig. 6*. We use a commercially available combination of crystal and photomultiplier for counting the scintillations. This method of counting is readily reproducible because the gamma rays are not significantly absorbed by the brass and the vial, and the crystal encloses the vial so well that it

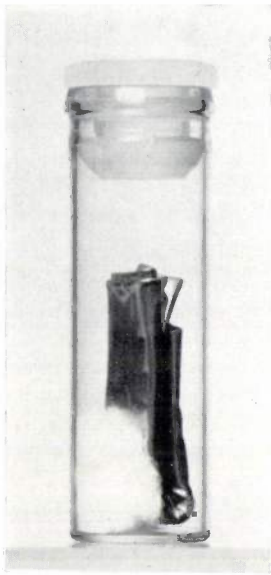


Fig. 5. A vial containing a folded brass foil with ground-off radioactive material and the wadding used for cleaning the specimen, ready for insertion in the scintillation counter.

Fig. 6. For measuring the gamma radiation, the vial in fig. 5 is placed in a well-type scintillation crystal *C*, which receives a considerable part of the radiation and is mounted on a photomultiplier tube *M*.

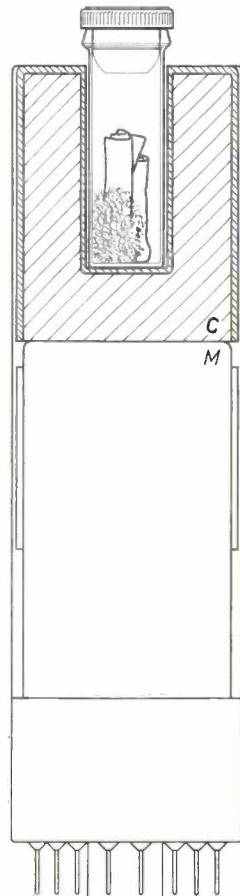


Fig. 6

receives a substantial part of the radiation (usually between 20 and 70%, depending on the energy of the gamma quanta). If beta radiation is to be measured it is necessary — owing to the strong absorption — to prepare the specimens very carefully. Normally the brass foil has to be dissolved and the radioactive material chemically separated. For the actual measurement a Geiger counter suffices, which is much cheaper than the equipment needed for measuring gamma radiation.

The thicknesses of the removed layers vary from a few microns to several hundred microns. The preferred thickness is about $20\ \mu\text{m}$. From the example given in fig. 1, however, which relates to measurements done with the apparatus described here, it can

be seen that good results are also obtained with layer thicknesses of a few microns.

The thinner the layers the more important it is that each layer should have a uniform thickness, in other words be evenly ground. The base plate *U* of the machine should therefore be scrupulously flat and the grinding table *G* and the intermediate plate *E* accurately flat and plane-parallel. The carrier disc *D* and the specimen can be ground plane-parallel on the machine itself. As regards the specimen, this must of course be done before diffusion takes place. When fixing the specimen with wax, care is needed to ensure that no wax comes between specimen and carrier disc.

Finally, it is important that the oil films between *U* and *E* and between *E* and *G* should be plane-parallel. We have achieved good results by using thin oil and providing the grinding plate and the intermediate plate *E* underneath with a spiral groove, which pumps the oil inwards while the machine is turning³⁾. These plates also contain radial grooves underneath, along which the oil returns and is thus kept circulating. The housing *I* is filled with oil up to the horizontal dashed line in fig. 3. A cover plate *A*, containing a recess for the grinding table, protects the oil from dust. To prevent the oil being completely forced out when the machine is stationary, we use oil that adheres well to the metal, being the type used to lubricate the bed of planing machines.

After successive grinding operations the specimen has been found to remain flat and plane-parallel to within $1\ \mu\text{m}$; the accuracy is probably even better, but it is difficult to establish this with certainty. With the intermediate plate turning at 25 revolutions per minute the grinding time per layer is between one minute and half an hour, depending on the thickness to be ground away, the material of the specimen and the diamond powder used.

L. M. L. J. LEBLANS *),
M. L. VERHEIJKE *)

³⁾ This kind of bearing will be dealt with in an article by E.A. Muijderland, which will shortly be published in this journal.

*) Philips Research Laboratories, Eindhoven.

INHOMOGENEITIES IN DOPED GERMANIUM AND SILICON CRYSTALS

by J. A. M. DIKHOFF *).

548.4:546.28

The demands made on the quality of doped germanium and silicon in science and industry are steadily increasing. This has stimulated research into the nature and genesis of inhomogeneities which are not normally detected by routine measurements on complete crystals. The article below gives a survey of the present state of knowledge on this subject, illustrated by a number of photos. Most of these show striation patterns which can occur in different cases, and which often give a clear record of what has happened during the growth of the crystal.

The technique of making rod-shaped germanium and silicon crystals containing desired amounts of impurities ("dope"), which are used for the production of transistors and other semiconducting switching elements, has in recent years reached a

Since these inhomogeneities can give the manufacturer of transistors a great deal of trouble, a number of years ago we started an investigation into their nature and the way they are produced. In this article we shall discuss three of the most important sorts of

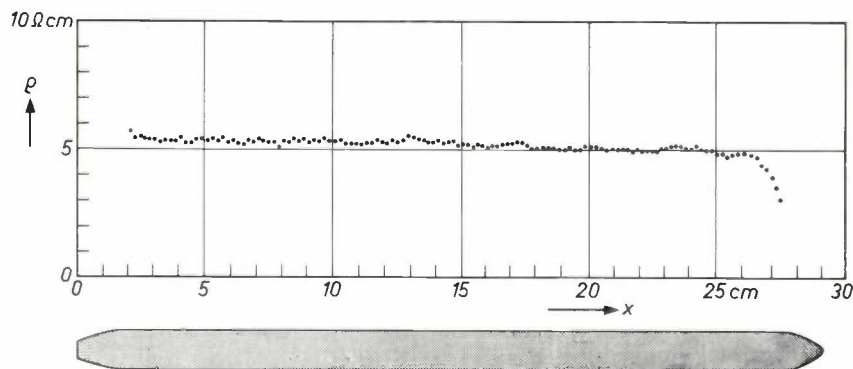


Fig.1. It is now possible to make doped rod-shaped crystals of germanium and silicon whose resistivity ρ shows no systematic variation and only slight fluctuations in an axial direction. The graph shows measurements on a germanium crystal doped with indium.

high state of perfection. It is now possible to make such doped crystals in which the concentration of impurities not only has the desired overall value but is also remarkably constant throughout the whole crystal¹⁾. The constancy of the concentration of dope is normally checked by measuring the resistivity ρ . An example of the result of such a measurement is shown in *fig.1*, in which the resistivity ρ is plotted against the distance x measured from one end of the crystal.

It has been found that rods which give a very nice ρ, x diagram may still exhibit considerable inhomogeneities, so much so in fact that they are sometimes unsuitable for their intended purpose. As an example of this, *fig.2* shows the variation of ρ along a diameter of a transverse section of a germanium single crystal doped with antimony.

inhomogeneities, and briefly indicate how they can be prevented (in so far as this is possible). These three sorts are: 1) striations, 2) cores and 3) inclusions²⁾.

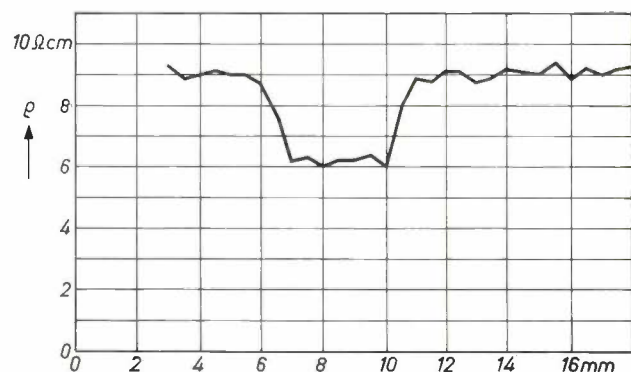


Fig.2. The variation of the resistivity ρ along a diameter of a transverse section of an inhomogeneous germanium crystal doped with antimony.

*) Philips Research Laboratories, Eindhoven.

¹⁾ See e.g. J. Goorissen, Philips tech. Rev. 21, 185-195, 1959/60, or chapter 6 (by B. Okkerse) of the Handbook of semiconductor electronics, 2nd edn. (editor L. P. Hunter), McGraw-Hill, New York 1962.

²⁾ Part of the results of this investigation, in particular with reference to cores, has already been published in: J.A.M. Dikhoff, Solid-state electronics 1, 202, 1960; references to previous investigations in this field are also given in this paper.

To begin with, we shall recapitulate some of the most important concepts of the theory of the solidification of binary mixtures, and give a brief description of the making of rod-shaped crystals by the "pulling" method.

The solidification of a binary mixture

In order to describe what happens at the solid-liquid interface during the solidification of a binary mixture, we make use of the phase diagram (fig.3).

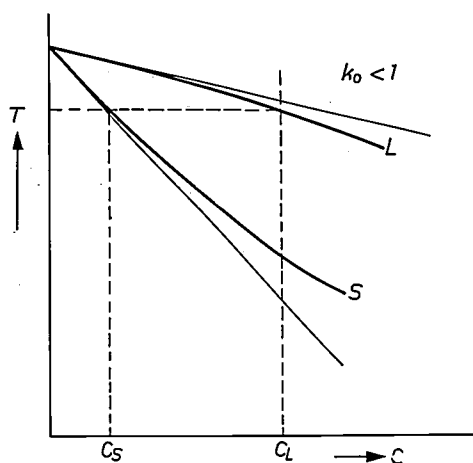


Fig.3. Part of the phase diagram of a binary mixture. At a certain temperature T the equilibrium concentrations C_S and C_L of the solute in the solid and liquid phases respectively are not equal. For low concentrations, the curves S and L which give the variation of C_S and C_L with T may be approximated to by straight lines. The ratio C_S/C_L , the distribution coefficient k_0 , does not depend on the concentration in this case. When, as in the case represented in the diagram, T decreases with increasing concentration, $k_0 < 1$.

This diagram shows how the freezing point of a liquid solution (curve L) and the melting point of a solid solution (curve S) vary with concentration. The points on the two curves at a given temperature correspond to the concentrations C_S and C_L of the solute in the solid and liquid phases in equilibrium with one another at this temperature. As may be seen, C_S and C_L are not equal.

For small values of C_S and C_L , the curves S and L may be approximated to by straight lines; the ratio C_S/C_L is then equal to the constant k_0 , which is known as the distribution coefficient. For the solutions we shall be dealing with in this article, the value of k_0 normally differs considerably from unity; for a solution of indium in germanium, for example, k_0 is about 0.001.

If a melt of concentration C situated in a long, narrow boat is allowed to solidify slowly from one end, the concentration in the first portion to solidify will be equal to $k_0 C$, i.e. much less than in the liquid. A large amount of the impurity has thus been driven out of the volume in which solidification has occurred. In the extreme case that the excess impurity is im-

mediately distributed throughout the liquid phase by vigorous stirring, the above remains true as solidification proceeds — except that C gradually increases as a result of this expulsion of impurity from the solid phase.

In practice, however, the stirring is never as good as this. There is always a layer of liquid near the solid-liquid interface in which transport of the impurity can only occur by diffusion. The concentration in this "diffusion layer" is thus greater than in the body of the liquid. As a result, the concentration C_S in the solid phase is also higher than would be the case with perfect stirring. The ratio k of C_S to the concentration C in the liquid outside the diffusion layer is thus greater than k_0 . This ratio k is known as the segregation coefficient. Its value is determined by the thickness of the diffusion layer (i.e. by the efficiency of the stirring) and by the rate at which the solid-liquid interface moves; as this rate is greater, there will be a greater concentration of the impurity in front of the interface so that k will be greater. The dependence of k on the growth rate and the degree of stirring will keep on coming up in this article.

The pulling method

Rod-shaped germanium crystals are normally made by Czochralski's method, better known as the "pulling method" ¹⁾. In this method, a seed crystal fixed on the end of a rotating shaft is lowered until it just touches the surface of a quantity of the molten material. The supply of heat to the melt is then reduced somewhat, and the seed crystal is slowly raised. In this way a single crystal is formed on the end of the seed. The value of the segregation coefficient k is here determined, apart from k_0 , by the pulling rate f and the angular velocity ω of the shaft; the latter quantity (together with the kinematic viscosity of the liquid and the diffusion constant of the impurity in question) determines the thickness of the diffusion layer.

Striations

It was found in 1953 ³⁾, during an investigation of the way in which the segregation coefficient k depends on the pulling conditions, that when a germanium crystal is rotated very slowly during pulling (e.g. 4 r.p.m.), periodic changes in concentration are produced along the length of the crystal. The variation of the concentration was investigated with the aid of radioactive impurities: as soon as a crystal had been pulled, it was sawn lengthways and

³⁾ J. A. Burton, E. D. Kolb, W. P. Slichter and J. D. Struthers, J. chem. Phys. 21, 1991, 1953.

an autoradiogram was made of the surface thus exposed. With crystals which had been rotated slowly, the autoradiogram showed transverse lines; crystals which had been rotated quickly showed no such lines.

It was found later that crystals which had been pulled with a fast rate of rotation also showed such lines ("striations"); but these lie so close to one another that they are not resolved in the autoradiogram. There is even less chance of finding them by routine measurements of the resistivity ρ . A variation of ρ as shown in fig.2 is due to another sort of inhomogeneity. The existence of striations very close to one another can only be demonstrated by methods with a high resolving power.

One of the most important of these is the method of pulsed copper-plating⁴⁾. Here too the rod-shaped crystal is cut open lengthways, and the exposed surface is dipped in a solution of a copper salt. A current is then passed through the solution, the crystal acting as the negative electrode. Since the zones of differing concentration also have different conductivities, more copper is deposited on the zones which conduct better. The current is periodically interrupted, to prevent the desired effect from being disturbed by local exhaustion of copper salt in the solution; during the periods in which the current is cut off, the concentration of the copper in solution is evened out by diffusion. A crystal which has been treated in this way is shown in fig.4. The method of pulsed copper-

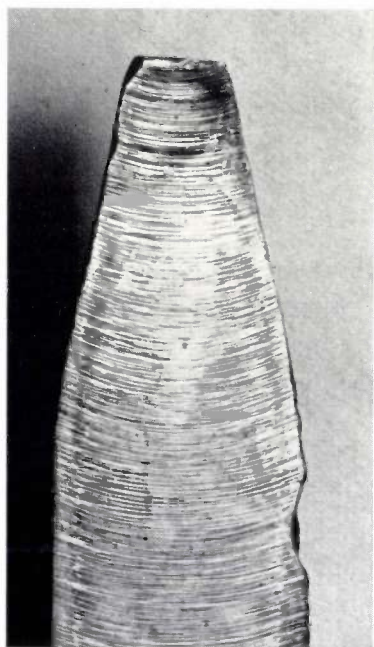


Fig.4. Longitudinal section of a crystal, with the striations made visible by pulsed copper-plating. (Growth direction from top to bottom; this is true of all the longitudinal sections reproduced in this article.)

⁴⁾ See P. R. Camp, *J. appl. Phys.* **25**, 459, 1954. The method has been further developed and modified by J. Bloem for N-type germanium (unpublished).

plating can detect very slight concentration differences; the resolving power is such that striations can still be clearly observed when they occur at intervals of 10 μm .

It is also possible to make the striations visible by connecting the voltage source the other way round: more material is then dissolved from the zones with higher conductivity, so that grooves are produced in the surface of the crystal.

In heavily doped crystals, the striations can be made visible simply by etching (e.g. in a mixture of HF, HNO₃, and alcohol). The resolution is even better here, being about 1 μm (see fig. 5).

Two other, very elegant methods which also have

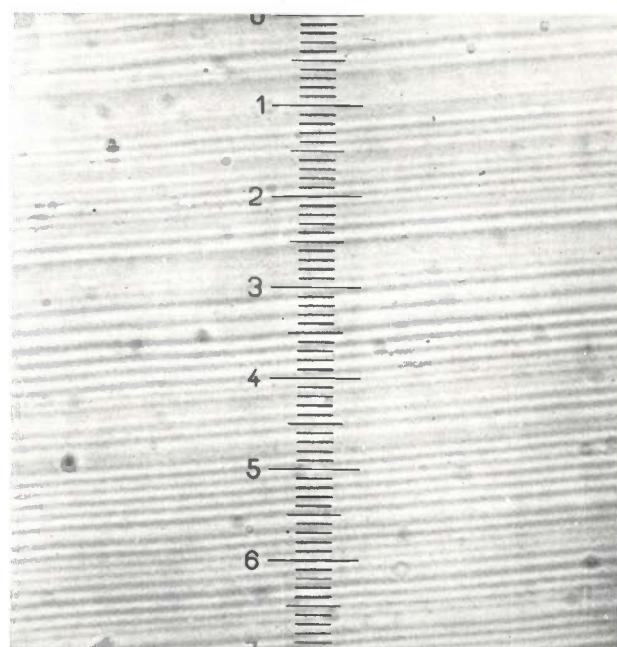


Fig.5. Detail of photo of striations in germanium heavily doped with gallium, which have been made visible by etching. The distance between successive striations is only 2 μm (magnification 600 \times).

a high resolution are based on certain aspects of the diffraction of X-rays. One of these makes use of the anomalous-transmission effect⁵⁾, while the other has come to be known as Lang's method⁶⁾. A good example of a photo made by the latter method is shown in fig. 6.

The fact that the very fine striations occurring in crystals which were rotated quickly during pulling can be demonstrated by pulsed copper-plating is an indication that these striations, like those found in slowly rotated crystals, correspond to zones of different concentration. A second argument for this is that the striations can be made to disappear by heating the crystal to a high temperature, for a length of time which has been found to depend directly on

⁵⁾ See e.g. B. Okkerse, *Philips tech. Rev.* **21**, 340-345, 1959/60.

⁶⁾ See e.g. A. E. Jenkinson, *Philips tech. Rev.* **23**, 82-88, 1961/62.

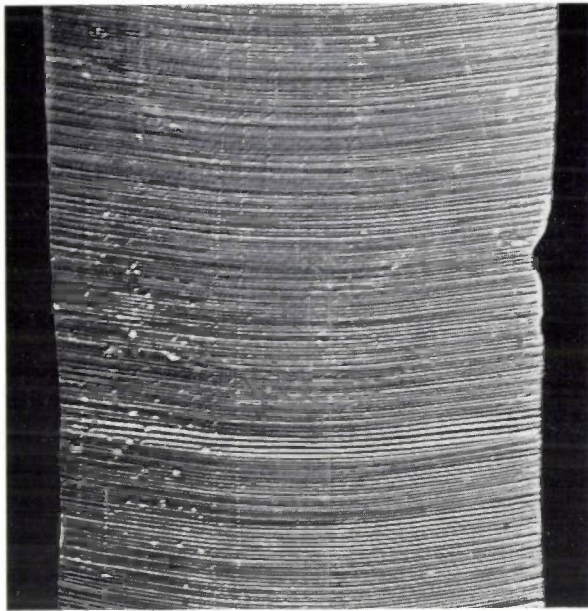


Fig.6. Striations in germanium crystal heavily doped with gallium (10^{20} atoms/cm³), made visible by X-rays according to Lang's method⁶). (Photo: A. E. Jenkinson, Mullard Research Laboratories, Salfords, England.)

the diffusion coefficients of the impurities involved. A third argument is based on the results of the following experiment. Copper is allowed to diffuse into a crystal which has been doped with antimony in such a way that the Sb concentration in a certain direction increases linearly (or at least monotonically) with distance. Since Cu diffuses easily, it will soon be uniformly distributed throughout the crystal. One end of the crystal will then be *P*-type, owing to the excess of Cu there, and the other end will be *N*-type, owing to the excess of Sb. Where the excess of Cu gives way to an excess of Sb, one would thus expect to find a *P-N* junction. In fact, a region is found with a number of *P-N* junctions. This means that the concentration of Sb must exhibit a ripple (fig.7).

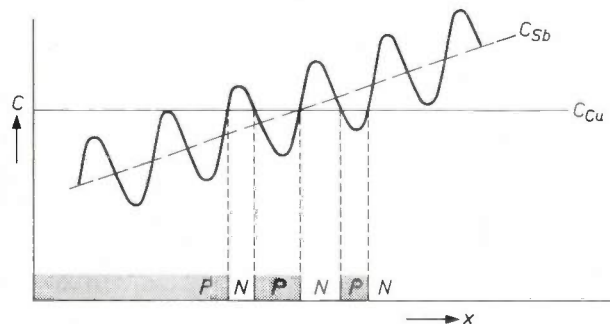


Fig.7. If a certain amount of copper is allowed to diffuse uniformly throughout a germanium crystal which has been doped with Sb in such a way that the Sb concentration increases linearly with the distance x (broken line), not one but a number of *P-N* junctions are found close together where the excess of copper gives way to an excess of antimony (concentrations C_{Cu} and C_{Sb} respectively). This proves that the concentration of antimony exhibits a ripple. The amplitude of this ripple can be calculated from the slope of the broken line and the width of the region in which the *P-N* junctions occur.

The distance between *P-N* junctions is exactly equal to that between striations.

Form and origin of the striations

When a pulled crystal is sawn through perpendicular to its length instead of lengthways, a single spiral striation is found which fills the whole of the exposed surface (fig.8). This means that the striations found in a longitudinal cross-section (fig.6) must not be seen as the intersection of this surface with an equal number of curved surfaces, but as the intersection of the surface with one helical surface.

There is no doubt that the striations in a pulled crystal are usually caused by the action of pulling. The fact that the distance between striations is exactly equal to the distance the crystal grows per revolution already shows that the production of the striations has something to do with the rotation of the crystal during pulling. Both this fact and the fact that the striations are the intersection of the plane of

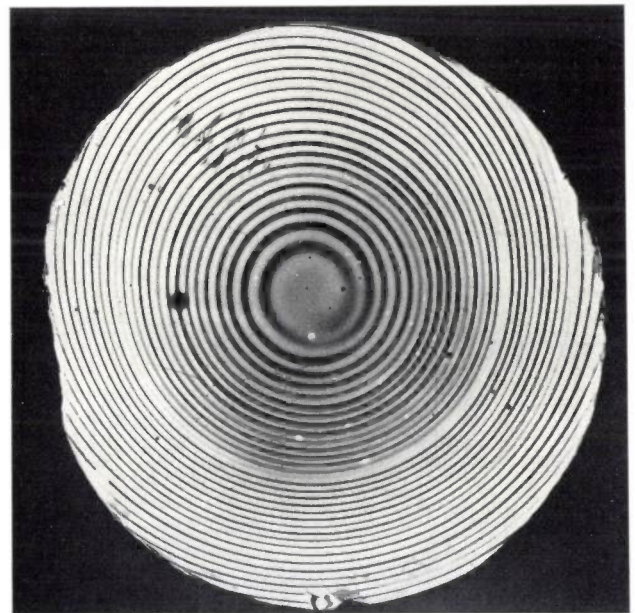


Fig.8. A transverse section of a pulled crystal shows only one striation, which has the form of a spiral.

the section with a helical surface, can be explained as results of the thermal asymmetry which afflicts nearly every pulling installation. What happens as a result of such asymmetry during pulling may easily be seen with reference to fig.9. Because the temperature distribution in crystal and melt is not symmetrical about the long axis of the crystal, the crystal grows e.g. more on the left than on the right. Since the crystal is rotated, each sector in turn passes the region of rapid growth. The crystal thus becomes a sort of helix of material which has solidified quickly, filled up with a helix of material which has solidified slowly. Since the segregation coefficient depends on

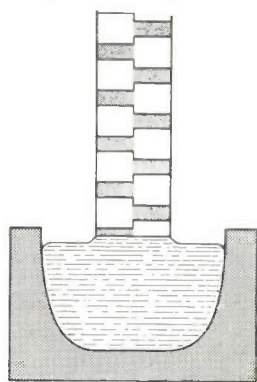


Fig. 9. The helical surface which is responsible for the striations is produced because the crystal grows faster in one part of the crucible than in the rest, and is also rotated. The shaded parts of the crystal in the figure represents the parts which have grown more slowly.

the growth rate (see introduction), one of these helices contains more dope than the other; the one with the higher concentration is identical with the above-mentioned helical surface.

Since the above-mentioned thermal asymmetry of the pulling installation can hardly be avoided, the same can be said of the formation of striations. This form of inhomogeneity has no adverse effects on the semiconducting devices made from the crystal in question; when one works with a pulling installation whose thermal symmetry is as good as possible, the variations in the concentration are so slight that they play no role at all.

Although as we have seen, the striations found when a crystal is cut through lengthways are intersections of the plane of the section with a *helical* surface, they still give a good idea of the shape of the growth interface. If the crystal were cut through along a plane through the axis of the helix, one should in principle obtain a pattern like that shown in *fig. 10*. Each of the lines situated at one side of the

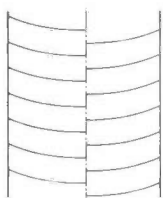


Fig. 10. Sketch of the form which the striations should in principle have in a longitudinal section through the axis of the helical surface (cf. *fig. 9*).

axis then gives an exact picture of the growth surface in a certain plane on the quick-growing side.

Successive lines show situations occurring at intervals of time equal to the period of revolution. The lines on the other side of the axis may be regarded as "exposures" each taken half a period later. The growth striations are thus very useful for studying the form of the growth interface. We shall meet examples of their use for this purpose in the following sections.

"Fundamental" striations

Striations are found not only in crystals which have been pulled in the normal way, but also in

crystals which were not rotated during pulling⁷⁾. They are also found in crystals made by horizontal zone melting⁸⁾. Although one might imagine that these were due to a certain jerkiness in the operation of the pulling mechanism, the particular instrumental cause is not very clear. Sometimes a further fine striation pattern is found between the "normal" striations of a pulled crystal⁷⁾. In particular these latter suggest that some striations may be due to some fundamental property of the growth process. One might for example imagine that the flow of heat and/or impurities away from the growth interface might not be continuous, but have the character of a relaxation vibration.

So far this problem has not been definitely solved. The result of the following experiments carried out by us is however a strong argument for the existence of "fundamental" striations. In these experiments during the pulling of a crystal, the high-frequency generator which warms the melt was switched off, and shortly afterwards the rotation of the crystal and the pulling were stopped. After all possible instrumental causes of the production of striations had thus been eliminated, the crystal was rapidly withdrawn from the melt and the drop hanging on its end allowed to solidify (this takes about 15 s). It was found that these solidified drops also exhibited striations. *Fig. 11* shows an example of this.

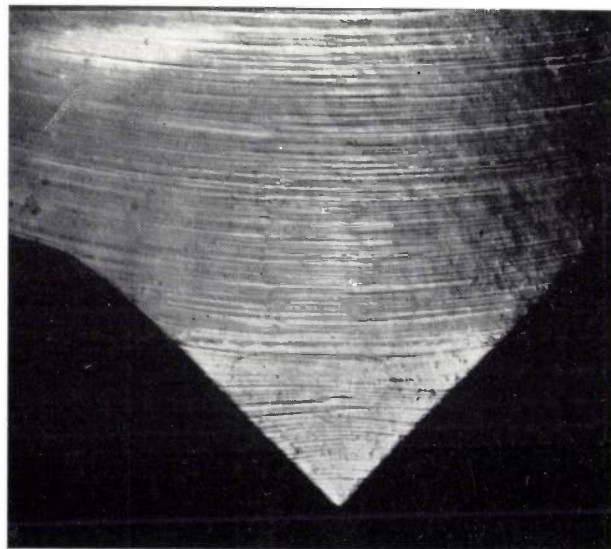
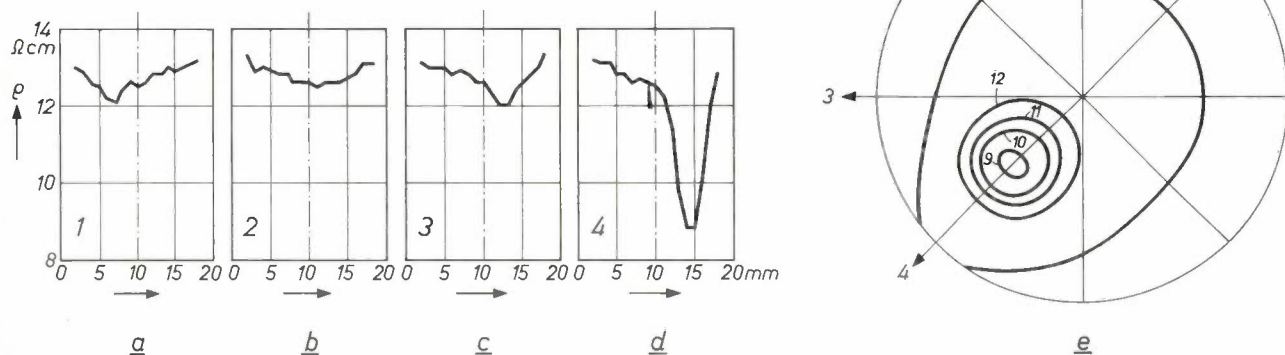


Fig. 11. The drop which remains hanging on a crystal withdrawn from the melt (the point bounded by straight lines in the photo) also exhibits striations on solidification. This indicates that striations can also be produced by causes which have nothing to do with the instrumentation of the pulling method ("fundamental" striations).

⁷⁾ H. C. Gatos et al., *J. appl. Phys.* **32**, 2057, 1961.

⁸⁾ H. Ueda, *J. Phys. Soc. Japan* **16**, 61, 1961.

Fig.12a to d. Variation of the resistivity ρ along the diameters denoted by the figures 1 to 4 in e, in a transverse section of a crystal with a "core". In e may be seen a number of lines of equal ρ .



Cores

Sometimes a pulled crystal is found to contain a region whose conductivity deviates from the desired value and whose dimensions far exceed those of the striations. Such a region, or "core", is often roughly a cylinder parallel to the long axis of the crystal and extending throughout its whole length. This can be demonstrated by making transverse sections of the crystal at various points and measuring the variation of ρ along various diameters in each section. Corresponding diameters from different sections are found in this way to give curves of similar form. For a diameter which passes through the core, the form of this curve is similar to that of fig.2. Along diameters which do not pass through the core the value of ρ shows no deviation (fig. 12).

The core can very elegantly be made visible by making a longitudinal section of the crystal in a suitable plane and "developing" the striations e.g. by pulsed copper-plating. Two examples are shown in fig. 13.

Closer inspection of the striations shows that these are linear within the core (fig.14). This fact is directly connected with the way in which the core is formed. Investigation has shown that in crystals with a core, the growth interface exhibits a facet during pulling. Cores are only produced if the growth interface is convex (i.e. if the end of the crystal is convex; see e.g. the striation patterns in figs. 6 and 13) and if a $\langle 111 \rangle$ axis makes not too large an angle θ with the long axis of the crystal; the facet is then part of a $\{111\}$ face perpendicular to the $\langle 111 \rangle$ axis in ques-

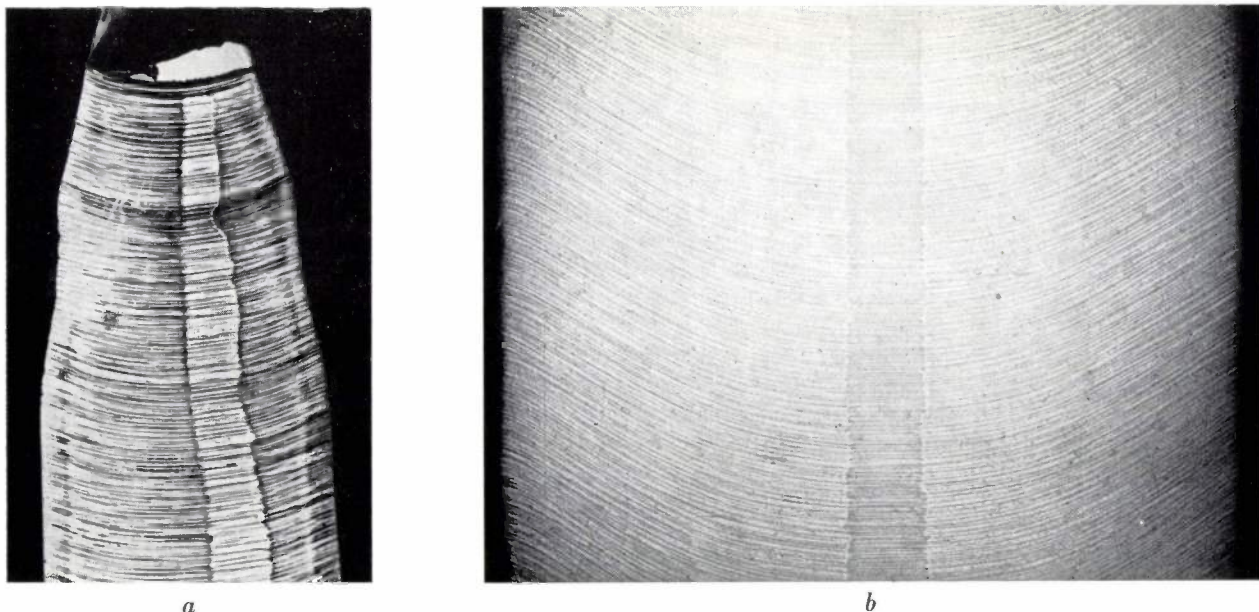


Fig.13. Two crystals with a core made visible by pulsed copper-plating: a) a germanium crystal and b) a silicon crystal. The germanium crystal was pulled, the other was made by the floating-zone technique¹⁾.

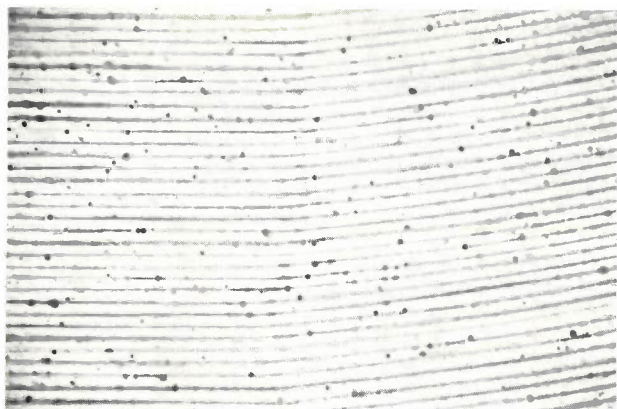


Fig.14. Detail of fig.13a. It may be clearly seen that the striations in the core (left-hand side of the figure) are straight lines.

tion ⁹⁾ (since germanium and silicon are both cubic). Fig.15 shows the striations in a transverse section of a crystal with a core; here too the striations are linear within the core. Finally, fig.16 shows the underside of a crystal which has been quickly withdrawn from the melt; the facet may be clearly seen.

The position of the facet is determined by the angle θ ; it is situated further from the middle of the crystal as θ is larger. It appears that the solid-liquid interface becomes flat round about the spot where the curved interface in the absence of a facet would be tangent to a $\{111\}$ face. The method of avoiding such cores follows directly from this fact; θ must simply be made so large that a $\{111\}$ face is nowhere tangent to the growth interface. It is not necessary

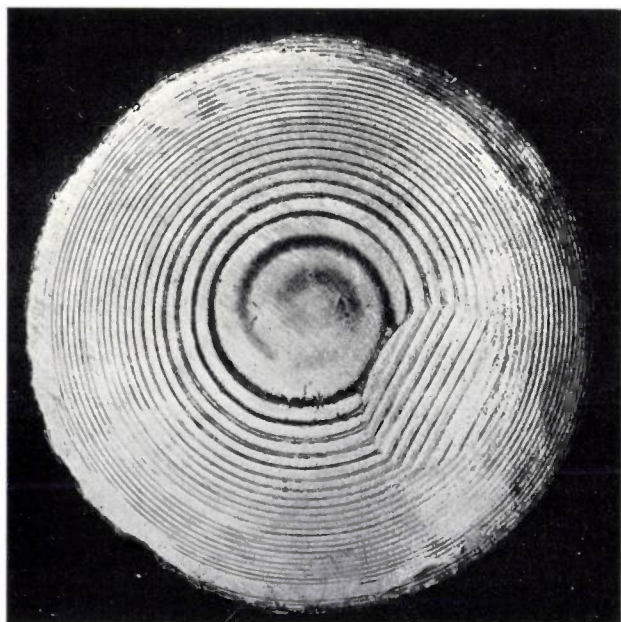


Fig.15. Just as in a longitudinal section of a crystal with a core, the striations in the core are also straight in a transverse section (cf. fig.14).

⁹⁾ See the article ²⁾ quoted above.

to make θ very large for this purpose; one can also try to make the temperature distribution such that the curvature of the growth interface is slight. If the temperature distribution can be made so favourable that the interface is naturally almost flat, it is also possible to make θ very small: the whole growth interface then becomes one big "facet".

Measurements of the resistivity of germanium crystals doped with Sb have shown that the ratio of the resistivity in the core to that in the rest of the crystal is constant (about 2/3; see fig.2) over a wide

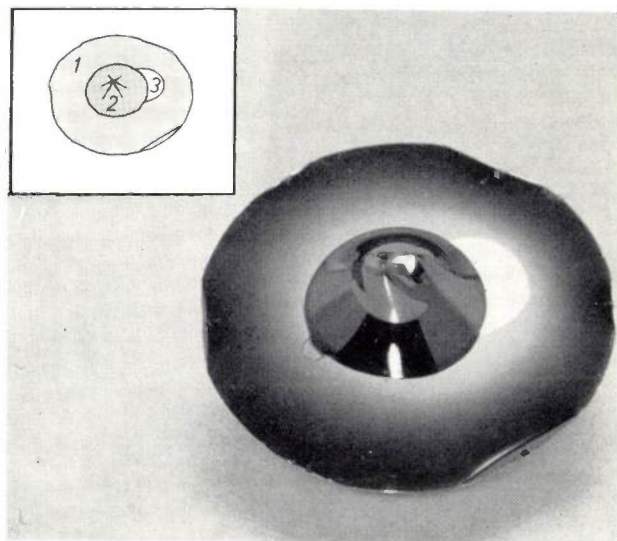


Fig.16. Underside of a crystal withdrawn from the melt whose growth interface had a flat part (facet). The inset helps to identify the various parts of the photo: 1 curved part of the growth interface, 2 solidified drop which remained hanging on the crystal when it was withdrawn from the melt, 3 the facet.

range of concentrations (values of ρ from 0.05 to 20 Ωcm). It thus appears that the value of the segregation coefficient is different for the facet. A similar phenomenon is found with other impurities; the quotient a of the segregation coefficient on the facet (k_f) and that on the rest of the growth interface (k_e) has a value which is characteristic of the impurity in question. A number of these values are shown in Table I.

Table I. The values found for the ratio a of the segregation coefficient of several impurities on the facet (k_f) to that on the rest of the growth interface (k_e) for pulled germanium crystals. These values apply to a pulling rate of 1 mm per minute and a rotation rate of 50 r.p.m.

Dope	$a (=k_f/k_e)$
P	2.5
As	1.8
Sb	1.45
Bi	1.65
Ga	0.85
In	1.4
Tl	1.2

The same effect is also found in other materials. An example which is remarkable for two reasons is the case of indium antimonide doped with tellurium¹⁰). Not only is α unusually large in this case (about 8), but $k_f > 1$ while $k_e < 1$. No theory has yet been produced which can give a satisfactory quantitative explanation of the phenomena described.

The formation of a facet is a direct consequence of the fact that the growth of the crystal is not equally easy in all parts of the solid-liquid interface. If we consider a cubic crystal for the sake of simplicity, the lattice points near the solid-liquid interface will be occupied as shown in *fig.17a*. The growth of the stepped parts of this interface requires merely that atoms fill up the spaces indicated by \times in *fig.17b*. This is quite easy, since the surface energy is hardly

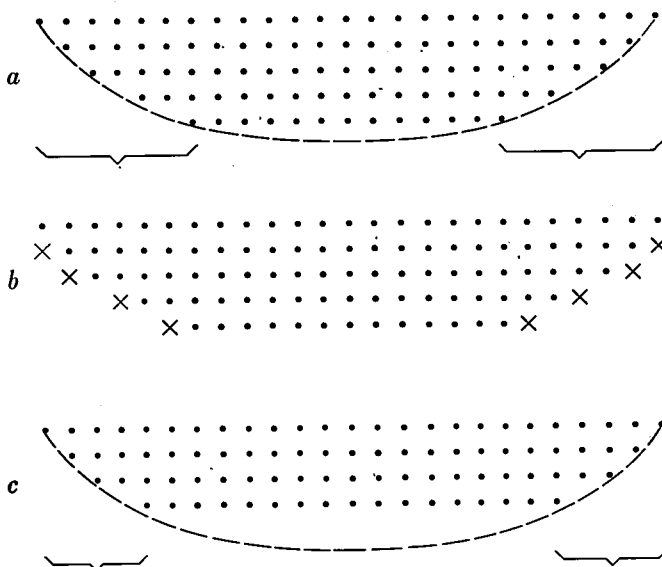


Fig.17. a) Schematic representation of a curved, non-moving, solid-liquid interface of a crystal with a cubic lattice. The outer part of the interface (see brackets) is stepped, while the inner part contains a region in which all atoms lie in one plane. b) The stepped parts of the crystals can easily grow. Atoms only need to fill up the spaces marked by \times in the figure, which requires little energy. Growth on the flat part requires much more energy, i.e. considerable supercooling. c) Growth interface with facet. The broken line represents the isotherm in which the rest of the interface is situated.

altered in the process. There are no such steps where atoms can be added on the flat part of the crystal; this part does not grow until such a step has been formed somewhere. A single atom is not enough for this purpose: a group of atoms (a "nucleus") is necessary. The formation of such a nucleus requires a certain amount of energy, whose value varies with the crystallographic orientation of the surface. In some cases this energy is quite large, so that the formation of a nucleus requires appreciable super-

cooling. The flat part of the solid-liquid interface cannot therefore coincide with the isothermal surface in which the rest of the interface is situated, but will lie somewhat behind this. It is thus larger than in the absence of supercooling, i.e. it forms a facet on the interface (*fig.17c*).

Similar considerations make it likely that facet formation will occur in crystals of other lattice types when there are faces on which nuclei are not formed easily. In substances like Ge and Si with the diamond structure, the $\{111\}$ faces are apparently such faces.

If a stable nucleus is once formed on a facet, it grows very fast laterally, because of the strong supercooling. Growth is then delayed until a new nucleus is formed, and so on. While the crystal thus grows uniformly on the curved parts of the solid-liquid interface, growth on the facet occurs in jumps; the average growth rate is naturally the same throughout.

The fact that the facet has a different segregation constant from the rest of the growth interface can be explained qualitatively by assuming that a certain adsorption (or desorption) of impurities occurs at the interface. This would have no effect on the final concentration of impurity in the solid phase when solidification was slow, as on the curved parts of the interface; but part of the adsorbed impurities could be frozen in on a part of the interface e.g. a facet where growth was fast. The concentration of impurity in the solid phase would then be greater here than in the rest of the crystal; with desorption it would be less¹¹).

We may finally mention that it is not impossible that this adsorption or desorption should depend on the crystallographic orientation of the surface in question.

Inhomogeneities due to constitutional supercooling; inclusions

Heavily doped material, such as that used for the manufacture of tunnel diodes, sometimes contains regions consisting of nearly pure dope; we shall call such regions *inclusions*. It has been found that such inclusions are formed only in crystals which are pulled in such a way that "constitutional supercooling" occurs in the liquid just in front of the growth interface. We shall now briefly explain what constitutional supercooling is¹²), and how it can lead to the formation of inhomogeneities. Inclusions are

¹¹) These ideas have been given quantitative expression by A. Trainor and B. E. Bartlett, *Solid-state electronics* 2, 106, 1961.

¹²) The existence of constitutional supercooling was first indicated by J. W. Rutter and B. Chalmers, *Canad. J. Phys.* 31, 15, 1953. A theoretical treatment of this phenomenon with reference to the pulling process has been given by D.T.J. Hurle, *Solid-state electronics* 3, 37, 1961. An experimental test of this theory and a description of the form of the solid-liquid interface in Ge heavily doped with Ga may be found in W. Bardsley et al., *Solid-state electronics* 3, 142, 1961 and 5, 395, 1962.

¹⁰) K. F. Hulme and J. B. Mullin, *Phil. Mag.* 4, 1286, 1959 and J. B. Mullin and K. F. Hulme, *Phys. Chem. Solids* 17, 1, 1960.

the most extreme form of the inhomogeneities which can be produced in this way.

As has been mentioned in the introduction, when the distribution coefficient $k_0 < 1$, the concentration $C(x)$ of dope in the liquid just in front of the growth interface is higher than elsewhere. The variation of the concentration with the distance x from the interface is sketched in *fig.18a*; the con-

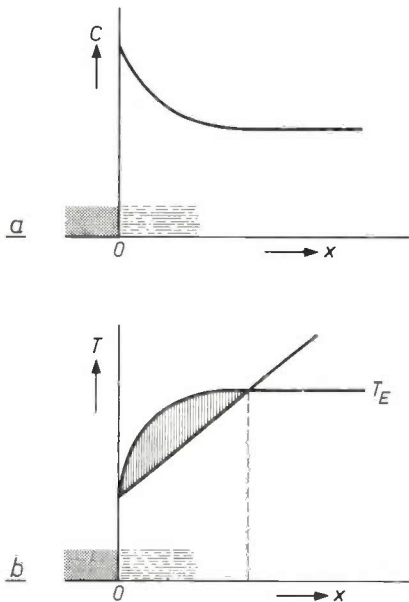


Fig.18. a) The variation of the concentration $C(x)$ in the melt near the growth interface as a function of the distance x from that interface. b) The variation of the equilibrium temperature T_E with x , which may be deduced from the above. If the temperature gradient dT/dx at $x=0$ is less than the gradient of T_E , constitutional supercooling occurs in the layer where $T < T_E$.

centration is maximum at the growth interface. If one determines with the aid of the phase diagram the equilibrium temperature T_E corresponding to $C(x)$ at each point, one obtains a curve like that shown in *fig.18b*. The equilibrium temperature $T_E(0)$ at the growth interface is lower than at some distance from this interface. If now the temperature gradient dT/dx in the liquid near the interface is less than the gradient dT_E/dx of the equilibrium temperature, then — even though T is everywhere greater than $T_E(0)$ — part of the liquid will be supercooled. This is what is known as constitutional supercooling. The minimum value of dT/dx necessary to avoid supercooling is higher the more concentrated the liquid, the higher the pulling rate, the thicker the diffusion layer (i.e. ω smaller) and the smaller the distribution coefficient k_0 .

A similar argument holds for $k_0 > 1$; here too constitutional supercooling is possible.

If the constitutional supercooling is not too strong, it does not lead to the spontaneous formation of

crystal nuclei in the liquid. (Molten germanium can be supercooled by several tens of degrees without anything happening.) At the solid-liquid interface, however, something unusual does happen: the normal convex (or concave) shape of the interface is no longer stable in the presence of supercooling. This can be easily seen by considering what happens to a small projection which happens to form on the surface of the crystal. Since the supercooled layer has a certain thickness, such a projection grows still further instead of lagging behind until it disappears, as would occur in a stable situation. During this growth of the projection, the excess impurity diffuses out laterally as well as in the direction of growth of the crystal as a whole. The concentration of dope in the liquid in the immediate vicinity of the projection is thus increased, i.e. T_E is decreased. Since the heat of solidification is also led off laterally to a certain extent, the liquid round the projection will also be warmer than elsewhere at the same distance from the growth interface. These two effects, the decrease in T_E and the increase in T , combine to abolish the supercooling in the immediate vicinity of the projection. Other projections can thus only be formed a certain distance away.

In the long run, the growth interface acquires a "cell" structure (*fig.19*). This structure of the interface is stable, and can persist for some considerable time.

It is understandable that the projections from the growth interface of a Ge or Si crystal are just as likely to show $\{111\}$ facets as is a normal interface. In fact, the strong curvature of these projections makes it practically certain that such a facet will occur. The shape of the projections (and thus of the growth interface as a whole) is therefore strongly

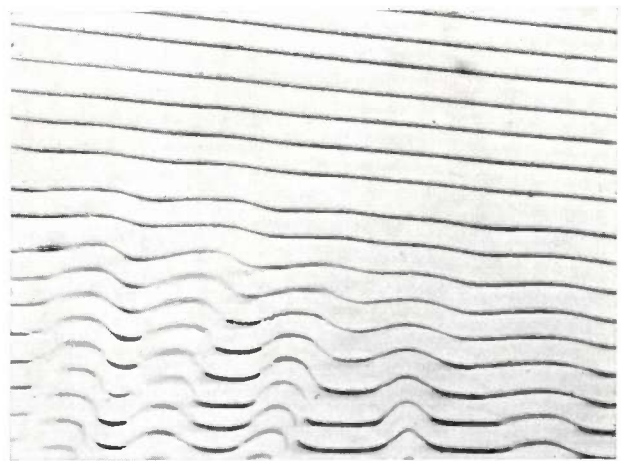


Fig.19. Beginning of the formation of the cell structure exhibited by the growth interface in cases of constitutional supercooling. The striations in a longitudinal section of the crystal are then wavy lines. (Magnification $200\times$.)

dependent on the orientation of the crystal in cases of constitutional supercooling.

The differences in temperature and dope concentration between the liquid at the tops of the projections and in the "valleys" will lead to considerable differences in segregation coefficient between these two spots. The portions of the crystal formed by freezing of the liquid in the valleys will have a considerably higher dope concentration than the rest of the crystal.

This process of cell formation is not restricted to crystal formation. It may be generally stated that where temperature inversion occurs, a plane surface of constant temperature will not be stable and cells will be formed. In 1901, Bénard found that if the bottom of a horizontal layer of liquid was kept warmer than the top, a cellular pattern of convection currents was produced. The liquid rises in the middle of the cells and falls at the edges¹³). A similar effect is found in horizontally enclosed layers of air, but here the flow is down in the middle and up at the edges¹⁴). In meteorology the formation of certain kinds of cumulus clouds has been suggested as being due to the production of Bénard cells.

As may be seen from fig.19, the course of the phenomena caused by constitutional supercooling can be followed very clearly by making the striations visible. Fig.20 shows three more cases of cell forma-

¹³) See e.g. H. J. V. Tyrrell, *Diffusion and heat flow in liquids*, Butterworths, London 1961, chapter 11.

¹⁴) Further details may be found in J. G. A. de Graaf, thesis Utrecht, 1952, who studied the air flow in enclosed layers in connection with the thermal insulation of buildings.

tion in germanium strongly doped with gallium (about 10^{20} Ga atoms per cm^3). In fig.20a we see how cells can be formed by raising the pulling rate, and can be caused to disappear again by pulling more slowly; fig.20b shows a similar experiment, except that here the pulling rate was increased again before the cells were quite destroyed. It may be seen that the pattern remains nearly constant throughout the experiment, which demonstrates its stability. Fig.20c shows the cell formation in a crystal pulled in a $\langle 100 \rangle$ direction. Facet formation then causes the projections to be pyramidal (or tent-shaped).

Nature and origin of inclusions

The occurrence of inclusions may be regarded as an extreme form of inhomogeneous segregation due to a cellular structure of the growth interface. It is supposed that they arise when a number of projections fuse at a given moment, enclosing the very concentrated liquid situated between them. Since the temperature in the crystal decreases considerably with the distance from the (external) solid-liquid interface, the enclosed drop begins to solidify at the top. As we have seen, when solidification occurs in this way and the segregation constant k is small compared to 1, most of the impurities will be concentrated in the last part of the liquid to solidify (at the bottom of the drop); it is this part (often a eutectic mixture) which forms what we here call the inclusion.

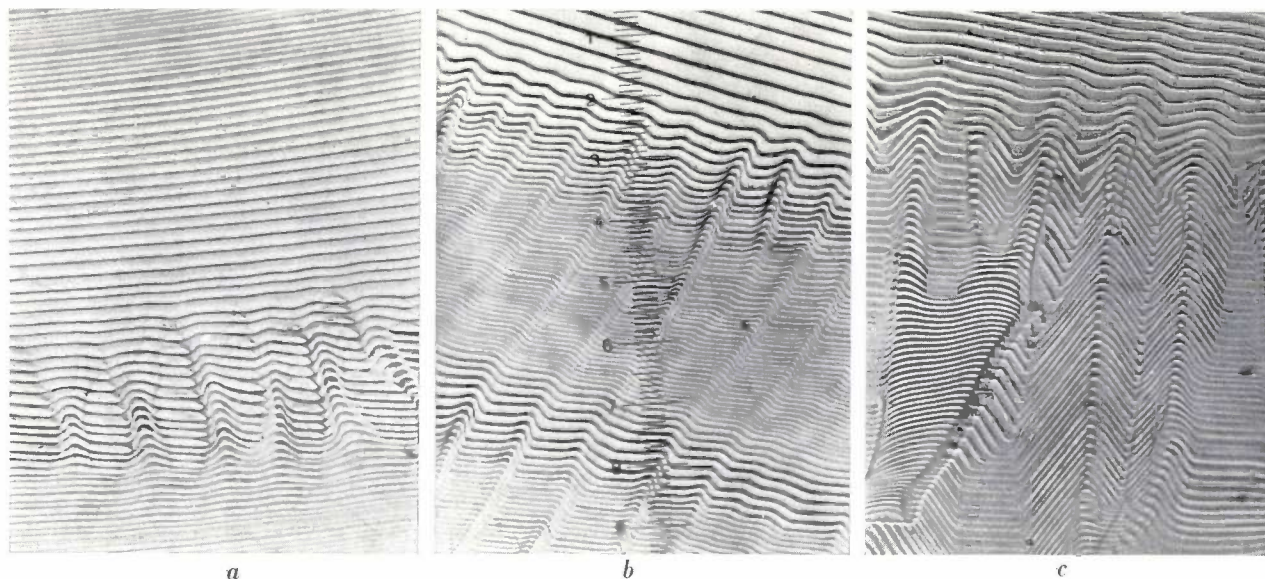


Fig.20. a) Example of a crystal where constitutional supercooling was produced in the melt by raising the pulling rate. The growth interface exhibits a ripple which steadily increases in magnitude. After some time the pulling rate was decreased again — visible from the smaller distance between striations; the amplitude of the ripple then decreases and it finally disappears altogether. b) As in (a), except that the pulling rate was here increased again during the experiment, before the ripples had

completely disappeared. The same pattern is observed throughout the whole operation, which shows the stability of the ripple structure. Both these crystals were pulled in the $\langle 111 \rangle$ direction. The tops of the projections from the growth surface are flattened by facet formation. c) If a germanium crystal is pulled in a $\langle 100 \rangle$ direction under conditions of constitutional supercooling, the projections from the growth interface are given the form of a pyramid or tent by the facet formation.

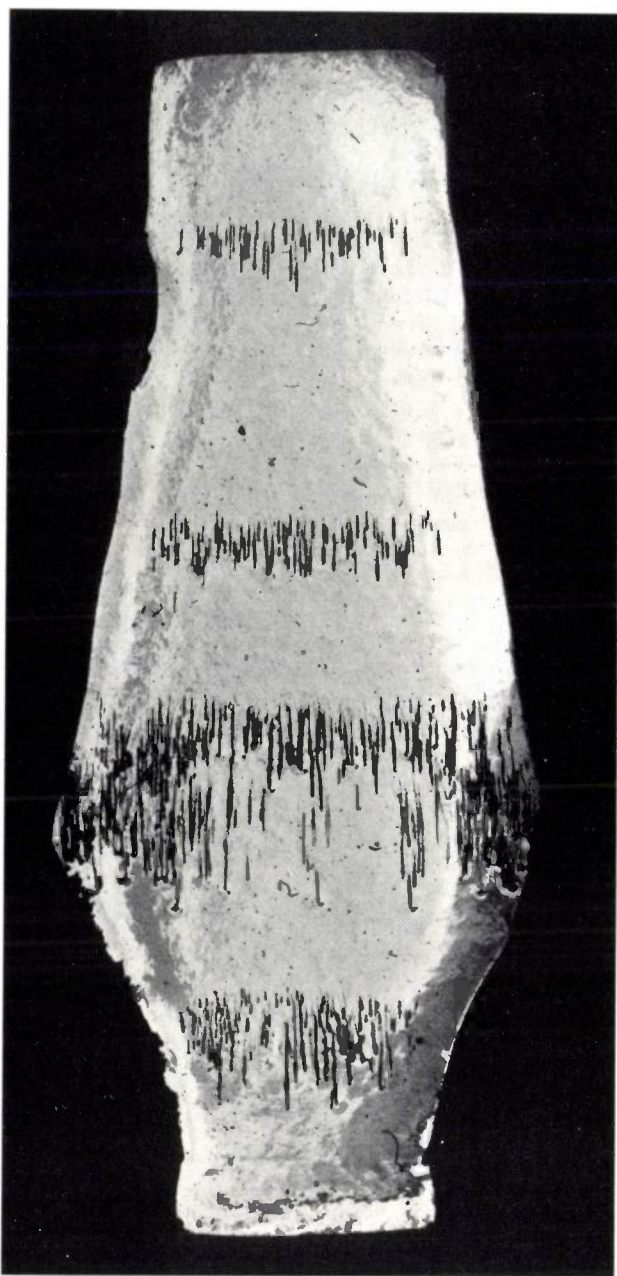


Fig.21. Inclusions in a Ge crystal pulled in a $\langle 110 \rangle$ direction. The dark vertical lines are the tracks made by enclosed drops. During the pulling of this crystal, the pulling rate was several times increased, so as to lead to constitutional supercooling and hence to the production of inclusions, and then decreased again after a short time. This is the reason why four groups of lines can be seen, each group beginning roughly in a horizontal plane.

We have implicitly assumed above, to simplify the argument, that an enclosed drop solidifies on the spot. In fact this is not so: it continues to move for some time in the direction of growth. This may be compared with the progress of the molten zone in "temperature-gradient zone melting": material is dissolved on the warm side of the zone, and is deposited on the cold side¹⁵. Finally, however, the

¹⁵ See W. G. Pfann, *Zone melting*, Wiley, New York 1958, chapter 9.

drop comes to a stop and forms an inclusion as described above (figs. 21 to 25). This progress of the enclosed drop is the reason why the fusing together of the projections cannot be seen in the striation pattern.

The fact that the region through which the enclosed drop has travelled also shows striations has led to the suggestion that these are "fundamental" striations. Calculation has however shown that the small temperature variations at the solid-liquid interface which, according to the argument on p. 198, are the reason for the formation of the normal striations, penetrate some distance into the crystal — to be precise, the amplitude decreases exponentially, with a characteristic length of a few mm. They are therefore very well able to influence the solidification of the enclosed drops.

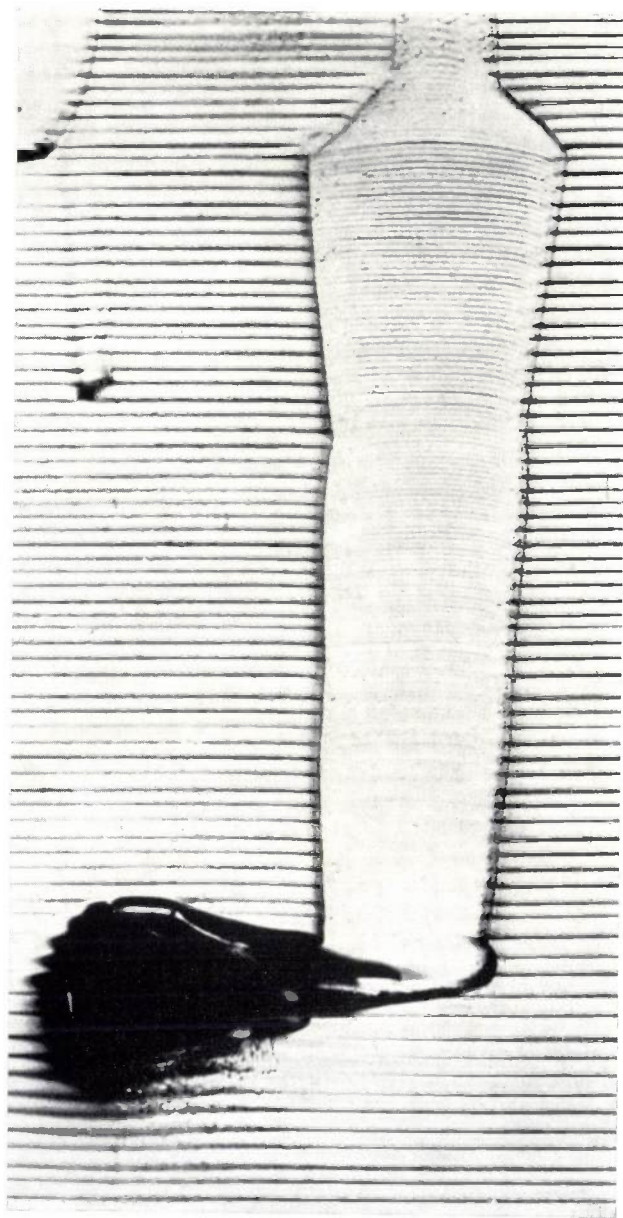


Fig.22. Highly magnified ($200\times$) striation pattern of part of a crystal which has been traversed by an enclosed drop. The dark patch represents the inclusion formed by the drop at the end of its path.



Fig. 23

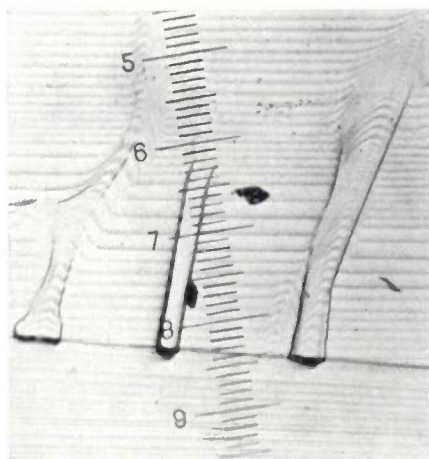


Fig. 24

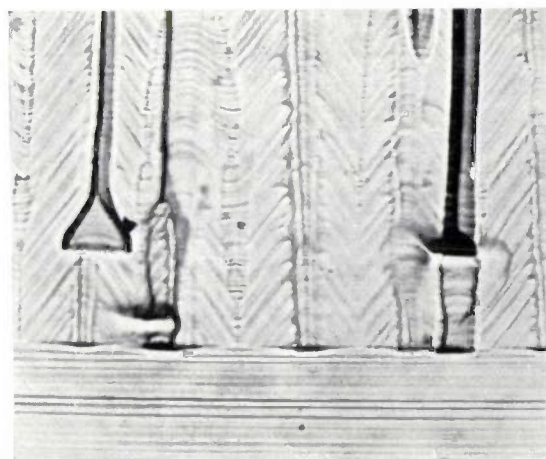


Fig. 25

Fig. 23. Striation pattern of part of a crystal in which a valley of a cellular growth interface gives way to a zone traversed by an enclosed drop. In the valley (top left) the distance between striations is equal to that in the projections, while in the zone traversed by the drop the striations are closer together. (Magnification $110\times$.)

Fig. 24. Striation pattern (magnification $120\times$) of part of a crystal grown with a cellular solid-liquid interface, in which the tracks of three enclosed drops can be seen. At a certain

moment, the pull rate was decreased and the melt was given such a big heat pulse that the crystal melted a little at the end before growing further. The striations below this point are again completely regular.

Fig. 25. As in fig. 24. The striation pattern above the melt-back boundary is highly irregular. The fact that the pattern below this boundary is again regular indicates that despite the constitutional supercooling the material remains monocrystalline. (Pulled in $\langle 100 \rangle$ direction, magnification $80\times$.)

The striation patterns of fig. 19 *et seq.* clearly show that constitutional supercooling, while giving rise to inhomogeneities, need not lead to the production of polycrystalline material. Even the crystal of fig. 25 was a single crystal, as may be seen after being partly melted back. It is true however that regions where the growth interface had a cellular structure, and in particular regions in and around the zones traversed by an enclosed drop, have a great dislocation density. This can be demonstrated both by the etch-pit technique and with the aid of the anomalous-transmission effect for X-rays. The stresses caused by the differences in lattice constant corresponding to the concentration differences are apparently partly compensated by dislocations.

A remarkable property of these dislocations is that they do not normally extend beyond the region containing the inhomogeneities. If one carefully pulls a dislocation-free crystal¹⁶⁾, then alters the conditions so that constitutional supercooling occurs, and finally returns to the original conditions, dislocations will be found mainly in the middle of the crystal. This shows that most of these dislocations form closed rings.

The occurrence of inhomogeneities produced by

constitutional supercooling can also be prevented, even in very heavily doped crystals. The temperature gradient must be made very steep, and for the rest it is only necessary to choose suitable values for the pulling and rotation rates. For example, by pulling slowly we have succeeded in making homogeneous dislocation-free germanium crystals with a gallium content of about 4×10^{20} atoms/cm³, i.e. nearly 1 wt.%. This content approaches the limit set by the solubility of the gallium.

Summary. Pulled doped germanium and silicon crystals which show no serious axial variation of the resistivity on routine examination can nevertheless be locally inhomogeneous. They can exhibit striations, cores and inhomogeneities due to constitutional supercooling, of which latter inclusions are an extreme form. Striations are produced by thermal asymmetry of the pulling installation, and are difficult to remove completely. In a longitudinal section they give a very good idea of the shape of the growth interface at various moments. Cores are produced when the growth interface contains a $\{111\}$ facet; the segregation coefficient on this facet differs from that on the rest of the interface. When doping is heavy, constitutional supercooling easily occurs in the melt in front of the growth interface. The growth interface then acquires a cell structure owing to the growth of projections. The "valleys" in between these projections are filled with relatively concentrated liquid, which solidifies to give more strongly doped material. Enclosure of this liquid by fusion of projections leads to the formation of inclusions. Cores can be prevented by a suitable crystallographic orientation of the seed crystal, and inclusions by suitable pulling conditions. It has been found possible in this way to pull Ge crystals doped with Ga in amounts barely less than the solubility, which were still free from inhomogeneities and dislocations.

¹⁶⁾ For the production of dislocation-free crystals and for various methods of investigating dislocations see the article quoted in ⁵⁾.

DETERMINING MAGNETIC QUANTITIES BY DISPLACEMENT MEASUREMENTS

by U. ENZ *) and H. ZIJLSTRA **).

621.317.44

For research on ferromagnetic materials, which has been in progress in the Philips laboratories for a considerable time now, the authors have built three instruments by which the magnetostriction, the magnetic anisotropy and the magnetization of these materials can be measured with a precision of approx. 1%. Up-to-date instrumentation can give a higher degree of precision, but wherever the above precision, which suffices for nearly all practical and many theoretical purposes, is acceptable, these measurements can be carried out with very simple equipment. In all three instruments the relevant magnetic property produces a displacement of a ferroxcube core or a coil, and this is measured with an established type of measuring bridge (PT 1200). These instruments, designed for use in our laboratories, have been used for many measurements and found to be satisfactory.

The magnetization of a sample of ferromagnetic material in a magnetic field is generally accompanied by magnetostriction, i.e. a change in its dimensions. If the sample is a single crystal, it will also tend to assume such a position that a preferred direction becomes parallel with the field, thus minimizing the magnetic anisotropy energy. The above three magnetic quantities together give a fairly complete picture of the magnetic properties of the sample. For measuring these quantities we have designed and built three instruments that can be conveniently operated and yet attain a precision of 1%. The measuring method of each instrument is based on the same principle: the relevant magnetic property (or rather its variation) is converted to a displacement of a ferroxcube core or to that of a coil. Because of this displacement there is a change in the coupling between two stationary coils forming a bridge circuit together with two other impedances. These two impedances are part of a commercially available device (measuring bridge PT 1200), which both feeds the bridge with an alternating current of 4 kc/s, and amplifies, rectifies and measures its output voltage. The magnitude of the displacement can either be read off an incorporated measuring instrument or be registered by means of an x-y-recorder as a function of e.g. the magnetic field strength or time. A further common feature of the three instruments is that the variation of the magnetic quantities as a function of temperature can be very easily determined. In all three cases the instruments are calibrated with the aid of samples whose magnetic properties are known.

Magnetostriction

When a non-magnetized rod of some ferromagnetic material is placed in a magnetic field that is

parallel to the axis of the rod, then the length l of the rod will change by an amount Δl . The other dimensions will primarily change in such a way that the volume of the rod remains constant. The magnetostriction λ is defined as $\Delta l/l$. In single crystals, λ assumes different magnitudes along different crystallographic directions. Most measurements, however, are made on polycrystalline material without texture, so that the same "average" value is found for all directions. The value of λ generally increases with increasing magnetic field strength up to the point of magnetic saturation. For most ferromagnetic substances its magnitude, either positive or negative, is then of the order of 10^{-5} and remains constant beyond that point.

In practice magnetostriction manifests itself in the humming noise produced by transformers and smoothing coils ¹⁾: the dimensions of the ferromagnetic core alternate at twice the frequency of the electric current. One useful application of magnetostriction is the generation of ultrasonic vibrations ²⁾. Magnetostriction is also of theoretical significance for studying the atomic processes that cause magnetism.

Fig. 1a shows a cross-section of the instrument for measuring magnetostriction. Test bar P , with a length l of about 5 cm, rests in the hollow cone in the bottom of quartz tube A . The variation in length Δl produced when the magnetic field is switched on is transferred by quartz rod Q to pin T . This pin is part of a commercially available type of dynamometer (PR 9310). The dynamometer contains two coils L and L' and ferroxcube core F . The ferroxcube core is mounted on pin T , the latter being held by leaf-springs B and B' in a position where it can only move lengthways. If core F is displaced over a

*) Philips Research Laboratories, Eindhoven.

**) Philips Radio, Television and Record-Playing Apparatus Division, Metallurgical Laboratory, Eindhoven.

¹⁾ See e.g. E.W. van Heuven, The noise emission of ballasts for fluorescent lamps, Philips tech. Rev. 18, 110-119, 1956/57.

²⁾ See e.g. C.M. van der Burgt, Ferroxcube material for piezomagnetic vibrators, Philips tech. Rev. 18, 285-298, 1956/57.

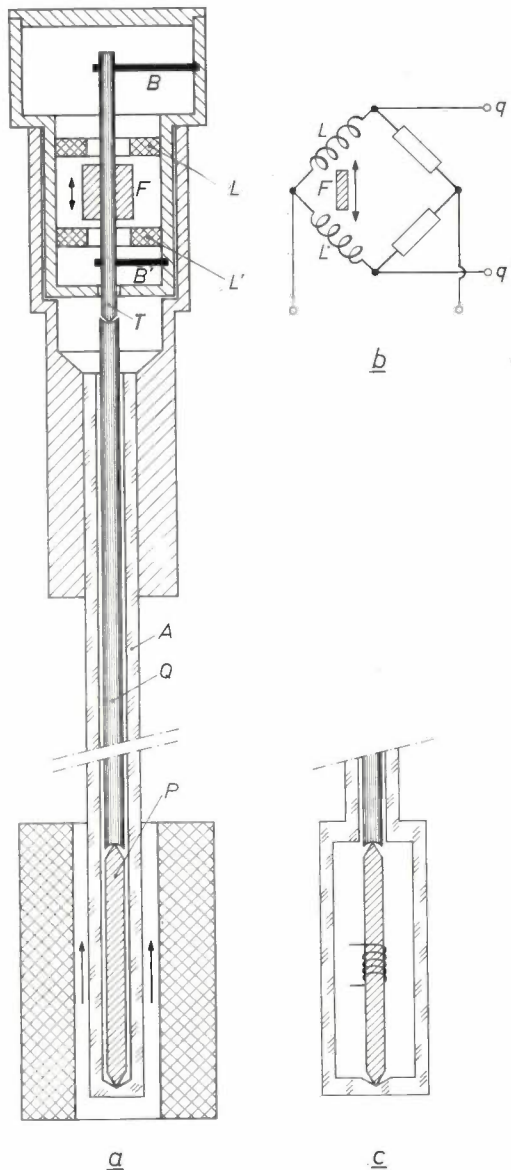


Fig. 1. a) Schematic cross-section of the instrument for measuring magnetostriction. Test bar *P* rests in the hollow cone in the bottom of quartz tube *A*. The change in length Δl of test bar *P* caused by the magnetic field set up by a solenoid (see arrows) is transferred by quartz rod *Q* to pin *T*, the latter being part of a commercially available dynamometer (PR 9310). The pin, supported by leaf-springs *B* and *B'*, is fitted with a ferrocube core *F* whose displacement over distance Δl changes the inductances of the two coils *L* and *L'*. The potential difference thus set up between the points *q* and *q'* (b) is measured by a measuring bridge (PT 1200), which is likewise commercially available. c) Modified version of quartz tube *A*, as explained under fig. 4.

distance Δl , the self-inductances of *L* and *L'* change, which unbalances a bridge circuit, producing a potential difference between points *q* and *q'* (fig. 1b). This potential difference is amplified and rectified in the measuring bridge, producing a deflection on the measuring instrument (fig. 2). This deflection is proportional to Δl and hence to the magnetostriction λ . The smallest deflection that can be read off the measuring bridge is about $0.01 \mu\text{m}$. For a value of λ of

2×10^{-5} and a test-bar length of 5 cm, this corresponds to a measuring precision of 1%.

The length of the quartz rod and tube must be such that the test bar and measuring probe are about 20 cm apart, allowing the rod to be placed within a large solenoid. By means of this solenoid (fig. 2), field strengths up to $1.6 \times 10^6 \text{ A/m}$ (20 000 Oe) can be produced, which makes it possible to measure into the saturation region of most ferromagnetic substances.

The pressure of the leaf-springs (a few grammes) is adequate to ensure a backlash-free contact between pin *T* and rod *Q*. Quartz rod *Q* and test bar *P* are cemented together to form a rigid unit. Since the leaf-springs do not allow lateral movement of the pin and the lower end of the test-bar rests in a hollow cone, *Q* and *P* are kept free of the wall, so that the whole assembly moves without friction.

The saturation magnetostriction is of the same order of magnitude as the thermal expansion at a temperature difference of 1°C . Therefore in order to retain a precision of 1%, the temperature during the measurement must remain constant within 0.01°C . Since the measurement, which is simply a comparison of the meter readings before and after the field is switched on, takes very little time, the desired temperature stability can be easily realized.

The variation of the magnetostriction as a function of temperature can be measured from -196°C to 700°C by surrounding quartz tube *A* with a bath of cold liquid or with a small furnace. The temperature of the test bar is then measured with the aid of a thermocouple. Because of the small dimensions of the bar and the short duration of each measurement, only a small amount of coolant or

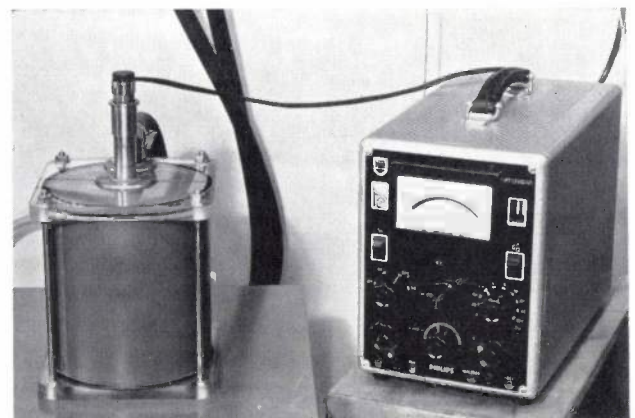


Fig. 2. Set-up for measuring the magnetostriction. On the left is the solenoid for generating a field of known strength, into which the quartz tube holding the test bar has been inserted. The measuring bridge PT 1200 is shown on the right. The strongest field that can be set up by the solenoid ($1.6 \times 10^6 \text{ A/m}$) is sufficiently strong to saturate most ferromagnetic substances.

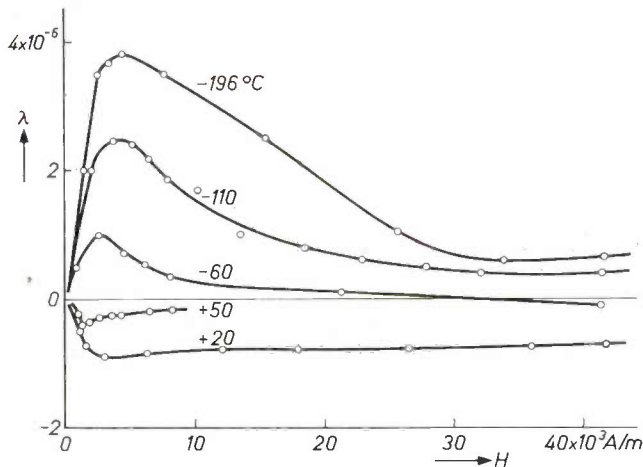


Fig.3. Magnetostriction λ of a manganese-ferro-ferrite as a function of the field strength H , at different temperatures. This ferrite is frequently used because of its high magnetic susceptibility in e.g. telephony in Pupin coils. From these and other measurements, this high susceptibility could be explained. (Cf. U. Enz, Proc. Instn. Electr. Engrs. **109 B**, suppl. No. 21, 246, 1962.)

a low furnace power is required. Fig. 3 is an example of a few curves obtained with the instruments.

Fig. 4 finally shows three versions of the instrument. The one just described is shown on the left. The version shown in the centre allows free access to the test bar (see also fig. 1c). A few turns of wire whose terminals are connected to a ballistic galvanometer can be wrapped round it. It is thus possible, whilst measuring the magnetostriction, to determine the change in flux and from this the magnetization of the test bar. With the right-hand version the magnetostriction of samples of annular form can be measured.

Magnetic anisotropy

If a monocrystalline sample of some ferromagnetic material is to be magnetized to saturation, we find that this does not require the same energy in every direction. There are some directions in which this energy is a minimum; these are the preferred directions of magnetization. In most cases they appear to be parallel to certain simple crystallographic directions, e.g. with ferroxdure ($\text{BaFe}_{12}\text{O}_{19}$) the preferred direction is parallel to the hexagonal axis. A crystal is usually divided into a large number of regions that have already been magnetized to saturation (the well-known Weiss domains), each being magnetized along one of the preferred directions.

The sample is placed in a magnetic field strong enough to bring it to saturation, whatever its crystal orientation with respect to the field. In order to rotate the sample about an axis perpendicular to the field, we must apply to it a couple with a moment M which supplies the energy ΔE required to turn the magnetization through an angle θ with respect to

the relevant preferred direction. This energy ΔE , called the *magnetic anisotropy energy*, is a periodic function of the angle θ between the field and the relevant preferred direction. This function can be written in the form of a power series and the magnetic anisotropy of a specific material characterized with the aid of the coefficients of this series. With ferroxdure all coefficients but one are zero, which leads to the very simple formula:

$$\Delta E = K_1 \sin^2 \theta.$$

The moment M is found by differentiating ΔE with respect to θ . For ferroxdure this yields:

$$M = \frac{d}{d\theta} \Delta E = K_1 \sin 2\theta. \quad (1)$$

This shows that K_1 , and in other cases also the remaining coefficients K_2, K_3 , etc., can be determined by measuring M as a function of θ . This is the prin-

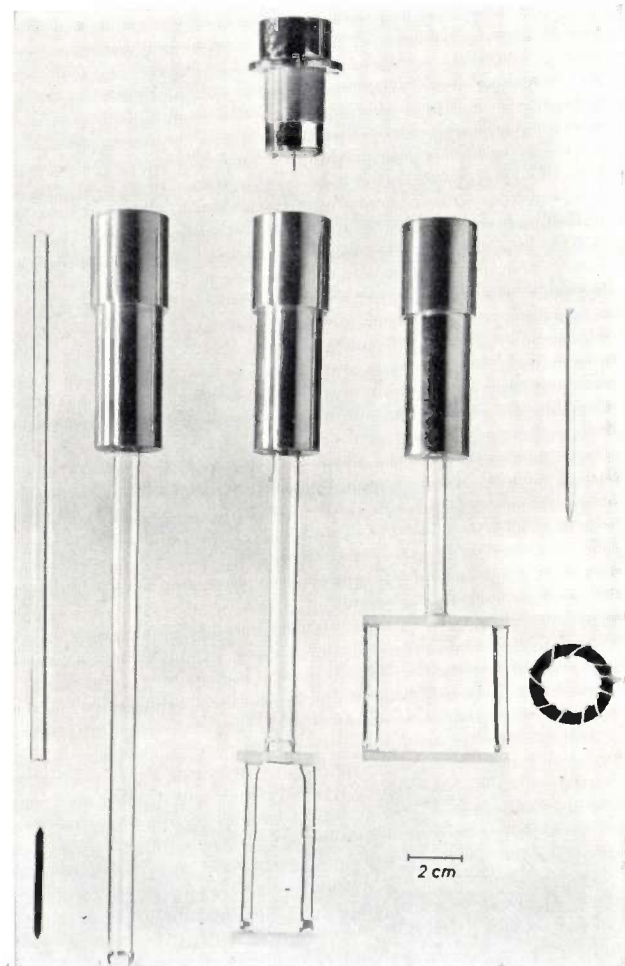


Fig.4. Various versions of the instrument for measuring magnetostriction. On the left is the version of fig. 1a. With the one in the centre it is possible to measure at the same time the variation of inductance in the test bar and thus to determine the magnetization (see fig. 1c). For this purpose a wire winding on the test bar is connected to a ballistic galvanometer. The magnetostriction of annular samples can be measured with the type shown on the right. In this case the magnetic field is produced by a current passed through the wire wound on the ring.

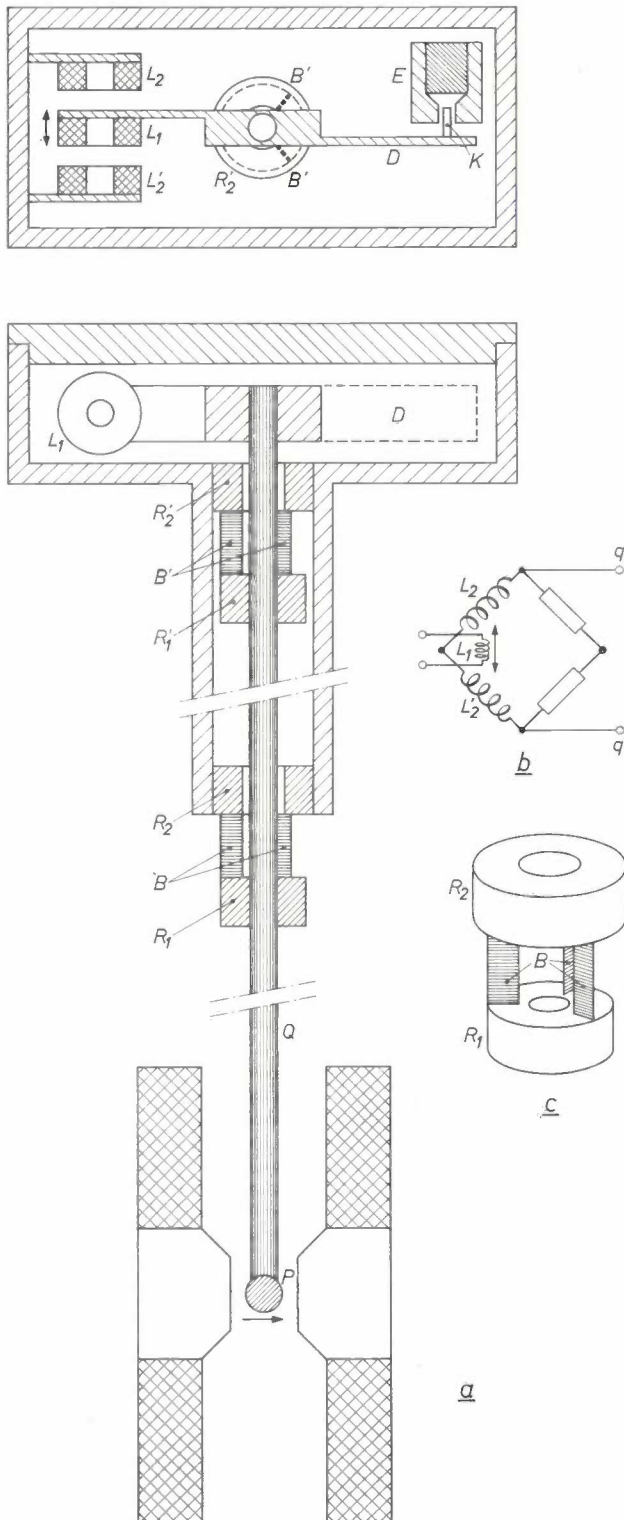


Fig. 5. a) Schematic cross-section of the instrument for measuring the magnetic anisotropy. Quartz bar Q is held by means of rings R_1 and R_1' and leaf-springs B to the rings R_2 and R_2' of the housing in such a way that it can only turn about its longitudinal axis (see also c). If a magnetic field (see arrow) exerts a couple upon the spherical single-crystal sample P , then coil L_1 mounted on cross-bar D is moved out of its equilibrium position halfway between coils L_2 and L_2' . The resulting potential difference between points q and q' (b) can again be read from the measuring bridge PT 1200. Fitted to the other arm of the cross bar is a piece of copper K , situated in the field of permanent magnet E , for damping possible vibrations.

ciple on which the instrument shown in fig. 5a operates.

Sample P is a spherical single crystal, a few millimetres in diameter, cemented to the lower end of a quartz rod Q ³⁾. The bar is clamped into two rings R_1 and R_1' , fitted by means of radially arranged leaf-springs B to immovable rings R_2 and R_2' (see sketch in fig. 5c). This allows the rod to turn through a moderate angle about its axis whilst motion in other directions is prevented. The top of the rod is fitted with a cross-bar D . Its left arm carries coil L_1 , through which an alternating current of 4 kc/s is passed, and which, together with two coils L_2 and L_2' , forms a differential transformer. Coils L_2 and L_2' have the same specification and are circuited in such a way that L_1 , when its position is halfway between the two coils, induces in them equal voltages of opposite sign, so that the potential between points q and q' (fig. 5b) is zero. Any displacement of L_1 causes a potential difference between q and q' , which is again amplified, rectified and measured by measuring bridge PT 1200. The measuring bridge also supplies the alternating current feeding the differen-

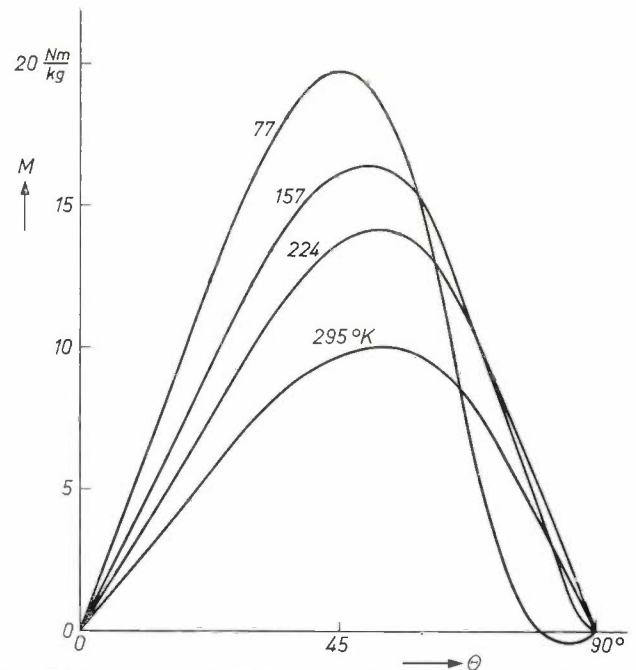


Fig. 6. The moment M of the couple that must be exerted on a single-crystal ferromagnetic sample of 1 g to maintain a preferred direction at an angle θ with the field, recorded as a function of angle θ , at various temperatures. Values of K_1 , K_2 , etc. can be derived from this diagram. The measurements were carried out on the compound $Ba_3CoZnFe_{24}O_{41}$ (a ferroxlana) very suitable for HF applications. This compound owes its remarkable properties to the fact that it has a preferred plane of magnetization. (Graph reproduced from: F. K. Lotgering, U. Enz and J. Smit, Philips Res. Repts. 16, 441, 1961. See further A. A. Aldenkamp, C. P. Marks and H. Zijlstra, Rev. sci. Instr. 31, 544, 1960.)

³⁾ A spherical shape was preferred as this eliminates the influence of the form anisotropy.

tial transformer. The right arm of cross-bar D is fitted with a small piece of copper K situated in the field of a permanent magnet E . Possible vibrations of the system are damped by the eddy currents induced by the magnet in the copper.

If the sample is situated in the field in such a position that one of its preferred directions is at an angle θ to the field, the bar will rotate about its axis through a small angle φ where the couple exerted by the leaf-springs on the bar balances the couple exerted by the field on the sample. The displacement of coil L_1 corresponding to φ results in a deflection of the measuring instrument proportional to moment M of the relevant couples. Knowing M , the value of K_1 can be calculated from (1).

The variation of the anisotropy with temperature can be measured just as simply as with the first instrument. As an example, some measuring results have been plotted in *fig. 6*. We see that the curves are only approximate sinusoidal functions of (1), which indicates that one or more of the coefficients K_2, K_3 , etc. are not zero. In order to determine the magnitude of these coefficients as well, the measurement must be carried out over the whole region $0 < \theta < 180^\circ$. It is therefore of great advantage that this set-up is very suitable for automatic recording. To this end the measuring instrument rotates about its axis with respect to the field at the rate of about 1 r.p.m., by means of a simple auxiliary device. This rotation is transmitted via gears to the arm of a potentiometer connected to the measuring instrument. The voltage across the potentiometer, being proportional to the angle θ , is applied to an x - y -recorder together with the output voltage of the measuring bridge, which is

proportional to the moment M . In this way the recorder automatically plots the variation of M with θ . The complete set-up is shown in *fig. 7*.

Magnetization

A magnetic field non-homogeneous in a given direction, e.g. in the z -direction, will exert on a ferromagnetic sample a force F parallel to that direction, proportional to the mass m of the sample as well as to the gradient dH/dz in this direction. We can therefore put:

$$F = m\sigma \frac{dH}{dz} \quad \dots \dots \dots (2)$$

The proportionality constant σ in this expression

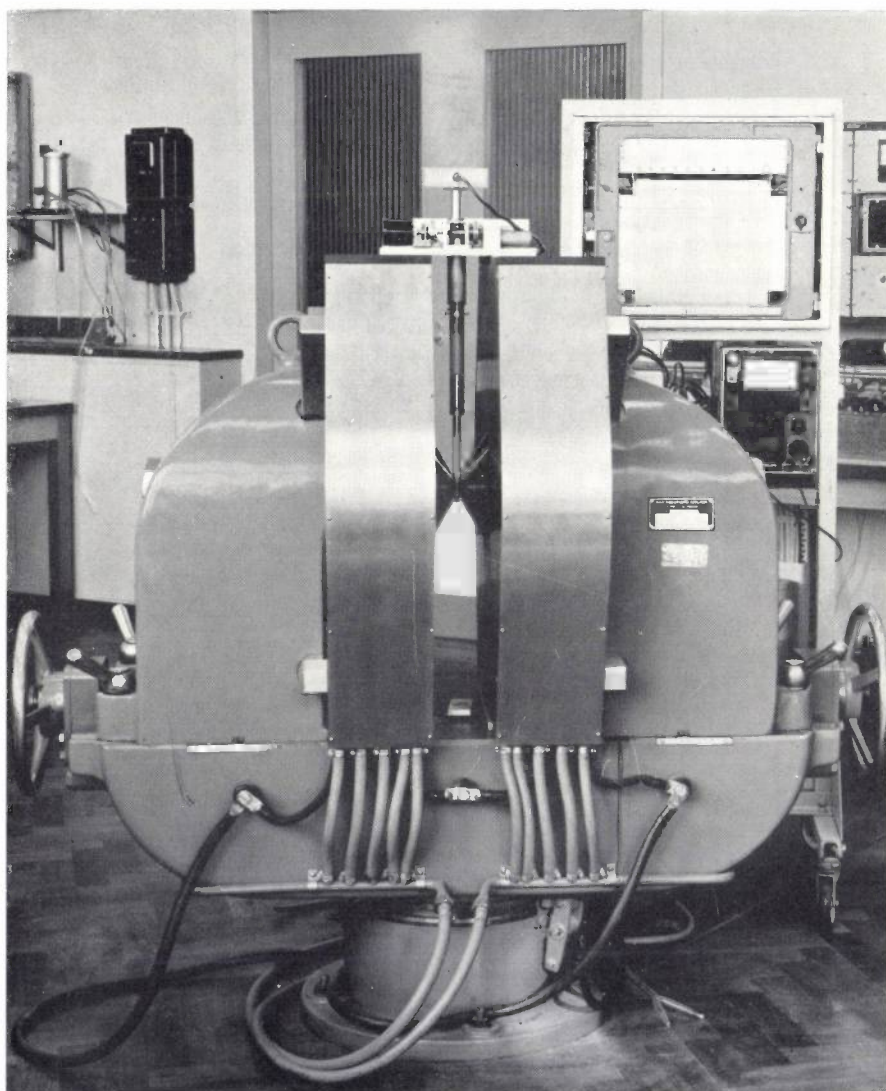


Fig. 7. Complete set-up for measuring the magnetic anisotropy. The specimen is placed between the pole shoes of the large electromagnet. On top of the magnet rests the auxiliary device by which the measuring instrument is rotated at approx. 1 revolution per minute about its longitudinal axis. Behind the magnet can be seen the x - y -recorder by which moment M is recorded as a function of angle θ . Below the x - y -recorder is the measuring bridge PT 1200.

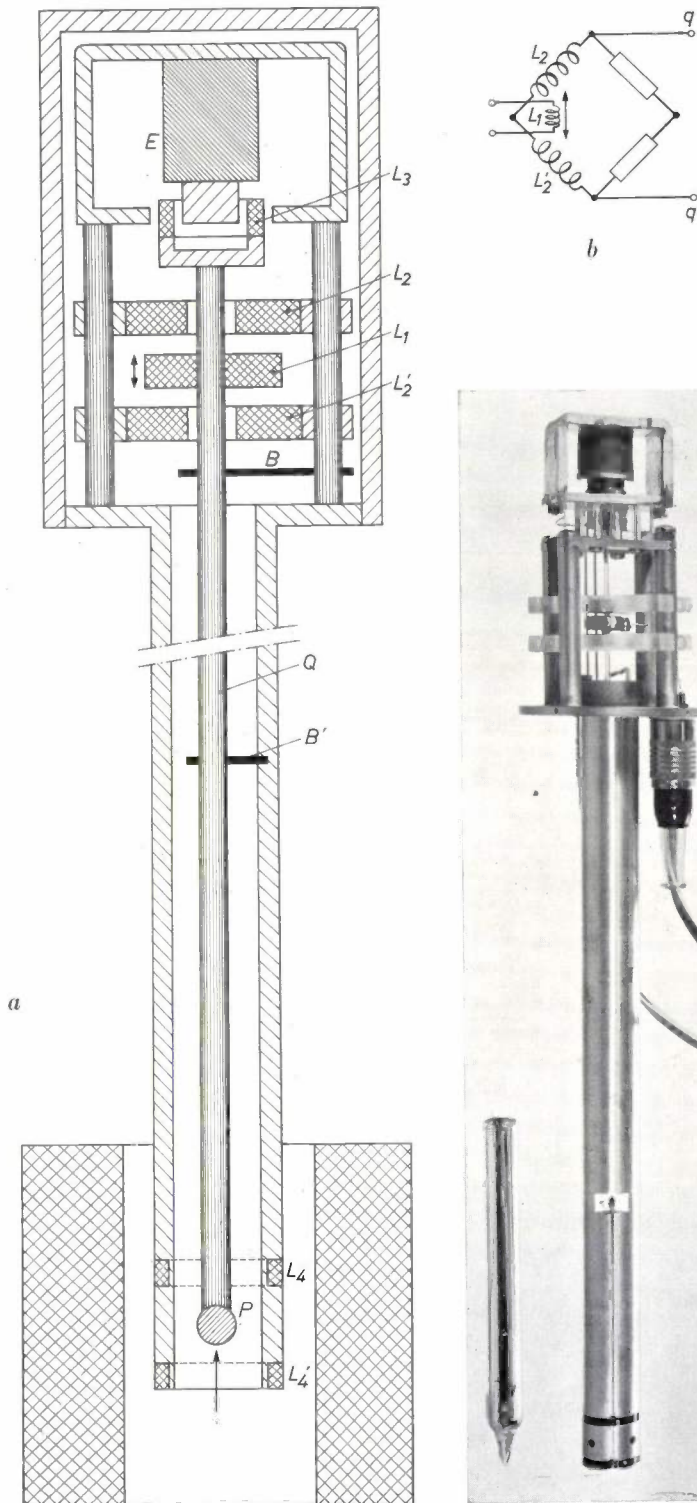


Fig. 8

is the *magnetization* per unit mass. Instead of $m\sigma$ we can also put in (2) the product of the volume V of the sample and the magnetization I per unit volume. The magnitude of I derived from this will not be very accurate as a rule, since most ferromagnetic materials are porous, so that their true volume cannot be precisely defined.

σ can be determined by measuring F when m and dH/dz are known, and this is done with the instrument shown in

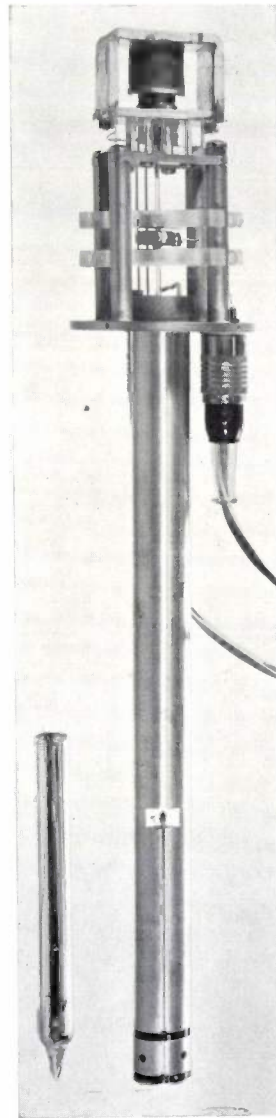


Fig. 9

Fig. 8. a) Schematic cross-section of the instrument for measuring the magnetization. Bar Q is held by the leaf-springs B and B' and is fitted at its lower end with the spherical sample P and at the top with coil L_3 , which forms part of a loudspeaker system, with E as permanent magnet. Coils L_4 and L_4' produce a field with constant gradient dH/dz , which exerts a force upon the sample magnetized by the field of the solenoid. The resulting displacement, however, is reduced to zero by varying the current through L_3 , the differential transformer (L_1 , L_2 and L_2') incorporated in a bridge circuit (b), in combination with measuring bridge PT 1200, serving as zero indicator. The current through L_3 is a measure of magnetization.

Fig. 9. The instrument for measuring the magnetization with its cover removed. To the left of the instrument is a small Dewar flask which can be fitted into it, so that for measuring the magnetization at low temperatures only the sample and a small section of the quartz rod have to be cooled down.

fig. 8a and fig. 9. A long, thin quartz rod Q is supported by leaf-springs B and B' in the same way as indicated for the displacement meter in fig. 1, so that only lengthways movements are permitted. Cemented to the lower end of the bar is the sample P (usually a sphere a few mm in diameter). Fitted to the upper end of the bar is coil L_3 of a loudspeaker system, fitting very closely in the circular air-gap of a permanent magnet E ⁴). Also fitted to the bar is a second coil L_1 which, together with two stationary coils L_2 and L_2' , forms a differential transformer. Two grooves in the casing at the height of the sample hold two coils L_4 and L_4' by which a magnetic field of a known and constant gradient dH/dz can be generated over a length of about 1 cm (see fig. 10).

In order to magnetize the sample, the narrow part of the instrument is placed inside a solenoid, the fields that can thus be generated being strong enough to saturate most materials. When the current through coils L_4 and L_4' is switched on, a field having a constant gradient is superimposed upon the field of the solenoid, and the sample is subjected to a small force of the same order of magnitude as its weight, causing a small displacement of coil L_1 . This displacement is found just as in the anisotropy instrument,

⁴) The device built by Foëx and Forrer (J. Phys. Radium 7, 180, 1926) likewise employs a loudspeaker system in this place.

but the measuring procedure is somewhat different here. In this case we determine the current through coil L_3 necessary to compensate the force exerted by the field of magnet E upon coil L_3 , using the measuring bridge as a null indicator. This method was preferred because the sample always remains in the same position relative to L_4 and L_4' , thus avoiding any errors due to the gradient dH/dz not being exactly uniform.

It is obviously desirable for the magnetization σ in the sample to be as homogeneous as possible, and since σ depends upon the field strength, this implies that the variation ΔH of H across the diameter of the sample should be small relative to H . This is fulfilled since with variations in H from 80×10^3 to 1600×10^3 A/m, ΔH amounts to approx. 3×10^3 A/m.

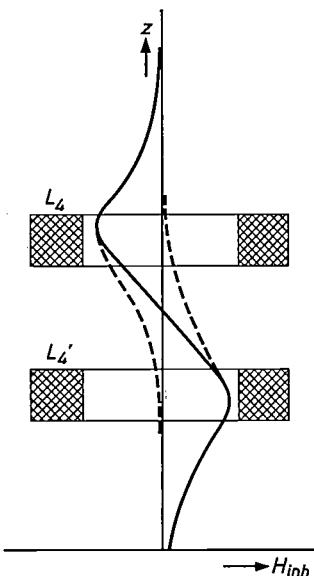


Fig. 10. A non-homogeneous magnetic field H_{inh} with a constant gradient dH/dz is produced by means of two identical coils L_4 and L_4' through which currents are passed in opposite directions. The fields set up by the coils are shown by the dotted lines. The resultant of the two fields has a constant gradient over a distance of approx. 1 cm.

Another source of errors has been eliminated by using coil L_1 instead of a ferroxcube core as is used in the instrument for measuring the magnetostriction. The influence of the powerful stray field of the solenoid on the ferroxcube core could attain the same order of magnitude as the force on the sample produced by the gradient dH/dz . But since an alternating current of 4 kc/s is passed through coil L_1 , the field of the solenoid, averaged over time, does not exert any force upon the coil.

The measuring method is particularly suitable for quickly establishing the relation between the mag-

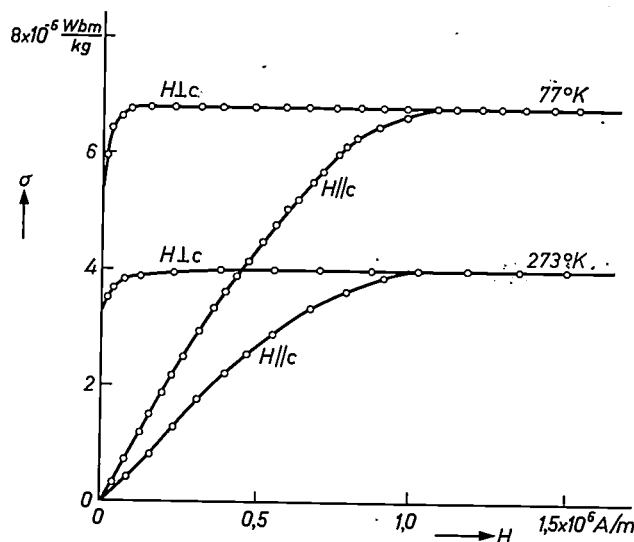


Fig. 11. Magnetization σ of a single crystal of $Ba_2Zn_2Fe_{12}O_{22}$ as a function of the field strength H at different temperatures. From similar measurements of the magnetization of single crystals along various crystallographic axes, in the present instance perpendicular or parallel to the hexagonal axis (c) of the specimen, conclusions regarding the magnetic structure of the substance can be drawn. (Graph reproduced from: U. Enz, J. appl. Phys. 32, suppl. to No. 3, 22S, 1961. See also: H. Zijlstra, thesis, Amsterdam 1960.)

netization and the field strength. Here again, the influence of temperature can be readily examined. The inner diameter of the casing surrounding the sample (16 mm) is sufficient to accommodate auxiliary devices and means for controlling the temperature. On the left in fig. 9 is shown a small Dewar flask fitting inside the casing. For a variable temperature below room temperature, a thin coiled copper tube is employed through which cold nitrogen is blown at a controlled rate. For the range above room temperature up to 700 °C, a small furnace is available. In fig. 11 are plotted a number of curves measured with the instrument.

Summary. Three instruments are described for measuring magnetostriction, magnetic anisotropy and magnetization. In each, the magnetic quantity is determined by measuring the displacement of a ferroxcube core or a coil. This displacement varies the coupling between two coils, which is measured by connecting them to a measuring bridge PT 1200. The samples of the ferromagnetic materials on which the measurements are carried out are 5 cm long rods for magnetostriction measurements and small spheres of a few mm diameter for the other two measurements. For the desired precision of 1%, the design of the instruments has been kept as simple as possible, so that they can be conveniently and quickly operated. By a few simple additions to the equipment, the variation with temperature of the three magnetic quantities can be established.

RECENT SCIENTIFIC PUBLICATIONS BY THE STAFF OF THE PHILIPS LABORATORIES AND FACTORIES

Reprints of those papers not marked with an asterisk * can be obtained free of charge upon application to the Philips Research Laboratories, Eindhoven, Netherlands, where a limited number of reprints are available for distribution.

- 3176:** C. Wansdronk: On the mechanism of hearing (thesis Leiden, Nov. 1961).
- 3177:** H. M. Jongerius: Measurements of optical excitation functions of the mercury atom (excitation by electrons) (thesis Utrecht, Dec. 1961).
- 3178:** H. L. Spier: Influence of chemical additions on the reduction of tungsten oxides (thesis Eindhoven, Nov. 1961).
- 3179:** C. Z. van Doorn: Colour centres in potassium chloride (thesis Utrecht, June 1962).
- 3180:** H. Elings: Experiences with 5-amino-3-phenyl-1-bis(dimethylamido) phosphoryl-1,2,4-triazole, a new fungicide controlling powdery mildew (Proc. Brit. Insecticide and Fungicide Conf. 1961, Vol. 2, pp. 451-459, 1962).
- 3181:** A. J. Pieters: Triphenyl tin hydroxide, a fungicide for the control of *Phytophthora infestans* on potatoes, and some other fungus diseases (as **3180**, pp. 461-470).
- 3182:** J. Meltzer and K. F. Jacobs: 2,4,5,4'-tetrachloro-diphenyl sulphide, an acaricide with ovo-larvicidal properties (as **3180**, pp. 499-505).
- 3183:** P. A. H. Hart: Partition effects in transverse electron beam waves (J. appl. Phys. **33**, 2401-2408, 1962, No. 8).
- 3184:** J. A. W. van Laar: The durability of paint coatings (Corrosion prevention & control **8**, No. 12, 32-42, 1961; **9**, No. 1, 35-42, 1962; **9**, No. 3, 57-60, 1962; **9**, No. 7, 31-32, 1962).
- 3185:** J. E. Cook and W. J. Oosterkamp: Protection against radiation injury (Internat. Tables for X-ray Crystall., Vol. III, pp. 331-338, Kynoch Press, Birmingham 1962).
- 3186:** W. Elenbaas: Dissipation calorifique par convection libre sur la surface interne de tubes verticaux (Journées internat. Transm. Chaleur, Paris 1961, Vol. I, pp. 379-384, publ. Inst. Français Combust. Energie, Paris 1962). (Heat dissipation by free convection on the inside surface of vertical tubes; in French.)
- 3187:** H. J. G. Meyer: On the low temperature limit of mm-wave cyclotron resonance line widths (Physics Letters, Amsterdam, **2**, 259-260, 1962, No. 5).
- 3188:** J. J. van Loef and W. van Dingenen: The influence of hydrogen on the magnetic scattering of neutrons by a nickel-palladium alloy (Physica **28**, 917-918, 1962, No. 9).
- 3189:** A. Venema: Processes limiting the ultimate pressure in ultra high vacuum systems (1961 Trans. 8th Nat. Vacuum Symp. + 2nd Int. Congress on Vacuum Sci. and Technol., Washington D.C., Vol. 1, pp. 1-7, Pergamon Press, Oxford 1962).
- 3190:** A. van Oostrom: A Bayard-Alpert type ionization gauge with a low X-ray limit (as **3189**, pp. 443-450).
- 3191:** B. D. H. Tellegen: Magnetic-dipole models (Amer. J. Phys. **30**, 650-652, 1962, No. 9).
- 3192:** J. H. Aalberts and M. L. Verheijke: The solid solubility of nickel in silicon determined by neutron activation analysis (Appl. Phys. Letters **1**, 19-20, 1962, No. 1).
- 3193:** F. de Jager and P. J. van Gerwen: CO-modulation, a new method for high-speed data transmission (IRE Trans. on information theory IT-**8**, S 285-S 290, 1962, No. 5).
- 3194:** H. J. Vink: Wechselwirkungen zwischen Störstellen in Halbleitern (Festkörperprobleme I, pp. 1-19, Vieweg, Brunswick 1962). (Interactions between lattice defects in semiconductors; in German.)
- 3195:** J. Dieleman: Influence of solvent-shared association on the electronic spectra of aromatic hydrocarbon negative ions (thesis V.U. Amsterdam, Dec. 1962).
- 3196:** J. W. L. Köhler and J. R. van Geuns: A small liquid-oxygen generator using the gas-refrigerating machine (Annexe 1961-5 au Bull. Inst. Int. Froid, pp. 65-70).
- 3197:** W. F. Druyvesteyn and D. J. van Ooijen: Influence of cold-rolling at 78 °K on the superconducting transition of lead (Physics Letters, Amsterdam, **2**, 328-329, 1962, No. 7).
- 3198:** W. van Gool and G. Diemer: Association of centers in zinc sulfide (Kallman and Spruch, Luminescence of organic and inorganic materials, pp. 391-401, Wiley, New York 1962).
- 3199:** A. Brill: Absolute efficiencies of phosphors with ultraviolet and cathode-ray excitation (as **3198**, pp. 479-493).
- 3200:** H. G. van Bueren, J. Haisma and H. de Lang: A small and stable continuous gas laser (Physics Letters, Amsterdam, **2**, 340-341, 1962, No. 7). See also Philips tech. Rev. **24**, 95-97, 1962/63 (No. 3).

- 3201: R. Bleekrode, J. Dieleman and H. J. Vegter: Electron spin resonance on Mn in GaAs (Physics Letters, Amsterdam, 2, 355-356, 1962, No. 7).
- 3202: H. B. G. Casimir: Technological advance: a stimulus to basic research (Cherwell-Simon Memorial Lectures 1961 and 1962, pp. 6-24, Oliver and Boyd, Edinburgh/London).
- 3203: N. V. Franssen: The mechanism of the human voice and wind instruments (4th Int. Congress on Acoustics, Copenhagen 1962, publ. No. G12).
- 3204: C. M. van der Burgt and A. L. Stuijts: Low-porosity ferrites for high-intensity ultrasonic radiators (as 3203, publ. No. K22).
- 3205: E. de Niet, K. Teer and D. L. A. Tjaden: Magnetic recording of audio signals at low tape speeds (as 3203, publ. No. N11).
- 3206: C. M. van der Burgt and E. E. Havinga: Finite-strain response of the piezoelectric transducer ceramics Pb-Ba and Pb-Sr zirconate-titanate (as 3203, publ. No. N18).
- 3207: A. van Oostrom: Field emission cathodes (J. appl. Phys. 33, 2917-2922, 1962, No. 10).
- 3208: A. Claassen and L. Bastings: A study of interferences in the iodometric determination of copper in fluoride medium (Z. anal. Chemie 191, 401-408, 1962, No. 6).
- 3209: L. E. Vrenken: High-output fluorescent lamps with circular cross section — The influence of the lamp diameter (Illum. Engng. 57, 683-687, 1962, No. 10).
- 3210: N. F. Verster, H. L. Hagedoorn, J. Zwanenburg, A. J. J. Franken and J. Geel: Some design features of the Philips AVF prototype (Nucl. Instr. Meth. 18/19, 88-92, 1962).
- 3211: H. L. Hagedoorn and N. F. Verster: Orbits in an AVF cyclotron (Nucl. Instr. Meth. 18/19, 201-228, 1962).
- 3212: N. F. Verster and H. L. Hagedoorn: Computer programs for an AVF cyclotron (Nucl. Instr. Meth. 18/19, 327-335, 1962). See also Philips tech. Rev. 24, 106-120, 1962/63 (No. 4/5).
- 3213: H. L. Hagedoorn and N. F. Verster: Analogue computer studies for an AVF cyclotron (Nucl. Instr. Meth. 18/19, 336-337, 1962).
- 3214: G. Meijer: Photomorphogenesis influenced by light of different spectral regions (Advng. Front. Plant Sci. 1, 129-140, 1962).
- 3215: J. H. Stuy: Transformability of Haemophilus influenzae (J. gen. Microbiol. 29, 537-549, 1962, No. 3).
- 3216: C. Haas: On diffusion, relaxation and defects in ice (Physics Letters, Amsterdam, 3, 126-128, 1962, No. 3).
- 3217: D. J. van Ooijen, J. H. N. van Vucht and W. F. Druyvesteyn: Superconductivity of NbSn₂ (Physics Letters, Amsterdam, 3, 128-129, 1962, No. 3).
- 3218: J. J. Wilting: Die Entwicklung auf dem Gebiete der Transistorumformer für Fluoreszenzlampe (Bull. Schweiz. Elektrotechn. Ver. 53, 1082-1091, 1962, No. 22). (Developments in transistorized converters for fluorescent lamps; in German.)
- 3219: M. L. Verheijke: Calculated efficiencies of a 3 × 3 in. NaI(Tl) well-type scintillation crystal (Int. J. appl. Rad. Isot. 13, 583-585, 1962, No. 10).
- 3220: N. W. H. Addink and A. W. Witmer: Spectrochemical analysis of impurities present in semiconductors and semiconductor materials in the part per billion range (IX. Colloquium spectroscopicum internationale, Lyon 1961, Vol. II, pp. 340-354).
- 3221: A. W. Witmer and N. W. H. Addink: New graphite-backed electrode for spectrochemical analysis of metals independent of original sample shape (as 3220, Vol. II, pp. 405-412).
- 3222: H. Groendijk: Amplification by longitudinal waves in beam-plasma systems (1962 North-east Electronics Res. and Engng. Meeting, NEREM Rec. 4, 184-185, 1962).
- 3223*: J. S. van Wieringen: Paramagnetic ions as impurities in crystals (and glasses) (Landolt-Börnstein, Zahlenwerte und Funktionen aus Physik, etc., 6th edition, Vol. II, Part 9, pp. 4-17 to 4-42, Springer, Berlin 1962). (Tables in German, introduction also in English).
- 3224: H. J. L. Trap and J. M. Stevels: Nouveaux types de verre présentant une conductibilité électronique (Verres et Réfract. 16, 337-343, 1962, No. 6). (New types of glass showing electrical conductivity; in French).
- 3225: N. W. H. Addink, H. Kraay and A. W. Witmer: The putting to advantage of the absorbing qualities of diluting agents for obtaining 45 degree calibration curves in X-ray fluorescence analysis (as 3220, Vol. III, pp. 368-384).
- 3226: S. van Houten: Investigation of the conduction mechanism in transition metal oxides by means of internal friction measurements (Rep. int. Conf. on the physics of semiconductors, Exeter 1962, pp. 197-201, publ. Inst. Phys./Phys. Soc., London 1962).
- 3227: S. M. de Veer and H. J. G. Meyer: Infra-red absorption by free electrons in germanium (as 3226, pp. 358-366).
- 3228: A. C. Aten, C. Z. van Doorn and A. T. Vink: Direct and phonon-assisted optical transitions in zinc telluride (as 3226, pp. 696-702).
- 3229: H. J. van Daal, W. F. Knippenberg and J. D. Wasscher: Mobility of electrons and holes in hexagonal silicon carbide (as 3226, pp. 783-789).

- 3230:** J. van Laar and J. J. Scheer: Influence of band bending on the photoelectric emission of silicon (as **3226**, pp. 827-831).
- 3231:** H. Bremmer: Electromagnetic wave propagation around the earth (Summer school Varenna 1961, Centro Internazionale Matematico Estivo, Istituto Matematico dell'Università, Rome 1962).
- 3232:** H. Bremmer: The pulse solution connected with the Sommerfeld problem for a dipole in the interface between two dielectrics (Electromagnetic waves, editor R. E. Langer, pp. 39-64, Univ. Wisconsin Press, Madison 1962).
- 3233:** Chr. Meyer: Einige Anwendungen von Entladungsblißröhren in der medizinischen Photographie (I. Int. Kongress für medizinische Photographie und Kinematographie, Düsseldorf 1960, pp. 314-316, Thieme, Stuttgart 1962). (Some applications of flash-discharge tubes in medical photography; in German.)
- 3234:** F. Th. Backers and J. H. Wessels: Magnetische Fernsehaufzeichnung mit einer Einkopf-Anlage (Nachrichtentechn. Z. **15**, 644-649, 1962, No. 12). (Magnetic recording of television signals using a single head system; in German.)
See also Philips tech. Rev. **24**, 81-83, 1962/63 (No. 3).
- 3235:** C. A. A. J. Greebe: The physical properties of grown *P-I-N* junctions in silicon carbide (thesis Eindhoven, June 1962).
- 3236:** A. M. Kruithof, A. A. Padmos, J. de Vries, J. de Groot and A. L. Zijlstra: Spannungsoptische Bestimmung der Wärmeausdehnungen von Gläsern und Metallen (Sprechsaal für Keramik Glas Email **95**, 464-467, 484-487, 518-520 and 691-694, 1962, Nos. 17, 18, 19 and 24; **96**, 36-39, 1963, No. 2). (Determination of thermal stresses in glass and metals by means of stress birefringence; in German.)
- 3237:** M. J. Sparnaay: Free energy calculations of diffuse double layer systems. The "secondary minimum" (Emulsion rheology, pp. 27-40, Pergamon Press, Oxford 1963).
- 3238:** W. J. Witteman: On vibrational relaxations in carbon dioxide (thesis Eindhoven, March 1963).
- 3239:** A. H. Boonstra, J. van Ruler and M. J. Sparnaay: On the influence of various ambients on the surface conductivity of germanium surfaces (Proc. Kon. Ned. Akad. Wetensch. **B 66**, 64-69, 1963, No. 2).
- 3240:** A. H. Boonstra, J. van Ruler and M. J. Sparnaay: Surface states on cleaned and oxidized germanium surfaces (Proc. Kon. Ned. Akad. Wetensch. **B 66**, 70-75, 1963, No. 2).
- 3241:** J. W. Steketee and J. de Jonge: Sensitized photoconductivity in anthracene (Proc. Kon. Ned. Akad. Wetensch. **B 66**, 76-79, 1963, No. 2).
- 3242:** J. H. N. van Vucht: Interaction of Th_2Al and related getters with hydrogen (thesis Eindhoven, March 1963).
- 3243:** C. Weber: A new resistor network for solving Laplace's equation (Proc. IEEE **51**, 252, 1963, No. 1).
- 3244:** J. Haisma and H. de Lang: Mode patterns obtained by tuning a small gas laser (Physics Letters, Amsterdam, **3**, 240-242, 1963, No. 5).
- 3245:** J. J. Scheer and J. van Laar: Photo-emission from semiconductor surfaces (Physics Letters, Amsterdam, **3**, 246-247, 1963, No. 5).
- 3246:** B. Bölger, J. A. W. van der Does de Bye, H. Kalter and H. J. Vegter: Laser action in a GaAs junction (Physics Letters, Amsterdam, **3**, 252, 1963, No. 5).
- 3247:** W. J. Oosterkamp and C. Albrecht: The evaluation of fluoroscopic screens and X-ray image intensifiers (Technological needs for reduction of patient dosage from diagnostic radiology, editor M. L. Janower, pp. 251-270, publ. Thomas, Springfield, Ill. U.S.A., 1963).
- 3248:** H. B. G. Casimir: Über die statistische Begründung des Nernstschen Wärmethorems (Z. Phys. **171**, 246-249, 1963, No. 1). (On the statistical basis of Nernst's heat theorem; in German.)
- 3249:** P. J. Severin: Some dynamic aspects of the cathode fall region in a D.C. glow discharge (Physica **29**, 83-92, 1963, No. 1).
- 3250:** H. J. van Daal, W. F. Knippenberg and J. D. Wasscher: On the electronic conduction of α -SiC crystals between 300 and 1500 °K (Phys. Chem. Solids **24**, 109-127, 1963, No. 1).
- 3251:** J. R. van Geuns: Eine kleine Luftzerlegungsanlage mit zwei Gaskältemaschinen zur Gewinnung von flüssigem Sauerstoff (Kältetechnik **15**, 5-10, 1963, No. 1). (A small air fractionating installation with two gas refrigerating machines for the production of liquid oxygen; in German.)
- 3252:** A. Claassen and L. Bastings: The determination of lead in carbon and low-alloy steel according to British Standard 1121 : Part 41 : 1960 (Analyst **88**, 67-68, 1963, No. 1042).
- 3253:** A. van Oostrom: Temperature dependence of the work function of single crystal planes of tungsten in the range 78-293 °K (Physics Letters, Amsterdam, **4**, 34-36, 1963, No. 1).
- 3254:** C. A. A. J. Greebe: On the frequency dependence of the acousto-electric effect in piezo-electric semiconductors (Physics Letters, Amsterdam, **4**, 45-46, 1963, No. 1).
- 3255:** K. G. Srivastava: A magnetic study of some compounds having the K_2NiF_4 structure (Physics Letters, Amsterdam, **4**, 55-56, 1963, No. 1).

Philips Technical Review

DEALING WITH TECHNICAL PROBLEMS
RELATING TO THE PRODUCTS, PROCESSES AND INVESTIGATIONS OF
THE PHILIPS INDUSTRIES

A PULSED MAGNETRON FOR $2\frac{1}{2}$ mm WAVES

by G. H. PLANTINGA *).

621.385.6:621.3.032.61

The development of tubes for operating at ever shorter wavelengths has not yet come to an end, as evidenced by the recent completion of a magnetron for $2\frac{1}{2}$ mm waves, described in this article. As far as we know, this is the first magnetron for this wavelength to give satisfactory results. It is capable of delivering a power of 2.5 kW in pulses of 0.1 μ s duration, the mean power being 0.5 W.

Some years ago a range of pulsed magnetrons developed in our laboratories was described in this journal¹⁾. This development was mainly directed towards the attainment of shorter operating wavelengths. The magnetron with the shortest wavelength in this range was a 4 mm tube. A magnetron for $2\frac{1}{2}$ mm waves has now appeared, some aspects of which will be dealt with in this article.

The principal application of magnetrons of the above-mentioned range was said to be radar. Although $2\frac{1}{2}$ mm waves are less suitable for radar because of their severe attenuation in the atmosphere, due to the presence of an oxygen absorption line at this wavelength²⁾, 4 mm is certainly not the shortest wavelength for radar purposes. Now that it has proved possible to build a $2\frac{1}{2}$ mm magnetron, there is nothing to stop the production of magnetrons for wavelengths between 4 and $2\frac{1}{2}$ mm, a band for which a need has recently arisen in the field of radar. The applications of the $2\frac{1}{2}$ mm magnetron, however, are mainly in the field of *physical measurements*³⁾.

Examples that come to mind are measurements in plasma research.

The smallest version of the above-mentioned range of magnetrons, the 4 mm tube, followed from an 8 mm type. After the development of this tube it seemed obvious to try to reduce the wavelength again by a factor of 2. Why the range of magnetrons cannot be extended in exactly this way will presently be explained. Some problems inherent in this scaling-down process will be discussed. Attention will also be paid to special details of construction, where the small dimensions of the essential components created problems. In conclusion a number of measurements will be described.

A photograph of the $2\frac{1}{2}$ mm magnetron (without the magnet) is shown in *fig. 1*.

Scaling down

Although the magnetron is one of the oldest of the microwave tubes⁴⁾ and has been the subject of considerable research over the years, there is still no completely satisfactory theory for this type of tube⁵⁾.

*) Philips Research Laboratories, Eindhoven.

¹⁾ J. Verweel and G. H. Plantinga, A range of pulsed magnetrons for centimetre and millimetre waves, Philips tech. Rev. 21, 1-9, 1959/60.

²⁾ J. H. van Vleck, Phys. Rev. 71, 413-424 and 425-433, 1947. See also H. Bremmer, Philips tech. Rev. 15, 150, 1953/54.

³⁾ The same applies to the waveguide equipment for 2 mm microwaves, previously described in this journal: C. W. van Es, M. Gevers and F. C. de Ronde, Philips tech. Rev. 22, 113-125 and 181-189, 1960/61.

⁴⁾ See e.g. K. Posthumus, Principles underlying the generation of oscillations by means of a split anode magnetron, Philips Transmitting News 1, No. 3, 11-25, 1934, or K. Posthumus, Oscillations in a split anode magnetron, Wirel. Engr. 12, 126-132, 1935.

⁵⁾ See Vol. I and II of Crossed-field microwave devices, edited by E. Okress, Acad. Press, New York 1961.

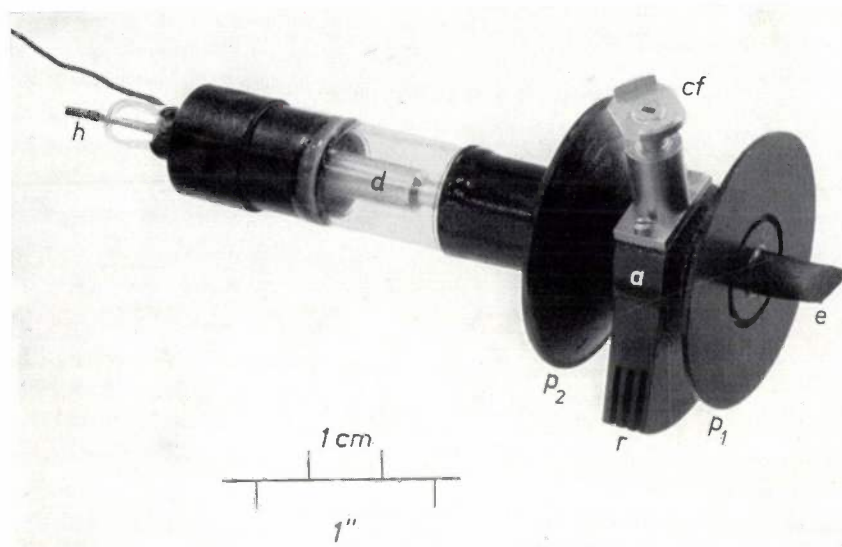


Fig. 1. Pulsed magnetron (without magnet) for $2\frac{1}{2}$ mm waves. It can deliver an output of 2.5 kW in pulses of 0.1 μ s duration.

h heater connection. *d* cathode cylinder. *a* anode block. *cf* claw flange³⁾ for connection to the waveguide through which the RF energy is extracted. *p*₁, *p*₂ pole pieces. *r* cooling fins. *e* pinch-sealed copper exhaust.

The design of a new magnetron is therefore governed to a very large extent by empirical knowledge of existing types. In general the aim will be to design a new magnetron as a modification of a type that has already proved itself in practice.

Magnetrons for shorter wavelengths can most simply be designed by modification on the principles of a *scaling law*¹⁾. Suppose that a given magnetron having a magnetic field with induction B delivers at a given anode current and anode voltage a certain power output with a wavelength λ . If we now scale up an existing magnetron so that its linear dimensions all become p times larger, and if we make the magnetic induction equal to B/p , then this magnetron at the same current and voltage will deliver the same power output at the wavelength $p\lambda$.

This principle applies exactly only provided the specific conductance at any given position in the new magnetron is $1/p$ times the specific conductance at the corresponding position in the old magnetron, and provided also that the same proportionality holds for the electric field-strength at the cathode. The first condition is never fulfilled, nor usually is the second one. Moreover, in the case of scaling down ($p < 1$), the saturation of the available ferromagnetic materials often makes it difficult to meet the requirement of a higher induction (B/p). Nevertheless a scaling law is very useful for gaining insight into the influence of the various parameters.

A scaling law was used in the development of the range of magnetrons described in the article under reference¹⁾. One can attempt to continue this range by scaling down to a tube for e.g. 2 mm waves. First, however, one should know the consequences of proportionately reducing the dimensions of the smallest tube in the series (the 4 mm magnetron).

Proportional scaling-down from the 4 mm magnetron

The following considerations are based on the operating region of the 4 mm magnetron. This region is characterized by the following values: magnetic induction $B = 1.5-1.9$ Wb/m², anode voltage $V = 11-16$ kV, anode current $I = 7-14$ A.

A 2 mm magnetron which is a scaled-down version of the 4 mm type possesses, according to the scaling law, a corresponding operating region with the same values of voltage and current; the corresponding induction values, however, must be $(4/2) \times (1.5-1.9) = 3.0-3.8$ Wb/m². The effective emissive area of the cathode of the 4 mm magnetron is 0.07 cm², so that the current density at the cathode reaches the appreciable value of $(7-14)/0.07 = 100-200$ A/cm². A current density of this magnitude is only possible as a result of the secondary emission caused by the electrons returning to the cathode, i.e. back-bombardment⁶⁾. The cathode of the 2 mm magnetron would have to be capable of delivering an even greater current density, namely from 400 to 800 A/cm². It is questionable whether current densities in excess of 400 A/cm² are to be achieved with any known type of cathode.

With linear scaling-down, the specific dissipation increases in inverse proportion to the square of the scaling factor p . This need not in principle entail a higher average anode temperature, because the higher specific dissipation can be countered with better cooling. What cannot be compensated in such a relatively simple manner, however, is the greater temperature increase of the bombarded anode surfaces during the pulses. The energy conducted away from the bombarded anode surface during a pulse is

⁶⁾ See J. Verweel, Philips tech. Rev. **14**, 44, 1952/53.

very small compared with the energy supplied with each pulse. During the pulses the temperature at the surface therefore rises rapidly. After the pulse most of the energy is transferred by conduction to other parts of the anode which, as we have said, can be prevented from getting too hot by more effective cooling. It is not possible, however, to improve the cooling of the bombarded area of the anode. An increase in the specific dissipation therefore means that the temperature of the effective anode surface will inevitably become higher during the pulses (we shall henceforth refer to this as peak heating).

The temperature increase at the surface of a body to which a specific power of W watts per cm^2 is supplied in a pulse of τ seconds duration can be calculated if a few simplifying assumptions are made. Assuming that the heat is conducted away only in the direction perpendicular to the surface, and neglecting radiation, we find that the temperature increase ΔT at the end of the pulse is given by the following expression ⁷⁾:

$$\Delta T = \frac{2W}{\sqrt{\pi k C}} \sqrt{\tau} \dots \dots (1)$$

Here k is the thermal conductivity of the medium (in $\text{W/cm}^\circ\text{C}$) and C the heat capacity per unit volume (in $\text{Ws/cm}^3^\circ\text{C}$). This formula is a reasonably good approximation for the peak heating of a magnetron anode. These anodes are made of copper, and the thermal conductivity and heat capacity of copper are respectively $k = 3.9 \text{ W/cm}^\circ\text{C}$ and $C = 3.5 \text{ Ws/cm}^3^\circ\text{C}$. Using these values we can write eq.(1) in the following form:

$$\Delta T = \frac{31 P \sqrt{\tau}}{\varphi \lambda^2} \dots \dots (2)$$

Here P is the power (in watts) which, during a pulse is lost in the anode as heat, and $\varphi = A/\lambda^2$, where A is the effective anode surface (A and λ^2 expressed in mm^2 , τ in seconds). According to the scaling law, φ remains constant upon a linear scaling. Consequently it follows from (2) that, for a scaling-down at a given value of P , the peak heating can only be kept unchanged by shortening the pulse duration τ in proportion to the fourth power of the scaling factor p ; this soon sets a practical limit to the scaling-down process.

One of the specifications for the new magnetron was that it should be capable of operating at maximum pulse durations of about $0.1 \mu\text{s}$. For the 4 mm magnetron $\varphi = 0.39$. Using this value as the basis

for scaling down, we can calculate from (2) the peak heating to be expected for other tubes — assuming they can be made. Fig. 2 was constructed for one operating point: $P/\varphi = 460 \text{ kW}$, the peak heating thus calculated being plotted as a function of wavelength and for various values of τ . It can at once be seen from this figure that such an operating point is impossible for a tube of 2 mm wavelength, with $\tau = 0.1 \mu\text{s}$, for the peak heating would be more than 1100°C , and the melting point of copper is 1083°C . At a wavelength of 2 mm the graph only gives practical values at pulses of $0.01 \mu\text{s}$ or shorter.

The conclusion must be that a 2 mm magnetron, derived from a 4 mm version, is not a practical proposition.

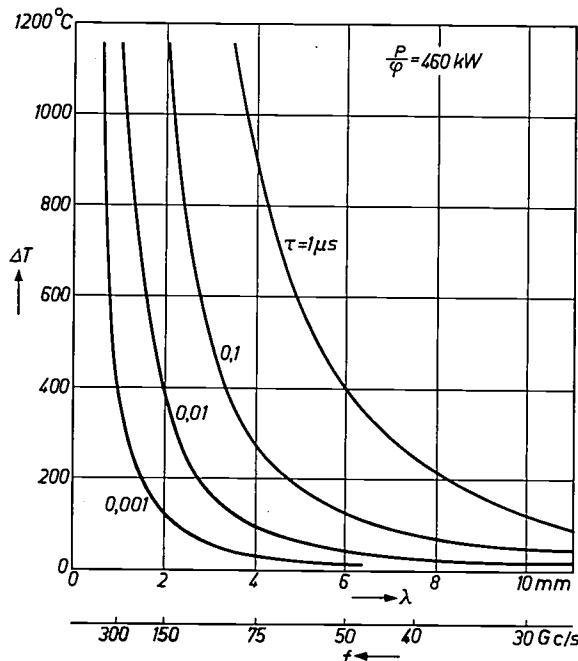


Fig. 2. The peak heating ΔT (calculated from (2)) at the surface of a magnetron anode as a function of wavelength λ , at constant $P/\varphi (= 460 \text{ kW})$ and with the pulse duration τ as parameter.

Table I presents some data of the 4 mm magnetron and of 2½ and 2 mm designs derived from it (the characteristic values B_0 and V_0 at the foot of the table will be discussed later). The table indicates that a 2½ mm magnetron can be regarded as a borderline case, for the operating region of such a tube will be very small compared with that of the 4 mm tube. This is evident from the very high values of magnetic induction, current density and peak heating. Nevertheless, we decided to start on the development of a magnetron for 2½ mm waves. Our decision was prompted by the possibility of modifying the structure of the resonator system in a way that promised favourable results, while the very object

⁷⁾ W. J. Oosterkamp, Problemen bij de constructie van technische röntgenbuizen, thesis Delft, 1939. (Problems in the construction of technical X-ray tubes; in Dutch.)

Table I. Data of the 4 mm magnetron and of scaled-down designs for a 2½ and 2 mm magnetron. In all cases there are 18 resonant cavities. Owing to the high values of magnetic induction, current density and peak heating, the 2 mm design is not a practical proposition, while the 2½ mm tube is a borderline case.

Wavelength (mm)	4	2.5	2.0
Magn. induction (Wb/m ²)	1.5-1.9	2.4-3.0	3.0-3.8
Anode voltage (kV)	11-16	11-16	11-16
Anode current (A)	7-14	7-14	7-14
Current density at cathode (A/cm ²)	100-200	260-500	400-800
Output power (kW)	5-40		
Peak heating (°C)	120-280	300-700	480-1100
Pulse duration (μs)	0.1	0.1	0.1
Charact. } B ₀ (Wb/m ²)	0.9	1.45	1.8
values } V ₀ (kV)	3.8	3.8	3.8

of the exercise was to determine the extreme limit. The modification referred to consisted in increasing the number of resonant cavities from 18 to 22.

Increasing the number of resonant cavities

Some insight into the effects of increasing the number of resonant cavities can be obtained by examining the equation formulated by Hartree as a starting condition for the oscillation of a magnetron. The Hartree equation gives the minimum value which the anode voltage *V* must have at a given magnetic induction *B* in order for oscillation to be possible, and may be written ⁶⁾

$$\frac{V}{V_0} = \frac{2B}{B_0} - 1. \dots \dots (3)$$

*V*₀ and *B*₀ are magnetron characteristics, given by

$$V_0 = 2 \pi^2 c^2 \frac{m}{e} \left(\frac{d_a}{N\lambda} \right)^2 \dots \dots (4)$$

and

$$B_0 = 8 \pi c \frac{m}{e} \frac{1}{\left(1 - \frac{d_k^2}{d_a^2} \right) N\lambda} \dots \dots (5)$$

Here *N* is the number of resonant cavities, *d*_a the diameter of the central aperture in the anode, *d*_k the diameter of the cathode, *c* the velocity of light, *e* and *m* the charge and mass of an electron. The condition (3) is valid only for magnetic fields with an induction greater than *B*₀ ⁸⁾.

The following remarks may be made on these characteristic quantities: if *d*_a is varied in proportion to *λ* there is no change in *V*₀ and if the ratio *d*_k : *d*_a is constant, *B*₀ varies inversely with *λ*. This is what is to be expected from the scaling law.

⁸⁾ G. A. Espersen and B. Arfin, Philips tech. Rev. 14, 88 and 89, 1952/53.

From eq. (4) and (5) it follows that increasing the number of resonant cavities *N* results in a decrease in the characteristic values *V*₀ and *B*₀. Other relative values remaining equal, this also entails lower values of *V* and *B* at the relevant operating point. Now in practice there will never be only one parameter varied at a time. If the number of resonant cavities is increased, for example, the diameter *d*_a of the anode aperture around which the cavities are grouped will also be enlarged, since the thickness of the partitions between the cavities cannot be reduced ad libitum. Enlarging *d*_a would reduce the advantageous influence of the increased *N* on *V*₀ (see eq. 4), but at the same time, as a result of the larger surface area, it has the favourable effect of reducing the heating of the anode during the pulses (of the same power). An increase of *N* will also usually entail making the cathode diameter *d*_k larger, so that *B*₀ remains roughly inversely proportional to *N*.

There is a limit to the extent to which the number of resonant cavities can be increased; too many cavities would jeopardize the stable operation of the tube in the required mode of oscillation (the π mode) ⁹⁾. A sharply defined upper limit for the number of cavities of an open "rising-sun" system — as used in the 4 mm magnetron, with *N* = 18 — cannot be given. An experimental magnetron with 22 cavities for a wavelength of 12½ mm has long been known ¹⁰⁾. The resonator system of the 2½ mm magnetron was derived by roughly scaling down from the system used in the 12½ mm tube. Fig. 3 shows a photograph taken along the axis of the resonator system for 2½ mm.

The scaling-down process obviously affects the construction of the tube. In the following we shall examine some of the principal constructional aspects of the 2½ mm magnetron, a schematic cross-section of which is shown in fig. 4.

Components of the 2½ mm magnetron

The anode block

The anode block of magnetrons with a rising-sun resonator system is made by a hobbing method ⁹⁾. The hob consists of a steel "negative" of the rising-sun system, which is forced into a block of copper. For the 2½ mm systems this is done at room temperature, whereas the hobbing of the larger resonator systems is done at a temperature of about 550 °C. The hob is made by a grinding process in which *N*

⁹⁾ G. B. Collins, Microwave magnetrons, M.I.T. Radiation Lab. Series, part 6, McGraw-Hill, New York 1948.

¹⁰⁾ See p. 790 of the book cited in ⁹⁾. Not enough is yet known about the possibility of increasing *N* still further. See G. H. Plantinga, Proc. 4th int. Congress on microwave tubes, Scheveningen 1962, pp. 202-205, Centrex, Eindhoven 1963.

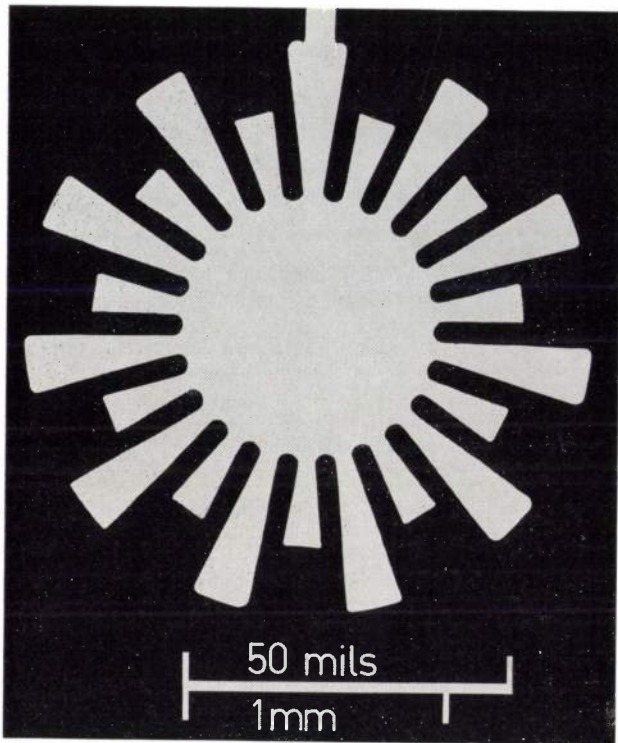


Fig. 3. Axial photograph of the resonator system of the 2½ mm magnetron. It is an open "rising-sun" system with 22 resonant cavities.

slots are ground into a solid steel cylinder; the width of the slots is equal to the required thickness of the cavity walls. Following this, the ½N ribs of the tool that correspond to the small cavities are ground to size.

While it was by no means simple to make a hob for a 4 mm magnetron, the grinding of a 2½ mm hob that meets reasonable demands of precision is even more of a problem. The diameter of the hob must be 2.15 mm, and into this 22 slots 80 μm wide and 0.60 mm deep have to be ground. Dimensions as small as this obviously call for precision-grinding of an exceptionally high order. The slots are ground out with a grinding disc which must be slightly thinner than 80 μm. Special care is needed in lining

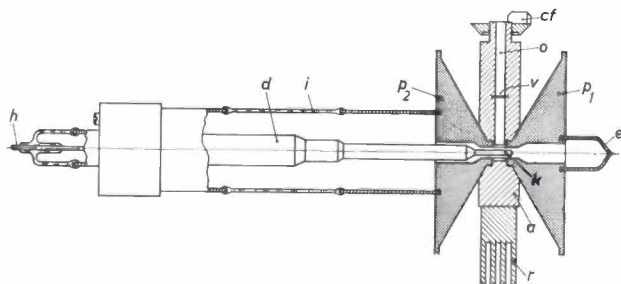


Fig. 4. Cross-section of the 2½ mm magnetron. *i* insulating glass sleeve. *k* cathode. *o* output waveguide. *v* vacuum-tight glass window. Meaning of other letters as in fig. 1.

Many details have been omitted here for the sake of clarity. See fig. 6 for the method of fixing and centering the cathode, and fig. 11 for the output system.

up the disc before grinding can start. The required alignment precision is achieved by adjusting the temperature of the cooling air supplied to the grinding machine as the last correction to the position of the disc. The same method ensures that, during the grinding operation, there can be no change in the position of the grinding disc in relation to the hob; displacements due to varying expansion of components of the grinding machine — as a result of slight fluctuations in ambient temperature — are compensated by adjustment of the temperature of the cooling air.

The dimensions of the 2½ mm rising-sun system are given in Table II. Fig. 5 gives an idea of the size of the 2½ mm hob, which is capable of making more than 100 anode blocks¹¹⁾; one of them can be seen in fig. 3.

Table II. Dimensions of cathode and resonator system of the 2½ mm magnetron.

Cathode	diameter 0.60 mm
Anode	} diameter of hole 0.95 mm height 1.20 mm
Small cavities	
Large cavities	depth 0.60 mm
Vanes	thickness 0.080 mm

¹¹⁾ This is a great advantage of hobbing compared with the method of spark machining sometimes used, where the tool is worn out after making only a few anode blocks.

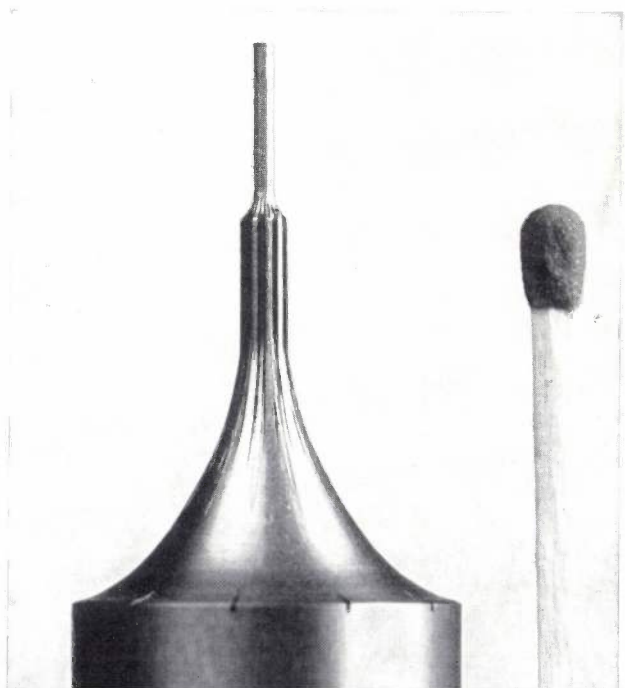


Fig. 5. Tool for hobbing 2½ mm magnetrons. With one such tool more than 100 anode blocks can be made.

The cathode

In most magnetrons the cathode is fixed to and insulated from the anode block by means of a small glass sleeve. Usually the cathode is mounted by sealing this sleeve to the anode. In the 2½ mm magnetron the emissive part of the cathode has a diameter of 0.60 mm, and the diameter of the anode aperture is 0.95 mm. It is obvious that in this case sufficiently accurate centering of the cathode in the anode aperture is not possible using a sealing method. Centering was already a problem with the 4 mm tube. In that case the solution was found by a method of assembly in which the cathode is soldered to a sleeve which is sealed beforehand to a glass insulator³). This method was not sufficiently accurate for the 2½ mm magnetron since the glass insulator, which is part of the cathode mounting, is never entirely free from stresses. These are produced, for example, when the cathode is soldered in. During the heating of the magnetron in the evacuation process, the stresses cause slight deformations, resulting in a displacement of the emissive part of the cathode in relation to the centre of the anode aperture. This is impermissible in this tube.

For the 2½ mm tube a method of centering the cathode was therefore devised which made it possible to correct the position of the emissive part after evacuating the tube; once this has been done, however, there must be no chance of a spontaneous change in the position of the cathode. The method adopted is described below. During the correction operation an electrical signal indicates whether the cathode is in fact coaxially situated in the anode aperture.

The method of fixing the cathode is shown schematically in fig. 6. Sealed to the glass insulator *i* is a cylindrical metal body with two flanges (*f*₁ and *f*₂) which are interconnected by a very thin wall *w*. The flange *f*₃ of the cathode body *d* is clamped between the flanges *f*₁ and *f*₂ in such a way that slight radial movements are still possible. With the aid of a centering jig the position of the cathode in the anode aperture can now be corrected because the thin wall *w* permits sufficient local deformation. The correction is effected by pressing a steel ball *b* inwards by means of a lever *l*. The jig has four such balls and levers, so that the cathode, after setting up the jig, can be moved in two radial directions perpendicular to each other. Three screws *s* in the flange *f*₁ make it possible, after centering, to clamp the cathode flange *f*₃ by deformation of the base of the screw holes. After some time, presumably owing to the formation of a pressure joint, the flanges *f*₁ and *f*₃ seize together, so that no further displacement of the cathode is possible.

Unlike other magnetrons, in which the cathode can still be centered after assembly in the tube, the 2½ mm magnetron is released from the jig after centering. This is an important practical advantage.

The fact that the cathode can still be displaced slightly would not of course be sufficient in itself for accurate centering if there were not at the same time a means of indicating the eccentricity. An optical indication here is ruled out. An electrical indication is therefore adopted, making use of a characteristic feature of the static — i.e. non-oscillating — magnetron. In a static magnetron the electrons, under the influence of the static electric and magnetic fields, describe curved trajectories between cathode and anode. When the magnetic field is increased and the electric field kept constant, the curvature of the trajectories increases until, at a certain critical magnetic induction, the electrons — putting the matter rather simply — no longer reach the anode, so that the anode current becomes discontinuously zero. The critical induction *B*_{cr} is easily calculated for a planar magnetron⁶). One finds:

$$B_{cr} = \sqrt{\frac{2m}{e}} \frac{\sqrt{V}}{d} \dots \dots (6)$$

Here *d* is the distance between cathode and anode. At a constant anode voltage *V*, then, *B*_{cr} is a measure of the distance *d*, and the latter follows from (6) as a

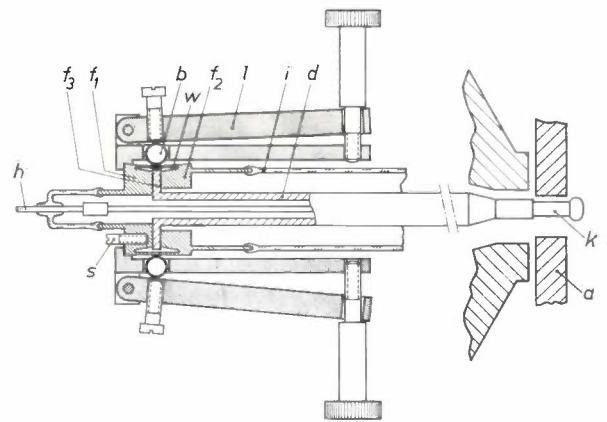


Fig. 6. Mechanism for fixing and centering the cathode in the 2½ mm magnetron. *a* anode. *k* emissive portion of the cathode (here drawn off-centre in the anode aperture). *h* heater connection. The flange *f*₃ of the cathode body *d* is clamped between the flanges *f*₁ and *f*₂ of a cylindrical body which is sealed to the glass insulator *i*. Around this assembly is placed the aligning jig, shown shaded, consisting primarily of four levers *l* with which steel balls *b* can be pressed inwards. The balls thereby deform the thin wall *w* which interconnects flanges *f*₁ and *f*₂, and in so doing shift the flange *f*₃ (and hence the cathode) radially. The degree of eccentricity of the cathode follows from electrical measurements (see figs. 7 and 8). When the coaxial position is found, the cathode is fixed by tightening three screws *s*; this deforms the base of the screw holes so that the flange *f*₃ is rigidly clamped between flanges *f*₁ and *f*₂. This being done, the jig is removed. After some time flanges *f*₁ and *f*₃ seize together, making any further displacement of the cathode impossible.

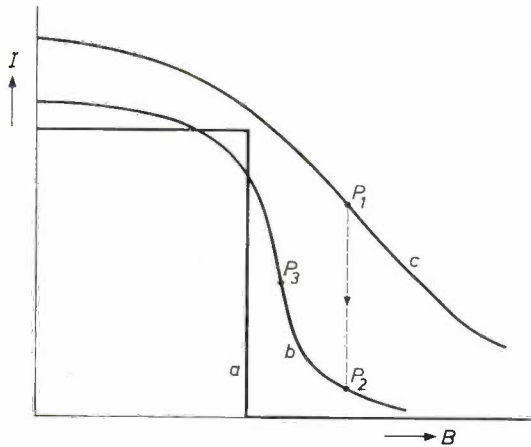


Fig. 7. Anode current I of a non-oscillating magnetron as a function of magnetic induction B at constant anode voltage (schematic). Curve a : cathode coaxially aligned in the anode aperture. Curve b : cathode off-centre. Curve c : cathode still farther off-centre.

function of B_{cr} . At a given anode voltage the value of B_{cr} can be used for determining the position of the cathode in relation to the anode.

In reality, of course, the magnetrons are cylindrical. The position of the cathode can still be determined on the same principle, but the position cannot be expressed so simply in terms of B_{cr} . For if the cathode is situated *eccentrically* in the anode aperture, then with increasing magnetic induction and constant anode voltage the electrons at the side of the cathode farthest away from the anode (where the electric field is weakest) will fail to reach the anode before those at the other side. We cannot therefore in this case distinguish one discrete value for B_{cr} ; instead there is a region in which the current gradually decreases as the induction increases. This is represented for various degrees of eccentricity by curves b and c in *fig. 7*.

The shape of the curve $I = f(B)$ is therefore an indication of the measure of eccentricity of the cathode. For zero eccentricity the simplified theory again gives one discrete value for the critical induction, viz:

$$B_{cr} = \sqrt{\frac{32m}{e}} \frac{\sqrt{V}}{\left(1 - \frac{d_k^2}{d_a^2}\right) d_a} \quad (7)$$

For a coaxial cathode, then, the characteristic has the discontinuous form of curve a in *fig. 7*.

The procedure during centering is as follows. First the magnetic induction is set to a value at which the anode current is considerably lower (e.g. by half) than at $B = 0$. The cathode is then displaced slightly in one of the two directions allowed by the jig. If the result is a drop in anode current, this is an indication that the cathode has moved closer towards the

coaxial position. The operating point in the graph $I = f(B)$ (*fig. 7*) has then shifted to another curve, e.g. from P_1 on curve c to P_2 on curve b . The cathode can now be moved farther in the same direction, but first it is useful to reduce the induction slightly: the effect of this is to move the operating point to a steeper part of the same curve (e.g. from P_2 to P_3), which improves the sensitivity of the indication. The optimum position in the direction of displacement is reached when the anode current is minimum. The same procedure is then repeated in the other direction of displacement. In this way highly accurate centering is achieved.

Fig. 8 shows two experimental $I = f(B)$ curves. The curve on the right was plotted before adjusting the cathode, the one on the left shows the result of measurements on the coaxial configuration. In both

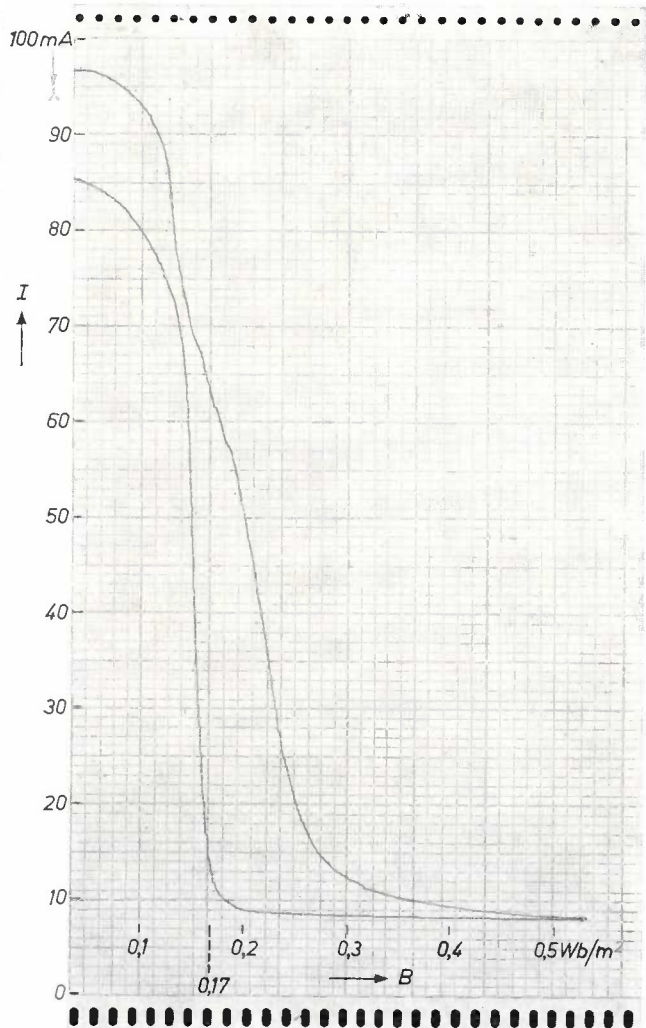


Fig. 8. Recording showing the anode current I of a non-oscillating 2½ mm magnetron versus magnetic induction B at 50 V anode voltage. The right-hand curve relates to an off-centre position of the cathode; the left-hand curve was obtained after careful coaxial alignment of the cathode. The critical induction calculated from eq.(7), $B_{cr} = 0.17 \text{ Wb/m}^2$, fits the latter curve.

sets of measurements the anode voltage was 50 V. At this value equation (7) gives $B_{cr} = 0.17 \text{ Wb/m}^2$. This result is in good agreement with the latter curve.

There is, incidentally, a considerable discrepancy between experiment and theory, for according to eq. (7) one would expect a step-function curve with the discontinuity at $B = B_{cr}$. It would take us too far to go into the reasons for this difference. It will be enough here to comment on the "tail" of the curve. That the current does not drop to zero at high values of B can be explained by the fact that the emission from the cathode is not limited to the part referred to as the emissive area. There are other parts, in particular at the ends, that also emit electrons. These electrons traverse parts of the magnetic field where the induction is lower than that prevailing inside the anode aperture. If the induction here is higher than the critical value, this will not necessarily prevent some of the other electrons mentioned from reaching the anode.

In the experimental magnetron on which the curves in fig. 8 were recorded, no measures were taken to prevent end emission.

A photograph of the cathode used in the $2\frac{1}{2}$ mm magnetron — an *impregnated cathode*¹²⁾ — can be seen in fig. 9. The favourable properties of this type of cathode are again evident in this tube, current densities being measured up to 400 A/cm^2 .

The output circuit

The high-frequency energy generated in a magnetron is extracted via a waveguide. The latter requires a vacuum-tight seal, designed so as to minimize power losses by reflection and absorption at the operating frequency (π mode). The seal should also reflect as little as possible at other frequencies, in particular the frequencies of some other modes of operation than the π mode. If there is any strong reflection at another mode, that mode is decoupled from the external load, and the only load is formed by internal (circuit) losses. It is known that oscillation can easily occur in a weakly damped mode⁹⁾. If Hartree's

¹²⁾ R. Levi, Dispenser cathodes, III. The impregnated cathode, Philips tech. Rev. 19, 186-190, 1957/58.

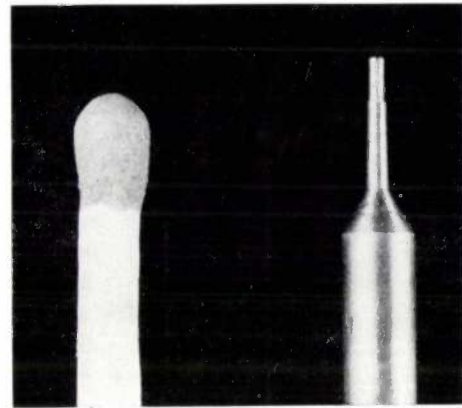


Fig. 9. The cathode of the $2\frac{1}{2}$ mm magnetron. It is an impregnated type¹²⁾, capable of delivering 400 A/cm^2 .

condition for this mode is roughly equal to that for the π mode, eq. (3), the magnetron's operation in the π mode can be disturbed.

An output circuit more than capable of meeting these requirements has long been known for the centimetre range. Curve I in fig. 10 shows for this circuit the modulus of the reflection coefficient r as a function of the frequency f . In the frequency range represented $|r|$ is nowhere greater than 16%. The attenuation does not exceed 0.07 dB. If this output circuit for the 3 cm range were to be scaled down for the $2\frac{1}{2}$ mm range, the result would again be curve I for $|r|$, but now with the lower frequency scale. For technical reasons, however, exactly proportional scaling-down was not possible. The resultant $2\frac{1}{2}$ mm circuit therefore has a slightly different frequency characteristic, represented by curve II in fig. 10. As can be seen, a reflection peak of about 50% occurs in the region of 135 Gc/s. This presents no difficulties, however. At the operating frequency of the magnetron the reflection is only about 10% and the attenuation here is less than 0.3 dB.

The construction of the output system to which curve II relates is shown, somewhat simplified, in fig. 11. The glass window providing the vacuum-tight seal for the waveguide is $100 \mu\text{m}$ thick.

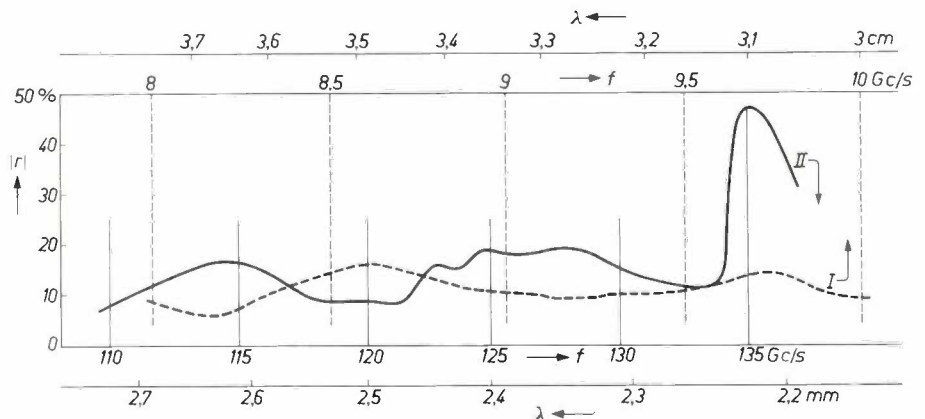


Fig. 10. Curve I: measured absolute values $|r|$ of the reflection coefficient of a 32 mm output system, as a function of frequency f (upper scale). Exactly proportional scaling-down of this circuit to $2\frac{1}{2}$ mm would show the same curve for $|r|$ on the lower frequency scale. Such a circuit, however, is not technically feasible. Curve II was measured on a slightly different circuit for $2\frac{1}{2}$ mm.

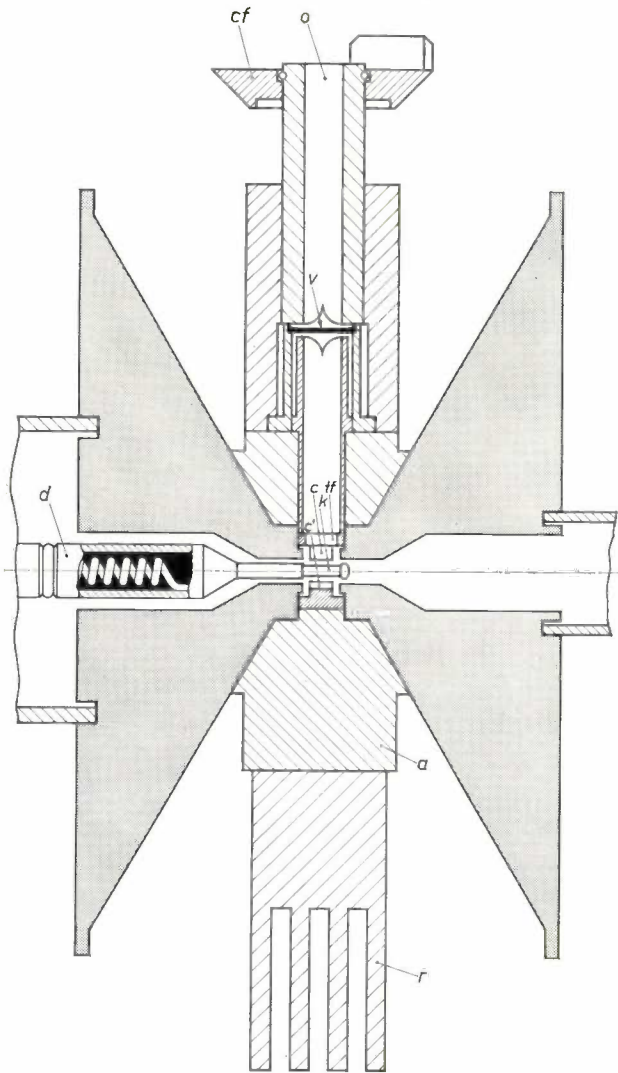


Fig. 11. Cross-section of the 2½ mm magnetron showing the output system with the vacuum-tight window *v* in more detail than in fig. 4. One of the large resonant cavities can be seen (*c*) and one of the small ones (*c'*). *ff* is a quarter-wavelength impedance-matching transformer. A part of the heater inside the cathode is shown. Other letters as in fig. 4.

Measurements on the 2½ mm magnetron

Some of the measurements necessary in the assembly of the tube have already been mentioned. We have shown how the measurement of the *I-B* characteristic (fig. 8) is used for the alignment of the cathode, and we have also referred to reflection measurements on the output system (fig. 10). As regards the latter measurements it may be noted that the transmission properties of the window can still be checked after the window has been sealed in, before the final assembly — unlike the method of assembly used for the larger predecessors of the 2½ mm tube.

Another measurement required during assembly relates to the coupling of the resonator system to the output waveguide. The coupling used is a quarter-

wavelength transformer (fig. 11). This is a $\frac{1}{4}\lambda$ section of waveguide (λ being the wavelength in the guide) the characteristic impedance of which is such that the low impedance offered by the resonator system is roughly matched to the high impedance of the output waveguide. The dimensions of the impedance-matching transformer, like those of the magnetron, are very small: the cross-section of the waveguide is 0.093×2.00 mm. The dimensions are so critical that, after the transformer has been fitted — even though it was made with the greatest precision — the coupling generally requires some additional correction. This is done by slightly deforming part of the transformer. Only after this has been done can the window be mounted. The coupling factor is measured with a bridge circuit, using a hybrid T and a variable impedance (see the articles under ref. 3)); for the 2½ mm magnetron the usual setting is 1.5. The quality factor Q_u of this type of tube unloaded is roughly 400.

The output power of the 2½ mm magnetrons is measured by a conventional water-load, in which water passes through a glass pipe fitted in the waveguide. Dimensioning is such that the power delivered to the waveguide is completely dissipated in the water, so that the power can be calculated from the temperature difference between the water entering and leaving the pipe, together with the rate of flow. The dimensions involved in this method for 2½ mm wavelength are again very small: in our arrangement the outside diameter of the glass pipe is 0.45 mm, the wall thickness about 0.07 mm. The flow rate of the water can be adjusted so that an average power of 0.2 W (or of 1 kW in pulses of 0.1 μ s with a repetition frequency of 2000 per second) produces a temperature increase of 4 °C.

Table III below gives various characteristic values measured on a given 2½ mm magnetron. The tube delivers a power of 2.5 kW in pulses of 0.1 μ s at a magnetic induction of 2.5 Wb/m²,

Table III. Some characteristic values measured on a 2½ mm magnetron.

Output power:	
peak value	2.5 kW
average value	0.5 W
Magnetic induction	2.5 Wb/m ²
Anode voltage	9 kV
Anode current	14 A
Current density	400 A/cm ²
Pulse duration	0.1 μ s
Pulse repetition frequency	2000 s ⁻¹
Peak heating	600 °C
Frequency	120 Gc/s
Coupling factor	1.5
Q_u	380

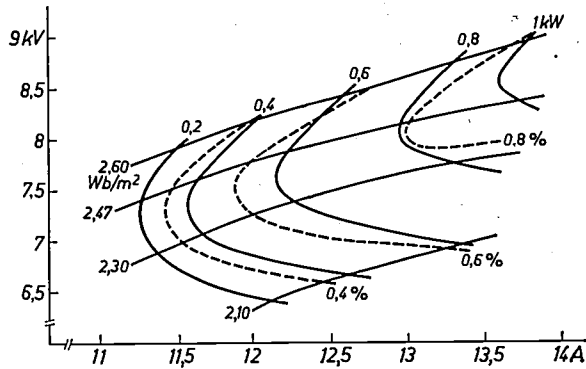


Fig. 12. Performance chart of a $2\frac{1}{2}$ mm magnetron, for a frequency of 120.4 Gc/s, a pulse duration of $0.1 \mu\text{s}$ and a pulse repetition frequency of 2000 per second. The chart shows contours of constant output power, constant efficiency and constant magnetic induction.

an anode voltage of 9 kV and an anode current of 14 A. These values can be used for estimating the peak heating of the anode, giving a value of roughly 600°C .

Note again the very high current density of 400 A/cm^2 delivered by the impregnated cathode employed in this tube.

Fig. 12 shows the performance chart for a $2\frac{1}{2}$ mm magnetron. The chart gives contours of constant magnetic induction, constant output power and constant efficiency.

Several members of our laboratories have contributed to the realization of the magnetron described. The hob was ground by H. J. Ronde in cooperation with M. C. Verhagen, who supervised the assembly of the tubes; F. Lingers had an important part in the construction of the cathode centering device; the cathodes were made by J. R. Blatter, and all the measurements described were done by H. Tjassens.

Summary. A $2\frac{1}{2}$ mm magnetron has now been added to the earlier described range of pulsed magnetrons, which ended with a 4 mm tube. Unlike the previous tubes in the range, which were scaled-down versions of a 32 mm magnetron with 18 cavities, the $2\frac{1}{2}$ mm tube has a resonator system consisting of 22 cavities. The article describes the anode block and the hobbing method used for making it, the cathode (an impregnated type) and the procedure by which it is aligned in the anode aperture after evacuation of the tube, and the output system. The $2\frac{1}{2}$ mm magnetron can deliver a power of 2.5 kW in pulses of $0.1 \mu\text{s}$. Some measurements on the magnetron are discussed and a performance chart is given.

FAST AND ACCURATE MAGNETIC MEASUREMENTS ON SAMPLES WEIGHING A FEW MILLIGRAMMES

by G. W. van OOSTERHOUT *) and L. J. NOORDERMEER **).

621.317.42

In research and development work on magnetic materials it is important to be able to measure quickly and accurately the magnetic moments of samples weighing only a few milligrammes. Such measurements provide the basis for determining important magnetic properties, such as saturation magnetization, coercive force and remanence. An apparatus designed for this purpose is described in this article.

In the development of magnetic materials it is important to know at an early stage whether a particular material is suited to the purpose for which it is intended. This applies especially to materials — usually in powder form — for magnetic recording¹⁾. At present it is not yet possible to decide from magnetic measurements on a powder whether the material is suitable for making e.g. magnetic tape. For this purpose it is still necessary to produce an experimental tape. It is, however, possible, by measuring the coercive force, saturation magnetization and remanence of the material, to see whether it is definitely *unsuitable*. The making of experimental tapes can thus be limited to materials that have at least some chance of success.

For experimental purposes it is useful if the measurements can be carried out on small samples. One of the advantages is that only small quantities need be made of the substances to be investigated, so that full benefit can be derived from the advantages of preparative chemistry on a small scale. Some ten years ago it was still a very difficult matter to perform magnetic measurements on samples weighing as little as a few milligrammes. One of the few properties that could be measured on small samples was the saturation magnetization²⁾. In 1954 a method was developed in Philips Research Laboratories for rapidly and accurately measuring the magnetic moment of very small samples³⁾. The method was intended at the time for measurements on galvanically deposited magnetic material. Since the proper-

ties of such materials depend on the thickness of the deposited layer, it was necessary to measure samples weighing a few milligrammes. The set-up designed to this end has gradually grown to be a useful tool for investigations concerning magnetic tape: firstly, for the above-mentioned selection of materials (powders), and secondly for measurements on finished tape. The apparatus is capable of measuring a magnetic moment as small as about 1.5×10^{-12} Vsm, which is the saturation moment of about 6×10^{-3} mg of iron.

After this apparatus had been used with good results for several years, the question arose as to whether its sensitivity could be increased sufficiently to permit the study of phenomena connected with the print-through effect. This effect occurs in a tape wound on a spool, and is due to the magnetization pattern in a winding being taken over by adjacent windings. Bound up with this effect are the weak magnetizations caused by the stray field of the magnetic tape itself, and which are therefore of the order of one thousandth of the remanence. In order to measure such weak magnetizations on a length of magnetic tape of e.g. 1.5 cm, a considerably higher sensitivity was needed.

In the following we shall first briefly describe the principle of the method of measurement and explain how the coercive force, the remanence and the saturation magnetization can be derived from measurements of a magnetic moment. We shall then consider the steps taken to increase the sensitivity sufficiently to permit the detection of a magnetic moment of about 7.5×10^{-14} Vsm (the saturation moment of 3×10^{-4} mg of iron). The article concludes with a few examples, including measurements concerning print-through.

Principle of the method

The principle of the method of measurement is illustrated in *fig. 1*. The sample under study — which, as mentioned, usually consists of a little powder or a piece of magnetic tape — is applied over a length of

*) Philips Research Laboratories, Eindhoven.

***) Formerly with Philips Research Laboratories, Eindhoven.

1) For a general introduction to magnetic recording, see: W. K. Westmijze, *The principle of the magnetic recording and reproduction of sound*, Philips tech. Rev. 15, 84-96, 1953/54.

2) G. W. Rathenau and J. L. Snoek, *Apparatus for measuring magnetic moments*, Philips Res. Repts. 1, 239, 1946.

3) G. W. van Oosterhout, *A rapid method for measuring coercive force and other ferromagnetic properties of very small samples*, Appl. sci. Res. B6, 101-104, 1956/57. A method based on the same principle is described by: S. Foner, *Vibrating sample magnetometer*, Rev. sci. Instr. 27, 548, 1956. For an improved version of this instrument, see: S. Foner, *Versatile and sensitive vibrating-sample magnetometer*, Rev. sci. Instr. 30, 548-557, 1959.

about 1.5 cm around a thin bar (diameter e.g. 2 mm) of non-magnetic material, preferably glass. The sample is magnetized in the direction of the bar axis. One end of the bar is connected to the speech coil of a loudspeaker. When the loudspeaker is connected to an alternating-current source, the sample moves to and fro axially with the bar. Identical search coils are placed around the ends of the sample, coaxially with the bar. When the sample is in vibration, an e.m.f. is induced in these two coils. The coils are connected in series opposition (astatic coils), so that interfering e.m.f.'s induced in the coils by fields from

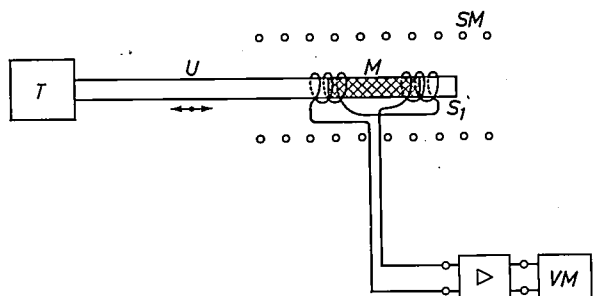


Fig. 1. The magnetic moment of a small sample M of magnetic material is measured by causing the sample to vibrate inside an astatic pair of coils S_1 . The sample (usually a powder or a piece of magnetic tape) is applied over a length of about 1.5 cm to the surface of a bar U which, driven by a loudspeaker system T , moves to and fro in the axial direction. VM electronic voltmeter, preceded by an amplifier. SM solenoid which can generate a homogeneous external magnetic field at M .

extraneous sources cancel each other. On the other hand the e.m.f.'s produced by the sample reinforce one another. The resultant alternating e.m.f. is amplified and measured with an electronic millivoltmeter, the deflection of which is a measure of the magnetic moment of the sample.

Determination of saturation magnetization, coercive force and remanence

The saturation magnetization of a material is determined by measuring the magnetic moment of a sample of known weight in the magnetically saturated state. The measurement must of course be done in a strong external field, which has the direction of the vibrating bar and keeps the sample in the saturated state. This field is supplied by a solenoid, fitted coaxially with the bar and the search coils, or by an electromagnet, with holes in the pole pieces for the bar to pass through. As a rule the direct current through the solenoid or through the electromagnet shows a slight ripple, so that the external field contains an alternating component. This does not induce an e.m.f. in the astatic coils and therefore causes no trouble.

When the external field is reduced to zero and the magnetic moment measured again, one can determine from this the remanence of the material.

The coercive force is measured by letting the external field grow in the reverse direction until the e.m.f. induced in the search coils reaches zero. The magnetization of the sample is then zero, and the strength of the external field is equal to the coercive force.

When interpreting the measurements, account should be taken of the demagnetizing field of the sample itself. This applies in particular to remanence measurements. These complications of interpretation are not, however, characteristic of the method of measurement described here, and therefore will not be dealt with in this article.

During the measurement the sample is shifted in relation to the search coils until the induced e.m.f. is maximum. Since the signal is in the form of an alternating voltage that can readily be amplified, the sensitivity of this method is substantially higher than that of the ballistic methods formerly used.

For the purpose of absolute measurements the apparatus is calibrated, using, for instance, a nickel sample of known weight which is magnetized to saturation (for nickel 0.7×10^{-4} Vsm/kg). The nickel sample is fitted over the same length of the bar in order to eliminate the influence of the shape of the samples.

Measuring arrangement with compensating device

In the measurement under fig. 1 the e.m.f. produced depends on the amplitude and the frequency of vibration of the sample. These two quantities are not entirely constant, which limits the accuracy of the measurement. We have eliminated this limitation by adopting a compensating method. Mounted at another point on the bar carrying the sample is a small permanent magnet of platinum-cobalt⁴⁾, surrounded by a second astatic pair of coils S_2 (fig. 2). The magnet and the sample are rigidly connected to each other, and therefore vibrate identically. The voltages induced in the two pairs of coils consequently depend in the same way on amplitude and frequency, so that changes in these quantities do not affect the ratio between these voltages.

This ratio is measured with a compensating circuit. The electronic millivoltmeter, again preceded by an amplifier, now serves as a null instrument. The setting q of the voltage divider R_2 at which the null instrument shows no deflection is a measure of the

⁴⁾ Because of its low temperature coefficient and low sensitivity to extraneous fields, platinum-cobalt is eminently suited for use as a standard magnet. See: R. A. Mintern, Platinum alloy permanent magnets, *Platinum Metals Rev.* 5, 82-88, 1961.

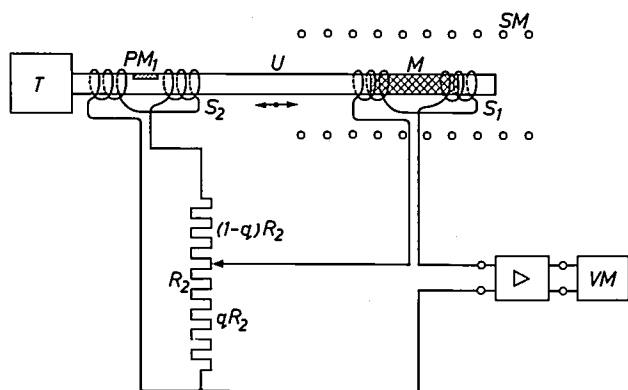


Fig. 2. Refinement of the method in fig.1: the e.m.f. induced by the sample M in the pair of coils S_1 is compensated by an e.m.f. induced by a platinum-cobalt magnet PM_1 in the pair of coils S_2 . This makes the measurement insensitive to changes in the amplitude and the frequency of vibration. The millivoltmeter VM now acts as a null instrument. The setting q of voltage divider R_2 is a measure of the magnetic moment. Meaning of the other symbols as in fig.1.

required magnetic moment. Calibration can again be carried out using a sample of known magnetic moment.

The essentials of the circuit actually employed are shown in fig. 3. The coils S_1 , containing the sample under measurement, are connected to the calibrated,

stepwise variable voltage divider R_1 , with which a part $E_x = pE_1$ of the voltage E_1 across R_1 can be taken off. In the successive steps of this voltage divider, p has the values 1, 1/3, 1/10, 1/30, 1/100, 1/300 and 1/1000. In this way E_x can be made smaller than the voltage E_2 produced by the permanent magnet vibrating in S_2 . The setting q of R_2 is then adjusted until the null instrument shows no deflection, after which q can be read off to three decimal places. In this connection E_2 is chosen such that it is about 1000 times greater than the smallest voltage detectable with the null instrument. For this purpose R_2 is connected to the fixed voltage divider R_3-R_4 .

Owing to the inductances of the pairs of coils S_1 and S_2 , the currents through R_1 and R_2 will show phase differences with respect to the vibration of the bar. Only when these differences are identical will the currents be in phase, which is necessary for exact compensation. To make the phase shifts equal, a resistance R_5 is put parallel with the coils S_2 . For given pairs of coils S_1 and S_2 , the resistance R_5 only has to be adjusted once.

The combination of amplifier (about $1000\times$) and electronic millivoltmeter as null instrument makes it possible to observe voltages of 20 nanovolts. Special measures have been taken to turn this high sensitivity to good advantage. The compensating circuit and the amplifier are magnetically screened. The amplifier is fitted with low-noise valves at the input, and is made selective by means of a bandpass filter for the vibration frequency of the sample (125 c/s) with a pass band of 30 c/s. Moreover, the mains harmonics at 100 and 150 c/s are additionally suppressed. A photograph of the measuring arrangement is shown in fig. 4.

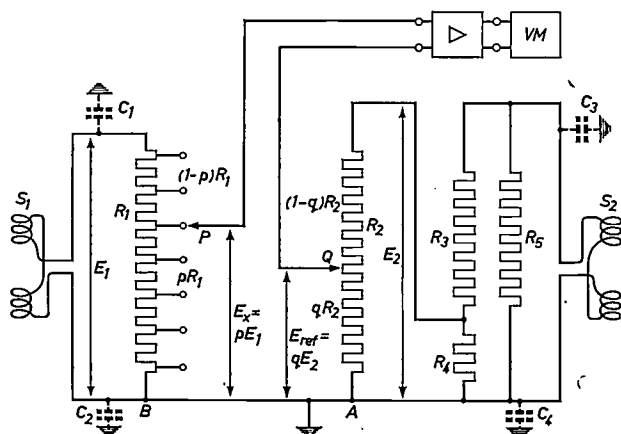


Fig. 3. Essentials of the compensating circuit. The pair of coils S_1 , inside which the sample vibrates, is connected to a calibrated voltage divider R_1 . The platinum-cobalt magnet vibrates inside the pair of coils S_2 . A fraction E_2 of the e.m.f. induced in S_2 appears across the voltage divider R_2 via the fixed voltage divider R_3-R_4 . R_5 is a resistor with which the phase difference between the compared voltages E_x and E_{ref} can be reduced to zero. When the circuit is earthed as shown here, no trouble is experienced from the four stray capacitances C_1, C_2, C_3 and C_4 , which are produced by the electrical screening of the cables interconnecting the pairs of coils and the compensating circuit. Now, however, points P and Q , between which the voltage must be reduced to zero, both have a certain potential with respect to earth. For this reason it is necessary to use a difference amplifier ⁵⁾.

Stray capacitances

Care was taken in the design of the circuitry to avoid interference from stray capacitances. The pairs of coils S_1 and S_2 are connected to the compensating circuit by cables with earthed screening. These cables therefore have a capacitance to earth of a few hundred pF. At a frequency of 125 c/s a capacitance of 100 pF represents an impedance of more than 10^7 ohms. This is very high compared with the resistances, of the order of 1000 ohms, used in the measuring circuits. The stray capacitances therefore have no significant influence on the amplitudes of the voltages that have to compensate each other. On the other hand the slight phase shifts which they give rise to in these voltages result in a perceptible difference voltage (fig. 5). This causes no trouble provided the phase shifts are independent of the settings of the voltage dividers R_1 and R_2 (fig. 3), for the phase correction by means of R_5 relates to a phase shift of this kind. The phase shifts will be independent of the settings of the voltage dividers when no currents flow through the two control contacts P and Q . If the null instrument has an infinitely high input impedance — or if we imagine it to be removed for a

⁵⁾ See e.g. G. Klein and J. J. Zaalberg van Zelst, General considerations on difference amplifiers, Philips tech. Rev. 22, 345-351, 1960/61, and by the same authors: Circuits for difference amplifiers, I and II, Philips tech. Rev. 23, 142-150 and 173-180, 1961/62.

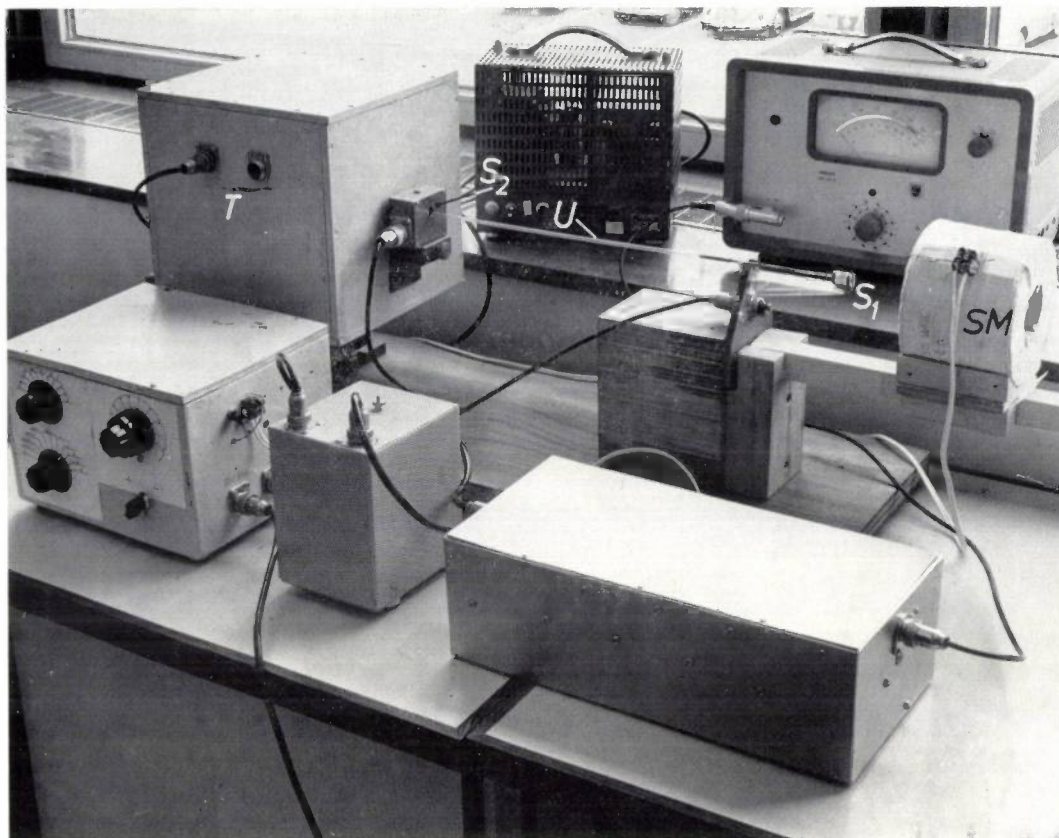


Fig. 4. The apparatus for measuring magnetic moments by the compensation method. S_1 and S_2 are the astatic pairs of coils, inside which, respectively, the sample and a small platinum-cobalt magnet (both fixed to the bar U) are caused to vibrate. Left, the loudspeaker system T for the drive. In the foreground, from left to right: the compensator (including the difference amplifier), a standard amplifier ($1000\times$) and a bandpass filter. In the background: the amplifier that drives the loudspeaker system, and the electronic millivoltmeter (the null instrument). The solenoid SM is mounted on a carriage and can be slid around the coils S_1 .

moment — then the control contacts in a circuit as in fig. 3 will certainly carry no current. No trouble is then experienced from the stray capacitances. The same then applies when the input impedance of the null instrument is not infinitely high, for once compensation has been effected it makes no difference whether the null instrument is connected or disconnected.

In fig. 3 none of the terminals of the null instrument are earthed, in other words the first amplifying stage must be designed as a difference amplifier⁵). It is in fact impossible

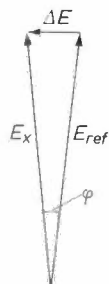


Fig. 5. A small phase difference φ between the voltages E_x and E_{ref} , which are to compensate each other, gives rise to a relatively large voltage difference ΔE .

to earth the circuit at one of the terminals of the null instrument, for in that case a current could flow via this earth connection and the stray capacitances through the control contact

connected to the earthed terminal. Movement of this contact would then not be entirely without influence on the current distribution in the circuit, and would in general cause slight phase shifts, making exact compensation impossible.

The vibration frequency

In the original measuring arrangement (with no compensating device) the sample was set in motion by a loudspeaker system operating on 50 c/s. Since the sensitivity was relatively low, little inconvenience was experienced from interfering fields of 50 c/s and multiples of it. When, however, the sensitivity was increased by introducing the compensation method, these fields became troublesome. Little could be done with filters because of the fact that the frequency of the desired signal was also 50 c/s. It was therefore necessary to choose a different vibration frequency.

A second source of interference that influenced the choice of frequency was the noise of the first amplifier tube. This noise contains a component which is

inversely proportional to the frequency⁶⁾. From these considerations it is evident that the frequency should be chosen as high as practicable, avoiding as far as possible multiples of 50 c/s. A limit is set to the height of the frequency, however, by considerations of noise nuisance and by the acceleration forces, which are proportional to the square of the frequency and threaten the connection between sample and bar. The frequency finally decided upon was 125 c/s.

The vibrator

The mechanical part of the vibrator is sketched in fig. 6. The bar, which carries the sample and the platinum-cobalt magnet, is fixed to a spring of a type that combines high lateral stiffness with a long life⁷⁾. On the left in fig. 6 can be seen the loudspeaker coil and the loudspeaker magnet. The current through the loudspeaker coil is supplied by an amplifier which receives its input signal from a second platinum-

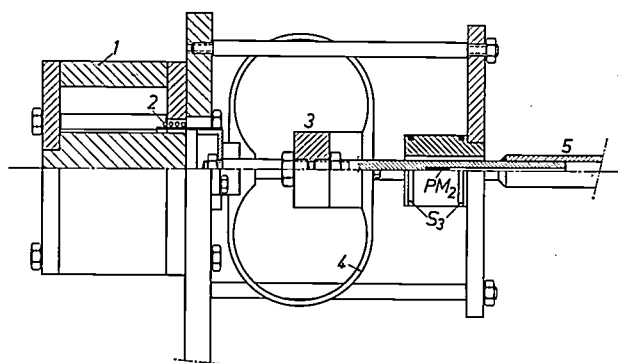


Fig. 6. The vibrator. 1 loudspeaker magnet, 2 speech coil, 3 mass of the vibrating system with which the frequency is adjusted, 4 spring (the vibrator contains two of these springs), 5 coupling piece for the bar carrying the sample and the magnet for the compensation voltage. PM_2 , platinum-cobalt magnet fixed to the same bar and contained inside a third astatic pair of coils S_3 , connected to the input of the amplifier which drives the current through the speech coil (see fig. 7).

cobalt magnet fixed to the vibrating bar, and contained in a third pair of coils S_3 . Because of this feedback the system is able to oscillate at its natural (mechanical) frequency (fig. 7). The amplitude of the vibration is limited to about 1 mm by shunting across the amplifier output a small incandescent lamp, mounted opposite to a photo-resistor⁸⁾ shunting the input of the amplifier.

⁶⁾ See K. S. Knol, Noise; a general survey, Philips tech. Rev. 20, 50-57, 1958/59.
⁷⁾ Another application of a spring of the same type is described in: B. Bollée and F. Krienen, The CERN 600 MeV synchrocyclotron at Geneva, III. The tuning-fork modulator, Philips tech. Rev. 22, 162-180, 1960/61, especially p. 169.
⁸⁾ N. A. de Gier, W. van Gool and J. G. van Santen, Photoresistors made of compressed and sintered cadmium sulphide, Philips tech. Rev. 20, 277-287, 1958/59, esp. p. 286.
⁹⁾ These measurements were made by B. J. G. Hamer.

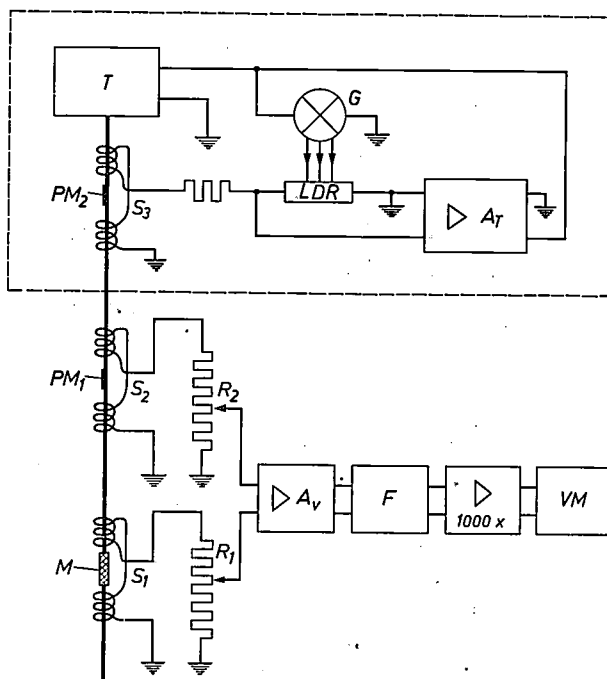


Fig. 7. The pair of coils S_3 , in which the magnet PM_2 vibrates, is connected to the input of an amplifier A_T , which feeds the speech coil of the vibrator T . Due to this feedback the system vibrates at its natural (mechanical) frequency. The photo-resistor LDR, connected to the input terminals of A_T , and the electric lamp G connected to the output terminals of A_T ensure that the vibration amplitude is limited to about 1 mm. A_v is the difference amplifier, F the bandpass filter.

Examples of applications⁹⁾

Fig. 8 gives an example of coercive-force measurements. The coercive force here is determined as a function of the thickness of a galvanically deposited layer of a Co-Ni-P alloy. The shape of the curve is

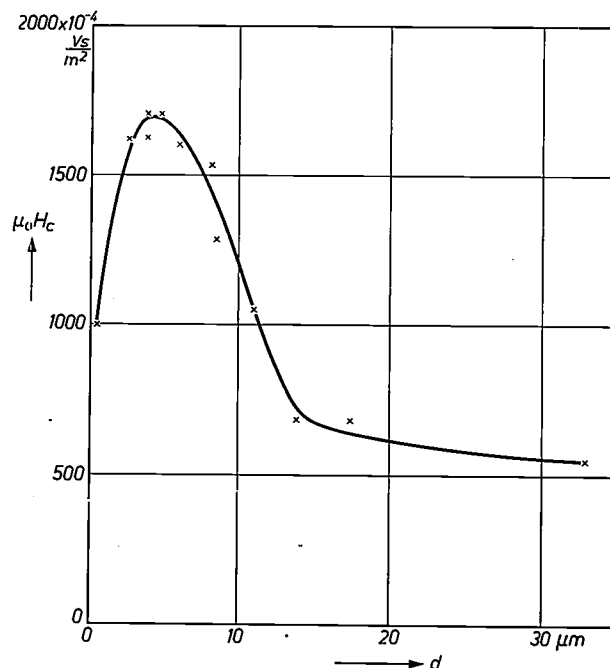


Fig. 8. Coercive force of a galvanically deposited layer of Co-Ni-P as a function of layer thickness d . The quantity of material varies from 0.4 to 50 mg.

most remarkable, the coercive force showing a pronounced maximum at a layer thickness of about $5 \mu\text{m}$. With increasing layer thickness the quantity of material increased from 0.4 to 50 mg. These measurements were done with the relatively insensitive arrangement, without compensating device.

As a second example *fig. 9* shows two remanence

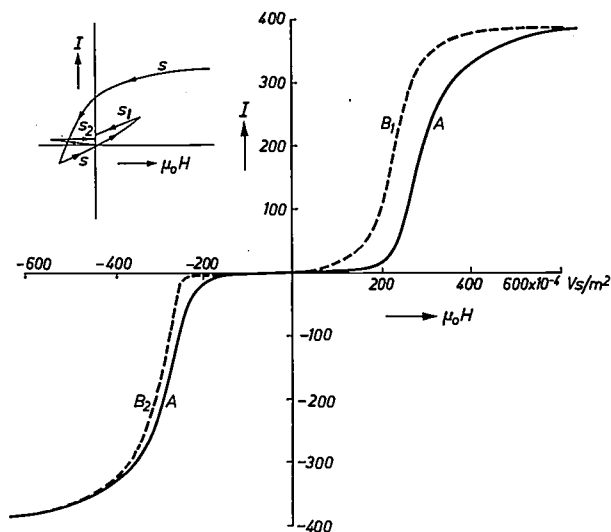


Fig. 9. Remanent magnetization produced in a piece of magnetic tape which — starting from a non-magnetized state — was magnetized by a field of the magnitude indicated on the abscissa (remanence curve). The two curves *A* and *B* (with branches B_1 and B_2) relate to different non-magnetic initial states: the symmetric curve *A* relates to conventional anhysteretic demagnetization, curve *B* to a demagnetizing process following the path indicated by *s* in the inset. The difference between branches B_1 and B_2 is due to the fact that the magnetizing field for these branches was respectively equal and opposite in direction to the field in which the sample was saturated (paths s_1 and s_2 in the inset). Quantity of material approx. 1.5 mg. Vertical scale not calibrated.

curves *A* and *B* measured on one sample weighing 1.5 mg, using the set-up with compensating device. The procedure for measuring a remanence curve is as follows. First, the sample is demagnetized. Next, it is exposed for a short time to a magnetizing field. The field is then switched off and the residual magnetization measured. This being done, the sample is again demagnetized, and the measurement is repeated for a different value of the magnetizing field, and so on. The measured values of remanence plotted against the magnetizing field producing them result in a remanence curve. As the magnetization field increases in strength the remanence curve of course approaches saturation remanence. Of the two remanence curves in *fig. 9* curve *A* was obtained after conventional demagnetizing in an alternating field, the initially high amplitude of which is slowly reduced to zero (anhysteretic demagnetization). Curve *B*, with branches B_1 and B_2 , relates to the same sample, but in this case the non-magnetic state

was reached along the path marked by *s* in the inset. The marked difference between curves *A* and *B* demonstrates the fact that the state of a magnetic material is in general by no means unambiguously defined by the point corresponding to that state in the *I-H* plane, but depends on the manner in which this point is reached. Only in the saturation state this is not the case. In order to obtain a material in a well-defined magnetic state, it is therefore necessary to start from saturation. This evidently also applies to the non-magnetic state.

The third example is the remanence curve of a piece of magnetic tape, measured with the sensitive version of the apparatus, where the accurate measurements were made even in the region of very low remanence (*fig. 10*). These low remanence values are important in connection with the print-through effect mentioned at the beginning of the article.

The fourth example relates to a study of the effect of grinding upon the magnetic properties of a powder¹⁰), the magnetic properties being investigated as a function of the grinding time. Since small samples could be used, it was possible to take ten samples from a charge of only 10 g in the ball mill without

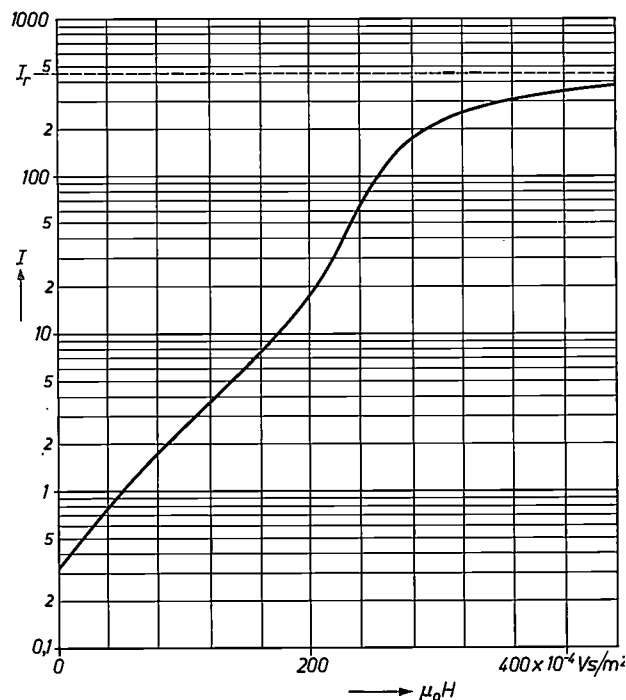


Fig. 10. Remanence curve for a piece of magnetic tape over a wide range of remanence values *I* (log scale for *I*). I_r is the saturation remanence. The processes responsible for print-through take place at values of $\mu_0 H$ smaller than roughly $40 \times 10^{-4} \text{ Vs/m}^2$. Quantity of material approx. 1.5 mg. Remanence values of one thousandth of the saturation value can still be measured on samples as small as this. Vertical scale not calibrated.

¹⁰) G. W. van Oosterhout and C. J. Klomp, On the effect of grinding upon the magnetic properties of magnetite and zinc ferrite, *Appl. sci. Res.* B9, 288-296, 1962 (No. 4/5).

appreciably changing the size of the charge. This size has a considerable influence on the grinding conditions.

Finally, it may be mentioned that the method of measurement described here is also used in geological

investigations for studying the "frozen-in" magnetism of rocks. From these measurements conclusions can be drawn about the earth's magnetic field at the time when the magnetism was frozen in (palaeomagnetism).

Summary. When a sample of a magnetic material — which possesses a magnetic moment — is caused to vibrate inside a coil, an alternating e.m.f. is induced in the coil. Since this e.m.f. can easily be amplified, a basis is thus provided for magnetic measurements which are much more sensitive than ballistic measurements. In this way magnetic measurements can be done on samples weighing only a few milligrammes. The use of an astatic pair of coils eliminates interference from extraneous alternating fields. The accuracy is increased by compensating

the induced e.m.f. with an e.m.f. generated in a second astatic pair of coils, in which a small permanent magnet, rigidly fixed to the sample, vibrates. Small variations in the amplitude and the frequency of vibration then do not influence the results. With a set-up based on this principle, developed and used in Philips Research Laboratories for the investigation of magnetic-recording materials, it is possible to measure a magnetic moment of 7.5×10^{-14} Vsm, i.e. the saturation moment of 3×10^{-4} mg of iron. Methods of suppressing interference are discussed.

ULTRASONIC DELAY LINES AND THEIR APPLICATIONS TO TELEVISION

by C. F. BROCKELSBY *) and J. S. PALFREEMAN *).

534.321.9-14/-16

Ultrasonic delay lines and their applications have been studied at the Mullard Research Laboratories for the past 15 years. The subject has long outgrown the space that can normally be allowed in a journal and in fact its theory and practice, together with many design details of delay lines, have recently been dealt with in a book ²⁾ published by the above authors in conjunction with R. W. Gibson. In the present article the limitation to one special though noteworthy field of application has offered the opportunity to consider the main problems of ultrasonic delay lines and to discuss some of the developments by M.R.L., while at the same time an idea is given of the variety of types of delay lines that exist and of the characteristics that can be achieved.

In many applications it is necessary to delay an electrical signal for a given period and to recover the signal after this time without appreciable distortion. The need for such a delay arose in the early days of telephony, and electrical delay circuits were developed to provide the comparatively short delays needed.

The delay systems used consisted of electrical transmission lines using lumped or distributed components, e.g. a coaxial cable; the required delay was achieved at the expense of attenuation and often some distortion of the signal. Such systems are practicable for obtaining delays up to a few microseconds in length, and where the bandwidth of the signal is not large. In modern electronics, however, applications occur for delay systems having delays of a few milliseconds with bandwidths of several Mc/s. It is to satisfy these requirements that ultrasonic delay lines have been developed.

In an ultrasonic delay system the electrical signal (oscillation of electric potential) to be delayed is converted into a corresponding mechanical vibration (i.e. described by the same function of time) and launched into a suitable solid or liquid delay medium. The designation "ultrasonic" simply stems from the fact that the electrical signals will usually have frequencies higher than 20 kc/s, putting the corresponding mechanical vibrations into the ultrasonic range. The velocity of mechanical waves in liquids and solids lies in the range 1-6 km/s, a factor approximately 10^5 lower than the velocity of an electrical signal along a coaxial cable. Thus a long delay can be obtained using a comparatively short path length in the medium, for example if fused quartz is used as the delay medium; a delay of approx. 2.5 ms can be obtained in a path length of 10 metres. After the mechanical wave has travelled a distance such that

the vibration has undergone the required delay, it is converted back into an electrical signal.

The first application of ultrasonic delay line techniques was in the pre-war "Scophony" television receiver where use was made of the variations in density of the water in a system resembling a delay line to provide optical readout of the video signal (see page 243). Ultrasonic delay line systems first came into prominence, however, during the Second World War, and pioneer work at the British Telecommunications Research Establishment (now known as the Royal Radar Establishment) later resulted in the development of a water delay line for use as an information storage device in Doppler radar. Meanwhile, in 1942, the first ultrasonic delay line to be used for a wartime application was produced at the Bell Telephone Laboratories, a mixture of water and ethylene glycol being used as the delay medium. It was soon discovered that mercury was a more suitable delay medium and many radar systems were developed using mercury delay lines.

Early work at the Telecommunications Research Establishment (1943) showed that vitreous fused quartz was likely to prove a valuable solid delay medium at frequencies at least up to 10 Mc/s. Much basic work on the properties of solid delay media was carried out at the Massachusetts Institute of Technology and the Bell Telephone Laboratories. Solid delay lines are extensively used nowadays and suitable designs enable long delays to be obtained in a compact space (see page 242). In 1949 Bradburd showed that magnetostrictive wire could also be conveniently used as an ultrasonic delay medium.

Although ultrasonic lines were originally developed as information storage devices in the radar field, their field of application has widened considerably in the last few years. They are now used extensively in digital and analogue computers, in communications networks, and in instrumentation based on pulse

*) Mullard Research Laboratories, Salfords (Surrey), England.

timing¹⁾. Several applications of ultrasonic delay techniques occur in the field of television and the discussion of ultrasonic delay lines in this article, after a general introduction to such lines, will con-

centrate on this group of applications (page 243 ff.). They are found to occur in the television studio, in the research laboratory, and in some possible kinds of domestic receiver.

I. THE DIFFERENT TYPES OF DELAY LINES, AND GENERAL CONSIDERATIONS²⁾

From the above it follows that an ultrasonic delay line consists basically of three components. First there is a device known as a transducer which converts the electrical signal into a mechanical vibration. Second there is the delay medium through which the mechanical signal travels and undergoes the required delay. Finally there is a second transducer which converts the mechanical vibration into the required electrical signal.

Ultrasonic delay lines may be divided into three main categories, using *wires*, *liquids*, and *extended solids* respectively as the delay media. These three types of line differ markedly in the mode of vibration employed for transmission and hence in the form of transducer required. Some principles of delay lines will now be explained using the comparatively simple wire line as an example. General considerations applying to liquid and solid lines will be given afterwards, followed by some details of these lines.

Wire delay lines

In a wire delay line the electrical signal is converted into a mechanical oscillation of a magnetostrictive wire or tube. A magnetostrictive material will undergo reversible expansion or contraction in the direction of an applied magnetic field, owing to internal stresses arising as the magnetic dipoles are diverted from their preferred orientations. Conversely a mechanical deformation of such a material will give rise to a magnetic flux. Thus by passing a fluctuating current through a coil surrounding the wire a longitudinal mechanical wave can be launched down the wire, and this wave can be detected at the output end of the line by another coil surrounding the wire, the change of magnetic flux through this coil giving rise to the desired electrical signal.

Magnetostriction is a square law effect, i.e. both positive and negative currents through the input coil will

cause deformation of the wire in one sense only. In order to obtain a more linear characteristic, bias must be provided by means of a current or by a magnet as shown in *fig. 1*.



Fig. 1. Wire delay line. The electrical input signal fed to the input transducer Td_i launches an acoustic wave down the wire W ; this wave induces a voltage in the coil of the output transducer Td_o . Reflections from the ends of the wire are prevented by the use of absorbent terminations Abs .

The delay obtained may be adjusted if necessary by sliding the coil along the wire, and this is a useful facility. Since signals may travel in either direction along the wire, absorbent terminations must be placed at each end of the wire to prevent reflections.

If a direct current is passed down the wire in addition to the alternating signal current in the coil, a helical magnetic field with alternating pitch results. Under these circumstances the signal is propagated as a *torsional* vibration. This has the advantage that a greater delay is obtained using the same length of wire. Another advantage is that the line may be coiled into a spiral for compactness of layout, as shown in *fig. 2*. This is not possible with a

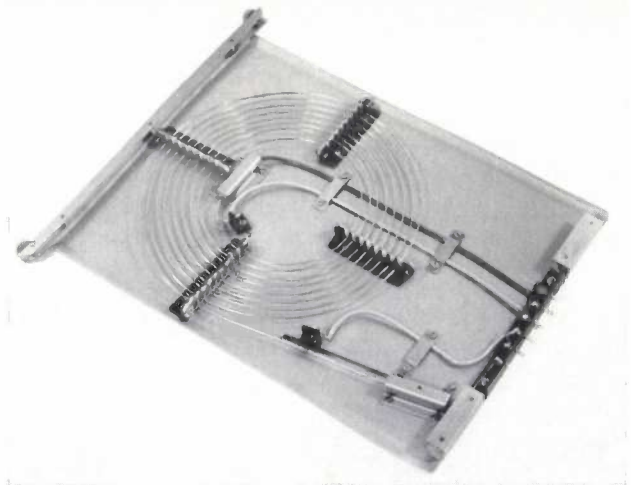


Fig. 2. Practical wire delay line (Mullard). A torsional wave is propagated down the line by passing a direct current along the wire itself in addition to the signal current in the coil. The wire itself is coiled into a spiral for convenience of layout.

¹⁾ See for example H. A. Dell, D. S. Hobbs and M. S. Richards, *An automatic particle counter and sizer*, Philips tech. Rev. **21**, 253-267, 1959/60.

²⁾ A detailed account of most of the information contained in the first part of this article is given in the book: *Ultrasonic delay lines*, by C. F. Brockelsby, J. S. Palfreeman and R. W. Gibson, published by Iliffe, London 1963. A list of references to the literature on the history of delay lines and on many developments mentioned in this article is also given in this book.

compressional vibration since bending of the wire would cause excessive frequency dispersion (differences in velocity of travel along the wire for different frequency components of the signal) resulting in excessive distortion. This effect never becomes serious for a torsional vibration even if the wire is bent.

Efficient conversion of electrical to mechanical energy is achieved only at frequencies near the mechanical resonance of the transducer: the resonance frequency is the centre frequency of the frequency band transmitted by the delay line. In the conventional designs of figs. 1 and 2 the transducer consists of the coil together with that portion of the wire in which it produces an appreciable magnetic field. This means that for high frequency applications the excited length of the wire, enclosed by the coil, must be extremely short, and the difficulty of making very short coils thus imposes a practical limit of about 1 Mc/s on the centre frequency. Because of this limitation wire delay lines are little used in television applications. In addition wire lines always degrade the signal owing to the existence within the material of inhomogeneities and grain boundaries at which reflection and refraction occur, thus limiting the usable bandwidth; the degradation is enhanced if the wire is coiled. Despite these limitations, however, wire delay lines are used in the field of digital computing where frequencies are lower and a lower bandwidth is acceptable.

The output signal of a wire delay line (and for that matter, of other delay lines too) is basically the second differential of the input, since the input and output transducers respond to changes in flux only. For sinusoidal operation this is of little consequence, since the shape of a sine wave is unchanged by differentiation. For arbitrary signals the differentiation will result in a linear distortion, and a compensation (de-emphasis of higher frequencies) may be necessary in the output. In digital computing, however, linearity is not important.

The choice of the delay line material depends chiefly on the intensity of the magnetostrictive effect. The velocity of propagation and the damping per unit length (or rather per unit delay time) should also be taken into account, but the first requirement does not leave much choice: nickel, nickel alloys or a special iron-cobalt alloy ("Permendur") are used for most applications of wire delay lines.

Liquid and solid delay lines: propagation patterns, transducer behaviour

Liquid and solid delay lines have a number of important problems in common, especially those

relating to the patterns of wave propagation and to the energy flow between external circuit, transducer and delay medium and vice versa. These problems will be considered first and separate sections will be devoted to the design of transducer and choice of delay medium for a) liquid and b) solid delay lines.

Both for liquid and solid lines the transducers are based on the piezoelectric effect. A piezoelectric material is one which undergoes reversible deformation on application of an electric field and which gives rise to a field when it is strained. Crystalline quartz exhibits this phenomenon, and some polarised ferroelectric ceramic materials behave in a very similar manner. A thin circular slice of crystalline quartz cut in a suitable orientation from a monocrystal is often used as transducer. The electrical input signal is applied to thin metal film electrodes coated on each face of the crystal wafer. The field produced causes a varying deformation of the crystal, thus launching a mechanical wave in the delay line medium which is in contact with one of the faces. The resultant wave travels through the delay medium along a path that will be discussed presently, ultimately arriving at the output end of the line where it produces a mechanical deformation of an identical crystal which forms the output transducer. This gives rise to an electric field in the crystal, and the signal is detected as a voltage signal on the electrodes.

Closer consideration of the process reveals that the size and orientation of the transducer used are of considerable importance in determining the properties of the line. Consider a circular disc transducer of diameter d radiating ultrasound of wavelength λ into an unbounded medium. If the transducer were a point source it would radiate spherical waves and the fraction of energy received by a receiver would depend only on the solid angle which it subtended at the source. The transducer not being a point source, it may be shown that the energy is emitted as a beam parallel to the transducer axis up to a distance approximately d^2/λ from the source. The region where the wave is defined by this beam is known as the "near field" (or Fresnel zone), and if the output transducer, also of diameter d , is placed within this region it will receive substantially all the energy radiated. Ideally, the transducers should always be chosen of such a size that the path traversed by the wave in the medium lies within the near field. Since the size of the transducers is limited, however, this is not practicable if the delay required is long.

At distances greater than d^2/λ from the source the energy is distributed in a diffraction pattern, constituting a number of lobes when plotted in a polar

diagram. This region is known as the "far field" (or Fraunhofer zone). Most of the vibration energy is contained in the principal lobe of this pattern, and the output transducer must be positioned to receive this lobe. It will then receive a fraction of the transmitted energy which is directly proportional to the area of the transducer and inversely proportional to the square of its distance from the source; the fraction of energy received is thus proportional to the solid angle which the receiver subtends at the source, but it is still much larger than that which it would receive from a point source.

In order for the incident signal to produce a disturbance which is in phase at all points across the face of the output transducer, this device must be aligned approximately normal to the incident beam. This situation, however, is not strictly necessary. More generally, a polar diagram can also be drawn for the response of the output transducer, making the situation entirely symmetrical: in fact it may be demonstrated that the energy transfer through a delay system is independent of which transducer is the input and which is the output.

In order to obtain the required delay, the path traversed by the wave in the medium may need to be several metres long; to obtain a straight path of this length is often difficult and sometimes impossible. For this reason a "folded" path must be used, in which the signal is deliberately made to undergo reflections from the boundaries of the medium during its passage from input to output. At each reflection the shape of the diffraction pattern is slightly altered but in practice such changes may usually be neglected. Each reflection may be regarded as specular, and the delay system may be approximated by a model in which the two transducers are separated by a distance equal to the total path traversed by the wave in the medium.

Since d^2/λ is the governing parameter, the transition from near field to far field will be seen to occur at larger distances the higher the frequency. In other words the principal lobe of the propagation pattern will be narrowest for the highest frequencies contained in a signal and this will cause a relative loss of *low frequency* intensity received at the output when the wave has travelled a long distance in the delay medium. On the other hand a certain amount of the wave energy is dissipated in the medium owing to viscous damping and thermal effects, and in solids losses also occur due to scattering of the signal by inhomogeneities in the medium. These losses in all cases increase with frequency, in some cases even according to a square law (see page 240), entailing a relative loss of *high frequencies* at long

delays. Both effects combined are responsible for a fundamental limitation of delay lines: long delays can only be achieved at the expense of useful bandwidth. However, the bandwidth is also limited by several other factors, which will be discussed below.

Since in the far field some of the energy transmitted is contained in the minor lobes of a diffraction pattern, it is possible for signals to arrive at the output having traversed paths different from that defined for the main signal. If these "secondary" signals happen to be incident at an angle corresponding to one of the minor lobes of the output transducer polar diagram they will be detected; these signals have in general undergone delays different from that experienced by the main signal and thus constitute a source of interference which may be particularly noticeable in lines where many reflecting surfaces are present, and in lines where the attenuation is appreciable: secondary signals which have travelled on a much shorter path than the main signal will then have a relative advantage. One task of the delay line designer is to minimise these spurious signals: they should be at least 50 dB weaker than the wanted signal. This may be achieved by using transducers of the largest lateral dimensions conveniently practicable, in order to confine most of the energy transmitted and received to the principal lobe of the polar diagram of each transducer; some improvement may also be obtained by putting absorbent material on walls of the delay line which cause particularly troublesome reflections, or by grinding these faces away to alter the direction of the reflection wave.

One commonly encountered unwanted signal is the "third-time-round" signal which is reflected by the output transducer, returns by the same path to the input, and is reflected back to the receiver again. This signal can be reduced to negligible amplitude at any particular frequency by tilting the output transducer through a small angle θ . This angle is chosen so that, while the main signal still falls within the principal lobe of the output transducer polar diagram, the angle of incidence of the third-time-round signal (3θ) corresponds to the first minimum of this polar diagram. This will only be effective for a narrow frequency band since the angular spacing of the lobes of the diffraction pattern depends on the frequency.

Other important considerations common to both liquid and solid delay lines, as stated above, refer to the behaviour of the transducers and their coupling to the delay medium. This will be very roughly described in the following paragraphs. The subject is rather complex and a full treatment would require much more space than can be allowed here.

In the static or quasistatic case (i.e. at low frequencies) a constant fraction k^2 of the electrical energy supplied to a piezo-electric crystal is stored as elastic energy in the deformed crystal; k is called the electromechanical coupling coefficient of the transducer material. On first sight it would seem that for efficient energy conversion at any frequency, k should be as large as possible. This condition, however, is neither sufficient nor necessary. That it is not sufficient is seen by considering the mechanical response of the crystal wafer to a given electrical input. The response will be greatest (i.e. resonance will occur) when the wafer thickness, measured in the direction of propagation, is equal to half the wavelength (or an odd multiple of it) of the ultrasound in the transducer material. If the thickness is an even multiple of it, the response is zero and thus a transducer chosen to give maximum response at e.g. 10Mc/s will give zero response (and zero energy conversion) at 20Mc/s — whatever its value of k . On the other hand it can be seen that a high k is not strictly necessary. A transducer crystal may be represented very approximately by a capacitance in parallel with a resistance representing the mechanical strain energy flowing out from the crystal (radiation resistance). No energy is *dissipated* in the system even when k is low, since the portion of the electrical energy which is *not* converted into mechanical strain energy is stored in the transducer capacitance and released when this capacitance is discharged.

Thus, k is not a direct measure of the efficiency of a transducer, this depending in addition on the internal losses and external loading of the transducer crystal, and should be discussed in terms of *energy flow*. Nevertheless, the coupling coefficient k is of fundamental importance and controls some aspects of transducer performance.

In the first place, if k is low (i.e. $k^2 \ll 1$) then the effect of the electrical terminations on the behaviour of the transducer may be neglected. If the voltage drive is constant then the mechanical response of the transducer at the resonant frequency is determined by the ratio of the "acoustic impedance" of the medium to that of the transducer. For a progressive wave the acoustic impedance of a material is defined as the complex ratio of the stress in the medium at any point to the "particle" velocity, and is directly analogous to impedance in electrical systems. The specific acoustic impedance may be shown to be equal to the product of the density of the medium and the velocity of the acoustic wave³⁾. Thus, if the

coupling coefficient k is low, the acoustic response at the resonant frequency is determined by the relative densities of the transducer and delay medium and the relative velocities of the acoustic wave in the two materials.

For a low- k transducer, loaded on one face only, it may be shown that the *fractional bandwidth* $\Delta f/f$, where $\frac{1}{2}\Delta f$ is defined by a decrease in response of 3 dB, is very approximately equal to $2/\pi$ times the ratio of the specific acoustic impedance of the medium (Z_1) to that of the transducer (Z_0)²⁾. Thus, if the medium has a much lower acoustic impedance than the transducer, the fractional bandwidth is small, and it will be higher the more the impedance of the medium approaches or surpasses that of the transducer; see *fig. 3*. The most suitable condition, however, is obtained if these impedances are equal ($Z_1/Z_0 = 1$). The transducer and delay medium are then said to be matched acoustically and in that case the amount of energy reflected from the boundary

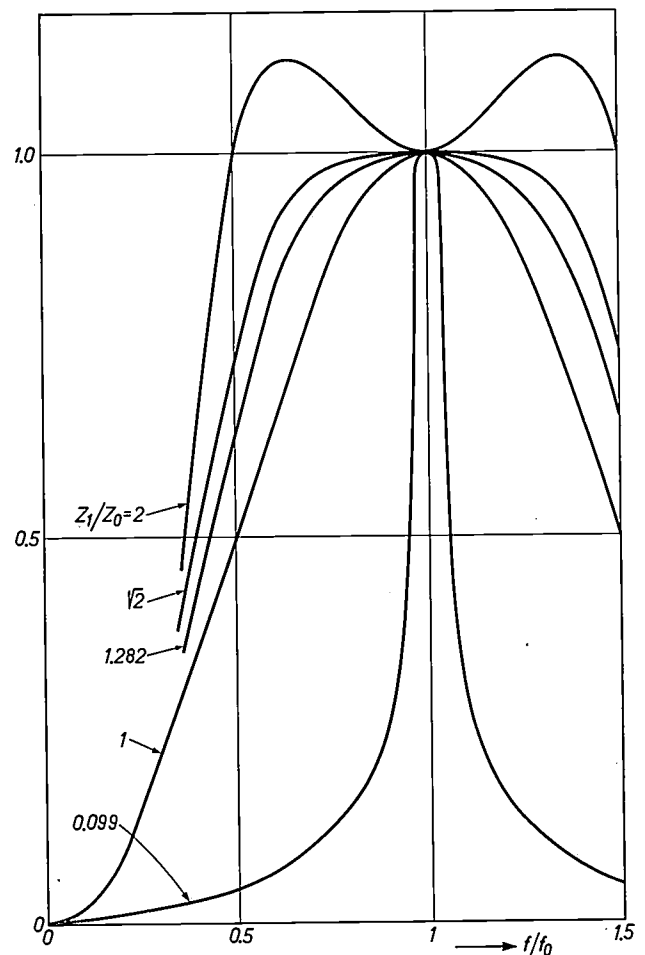


Fig. 3. Response of an X-cut quartz crystal transducer, unbacked, in a liquid medium, with various ratios Z_1/Z_0 of the specific acoustic impedance of the medium to that of the transducer. For water $Z_1/Z_0 = 0.099$; for mercury $Z_1/Z_0 = 1.282$.

³⁾ T. F. Hueter and R. H. Bolt, *Sonics*, Wiley, New York 1955.

between them is zero. Any energy which is reflected from the face of the output transducer produces no output and is not detected at the output except as an unwanted signal (the "third-time-round" signal mentioned above). This troublesome effect, therefore, is minimised by the acoustical matching. The fractional bandwidth in this case evidently is given by $2/\pi$, which is a sizeable portion of the ideal value 2 that would be permitted by the resonance behaviour of the vibrating wafer considered above (cf. the example of maximum response at 10Mc/s, when the response can differ from zero in the band between 0 and 20Mc/s).

When using the concept of energy flow the mechanical wave entering the output transducer should also be considered. Part of its energy will be used for producing the output signal, but in a low- k material a relatively large part of the wave energy will not be made use of in this way and will proceed to the back of the transducer. If this face is loaded with a material of negligible acoustic impedance, such as air, then energy which is incident on this face is almost totally reflected and may again give rise to a third-time-round signal. In a practical delay line it is therefore often desirable to "back" the transducer with an absorbent medium of acoustic impedance similar to that of the transducer.

When the coupling coefficient k is high, the electromechanical response of the transducer depends not only on the ratio of the acoustic impedances but also on the electrical terminations of the system. In this case acoustical matching is not so important since an appreciable part of the mechanical power is usually converted into electrical output power and for this reason is not liable to reflection.

To conclude these general considerations the importance of a low attenuation of the signal in the medium should be stressed. As will be shown later, the electrical terminations which must be used to obtain an electrical bandwidth comparable to the acoustic bandwidth result in a voltage loss of perhaps 40 or 50 dB, if low- k transducers are used. The total voltage transfer ratio V_{in}/V_{out} should not exceed 60 or 70 dB, since a convenient level for the input signal is of the order of one volt and the output signal should not be reduced to much less than 1 mV, lest the effect of electrical noise in the output circuit should become appreciable. Thus, the loss in the medium should not amount to more than 20 dB. When long wide-bandwidth delays are required, this low loss value is only possible if the attenuation per unit delay is very small indeed. This will normally confine the choice of media to an extremely limited number of materials.

Liquid delay lines: delay medium and design

Mechanical vibrations in liquids can only be supported in a compressional mode, torsional or shear oscillations being impossible. An X-cut crystalline quartz wafer undergoes a compressional change under the influence of an electrical field and may therefore be used as a transducer in a delay line employing a liquid delay medium.

The choice of the liquid delay medium is determined by its acoustical properties and by those of the transducer. The attenuation of most liquids is too high; apart from the liquefied monatomic gases, only mercury, water, and the lower alcohols have a low enough attenuation. In addition, since the value of k , the electromechanical coupling coefficient, is only 0.1 for crystalline quartz, a large fractional bandwidth can only be obtained if the specific acoustic impedance of the transducer is similar to that of the delay medium. In this case this requirement means that the transducer must be loaded with a medium of high density. It is found that mercury and crystalline quartz are approximately matched acoustically.

Since mercury is a conductor, it is only necessary for the back of the transducer to be coated with a gold film electrode. The other electrode of the transducer consists of the mercury in contact with the front face.

Ferroelectric ceramic transducers have higher values of the electromechanical coupling coefficient, typical values being 0.45 for compressional waves and 0.65 for shear waves. However, these materials have the disadvantage that it is very difficult to obtain the extremely thin samples necessary for use at very high frequencies. For this reason the practical limit on the use of ceramic transducers is about 20Mc/s.

If the mercury delay medium is in contact with a steel surface, then a wave striking the liquid/solid interface at an angle of more than 10° to the normal will undergo total reflection. This property is employed in the variable mercury delay line illustrated in *fig. 4*. The signal from the input transducer travels through the mercury and falls on the steel "corner reflector" as shown. Here the signal suffers two reflections at approximately 45° and is thus reflected back to the output transducer which is mounted beside the input. The reflector is mounted on a piston, so that the path-length in the medium can be changed. Thus a liquid delay line can be made continuously variable in length, and this is of considerable importance in some television applications.

This property of total internal reflection is also employed in the fixed path length delay line shown

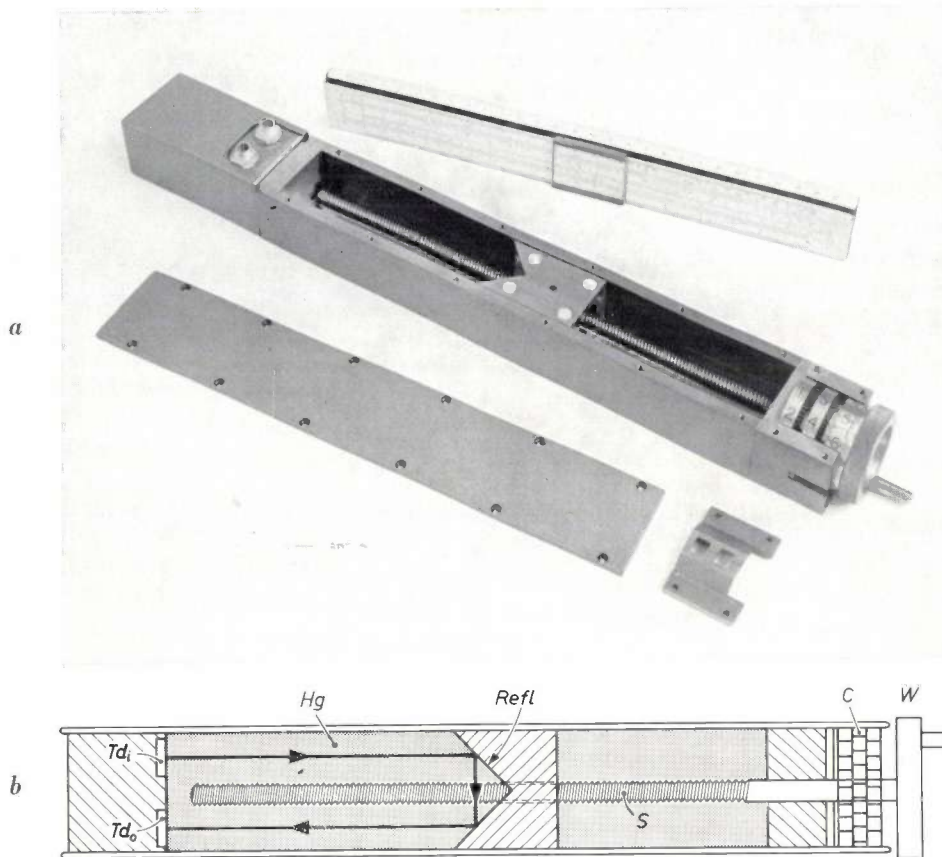


Fig. 4. a) Variable mercury delay line, with lid removed. b) Path of waves in the line. Td_i input transducer. Td_o output transducer. The delay is varied by changing the position of the corner reflector $Refl$, mounted on a sliding piston driven by a precision lead screw S . This screw is cut with the exact pitch to make 1 revolution correspond to $10 \mu s$ change of delay. W driving wheel. C revolution counter. (Photograph from: C. F. Brockelsby, *Ultrasonic mercury delay lines*, *Electronic and Radio Engr.* **35**, 446-452, 1958.)

in *fig. 5*. In this system many reflections occur as the signal traverses its "billiard table" path from input to output and a comparatively long path can be obtained in a reasonably small space.

The classical theory of absorption of sound in liquids predicts an attenuation constant which is proportional to the square of the frequency. The molecules of most liquids have rotational and vibrational degrees of freedom which are neglected by classical theory, and which result in attenuation constants higher than those predicted. Mercury however is monatomic and agrees well with the theoretical predictions at frequencies below 50 Mc/s.

It is the quadratic variation of the attenuation constant which limits the frequency at which a given delay can be obtained in a practical system using mercury as the delay medium. As the transducer resonant frequency is raised, the fractional bandwidth of the line at first remains constant. As the frequency is raised further, however, the mercury attenuation at the high frequency extremity of the passband becomes increasingly significant; this both limits the bandwidth and depresses the frequency

of maximum response to a value below the crystal frequency. Thus at television frequencies long delays are difficult to obtain if the required bandwidth is to be preserved. The characteristics of some typical mercury delay lines, including those illustrated in figures 4 and 5, are given in *Table I* on page 241.

Solid delay lines: delay medium and design

Solid materials are, in general, capable of supporting two types of vibration, namely compressional waves and shear waves. In a solid ultrasonic delay line shear waves are chosen for two reasons. First, shear waves travel more slowly through a solid medium than compressional waves, and thus a longer delay may be obtained in a given path length. Second, and more important, when a dilatational wave is reflected from the boundary of the delay medium then in general shear waves are also generated. These waves are propagated in a direction different from that taken by the reflected compressional wave, and travel through the medium with a different velocity; they may thus give rise to spurious signals at the output transducer. If shear

Table I. Physical and electrical characteristics of some typical liquid and solid delay lines suitable for use in television applications.

Delay medium	Transducers	Delay	Band-centre	Bandwidth	Insertion loss V_{in}/V_{out} dB	Input and output capacitance pF	Largest spurious signal, dB below wanted signal
		μs	Mc/s	Mc/s			
Mercury	X-cut quartz crystal	25	15	6	65	31	46
"	"	30-330 *)	14.3-15.5	6.8-7.6	61-65	31	35
"	"	1000 **)	7.5	3	69	44	33
Fused quartz	Y-cut quartz crystal	33.3	59	28	48	80	50
"	"	2500	29	7	38	180	40
Lime soda glass	Lead zirconate-titanate type Piezoxide 3	64	4.4	2.5	10-20 ***)	1000-2000 ***)	40

*) Illustrated in fig. 3.

**) Illustrated in fig. 4.

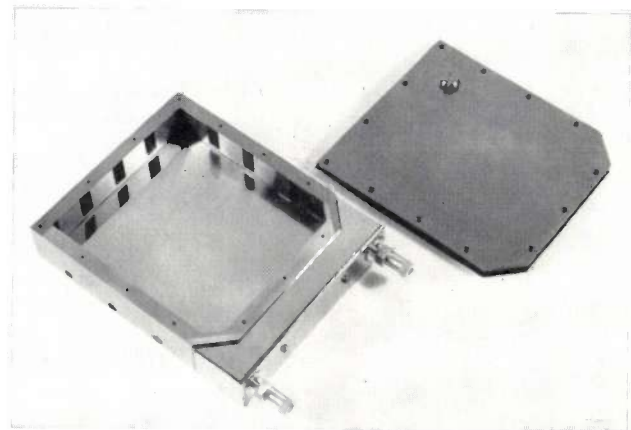
***) The insertion loss of this line depends on source and termination impedances; the capacitances vary widely over the passband.

waves are used initially, however, and are polarised parallel to the reflecting surface (i.e. normal to the plane of incidence of the wave on the reflecting surface), then they are simply reflected at each impact with no such "mode conversion". The geometrical design of the delay line configuration is thereby greatly simplified.

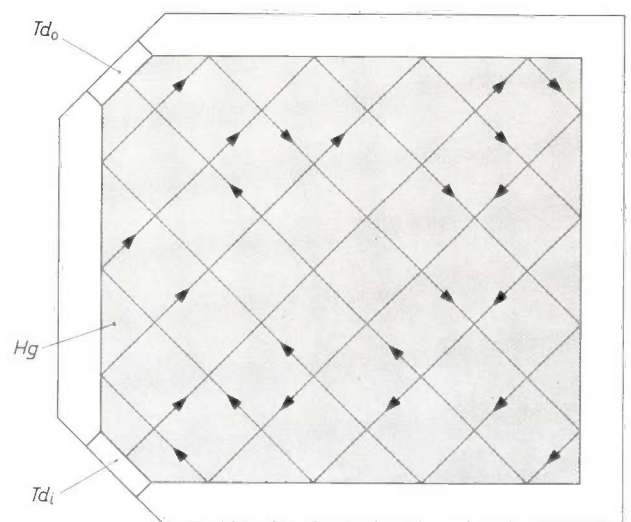
The piezoelectric transducer used to generate the shear vibration normally consists of a Y-cut crystal-line quartz wafer; alternatively a polarised ferroelectric material can be used. The transducer is coated on both faces with metal film electrodes as before and bonded on one face to the delay medium by means of a material which should be acoustically matched to both the transducer material and the delay medium. Indium is often used to make the bond because it has good adhesive properties and its acoustic impedance has a suitable value.

Consider now the choice of the medium. Single crystals are difficult to use since their elastic constants are not normally the same in all directions. Polycrystalline materials are unsuitable for wide-passband delay lines since the ultrasonic waves interact with the grain structure of the medium at high frequencies causing scattering. The material currently considered most suitable as a delay medium is vitreous silica (fused quartz), which has an extremely low attenuation. For short delays mixed oxide glass may be used, although the attenuation in this medium is much greater and it cannot be made as homogeneous as fused quartz.

If large pieces are called for, even fused quartz is difficult to make with the required homogeneity, and the cost will be very high. For producing a long delay in a single piece of quartz, the path traversed by the beam is therefore folded, as in the case of the



a



b

Fig. 5. a) "Billiard table" type of mercury delay line, with lid removed. b) Path of waves in the line. The signal propagated by the input transducer travels through the mercury by the billiard table path shown, and thus undergoes a long delay in a comparatively small volume of mercury. (Photograph from: C. F. Brockelsby, Ultrasonic mercury delay lines, *Electronic and Radio Engr.* 35, 446-452, 1958.)

mercury delay line shown in fig.5. In fig.6 some practical delay line geometries of varying complexity are illustrated. The longest delays are obtained by using the complex fifteen-sided line shown in fig.6d. The delay may then be doubled by using the double-decker configuration shown in the photograph of fig.7. In this system the input transducer launches a signal into the lower half of the line; after traversing the path shown in fig.6 the signal strikes a corner reflector which transfers it to the upper half of the

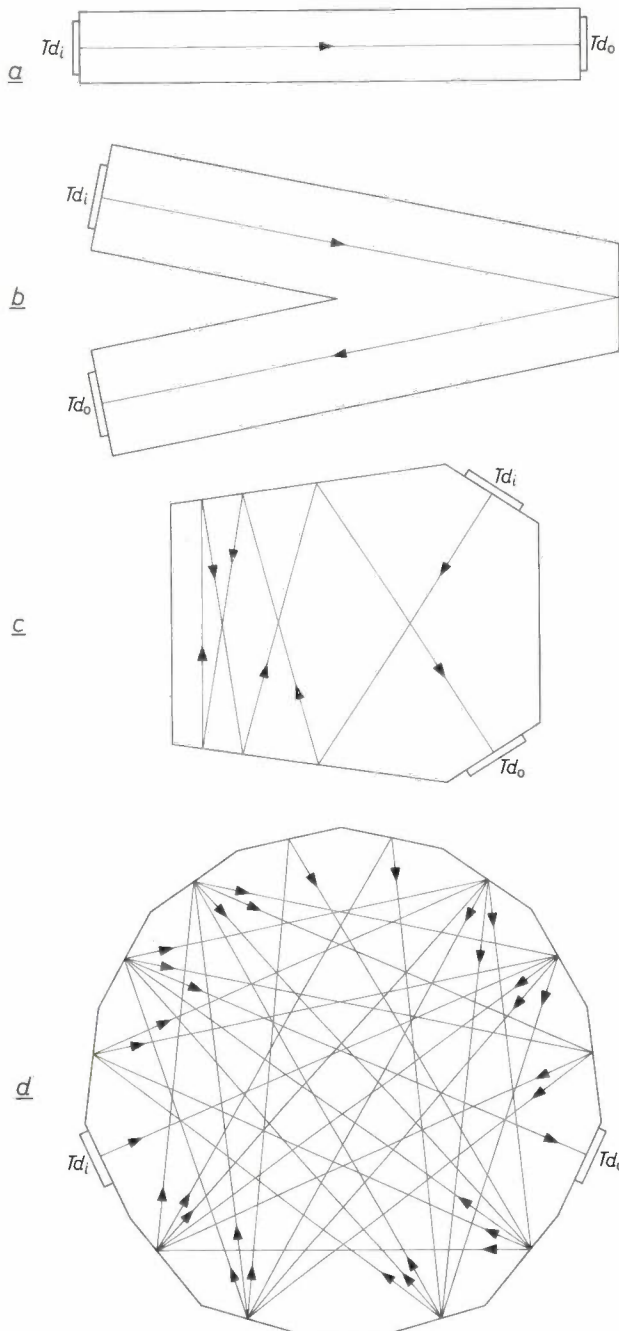


Fig. 6. Different configurations of solid delay lines, e.g. in fused quartz. Large pieces of quartz of suitable homogeneity are expensive and difficult to make. When long delays are required the configuration is made such that the signal must undergo many reflections in its passage through the line.

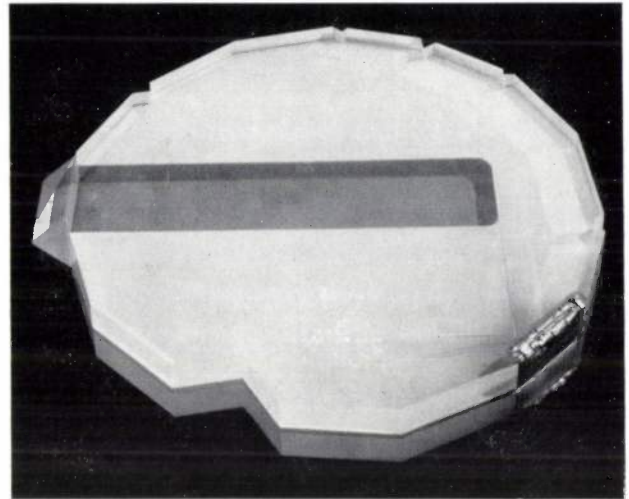


Fig. 7. "Double-decker" quartz delay line. In this configuration two of the complex fifteen-sided delay lines shown in fig. 6d are placed on top of each other and are connected by means of a corner reflector, in order to double the delay obtained. Edges of the line which give rise to troublesome reflections are ground away.

line. The signal then follows an identical path (in reverse) in this portion of the line, and finally arrives at the output transducer where it is reconverted into an electrical signal. This system has the additional advantage that the probability of secondary signals travelling on different paths from the input to the output transducer is reduced to practically zero.

Fused quartz has a lower attenuation per unit delay than mercury at a given frequency and thus much longer delays may be achieved in this medium. Delays of several milliseconds may be obtained at a centre frequency of 30 Mc/s with a bandwidth of 8 Mc/s. The characteristics of some typical solid delay lines are also given in Table I.

It is worth mentioning at this point a metal strip delay line which has recently been developed in the United States⁴⁾. A ceramic transducer is bonded to the end of the strip which is made from a metal having a low acoustic attenuation, and is used to propagate shear waves down the interior of the strip. It may be shown that if the thickness of the strip is less than half the wavelength of the highest frequency component of ultrasound present, then the signal travels down the line without dispersion. The width of the strip may be made large compared with the wavelength to provide mechanical rigidity and to enable transducers of convenient size to be bonded to the end. Ultrasonic energy striking the edges of the strip is absorbed by means of adhesive tape. The advantage of this form of delay line is that it may be bent or rolled up without loss of performance, and although its attenuation is greater than that of fused

⁴⁾ A. H. Meitzler, IRE Trans. UE-7, 35, 1960.

quartz, a delay of 10 milliseconds has been achieved with a video bandwidth of 2Mc/s.

Input and output circuits

In order to obtain optimum performance from an ultrasonic delay line it is necessary that the electrical source and load impedances should be chosen correctly. This choice is determined by the nature of the transducers used and by their coupling to the delay medium.

It has already been mentioned that a transducer for use with solid or liquid delay lines may be represented very approximately by a capacitance in parallel with a resistance (in reality this is valid only at the centre of the passband). If the transducer is a quartz crystal which has a low value of the coupling coefficient k , this effective parallel resistance is very high compared with the reactance of the transducer capacitance within the passband, and, as previously stated, the acoustic response of the line is not significantly dependent on the electrical terminations. A satisfactory *mechanical* bandwidth (fractional bandwidth $2/\pi$) is then achieved by acoustical matching of transducer and delay medium. The electrical circuit of which the transducer forms a part evidently should have at least the same bandwidth. To this end it is necessary to damp the circuit with a shunt resistance (alternatively a suitable four-terminal matching network may be used). A typical quartz transducer for a solid delay line may be represented electrically by a 10 k Ω resistance in parallel with a 200 pF capacitance. The damping resistor required to terminate this system might be

as low as 75 Ω . (The capacitance of course must be tuned to the crystal frequency by means of a parallel inductance.) The output of the delay line system may then be regarded as a constant current generator, and the effect of the damping resistor is to produce a voltage insertion loss V_{in}/V_{out} which depends largely on the ratio of termination impedance to source (transducer) impedance, and in this case is of the order of 40 dB. To reduce this voltage loss it is important to keep stray capacitance to a minimum and thus maximise the value of the damping resistance necessary to produce the required electrical bandwidth. A similar electrical bandwidth is, of course, necessary for the driving circuit.

In the case of ceramic transducers, which have *high* coupling coefficients, the effect of a parallel damping resistor is by no means so simple. The shunt radiation resistance of the transducer is now comparable with the reactance of the capacitor and both vary appreciably over the passband. The optimum driving and receiving circuits can then be predicted exactly only by laborious calculations; a good account of the effect of electrical and mechanical terminations on the loss and bandwidth of delay systems using ceramic transducers is given by Thurston⁵⁾.

The electrical characteristics of wire delay lines, where coils are used as input and output transducers, are entirely different from those of solid and liquid lines. However, as previously mentioned, wire delay lines are seldom used in television applications; for this reason no further treatment of the relevant electrical circuitry will be given.

II. APPLICATIONS TO TELEVISION

1) *The "Scophony" receiver*

The earliest application of ultrasonic techniques in the field of television was in the pre-war "Scophony" mechanical scanning receiver, in which use was made of the *optical* properties of a liquid delay line when an ultrasonic signal was present in the line.

A television picture is always transmitted as an array of horizontal lines. During one "field" period the video signal corresponding to every alternate line in the picture is transmitted, during the next field period the transmission consists of those lines omitted during the previous scan. The two sets of lines are "interlaced" by the receiver to describe the complete picture or "frame".

In the "Scophony" receiver⁶⁾, the video information corresponding to each line of the picture was modulated onto a 10 Mc/s carrier and applied to the input transducer of a delay line, which used water as the delay medium. Absorbent material was placed at the output end of the line, since no electrical output was required. Under the influence of the carrier alone the periodic variations in the density and hence in the refractive index of the water cause it to behave as a diffraction grating, the spacing of the lines being equal to the wavelength of the ultrasound in the

⁵⁾ R. N. Thurston, IRE Trans. UE-7, 16, 1960.

⁶⁾ J. H. Jeffree, "Television" 9, May 1936, p. 260, and British Patent No. 439 236.

water. If a parallel beam of light is allowed to pass through the medium, then the amount of light diffracted away from the zero order maximum into subsidiary maxima by any part of the grating is proportional to the amplitude of the periodic variations in the refractive index of the medium at that point.

The system used is illustrated in *fig.8*. Light from an illuminated slit is collimated to pass through the delay line as a parallel beam. The 10Mc/s carrier, modulated with the picture information, is applied to the delay line, which is of such a length as to accommodate a wave train corresponding to one complete line of the picture. The signal corresponding to each picture element causes an amount of light proportional to the amplitude of this signal to be diffracted away from the zero order maximum for that section of the delay line. The undeviated zero order beam which is thus modulated in intensity across its width, is focussed onto the screen of the receiver by a lens and rotating mirror system as shown. A given progressive picture point on the delay line is arrested by the rotating mirror system to produce a stationary picture point on the screen; this point will be present for the complete line duration, and the same applies to other points of the picture line. A further rotating mirror system, not shown in *fig.8*, is used to provide the "frame scan", i.e. to combine the successive lines of the picture to produce the complete display.

The "Scophony" receiver suffered from all the usual problems of mechanical scanning systems; the chief of these was the difficulty in synchronising the extremely high speed motor (30 000 r.p.m.) which drives the rotating mirrors providing the stationary picture. For this reason the "Scophony" receiver was soon superseded by the electronic scanning receivers in use today. However, the principle of using ultra-

sonic techniques in order to provide optical readout of an electrical signal is still of interest as a means of high speed data processing, for certain special applications. Bandwidths of 40 Mc/s may be achieved, together with the facility of simultaneous display or inspection of bits of information fed in sequentially over a period of many microseconds. An application of such a technique will be described later in the section on systems conversion.

2) Inertia compensation for a vidicon tube

Ultrasonic delay lines have been used by Hughes ⁷⁾ (1961) to correct for effects due to moving objects in the well known vidicon television camera tube. In this tube the light from the object in the field of view of the camera falls on a photoconductive layer of antimony trisulphide producing a pattern of conductivity which at any point corresponds to the brightness of the picture observed. In order to convert this pattern into an electrical signal the photoconductive layer is scanned by a beam of electrons, in two fields with interlaced lines as previously described.

Difficulty arises in the vidicon tube when the image on the photoconductive layer is not erased completely by each scan. Owing to the finite decay time of the layer, the signal obtained on scanning consists of the new information plus a certain percentage of the previous information. This effect, which is only noticeable under conditions of poor illumination, results in the "smearing" of the image of a moving object.

Hughes has used the following method in order to correct for this effect. Part of the signal from each line in a field was delayed by one field period (16.651 ms on the US system) and subtracted from the signal due to the corresponding line on the next

field, which is the one *adjacent* to it in the picture. The fraction of the signal used for the correction was 10-40%. Since this signal is merely a correction to the main signal, an appreciable improvement may be obtained even when using a low bandwidth delay line, and the line used was of the torsional magnetostrictive type with a bandwidth of 600 kc/s on a 800 kc/s carrier.

⁷⁾ W.L. Hughes, IRE Trans. PGBC-7, No. 3, p. 8, 1961.

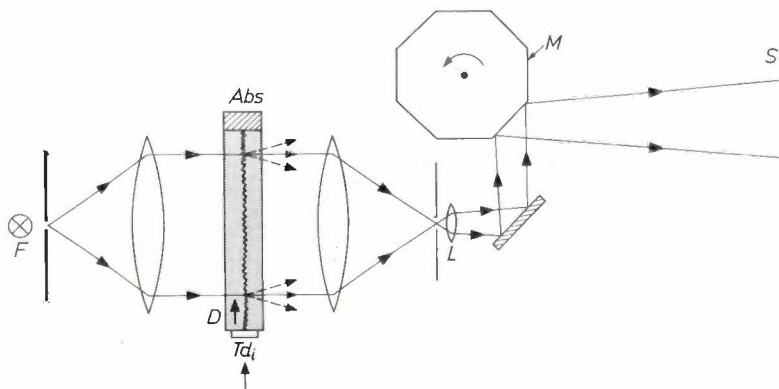


Fig. 8. Display system of the "Scophony" television receiver (1936). A flat light beam from a source *F* passes through the delay line *D* and is locally affected in intensity by the wave originating from the video signal. The transmitted beam is focussed by lens *L* on the screen *S*. Any progressive picture point in the line is arrested by the rotating mirror *M* to produce a stationary picture point on the screen.

The correction was inadequate in that the signal should ideally have been delayed by *two* field periods and applied to the *corresponding* line on the next frame. This would have been more difficult to achieve owing to the very long delay required. However, although interlace was ignored in this way, and the bandwidth was low, a useful reduction of smear was achieved with this experimental system.

An alternative form of television camera tube, the image orthicon, employs a photoemissive cathode and does not exhibit "smear". For this reason the vidicon is little used in television broadcasting except under conditions of high illumination or in applications where its comparatively small size is of advantage. In addition, in a more recently developed tube of the vidicon type, the "Plumbicon"⁸⁾, lead oxide is used as the photoconductive material; in this case the "smearing" effect is hardly noticeable. Thus it appears that smear correction will seldom be necessary in future television applications.

3) Vertical aperture correction

Ultrasonic delay line techniques may also be used to correct for another fault of a television camera tube, viz vertical aperture distortion.

The electron beam in the pick-up tube as well as in the picture tube must scan the discrete lines from which the television picture is formed (say 405 lines per picture). The effective diameter of the scanning spot formed by the beam of electrons in the pick-up tube, however, cannot be made as small as would be required for the ideal line width. Thus the signal generated when scanning one line is diluted with information from the adjacent lines. This effect is known as vertical aperture distortion and will obviously reduce the definition of the picture produced in the receiver. A *horizontal* aperture distortion also exists: whereas the television transmitter is designed to have a bandwidth such that frequencies corresponding to $\frac{5}{4} \times 405$ changes from black to white along one picture line can be coped with, the diameter of the scanning spot overlapping several of these changes will prevent the resolution of all these picture elements in the receiver. This horizontal distortion, which strongly resembles the effect of a finite slit width in scanning sound film or magnetic tape recording, can be approximately corrected by use of electronic circuits. Correction of the *vertical* aperture distortion, however, has to deal with the admixture of information pertaining to picture elements scanned one complete picture line period

before or afterwards and is possible only by using delay line techniques.

An extra difficulty arises from the way in which the picture is scanned. Since two fields are interlaced in order to describe one complete picture, or frame, it follows that in order to correct one line of a frame for the admixed information of adjacent lines, it would be necessary to store the information not for one line (96 μ s on the 405 line 50 c/s system used in Great Britain) but for one field period (20 ms).

For simplicity it is proposed first to ignore interlace and to correct each line with the information stored in the adjacent lines of the same field. To perform this correction at all adequately, each line must be corrected with the signal due to the subsequent line in the field as well as the preceding one. The system used is illustrated in *fig. 9*. The main

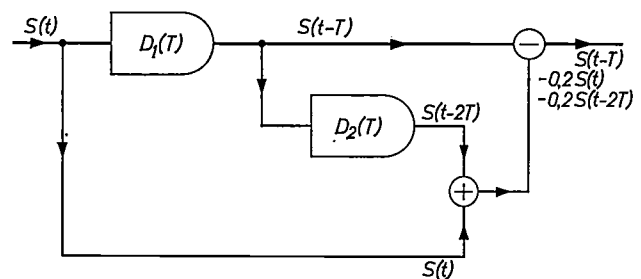


Fig. 9. Vertical aperture correction using two "one-line" delay lines D_1 and D_2 . The input signal $S(t)$ delayed by one line period T is used as the main signal, $S(t-T)$. This signal is then combined with 10-20% of the signal from the previous line, $S(t-2T)$, which has been delayed by $2T$, and the same proportion of the signal from the subsequent line, $S(t)$, which has undergone no delay.

signal is delayed by one line period, i.e. 96 μ s; from this is subtracted a part of the signal from the *preceding* line of that field, which has undergone a delay of twice the line period, and part of the signal from the *subsequent* line, which is made available in advance by bypassing the main delay line. Dependent on the vertical aperture distortion in the signal, the fraction of the signal from the adjacent lines needed for the correction is 10-20%.

Since this correction involves delaying the main signal, the delay line used must be one with a bandwidth sufficient to accommodate the video information. For the 405-line, 50 c/s system in which double sideband modulation is used, the delay line must have a bandwidth of 6 Mc/s. In order to prevent appreciable distortion, the frequency characteristic of the line should be flat to within 1 dB over the whole band. In addition, the delay line must be variable in length if the line system is synchronised to the mains, since the frequency of the mains may drift appreciably. A variable mercury delay line is suitable for this application and it is possible to use

⁸⁾ E. F. de Haan, A. van der Drift and P. P. M. Schampers, The "Plumbicon", a new television camera tube, Philips tech. Rev. 25, 133-151, 1963/64 (No. 6/7).

a servo mechanism to adjust the length of the line and to provide automatic control of the vertical aperture correction. If, however, the line system is controlled by a crystal-locked oscillator then no adjustment should be necessary and a solid delay line may be used.

Using the system described, a very marked improvement in picture quality may be obtained. Gibson and Schroeder⁹⁾ (1960) and Howorth¹⁰⁾ (1962) have described systems of this kind. However, in order to perform this correction in the most effective manner interlace should not be ignored, and each line should be corrected with information from the adjacent lines in the *frame* instead of the field. The system used should then be essentially the same as that shown in fig. 9 with the exception that the delays involved are now equal to one field period (20 ms).

Since this long delay is required for the main signal, which however should not suffer any loss of definition, a rather difficult problem has to be solved. As previously mentioned, the most suitable delay medium for providing long delays at large bandwidth is fused quartz. However, using existing techniques, it is not possible to construct a single delay line of 20 ms delay even using fused quartz, since the path length required is 80 metres. A piece of quartz of the required size and homogeneity cannot at the moment be obtained; in any case the attenuation in this path length would be too great. It is therefore necessary to use a number of shorter delay lines to achieve this delay, with repeating amplifiers to boost the signal after passage through each section. A 20 ms delay which has been made by Mullard consists of eight lines each of 2.5 ms delay. This system has a bandwidth of 8 Mc/s with a centre frequency of 30 Mc/s.

As previously stated, if the line system is synchronised to the mains frequency then the delay used must be variable. In order to achieve this, the cascade of quartz delay lines is made with a delay slightly less than 20 ms. The remainder of the delay is provided by means of a short mercury delay line which may be fitted with a servomechanism to keep the delay matched to the mains frequency, as described above. This servomechanism might also be used to compensate for variations in temperature, although it is also possible to stabilise the temperature at a constant value by use of a thermostat. This should preferably be set to a value between 50 °C

and 70 °C, since the attenuation in fused quartz is lower in this temperature region than at room temperature.

It would, incidentally, be possible to feed the mechanical signal from the final section of the quartz delay line directly into the mercury line without the use of an intermediate repeater amplifier and the two associated transducers. This might be done as shown in fig. 10. The shear wave in the quartz undergoes a reflection at a plane such that the plane of incidence is not normal but parallel to the polarisation of the shear wave, and at such an angle of incidence that the wave is converted entirely into a compression wave. The resultant signal may now be used to propagate a compressional wave in the mercury which is held in a steel container bonded to the end of the quartz.

Since the delay line required for this ideal form of vertical aperture correction is so complex, it would be convenient if a single delay line could be used to provide both the 20 millisecond delays needed. In fact, this may be done by using two separate carrier

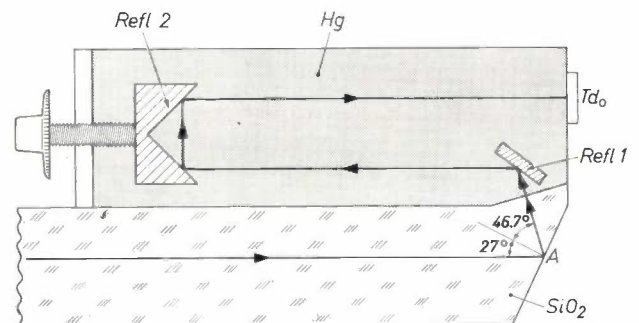


Fig. 10. Combination of a fused-quartz delay line with a variable mercury delay line. At the point *A* the plane and angle of incidence of the vertically polarised shear wave in the fused quartz delay line (SiO_2) are such that the signal is converted entirely into a compression wave. This wave then passes directly into the mercury delay line, with reflector *Refl 1* and adjustable corner reflector *Refl 2*, by means of which the delay of the composite line may be adjusted.

frequencies in the 8 Mc/s pass-band of the delay line. A possible system is illustrated in fig. 11. If the centre frequency of the delay line is 30 Mc/s, the main video signal is passed through the delay line as a single-side-band modulation (width 4 Mc/s) on a 26 Mc/s carrier. This is then combined with a fraction of the signal from the subsequent line in the next field which has undergone zero delay, and with that from the previous line of the preceding field which, having traversed the delay line once on a 26 Mc/s carrier is then passed through the delay line once more on a 34 Mc/s carrier. Filters are used to prevent mixing of the two signals.

Owing to attenuation in the delay lines, and noise in the amplifiers used, the improved definition

⁹⁾ W. G. Gibson and A. C. Schroeder, *J. Soc. Motion Picture and Television Engineers* **69**, 395, 1960.

¹⁰⁾ D. Howorth, B.B.C. Research Department Report **T-085**, 1962.

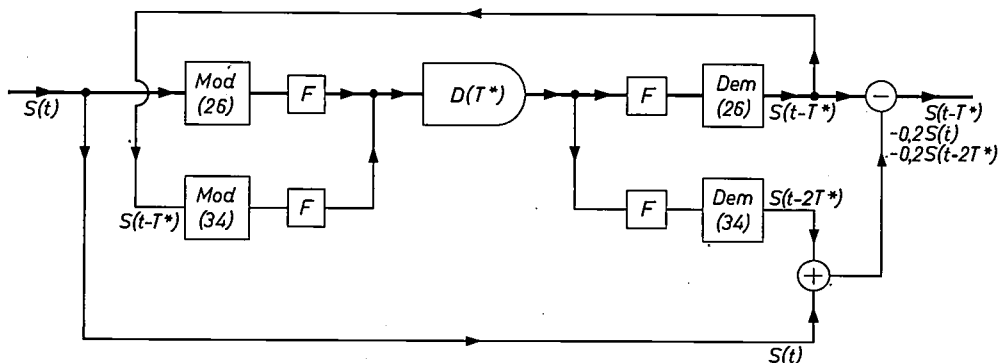


Fig. 11. Vertical aperture correction using signals delayed by one field period. This system is similar to that shown in fig.9, except that a single delay line D is used to provide both the one-field-period delays required. This is done by passing the signal with a bandwidth of 4Mc/s once through the line as single-side-band modulation on a 26Mc/s carrier, by means of a modulator Mod (26) and a demodulator Dem (26), with suitable filters F , and then again on a 34 Mc/s carrier; the centre frequency of the 8 Mc/s passband of the delay line is 30 Mc/s.

resulting from both these methods of vertical aperture correction is paid for by some small deterioration in the signal-to-noise ratio. However, since the signal-to-noise ratio of the delay system is normally of the order of 50 dB, the overall result is a considerable improvement in picture quality.

4) The "Secam" and the "PAL" colour systems

In the previous applications described in this article an ultrasonic delay line was employed to reduce the effect of one line of a television picture on the adjacent lines, and thus to improve definition. In the "Secam" system¹¹⁾ of colour television, which was proposed a few years ago, a similar process is used for a purpose opposite to that of the previous case: a delay line is used to store one line of the picture so that it may *add* information to the subsequent line.

Every colour television system should preferably be "compatible" i.e. it must be possible to receive the total signal as a black-and-white picture on a normal black-and-white receiver. Three signals are transmitted; one is a luminance signal which defines the brightness or luminance of each element of the picture just as in a black-and-white system. The other two signals contain the colour information and define the hue and saturation of the colour at each point of the picture. These are transmitted as the red and blue colour difference signals, one describing the amount by which the red signal differs from the luminance signal and the other similarly describing the blue. The green signal is that remaining when the red and blue signals have been subtracted from the luminance signal. In the "Secam" system these colour signals are not transmitted simultaneously, as in the N.T.S.C. system, but on alternate lines of

each field. The receiver displays each line of the picture by using directly the information being received at that moment (say the blue) whereas for the other colour difference (red) it employs the information which was transmitted on the previous line of that field. This sharing of half the colour information between adjacent lines of each field entails some loss of precision in the colour detail since the mixing process has introduced errors similar to those which the vertical aperture correction previously described sought to remove. However, these errors to a first approximation are in the colour of the picture rather than in its luminance, and the eye is less sensitive to loss of colour definition.

In order to effect this combination of colour information from adjacent lines of a field, a "Secam" receiver requires a device which is capable of storing the colour signal for one line period (64 μ s on the 625 line 50 c/s system which will be used for colour television in Europe). Since the transmitter is to be crystal controlled rather than locked to the mains frequency, this delay need not be variable and thus it is not necessary to use a mercury delay line. In addition, the delay is comparatively short, the centre frequency is low (4.43 Mc/s), the required bandwidth is only 2 Mc/s and some attenuation can be tolerated at the edges of the passband. Thus a suitable delay line can be made using *glass* as the delay medium. Glass has the disadvantage that the velocity of shear waves in the delay medium varies slightly from sample to sample, and that each line must be individually checked and adjusted to give the required delay, which must be correct to within 0.05 μ s. Such adjustment involves grinding away one of the reflecting edges of the line, and this is normally difficult since errors may be introduced in the direction of the reflected beam. However, by use of the delay path geometry shown in fig. 12 this

¹¹⁾ P. Cassagne and M. Sauvanet, Ann. Radioélectrique 16, 109, 1961.

adjustment is simplified. If the longest edge of the delay line body, on which two reflections occur, is ground away, then any variation in the direction of the wave in the plane of the paper, introduced at the first reflection by errors in the angle of grinding, is compensated at the second reflection. Such compensation is important if the received signal is to fall within the central lobe of the polar diagram of the output transducer.

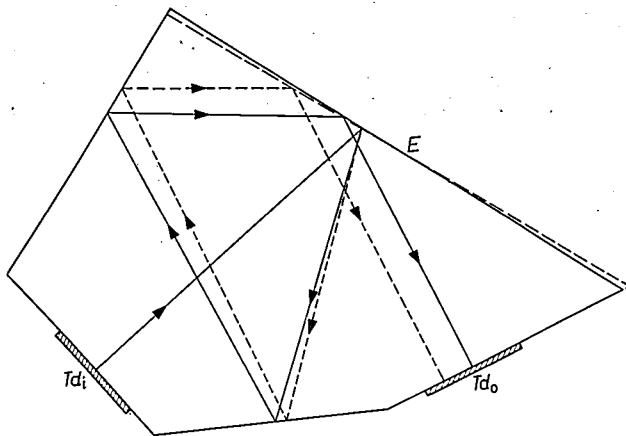


Fig. 12. Path geometry in a glass delay line for use in "Secam" and "PAL" colour television systems. This diagram shows how deviation of the ray, caused by an error in the angle at which the first reflecting surface *E* is ground away, is compensated by the second reflection at this surface. The error in grinding has been considerably exaggerated for convenience of drawing. (J. S. Palfreeman and R. W. Gibson, British patent applied for.)

It is necessary that the delay obtained should not vary significantly over the temperature range in which the receiver normally operates. In some recent experimental delay lines made from Philips type 18 glass, the temperature coefficient of the delay is about $0.001 \mu\text{s}/^\circ\text{C}$, so the temperature can rise or fall by about 50°C before the picture is degraded.

It is important in this application that the amplitude of signals arriving at the output transducer of the delay line at the wrong time should be kept to a minimum, since these would produce areas of colour in the wrong place. In the design shown in fig. 12 these spurious signals are kept at a level of -35 to -40 dB, which could be extended to -50 dB if necessary.

The insertion loss of these delay lines is between 20 and 25 dB if symmetrical terminations are used (i.e. if the internal resistance of the signal source is equal to the load resistance) and if the resistance value is optimized for maximum flat bandpass characteristics. The insertion loss may be up to 12 dB better for asymmetrical terminations. This loss has to be made up by an amplifier coupled to the delay line. The component values and circuit parameters are not critical.

In the N.T.S.C. system the colour difference signals are transmitted simultaneously but separated in phase. In another system for colour television, the "PAL" system¹²⁾, the phase of one of these signals is *inverted* on alternate lines. It has recently been proposed for the receiving equipment which decodes and separates the two signals to store the colour information in a particular picture line for one line period and to add or subtract it to that received for the next line. However, since it is important that the two signals are mixed in the correct phase, the delay line used must be accurate to within a fraction of the subcarrier period, i.e. a few nanoseconds. In addition, the delay must maintain this value over the frequency band of the colour signal and over the temperature range of the receiver.

5) Study of multipath effects

The picture displayed by a television receiver frequently suffers from what are known as multipath effects. These effects are due to the arrival at the receiving antenna of two (or more) signals, one direct from the transmitter and the other by a different path, perhaps by reflection from a passing aircraft. If the reflected signal is received at appreciable strength in comparison to the direct signal a "ghost" picture is observed as shown in fig. 13. As the aircraft moves, the path difference, and hence the time delay between the two signals, varies. Thus, the phase and position of the reflected signal is constantly changing and this may give rise to a beat effect or "flutter" on the screen of the receiver.

When a new receiver is being designed, or when a new system (e.g. colour television) is being developed in the laboratory it is important to study the effects of reflected signals on the received picture. Since it is inconvenient to use real aircraft to produce the reflected signal, and in any case the exact reflection is not readily repeatable, the reflected signal must be produced by artificial means.

A variable mercury delay line can be used for this purpose¹³⁾. In the system illustrated in fig. 14, the test signal, from either a live television transmitter or from a local test pattern generator, was modulated onto a carrier of a suitable frequency, viz 15 Mc/s, and applied to two transmission paths. One of these consisted of a short fixed delay of $30 \mu\text{s}$ and the other included a variable delay line, the delay of which could be varied continuously from $25 \mu\text{s}$ to $300 \mu\text{s}$. In series with the variable delay was an attenuator.

¹²⁾ W. Bruch, Farbfernsehsysteme — Überblick über das NTSC-, SECAM- und PAL-System, Telefunken-Z. 36, 70-88, 1963 (No. 1/2).

¹³⁾ C. F. Brockelsby, Electronic Design, Oct. 1957, p. 36.

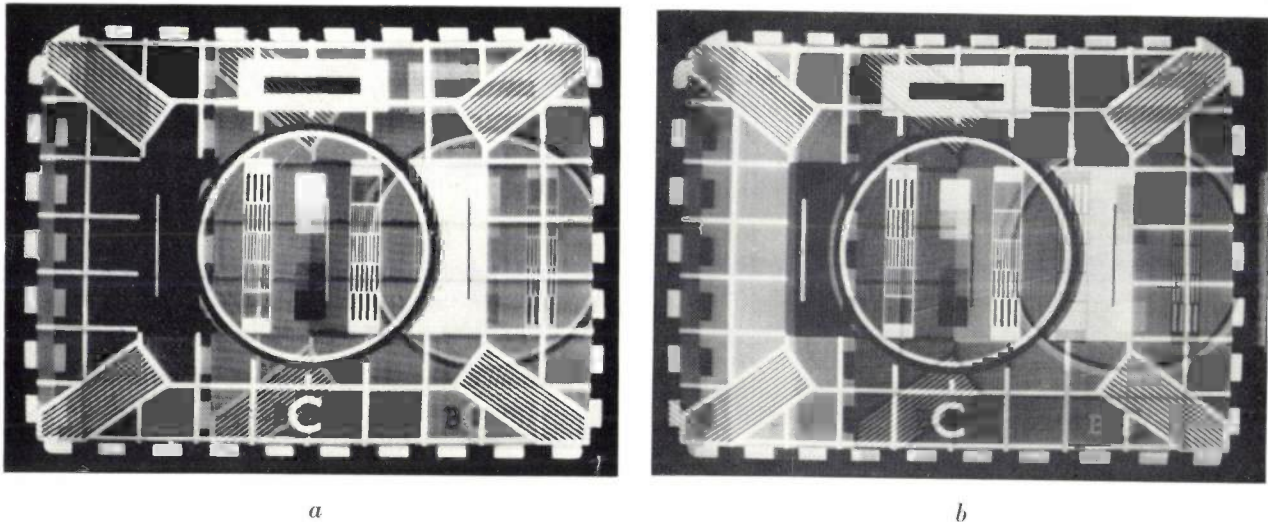


Fig. 13. Ghost images produced by signal reflections, e.g. at a passing aircraft.
 a) Reflected signal in phase with main signal.
 b) Reflected signal out of phase with main signal.

After passing through the delay lines the signals from the two paths were combined and their frequency changed back to the original carrier frequency, which was applied to the receiver under test. By altering the variable delay the effective path difference between the two signals could be changed, and by adjusting the attenuator the strength of the reflected signal could be controlled.

The variable delay line used was a mercury delay line similar to the line illustrated in fig. 3. In order to simulate the effect of a moving aircraft the lead screw driving the sliding piston was driven from a Velodyne motor. The input to the Velodyne amplifier was a voltage to which the motor speed was proportional. The delay could then conveniently be programmed by supplying the Velodyne control voltage from a potentiometer.

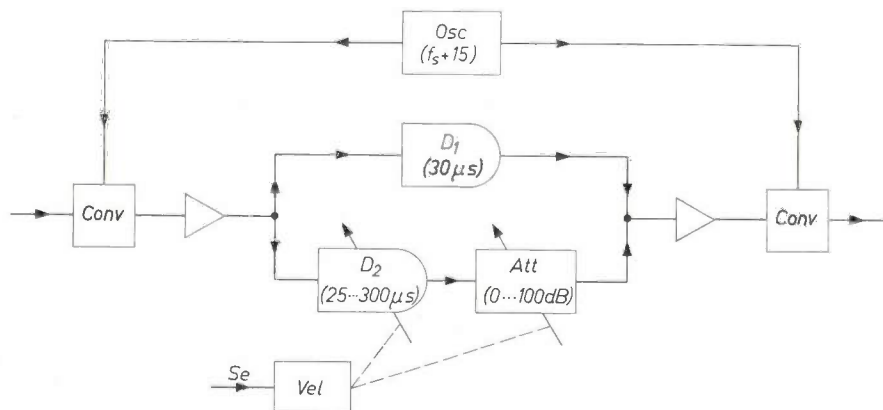


Fig. 14. Aircraft reflection simulator using a variable liquid delay line. The signal passing through the fixed $30\mu\text{s}$ delay line D_1 represents that arriving at the receiving antenna directly from the transmitter. The signal passing through the variable delay line D_2 and attenuator Att represents that reflected from a passing aircraft; the amplitude and phase of this signal may be varied. Both the delay line and the attenuator are driven by a Velodyne motor Vel , whose control voltage can conveniently be programmed (servo system Se).

At a carrier frequency of 15Mc/s the delay line system had a bandwidth of 8Mc/s for a $300\mu\text{s}$ delay. Working at a received signal level of 3mV a signal-to-noise ratio of 50dB was achieved. The insertion loss of the line was around 50dB , so the input transducer required a drive of about one volt which could readily be provided with adequate linearity by a small receiving tube.

Gander and Mothersole¹⁴ (1958) have given a detailed description of such a system. They found this application of delay line techniques particularly useful when appraising a new television system such as the N.T.S.C. colour system.

6) Systems conversion

It is frequently required to convert a television video signal from one scanning system to another, e.g. from 625 to 405 lines per picture. Such conversion is a regular requirement when programmes are relayed between countries using differing line systems. The conventional technique is to display the input signal on a cathode ray tube of relatively long persistence, and to examine this with a television camera tube working on the line system

¹⁴) M. C. Gander and P. L. Mothersole, *Electronic Engng.* **30**, 408, 1958.

required¹⁵). This process may introduce noise in the conversion of video signals into a display and vice versa, and may produce loss of definition and smearing of moving images due to the persistence of the phosphor. Moreover, moiré-effects are virtually unavoidable with this technique. Other possibilities for a systems conversion are therefore of interest.

In most countries the field period of the television system is equal to the period of the mains. It therefore follows that in general systems conversion involves a change in the field period as well as in the number of lines. However, in many cases it appears that the field periods of the input and output signals may be equal and that conversion may involve only a change in the number of lines per field. For example, in Great Britain it is proposed to use a 625-line camera, but to transmit the picture simultaneously on both 625 lines and 405 lines using the same field period. Conversion without change of the field period is known as synchronous conversion and Lord and Rout¹⁶ (1962) have recently described a standards converter which uses ultrasonic delay line techniques in order to effect such a conversion.

In order to effect the change from one line system to another, two processes must be performed. First, by selective rejection or repetition of information the number of lines in the field must be changed to suit the new standard. Secondly, the information in each line must be redistributed to the time scale of the

new line system. This would involve, for instance, stretching a 64 μ s "625" line into a 96 μ s "405" line.

As a simple example the reduction of the number of lines by a factor $\frac{3}{4}$ may be considered as shown in *fig.15*. This conversion is done simply by discarding every fourth line of the field. However, when the lines are now displayed on the new system they will be distributed as shown by the dotted lines. An originally straight inclined row of picture elements *A, B, C, D, E, F, G, H* will thus appear as a discontinuous line *a, b, c, e, f, g*.

Moreover the process of discarding the fourth line, which contains picture element *D*, must not result in the loss of the information contained in this line. This is avoided by correcting each of the remaining lines with information from the adjacent lines, suitably weighted in magnitude as shown in *fig.16*. Output line 1 is reproduced as before; output line 2 however is displayed between input lines 2 and 3 and thus contains information from line 2 (e.g. *B* displayed at point *b₁*) and information from line 3 (point *c₁*). Output line 3 similarly contains both information from input line 3 (*c₂*) and from input line 4 (*d₁*). In this way interpolation is achieved which results in a reduction of the original distortion of the inclined row of points at the expense of some loss of horizontal definition.

In the process described by Lord and Rout it is proposed that a one-line delay should be used to permit the required interpolation to be performed. This system is illustrated in *fig. 17*. The input signal is split into two parts. One part is fed into a one-line delay; the other is multiplied by an "interpolation function" *F* and is fed into one input of an adder.

¹⁵ J. Haantjes and Th. G. Schut, A line converter for the international exchange of television programmes, Philips tech. Rev. 15, 297-306, 1953/54.

¹⁶ A. V. Lord and E. R. Rout, I.E.E./I.R.E. Int. Telev. Conf., London, June 1962.

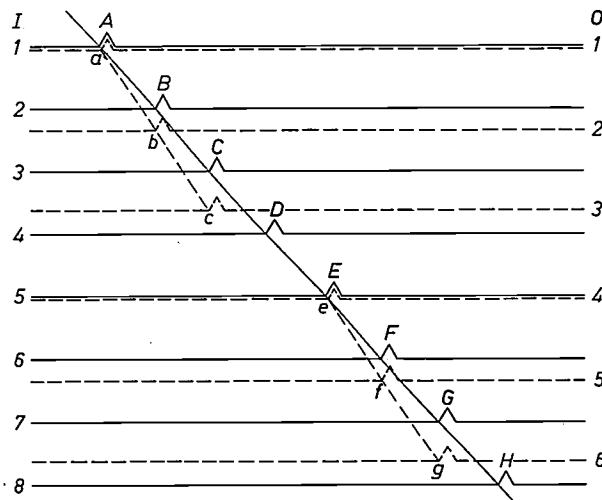


Fig. 15. Standards conversion by simply discarding (or adding) picture lines. In this diagram the number of picture lines is reduced by a factor $\frac{3}{4}$ by discarding every fourth line. *I* numbering of input lines, *O* numbering of output lines. An originally straight diagonal row of picture points *ABCDEFGH* is thus transformed into the zigzag row *abcefg*.

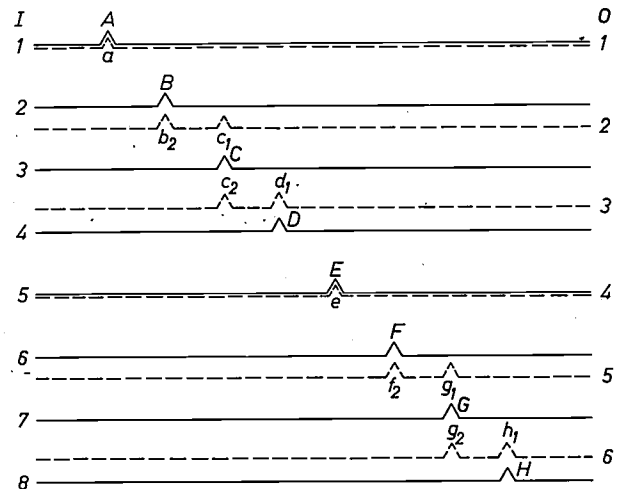


Fig.16. Standards conversion with interpolation. This process differs from that shown in *fig. 15* in that each of the remaining picture lines on the new system is corrected with information from the adjacent lines suitably weighted in magnitude. Thus no picture information is lost and the resultant distortion is reduced.

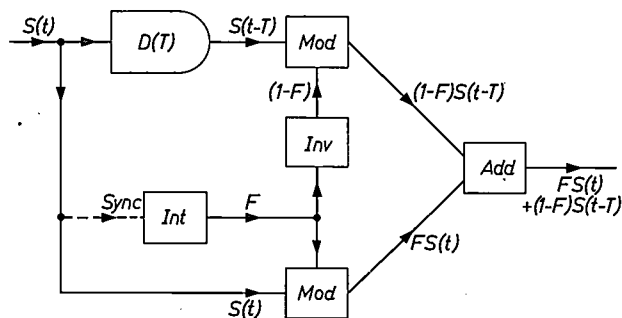


Fig. 17. The interpolation described in fig.16 may be performed using a delay line as shown. The delay is equal to one input line period T . The value of the interpolation function F produced in the generator *Int* (which is synchronised with the line frequency of the input video signal) at any time determines the proportion of information from each input line present in the resultant output line. *Mod* modulators, *Inv* inverter, *Add* adder.

In this unit the signal is combined with that corresponding to the previous line of the field which, after passing through the delay line, is multiplied with the complement of the interpolation function $(1-F)$. The output of the adder is the interpolated signal on the new line system which must now be converted to the new line period.

The value of the periodic interpolation function F at any instant determines the proportions in which the information from each of the two adjacent input field lines is combined to produce the resultant line. For example, when F is 0.3 then 30% of the resultant signal consists of information from the input line $S(t)$ and 70% of information from the previous line $S(t-T)$. In the simple example under consideration F must have a period equal to four input lines since every fourth line is discarded. In practice the interpolation function will be of sawtooth form.

The one-line delay proposed may conveniently consist of a variable mercury delay line of the type previously described if it is required to adjust the delay to compensate for variation of the mains frequency, or a fused-quartz line if the system is synchronised to a crystal controlled frequency.

It is possible, though by no means certain in the case of moving images, that a more satisfactory result would be obtained if the interpolation were performed using, not adjacent lines in the field, but adjacent lines in the picture. For this case a one field period delay would be required and the 20ms quartz delay line system previously described could be used in this application.

The remaining process in the conversion is the expansion of each of the selected lines to the line period of the new system. This may be achieved by feeding the information contained in the picture line into a storage system, such as an analogue computer store, and reading it out again at a rate determined

by the output line period. The computer store might employ magnetic tape as the storage medium. Alternatively, this store might consist simply of a series of capacitors, one for each element of the picture line¹⁷). For reading-in and reading-out, two electronic rotary switches are provided, each with a number of contacts equal to the number of picture elements (and capacitors). During one input line period the input switch arm rotates steadily to charge each capacitor with a charge proportional to the signal amplitude of the appropriate picture element. The output switch arm "samples" the charge on all the capacitors in a total time equal to the output line period.

This line stretching may, however, also be performed by a combination of ultrasonic delay line techniques and optical picture handling such as the "Scophony" receiving system previously described. In that system a rotating mirror was provided in order to prevent a continuous progression of picture points across the screen. By adjusting the speed of rotation these points may be made to pass a photosensitive device, e.g. a photomultiplier, at any desired rate, and thus the input signal may be reconverted into an electrical signal, the duration of the output signal corresponding to one input line being adjustable to any required value.

In practice, the system used would be somewhat different from the "Scophony" receiver: a more linear conversion of electrical signal into optical modulation may be obtained if use is made of the photoelastic properties of fused quartz to effect the required conversion¹⁸). A fused quartz bar, under the influence of a stress, will produce rotation of the plane of polarisation of polarised light passing transversely through it; this property is frequently used as a method of stress analysis. If such a bar is placed between two crossed polarisers then, in the absence of stress, no light will pass through the system. If stress is present in the bar, however, then light which has passed through the bar will have a component polarised in the plane of the analyser, and this will be received by the photomultiplier. Thus a video signal applied to a transducer bonded to the bar will result in a video frequency modulation across a beam of light transmitted.

The system just described would however have a square law response, because a stress of either sign would allow light to pass through. To give the required linear characteristic, optical bias to a state

¹⁷ P. Rainger, I.E.E./I.R.E. Int. Telev. Conf., London, June 1962.

¹⁸ C. F. Brockelsby, J. S. Palfreeman and R. W. Gibson, British patent applied for.

mid-way between extinction and full transmission is provided by including an optical quarter-wave plate. A certain amount of light is then transmitted when there is no stress in the bar, and it is this amount which is modulated when a video signal on a carrier is applied to the transducer.

A complete line stretching system using a photoelastic delay line is shown in *fig. 18*. The input signal

applied to the delay line causes an amount of light to be transmitted through the system whose local intensity depends on the signal amplitude present in the delay line at any point. As in the "Scophony" receiver, the delay line is imaged on a screen by a lens system; at one point on this screen a slit allows the incident light to fall on a photomultiplier. The speed of the rotating mirror is adjusted so that the picture elements of a complete picture line will pass across the photomultiplier slit in a time equal to the output line period. In this way the required time expansion of the picture line may be achieved. In view of the very high rate on information handling required, such a system may prove more attractive than one using a computer store.

It would be possible to dispense with the rotating mirror and to use instead a moving light source. This source might conveniently consist of a spot of light on the screen of a cathode ray tube, although in practice a vertical line of light would be used to reduce phosphor noise and screen burn. By electronically sweeping the spot (or the vertical line) across the screen in a horizontal direction at an appropriate speed, the picture points may be made to pass the photocell at the required rate.

Alternatively the moving light source might be produced by using a second photoelastic delay line, in which a single pulse is travelling, to "gate" part of a parallel beam of light. By using an optical system of appropriate magnification, an image of this moving source may be made to scan the original delay line at the correct rate and thus produce the required change of time scale.

Since rotating mirrors are difficult to synchronise at high speed, both these electronically controlled

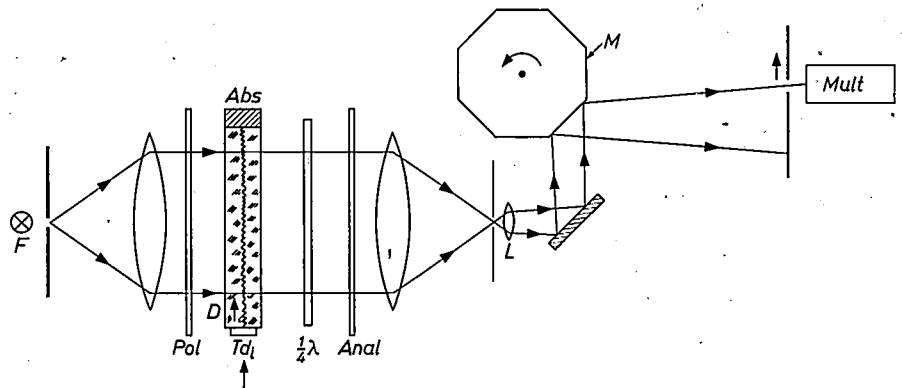


Fig. 18. Line stretching in systems conversion. The system illustrated is similar to the "Scophony" receiver shown in *fig. 8*. A solid photoelastic delay line is used in conjunction with a polariser (*Pol*), analyser (*Anal*) and $\frac{1}{4}\lambda$ -plate, and the speed of rotation of the mirror *M* is adjusted so that the picture points corresponding to each input line move across the slit of the photomultiplier (*Mult*) in a time equal to the desired output line period.

scanning systems offer considerable practical advantages.

The rather sophisticated combination, in this last instance, of several delay lines for interpolation and for a mechanical change-of-rate via optical scanning seems to us a fitting conclusion of this review of delay-line applications in television.

Summary. In ultrasonic delay lines use is made of the low velocity of mechanical waves in solids and liquids to effect a delay of wide-bandwidth electrical signals for times ranging from a few microseconds to several milliseconds. An ultrasonic delay line consists of three components: an input transducer which converts the electrical signal into an identical mechanical wave; the delay medium; and an output transducer which converts the mechanical wave back into an identical electrical signal (whose frequency is usually much higher than 20kc/s — hence the name "ultrasonic"). Ultrasonic delay lines fall into three categories, using wire, a liquid and an extended solid respectively as the delay medium. In general only solid and liquid lines are used in television applications. When a delay of one picture line period is required a mercury delay line can be used; when a delay of one field period is needed a fused-quartz delay line is better. Wafers of crystalline quartz or of a ferroelectric ceramic are used as transducers for solid and liquid delay lines. It is important that the transducers should be of sufficient size to transmit and receive mechanical signals mainly over narrow ranges of angle. Low-*k* transducers should be matched in mechanical impedance to the delay medium. For high-*k* transducers electrical adaptation to the input and output networks is more difficult to calculate. A table of the characteristics of some typical delay lines is given in the text.

Applications of ultrasonic delay lines in the field of television are described. The earliest application was in the "Scophony" receiver where the variations in density of water accompanying a mechanical wave were used to modulate the intensity of a light beam across its width and to provide the display. A delay of one field period has been used to correct for the effects of smear in the vidicon television camera tube. A delay of one line or one field period may be used to provide correction of "vertical aperture distortion" in television camera tubes. A delay line of one line period delay is incorporated in a receiver for the "Secam" and "PAL" systems of colour television. A variable mercury delay line has been used to simulate the effects of reflections from aircraft on television reception. Finally, it has recently been proposed to use one or more delay lines in a system providing synchronous conversion between two television line systems, e.g. from 625 to 405 lines per picture.

Philips Technical Review

DEALING WITH TECHNICAL PROBLEMS
RELATING TO THE PRODUCTS, PROCESSES AND INVESTIGATIONS OF
THE PHILIPS INDUSTRIES

NEW FORMS OF BEARING: THE GAS AND THE SPIRAL GROOVE BEARING

by E. A. MUIJDERMAN *).

621.822.5-621.892.9

- I. THE CONTACTLESS BEARING PRINCIPLE
- II. GAS BEARINGS
- III. SPIRAL GROOVE BEARINGS

Although the use of oil to counteract friction was known to the Ancient Egyptians forty centuries ago, the idea of substituting air for lubricating oil was not conceived until the second half of the 19th century. This suggestion, put forward by Hirn, was not taken up immediately, and could not be taken up until certain prerequisites had been fulfilled. One necessary condition was the development of a new form of bearing, the contactless bearing. Part I of the article which follows explains the principles on which the contactless bearing is based.

For more than half a century all practical types of contactless bearing were lubricated with oil or other liquids. The development on a large scale of air or gas bearings (Part II) which worked on the same principles, and which were first demonstrated by Kingsbury in 1897, began round about 1950. They are now being employed in nuclear reactors, turbo-jet engines and gyroscopic compasses, in the textile and food industries, and in dentists' drills.

In Part III of the article, having sketched in a background of these quite recent developments, the author goes on to describe a further innovation — the spiral groove bearing. This opens up new possibilities not only by reducing coefficients of friction but also by permitting a reduction in the size of the bearing. Amongst the topics discussed are a spherical-type spiral groove bearing which has a diameter of only 3 mm.

I. THE CONTACTLESS BEARING PRINCIPLE

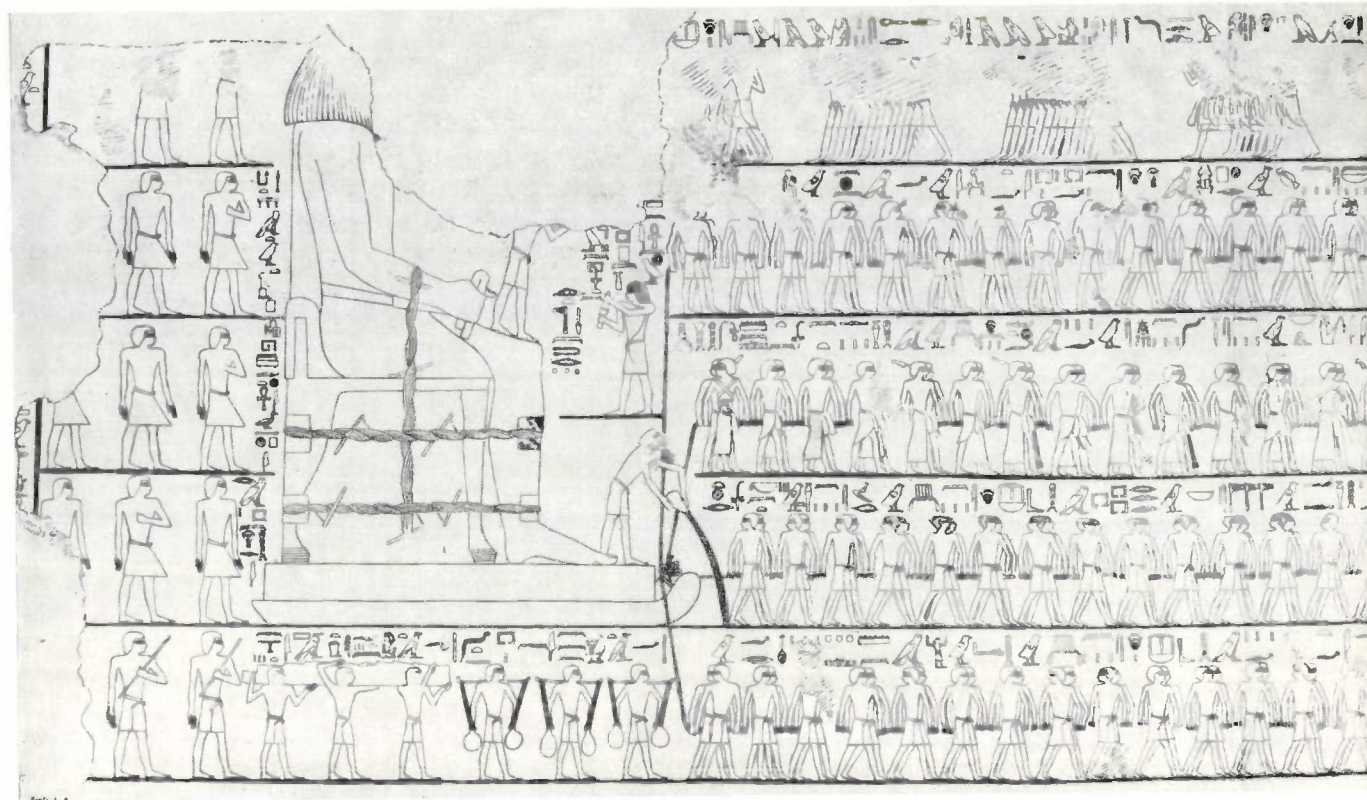
The rotation of a shaft or spindle in bearings involves friction and wear which, for obvious reasons, must be kept within bounds by some means or other. A common practice is to use oil as a lubricant (*fig. 1*); alternatively, the shaft can be allowed to turn in ball-bearings (*fig. 2*). This does not exhaust the possibilities, and in the present article we shall be concerned with bearings which, essentially, rely on a clearance being maintained between the shaft and the surface of the bearing oil or any one of a whole range of other fluids being used as separating medium.

The oldest representative of this class is the

oil-lubricated *journal bearing*. In 1883 Tower discovered that its good properties were not just a consequence of oil lubrication, as had been thought. One can regard the journal bearing as a forerunner satisfying the conditions for maintaining the clearance between the surface of the shaft and the bearing before these conditions were recognized. Present-day understanding of these conditions makes it possible to design a great variety of bearings in which separation of the shaft and bearing surfaces is a fundamental feature. Our proposed name for the whole class is "contactless bearings".

Magnetic bearings, in which the spinning shaft is supported by magnetic fields, must also be included in the contactless class. These bearings, which can be used for certain specialized applications, have

*) Philips Research Laboratories, Eindhoven.



already been dealt with in this review¹). Here it is only proposed to discuss contactless bearings in which a viscous fluid separates the bearing from the shaft or spindle (full-film lubrication). Either a liquid or a gas can be used for this purpose; a gas, after all, also possesses viscosity, if only to a small degree. In the present article a particular point will be made of going rather more fully into gas lubrication, which is being employed on an increasing scale in all kinds of applications²).

"Hovercraft" in motion are supported on an air-cushion that separates them from the surface of the earth or the sea. Separation is achieved by virtue of inertial forces set up in the medium, and does not depend on viscosity forces as in the case of the contactless bearings just referred to. Surface-separating effects in which viscosity forces play the major part can only be obtained with very small clearances.

The *spiral groove bearing* is a recently developed type in which either a liquid or a gas, or even grease, will act as separating viscous fluid. The merits of the new type can only be stated very summarily in this introductory account. Its outstanding features are the low coefficients of friction that can be achieved

with it, and the small dimensions it can be given. For example, cheap, highly wear-resistant and almost frictionless spiral groove bearings have been made that have a diameter of only 3 mm. To get a really clear idea of the properties of the spiral groove bearing, we must consider it against the background of contactless bearing properties in general.

Two categories will now be discussed in turn: contactless bearings with an external pressure source ("pressurized bearings"), and "self-acting" contactless bearings. Since spiral groove bearings fall into the latter category, it will be accorded all the greater attention.

Contactless bearings with an external pressure source

At the Industrial Exhibition held at Paris in 1878, it was shown how a heavy object could be moved almost frictionlessly over a smooth steel base-plate. The object had four legs which rested on the base-plate in the manner shown schematically for one leg in *fig. 3a*. To create a clearance between the base-plate and the sliding block, which was carrying its share of the overall weight of the object, it was necessary to build up sufficient pressure in the lubricant between the block and the plate by means of a pump. Creating a strong enough *upward thrust* (or "lift") is no problem, but the requirement of *stability* also has to be satisfied: if the clearance (or layer thickness) h changes, then forces opposing the

¹) F. Th. Backers, A magnetic journal bearing, Philips tech. Rev. 22, 232-238, 1960/61.

²) One of the first publications having an important bearing on present-day gas lubrication practice was G. W. K. Ford, D. M. Harris and D. Pantall, Proc. Inst. Mech. Engrs. 171, 93, 1957.

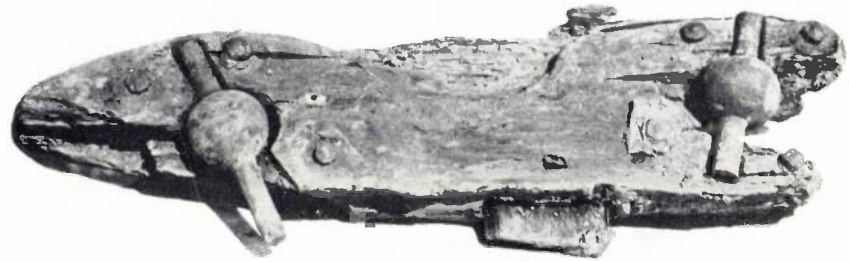


Fig. 2. Remains of a ball bearing found in one of two Roman ships that were raised round about 1930 out of the lake of Nemi. On the evidence of coins and inscriptions discovered in and near the ships it is fairly certain that they were built by the emperor Caligula (about 40 A.D.) and that they sank during the time of Nero. This 4.5 cm diameter ball bearing seems to have helped to support a turntable. The load was at the same time borne by the shafts, so strictly speaking this was a forerunner of the modern ball bearing rather than an early example of it.

The ships, which were housed in a special museum, were entirely destroyed by fire during the fighting that took place in the outskirts of Rome in 1944. See G. Ücelli, *Le navi di Nemi*, Libr. dello Stato, Rome 1950, p. 191 et seq., from which book the above photograph has been reproduced, with the permission of the author.

Fig. 1. Egyptian tomb painting dating from about 1650 B.C. A slave is pouring oil in front of a sledge bearing a statue of Pharaoh Tehuti-Hotep. Three porters carrying flasks of oil may be seen behind the slaves who are pulling the sledge. This is the oldest known picture representing the use of oil as a lubricant. (Reproduced from P. E. Newberry, *Archaeological Survey of Egypt, El Bersheh, Part I, The tomb of Tehuti-Hotep.*)

change must arise, with the result that the clearance remains more or less constant.

Stability might be obtained by employing a pump giving a constant output (e.g. a gear pump). When the clearance h decreases, the flow resistance of the gap increases, and if the pressure remains the same, less of the fluid will be able to escape from the gap (under laminar flow conditions, leakage is proportional to h^3). But this is impossible because the delivery rate is constant, so the pressure in the gap will increase and the gap will widen again.

Often, particularly where the fluid is a gas, pumps are employed that supply a constant pressure; that

is the case we are concerned with in fig. 3a. Here the same stabilization effect is obtained by inserting a flow restrictor r between the pump and the gap. Fig. 3b shows pressure distributions over the sup-

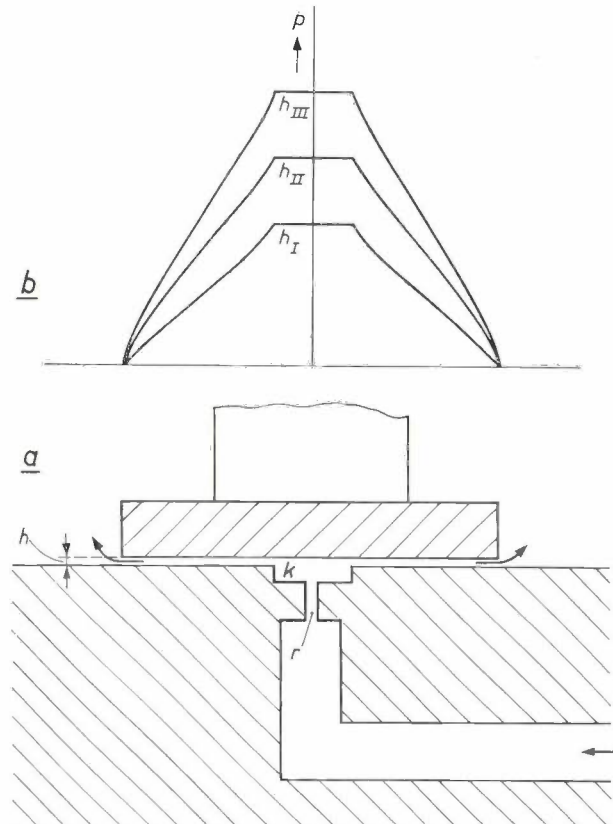


Fig. 3. (a) Principle of a contactless bearing with an external pressure source, the first application of which was in an exhibit called "le chemin de fer en glace" demonstrated at the 1878 Industrial Exhibition in Paris. This was a vehicle on "lion's feet" that was able to skim over a smooth steel surface. A pump working at a constant pressure forces a viscous fluid (which was oil in the "skating railway") through a constriction r , a chamber k and the gap (of height h) between the two surfaces to be separated, the fluid then escaping to the exterior. The constriction has a stabilizing effect, as will be clear from diagram (b).

(b) The pressure p in the gap as a function of place for three gap height values ($h_I > h_{II} > h_{III}$). Any reduction in the gap height gives rise to an increase in pressure over the whole of the base-line, and thus to forces opposing the decrease in h . (The above curves relate to the case where the supporting fluid is compressible, but the conclusion is equally valid for an incompressible fluid.)

porting surface at various values of the gap height h . As before, if the gap shrinks, the pressure inside it will increase. This can be explained on the analogy between the pressure fall-off over the base-plate surface and the potential drop along an electrical circuit consisting of a constant voltage source, a fixed resistor (the flow restrictor) and a variable resistor (the gap) connected up in series: if the variable resistance is increased, more of the available potential difference will appear across its terminals.

Self-acting bearings

In the second category of contactless bearings, the self-acting kind, the pressure is built up from *within* the bearing. There are various ways of generating this but we shall only deal with the most important, which is exploited in self-acting bearings based on the *convergence* or *wedge effect*.

Between the flat block and base-plate in *fig. 4* is a wedge-shaped space; if the block is kept at an angle to the base-plate and moved through a viscous fluid in direction U , the fluid forced under the block will build up a pressure on it. We shall assume for the time being that the fluid is incompressible and that the flow caused by the movement of the block is steady and laminar, and we shall neglect the effects due to the fact that the block has a finite breadth L . Suppose that the pressure in the gap is everywhere the same; if the block is moving through a fluid of density ρ at a velocity of U relative to the base-plate, the extreme layer thicknesses being h_1 at the front and h_2 at the back, then fluid will pass under the front edge at the rate of $\rho U L h_1 / 2$ volumes per unit time, and leave the wedge-shaped space via the rear edge at the rate of $\rho U L h_2 / 2$ volumes per unit time. But this does not satisfy the condition for continuity — more fluid is entering the space than

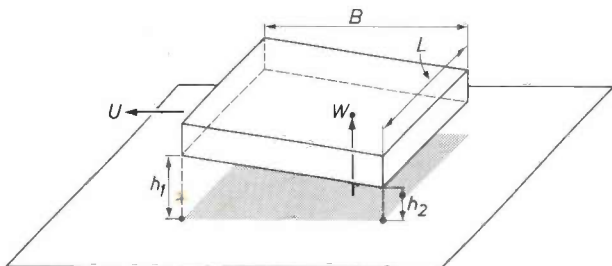


Fig. 4. To illustrate the principle of a self-acting bearing, based on the convergence or wedge effect. A flat block inclined to a base-plate in such a way that their opposed surfaces converge (in the case shown here, the gap in between is strictly cuneiform — a right triangular prism) is displaced through a viscous fluid at a velocity of U . Pressure thus builds up between the block and the base-plate with the result that a lifting force W is exerted on the block.

Movement of the block in the opposite direction would result in a fall-off in pressure in the gap, with the result that the block would be acted upon by a force opposite to W .

is leaving it. Pressures between the block and the base-plate must therefore build up in such a way as to produce a velocity distribution that will ensure that fluid enters and leaves the gap at the same rate (*fig. 5*).

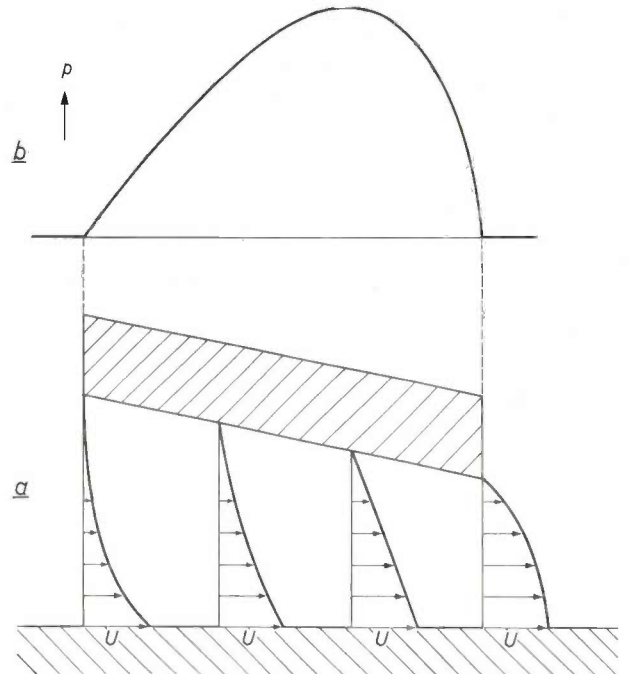


Fig. 5. (a) Velocity distribution and (b) pressure distribution in the incompressible viscous fluid filling the wedge-shaped space in *fig. 4*. The flat block is at rest and the base-plate is moving at a velocity U , dragging with it the fluid in the neighbouring boundary layer. The pressure is at a peak roughly half-way along the block, and at this point there is a linear increase in the velocity along a perpendicular drawn to the base-plate.

As has already been observed, the journal bearing was being used long before its essential mode of functioning was understood. We now know that the load on the spinning shaft causes it to lie somewhat eccentrically inside the journal bearing, so that the gap converges (*fig. 6*) in much the same way as the wedge-shaped space between block and base-plate. Provided the plain bearing is adequately lubricated the convergence effect will prevent the shaft from rubbing against the bearing bush. For a long time it was not understood why 19th-century journal bearings should be less subject to friction and show less wear than thrust bearings of the same period.

Tower cleared the way for an explanation of this fact when he discovered that the pressure in a journal bearing could (at points near the convergence) attain a local value considerably higher than that calculated on the assumption that the load was evenly distributed over the superficial area of the bearing. He became aware of this when he attempted to use a cork for stopping up a hole that had been drilled in

a journal bearing. Observing that the cork repeatedly worked itself out of the hole, Tower conceived the idea that it was under high pressure and that this might be the reason for the journal bearing's good properties. Experimental data on the pressure distribution in a journal bearing investigated by him, which were published in 1883/5, attracted wide notice. Amongst those whose interest was aroused was a theoretician, Reynolds, who succeeded as early as 1886 in explaining Tower's data in terms of the wedge effect we have just been discussing³⁾.

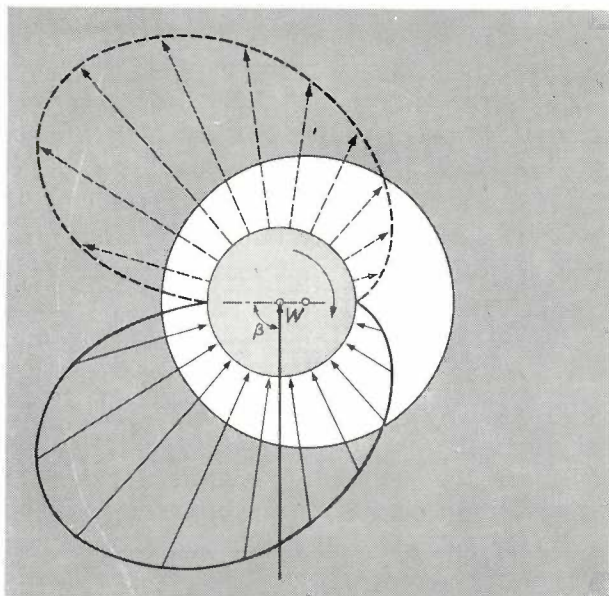


Fig. 6. Build-up of pressure inside a journal bearing lubricated with an incompressible fluid (schematic representation with bearing clearance greatly exaggerated). The fully-drawn arrows represent pressures above atmospheric, the dashed arrows pressures below it. Excess pressure arises where the bearing surfaces converge in the direction of shaft rotation; a fall-off in pressure occurs where they diverge.

The case to which the above diagram relates is the purely theoretical one in which the two pressure patterns are mirror images. In practice, the excess pressures generated are often much greater than the fall-off in pressure the latter being limited by the vapour pressure of the lubricating fluid. The non-symmetrical pressure build-up obtained in practice leaves the shaft in a different equilibrium position from that shown above, an angle β that is smaller than 90° being enclosed between the gravity vector and the line through the shaft centre and the points of closest convergence. The equilibrium position of the shaft is also dependent on the compressibility of the fluid. For a more detailed account of how pressure builds up in a journal bearing, reference should be made to the literature²⁾.

This newly acquired knowledge was to be applied about ten years later to thrust bearings. At that time attention was being devoted to the problem of taking up the reaction of the water on a rotating ship's screw, transmitted through the propeller shaft to the ship itself. The arrangement employed prior to 1898 consisted, in principle, of a flat circular plate parallel

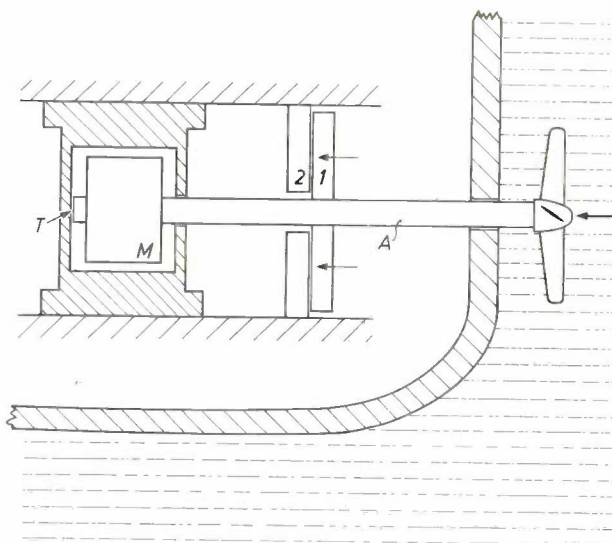


Fig. 7. A marine engine *M* drives the ship's screw via a long shaft *A* passing through a "tunnel" in the hull. The thrust exerted by the water on the screw, when this is turning, cannot of course be passed on to the hull of the ship by the bearing *T* supporting the crankshaft end in the engine housing. The thrust may amount to 150 or 200 tons, and it has to be taken up by a special bearing consisting essentially of a collar *1* which is fixed to the shaft and which presses against a stationary circular plate *2* built into the frame of the ship. The severe wear occurring in this type of thrust bearing led to the adoption of the Michell bearing.

to and bearing upon a similar fixed plate, the rubbing surfaces being lubricated with oil (fig. 7). Wear was considerable, and the load-carrying capacity was very poor. The idea of fitting one of the circular plates with a ring of pivoted blocks (fig. 8) occurred independently to Kingsbury (1898) and Michell (1905). Each

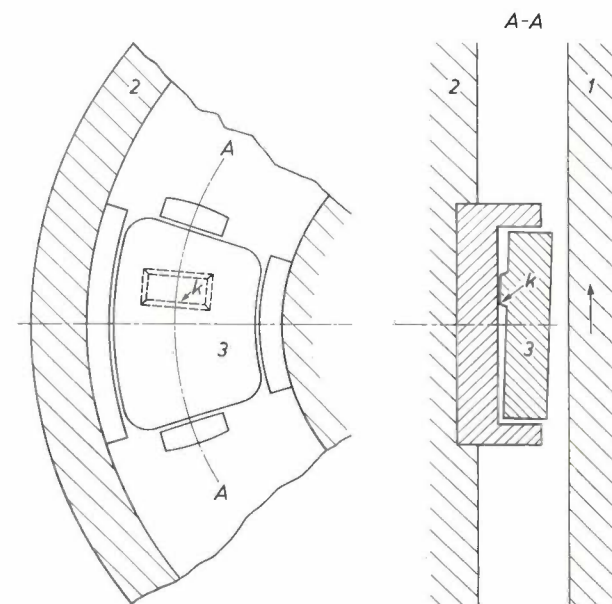


Fig. 8. The Michell bearing consists of a plane collar *1* and a circular plate *2* around whose edge are fitted slipper blocks *3* able to tilt about a pivoting edge *k*. The pivoting edge is given a position such that each block automatically adjusts itself for maximum load-carrying capacity (see the literature⁴⁾²⁰⁾ referred to in the text).

³⁾ B. Tower, Proc. Inst. Mech. Engrs. **34**, 632, 1883; **35**, 29, 1884; **36**, 58, 1885. O. Reynolds, Phil. Trans. Roy. Soc. **177A**, 157, 1886.

block introduces a wedge-shaped constriction into the space between the plates. If the pivoting ridge is correctly placed the pad will automatically take up a position such that, under the conditions prevailing, the bearing has optimum load-carrying capacity. In this way it is possible to create a complete clearance between the plates, even when they are subject to strong compression. Known as a Michell bearing⁴⁾ in Europe, this type is generally referred to in America as a Kingsbury bearing.

The *step bearing*, another contactless thrust type, is of later date and rather simpler construction. Here rectangular ridges serve to bring about the constriction that is an essential feature of contactless bearings. Although the space between the plates is not wedge-shaped in the true sense of the word, any more than it is in the spiral groove bearing that will be discussed below, the convergence effect is achieved just the same. These differences in construction involve no fundamental change in the principle. We can therefore quite reasonably study the wedge configuration in fig. 4 for the purpose of gaining some insight into the basic properties of the self-acting bearing.

By integrating the pressure built up in the gap over the inclined surface, whose length is B , we obtain the lift W exerted on the inclined block:

$$W = \frac{C_1 \eta U B^2 L}{h_2^2}, \dots \dots (1)$$

where η is the viscosity and C_1 , to a first approximation, is a function of h_1/h_2 alone. The quantities h_1 , h_2 , U and L have already been defined. When a set of such blocks is incorporated in a thrust bearing, the total lift or load-carrying capacity of the bearing can be arrived at by treating B as the sum of the average tangential length of all the blocks. (If end effects are taken into account, which means allotting L a finite value, it will be found that C_1 also depends to some extent on the $L : B$ ratio.) The frictional force F in the same bearing is:

$$F = \frac{C_2 \eta U B L}{h_2}, \dots \dots (2)$$

where C_2 is likewise a function of h_1/h_2 alone. We shall refer to C_1 and C_2 as the bearing coefficients. The bearing will adjust itself to a value of h_2 , the smallest layer thickness, that is dependent on operating conditions, i.e. the speed U and the load or required load-carrying capacity W . If the blocks are rigidly mounted on the shaft or bearing the difference between h_1 and h_2 will remain constant, so that if h_2

changes, the h_1/h_2 ratio and the bearing coefficients C_1 and C_2 will change too. If the blocks are pivoted, as in the Michell bearing, shown in fig. 8, h_1/h_2 can remain constant whatever the inclination of the block.

The ratio between frictional force and load-carrying capacity, $f = F/W$, is called the coefficient of friction of the bearing because it has much the same significance as the familiar coefficient of dry friction. It follows from (1) and (2) that

$$f = \frac{C_2}{C_1} \frac{h_2}{B}, \dots \dots (3)$$

which indicates, perhaps rather surprisingly at first sight, that the friction coefficient of a bearing does *not* depend on the viscosity of the lubricant used e.g. oil or air.

The following formulae, analogous to (1) and (2), can be derived for a *journal bearing*, of radius r , in which a shaft is spinning with an angular velocity ω :

$$W = \frac{K_1 \eta \omega r^3 L}{(\Delta r)^2}, \dots \dots (4)$$

$$P = \frac{K_2 \eta \omega^2 r^3 L}{\Delta r}, \dots \dots (5)$$

The quantity P given by the second formula is the rate at which energy is dissipated by friction; Δr is the uniform clearance around the shaft when it is in the exact centre of the bearing bush. Since the situation is slightly different from that in the thrust bearing, we have different bearing coefficients to deal with, K_1 and K_2 . These depend, amongst other things, on the degree to which the shaft sinks into the lubricating film, or in other words on its eccentricity with respect to the bearing bush. The eccentricity of the shaft is analogous to gap height h_2 in the thrust bearing. (If end effects are taken into account, L being allotted a finite value, K_1 and K_2 are found to be dependent, in addition, on the ratio r/L .) Like h_2 , the shaft eccentricity adjust itself to a value dependent on operating conditions; again depending on operating conditions, the bearing coefficients vary over ranges whose extreme values, in practice, may differ by a factor of about 5.

Some important conclusions can be drawn directly from the above formulae.

From either (1) or (4) we can see that the shaft speed must exceed a certain minimum if a self-acting bearing is to develop any load-carrying capacity. Inevitably, then, starting from rest will involve wear, an important factor that will be discussed at greater length in Part II. We can further infer from (4)

⁴⁾ See for example G. Vogelpohl, *Betriebssichere Gleitlager*, Springer, Berlin 1958,

that in so far as it is possible to reduce the diametral clearance ($2\Delta r$), doing so will allow the desired load-carrying capacity to be achieved at a lower speed. The implication is that very narrow bearing clearances can be a vital requirement, particularly where the lubricant is air (which has a small η). For one special application, American engineers went so far as to design and build a journal air bearing in which the diametral clearance around the shaft was only $0.6 \mu\text{m}$ ⁵). That the demands on technology and materials are extreme in such a case (the only suitable materials are ceramics) will be obvious. It is partly on that account that work on air bearings did not really get into its stride until about 1950.

Formula (1), as it stands, is not entirely valid for very high shaft speeds. In a thrust bearing under a certain constant load, an increase in shaft speed will not in the first instance involve any change in the pressure built up in the bearing because the smallest layer thickness h_2 will increase accordingly, automatically adjusting itself to the required load-carrying capacity. But in practice h_2 can only widen to a limited extent, seeing that normally a shaft is

held in *two* thrust bearings. Once h_2 has reached this limit, any further increase in shaft speed will involve an increase in bearing pressure and give a surplus of load-carrying capacity, which is of no use, but which will result in increased friction in accordance with formula (2).

Much the same applies when the speed of a shaft in a journal bearing is increased, though the implications are not quite so evident in formula (4). As has already been explained, the shaft adapts itself to a given load by assuming a certain degree of eccentricity with respect to the bearing bush, this being associated with a K_1 value such that the bearing develops exactly the required load-carrying capacity. The higher the speed, the smaller will be the degree of eccentricity and the value of bearing coefficient K_1 , but a limit is reached once the shaft has come to lie dead-centre in the bearing. If the speed is further increased, K_1 will remain constant and surplus load-carrying capacity and increased friction will again be the result.

The themes developed so far will be taken up again at an early point in Part II of this article.

II. GAS BEARINGS

Air versus oil

In Part I an attempt has been made to explain the principles which enable an air or gas bearing to function. Before these forms of bearing are examined more closely it is natural to inquire what are the advantages of using air or some other gas as lubricant in a contactless bearing.

Oil was the lubricant in an application of the contactless bearing principle exhibited in Paris in 1878. The oil pumped under the sliding blocks had to be collected in a tank and recirculated. It is interesting to compare this contrivance with a very similar one now being used for a purpose of which nobody in 1878 is likely to have had any inkling. The allusion is to a space flight simulator (*fig. 9*). Here the lubricant is air which is pumped under the supporting pads. One convenient feature of air as a lubricant is immediately obvious: it can simply be allowed to escape into the surrounding atmosphere; it does not need to be collected or circulated; and the user has no need to worry about the lubricant gradually getting dirty, and about the complications this normally gives rise to. This property of air was pointed out by Kingsbury as early as 1897, when he

was demonstrating an air-lubricated journal bearing⁶): "The atmosphere furnishes a bath of the lubricant, thus maintaining a constant supply of constant quality". Contamination of the lubricant is one problem, contamination of its environment by the lubricant is another: the latter danger, which persists despite all the ingenuity the designer may devote to making his bearings leak-proof, rules out the use of oil in machinery for processing food, for example, or for manufacturing textiles or other materials that would be spoilt by contact with oil. In such cases air lubrication is clearly the method of choice.

There are other cases in which oil lubrication is unsuitable for purely practical reasons, and in which the gas bearing offers a way out of the difficulty. Examples are machines whose bearings must work at very low or very high temperatures, temperatures at which oil would congeal or break down chemically. Cases of this kind will be referred to in the section on typical applications of gas bearings.

In addition, however, we may point out that a big advantage of gas as compared with oil lubrication, predictable on purely theoretical grounds, is the fact that gas bearings are inherently more suitable for

⁵) The bearing was developed by the Minneapolis-Honeywell Regulator Company; see *Machine Design* 32, no. 13, p. 39, 1960.

⁶) A. Kingsbury, *Experiments with an air-lubricated journal*, *J. Amer. Soc. Naval Engrs.* 9, 267-292, 1897.

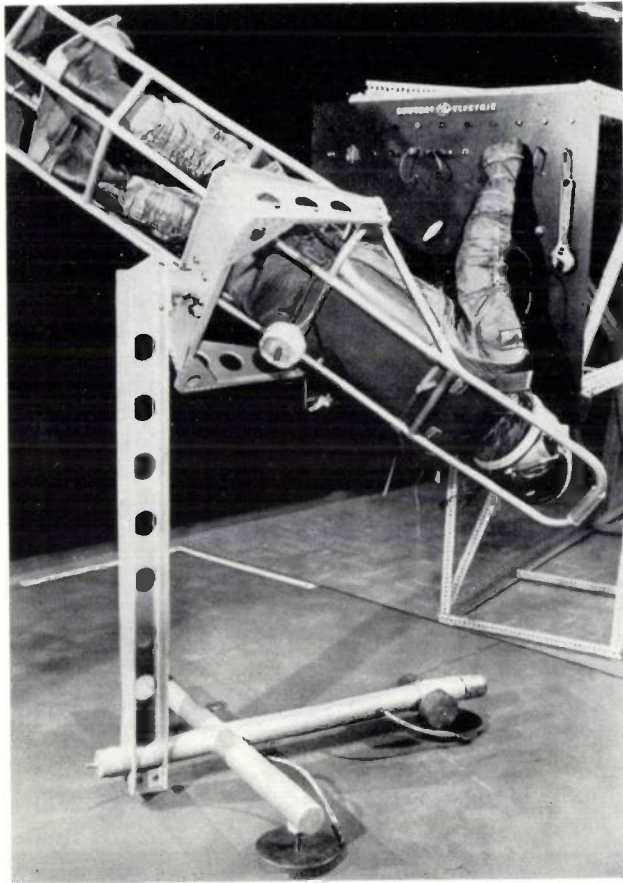


Fig. 9. Space travel simulator built by General Electric. The trainee astronaut is strapped into a frame mounted in a universal joint and supported on air-lubricated pads which glide almost frictionlessly over the floor (the principle being exactly the same as that of the "skating railway" exhibited at Paris in 1878). The simulator is used for investigating one of the consequences of weightlessness, namely the absence of friction. Normally, friction is an aid to locomotion and other bodily movements. In the appliance shown here, movement of any part of the body results in displacement of the rest of the body in the opposite direction. It appears to be possible to perform maintenance routines in these circumstances, but the work raises the subject's oxygen consumption to 30% or 40% above normal.

very high shaft speeds. This property is bound up with the limitations on eccentricity and smallest layer thickness that were pointed out in the final paragraphs of Part I. A shaft whose speed is continuously increased will finally take up a position exactly central with respect to the bearing (similarly, in the case of a thrust bearing, a point will be reached at which h_2 cannot widen any further). If the speed is still further increased the bearing will develop excess load-carrying capacity, and the frictional losses P will soon become prohibitive. An obvious remedy would be to reduce the radius r and/or the length L of the bearing by an amount such as to cancel out the surplus load-carrying capacity. But if the bearing cannot be redimensioned without a dangerous loss of mechanical strength, the only way of overcoming dead-centre running will be to switch

to a lower-viscosity lubricant. In a manner of speaking, oil is too good a lubricant, since its load-carrying capacity at high speeds is too great. Formula (5) reveals that by using air, whose η is roughly 10 000 times smaller than that of oil, it is possible to increase the shaft speed by a factor of 100 or the dimensions of the bearing by a factor of 10 without any change in frictional losses, provided other conditions likewise remain the same. In reality, comparing air with oil is not quite so straightforward because it is normal to design gas bearings for smaller film thicknesses; but this does not detract from the general validity of the above conclusion and we shall see that fast shaft speeds are a prominent feature in typical applications of the gas bearing principle.

Comparison between self-acting and externally pressurized gas bearings ⁷⁾

The self-acting gas bearing differs from the externally pressurized type in being of simpler design and having greater reliability (since the supply of gas under pressure cannot break down). Another big difference between the two categories concerns their starting characteristics. As has already been pointed out, formulae (1) and (4) show that a self-acting bearing cannot develop a load-carrying capacity at zero shaft speed; the lift increases with speed, linearly to begin with. Shaft speed, in the first instance, has no influence on the load-carrying capacity of bearings of the other type; this is merely a matter of the pressure provided by the pump. In the self-acting bearing, then, starting produces wear, and it is only when the shaft has attained a certain speed that the clearance between the bearing surfaces is large enough to reduce friction and wear to the desired low levels. This means, firstly, that self-acting bearings must be made of hard, wear-resistant materials ⁸⁾, and secondly, that they must be designed in such a way that separation between the bearing surfaces occurs at the lowest possible shaft speed. As already stated, American engineers, with these aims in mind, have made bearings fitted with ceramic bushes and having a diametral clearance of only 0.6 μm .

Obviously, because their load-carrying capacity depends on shaft speed, self-acting bearings will be less suitable in cases where a low speed is desired, or where the shaft speed is subject to wide variations.

⁷⁾ In dealing with liquids, we have to remember that they are far less compressible than gases. With that reserve, much of what is said here would apply equally well to contactless bearings lubricated with liquids.

⁸⁾ This consideration is not of such great importance in oil-lubricated bearings since, under starting conditions, there is always a thin film of oil to provide "boundary lubrication" and so reduce friction and wear to some extent.

The two classes cannot be further compared without taking the *compressibility* of the working fluid into account.

Limits to load-carrying capacity

Formula (1) was derived for a wedge-shaped gap through which, it was assumed, an *incompressible* fluid was passing. The condition for continuity, we said, was that no difference $\rho ULh_1/2 - \rho ULh_2/2$ should exist between the quantity of fluid entering and the quantity of fluid leaving the gap. We also assumed that such a difference was prevented from arising by a build-up of pressure in the gap, this build-up being responsible for the lift exerted on the underside of the block. Any change in the density ρ of the fluid was not taken into account. Now, what happens if there is in fact such a variation? Then the extra lift obtained by increasing the relative speed of the surfaces will fall off steadily with each increment of velocity because of the density variation involved, till a limit is reached at which it is *only* the density variation that is preventing a difference from arising between the quantities of fluid entering and leaving the gap. In this limiting case, then, speed has ceased to play any part in building up pressure (and so has viscosity). *Only the pressure p_i of the surrounding atmosphere is of importance in the limiting case.* A straightforward calculation⁹⁾ shows that in these circumstances the pressure in the gap approaches

$$p_{\max} = p_i \frac{h_1}{h_2} \quad \dots \dots \dots (6)$$

Thus the load-carrying capacity of a self-acting bearing is limited; but that of an externally pressurized bearing can always be increased, simply by stepping up the pump pressure.

For reasons like these, self-acting bearings are most likely to be used, in practice, for taking up relatively light loads, whereas a bearing with an external pressure source will often be the best solution to the problem of taking up a relatively heavy load.

Compressibility is not the only factor limiting the load-carrying capacity of a self-acting bearing. Other limitations come into play in cases where the gap height or clearance is of the same order as the mean free path of the gas molecules. A gradual transition from viscous to inertial flow at high shaft speeds may also have the effect of limiting capacity; this change in flow conditions is liable to occur in externally pressurized as well as in self-acting bearings, though in practice it does not limit the capacity of bearings in the former class. These pheno-

mena, which assume some importance in extreme cases, cannot be gone into here, and the reader is referred to the literature on the subject⁹⁾¹⁰⁾¹¹⁾.

Limits to stability

Mention of the instability phenomena to which contactless bearings are liable takes us into a difficult field which is still far from being fully explored. Because of their great importance we must touch upon these phenomena in passing, but for a fuller study the reader must consult the literature⁹⁾¹¹⁾.

In the simplest possible terms, a contactless bearing can be regarded as a damped system possessing mass and springiness. A system of this kind has a natural frequency which, according to a well-known formula, is roughly equal to the square root of its stiffness/mass ratio. A periodic disturbance — consequent on rotor unbalance in the case of a journal bearing, for example — will set the system into forced vibration. In the case of the unbalanced journal bearing, the frequency of the vibration will be equal to the rotor speed in r.p.m. If this happens to be the same as the natural frequency of the system, resonance effects will occur. In general, designers try to obviate such resonances by giving the bearing a natural frequency high above that of any possible disturbing effect, or ensuring that it will pass quickly through the range of critical frequencies.

The system may also get into a state of *self-sustained vibration* which is due, not to any lack of balance, but to the particular way the stabilizing force varies as a function of the layer thickness. In a radial self-acting bearing which is running dead-centre — a state of affairs that is undesirable for this as well as for the previously mentioned reason — the variation in question may give rise to what is known as “half-speed whirl”. This is a dangerous and destructive phenomenon in which the shaft axis whirls around the centre-line of the bearing at a speed approaching half the angular velocity of the shaft, its distance from the centre-line gradually increasing. The shaft may thus start chattering in the bearing. Both journal and thrust bearings in the externally pressurized type may be subject to a similar kind of vibration if the gap height or the volume of the “chamber” (see fig. 3) is large. The latter phenomenon, which is comparable with all known forms of relaxation vibration, is termed the “air hammer” (because air hammers are based on that particular kind of vibration).

¹⁰⁾ Gas lubricated bearings, a critical survey, U.S. Dep. Commerce, Office of Technical Services, 1958.

¹¹⁾ O. Pinkus and B. Sternlicht, Theory of hydrodynamic lubrication, McGraw Hill, New York 1961.

⁹⁾ See for example W. A. Gross, Gas film lubrication, Wiley, New York 1962, p. 64.

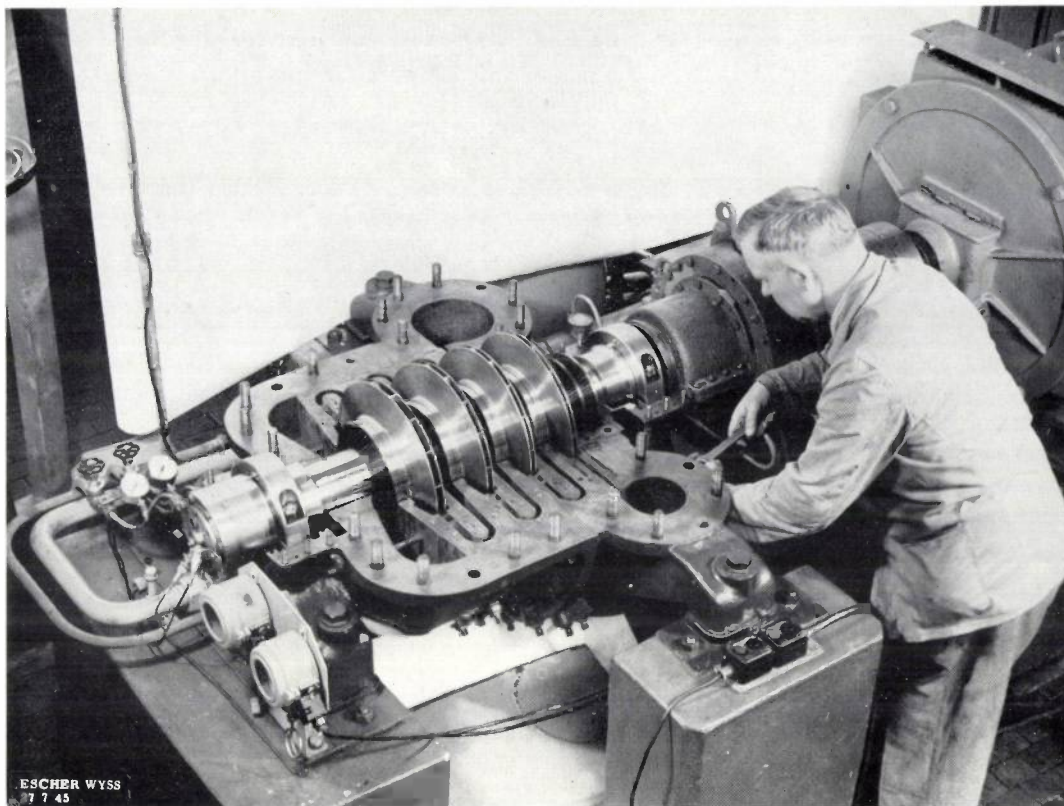


Fig. 10. Experimental four-stage centrifugal compressor made by Escher Wyss, partly dismantled. Gas bearings afford both axial and radial support for the shaft. Pipes and pressure gauges for the incoming gas supply for these bearings may be seen on the left. This compressor runs at higher speeds than normal oil-lubricated types, and is therefore able to produce higher compressions. At the same time the compressed gas is completely free from oil. (Reproduced from E. Loch, *Escher Wyss Mitteilungen* 33, no. 1/2/3, p. 118, 1960.)

In cases where one type of bearing may seem on the face of it to be the more suitable, instability phenomena may tip the scale in favour of the other type. If contactless bearings are to be further improved it is of the greatest importance that the forms of instability to which they are susceptible should be properly understood, and much of the research work at present being done in various laboratories does in fact have as its object the better understanding of these phenomena.

Some examples of gas bearing applications

Mention has already been made of certain applications that do not require a great deal of explanation. We shall now go on to consider applications having some special feature or other that must claim our fuller attention.

Spectacular, though still experimental, compressors embodying gas bearings offer a good example of the desirability and feasibility of working at higher speeds than normal, and so developing higher pressures than are possible with oil lubrication¹²⁾.

¹²⁾ E. Loch, *Escher Wyss Mitteilungen* 33, No. 1/2/3, p. 118, 1960.

Fig. 10 shows a four-stage centrifugal compressor, the main shaft of which is supported at left and right in thrust and journal bearings. The bearing gas intake ducts and gauges are clearly visible on the left. The self-acting type of bearing would obviously be less suitable here because the compressors are not kept in continuous operation, and the wear consequent on frequent starting would cause a lot of trouble. A further advantage of using gas bearings in this equipment is that the gas delivered under pressure is entirely free from oil. This is of particular importance when oxygen is being compressed, since the presence of oil would involve an explosion hazard.

Self-acting gas bearings are also employed in CO₂ circulators for nuclear reactors²⁾. As is well known, carbon dioxide gas is the coolant used in British atomic power stations like that at Calder Hall. Oil-lubricated bearings were unsuitable for the CO₂ circulators because oil has the tendency to break down under the action of irradiation. This fact gave a considerable stimulus to the development of gas bearings, the first successful application of which aroused a great deal of interest at the time. The con-

tinuously circulating CO₂ serves at the same time for lubricating the bearings, which together with the entire cooling system are self-contained — a great help in preventing the dissemination of radioactive

material. *Fig. 11* shows the circulator and the shaft suspension arrangements, which consist of two journal bearings *a* and *b* and a thrust bearing *c*. The last named is of the spiral grooved type that will be discussed at length in Part III of this article. *Fig. 12* is a photograph of the rotor assembly of the CO₂ circulator, the two bushes for the journal bearings appearing in the foreground.

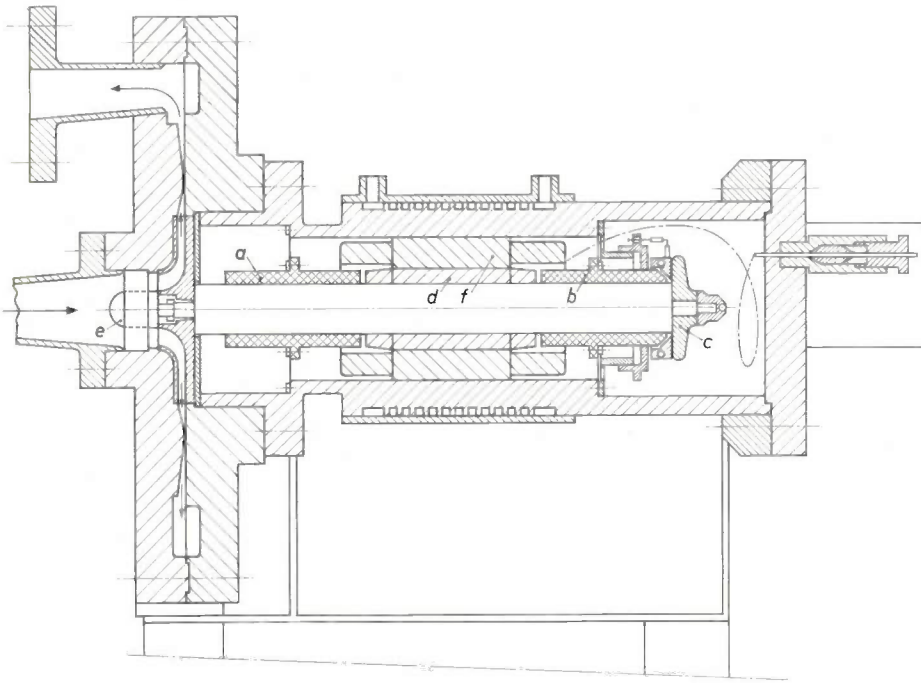


Fig. 11. CO₂ circulator for a nuclear reactor. The carbon dioxide gas used to cool the reactor (or, to put it more accurately, used to recover the heat developed in the reactor for exploitation elsewhere) is forced through the circuit by a radial fan *e* driven by an electric motor (stator *f*, rotor *d*). The arrows show the direction of the circulating gas. Since oil tends to break down chemically under the action of irradiation, gas-lubricated bearings have been incorporated in these circulators, the same CO₂ gas supply serving as lubricating fluid. The shaft is carried in two journal bearings; *a* and *b* are their bushes, and *c* is a spiral groove bearing for taking up the thrust (see Part III of this article). (This diagram and *fig. 12* are reproduced from G. W. K. Ford, D. M. Harris and D. Pantall, *Proc. Inst. Mech. Engrs.* 171, 93, 1957.)

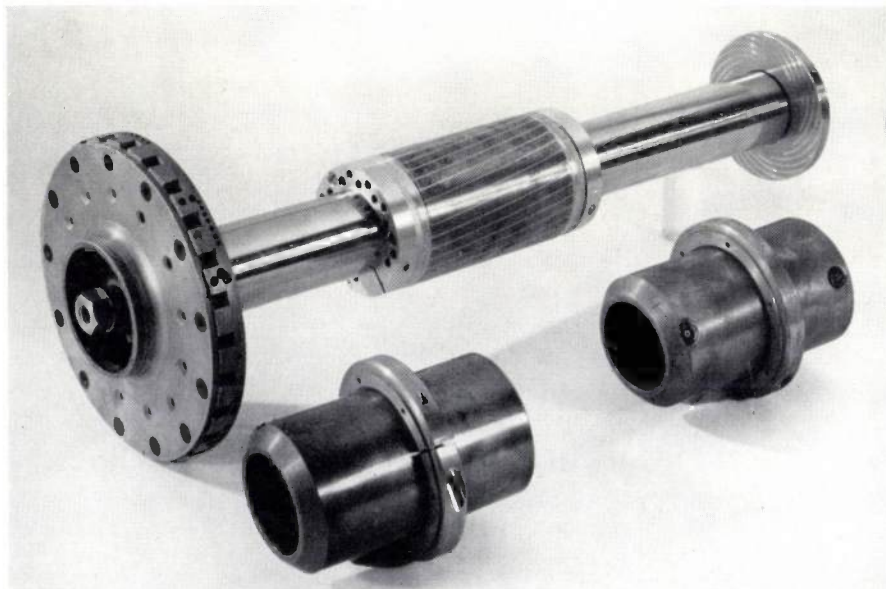


Fig. 12. Rotor assembly of the CO₂ circulator drawn in *fig. 11*, in which the gas circulated by the machine serves to lubricate its thrust and two journal bearings. In the foreground, the bushes for the journal bearings.

Gas bearings are now to be found in a whole series of smaller devices. Amongst some experimental devices made in our laboratory is a small rotor (*fig. 13*) for which compressed air supplies motive power as well as a supporting lubricating film. Because of the low friction losses, the rotor can be driven at speeds up to 450 000 r.p.m. without overheating. The same idea has been exploited in the newest types of dentists' drills. Turbo-jet engines and gyroscopic compasses also make use of gas bearings in view of the high speeds at which they are required to operate.

An interesting class of gas bearing applications is that in which the main consideration is to keep the friction constant rather than reduce it. It is mainly in connection with sensitive measurements that this demand is encountered. The set-up in *fig. 14* is for measuring, with the aid of an eddy-current dynamometer, the torque exerted by a miniature electric motor. This torque is small compared with the frictional couple that would arise if the rotor of the dynamometer,

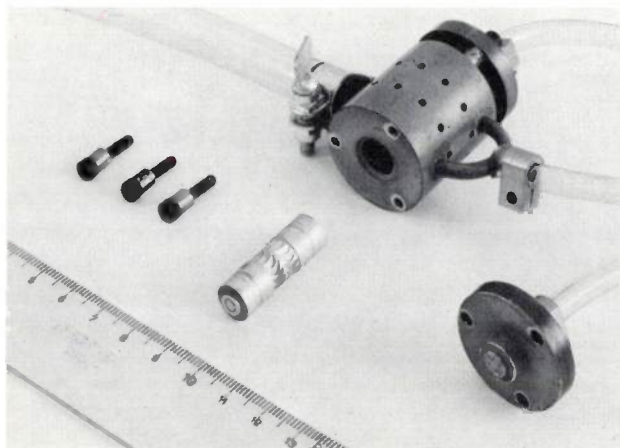


Fig. 13. Small experimental rotor which is driven and cushioned by compressed air. It can attain a speed of about 450 000 r.p.m. Recesses acting as turbine "buckets" have been milled in the rotor, which may be seen in the foreground. The split pipe entering the housing on the right supplies air for lubrication of the journal bearings on either side of the recesses. Thrust bearings are also provided, at both ends of the shaft. The front thrust bearing has been removed; four small orifices through which the air is blown (they have the same function as the restriction in fig. 3) may be seen in the middle.

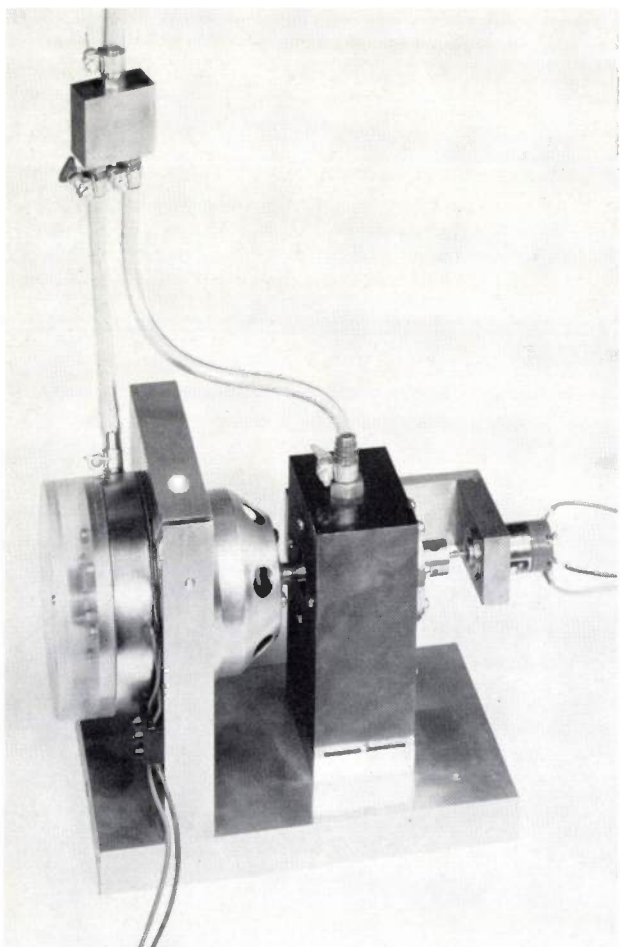


Fig. 14. Arrangement for measuring the torque delivered by a very small electric motor, mounted in the holder on the extreme right. The measuring instrument (left) contains a disc which is coupled to the motor spindle and which undergoes braking due to eddy currents; the braking couple is adjustable. To eliminate inaccuracies due to uneven bearing friction, compressed air is used to provide radial support for the disc, giving an extremely low and constant level of friction.

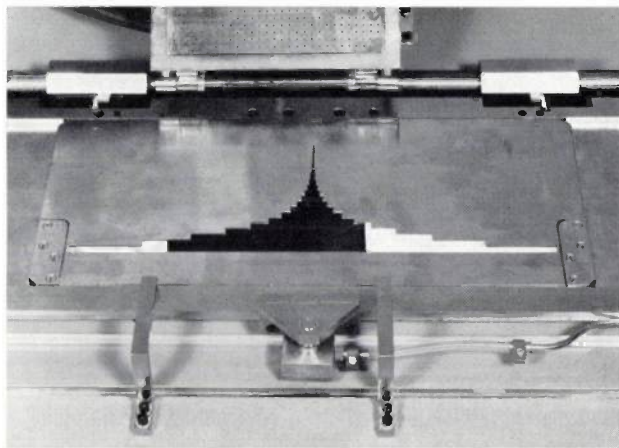


Fig. 15. Sensitometer for determining the sensitivity and other characteristics of photographic material. A masking pattern moves slowly across the instrument, with the result that the photographic material is exposed stepwise to light of known spectral composition and intensity from a source (not visible here) under the masking pattern. By means of a vacuum the material to be tested is held on a hinged grid, which in the photograph is in the raised position. It is necessary that the pattern should move with extreme smoothness and regularity if the desired aim, that of varying the exposure time in exactly determined steps, is to be realized. To ensure this, the carriage to which the masking pattern is fixed runs in tubular air-lubricated bearings that serve as guides (to the left and right of the grid hinges), and rests on a flat air-lubricated pad. The pipe supplying air to the pad can be seen in the foreground.

which gives the braking effect, were supported in ball-bearings, and inevitable small variations in the frictional couple would make the measurements very unreliable¹³). Something rather similar applies to the sensitometer¹⁴) appearing in fig. 15. Mounted on a carriage is a screen or masking pattern which serves to vary, as a function of place, the exposure time of photographic material placed underneath it. The problem was to make the translatory movement of the screen completely smooth. The slight jerks and hesitations involved by rolling over steel balls or the like, though these are practically imperceptible even to the careful observer, would have introduced quite impermissible discontinuities into the blackening pattern on the exposed film. Another advantage in the use of air as a lubricant, and which has already been referred to, is that of not contaminating materials it comes in contact with — in this case photographic film. As a final example of this class of application let us take an apparatus for calibrating acceleration pick-ups that has been developed elsewhere¹⁵). The pick-up is fixed to a carriage that is

¹³) The torque meter appearing in the photograph is based on damping caused by eddy currents, and was designed by W. Bähler of these Laboratories.

¹⁴) This instrument was the result of cooperation between our photochemical group and the Research Laboratories designers.

¹⁵) TNO-Nieuws 18, 154, 1963 (No. 3). In Dutch.

required to vibrate sinusoidally in an exactly defined way. Mechanical and electrodynamic excitation proved to have various drawbacks; either the movement was distorted out of the sinusoidal, or noise and interference were introduced by the ball-bearings etc. In the design just referred to, air was again used for supporting the carriage, which is held between two helical springs. The carriage is brought into free oscillation by displacing it and so compressing one of the springs. It is stated in the article cited that thanks to the very low frictional losses which remain constant within extremely narrow limits, very true sinusoidal oscillations are maintained for minutes at a time.

The last application to be discussed here falls into a quite different class. The device in question is to be found amongst other things in the magnetic-drum memories of computers, e.g. PASCAL. It is essential that there should be accurate transference of signals between the magnetic surface layer of the rotating drum and a fixed magnetic reading or writing head. But this will only be guaranteed if the clearance between head and drum surface is small and not subject to any great variation. In virtue of the air-bearing principle employed in PASCAL, a clearance of $8 \mu\text{m}$ is maintained between the head and the drum¹⁶⁾. In the applications discussed earlier, maintenance of a given separation between bearing surfaces was just a consequence of fulfilling the condition for stability essential to contactless bearing operation. Here the constant clearance has become an aim in itself.

Let us examine the air-bearing action exploited in PASCAL in rather greater detail, and with reference to numerical values deriving from an experimental set-up. Fig. 16 shows schematically how the reading or writing head is suspended. A weak spring (of stiffness $c_w = 1 \text{ N/mm}$) tends to press the head (of mass $m = 7$ grammes) against the rotating drum, but this force is opposed by the air in the more or less wedge-shaped space in between, which acts as a second, very strong spring (of stiffness $c_s = 300 \text{ N/mm}$). The desired clearance ($8 \mu\text{m}$) is main-

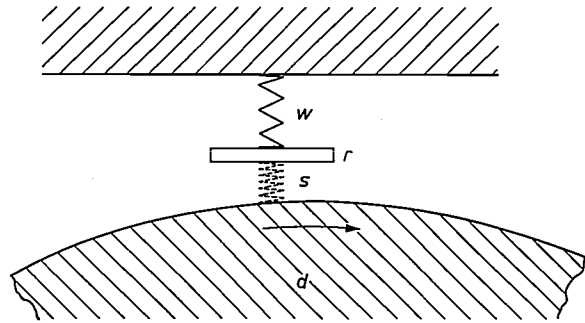


Fig. 16. Schematic drawing to show suspension of a magnetic head r for writing on to or reading off from a drum memory d such as is employed in the PASCAL computer. Spring w , which has a low stiffness value, tends to press the head against the rotating drum. In virtue of the convergence effect the air cushion between head and drum acts as a very strong spring s . Using this principle, it is possible to ensure that an $8 \mu\text{m}$ clearance will be maintained, with only very small variations, between the head and that part of the rotating drum surface which is passing it.

tained despite slow changes — temperature fluctuations, for example — but also despite fast ones due to “ripples” on the surface of the rotating drum. Let us suppose that the drum has an angular velocity of ω and that its surface shows a regular sinusoidal deformation, x peaks of amplitude \hat{h} being present around the perimeter. The sinusoidal rippling of the drum surface gives a regularly recurring impulse to the suspended magnetic head, and so sets it oscillating in a manner that is likewise sinusoidal. If its damping is zero the difference between the amplitudes of the two oscillations will be

$$\Delta \hat{y} = \frac{(x\omega)^2 / \omega_n^2}{1 - (x\omega)^2 / \omega_n^2} \hat{h},$$

where ω_n is the resonant angular frequency of the magnetic head:

$$\omega_n = \sqrt{\frac{c_s + c_w}{m}}.$$

Since in the case under consideration $c_w \ll c_s$, we may write

$$\omega_n \approx \sqrt{\frac{c_s}{m}} \approx 6000 \text{ rad/s}.$$

This is in fact quite close to the actual value of ω_n for the air-supported magnetic heads in PASCAL. On this basis, and taking $\omega = 300$, we find that if there are three ripples in the drum perimeter, the oscillating magnetic head will follow the rippling so closely that the clearance between the head and the drum surface will not vary by more than about 3% of the ripple amplitude.

With this example we close the part of the article concerning gas bearings, and turn our attention to bearings of the spiral groove type.

III. SPIRAL GROOVE BEARINGS

Instigation of the work on spiral groove bearings

Our work on spiral groove bearings in the Research Laboratories began in 1960, when we were consulted on the following problem. Would it be possible to make a wear-resistant thrust bearing able to take

up to about 1 kg thrust from a shaft rotating at at least 50 000 r.p.m., without incurring a power consumption much in excess of 1.5 watts? The bearing was to support the end of the shaft, and it had to be suitable for operation in a vacuum.

¹⁶⁾ The suspension system was designed by H. J. Hubers of this laboratory. See also J. H. Wessels, A magnetic wheel store for recording television signals, Philips tech. Rev. 22, 1-10, especially p. 6. In the case discussed in that article a constant clearance not exceeding $1 \mu\text{m}$ has been achieved.

To start with, it will be shown that none of the bearings so far discussed was likely to provide a ready solution to the above problem. Bearings involving sliding friction were out of the question, as also were ball-bearings and the like, on account of the wear they are subject to and also because the frictional losses would certainly be excessive. This narrowed the field to contactless bearings. As far as externally pressurized types were concerned, the

pump alone would be responsible for more than 2 watts power consumption. The self-acting class seemed to offer good prospects (as did magnetic bearings, but their possibilities in this connection were not investigated in detail).

Formulae for the load-carrying capacity of and the frictional force arising in a self-acting bearing were given in Part I (p. 258). Transformed for the general case of a thrust bearing, formulae (1) and (2) provide a basis for writing down the two conditions that now had to be satisfied:

$$W = \frac{K_1' \eta \omega r^4}{h_2^2} \geq 10 \text{ (newton)}, \quad \dots \quad (1a)$$

$$P = \frac{K_2' \eta \omega^2 r^4}{h_2} \leq 1.5 \text{ (watt)}. \quad \dots \quad (2a)$$

It will be recalled that W denotes load-carrying capacity and P frictional losses in the bearing; η is the viscosity, ω the angular velocity, r half the outside diameter, and h_2 the smallest gap height. The bearing coefficients (which are different again from those in equations 1, 2 and 4, 5) are denoted by K_1' and K_2' .

Dividing one condition into the other gives

$$\frac{W}{P} = \frac{K_1'}{K_2' \omega h_2} \geq \frac{10}{1.5} \text{ (seconds/metre)},$$

from which it follows that

$$h_2 \leq \frac{1.5}{10} \frac{1}{\omega} \frac{K_1'}{K_2'} \text{ (metres)}.$$

A Michell bearing was the type best fitted to the purpose. Inserting $\omega \approx 5000$ rad/s and optimum values for K_1' and K_2' , which calculation reveals to be 0.06 and 0.81 respectively, we obtain

$$h_2 \leq 2 \mu\text{m}.$$

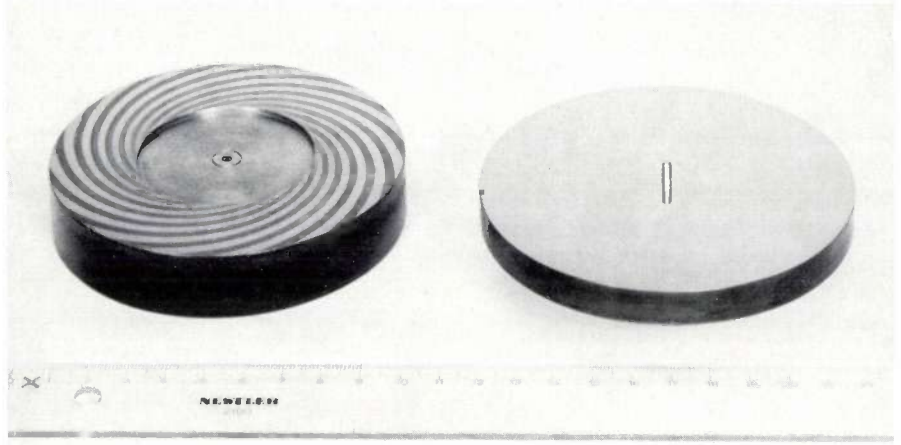


Fig. 17. Spiral groove bearing made in the Research Laboratories, consisting of a smooth and a grooved circular plate. When the plates are assembled and one is turned by hand with respect to the other (it must be turned in the right direction) complete separation occurs at a speed as low as one revolution per second, the air layer between the bearing surfaces then being about 11 μm thick.

So small a gap height may well be feasible, in view of the American achievements in connection with radial bearings⁵⁾, but at the time we felt very doubtful about the possibilities of building a bearing with such a small diametral clearance, and the prospect of doing so was not in any case an attractive one.

What else could be done? We were now reduced to looking for a bearing with a different kind of geometry, and having different coefficients, in order to yield a bigger K_1'/K_2' ratio. In physical terms, the problem was essentially one of reducing the coefficient of friction (see formula (3) in Part I).

The spiral groove idea

H. Rinia, of the Research Laboratories, suggested an arrangement in which a smooth circular plate rotated relative to a similar plate in which grooves had been cut (fig. 17). Lying oblique to the relative velocity vector of the two plates, the grooves would have a twofold effect. Firstly there would be a convergence effect; looked at in the direction of the velocity vector, the air or other fluid would be pushed out of the grooves into the smaller gap above the ridges. ~~This pump effect can be directed towards or away from the centre of rotation, depending on the direction of rotation and on the grooves.~~ Secondly, provided rotation was in the right sense the fluid would be pumped towards the centre, in consequence of the angle made by the grooves with the velocity vector at any given point, resulting in the plates being pushed apart. Having built the spiral groove bearing illustrated in fig. 17, we found that it sufficed to turn the upper plate by hand (at a speed of about one

¹⁷⁾ H. Rinia, Verslag gewone Vergad. Afd. Natuurk. Kon. Ned. Akad. Wetensch. (in Dutch), 70, 144, 1961 (No. 10).

revolution per second) in order to built up an air layer about 11 μm thick completely separating the two bearing surfaces.

The reader may wonder just what advantage, in terms of reduced friction (which was what we were after), is provided by the combination of effects just referred to. The situation can be summed up by saying that, whereas pressure is zero in the centre of the Michell bearing, because the relative velocity is zero at that point, the pumping action of the spiral groove bearing results in a pressure distribution that shows a sharp increase along a line drawn from the perimeter to the centre. In the spiral groove bearing, therefore, a bigger area contributes to load-carrying capacity *without this entailing any great increase in frictional losses*. A more quantitative account of the difference between the two types will be given below.

As we later discovered, work had already been done in various quarters on developing the spiral groove bearing. The first reference in the literature is a description of the principle by Gumbel in 1925¹⁸⁾; Gumbel did not apply for a patent. Whipple carried out the first calculations in 1949, and some time elapsed before these were allowed to be published. It was on the basis of his calculations that a spiral groove bearing was designed for the CO₂ circulator which was discussed in Part II and which is employed in reactor cooling systems¹⁹⁾.

It will however be as well to point out that Whipple undertook his calculations with an aim rather different from ours. He was looking into the possibilities of making a gas bearing that would be of simpler construction than the Michell bearing. He does not state explicitly that spiral groove bearings represent a possibility of reducing friction coefficients, and it is not therefore remarkable that he did not devote any further effort to the theoretical and experimental elaboration of this possibility.

Optimization of a spiral groove bearing

Now that a general line of investigation had been opened up, our main concern was to design a bearing with optimum performance. The first experimental version was very far from satisfying the requirements that had been laid down. A brief account will

now be given of the calculations that were undertaken with a view to arriving at optimum load-carrying capacity. Frictional losses as well as load-carrying capacity were taken into account in the full calculations²⁰⁾.

We started by considering a model consisting of rectilinear grooves and ridges — see *fig. 18*. Assuming steady-state operation of the model in an incompressible working fluid, the pressure distribution therein is described by the Laplace differential equation:

$$\frac{\partial^2 p}{\partial x^2} + \frac{\partial^2 p}{\partial y^2} = 0 \quad \dots \dots \dots (7)$$

No analytical solution can be found for the relevant boundary conditions. The simplest approximation was to consider two linear functions that would

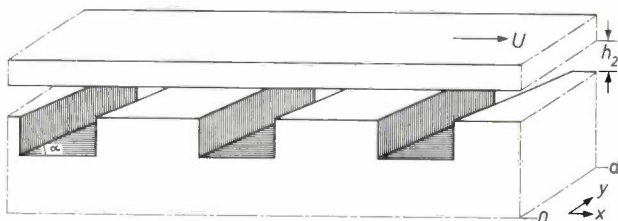


Fig. 18. Rectilinear groove model used in calculations for optimum spiral groove bearing.

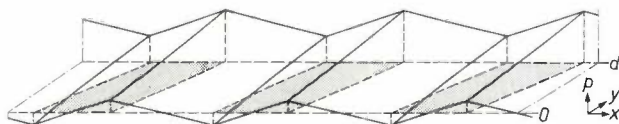


Fig. 19. First approximation to the distribution of pressures in the model appearing in *fig. 18*. This approximation still does not satisfy all the boundary conditions of the differential equation. By superimposing a correction which has been derived elsewhere, it is possible to obtain a distribution in which pressures are uniform along edges $y = 0$ and $y = d$, as they must necessarily be in reality.

satisfy the differential equation, one giving the pressure p_d above a ridge and the other giving the pressure p_g above a groove.

$$p_d = p_1 + A_1x + B_1y, \quad \dots \dots \dots (8)$$

$$p_g = p_2 + A_2x + B_2y. \quad \dots \dots \dots (9)$$

These two functions do not suffice to satisfy the boundary conditions at $y = 0$ and $y = d$; the approximation implies a sawtooth variation in pressure along these coordinates, as in *fig. 19*. The six parameters occurring in the above two functions were evaluated from the six remaining boundary

¹⁸⁾ L. Gumbel and E. Everling, *Reibung und Schmierung im Maschinenbau*, Kraysn Verlag, Berlin 1925. In particular, see p. 81. To judge from the fact that the spiral groove bearing figures in this book as an exercise problem, Gumbel did not rate its practical importance very high, and it may be that he underestimated the difficulties of exhaustive theoretical treatment.

¹⁹⁾ See Ford, Harris and Pantall²⁾ and also R. T. P. Whipple, *The inclined groove bearing*, A.E.R.E., T/R 622, revised Oct. 1958, and the same author's contribution to *First int. Symp. on gas-lubricated bearings*, Washington 1959, pp. 361-382.

²⁰⁾ For a more complete account of the solution to this problem, see E. A. Muijderland, *De Ingenieur* 75, W 35, 1963 (no. 10) and the same author's thesis, "Spiral groove bearings" (University of Delft, 1964). The theory was elaborated in close collaboration with J. A. Haringx of this laboratory.

conditions, deducible from the need for continuity and from the fact that equations (8) and (9) must necessarily yield the same values for pressures along the edge between ridge and groove-wall. We used the parameters thus obtained to calculate Δp , the mean difference of pressure between $y = 0$ and $y = d$. In the case where there is no net flow of working fluid in the y direction:

$$\Delta p = g(\alpha, \delta, \gamma) \frac{\eta U d}{h_2^2} \dots \dots (10)$$

Here η is the viscosity of the fluid, U the relative velocity of the bearing surfaces, h_2 the gap height above the ridges, and $g(\alpha, \delta, \gamma)$ is a function of the angle α at which the grooves are cut, the ratio δ between the groove depth and h_2 , and the ratio γ between the groove width and the ridge width. What

the groove would make an angle of 16° with the tangential direction; in other words, the groove had to have a logarithmic spiral shape. Also, at any point along the groove, the groove width must equal the ridge width ($\gamma = 1$). The groove depth was fixed by $\delta = 0.4$.

So far we had been working on the sole basis of equations (8) and (9), which only provide an approximation to the pressure distribution. For the manner in which corrections were introduced, reference should be made to the more detailed publication already cited²⁰), which also explains how the frictional couple in the actual spiral groove bearing was calculated.

The rear part of *fig. 21* shows the pressure distribution in an optimum spiral groove bearing employed to support a shaft-end. It will be seen that a "pres-

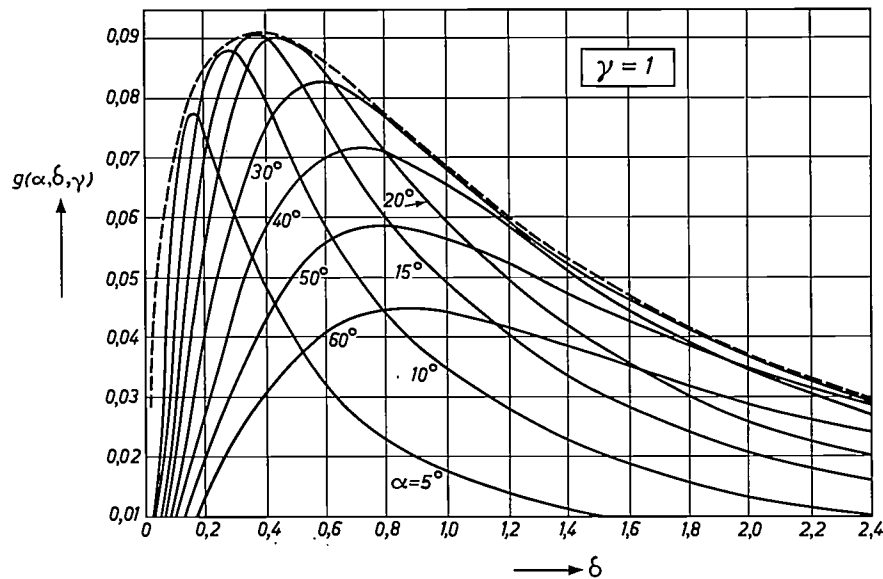


Fig. 20. Function $g(\alpha, \delta, \gamma)$ plotted against δ for $\gamma = 1$ and a set of different α values. An envelope enclosing this family of curves has been drawn as a dashed line. Inspection shows that the highest peak is that of the curve for $\alpha \approx 16^\circ$, this maximum being attained at $\delta = 0.4$.

we had to do was to choose α , δ and γ in such a way as to get the largest possible $g(\alpha, \delta, \gamma)$. We were able to deduce that γ must in any case be unity. In *fig. 20*, $g(\alpha, \delta, 1)$ has been plotted as a function of δ for various values of α . It will be noted that $g(\alpha, \delta, 1)$ reaches a peak when $\alpha = 16^\circ$ and $\delta = 0.4$.

In order to be able to apply findings from the simple model to a bearing plate in which spiral grooves had been cut, we imagined the latter to be broken up into a large number of small elements, each of which resembled the model. Each element had to contribute as much as possible to the lift afforded by the bearing plate; consequently each spiral groove had to be cut in such a way that at any point along its length, a line drawn tangentially to

sure hill", whose shape is somewhat reminiscent of an old-fashioned pudding basin, builds up over the whole circular bearing surface. To allow comparison, the pressure distribution over a Michell bearing consisting of six slipper blocks has been drawn into the front part of the figure. A separate "pressure hill" arises on top of each block, and it will be quite obvious that integrating the pressures above the whole set of slipper blocks will yield a much weaker total lift than integrating over the pudding-shaped hill created by the spiral groove bearing. Yet the total area of bearing surface occupied by the hills in the Michell bearing is not much less (about $\frac{3}{4}$) than that occupied by the single hill in the spiral groove bearing, and it is this area (because here the

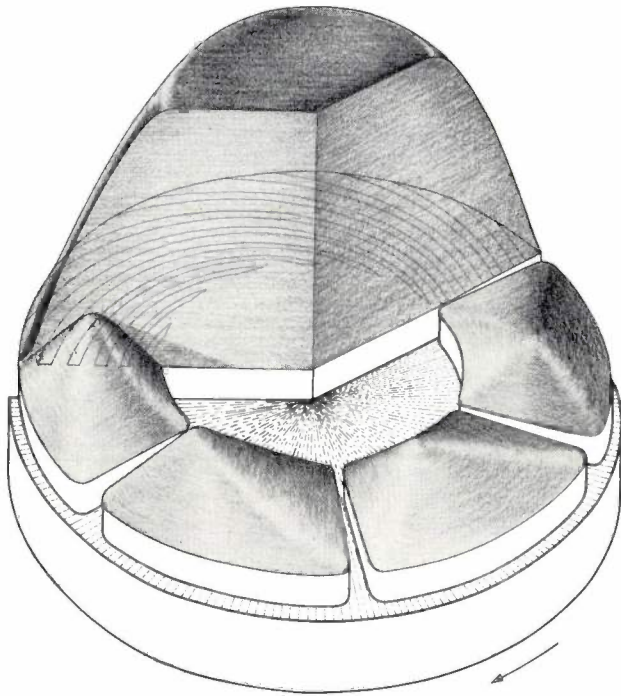


Fig. 21. Three-dimensional sketch showing calculated pressure distributions in an optimum spiral groove bearing (at the rear) and in a Michell bearing of the same size, equipped with a total of six slipper blocks (in front). A smooth upper member, rotating in the sense indicated by the arrow, is to be imagined above the fixed member with its grooves (or slipper blocks). The pressure prevailing at each point on the circular surface of the lower member has been plotted on a vertical scale that is the same for the two types of bearing. The volume of the big "pressure hill" or the total volume of the smaller "hill" is a measure of load-carrying capacity.

layer is the smallest) that determines the frictional losses.

Checking the theory

Measurements to check the theory were done with the apparatus shown schematically in fig. 22. The upper plate *a*, the one with the spiral grooves cut in it, was made to rotate at various speeds relative to the smooth plate *b*. A small ball bearing *c* was responsible for keeping the two plates properly centered. The couple transferred to the lower member by friction was measured with a small dial-reading dynamometer. The shaft was suspended both radially and axially with compressed air, in the manner described in Parts I and II of this article. By means of capacitance measurements we were able to determine the height of the gap between the two members of the spiral groove bearing.

Measurements of gap height at a given lift and speed yielded values roughly 12% in excess of those originally calculated. After working out the correction terms and improving the accuracy of the measurements, we managed to reduce the disparity

to 1%; ultimately, then, the agreement between theory and experiment could be regarded as highly satisfactory. Theoretical and experimental values of frictional torque were found on average to differ by 6%.

Results

The optimum spiral groove bearing that we designed and made along these lines has a K_1' coefficient greater by a factor of 8.6 than that of a Michell bearing used to support a shaft-end. The K_2' coefficient is also greater, but only by a factor of 1.2. This means that we have managed to make a bearing with a coefficient of friction 7.4 times smaller than that of a Michell bearing with the same radius and clearance. So far there is no other bearing in the self-acting class that has such a low coefficient of friction compared to the spiral groove type. Using the spiral groove bearing in question, the maximum clearance imposed by the problem outlined on p. 266 becomes $h_2 \leq 15 \mu\text{m}$. This condition can be fulfilled without great trouble.

We have achieved a further increase in the relatively high load-carrying capacity of the spiral groove

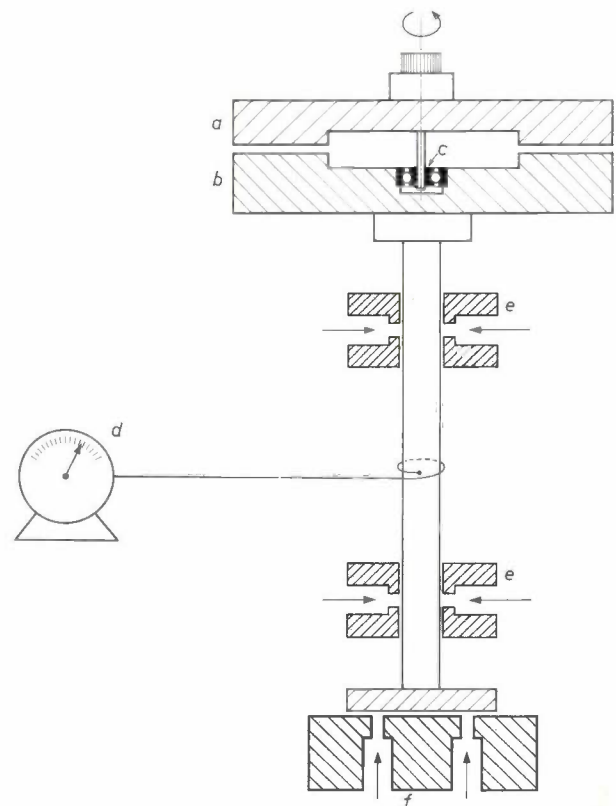


Fig. 22. Arrangement for measuring friction in a spiral groove bearing (schematic). The upper, grooved member *a* is caused to rotate at a given speed relative to the smooth plate *b*. The frictional couple exerted on member *b* is measured with a small dial-reading dynamometer *d*. A very small ball bearing *c* serves for centering the plates; axial air bearing *f* and the radial air bearings marked *e* are all externally pressurized.

bearing (it will be recalled that its K_2' is 8.6 times that of a corresponding Michell bearing) by redesigning the bearing surface in the form of a spherical cap. If a flat thrust bearing be compared with a spherical one having the same radius and operating at the same speed, it can readily be seen that the surface elements of the latter have, on average, a greater velocity relative to the fixed bearing surface. Moreover, the distances from centre involved in integrating over the surface elements are also longer in the case of the spherical bearing. As can be directly inferred from formula (1a), both factors make for greater load-carrying capacity. Indeed, this becomes so high as to amount to about 25 times that of a Michell bearing of the same diameter.

Other favourable features of a spherical as compared with a plane spiral groove bearing are that it is easier to centre and that, to some limited extent, it is able to take up a radial as well as an axial load.

Fig. 23 shows two spherical type spiral groove bearings using oil lubrication which have been made and tested in our laboratory. The diameter of the smallest spherical cap is about 3 mm; the cap and its concave seating are completely separated by an air film at 5000 r.p.m., with the bearing taking up a thrust of 1 kg. Under these conditions the pressure developed at the centre of the bearing is about 25 atm.

Applications

The possible applications of spiral groove bearings are not limited to cases where a low coefficient of friction is essential. Another feature of the bearing which is certainly just as important, particularly where small size is required, is the ease with which they can be made. A diameter of 3 mm, such as the smaller of the bearings shown in fig. 23, would be quite impossible for Michell-type bearings.

Spiral groove bearings can also be designed to take up thrust at points along the length of the shaft

THEATRI MACHINARUM HYDRAULICARUM Tomus II.

Ober: Schau-Platz der Wasser-Künste, Anderer Theil.

bestehend

In fernerer Fortsetzung der Künste und Maschinen, womit die Wasser aus der Tiefe zu erheben oder in die Höhe zu treiben;

Darbey so wohl falsche und unbrauchbare, die Fehler und Ursachen daraus zu erkennen, als auch viele nützliche und brauchbare zu finden, absonderlich aber eine deutliche Anweisung zu denen Maschinen, da das Wasser vermittelst des Feuers gehoben wird, darunter auch die allerneueste und ohnehin allerleichteste Art anzutreffen;

Deme beygefüget:

Ein Discurs oder Anweisung zu denen Wasser-Künsten, was eigentlich bey selbigen zu beobachten, und wie das *Theatrum Machinarum* hierbey zu gebrauchen.

Ein Werk, so nicht nur Künstlern, Kunstmeistern, Bergleuthen und Kunst-Steigern, ja allen, die selbst Hand anlegen, sondern auch Architectis, Ingenieurs, Commissarien, Beamten; überhaupt allen Hausvateren und Kunstliebenden, absonderlich aber der Jugend, solcher ein Erkenntnis und Fundament gar leicht bezubringen, sehr nützlich und nöthig.

Ausgefertiget und mit vielen Figuren versehen

von

Jacob Scupold, Mathematico und Mechanico,
Königl. Preussisch. Commerzien-Rath, der Königl. Preuss. und Sächs. wie auch Forstlichen Societäten der Wissenschaften Mitglied.

Zu finden bey dem Autore und Joh. Friedr. Gleditschens seel. Sohn.

Leipzig, druckt Christoph Zundel, 1725.

(instead of at the ends). Leakage takes place in consequence of the shaft passing through the bearing, the pumping action of which no longer serves to maintain a high pressure near the shaft; thus the pudding-shaped pressure hill collapses in the middle, becoming ring-shaped. A remedy for the loss of pressure has been found in the partial and herringbone types of spiral groove bearing (fig. 24). In the former type an effort has been made to limit leakage by leaving a large area ungrooved in the middle of the plate. The grooved outer portion, which provides the

§. 263.

Wie es nun eine pure Unmöglichkeit ist, eine einfache Maschine dahin zu bringen, daß sie auch nur einen einzigen Grad mehr Effect als die andere oder der gemeine Hebel mit einer scharffen Unterlage mache, vielweniger ist bey zusammengesetzten und durch viele Räder, Schrauben und dergleichen verstärkten Maschinen, etwas zu erhalten; denn diese auch mehrentheils mit grosser Last beschwehret werden. Und weil sie viel mehr Zapfen, Zähne, Getriebe und Flächen haben, die sich schleiffen, schleppen und stemmen, so folget daher eine so viel grössere Hinderniß und Widerstand der Kraft, daß sie viel weniger, als die Theorie ausweist, verrichten kan.

§. 264.

Dieser Widerstand, insgemein die Friction, von denen Deutschen und Werk-Weisern das Stocken oder Zwängen genannt, ist die vornehmste und Haupt-Ursache, warum eine Maschine nicht so viel thut als die andre, oder als die Theorie und Berechnung ausweist.

Die andre Haupt-Ursache aber ist eine ungeschickte Application der Kraft. Wer nun geschickt ist die Friction seiner Maschinen zu benehmen, und die Kraft recht nach der Kunst zu appliciren, der kan den andern Punct der Frage:

Ob die Maschinen zu verbessern?

auch mit ja beantworten, und vor einen Kunstverständigen passiren.

§. 265.

Daß uns die Friction die meiste Kraft raubet, ist auch an einem Last-Wagen zu sehen; denn ob er schon mit 50 ja 100 Centner beladen wäre, sollte man doch selbigen mit einem Finger auf einem recht gleichen und glatten plano horizontali fortziehen können; allein daß es etliche starke Pferde kaum vermögend, verwirflicher bloß die Friction, so die Räder an denen Achsen und ferner selbige mit ihren Fälgeln und Nägeln auf dem unebenen Pflaster oder Wegen machen.

§. 266.

Wer daher mit seinen Maschinen meist so viel ausrichten will, als die Theorie lehret, der schaffe so viel möglich alle Friction ab, welches geschieht:

1. Wenn die Maschine schnell gehet,
2. Daß sie nicht allzusehr beschwehret wird,
3. Daß wenig Theile und Stücke sind, die sich auf ihren Lagern bewegen, oder auf einander reiben, rutschen, schleiffen, oder stemmen müssen.
4. Daß alle solche Theile hart, glatt, rund, eben seyn, und nirgend an unglamer Schmiere ermangele.

Wie hiervon unterschiedliche Exempel im Theatro generali Tabula XXX. und XXXI. zu ersehen.

§. 267.

In this article in this issue, E. A. Muijderland cites some examples of expedients adopted in antiquity to reduce friction—the use of oil to make a heavily laden sledge run more easily, and the primitive ball-bearing fitted under a turntable. Now, over the long centuries during which Western technology was evolving, a point must sooner or later have been reached at which designers of machines, and for even greater reason those who had to build them, became all too aware of the important part that frictional losses were going to play in their ever more complicated and ambitious constructions. This awareness is clearly reflected in the writings of Jacob Leupold, a Prussian “*Mathematico and Mechanico*” (i.e. engineer), who published his *Theatrum Machinarum Hydraulicarum* at Leipzig in 1725. The book is largely devoted to the fundamental industrial problems of the time, dealing with the design of water-raising machines such as were required for pumping out mineshafts or supplying towns, estates or fountains. Leupold never neglects an opportunity of emphasizing the importance of reducing friction between the moving parts of machines. Here we reproduce the title-page of the second part of his work, the picturesque wording of which is characteristic of the age, and the page of text in which Leupold formulates his doctrines with forceful clarity. His advice to let the machine run fast (point 1 of § 266) should not be interpreted as a remarkable example of foresight into the operation of self-acting contactless bearings, for which a certain minimum shaft speed is necessary; what he had in mind is that slow and none too regular motion is liable to involve sticking and jamming (“*Stocken oder Zwängen*”). During these brief intervals of motionlessness, static friction becomes operative in place of dynamic friction.

pumping action, is thus separated by an area of high flow resistance from the central opening for the shaft, through which leakage occurs. Leakage has been cut out altogether in the herringbone bearing, an opposite pumping action being provided by the grooves on the inside. Since the area over which the pressure hill builds up is rather more restricted in these types of bearing, they are not of course ideal from the viewpoint of reducing friction. Even so, the coefficient of friction of a herringbone bearing is still rather smaller than that of a Michell bearing under

comparable conditions. A herringbone bearing that has been incorporated in an experimental hot gas engine ²¹⁾ in the Research Laboratories may be seen in *fig. 25*.

Another interesting variant is the conical type of spiral groove bearing. Its most notable property is its ability to take up a radial load as well as a thrust; as already stated, the spherical type is also able to do this, but only to a much lower degree. (Theoretical

²¹⁾ The practical development work was undertaken by R. J. Meijer and coworkers of this laboratory.

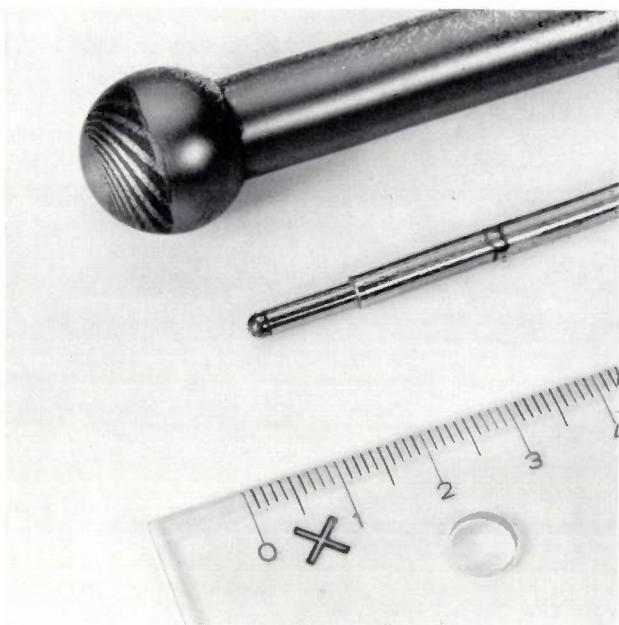


Fig. 23. Spindle-ends for spherical-type spiral groove bearings with diameters of 18 mm and 3 mm. The grooves are cut into hardened and polished steel balls (such as are used in ball-bearings) by an etching process. The surface of the metal is coated with light-sensitive lacquer, and the desired spiral groove pattern is transferred to this layer by a photographic printing method. Subsequent treatment in an etching bath affects only those areas of the layer that have been exposed to light, and only the steel under the exposed areas is attacked by the etchant (which might be FeCl_3 , for example).

Alternatively, the grooves can be cut into the concave member of the bearing. In this case the seating might be made of aluminium, for which FeCl_3 is also a suitable etchant.

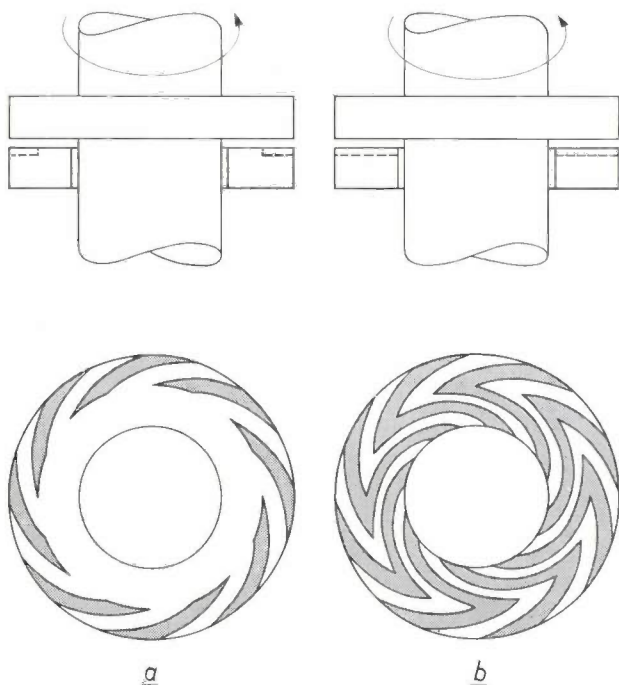


Fig. 24. Two types of spiral groove bearings suitable for taking up axial thrust from a shaft that passes through the bearing. (a) Partial spiral groove bearing, in which the grooved area is restricted to the outer margin of the plate. (b) Herringbone bearing.

studies have shown that nothing is gained, from the viewpoint of reduced friction, by cutting spiral grooves in a "pure" radial bearing.) Fig. 26 shows a conical spiral groove bearing that was recently designed in our laboratory for a small electric motor.

Optimum bearing coefficients for all the types discussed above are displayed in Table I.

Lubrication with grease

In conclusion, a word may be said about an unexpected finding that has engaged much of our attention over the past few years — the discovery that there is a lot to be gained by lubricating small spiral groove bearings with *grease*.



Fig. 25. A herringbone bearing employed in a hot gas engine developed in the Research Laboratories²¹⁾.

In bearings with diameters of only a few millimetres, lubrication starts to become a problem in itself. The provision of continuous or drip lubrication becomes disproportionately complicated and expensive. What we have particularly in mind here are small domestic and other appliances which are in operation at irregular intervals, and which must be able to run or to rest in any conceivable position.

If grease is used as a lubricant it will be sucked into the bearing clearance, just as oil is, in virtue of the pumping action of the spiral groove bearing; but it is obvious that grease will be far less liable than oil is to escape from the bearing during periods of rest. We have in fact established that after long periods of immobility in various

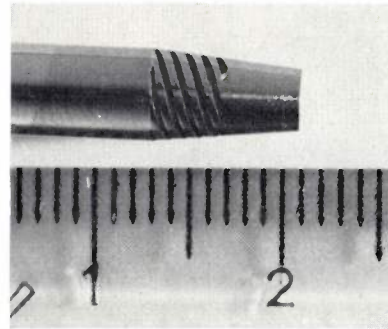
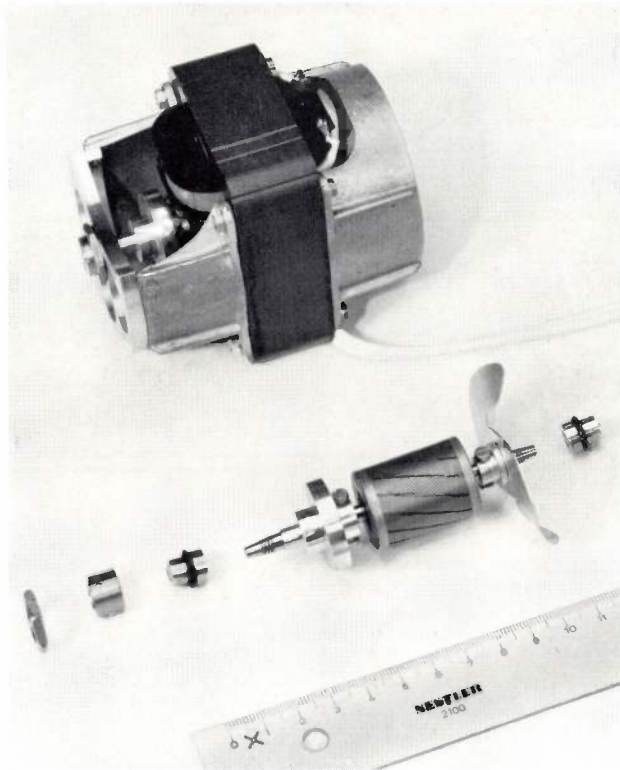


Fig. 26. Experimental type of miniature electric motor embodying a conical spiral groove bearing able to carry appreciable radial loads as well as taking up thrust. In front of it, the rotor of another motor of the same type, dismantled to give an "exploded" view. The photograph above shows one of the grooved spindle-ends. The bearing is grease lubricated.

positions, periods which had ranged from a few months to a year, lubrication conditions on restarting left nothing to be desired, complete separation of the bearing surfaces having occurred at the same relatively slow speeds as had been noted during the first trials. Further investigations are still proceeding.

One point we are interested in, in this connection, is whether the grease retains its good lubricating

properties when the bearing has been in operation for a lengthy time; whether its chemical composition alters, for example, or whether it is liable to drain out of the bearing in the course of a long hot spell during the summer. Ad hoc tests that have extended over periods varying from a few months to two years have so far failed to reveal any shortcoming whatsoever in this respect.

Table I. Various forms of thrust bearing, with calculated values of their K_1' and K_2' coefficients appropriate to optimum running conditions. All types are assumed to have the same outside diameter; that of flat bearings is twice the inside diameter. Half-diametral clearance (half the difference between the cup diameter and the ball diameter) is assumed in the case of the spherical cap bearing.

	Michell bearing	step bearing	spiral groove bearings			
			flat type for shaft-end	spherical cap	for mid-shaft support	
					partial	herringbone
K_1'	0.042	0.047	0.366	1.11	0.124	0.106
K_2'	22.0	ca. 25	2.9	2.8	8.1	10.2

Though they will still have to undergo the test of time in practical applications, we personally feel that these miniature grease-lubricated contactless bearings have good future prospects.

Summary. In this article types of bearing are discussed in which friction and wear are reduced to very small proportions by the agency of a viscous fluid (lubricant) that serves to maintain a small and more or less constant clearance between the bearing surfaces. A "contactless" bearing of this kind does not necessarily have to be lubricated with a liquid, such as oil; a gas is also effective. Particular attention is given to gas-lubricated bearings, which have been a practical possibility for the past 15 years or so. A distinction is made between two classes of contactless bearing, the externally pressurized types and the self-acting types. In a comparative account of the two classes,

some indication is given of the applications for which each is most suitable. Examples of gas bearing applications may be found in turbo-jet engines, gyroscopic compasses, nuclear reactors, dentists' drills etc.

On the basis of the self-acting contactless bearing a new type — the spiral groove bearing — has been developed, this work having largely been done in Philips Research Laboratories at Eindhoven. The main advantage of the new type is its very low coefficient of friction. A flat thrust bearing of the spiral groove type, designed to support a shaft-end, has a friction coefficient only about one-seventh that of a Michell bearing under comparable optimum conditions. Besides a low coefficient of friction, a variant in which the grooves are cut into a spherical cap has a load-carrying capacity about 25 times greater than that of a corresponding Michell bearing. Small spiral groove bearings having diameters of a few millimeters, and lubricated with grease, promise to be useful in small domestic and other appliances.

A 4 mm RADAR INSTALLATION

by H. ALLARIES *).

621.396.967.029.65

Radar installations operating at a wavelength of 8 mm are now widely employed in cases where a high degree of detail discrimination is required within a restricted area, e.g. for manoeuvring shipping in narrow and busy water-ways. This article describes an experimental 4 mm radar installation, built in Philips Research Laboratories, which uses various new tubes including a 4 mm magnetron and a 4 mm reflex klystron. The screen images obtained with this installation show that, although the maximum range is no more than a few kilometres, the detail discrimination at short distances is exceptionally good.

Various wavebands are at present in use for radar installations, the choice being determined by the operating range for which the installation is intended. Observations over distances up to several hundreds of kilometres require wavelengths of 25 cm¹⁾ and longer, distances up to about 100 km are covered with 10 cm waves, and for shorter ranges use is made of 3 cm waves and lower. In general it can be said that shortening the wavelength reduces the range of the installation. On the other hand, it improves the resolution, that is to say the power to discriminate on the radar screen between closely adjacent objects.

For certain special applications, for example where ships have to be manoeuvred in narrow and busy water-ways, this has led to the use of millimetre wavelengths. An article published earlier in this journal described an 8 mm installation²⁾. The range at such wavelengths is relatively small, but sufficient for the purpose. The resolution, however, is exceptionally high, making visible on the screen

large numbers of details which are of importance, for example, to navigation.

The availability of several new tubes — including a 4 mm magnetron and a 4 mm klystron — led to the construction in our Research Laboratories of a 4 mm radar installation. Part of it can be seen in *fig. 1*. This equipment has been used to investigate the effects of a further shortening of the wavelength on the resolution and range, and also the technical problems which this involves.

General design

To obtain the high est possible *radial resolution*, the transmitted radar pulses must be extremely short. On the other hand, the magnetron cannot work properly below a certain minimum pulse length. In practice the rule of thumb is used that the number of cycles in a pulse must be equal to the figure of merit *Q* of the cavity resonator system of the magnetron under optimum loading conditions. For most magnetrons this figure is roughly 200, which, at a wavelength of 4 mm, gives a minimum pulse length of 4 nanoseconds. The pulse length actually chosen is 5 nanoseconds. Theoretically this should result in a radial resolution of 0.75 m, but in practice it will be somewhat less favourable, owing to inevitable pulse distortion.

*) Philips Research Laboratory, Eindhoven.

¹⁾ A 25 cm radar is described by H. van Lambalgen and J. van der Plas in: The SGR 200 long-range surveillance radar at Schiphol Airport, Philips Telecomm. Rev. 22, 51-62, 1961.

²⁾ J. M. G. Seppen and J. Verstraten, An 8 mm-high resolution radar installation, Philips tech. Rev., 21, 92-103, 1959/60.

Though they will still have to undergo the test of time in practical applications, we personally feel that these miniature grease-lubricated contactless bearings have good future prospects.

Summary. In this article types of bearing are discussed in which friction and wear are reduced to very small proportions by the agency of a viscous fluid (lubricant) that serves to maintain a small and more or less constant clearance between the bearing surfaces. A "contactless" bearing of this kind does not necessarily have to be lubricated with a liquid, such as oil; a gas is also effective. Particular attention is given to gas-lubricated bearings, which have been a practical possibility for the past 15 years or so. A distinction is made between two classes of contactless bearing, the externally pressurized types and the self-acting types. In a comparative account of the two classes,

some indication is given of the applications for which each is most suitable. Examples of gas bearing applications may be found in turbo-jet engines, gyroscopic compasses, nuclear reactors, dentists' drills etc.

On the basis of the self-acting contactless bearing a new type — the spiral groove bearing — has been developed, this work having largely been done in Philips Research Laboratories at Eindhoven. The main advantage of the new type is its very low coefficient of friction. A flat thrust bearing of the spiral groove type, designed to support a shaft-end, has a friction coefficient only about one-seventh that of a Michell bearing under comparable optimum conditions. Besides a low coefficient of friction, a variant in which the grooves are cut into a spherical cap has a load-carrying capacity about 25 times greater than that of a corresponding Michell bearing. Small spiral groove bearings having diameters of a few millimeters, and lubricated with grease, promise to be useful in small domestic and other appliances.

A 4 mm RADAR INSTALLATION

by H. ALLARIES *).

621.396.967.029.65

Radar installations operating at a wavelength of 8 mm are now widely employed in cases where a high degree of detail discrimination is required within a restricted area, e.g. for manoeuvring shipping in narrow and busy water-ways. This article describes an experimental 4 mm radar installation, built in Philips Research Laboratories, which uses various new tubes including a 4 mm magnetron and a 4 mm reflex klystron. The screen images obtained with this installation show that, although the maximum range is no more than a few kilometres, the detail discrimination at short distances is exceptionally good.

Various wavebands are at present in use for radar installations, the choice being determined by the operating range for which the installation is intended. Observations over distances up to several hundreds of kilometres require wavelengths of 25 cm¹⁾ and longer, distances up to about 100 km are covered with 10 cm waves, and for shorter ranges use is made of 3 cm waves and lower. In general it can be said that shortening the wavelength reduces the range of the installation. On the other hand, it improves the resolution, that is to say the power to discriminate on the radar screen between closely adjacent objects.

For certain special applications, for example where ships have to be manoeuvred in narrow and busy water-ways, this has led to the use of millimetre wavelengths. An article published earlier in this journal described an 8 mm installation²⁾. The range at such wavelengths is relatively small, but sufficient for the purpose. The resolution, however, is exceptionally high, making visible on the screen

large numbers of details which are of importance, for example, to navigation.

The availability of several new tubes — including a 4 mm magnetron and a 4 mm klystron — led to the construction in our Research Laboratories of a 4 mm radar installation. Part of it can be seen in *fig. 1*. This equipment has been used to investigate the effects of a further shortening of the wavelength on the resolution and range, and also the technical problems which this involves.

General design

To obtain the high est possible *radial resolution*, the transmitted radar pulses must be extremely short. On the other hand, the magnetron cannot work properly below a certain minimum pulse length. In practice the rule of thumb is used that the number of cycles in a pulse must be equal to the figure of merit *Q* of the cavity resonator system of the magnetron under optimum loading conditions. For most magnetrons this figure is roughly 200, which, at a wavelength of 4 mm, gives a minimum pulse length of 4 nanoseconds. The pulse length actually chosen is 5 nanoseconds. Theoretically this should result in a radial resolution of 0.75 m, but in practice it will be somewhat less favourable, owing to inevitable pulse distortion.

*) Philips Research Laboratory, Eindhoven.

¹⁾ A 25 cm radar is described by H. van Lambalgen and J. van der Plas in: The SGR 200 long-range surveillance radar at Schiphol Airport, Philips Telecomm. Rev. 22, 51-62, 1961.

²⁾ J. M. G. Seppen and J. Verstraten, An 8 mm-high resolution radar installation, Philips tech. Rev., 21, 92-103, 1959/60.

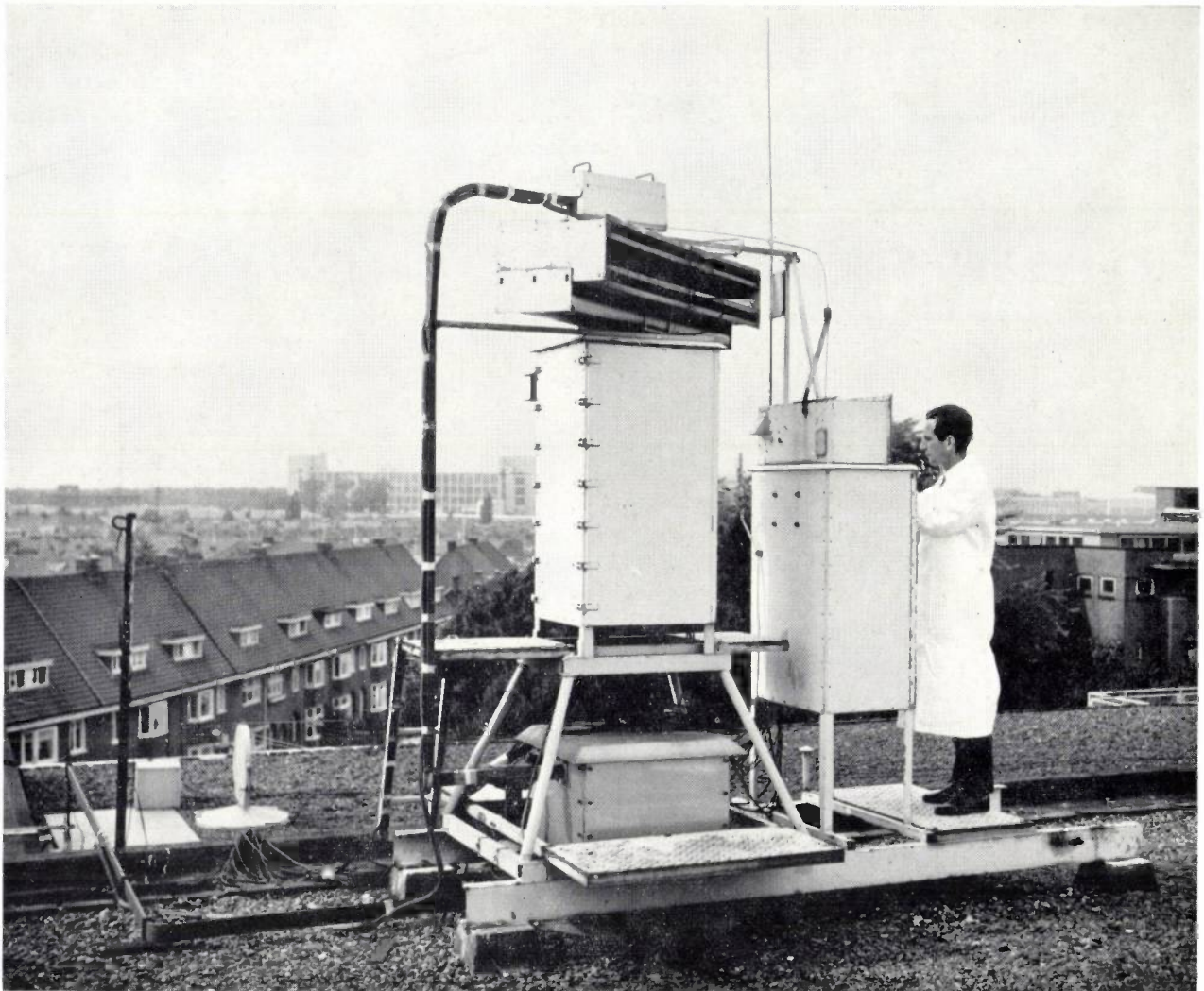


Fig. 1. Experimental 4 mm radar installation: the antenna system and part of the transmitter and receiver, mounted on the roof of the Eindhoven Research Laboratory.

The *tangential resolution*³⁾ is determined at every point by the width of the transmitted beam of RF energy. In installations of the type considered here it has to be remembered that the radar beam close to the antenna has roughly constant width, which is that of the antenna itself. At a certain distance away, depending on the aperture angle of the antenna, the beam becomes wider than the antenna by divergence. On the one hand, then, the antenna cannot be made too wide without adversely affecting the tangential resolution at very short ranges; on the other hand a narrow antenna has a large aperture angle, which results in a poorer tangential resolution on longer ranges. In the present case we compromised with an antenna width of 1.5 m. In the horizontal plane the antenna has an aperture angle (beam width) of 0.0027 radians, i.e. 0.15 degrees. From

this it can be calculated that the beam only becomes wider than the antenna itself at a distance of 560 m. Up to that point the tangential resolution is virtually constant and equal to 1.5 m.

At wavelengths of 3 cm and longer it is customary to use a common antenna for transmitting and receiving. To prevent the transmitted pulses from passing directly into the receiver, thereby overloading it, the receiver input during pulse transmission is short-circuited by means of a TR switch (duplexer) of the gas-discharge type. The firing (ionization) time of such switches, however, is in the order of several nanoseconds, so that with pulses as short as in millimetre radar they can provide no protection. For this reason, as in the case of the 8 mm radar installation, separate antennas are used for transmitting and receiving. Each antenna has the form of a very short parabolic cylinder, sandwiched between two flat, parallel plates ("cheese antenna", see fig. 1). Both antennas have the above

³⁾ See for example S. Silver, *Microwave antenna theory and design*, M.I.T. Radiation Laboratory Series No. 12, McGraw-Hill, New York 1949, Chapter 1.

mentioned width of 1.5 m. The vertical aperture is 35 mm, giving a beam width in the vertical plane of 6.7° . The directive gain of one antenna is $G_0 = 45$ dB.

If full use is to be made of the theoretical resolution, the cathode ray tube must be capable of displaying sufficient detail. The tube employed has a screen diameter of 40 cm, while the spot — provided the brightness is not excessive — can be reduced to a diameter of 0.5 mm. Therefore in order to obtain the optimum radial resolution of 0.75 m on the screen, the swept area should not exceed 300 m radius. Since the range of the installation is much greater, it is possible to switch over to areas with radii of 1 km and 3 km too; the screen does not then display all available radial details. For the *tangential* resolution it can be calculated that, within a 300 m range, the screen can display more details than the radar can detect, while the reverse is again the case for the other ranges.

A further design parameter, the *repetition frequency* of the radar pulses, can be given both as a minimum and a maximum. The minimum is governed by the consideration that the antenna, while traversing an angle of rotation equal to its beam width, must transmit at least one pulse, otherwise small objects would no longer be detected. The maximum speed of revolution of the antenna was fixed at $w = 120$ r.p.m., corresponding to an angular velocity of 4π rad/s. At the above-mentioned horizontal beam width of $\theta_h = 0.0027$ radians we thus arrive at a minimum pulse repetition frequency of $f_r \min = w/\theta_h = 4730$ c/s.

The maximum pulse repetition frequency is governed by two considerations. In the first place it must not be smaller than the time taken by a pulse to travel the theoretical range of the radar installation, there and back. As we shall see, in our case we can calculate for the latter a value of 4.7 km. If, to be on the safe side, we take the range to be 6 km, we then find a maximum pulse repetition frequency of 25 kc/s.

A second upper limit is set to the repetition frequency by the permissible thermal loading of the magnetron, or, to be more exact, by the permissible ratio between average power and peak power. This ratio, (called the duty cycle) which is equal to τf_r (τ being the pulse duration) can be roughly 1/5000 for the magnetron employed, giving for f_r a maximum permissible value of 40 kc/s.

Making f_r equal to the smaller of these two maxima we then obtain the maximum possible number of hits per target, i.e. as bright a display as possible. As will be seen, however, it proved necessary to reduce the pulse repetition frequency to 12.5 kc/s.

In order to turn to full advantage the possibilities offered by using such a short pulse duration ($\tau = 5$ ns), the receiver should have an adequate *bandwidth*. A larger bandwidth improves the pulse discrimination but increases the relative noise, thus reducing the sensitivity obtainable. A good compromise⁴⁾ is to choose the value of the bandwidth B between τ^{-1} and $2\tau^{-1}$. At the very short distances for which the 4 mm radar installation is intended, good pulse discrimination is more important than optimum sensitivity, for which reason we took $B = 2\tau^{-1} = 400$ Mc/s. Given the intermediate frequencies commonly used for radar and with conventional tubes, it would not be possible to achieve such a bandwidth; in this experimental installation, however, use is made of several travelling-wave tubes (four in cascade), allowing the choice of a 4 Gc/s intermediate frequency. The relative bandwidth is then only 10%.

We shall return to the design of the amplifier when we discuss the receiver. At this stage it is useful to note that a noise figure of $F = 222 \times$ was measured on the receiver. The apparent noise power at the input is equal to FkT_0B , where k is Boltzmann's constant and T_0 the standard noise temperature of 290 °K. The minimum detectable signal power S_{\min} is roughly equal to this:

$$S_{\min} \approx F k T_0 B = 3.61 \times 10^{-10} \text{ W.}$$

The range R_{\max} of the radar installation can now be calculated from the familiar formula:

$$R_{\max}^4 = P_0 \frac{A^2 \sigma}{4 \lambda^2 S_{\min}},$$

where P_0 is the peak power of the magnetron, A the effective area of the antenna and σ the reflecting area, normally put at 1 m^2 . After inserting this value and writing $P_0 = 20$ kW and $A = 0.042 \text{ m}^2$, we find for R_{\max} the value 4.7 km.

The foregoing data and some additional data of the installation are presented in *Table I*.

Table I. Data of experimental 4 mm radar installation.

Wavelength	λ	= 4 mm
Antenna width	h_h	= 1.5 m
Antenna height	w	= 35 mm
Maximum speed of revolution of antenna	v	= 120 r.p.m.
Pulse length	τ	= 5 ns
Pulse repetition frequency	f_r	= 12.5 kc/s
Peak transmitting power	P_0	= 20 kW
Average transmitting power	$P_0 \tau f_r$	= 1.3 W
Bandwidth	B	= 400 Mc/s
Centre frequency of IF band	f_m	= 4 Gc/s
Ranges		0.3 km; 1 km; 3 km
Noise figure of receiver	F_{tot}	= 23.5 dB
Conversion loss of crystal mixer	L_1	= 13.6 dB

⁴⁾ See J. F. Reintjes and G. T. Coate, *Principles of radar*, McGraw-Hill, New York 1952, p. 392 ff.

We shall now describe at greater length the main parts of the installation, viz: the transmitter, the receiver, the display unit and the various ancillary equipment.

The transmitter

Modulator circuit

The chief problem in designing the transmitter concerned the generation of the very short high-voltage pulses needed for setting the magnetron in oscillation. We shall therefore examine this problem in some detail.

To operate properly, the magnetron employed requires a voltage pulse with an amplitude of 17 kV. If, instead of insisting on a rectangular pulse, we

which has to be charged up in 5 ns to -17 kV. For a linearly rising voltage this calls for a continuous charging current $i = C\Delta V/\Delta t$ of 102 A. Compared with this the current of 3 to 4 A consumed by the oscillating magnetron itself is very small, and will therefore from now on be disregarded. The average power $\frac{1}{2}C(\Delta V)^2 f_r = 54$ W, required for charging, presents no particular problems either, but the very high charging current of 102 A would obviously make exceptionally high demands on the pulse-generating tube.

To avoid this difficulty we took as our starting point the consideration that the magnetron does not begin to oscillate before the cathode voltage has dropped to about -14 kV, so that before that time the shape of the voltage pulse is of little significance.

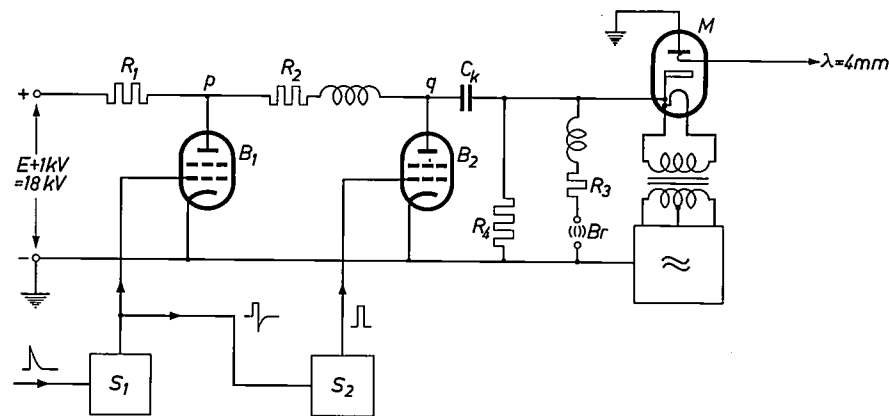


Fig. 2. Simplified circuit of the modulator. *M* 4 mm magnetron. The circuit must periodically supply to the magnetron cathode a negative voltage pulse of -17 kV, with a sufficiently short rise time to cause the magnetron to generate a wave train of 5 nanoseconds duration. The first part of the pulse is generated with *B*₁, the second with *B*₂. These tetrodes receive their triggering pulses from the respective blocking oscillators *S*₁ and *S*₂.

can be satisfied with a triangular pulse with a half-height width of 5 ns, then the rise time will also be 5 ns.

In practice the anode of the magnetron is always at earth potential, and cathode and filament are given a high negative potential by the pulse. The circuit supplying this pulse is called the modulator. The modulator circuit used in this installation, and which will now be discussed, is represented schematically in *fig. 2*.

In view of the high potential it receives, the magnetron filament has to be fed by means of a transformer. In spite of careful construction, the intrinsic capacitance of the transformer cannot easily be kept below 10 pF. Moreover the magnetron has an input capacitance of 5 pF, and the tube delivering the voltage pulse has an output capacitance of 10 pF. Adding to this roughly 5 pF for the wiring capacitance, we arrive at a total capacitance *C* of 30 pF,

It can be seen from *fig. 3* that the pulse is therefore built up in two parts, the first with a rise time of 50 ns and the second with a rise time of 5 ns. The

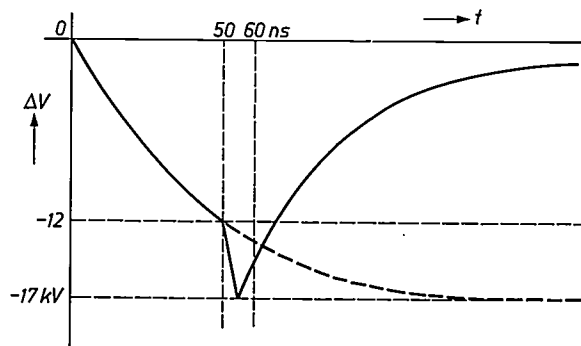


Fig. 3. The voltage pulse ΔV on the cathode of the 4 mm magnetron is built up in two steps. In the first part the voltage is made -12 kV negative in 50 nanoseconds, and in the second it is brought to -17 kV in 5 ns.

Without the measures described in the text, the cathode voltage at the end of the pulse would return to zero following the right-hand part of the solid curve.

second part of the pulse was generated by a tetrode type QEP 20/18, which can deliver a current of 30 A at a somewhat increased heater voltage. For a linearly rising pulse it is possible with a current of this magnitude to charge a capacitance of 30 pF to 5 kV in 5 ns. The first part of the pulse now has to bring the cathode potential from zero to -12 kV while the second part brings the cathode in 5 ns to -17 kV.

As can be seen from the diagram in fig. 2, two tubes B_1 and B_2 are used for the modulator, the anodes of which are connected in parallel via a resistor R_2 and coupled to the magnetron cathode via a capacitor C_k . For B_1 a type QB 5/1750 tetrode was chosen, while B_2 is the QEP 20/18 tetrode already mentioned.

When the circuit S_1 (which will presently be discussed, together with S_2) receives a triggering pulse, it applies to the grid of B_1 a pulse of 50 ns duration and 800 V amplitude. As B_1 is made suddenly conductive, the cathode voltage of the magnetron drops in 50 ns to -12 kV. Thereupon circuit S_2 applies to the grid of B_2 a pulse of 5 ns duration and 800 V amplitude. Since R_2 is a wire-wound resistor it has significant self-inductance. For a transient as fast as a pulse of 5 ns the impedance of R_2 is sufficient to ensure the almost complete separation of points p and q , so that during the voltage drop of 5 kV, caused by B_2 becoming conductive, only the above-mentioned capacitance of 30 pF needs to be charged up. Although the impedance of R_2 for the first part of the pulse is much lower, here too this resistance still plays a useful role; because of its presence the potential at point p drops somewhat faster than at point q . The result is that the power dissipated in B_1 is kept within permissible bounds.

After the end of the pulses from S_1 and S_2 , tubes B_1 and B_2 stop conducting and points p and q have again to be raised via R_1 to the original potential of $+18$ kV. Because of the various stray capacitances present, this takes place relatively slowly. Without further precautions, the cathode pulse would therefore acquire the long tail indicated in fig. 3. This is prevented by incorporating a spark gap in parallel with the cathode (Br in fig. 2). The charging current for the capacitance of the spark gap produces in resistor R_3 a voltage drop which delays the sparkover of the gap until just after the cathode voltage has reached its maximum value. This gives the voltage on the cathode of the magnetron the form shown in fig. 4. The leading edge of the pulse is thus built up in two steps over a high impedance, while the discharge of the relevant capacitances takes place via the spark gap and the low impedance of R_3 .

The spark gap is situated in a strong air current, with the object of rapidly extinguishing the spark. At the moment of extinction a certain residual charge may be present in the coupling capacitor C_k , which must be drained off through R_4 . This resistance must be small enough to allow all charge to leak away before the next pulse arrives. At the same time the potential at points p and q must then again have risen to 18 kV, which means that R_1 cannot exceed a maximum value. That maximum, however, should be chosen as high as possible to ensure that the power supply is not loaded too unevenly. A value of 100 k Ω proved to be a good compromise.

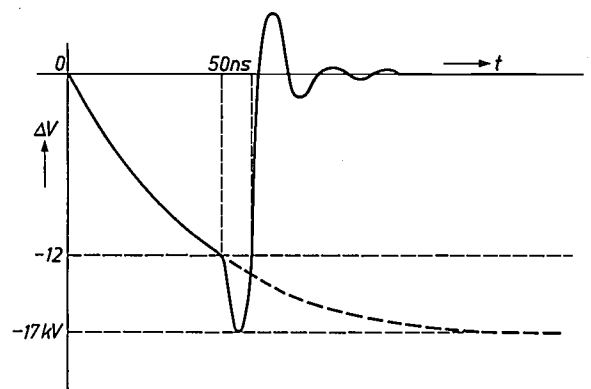


Fig. 4. By means of a spark gap (Br in fig. 2), the voltage on the cathode of the magnetron is very rapidly returned to zero at the end of the pulse.

The 50 ns pulse for the grid of B_1 in fig. 3 is generated in the blocking oscillator circuit S_1 , a diagram of which is shown in fig. 5. In order for tube B_1 to be made strongly conductive in a short time, the grid must be raised in the same time to a high positive potential, resulting in a high grid current, i.e. a low grid impedance. The special feature of the blocking oscillator circuit is therefore that it can supply a large current through a low impedance. For this purpose the four tetrodes type QQE 02/5, operated in parallel in this oscillator, have a high mutual conductance and an amply dimensioned cathode. An examination of this circuit shows that the current tapped from the autotransformer T_1 , to which transformer T_2 is connected, is the sum of the anode current, the grid current and the current through the voltage-limiting diode OA 211, i.e. a total of 20 A. From the secondary side of T_2 a current of 5 A is taken at a voltage of 900 V, approximately 2 A flowing through the terminal resistance of 440 ohms and the remainder being available for grid current.

The circuit S_2 in fig. 2, which delivers the pulse for the modulator tube B_2 , is a blocking oscillator of the same type as in fig. 5, but now using two QQE 02/5

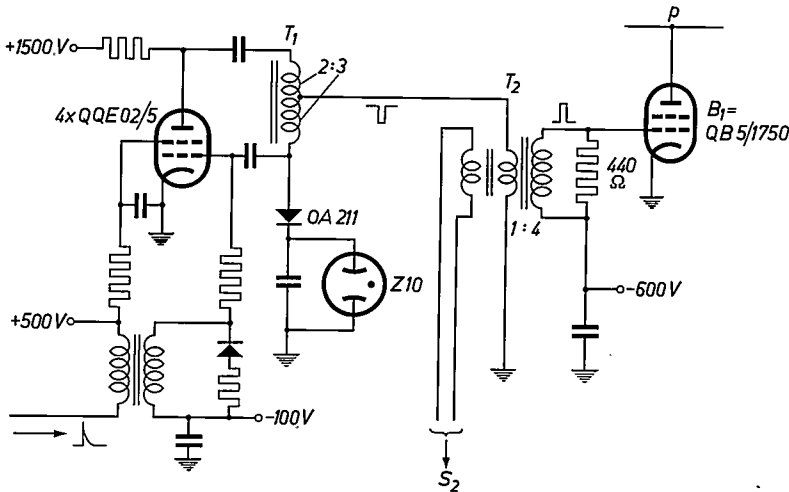


Fig. 5. Circuit diagram of the blocking oscillator S_1 , which supplies the driving pulse to the grid of B_1 in fig. 2.

voltages occurring in the circuits described gave rise initially to some flashover between the base pins of the tubes. This was overcome by applying silicon grease between the pins.

Overload protection

As mentioned when discussing the design, the theoretically permissible modulator pulse repetition frequency of 25 kc/s was not feasible and had to be reduced to 12.5 kc/s. The reason for this is that, although the magnetron does not begin to oscillate in the desired mode at a wavelength of 4 mm until the voltage is 14 kV,

tetrodes in parallel. The circuit diagram can be seen in fig. 6. The pulse that starts this oscillator is obtained from an auxiliary winding of transformer T_2 in fig. 5. The second blocking oscillator is required to start about 50 ns after the first; the necessary delay is provided by the grid resistor R_g together with coupling capacitor C_g . The length of the delay can further be regulated slightly with the potentiometer P .

it starts oscillating in another mode at a lower frequency earlier, owing to the rather slow initial rise of the anode voltage in our pulse (fig. 4). The energy thereby generated cannot leave the magnetron and causes extra heating of the cathode.

Since the pulse to be delivered by S_2 has to be much shorter than that from S_1 , additional measures are taken to limit the length of the pulse from the blocking oscillator. In the first place the autotransformer T_3 is rated for saturation. Secondly an extra stage containing four QQE 02/5 tetrodes is employed. As a result of the high negative bias of this stage, it can only be triggered by the peaks of the pulses from the oscillator.

To prevent damage to the cathode an H-bend is fitted directly to the output waveguide of the magnetron, i.e. a piece of rectangular waveguide bent over its short side. As can be seen in fig. 7, the wall of the bend is slotted on the outside, forming a kind of grille. While the 4 mm energy follows the waveguide, the light radiated from the hot cathode passes through the slots on to a photoconductor. The latter is incorporated in a circuit which automatically reduces the heater current of the magnetron if the light intensity, i.e. the operating temperature of the cathode, exceeds the permissible maximum.

The cores used for transformers T_3 , T_4 and T_5 are ferrocube cores with a diameter of 10 mm. The high

The 4 mm energy is finally conducted to the rotating antenna by means of a rotary joint of conventional construction.

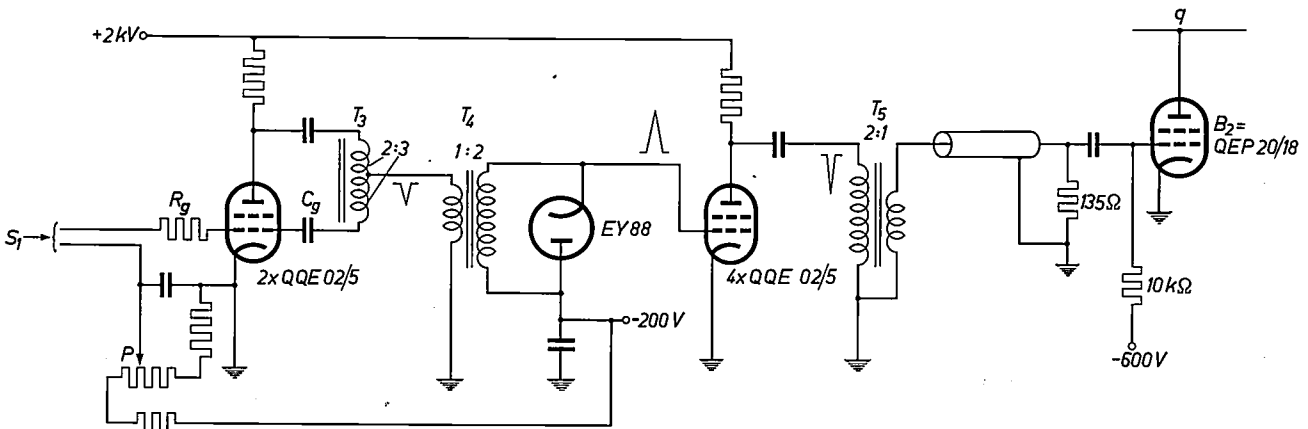


Fig. 6. Circuit diagram of blocking oscillator S_2 , with follower stage which supplies the pulse to the grid of B_2 in fig. 2.

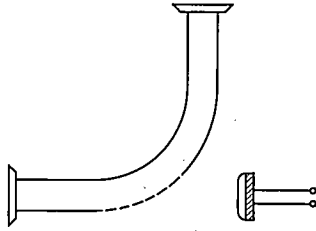


Fig. 7. *H*-bend in the output waveguide of the magnetron, slotted on the outside. The light radiated from the cathode passes through the slots to a photocell, and is used for automatically reducing the heater current to prevent thermal overloading of the cathode.

The receiver

The parts of the receiver are shown in *fig. 8*. The crystal mixer *K* is mounted directly above the receiving antenna *B*, from which it receives its signals via a rectangular wave guide and a rotary joint *C*. In the local oscillator a reflex klystron generates RF energy with a frequency of 71 Gc/s; the intermediate frequency is therefore 4 Gc/s (wavelength 7.5 cm). The local oscillator signal is mixed by means of a directional coupler.

The large bandwidth of 400 Mc/s required for the image quality does not of course present any problems at the signal frequency of 75 Gc/s, the relative bandwidth in this case being only 0.5%. Nor are there any difficulties in the IF amplifier, where the relative bandwidth is no more than 10%; we mentioned at the outset that the relatively high intermediate frequency of 4 Gc/s was chosen for this very reason. Because of this high intermediate frequency, however, a new problem arises in the crystal mixer: the difference of 4 Gc/s between the signal and the local oscillator frequency would require from the mixer device a relative bandwidth of more than 5% in order to be able to supply to the crystal the received signal together with the LO signal. This problem was solved by departing from the tuning procedure commonly used in radar installations for longer wavelengths. In the normal procedure the plunger in the waveguide which incorporates the crystal mixer is adjusted so as to produce the highest possible crystal current during the operation of the local oscillator; in other words the system is tuned to the local oscillator frequency. Making use of the fact that the available reflex klystron delivers sufficient local oscillator power, we decided to tune to the signal frequency. In spite of the mismatch the local oscillator then still delivers a current of 0.5 mA in the crystal mixer.

Another advantage of using such a high intermediate frequency is that a substantial part of the

local oscillator's contribution to the noise is eliminated. The local oscillator, too, generates a spectrum of noise frequencies, and the width of that spectrum is determined by the quality of the output cavity of the klystron. In radar operating on conventional wavelengths the mutual beat frequencies of the noise spectrum lie partly in the IF amplifier band, but at our high intermediate frequency they lie outside it.

The crystal with its cat's whisker is fitted in a mount which has the same inside dimensions as a 4 mm waveguide. To obtain a low intrinsic capacitance and a large mixing effect, the cat's whisker must be extremely thin at the point where it makes

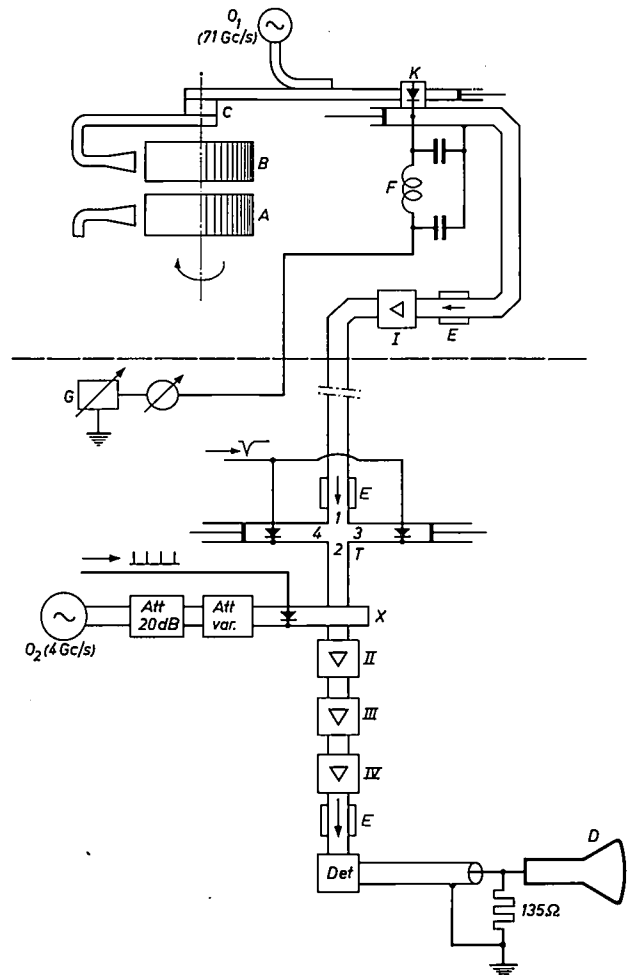


Fig. 8. Schematic survey of the 4 mm radar receiving system. *A* transmitting antenna. *B* receiving antenna. *C* rotary joint. *O*₁ local oscillator. *K* crystal mixer, in which the signal band of 400 Mc/s width is shifted from the signal frequency 75 Gc/s to the intermediate frequency 4 Gc/s (7.5 cm wavelength). *F* filter. *G* DC voltage source. *E* directional isolators. *I*, *II*, *III*, *IV* amplifying stages using travelling-wave tubes. *T* crystal switch, providing the swept gain. *X* cross-guide coupler. *O*₂ auxiliary oscillator, one purpose of which is to provide range marker rings on the screen. *Det* detector (disc-seal triode type EC 157). *D* cathode ray tube.

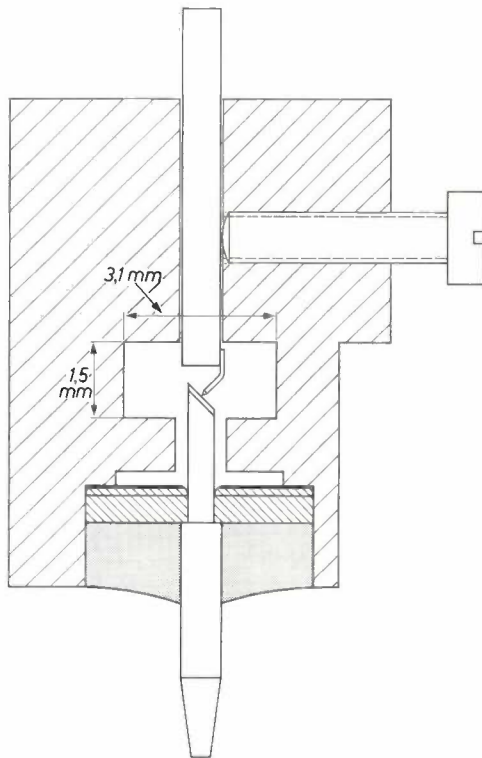


Fig. 9. Mount of the 4 mm mixing crystal, specially designed to minimize the length of the cat's whisker, this keeping the inductance as low as possible.

contact with the crystal wafer. A thin cat's whisker, however, implies a high series inductance which, in crystal mounts of conventional construction, is further increased by the fact that the cat's whisker has a loop in it, so that the point makes spring contact with the crystal.

This drawback has been overcome by the construction illustrated in fig. 9. A germanium wafer is mounted at an angle of 45° on the output pin. The cat's whisker is kept very short and has a diameter of only $20 \mu\text{m}$; the tip of the whisker is pointed electrolytically. The whisker is welded to a thick pin, which largely bridges the height of the waveguide. When the pin is rotated the whisker comes in contact with the crystal, the contact pressure being derived from a slight torsion in the thin whisker. Because of its higher electron mobility — and hence its lower resistance — germanium was chosen for the crystal wafer rather than silicon.

In spite of the above-mentioned precautions the conversion loss is high. This loss, which was found to be 14 dB, occurs partly at the crystal output. Although the capacitance here is kept as low as possible, in this case it is not compensated in the usual manner by means of a tuned circuit at the input of the IF stage.

With a view to keeping the bandwidth as large as possible, the 4 mm waveguide containing the crystal mount is coupled directly to a 7.5 cm waveguide for the IF output signal. As can be seen in fig. 10, the IF signal is conducted via a cylindrical pin coaxially through a hole in the common wall. The pin is at the same time a component of a crossbar coupling, the purpose of which is to obtain a good match between the crystal output and the 7.5 cm waveguide. The crossbar is not metallically connected to the wall of the waveguide but is led out capacitively, making it possible to measure the crystal current at this point. The test line contains, in addition to a filter

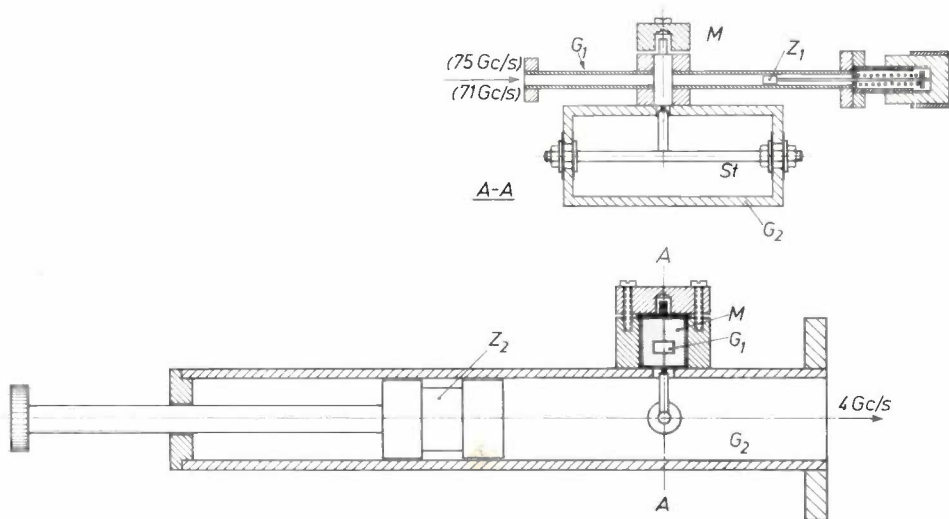


Fig. 10. Mechanical details of the mixer stage, showing the crystal mount M , the coupling to the 4 mm waveguide G_1 , which receives the radar signal (75 Gc/s) and the local oscillator signal (71 Gc/s), and the coupling to the 7.5 cm waveguide G_2 for the IF signal. The latter coupling is a crossbar type St . Both waveguides contain a tuning plunger (Z_1, Z_2); the plunger for the 4 mm guide, the adjustment of which is extremely critical, has practically no backlash.

for protecting the crystal from voltage surges, a variable biasing device for adjusting the crystal to the optimum operating point.

The IF signal passes along the 7.5 cm waveguide to the first travelling-wave tube (*I*), still fitted in the antenna pedestal. This guide contains a directional isolator, which prevents very strong radar echoes from causing repeated reflections, which would appear on the screen as a series of dots. The first amplifying tube is set to give a low noise figure for a moderate gain (18.5 dB). The former was measured at 9 dB (or $8\times$).

The signal from the first amplifying tube is conducted through a 12 metre-long waveguide to the installation in the operating room. This waveguide has a low and wide cross-section with a view to avoiding excessive dispersion, i.e. undue transit-time differences between the components of the very broad frequency spectrum, which would give rise to pulse distortion. The broader the guide, the lower these relative differences are.

In front of the second amplifying stage the waveguide contains another directional isolator, specially intended for suppressing reflections in the variable attenuator which follows next in the waveguide. The operation of this component can only be described here very roughly. It contains a magic *T* (see fig. 8), arms 3 and 4 of which contain diodes and shorting plungers⁵⁾. Immediately before the pulse is sent out the diodes are made conductive, as a result of which incoming signals are almost completely reflected and absorbed in the directional isolator. During the moment of transmission the receiver is therefore non-receptive. After this the diode current decreases exponentially, so that the signal transmission from arm 1 to 2 gradually increases. This time-dependent gain control, which appears as a localized gain control on the PPI tube, makes the brightness of the image more uniform in the radial direction.

The signal next passes a cross-guide coupler. By means of this coupler, which gives 20 dB attenuation, 4 Gc/s pulses can be added to produce range marker rings on the PPI tube. The 4 Gc/s signal can also serve for setting the subsequent amplifier stages *II*, *III* and *IV*, each of which contains a travelling-wave tube. Since stage *II* makes a much smaller contri-

bution to the total noise than stage *I*, it is set to give a somewhat higher gain (25 dB). The measured noise figure of this stage was 11.1 dB (i.e. $13\times$). Stage *III* has an even higher gain, of 35 dB. Its relative noise contribution is negligible and was therefore not measured. The last stage serves as a power amplifier and can deliver 10 W. The total gain of the four stages in cascade is between 90 and 100 dB.

The noise figure of a multi-stage receiver can be calculated using the familiar formula:

$$F = F_1 + (F_2 - 1)G_1^{-1} + (F_3 - 1)(G_1G_2)^{-1} + \dots + (F_k - 1)(G_1G_2 \dots G_{k-1})^{-1},$$

where F_i and G_i are respectively the noise figure and the gain of stage *i* of the receiver.

Considering the crystal mixer as the first stage of the receiver, it is better to introduce: $L_1 = \text{conversion loss} = G_1^{-1}$, and $n_1 = \text{noise temperature}^6) = F_1G_1$. We can then rewrite the formula as:

$$F = L_1 [n_1 + F_2 - 1 + (F_3 - 1)G_2^{-1} + \dots].$$

The measured conversion loss of the crystal was 23 (i.e. about 14 dB) and the measured noise temperature 2.5. For determining the noise figures of the various amplifier stages, use was made of a gas-discharge noise source for the 4 mm band⁷⁾. Substitution in the above formula of the separately measured values for the individual stages gives the earlier mentioned total noise figure of $222\times$ (i.e. 23.5 dB).

When adjusting the operating point of the various stages it was taken into account that the gain of a travelling-wave tube is not constant but decreases as the strength of the input signal increases. This relation can be influenced by a suitable choice of the voltage on the helix: see for example the schematic curves 1 and 2 in fig. 11. In the last two stages the helix voltage is chosen so that the gain only begins to decrease at very large signal strengths. The total gain therefore follows a curve as shown schematically by curve 3 in fig. 11. For the largest signals the curve of the gain as a function of input power is flat, which again contributes to the uniformity of the image brightness and makes a limiter for the CRT superfluous.

Detection of the output signal from the last amplifying stage is effected by a disc-seal triode type EC 157, the grid-cathode space of which is incorporated in the 7.5 cm waveguide as illustrated in fig. 12. The waveguide profile is shaped in such a way as to match the grid-cathode impedance to that of the

⁵⁾ For an explanation of the operation of the magic *T*, see: C. L. Ragan, Microwave transmission circuits, M.I.T. Radiation Laboratory Series No. 9, McGraw-Hill, New York 1948, p. 706. For diode switching in waveguides: R. V. Garver, J. A. Rosado and E. F. Turner, Theory of the germanium diode microwave switch, I.R.E. Transactions on microwave theory and techniques 8, 108-111, 1960. Applications of the magic *T* are discussed in an article by J. P. M. Gieles, Applications of microwave triodes, Philips tech. Rev. 22, 16-28, 1960/61.

⁶⁾ See for example H. C. Torrey and C. A. Whitmer, Crystal rectifiers, M.I.T. Radiation Laboratory Series No. 15, McGraw-Hill, New York 1948, pp. 213 and 227.

⁷⁾ See P. A. H. Hart, Standard noise sources, Philips tech. Rev. 23, 293-309, 1961/62.

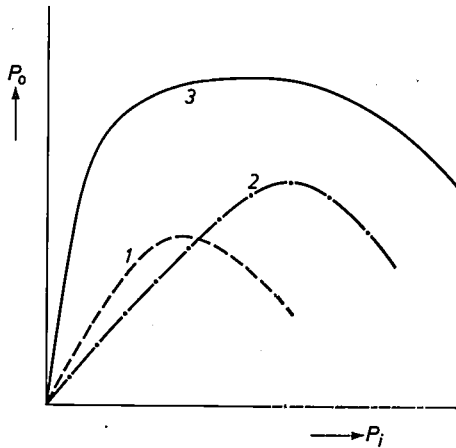


Fig. 11. Output signal power P_o of a travelling-wave tube as a function of signal input power P_i , represented schematically. At large input signals the gain decreases, finally becoming less than unity. By giving the four tubes in the receiver different operating points (e.g. curve 1 for tube III and curve 2 for tube IV) a total gain characteristic is obtained as represented schematically by curve 3. The curve flattens for strong signals.

waveguide while maintaining the required bandwidth of 400 Mc/s.

The choice of an EC 157 as detector was due to the fact that an experimental CRT was available which could be completely cut off by a negative bias as low as 6 V. This made it possible to dispense completely with a video amplifier, which, after the detector, would have needed a bandwidth of 200 Mc/s. This meant, however, that the detector had to be capable of delivering through its output impedance, formed by the 135 ohm coaxial cable through which the video signal is applied to the CRT, a current of at least $6/135$ A, i.e. about 50 mA; a crystal detector cannot readily be made to supply such a current.

The grid bias for the EC 157 is so chosen to make the tube work as an anodebend detector. The video

signal appears across an anode resistance of 1000 ohms and is supplied to the coaxial cable via a coupling capacitance of 470 nF. Incorporated in the supply line to the control grid of the CRT, by a method familiar in television engineering⁸⁾, is a small inductance designed to obtain the required bandwidth of 200 Mc/s in the transmission of the video signal. In order to be able to display the video signal on an oscilloscope, the terminating impedance for the coaxial cable is not fitted to the CRT but in a removable plug on the front panel of the PPI console.

No measures are taken for DC restoration⁹⁾ because most of the time there is no signal and therefore the charge displacement on the coupling capacitor of 470 nF is negligible.

Display unit and ancillary equipment

The main components of the display unit, apart from the CRT, are the sawtooth generator, which energizes the CRT deflection coil, and the servo system that synchronizes the deflection coil with the antenna. These devices follow familiar principles of construction and will not be described here in detail. It is, however, useful to note the considerable extent to which the currents and voltages to be delivered by the sawtooth generator are increased at the short ranges at which this radar installation operates. The echo from an object at a distance of 300 m away reaches the receiver 2 microseconds

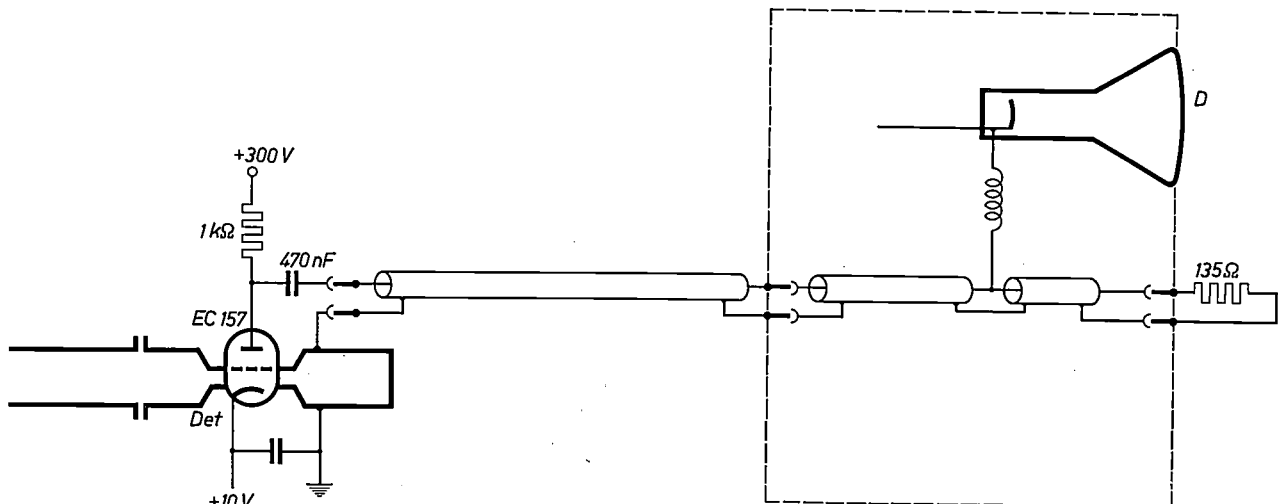


Fig. 12. The intermediate frequency detector is an EC 157 disc-seal triode, whose grid-cathode space is incorporated in the 4 Gc/s waveguide. Particulars of the connection to the cathode ray tube D are mentioned in the text.

⁸⁾ See G. E. Valley and H. Wallman, Vacuum tube amplifiers, M.I.T. Radiation Laboratory Series No. 18, McGraw-Hill, New York 1948, Chapter 2.
⁹⁾ See F. Kerkhof and W. Werner, Television, Philips Tech. Library, Centrex, Eindhoven 1952, Part I, p. 88.

after transmission of the radar pulse. Where the range is set to 300 m this means that the spot has to move from the centre of the tube to the periphery in $2 \mu\text{s}$. With a view to keeping the voltage across the deflection coil within reasonable limits we gave the coil relatively few windings, but this necessitated

ductive state must maintain a certain reserve of anode voltage, a supply voltage of 800 V was needed. The required current can be obtained with two E 130 L tubes in parallel.

The equipment further comprises, in addition to the power pack, all circuits needed for generating

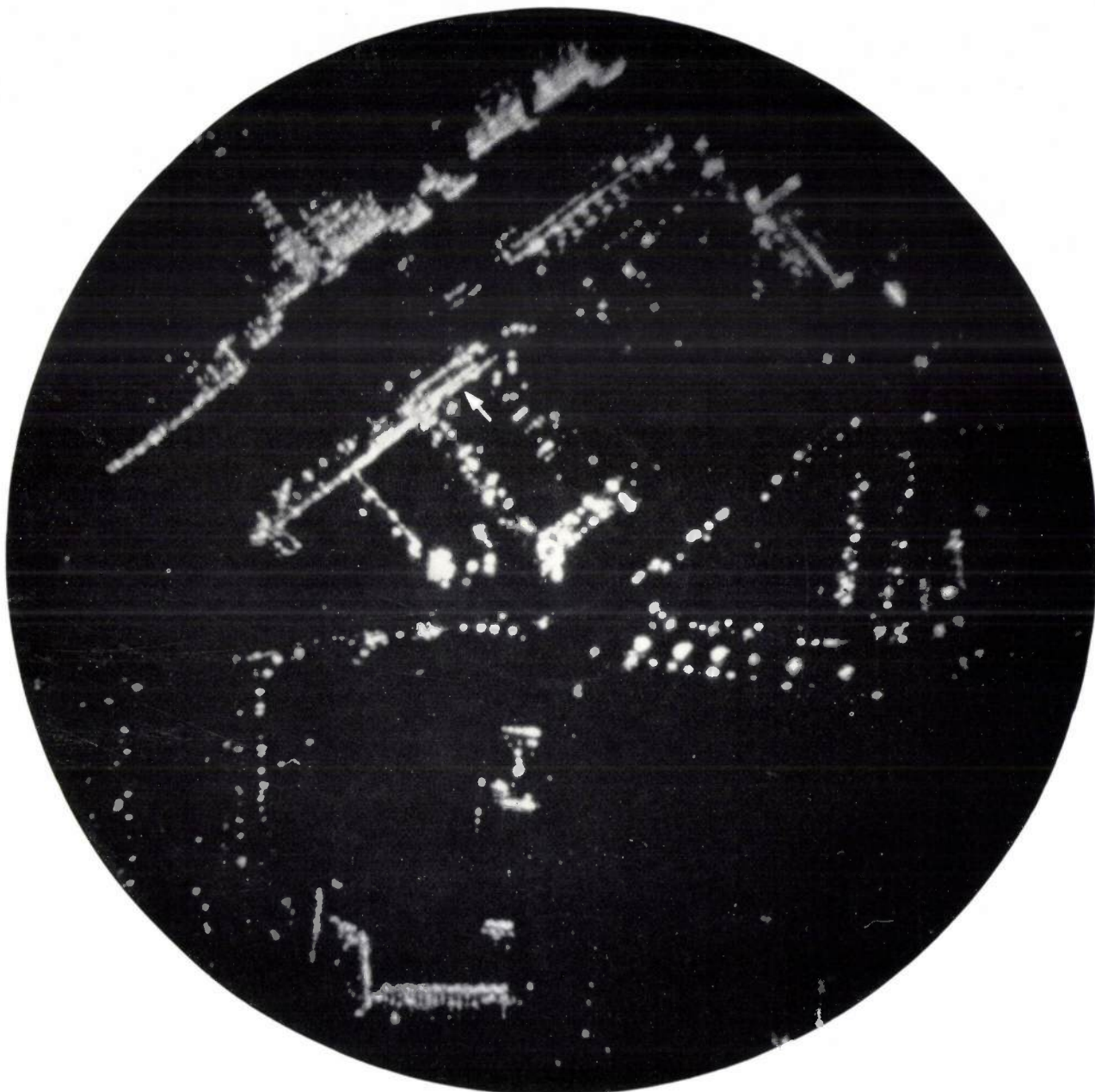


Fig. 13. The radar display covering the part of the town and the Philips factories immediately surrounding the Eindhoven Research Laboratories. The range was set here at 300 m.

a relatively high deflection current. From the inductance value obtained, $L = 800 \mu\text{H}$, and taking into account the number of ampere-turns required for the maximum deflection of the spot, the amplitude of the energizing current is easily calculated to be 1.5 A and the amplitude of the voltage 600 V. Since the output tube in the sawtooth generator in the con-

the various pulse and triggering signals. These signals are obtained by frequency division from the output signal of a crystal-controlled 1500 kc/s generator. The highest frequencies in the sequence are those used for producing the range marker rings on the PPI tube, while the lowest is the pulse repetition frequency (12.5 kc/s). Since, after a number of fre-



Fig. 14. Glass wall of a canteen on the roof of the Research Laboratories and the roof balustrade 3 m in front of it, each separately visible in the radar display in fig. 13 (marked by arrow). The tall factory buildings in the background can be seen top left on the radar screen.

quency divisions, the leading edges of the pulses may show some jitter, the leading edges of the pulses for the lowest frequencies are directly coupled with those of the oscillations of the crystal oscillator.

Performance and discussion

A radar display obtained with this installation when the range is set to 300 m is shown in fig. 13. At the point marked by an arrow it can be seen how the front wall of a building is separated in the display quite distinctly from a balustrade about 3 m in front of it. The actual situation on the site is shown in fig. 14. The rear wall of the building also appears in the display. This is bound up with the fact that the front wall consists to a large extent of glass and thus passes part of the 4 mm energy.

Fig. 15 shows the radar display of the same objects when the range is set to 1000 m. As can be seen, not many echoes are received beyond this range. The effective maximum range of the installation is therefore roughly 1 km, which is a lot shorter than the theoretical value of 4.7 km. There are several possible explanations for this.

a) The microwave energy passes at the transmitting side through about 1.5 m of waveguide, and at the receiving side through about 1 m. To minimize the losses the guide used for this purpose is the 5 mm type (WG 25) which is just narrow enough not to transmit energy in the wrong mode (TE_{02} mode). Further, red copper is used in-

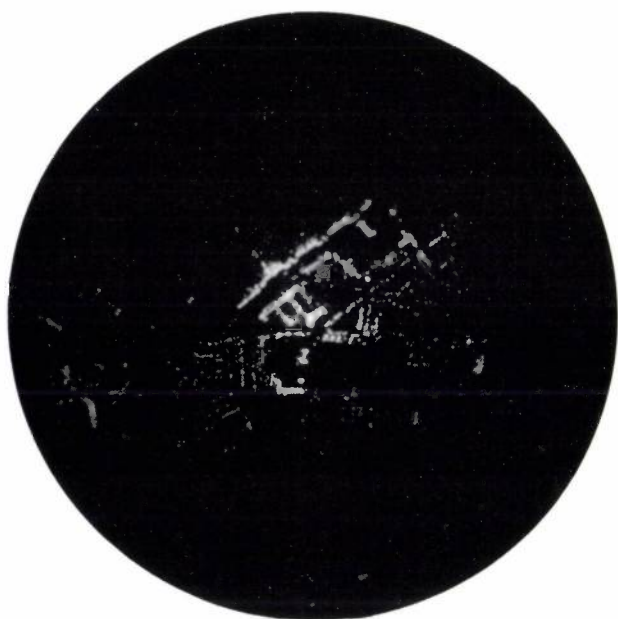


Fig. 15. As fig. 13, but with the range set at 1000 m. Beyond 500 m the amount of detail reproduced rapidly decreases.

stead of brass for the waveguide. The damping of the two sections of waveguide together is still 3.5 dB, however. Added to this are the losses of the two rotary joints, together amounting to 2.4 dB, so that the total damping in the microwave part is about 6 dB. It is possible to reduce the damping by shortening the waveguide connections, which might be done in the present installation for example by shifting the point of rotation of the antennas.

b) The influence of atmospheric losses, which occur during the propagation of energy in free space, is apparently relatively low. The pictures of the displays were taken in fine weather, and, as reported in the literature ¹⁰⁾, the absorption of 4 mm waves in oxygen is 0.2 dB/km and for uncondensed water vapour 0.05 dB/km at a degree of humidity of 44%. This adds up to 0.25 dB/km, which, for radar, where the energy travels twice the distance to the object, means 0.5 dB per km range. Compared with the damping mentioned under (a) this is not very significant.

In rain or mist the situation would be quite different. Under these conditions the following figures apply (including the radar multiplication factor of 2):

In mist		
of 0.23 g/m ³ (400 m visibility):	1.6 dB/km	
of 2.3 g/m ³ (100 m visibility):	10 dB/km	
In rain		
of 0.25 mm per hr. (drizzle):	0.4 dB/km	
of 1 mm per hr. (light rain):	1.6 dB/km	
of 16 mm per hr. (heavy rain):	16 dB/km	

To these figures we must add the 0.5 dB/km for absorption in oxygen and water vapour.

In mist, but particularly in rain, the loss in question is not so much due to absorption as to scattering. Part of the scattered energy will arrive in the receiving antenna and cause interference comparable to noise, blurring the echoes which are already attenuated by absorption. The effects of this scattering can be overcome to a large extent by using antennas that polarize the waves circularly instead of linearly.

c) The range formula, which we discussed when dealing with the design, is presumably limited in its application to 4 mm waves. There is reason to assume that the reflection of such short waves involves more losses than in the case of longer micro-

waves. As mentioned in connection with fig. 13, the 4 mm waves can readily pass through certain objects, such as glass walls. On the other hand, with waves as short as this there is a real chance of actual reflection from parts of an object, the reflected beam then being *directed*, and in general *not* back to the receiving antenna. All in all, then, the formula referred to gives only a first order approximation of the true range.

When dealing with the receiver we stated that the first travelling-wave tube has a noise figure of 9 dB (8×). Because of the high conversion loss of the crystal mixer (14 dB, see page 281) the noise figure of the first travelling wave tube has a fairly marked influence on the total noise ¹¹⁾. A considerable improvement can therefore be achieved by using a tube with lower inherent noise. Admittedly this does not have very much influence on the range, which is of course inversely proportional to the fourth root of the minimum detectable signal — the latter being directly proportional to the total noise — but it does mean that with less noise more echoes are visible within the swept area. In the experiment described here the main emphasis was placed on achieving the best possible resolution. For this purpose the less favourable noise figure of the first travelling wave tube was not felt to be a disadvantage.

¹¹⁾ This can be derived directly from the calculation given in small print on page 282: F_2 is the noise figure of the first tube; the term $n_1 = F_1 C_1$ beside F_2 is relatively small owing to the high conversion loss G_1^{-1} .

Summary. To investigate the extent to which the resolution of a short-range radar can be improved by using wavelengths shorter than the conventional 8 mm, tests were made with an experimental 4 mm installation. A high radial resolution depends on the transmitted pulses being as short as possible. The pulse length of 5 ns adopted is very close to the minimum required for the proper operation of the magnetron. To achieve the very short rise time for the magnetron pulses a modulator was built that delivers a voltage pulse in two steps. For the purpose of amplifying the received echo pulses without distortion the IF amplifier in the receiver should have a bandwidth of 400 Mc/s. The choice of a very high intermediate frequency, i.e. 4 Gc/s, allowed the relative bandwidth of the IF amplifier to be limited to 10%. Amplification at 4 Gc/s was made possible by using in the receiver four travelling-wave tubes connected in cascade. The crystal mixer before the amplifier is contained in a specially designed mount. The detector for the 4 Gc/s signal is a disc-seal triode type EC 157, which can deliver more video energy than conventional crystal detectors. Because of this and the use of an experimental CRT of exceptional sensitivity, a video amplifier between detector and CRT could be dispensed with.

¹⁰⁾ See C. W. Tolbert and A. W. Straiton, Attenuation and fluctuation of millimeter radio waves, IRE Nat. Conv. Rec. 5, Part 1, pp. 12-18, 1957.

RECENT SCIENTIFIC PUBLICATIONS BY THE STAFF OF THE PHILIPS LABORATORIES AND FACTORIES

Reprints of those papers not marked with an asterisk * can be obtained free of charge upon application to the Philips Research Laboratories, Eindhoven, Netherlands, where a limited number of reprints are available for distribution.

- 3256:** S. Duinker: Search for a complete set of basic elements for the synthesis of non-linear electrical systems (Network theory, pp. 221-250, Pergamon Press, Oxford 1963).
- 3257:** K. M. Adams: A review of the synthesis of linear three-terminal networks composed of two kinds of elements (as **3256**, pp. 65-73).
- 3258:** G. Blasse: The structures of $ZnLiVO_4$ and $ZnLiNbO_4$ (J. inorg. nucl. Chem. **25**, 136-137, 1963, No. 1).
- 3259:** D. J. van Ooijen and J. D. Fast: Electrical resistance of hydrogen-charged iron wires (Acta metallurgica **11**, 211-216, 1963, No. 3).
- 3260:** A. J. Th. Mollet and L. E. Vrenken: Fülldruckmessungen an Inhalten von 0,2 cm³ und grösser im Druckbereich von 20 bis 100 Torr (Vakuum-Technik **12**, 6-12, 1963, No. 1). (Filling-pressure measurements on volumes of 0.2 cm³ upwards in the pressure range from 20 to 100 torr; in German.)
- 3261:** A. J. Bosman and E. E. Havinga: Temperature dependence of dielectric constants of cubic ionic compounds (Phys. Rev. **129**, 1593-1600, 1963, No. 4).
- 3262:** C. McD. Hargreaves: Multiple-beam 'transmission-like' Fizeau fringes in the reflexion interference system (Nature **197**, 890-892, 1963, No. 4870).
- 3263:** D. Polder and A. Baelde: Theory of noise of transistor-like devices (Solid-state electronics **6**, 103-110, 1963, No. 2).
- 3264:** W. F. Druyvesteyn and D. J. van Ooijen: Influence of neutron irradiation at 78 °K on the critical field of superconducting lead (Physics Letters, Amsterdam, **4**, 170-172, 1963, No. 3).
- 3265:** C. J. M. Rooymans: Structure of the high pressure phase of CdS, CdSe and InSb (Physics Letters, Amsterdam, **4**, 186-187, 1963, No. 3).
- 3266:** G. Blasse: The crystal structure of some compounds of the type $LiMe^{3+}Me^{4+}O_4$ and $LiMe^{2+}Me^{5+}O_4$ (J. inorg. nucl. Chem. **25**, 230-231, 1963, No. 2).
- 3267:** J. S. C. Wessels: Separation of the two photochemical systems of photosynthesis by digitonin fragmentation of spinach chloroplasts (Proc. Roy. Soc., London, B **157**, 345-355, 1963, No. 968).
- 3268:** C. W. Berghout: The uniaxial magnetic anisotropy of the F.C.C. cobalt precipitate in copper (Phys. Chem. Solids **24**, 507-516, 1963, No. 4).
- 3269:** P. Massini: Aminotriazolylalanine: a metabolic product of aminotriazole from plants (Acta bot. neerl. **12**, 64-72, 1963, No. 1).
- 3270:** E. W. Gorter: Interactions in various magnetic compounds (J. appl. Phys. **34**, 1253-1259, 1963, No. 4^{II}).
- 3271:** C. J. M. Rooymans: A phase transformation in the wurtzite and zinc blende lattice under pressure (J. inorg. nucl. Chem. **25**, 253-255, 1963, No. 3).
- 3272:** C. Wansdronk: Threshold mechanism and masking by noise (J. Acoust. Soc. Amer. **35**, 726-728, 1963, No. 5).
- 3273:** J. D. Wasscher, W. Albers and C. Haas: Simple evaluation of the maximum thermo-electric figure of merit, with application to mixed crystals $SnS_{1-x}Se_x$ (Solid-state electronics **6**, 261-264, 1963, No. 3).
- 3274:** J. C. Courvoisier, W. Haidinger, P. J. W. Jochems and L. J. Tummers: Evaporation-condensation method for making germanium layers for transistor purposes (Solid-state electronics **6**, 265-270, 1963, No. 3).
- 3275:** G. Blasse: The structure of some new mixed metal oxides containing lithium (J. inorg. nucl. Chem. **25**, 743-744, 1963, No. 6).
- R 459:** J. Hasker and H. Groendijk: Measurement and calculation of the figure of merit of a cathode-ray tube (Philips Res. Repts **17**, 401-418, 1962, No. 5).
- R 460:** J. A. W. van der Does de Bye: Transient recombination in silicon carbide (Philips Res. Repts **17**, 419-430, 1962, No. 5).
- R 461:** L. J. van de Polder: Simple representation of the behaviour of a diode in converter circuits (Philips Res. Repts **17**, 431-450, 1962, No. 5).
- R 462:** U. Enz, J. F. Fast, S. van Houten and J. Smit: Magnetism of EuS, EuSe and EuTe (Philips Res. Repts **17**, 451-463, 1962, No. 5).
- R 463:** B. Okkerse: Anomalous transmission of X-rays in germanium. Part I: The imaginary part of the atomic scattering factor (Philips Res. Repts **17**, 464-478, 1962, No. 5).
- R 464:** F. van der Maesen, C. A. A. J. Greebe and H. J. C. A. Nunnink: Steady-state injections in semiconductors (Philips Res. Repts **17**, 479-512, 1962, No. 5).
- R 465:** R. Bleekrode, J. Dieleman and H. J. Vegter: Electron-spin resonance of Fe in GaAs (Philips Res. Repts **17**, 513-517, 1962, No. 5).

- R 466:** A. J. W. Duijvestijn: Electronic computation of squared rectangles (Philips Res. Repts 17, 523-613, 1962, No. 6). Thesis Eindhoven, 1962.
- R 467:** J. H. N. van Vucht: Equilibrium pressures in the system Th_2Al -hydrogen (Philips Res. Repts 18, 1-20, 1963, No. 1).
- R 468:** J. H. N. van Vucht: X-ray diffraction of Th_2Al containing hydrogen (Philips Res. Repts 18, 21-34, 1963, No. 1).
- R 469:** J. H. N. van Vucht: Neutron diffraction and proton magnetic resonance of deuterium and hydrogen solutions in Th_2Al (Philips Res. Repts 18, 35-52, 1963, No. 1).
- R 470:** J. H. N. van Vucht: The problem of order or disorder of hydrogen in $\text{Th}_3\text{Al}_4\text{H}_8$ (Philips Res. Repts 18, 53-60, 1963, No. 1).
- R 471:** H. de Lang: Ferromagnetic domain structure as a microscopic object (Philips Res. Repts 18, 61-64, 1963, No. 1).
- R 472:** C. A. A. J. Greebe and F. van der Maesen: Graphical approach to small injections in semiconductors (Philips Res. Repts 18, 65-70, 1963, No. 1).
- R 473:** J. J. van Loef: Influence of hydrogen on electric and magnetic properties of a nickel-palladium alloy (Philips Res. Repts 18, 71-74, 1963, No. 1).
- R 474:** W. Steinmaier: Thermodynamical approach to the growth rate of epitaxial silicon from SiCl_4 (Philips Res. Repts 18, 75-81, 1963, No. 1).
- R 475:** B. Okkerse and P. Penning: Anomalous transmission of X-rays in germanium. Part II: Effects due to elastic deformation (Philips Res. Repts 18, 82-94, 1963, No. 1). Continued from **R 463**.
- R 476:** M. T. Vlaardingerbroek and K. R. U. Weimer: On wave propagation in beam-plasma systems in a finite magnetic field (Philips Res. Repts 18, 95-108, 1963, No. 2).
- R 477:** M. J. Hogendijk: Random dense packing of spheres with a discrete distribution of the radii (Philips Res. Repts 18, 109-126, 1963, No. 2).
- R 478:** F. H. Stieltjes and G. Diemer: Two-carrier photoconductance (Philips Res. Repts 18, 127-146, 1963, No. 2).
- R 479:** W. Elenbaas: Rate of evaporation and heat dissipation of a heated filament in a gaseous atmosphere (Philips Res. Repts 18, 147-160, 1963, No. 2).
- A 60:** A. Klopfer: An ionization gauge for measurement of ultra-high vacua (1961 Trans. 8th Nat. Vacuum Symp. + 2nd Int. Congress on Vacuum Sci. and Technol., Washington D.C., Vol. 1, pp. 439-442, Pergamon Press, Oxford 1962).
- A 61:** R. Groth, E. Kauer and P. C. van der Linden: Optische Effekte freier Träger in SnO_2 -Schichten (Z. Naturf. 17a, 789-793, 1962, No. 9). (Optical effects of free carriers in SnO_2 layers; in German.)
- A 62:** H. G. Reik: Theoretische Untersuchungen zum Problem der heissen Elektronen in Halbleitern (Festkörperprobleme I, pp. 89-121, Vieweg, Brunswick 1962). (Theoretical studies on the problem of hot electrons in semiconductors; in German.)
- A 63:** H. G. Grimmeiss and R. Memming: Origins of the photovoltaic effect in vapor-deposited CdS layers (J. appl. Phys. 33, 3596-3597, 1962, No. 12).
- A 64:** H. Hörster and E. Kauer: Untersuchung der Kinetik von Gas-Feststoff-Reaktionen mittels elektrischer Messungen (Z. Elektrochemie, Ber. Bunsenges. physik. Chemie 66, 667-671, 1962, No. 8/9). (Study of the kinetics of gas-solid reactions, using electrical measurements; in German.)
- A 65:** N. Hansen: Chemisorption und Widerstandsänderungen an aufgedampften Zirkoniumfilmen (Z. Elektrochemie, Ber. Bunsenges. physik. Chemie 66, 726-731, 1962, No. 8/9). (Chemisorption and resistance changes in vacuum-deposited zirconium films; in German.)
- A 66:** A. Rabenau: Siliziumnitrid, ein keramisches Material für hohe Temperaturen (Ber. Dtsch. Keram. Ges. 40, 6-12, 1963, No. 1). (Silicon nitride, a ceramic material for high temperatures; in German.)
- A 67:** E. Andrich and T. van der Sterre: Aufbau und Eigenschaften von PTC-Widerständen (Elektron. Rdsch. 17, 63-64, 1963, No. 2). (Structure and properties of PTC resistors; in German.)
- A 68:** E. Schwartz: Die Änderung der Leistung in gestörten linearen Gleichstromnetzwerken (Arch. elektr. Übertr. 17, 198-202, 1963, No. 4). (Power changes in perturbed linear DC networks; in German.)
- A 69:** P. Gerthsen: Ein neues Verfahren zur Kristallzüchtung von hochschmelzenden Stoffen (Z. angew. Phys. 15, 301-307, 1963, No. 4). (A new procedure for growing crystals from substances with a high melting point; in German.)
- A 70:** G. Schiefer: Kleine Ferritantennen für Meterwellen (Arch. elektr. Übertr. 17, 289-294, 1963, No. 6). (Small ferrite aeriels for metre wavelengths; in German.) See also Philips tech. Rev. 24, 332-336, 1962/63 (No. 10).
- A 71:** P. Gerthsen and K. H. Härdtl: Eine Methode zum direkten Nachweis von Leitfähigkeitsinhomogenitäten an Korngrenzen (Z. Naturf. 18a, 423-424, 1963, No. 3). (A direct method for demonstrating conductivity inhomogeneities at grain boundaries; in German.)

Philips Technical Review

DEALING WITH TECHNICAL PROBLEMS
RELATING TO THE PRODUCTS, PROCESSES AND INVESTIGATIONS OF
THE PHILIPS INDUSTRIES

SOLID STATE MASERS AND THEIR USE IN SATELLITE COMMUNICATION SYSTEMS

by J. C. WALLING *) and F. W. SMITH *).

621.375.9:538.56

The design of a maser for practical applications calls for a combination of electronics and solid state physics. The article below discusses this combination. A full description is also given of the travelling wave maser which was built at the Mullard Research Laboratories for use in experiments with the satellites Telstar and Relay.

Introduction

It is now well known that the solid state maser amplifier provides the most sensitive available means of amplifying microwave radiation. It is potentially capable of permitting the detection of signals in the microwave region having energies of only a few quanta. The device has therefore excited considerable interest among radio astronomers and more recently among communications engineers. Indeed the spectacular success of the recent satellite communication projects Telstar and Relay was due, in no small part, to the use of solid state maser amplifiers in the receiving stations.

It is the purpose of this article to discuss the design, performance and applications of travelling wave maser (TWM) amplifiers with particular reference to the maser recently developed at Mullard Research Laboratories for use at the Communication Satellite Earth Station of the British General Post Office at Goonhilly Down, Cornwall. A preliminary account of this device has already been given elsewhere ¹⁾ **).

Satellite communications

The first experiments in communication via an artificial earth satellite were carried out in 1960 with equipment designed and constructed by Bell Tele-

phone Laboratories and using the 30 m diameter metallized balloon Echo I ²⁾ which was launched from Cape Kennedy into an almost circular orbit in August 1960 at an altitude of about 1600 km. Echo acts as a passive reflector of signals from a ground transmitter, and the scattered signal is received at other ground stations.

The path loss over the complete circuit may be shown to be

$$L = \frac{(4\pi)^3 d_1^2 d_2^2}{G_1 G_2 \lambda^2 \sigma}$$

where d_1 and d_2 are the path lengths from the two ground stations to the satellite, G_1 and G_2 are the aerial gains over an isotropic radiator appropriate to the two stations, λ is the wavelength and σ is the scattering cross section of the satellite; see fig. 1.

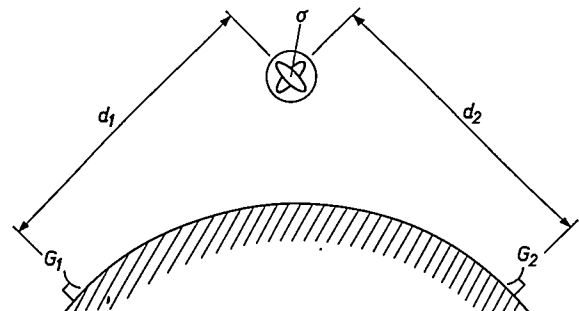


Fig. 1. Satellite communication scheme. The satellite has a scattering cross section σ , and the ground station aeri- als have gains of G_1 and G_2 .

*) Mullard Research Laboratories, Redhill (Surrey), England.

***) Note of the editor: In view of the fact that the Gaussian system is in common use in the current literature on masers, we have refrained from converting to the rationalized Giorgi system. For such a conversion see Appendix III.

¹⁾ J. C. Walling and F. W. Smith, Brit. Commun. and Elec., Aug. 1962.

²⁾ Bell Syst. tech. J. 40, no. 4, 1961.

From this expression the magnitude of the received signal can be calculated. Assuming that the transmitter and receiver aerials have gains of about 45 dB (a practical figure), then with the satellite (scattering cross section $\sim 730 \text{ m}^2$) in the most favourable position with respect to two stations 4800 km apart, we find that the path loss at 2400 Mc/s is about 180 dB and therefore with a 10 kW transmitter the received carrier power is 10^{-14} watt; signals of this order may easily be swamped by noise. For example, a good low noise receiver with 1 Mc/s bandwidth and a noise factor of 1.06 dB (equivalent noise temperature ³⁾ of 50 °K) has an equivalent input noise power of 0.7×10^{-15} watt and could thus, for this case, only realize a carrier-to-noise power ratio of about 10 dB.

Initial experiments were carried out with receivers of much narrower bandwidth than this to achieve satisfactory signal-to-noise ratios, and although the experiments were successful the use of a narrow bandwidth always severely limits the amount of information which can be put over the channel.

In a world-wide communication system it is desirable to use satellites at greater altitudes than the 1600 km at which Echo I is orbiting because of the need to obtain longer periods of mutual visibility between ground stations. However this invariably implies an even greater path attenuation and even smaller received signals.

The second generation of communication satellites, Telstar, developed by the Bell Laboratories and launched in 1963 ⁴⁾, and Relay, developed by R.C.A. for N.A.S.A. and launched in 1963 ⁵⁾, employs active repeaters in the satellite. The signal from one ground station is received in the satellite, frequency converted, amplified and re-radiated at a power level of about 2 watts (Telstar I and II) and 10 watts (Relay I). By introducing gain in the system in this way it is possible to work at greater satellite altitudes with longer periods of mutual visibility between ground stations and also to increase the band-

³⁾ When we speak of the equivalent noise temperature T of an amplifier we mean that the noise added to the signal by the amplifier is equivalent to that which would be generated by a matched resistive termination at temperature T radiating into the input waveguide of the amplifier. However the noise factor F of the amplifier is, according to the standard definition:

$$F = \frac{\text{input signal} / \text{input noise}}{\text{output signal} / \text{output noise}}$$

when the input is generated by a matched source at a temperature $T_s = 290$ °K. Hence:

$$F = 1 + \frac{T}{290}$$

⁴⁾ "The Telstar experiment", Bell Syst. tech. J. 42, no. 4, 1963.

⁵⁾ Programme and Conference Digest, I.E.E. Conference on Satellite Communications, Session 8, Nov. 1962.

width of the system. Furthermore, use of these greater altitudes is desirable in order that the active satellites avoid the van Allen radiation belts. More sophisticated aerials with gains above 55 dB have been built for these experiments and signals received from Telstar I at slant ranges (e.g. d_1 in fig. 1) of between 4000 and 10 000 kilometres were in the range between 10^{-12} and 10^{-13} watt. This follows from the ratio of power received at the aerial P_A to that radiated substantially isotropically by the satellite P_S which is:

$$\frac{P_A}{P_S} = \frac{G\lambda^2}{16\pi^2 d^2} \quad (G \text{ being the aerial gain}).$$

The bandwidth of the system using an active repeater in the satellite may be increased to about 25 Mc/s since the noise power introduced by a receiver with such a bandwidth and an equivalent noise temperature of 50 °K is now 1.75×10^{-14} watt and even at ranges up to 10 000 kilometres the carrier-to-noise power ratio is greater than 10 dB. Sophisticated modulation techniques such as wide-band frequency modulation with FM feedback in the receiver are currently used to improve further the overall signal-to-noise ratio ⁵⁾.

From the foregoing it is apparent that receivers with noise temperatures of the order of 50 °K or less are necessary if wide band satellite communication systems are to be successfully realized with practical satellite transmitter powers which, in the present state of the art, are limited to a few watts. Clearly then it is necessary to pay careful attention to the reduction of all sources of noise in the receiving system and it is thus desirable that the first stage amplifier should have the lowest possible noise temperature; this amplifier should then be a maser.

In the receiving system at Goonhilly Down the maser amplifier is mounted in a cabin at the back of a steerable, 26 metre diameter, parabolic antenna illustrated in fig. 2. Figure 3 is a photograph of the maser in its operating position in the cabin.

The combination of this antenna and the maser amplifier results in a receiving system having the necessary high directivity and very low noise temperature.

Basic principles of maser operation

Before describing a particular device we shall first make a brief re-examination of the basis of maser operation.

The fundamental principle of maser operation is indicated in the name ⁶⁾: microwave amplification

⁶⁾ J. P. Gordon, H. J. Zeiger and C. H. Townes, Phys. Rev. 99, 1264, 1955.

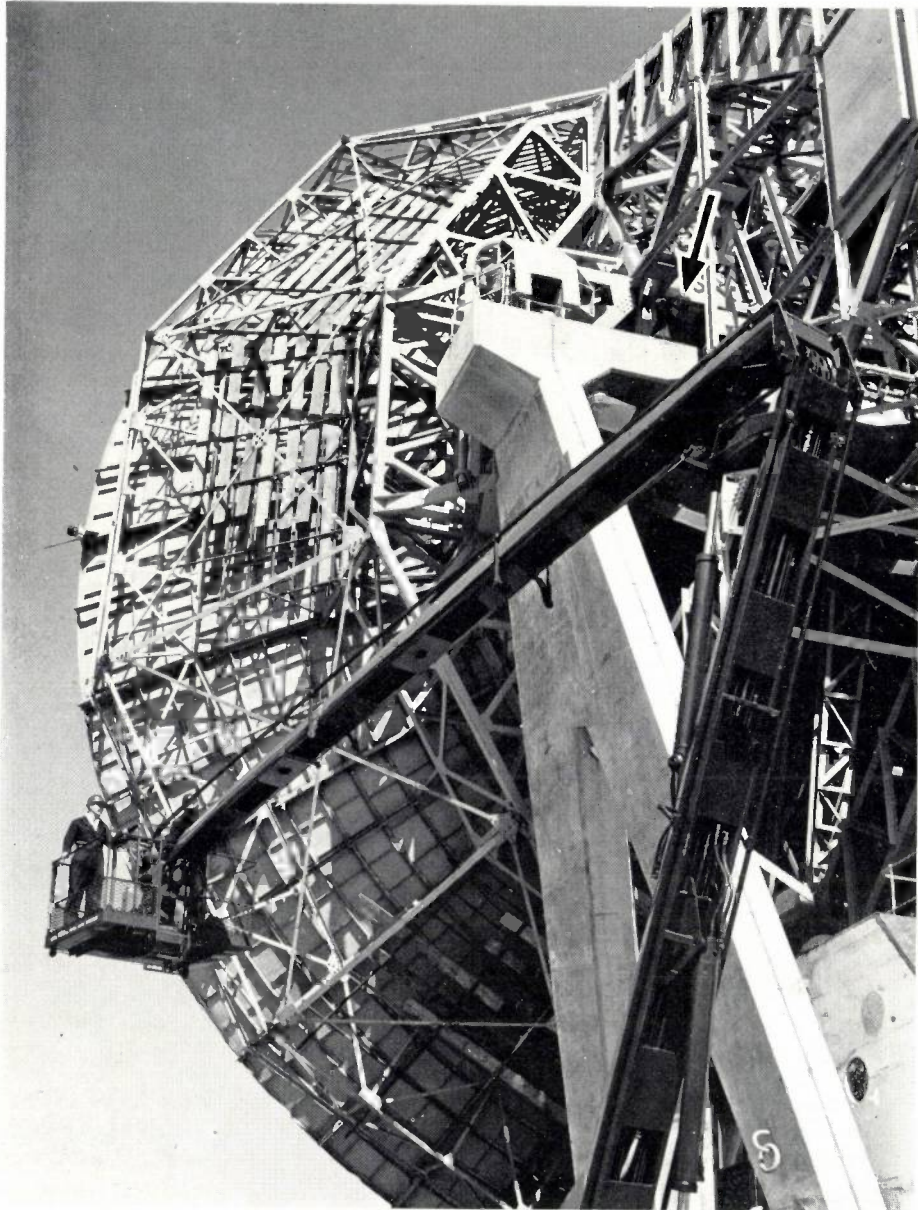


Fig. 2. The 26 meter diameter antenna at the Communication Satellite Earth Station at Goonhilly Down, Cornwall. This antenna is used for receiving signals from the Telstar and Relay satellites. The arrow indicates the cabin in which the maser is mounted. (Photo published by permission of the British G.P.O.)

by stimulated emission of radiation. The radiation is emitted from particles which make a transition from the upper to the lower of two quantum energy states. In the Bloembergen solid state maser the fundamental phenomenon which gives rise to the relevant energy states is paramagnetic resonance. We will first discuss paramagnetic resonance for the simple case of an assembly of free electrons and the stimulated emission which may occur in such a system.

Each electron in our assembly possesses a spin $h/4\pi$ and a magnetic moment of one Bohr magneton:

$$\beta = \frac{eh}{4\pi mc}, \dots \dots \dots (1)$$

where e = the electronic charge, h = Planck's constant, m = the electronic mass, and c = the free space velocity of light. If the system is subjected to the action of a static magnetic field H_0 , each electron can occupy one of two energy states often referred to as energy levels, the energy difference between the states being

$$\Delta E = 2 \beta H_0. \dots \dots \dots (2)$$

In thermal equilibrium the relative populations n_1 and n_2 of the two states are determined by Boltzmann statistics, i.e.:

$$\frac{n_2}{n_1} = \exp\left(-\frac{\Delta E}{kT}\right). \dots \dots \dots (3)$$

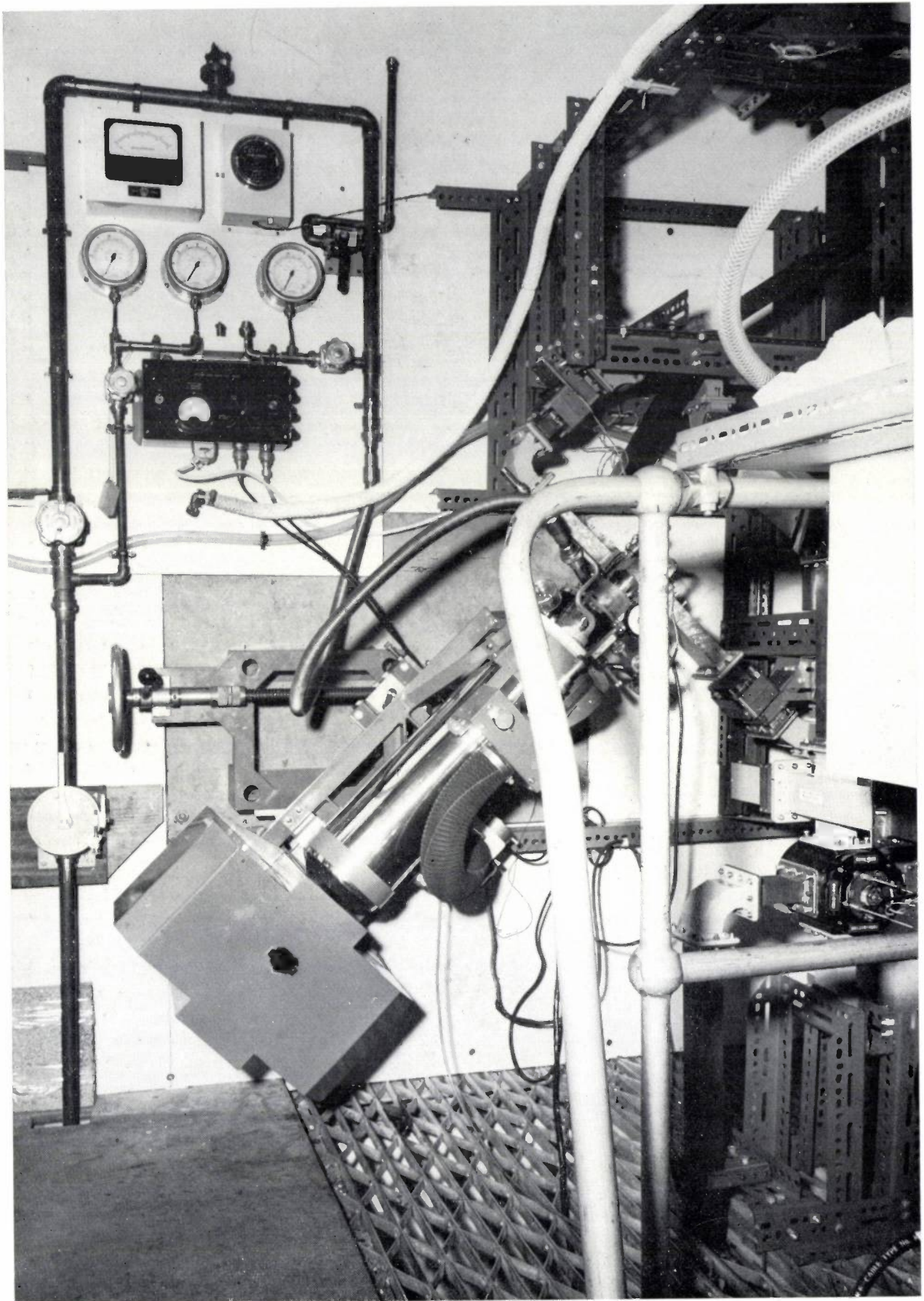


Fig. 3. Travelling wave maser amplifier in its operating position on the parabolic antenna shown in fig. 2. (Photo published by permission of the British G.P.O.)

where n_2 corresponds to the higher energy state. It was shown by Einstein ⁷⁾ that if electromagnetic radiation of frequency f given by

$$hf = \Delta E \dots \dots \dots (4)$$

is incident upon the system, transitions are *stimulated* from level 1 to level 2 and from level 2 to level 1, and that upward and downward transitions are equally probable. From equations (2) and (4):

$$f = \frac{eH_0}{2\pi mc} \dots \dots \dots (5)$$

This type of resonant interaction between a system of spins and a radiation field is known as paramagnetic resonance.

Certain features of this interaction can be understood in classical terms. The assembly of electrons when subject to the action of a magnetic field \mathbf{H} will have a net magnetic moment \mathbf{M} and a net angular momentum $1/\gamma \mathbf{M}$. The gyromagnetic ratio γ is equal to e/mc for free electrons. In general $\gamma = ge/2mc$, g being the spectroscopic splitting factor (equal to 2 for free electrons). The equation of motion for the angular momentum of the system is:

$$\frac{1}{\gamma} \frac{d\mathbf{M}}{dt} = \mathbf{M} \times \mathbf{H} \dots \dots \dots (6)$$

If we suppose that the magnetic field \mathbf{H} has a large static component $H_z = H_0$ and small time dependent components H_x and H_y varying as $e^{j\omega t}$, then M_z is time independent and for M_x and M_y we have:

$$\frac{dM_x}{dt} = j\omega M_x = \gamma M_y H_0 - \gamma M_z H_y,$$

$$\frac{dM_y}{dt} = j\omega M_y = \gamma M_z H_x - \gamma M_x H_0.$$

Writing $\omega_0 = \gamma H_0$ and resolving the (x, y) magnetization and field into left and right circularly polarized components:

$$M_x + jM_y = M_+ \quad \text{and} \quad M_x - jM_y = M_-,$$

$$H_x + jH_y = H_+ \quad \text{and} \quad H_x - jH_y = H_-,$$

we obtain:

$$M_+ = \frac{\gamma M_z}{\omega + \omega_0} H_+,$$

$$M_- = \frac{-\gamma M_z}{\omega - \omega_0} H_-.$$

These equations indicate that the interaction is of a resonant character, circularly polarized fields of

positive sense strongly exciting circularly polarized magnetization of the same sense at $\omega = \omega_0$, whilst for the opposite direction of applied field ($\omega = -\omega_0$) a resonant interaction is observed for the opposite sense of polarization. In this classical situation the magnetization executes a precessional motion about the direction of the applied static field with frequency ω_0 .

This classical analysis demonstrates that the phenomenon of paramagnetic resonance is due to an interaction between an RF magnetic field and the magnetic moment of the spin system, and that this interaction will only occur if the RF magnetic field is of the correct frequency and contains a circularly polarized component of appropriate sense.

The two energy levels of our earlier discussion might be regarded in the classical case as corresponding to the magnetic moments of individual electrons being aligned parallel or antiparallel to the applied field.

We have seen that in the two-level system transitions are stimulated between the two levels with equal probability in either direction. Downward transitions take place with the emission of radiation and upward transitions are accompanied by absorption. The radiation emitted in the downward transitions is coherent and in phase with the original stimulating field. However, although the probabilities of upward and downward transitions for each electron are equal, the number of upward transitions exceeds the number of downward transitions in a system initially in thermal equilibrium because of the Boltzmann distribution (eq. 3) between the levels, and thus the net effect is that of absorption of energy from the incident RF field.

The maser is based on the following idea: If by some means the distribution of electrons between the levels can be changed so that the number in the upper level exceeds that in the lower, the dominant paramagnetic resonance process would be that of stimulated emission rather than absorption, and since the emitted radiation is in phase with the stimulating radiation, amplification of the original signal would be observed. For readily available magnetic fields paramagnetic resonance occurs at microwave frequencies (2.8 Gc/s at 1000 Oe according to eq. (5)) and thus this phenomenon offers the possibility of microwave amplification.

Although there are means (reviewed by Wittke ⁸⁾) of inverting the populations of a solid state two-level system, the inversion is transient and continuous amplification cannot be obtained. It was

⁷⁾ A. Einstein, Phys. Z. 18, 121, 1917.

⁸⁾ J. P. Wittke, Proc. I.R.E. 45, 291, 1957.

not until 1956 when Bloembergen⁹⁾ proposed the three-level maser that a method of obtaining continuous amplification of an RF signal by a spin system became available.

Paramagnetic ions in crystals

In the three-level maser we are concerned, not with an assembly of electrons, but with paramagnetic ions in a crystal lattice.

The magnetic properties of paramagnetic ions may be rather complicated because we are concerned both with the spin and orbital motion of the unpaired electrons. Both spin and orbit have angular momentum and an associated magnetic moment. If the spin and orbital angular momenta are characterised by quantum numbers S and L respectively then the corresponding angular momenta and magnetic moments are:

$$\text{spin: } \frac{h}{2\pi} \sqrt{S(S+1)} \quad \text{and} \quad -\frac{g_s \beta h}{2\pi} \sqrt{S(S+1)},$$

$$\text{orbit: } \frac{h}{2\pi} \sqrt{L(L+1)} \quad \text{and} \quad -\frac{g_L \beta h}{2\pi} \sqrt{L(L+1)},$$

β being the Bohr magneton (1) and g_s and g_L the spin and orbital spectroscopic splitting factors. However since $g_s = 2$ and $g_L = 1$ there is no simple relation between the resultant magnetic moment and angular momentum. The latter is characterised by a quantum number J which is the vector sum of L and S and has magnitude $(h/2\pi) \sqrt{J(J+1)}$. The resultant magnetic moment is $-(g_J \beta h/2\pi) \sqrt{J(J+1)}$, g_J being the Landé splitting factor. When acted upon by a magnetic field such an ion can occupy one of $(2J+1)$ equally spaced energy levels.

Detailed treatment of the effect of the electric field produced by neighbouring ions of the crystal lattice on the paramagnetic ion lies beyond the scope of this article; for further discussion of this subject the reader is referred to the review article by Bleaney and Stevens¹⁰⁾. We may note however that the effect of this crystal field depends on its symmetry and on the relative magnitudes of the field and the spin-orbit coupling in the paramagnetic ion.

In most maser materials the effect of the crystal field is to cause large energy differences (corresponding to frequencies in the optical region of the spectrum) between states of different orbital motion and only the lowest of these levels is occupied

at ordinary temperatures (cf. equation 3). For example the ground state of the Cr^{3+} ion (the active ion in ruby — to date the most widely used maser material) is split by the action of a field of cubic symmetry into a low lying orbital singlet and two very much higher triplets (fig. 4a). Ions in the lowest state have

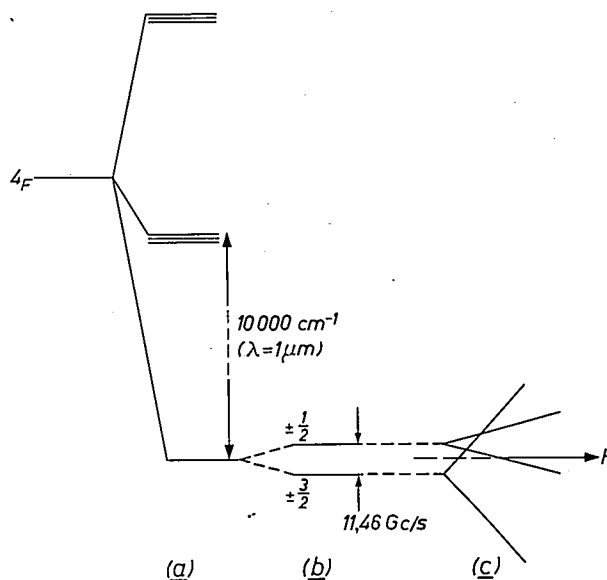


Fig. 4. Energy level diagram. The splitting of the ground state of the free chromium (Cr^{3+}) ion by a cubic crystal field with trigonal distortion.

a) Splitting of orbital levels by a crystal field of cubic symmetry. b) Partial lifting of four-fold spin degeneracy of lowest orbital level by combined action of axial field and spin orbit coupling (zero field splitting). c) Zeeman splitting of ground state levels in a magnetic field H .

no net orbital moment and the paramagnetism of this material is due solely to the electron spin. There are three unpaired electrons in this ion and thus four spin states all of which have the same energy (fourfold spin degeneracy). As a result of deviations of the crystal field from cubic symmetry and some residual spin orbit coupling, the fourfold degenerate lowest level is split into two doubly degenerate levels; this latter energy splitting is called the ground state zero field splitting and generally corresponds to frequencies in the microwave range (in ruby it is 11.46 Gc/s ; fig. 4b).

In the presence of a magnetic field each of the doubly degenerate ground state levels is further split and it is with these Zeeman levels (so called because this type of level splitting gives rise to the splitting of optical spectral lines first observed by Zeeman in 1896) of the ground state that we are concerned in the maser (fig. 4c).

The behaviour of the Zeeman levels depends on the magnitude and direction of the applied static magnetic field with respect to the crystal field. In the case in which the crystal is axially symmetrical

⁹⁾ N. Bloembergen, Phys. Rev. 104, 324, 1956.

¹⁰⁾ B. Bleaney and K. W. H. Stevens, Rep. Prog. Phys. 16, 108, 1953 — An introductory article on paramagnetic resonance by J. S. van Wieringen appeared in Philips tech. Rev. 19, 301, 1957/58.

and the static magnetic field is parallel to this axis, the ground state Zeeman level splitting is linearly dependent on the applied field and the corresponding spin states may be individually characterised by magnetic quantum numbers m ($mh/2\pi$ being the component of angular momentum along the magnetic field). Such states are called pure states. For an ion with three unpaired spins (such as Cr^{3+}) m can take the values $+\frac{3}{2}, +\frac{1}{2}, -\frac{1}{2}, -\frac{3}{2}$.

Only transitions between levels corresponding to $\Delta m = \pm 1$ (or 0) are allowed. However, in the general case in which the static magnetic field is not parallel to the axis of symmetry the energy differences between states do not vary linearly with the applied magnetic field. This is shown in *fig. 5*, which is the energy level diagram for the ground state levels of the chromium ion in ruby when the angle between the magnetic field and the axis of symmetry of the crystal field is 90° . Furthermore these energy states are not pure states but linear combinations of pure states; thus they can no longer be characterized by a single magnetic quantum number — such states are called mixed states. As a consequence of this mixing of states, transitions between any pair of ground state levels are allowed although all transitions are not of equal probability.

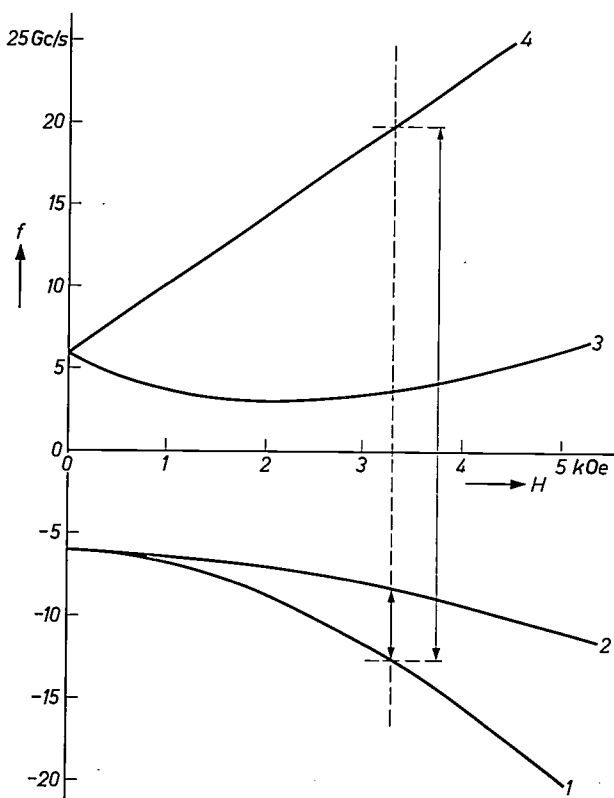


Fig. 5. Ground state Zeeman levels in ruby (Cr^{3+} in Al_2O_3) as functions of the magnetic field H . The magnetic field is at 90° to the three-fold axis of symmetry of the crystal field. The arrows indicate the operating pump transition 1-4 (30 150 Mc/s) and the signal transition 1-2 (4170 Mc/s) in a field of 3280 Oe.

The three level maser

We have now seen broadly what determines the ground state Zeeman levels of paramagnetic ions in a crystal and in 1956 Bloembergen proposed a simple means of producing a continuously inverted population distribution between a pair of these levels which provides the basis of the continuous wave solid state maser as we know it today.

Let us consider a system in which we have three unequally spaced Zeeman levels (*fig. 6*). We will

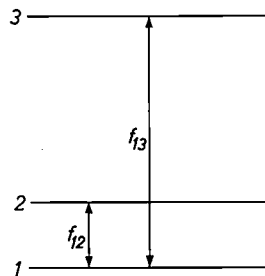


Fig. 6. Three energy level system. f_{12} signal frequency. f_{13} pump frequency.

suppose that we have *two* impressed signals which have frequencies f_{12} and f_{13} and which stimulate transitions between levels 1 and 2 and 1 and 3 with probabilities W_{12} and W_{13} respectively ($W_{12} = W_{21}$, $W_{13} = W_{31}$). In addition to the transitions stimulated by these external signals there are also spontaneous downward transitions and the thermal transitions which are responsible for the energy exchange between the spin system and the lattice and therefore determine the rate of approach to thermal equilibrium of a perturbed spin system — the “spin lattice relaxation”. These latter transitions are radiationless and their probabilities are different in the two directions; these probabilities are $w_{12}, w_{21}, w_{13}, w_{31}, w_{23}$ and w_{32} . The spontaneous transitions are very improbable at microwave frequencies and may be neglected in this discussion. If the three levels have populations n_1, n_2, n_3 then we may write:

$$\left. \begin{aligned} \frac{dn_1}{dt} &= -n_1(W_{13} + w_{13} + W_{12} + w_{12}) + \\ &\quad + n_2(W_{21} + w_{21}) + n_3(W_{31} + w_{31}), \\ \frac{dn_2}{dt} &= -n_2(W_{21} + w_{21} + w_{23}) + \\ &\quad + n_1(W_{12} + w_{12}) + n_3(w_{32}). \end{aligned} \right\} \quad (7)$$

If we have no impressed signals the thermal equilibrium populations of the levels are determined by

Boltzmann's law (equation 3) and it follows from the Principle of Detailed Balancing ¹¹⁾ that:

$$\left. \begin{aligned} \frac{w_{13}}{w_{31}} &= \left(\frac{n_3}{n_1} \right)_0 = \exp \left(- \frac{hf_{13}}{kT} \right) \\ \frac{w_{12}}{w_{21}} &= \left(\frac{n_2}{n_1} \right)_0 = \exp \left(- \frac{hf_{12}}{kT} \right) \\ \frac{w_{23}}{w_{32}} &= \left(\frac{n_3}{n_2} \right)_0 = \exp \left(- \frac{hf_{23}}{kT} \right) \end{aligned} \right\} \dots (8)$$

the subscript 0 signifying the magnitude in thermal equilibrium.

If we now make W_{13} very large, i.e., we make the amplitude of the signal at the frequency f_{13} very large, the transition at f_{13} becomes saturated, that is, the populations of levels 1 and 3 become equal and we find from (5) and (6) at equilibrium ($dn_1/dt = dn_2/dt = 0$):

$$\frac{n_2}{n_1} = \frac{w_{23} \exp(hf_{23}/kT) + W_{12} + w_{12}}{W_{12} + w_{12} \exp(hf_{12}/kT) + w_{23}} \dots (9)$$

If our signal at f_{12} is very small we may write $W_{12} = 0$ and hence

$$\frac{n_2 - n_1}{N} = \frac{w_{23} [\exp(hf_{23}/kT) - 1] - w_{12} [\exp(hf_{12}/kT) - 1]}{w_{23} [2 + \exp(hf_{23}/kT)] + w_{12} [2 \exp(hf_{12}/kT) + 1]} \dots (10)$$

in which $N = n_1 + n_2 + n_3 = 2n_1 + n_2$ is the total number of active ions involved. This equation expresses the fact that in a three level system the population of level 2 can be made to exceed that of level 1 by applying a large amplitude signal of frequency f_{13} (called the "pump") if

$$w_{23} [\exp(hf_{23}/kT) - 1] > w_{12} [\exp(hf_{12}/kT) - 1]. (11)$$

If both hf_{23} and $hf_{12} \ll kT$ this condition becomes:

$$w_{23}f_{23} > w_{12}f_{12} \dots (12)$$

In the absence of precise information concerning the relative magnitudes of the thermal transition probabilities w_{12}, w_{23} it is usually assumed that they are equal, which may not be too far from correct provided we are dealing with frequencies of the same order of magnitude. Making this assumption we see that a condition for maser action in a system of this kind is that the pump frequency ($f_{13} = f_{12} + f_{23}$)

should be greater than twice the signal frequency f_{12} .

Three level maser action is illustrated by the diagram of fig. 7 in which population is plotted against energy. The populations of levels 1 and 3 which result from applying the pump signal are indicated by the heavy lines. The lower the ambient temperature the larger the population difference ($n_2 - n_1$) becomes and thus masers are commonly operated at very low temperatures.

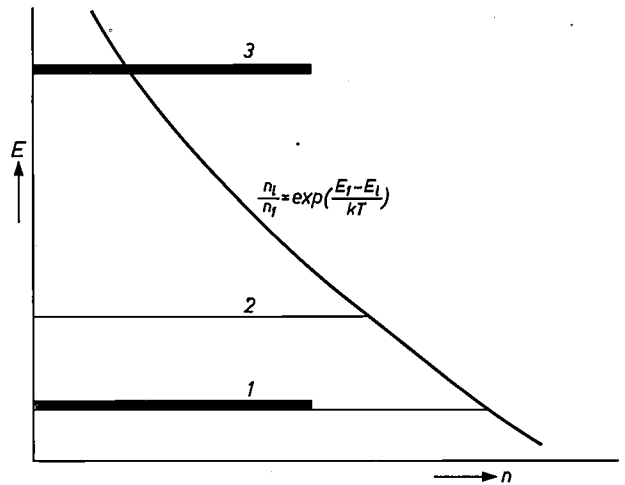


Fig. 7. Population inversion in a three-level system. Population is plotted horizontally for the three energy levels. The exponential curve indicates the Boltzmann distribution for thermal equilibrium at a given temperature. The heavy lines indicate the populations of levels 1 and 3 when the pump signal is applied. The relative population of level 2 is determined by the thermal transition probabilities w_{12}, w_{23} . For $w_{23}f_{23} > w_{12}f_{12}$ an inversion of population of level 2 is obtained. (In the opposite case, $w_{23}f_{23} < w_{12}f_{12}$, the populations of levels 2 and 3 would be inverted.)

The majority of solid state masers have used crystals in which the active ion is Cr^{3+} (e.g. ruby, chromicyanide, emerald, rutile) and here as we have seen we have four Zeeman levels in the ground state. Three-level maser action can still be obtained by choosing three of the four available levels although the rate equations are somewhat complicated, due to the greater number of relaxation processes which can now take place. Occasionally double pumping schemes in which all four energy levels take part can be used to advantage. In the case where the energy levels are completely symmetrical — which occurs in ruby, for example, when the angle between the static applied magnetic field and the symmetry axis is $\cos^{-1}(1/\sqrt{3})$ i.e. $54^\circ 44'$ — it is possible to employ "push pull" pumping, the signal transition being between levels 2 and 3 and pump transitions between levels 1 and 3 and 2 and 4, a pump of one frequency saturating both the 1-3 and 2-4 transitions ¹²⁾ (fig. 8).

¹¹⁾ According to this principle every process of transformation or exchange of energy which occurs in a system in thermodynamic equilibrium is invariably accompanied by an analogous reverse process and the two processes occur with equal frequency.

¹²⁾ G. Makhov *et al.*, Phys. Rev. 109, 1399, 1958.

It is convenient to relate the inverted population difference (Δn) to the thermal equilibrium population difference (Δn_0) through

$$\Delta n = -I \Delta n_0,$$

I being known as the inversion produced by the pumping scheme.

Transition probabilities

The probability W_{ij} that an applied RF magnetic field will stimulate transitions between a given pair of Zeeman levels i and j is a vital parameter in maser design. It can be calculated by means of perturbation theory but we will content ourselves by quoting the result of this calculation which is:

$$W_{ij} = W_{ji} = \frac{1}{4} \gamma^2 \varphi(f) |(A + jB)(H + jH')|^2, \quad (13)$$

and by briefly discussing this expression and the occurring symbols. γ is the gyromagnetic ratio already introduced:

$$\gamma = \frac{2\pi g\beta}{h} \dots \dots \dots (14)$$

$\varphi(f)$ is a normalized line shape function:

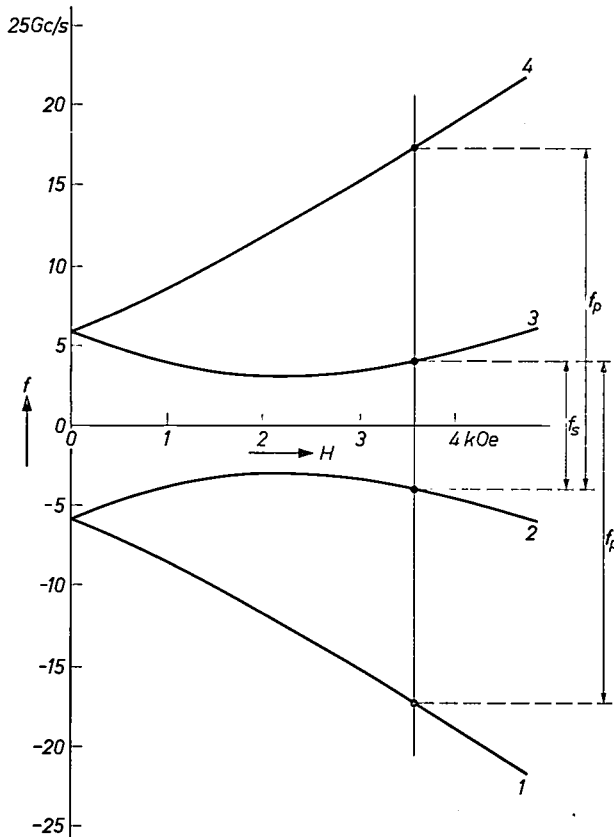


Fig. 8. Push-pull pumping. The ground state Zeeman levels in ruby are symmetrical when the magnetic field is at $54^\circ 44'$ to the crystal field axis. f_s frequency of signal inducing 2-3 transitions. f_p frequency of pump saturating both the 1-3 and the 2-4 transition.

$$\int_0^\infty \varphi(f) df = 1$$

which expresses the fact that because a given ion spends only a limited time in a particular energy state before exchanging its energy with another ion (or the lattice), the energy levels have a finite width and resonant interaction is obtained at signal frequencies not only equal to f_0 but also around f_0 . When interaction between neighbouring ions (dipole-dipole or spin-spin) is the dominant process, $\varphi(f)$ is a "Lorentzian line shape function":

$$\varphi(f) = \frac{2/T_2}{4\pi^2 (f-f_0)^2 + 1/T_2^2} \dots \dots (15)$$

T_2 is the relaxation time characterizing the interaction and is typically of the order of 10^{-9} s. T_2 determines the paramagnetic resonance linewidth $1/\pi T_2$. The RF magnetic field is represented by the term $H + jH'$ (that is, the actual RF magnetic field is the real part of $(H + jH') \exp(2\pi jft)$). H and H' are two mutually orthogonal magnetic field vectors.

A and B are two mutually perpendicular vectors (termed matrix element vectors) whose magnitude and direction can be calculated¹³ from a knowledge of the electron spin resonance spectrum of the ion in the particular crystal environment under consideration. For transitions between pure states, the magnitudes of A and B are equal and in general of the order of unity for allowed transitions (and zero for forbidden transitions). Thus for pure states eq. (13) expresses the fact that maximum transition probability is obtained when the RF field is circularly polarized and of the appropriate sense which is in agreement with the earlier classical analysis.

In general, however, we are not concerned with pure states and for a given transition A and B are not equal and depend both on the magnitude of the static magnetic field and the angle α between this field and the axis of symmetry of the crystal field. As an illustration of this the variation of A and B for two transitions in ruby is plotted in fig. 9 from the data of Chang and Siegman¹³.

By analogy with the classical model we may regard the crystal field as producing an anisotropic constraint on the precession of the magnetization and thus maximum interaction occurs in this case not with circularly polarized fields but with elliptically polarized fields of the appropriate ellipticity (A/B) and sense.

¹³ W. S. C. Chang and A. E. Siegman, Stanford Technical Report 156-2, 1958 (essential data from this report are quoted by J. Weber, Rev. mod. Phys. 31, 681, 1959).

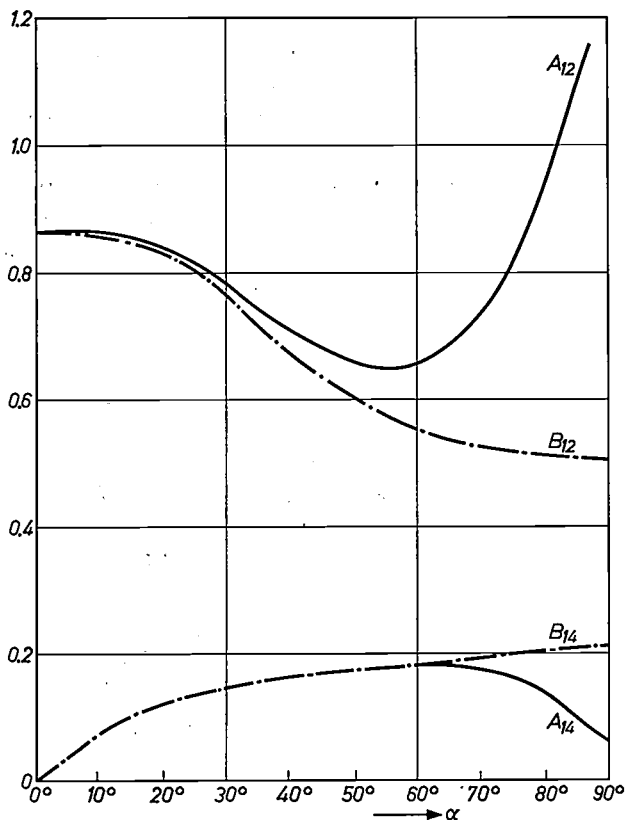


Fig. 9. The matrix element vectors A and B as a function of α , the angle between magnetic field and crystal field axis, for the $I-2$ and the $I-4$ transition in ruby in a magnetic field of 3000 Oe.

Choice of material for a maser

We can now state the conditions which a good maser material should satisfy. These are as follows:

- (1) The active ions should occupy equivalent sites in the crystal; otherwise in general at a given orientation of the crystal only ions on a certain site will take part in the interaction with the RF field.
- (2) The active ions should not have a nuclear magnetic moment. This would cause hyperfine splitting of energy levels and effectively decrease the number of ions available for maser action at a particular frequency.
- (3) The interaction between the spin system and the lattice should not be too strong if we are to saturate the pump transition fairly readily — this is another reason for operating at very low temperatures.
- (4) The material should be mechanically robust and should withstand repeated cooling to very low temperatures. For instance, chromium doped potassium cobaltcyanide ($K_3Co(CN)_6$) which is otherwise a very satisfactory material fails in this respect.
- (5) The material should be available as large single crystals.

Few, if any, materials fulfil all these requirements: synthetic ruby (chromium-doped aluminium oxide) comes very close and is widely used, emerald looks a promising material but is at present difficult to synthesize as large single crystals, chromium- and iron-doped rutile are also frequently used but present difficulties at high frequencies as a result of the very high dielectric constant which necessitates the use of very small microwave structures in the maser. A new material which is extremely interesting is chromium doped (Cr^{3+}) zinc tungstate¹⁴.

Maser devices; the travelling wave maser

Having seen how stimulated emission from a paramagnetic crystal can occur at microwave frequencies, we must now consider how it can be used in an amplifier. The strength of the interaction between the spin system and the RF magnetic field is, as we have seen, determined by the square of the amplitude of this field within the crystal (eq. 13) and it is therefore desirable, for a given signal power input to the maser, that this amplitude should be made as large as possible.

The simplest way of obtaining a large RF field within the crystal is to place it in a resonant cavity and this technique has been widely used¹⁵). Such a cavity maser can be constructed as a reflection device (fig. 10) in which the input and output signals

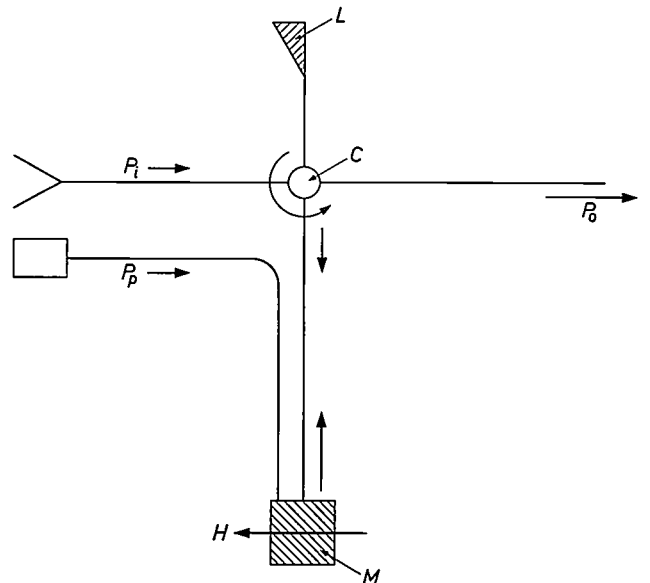


Fig. 10. Cavity maser circuit. P_p pump power. P_i signal input power. P_o signal output power. M maser cavity filled with active material. H static magnetic field. C circulator. L matched load.

¹⁴) L. G. van Uitert and S. Preziosi, J. appl. Phys. **33**, 2908, 1962.

¹⁵) H. E. D. Scovil, G. Feher and H. Seidel, Phys. Rev. **105**, 762, 1957; A. L. McWhorter and J. W. Meyer, Phys. Rev. **109**, 312, 1958.

are separated by means of a circulator¹⁶⁾ or as a transmission device with distinct input and output waveguides. In either case the device is regenerative, that is to say the energy which is emitted by an element of the maser material increases the RF field in the cavity and thus the rate of emission of energy from the element of material itself increases. As a consequence of this positive feedback the product of the bandwidth and the square root of the numerical gain for a single cavity device is constant,

A two port device employing this latter principle is known as a travelling wave maser (TWM) and the first working TWM was described by DeGrasse *et al*¹⁷⁾.

The situation in the TWM is quite different from that in the cavity device in so far as the energy emitted by an element of maser material leads to an increase in the RF field travelling in the structure and thus increases the rate of emission of energy from succeeding elements of material but does not react on the

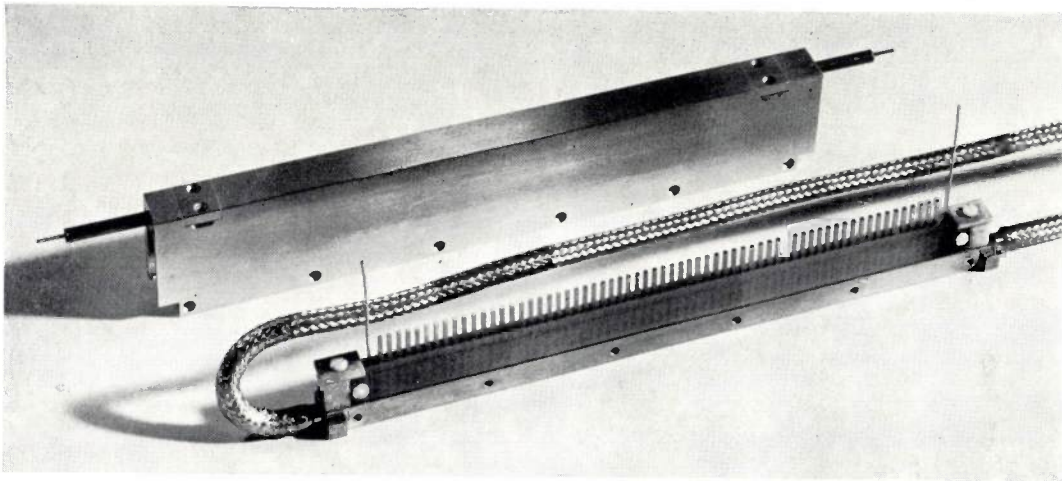


Fig. 11. Photograph of comb slow wave structure as used in a TWM.

and the gain is very sensitive to variations in load impedance and hence there is a tendency to oscillation at high gains. Although it is true that for multiple cavity devices larger bandwidths can be obtained at a given gain, the positive feedback is always present and so too is the possibility of self oscillation.

Another means of obtaining a large RF field is to use a slow wave structure in which the velocity of propagation of electromagnetic energy is substantially less than the free space velocity. Field concentration occurs in such a structure as a consequence of the simple law relating the stored energy per unit length (W_s) to the power P in a wave travelling in the structure which is

$$P = v_g W_s, \quad (16)$$

v_g being the group velocity. W_s is determined by the square of the RF fields integrated over the cross section of the structure and thus if, at a given power level, W_s is made large by velocity reduction so also is the RF field.

original element. Regeneration and oscillation in a TWM can then only occur as a result of reflections in the external circuitry.

The TWM thus has some important advantages over the cavity maser in that it is non-regenerative and has therefore no intrinsic tendency to oscillate. Furthermore, the bandwidth is determined mainly by the paramagnetic resonance linewidth of the sample, and decreases only slowly with increasing gain.

Moreover, as will be shown, the device can be constructed to be completely non-reciprocal and hence the need for ancillary non-reciprocal elements essential for cavity maser operation is removed. In addition, operation can be obtained over a very wide centre frequency range — some hundreds of megacycles in a single structure — the centre frequency being simply shifted by adjusting the magnetic field and the pump frequency. These features make the TWM the only really practical embodiment of the maser principle. A typical maser slow wave structure loaded with active material is shown in *fig. 11*.

¹⁶⁾ A. G. Fox *et al.*, Bell Syst. tech. J. **34**, 5, 1955.

¹⁷⁾ R. W. DeGrasse, E. O. Schulz-Du Bois and H. E. Scovil, Bell Syst. tech. J. **38**, 305, 1959.

Theory of the travelling wave maser

The small signal gain of the TWMM can readily be expressed in terms of two quality factors, Q_0 , the intrinsic quality factor of the propagating structure, determined by ohmic and dielectric power losses per unit length P_0 , and Q_m , the magnetic quality factor of the maser material which is determined by the power P_m emitted per unit length of the maser material:

$$\frac{1}{Q_m} = \frac{P_m}{2\pi f W_s}, \quad \frac{1}{Q_0} = \frac{P_0}{2\pi f W_s} \dots (17)$$

Let us consider an element of the TWMM of length dz (fig. 12). Energy is emitted by the maser material

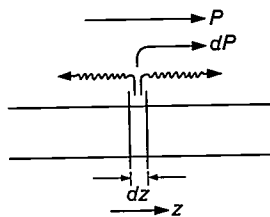


Fig. 12. Emission from an element of a TWMM.

in this element but, since only the forward travelling increments of field add in phase, virtually all the energy emitted by the element travels in the forward direction. Energy absorption also takes place in the element due to ohmic and dielectric losses and thus the change dP in power level P in the element is:

$$dP = (P_m - P_0)dz.$$

Using (16) and (17):

$$\begin{aligned} dP &= 2\pi f W_s \left(\frac{1}{Q_m} - \frac{1}{Q_0} \right) dz \\ &= P \frac{2\pi f}{v_g} \left(\frac{1}{Q_m} - \frac{1}{Q_0} \right) dz, \end{aligned}$$

whence the net gain (in dB) of a maser of length L is:

$$\begin{aligned} G_n &= 20\pi(\log_{10} e) \frac{fL}{v_g} \left(\frac{1}{Q_m} - \frac{1}{Q_0} \right) \\ &= \frac{27.3 fL}{v_g} \left(\frac{1}{Q_m} - \frac{1}{Q_0} \right) \dots (18) \end{aligned}$$

To obtain a high gain within a reasonable length L , Q_m must be made small, Q_0 large and v_g as small as is practicable. The first term of G_n is the "electronic gain" G , i.e. the gain which would be obtained if there were no structure losses.

Both v_g and Q_m are determined by the way in which we combine our propagating structure and active material and this is the main problem in designing a TWMM.

It is shown in the Appendix I that Q_m as defined above is given by

$$\frac{1}{Q_m} = \Delta n h \gamma^2 \frac{\varphi(f)\eta}{2(1+R)} [(A+B)^2 + R(A-B)^2 + 2\cos 2\Theta (A^2 - B^2)R^{\frac{1}{2}}], (19)$$

in which A and B are the signal transition matrix element vectors, previously defined; Δn is the inverted population density difference of the signal levels; $\varphi(f)$ is the line shape function, in many cases given by eq. (15); Θ is the angle between the larger of the two matrix element vectors and the major axis of the elliptically polarized RF magnetic field. R is a measure of the degree of ellipticity of the field polarization — for circular polarization $R = 0$ or $R = \infty$ depending on the sense of polarization, whilst for linear polarization $R = 1$ (cf. eq. 33). The factor η , the "filling factor", is the fraction of the total magnetic energy stored in the maser material (eq. 38).

The gain of the travelling wave maser is a function of frequency and by combining eq. (18) and (19) the instantaneous bandwidth of the device may readily be calculated. We find that for a Lorentzian line (i.e. $\varphi(f)$ given by eq. (15)) the bandwidth to half power points is:

$$B = \frac{1}{\pi T_2} \sqrt{\frac{3}{G_0 - 3}}, \dots (20)$$

G_0 being the uniform field peak electronic gain (in dB) of the TWMM and $1/\pi T_2$ the paramagnetic resonance line width (cf. eq. (15)). This relation is plotted for $T_2 = 4.9 \times 10^{-9}$ s in fig. 13¹⁸⁾.

The bandwidth of the TWMM may be increased at the expense of gain if we arrange that different sections of the device are acted upon by different static

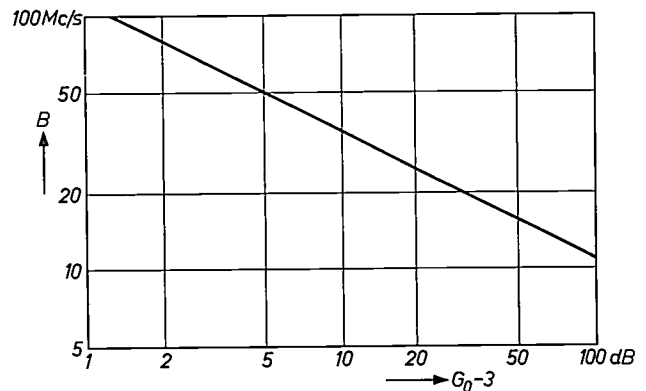


Fig. 13. Bandwidth B as a function of peak electronic gain G_0 for a TWMM in a uniform magnetic field, with $T_2 = 4.9 \times 10^{-9}$ s.

¹⁸⁾ The gain-bandwidth characteristics of the single cavity maser and the TWMM have been compared by DeGrasse *et al.*¹⁷⁾

magnetic fields, thus spreading the centre resonant frequencies of these sections.

This is the most powerful technique for increasing the bandwidth of the TWM and we shall consider three types of static magnetic field variation along the length of the structure. These are a single step occurring half way along the structure and linear and sinusoidal variations.

For these cases, assuming the line shape function $\varphi(f)$ of equation 15, the electronic gain G is given as a function of frequency by the following expressions:

1) single step:

$$G = \frac{G_0}{2} \left[\frac{1}{1 + (x + b)^2} + \frac{1}{1 + (x - b)^2} \right]. \quad (21)$$

2) sinusoidal variation:

$$G = \frac{G_0}{[(1 - x^2 + b^2)^2 + 4x^2]^{\frac{1}{4}}} \cos \left[\frac{1}{2} \tan^{-1} \frac{2x}{1 - x^2 + b^2} \right]. \quad (22)$$

3) linear variation:

$$G = \frac{G_0}{2b} \cdot \tan^{-1} \frac{2b}{1 + x^2 - b^2}. \quad (23)$$

In these expressions we have written:

$$\left. \begin{aligned} x &= 2\pi T_2(f - f_0) \\ b &= \pi T_2 \Delta f \end{aligned} \right\} \dots \dots (24)$$

G_0 is the peak electronic gain as in eq. (20). The factor Δf is the total spread in local centre resonant frequencies. As the centre resonant frequency is a function of magnetic field H (to be obtained e.g. from fig. 5), Δf is directly given by ΔH , the difference between the highest and the lowest field acting on the maser crystal. (Similar expressions to the above have been given by Ostermayer ¹⁹.)

It follows from these expressions that both single step and sinusoidal field variations produce gain frequency characteristics with a minimum at the centre frequency when the field staggering exceeds certain limits, e.g. fig. 14. For a single step this occurs when

$$b^2 > \frac{1}{3},$$

and for a sinusoidal variation when

$$b^2 > 2.$$

There is usually no practical advantage in increasing the bandwidth beyond the point at which the centre gain dip exceeds 3 dB.

In fig. 15 the ratio of peak electronic gain G_c to the uniform field peak electronic gain G_0 is plotted against the field-staggering parameter, $\pi T_2 \Delta f$, for

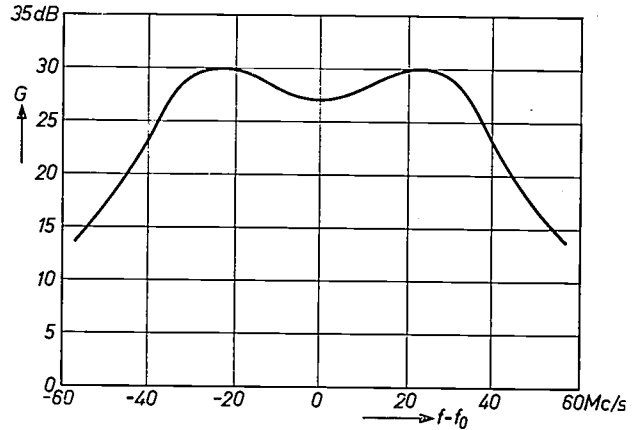


Fig. 14. Electronic gain G as a function of frequency in a TWM with a single step in the magnetic field. The curve represents eq. (21) for $G_0 = 50$ dB and $b = 1.0$.

the three types of field variation. In fig. 16 the 3 dB bandwidth resulting from the different types of field variation is plotted against peak electronic gain G_c for a TWM having a uniform field peak electronic gain G_0 of 50 dB. Clearly the field staggering parameter Δf corresponding to each point of fig. 16 can be derived from fig. 15.

An alternative technique to field staggering for increasing the bandwidth of a system employing a TWM as the first stage amplifier is to compensate the rather sharply peaked gain frequency characteristic of the uniform field maser by a suitable passive network in a subsequent stage of amplification — typically one of the intermediate frequency amplifiers. This technique which is known as gain equalization ²⁰, may be regarded to a first approximation as

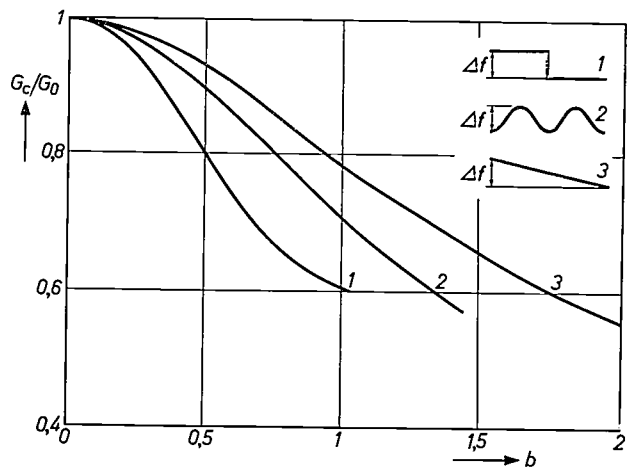


Fig. 15. Peak electronic gain G_c (relative to the uniform field peak electronic gain G_0) as a function of field-staggering parameter $b = \pi T_2 \Delta f$, for three types of field variation: 1. single step, 2. sinusoidal variation, 3. linear variation.

¹⁹ F. W. Ostermayer, 2nd quarterly report "Solid State Maser Research" B.T.L., 1960.

²⁰ W. J. Tabor and J. T. Sibilica, Bell Syst. tech. J. 42, 1863, 1963.

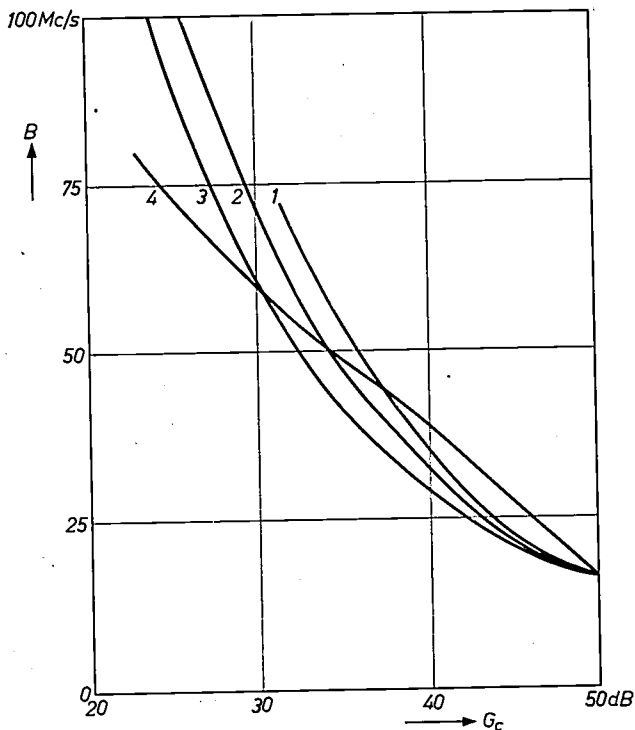


Fig. 16. 3 dB bandwidth B as a function of centre frequency electronic gain G_c for a uniform field peak electronic gain $G_0 = 50$ dB and $T_2 = 4.9 \times 10^{-9}$ s for three types of field variation and for gain equalization. 1 field variation: single step, 2 field variation: sinusoidal, 3 field variation: linear, 4 gain equalization (curve refers to system gain). (Curve 1 is not drawn in the region where the centre gain dip exceeds 3 dB.)

removing the peak of the uniform field gain characteristic (fig. 17). The 3 dB bandwidth of the system may then readily be calculated and is plotted in fig. 16 against effective system gain.

The noise temperature of the travelling wave maser

The most important characteristic of the TWM is its very low noise temperature. Calculation of the maser noise temperature is made in the Appendix and we find that the equivalent noise temperature is given to a good approximation by:

$$T_n = \frac{1}{(1 - a)} \left[aT_a + \frac{T_0}{I} \right] \dots (25)$$

In this equation a is the absorption coefficient of the input lead to the maser and T_a the mean temperature of this lead; T_0 is the ambient temperature of the active part of the maser and I is the inversion. Typically $T_0 = 4.2$ °K, $I \approx 3$, $a \approx 0.045$ (0.2 dB loss) and $T_a \approx 100$ °K, whence we find:

$$T_n = \frac{1}{0.955} [4.5 + 1.4] = 6.2 \text{ °K} \dots (26)$$

Evidently if the low noise potentialities of the maser

are to be fully realized, great attention must be given to reduction of loss in the input leads.

Design of a travelling wave maser

In designing a TWM the first consideration must be the choice of active material. To date, for masers operating with signal frequencies in the 1 - 10 Gc/s range, no better material than synthetic ruby has come to light. The optimum concentration of chromium ions in the ruby depends on the operating temperature proposed for the device, and if this is in the liquid helium range it is found that the largest value of the product $\Delta n_0 I T_2$ (hence the lowest value of Q_m) can be obtained at a chromium concentration of about 0.05 Cr³⁺ ions per 100 aluminium ions (0.05% ruby) — at higher concentrations multiple spin-spin interactions (cross relaxation) rapidly tend to reduce the inversion which may be obtained. In choosing the orientation of the ruby crystal with respect to the applied static magnetic field we look for a large transition probability at the signal frequency and freedom from low-order cross-relaxation effects which even at low concentrations can seriously affect maser operation²¹). For example, it is found that if a simple integral relation exists between the pump and signal frequencies, e.g.,

$$nf_s = mf_p,$$

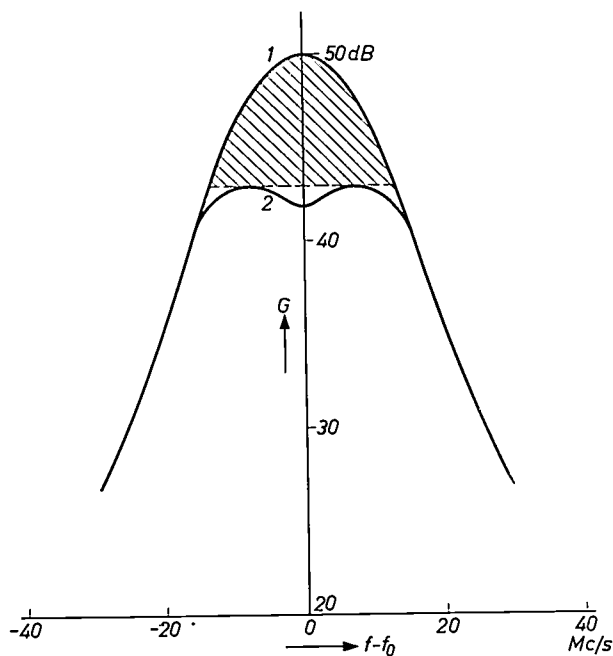


Fig. 17. Gain equalization. 1 Uniform field gain as a function of frequency — no equalization. 2 Effective gain as a function of frequency after equalization. The shaded area is the excess gain removed by equalization.

²¹ S. A. Ahern, P. A. Gould and J. C. Walling, J. Electronics and Control 9, 477, 1960.

there is a tendency for the pump frequency to saturate the signal transition, the tendency being particularly marked for low values of m and n . It is found that in ruby the best operation (for signal frequencies below 7 Gc/s) is obtained with the magnetic field at right angles to the three fold symmetry axis of the ruby and in this case the ground state Zeeman levels are as indicated in figure 5.

We can now use eq. (19) to ascertain what value of Q_m might be expected. For simplicity let us assume that the RF magnetic field is circularly polarized ($R = 0$) and has a frequency f_0 . Eq. (19) then becomes:

$$\frac{1}{Q_m} = \Delta n h \gamma^2 \eta T_2 (A + B)^2. \quad \dots (27)$$

Δn may be evaluated in terms of the chromium ion population density N , the signal frequency f , the ambient temperature T and the inversion I as follows.

We have:

$$N = n_1 + n_2 + n_3 + n_4,$$

and in thermal equilibrium (subscript 0):

$$N = n_{10} \left[1 + \exp\left(-\frac{hf_{12}}{kT}\right) + \exp\left(-\frac{hf_{13}}{kT}\right) + \exp\left(-\frac{hf_{14}}{kT}\right) \right] \\ = n_{10} c.$$

Therefore the equilibrium population difference between levels 1 and 2 is given by

$$(n_2 - n_1)_0 = \Delta n_0 = \frac{N}{c} \left[\exp\left(-\frac{hf_{12}}{kT}\right) - 1 \right]$$

and hence the inverted population difference

$$\Delta n = -I \Delta n_0 = -\frac{IN}{c} \left[\exp\left(-\frac{hf_{12}}{kT}\right) - 1 \right] \approx \frac{NIhf_{12}}{kTc}.$$

Thus:

$$\frac{1}{Q_m} = \frac{NIh^2f_s}{ckT} \gamma^2 \eta T_2 (A + B)^2.$$

Let us consider the particular case of a maser using ruby as the active material and operating in the 90° orientation (fig. 5) at a signal frequency of 4170 Mc/s, the signal transition being between levels 1 and 2. In this case we find using the tables of Chang and Siegman¹³ that the matrix element vectors are $A = 1.16$, $B = 0.56$. For 0.05% ruby $N = 2.35 \times 10^{19} \text{ cm}^{-3}$, $T_2 = 4.9 \times 10^{-9} \text{ s}$, and by pumping between levels 1 and 4 an inversion of about 2.5 (possibly better) may be obtained. The value of γ^2 is $3.09 \times 10^{14} \text{ gauss}^{-2} \text{ s}^{-2}$, $h = 6.62 \times 10^{-27} \text{ erg s}$ and $k = 1.38 \times 10^{-16} \text{ erg deg}^{-1}$. Therefore for this case:

$$\frac{1}{Q_m} = 3.54 \times 10^{-1} \frac{\eta}{cT}.$$

For an operating temperature of 1.5 °K we find that

$$c = 2.85,$$

and if we assume that $\eta = 0.20$:

$$\frac{1}{Q_m} = 1.66 \times 10^{-2}.$$

We may note that for waves propagating in the backward direction the sense of polarization is opposite to that for waves propagating in the forward direction. Thus for backward travelling waves we must write $R = \infty$ in eq. (19), so that the ratio of Q_m in the forward and backward directions is:

$$\left(\frac{A - B}{A + B} \right)^2 \approx \frac{1}{8}.$$

The device is thus, to some extent, intrinsically non reciprocal.

According to eq. (18) the gain in dB is proportional to the length of the structure. Various practical considerations such as the manufacture of the slow wave structure, the obtaining of large uniform single crystals of ruby and the provision of magnetic fields of high uniformity over a large volume tend to limit the length of the device. We will consider the case of a TWM operating under the above conditions and having a length of 10 cm. We find using eq. (18) that the forward electronic gain is:

$$G_0 = 0.63 r \text{ dB},$$

where r is the ratio between the free space velocity of light and the structure group velocity v_g , and is called the slowing factor.

Such a maser using a structure having a slowing factor of 100 will therefore have an electronic gain of 63 dB — the net gain of course will be less than this by the structure insertion loss. In a practical structure the polarization of the RF field may deviate from circularity and the complete form of eq. (19) must be used.

We see then that successful operation of masers of this type depends on the use of a propagating structure having a substantial slowing factor. Slow wave structures are familiar through their application in travelling wave tubes and in linear accelerators. In these devices, however, we are concerned with reducing the *phase* velocity of the propagating wave whereas in the TWM we wish to reduce the group velocity, and furthermore (with the construction of a non-reciprocal device in mind) to provide regions in the structure where the RF magnetic fields are substantially circularly polarised. Structures consisting essentially of arrays of parallel conductors have been found suitable and that most

widely used is the comb structure (fig. 11) which consists of an array of conductors approximately a quarter wavelength long at the signal frequency and short circuited at one end. (In this structure the RF magnetic field associated with the propagation lies in the plane normal to the extension of the conductors and is substantially circularly polarized, the sense of polarization being opposite on the two sides of the array of conductors. This means that by placing the active material on one side of the array it is possible to utilize the non reciprocal characteristics of the ruby already discussed. The device may be made to be completely non reciprocal if ferrite material, dimensioned so that ferrimagnetic resonance is obtained at the signal frequency for the same static magnetic field as is required by the ruby, is placed on the other side of the structure. In this way a resonant interaction between the magnetization of the ferrite and the backward travelling circularly polarized waves in the structure is obtained, thus backward travelling waves experience large attenuation whilst the forward travelling waves do not interact with the ferrite to any significant extent. If sufficient backward loss is provided for the loop gain to be less than unity when the structure is terminated by a short circuit, the device is completely stable. Furthermore, since the ferrite elements are at a very low temperature, any loss which they might introduce in the forward travelling wave does not significantly affect the maser noise temperature (Appendix II).

A 4170 Mc/s packaged travelling wave maser

As an example of a practical packaged TWM we will now describe briefly the amplifier designed and built at the Mullard Research Laboratories and used at the General Post Office satellite communication ground station at Goonhilly Down in Cornwall for experiments with the Telstar and Relay communication satellites.

Maser structure

The active material in this maser is 0.05% ruby used with the applied static magnetic field normal to the three-fold axis of symmetry of the crystal as described in the last section. The signal transition is that between levels 1 and 2 at 4170 Mc/s and a population inversion of about 2.7 is obtained by pumping between levels 1 and 4 at 30 150 Mc/s. These frequencies correspond to a magnetic field of 3280 Oe (fig. 5).

The ruby sample was cut from a large synthetic single crystal in the form of a rod, the *c*-axis being

inclined at an angle of 60° to the axis of the rod. The *c*-axis is therefore at an angle of 60° to the direction of propagation in the slow wave structure, in the plane normal to the array of parallel conductors.

The isolator material used in the maser described here is yttrium iron garnet (YIG) in the form of flat discs which are supported in a polycrystalline alumina slab. By suitable choice of the thickness of the discs (determining the shape demagnetizing factors) it is arranged that ferrimagnetic resonance occurs in the discs at the same static magnetic field as is required by the ruby. The required demagnetizing factor is calculated from the Kittel resonance equation²²⁾ which for flat discs mounted away from conducting walls may be written:

$$\omega = \gamma \left[H_0 - \frac{4\pi M_s}{2} (3N_z - 1) \right],$$

where H_0 is the applied magnetic field, N_z is the demagnetizing factor in the direction of H_0 , and $4\pi M_s$ is the saturation magnetization of the garnet at the operating temperature. Yttrium iron garnet is one of the few ferrimagnetic materials which are suitable for this application as it still has a relatively narrow ferrimagnetic resonance line at liquid helium temperatures.

The slow wave structure is a comb (cf. fig. 11) having the dimensions shown in fig. 18*b* and provides a slowing factor of 110. The assembly is shown in a cut-away view in fig. 18*a*.

The input signal is launched on to the comb structure through a coaxial line the centre conductor of which continues as the conductor *E* of fig. 19. This conductor terminates in a short length of coaxial line *X* the length of which may be adjusted by means of the short circuiting plunger *P*. Impedance matching is achieved by adjusting the position of this plunger and varying the proximity of the conductor *E* to the first conductor of the comb proper. A similar arrangement is provided at the output end.

An advantage of slow wave structures of the iterated conductor type is that they can be introduced in a magnetic equipotential plane of a rectangular waveguide propagating, say, an H_{01} mode, without substantially perturbing this propagation. The structure of fig. 18 will therefore propagate certain rectangular waveguide modes at frequencies above that corresponding to a free space wavelength of approximately 3 cm. In the present maser the pump energy propagates in such a waveguide mode and is introduced into the end of the slow wave structure

²²⁾ C. Kittel, Phys. Rev. 73, 155, 1948.

by a direct connection from rectangular waveguide, the broad face of the waveguide being parallel to the plane of the comb conductors. A pump power of about 30 mW is required to saturate the $1 \rightarrow 4$ transition.

The cryostat

The maser structure is housed in the tail of a stainless steel double dewar vessel (fig. 20), the magnetic field of 3280 Oe being provided by a permanent magnet as shown in fig. 3. Centre frequency ad-

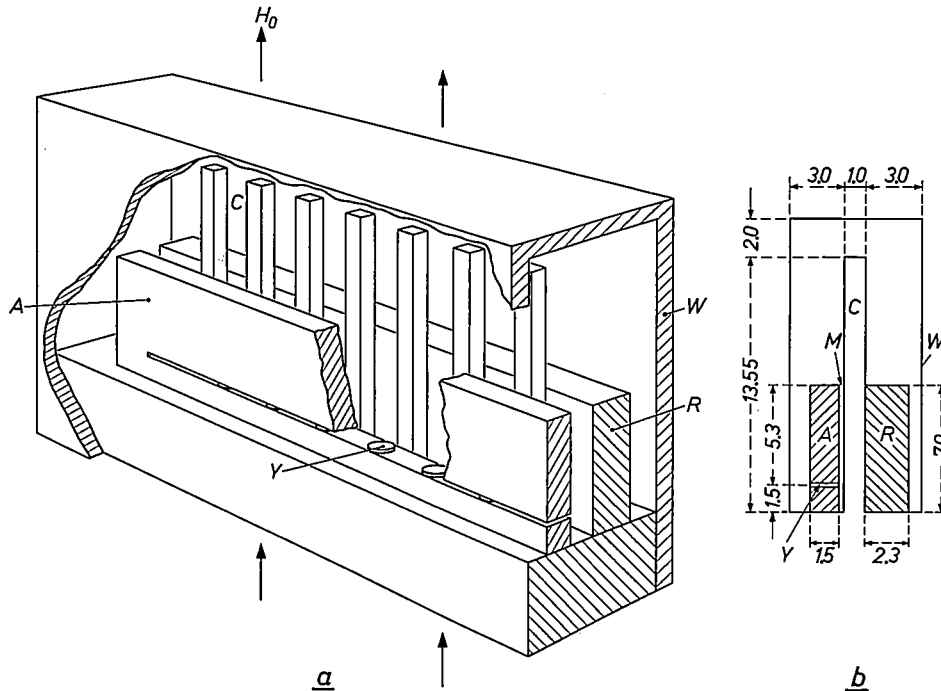


Fig. 18. Cut-away view (a) and cross section (b) of the 4170 Mc/s TWM. The dimensions are in millimeters. The slow wave comb structure C (pitch 2 mm) permits the propagation of waves with a group velocity of $1/110$ times the free space velocity of light, and with an RF magnetic field circularly polarized in a plane perpendicular to the extension of the comb conductors. The sense of polarization in a travelling wave is opposite on the two sides of the comb, and opposite for forward and backward waves. In the applied static magnetic field H_0 of 3280 Oe the Cr^{3+} ions in the single crystal ruby slab R (Al_2O_3 with 0.05% Cr^{3+}) are resonant at the signal frequency (4170 Mc/s, $1-2$ transition) and at the pump frequency (30 150 Mc/s, $1-4$ transition). At the signal frequency they amplify forward waves. The yttrium iron garnet discs Y , held in place by the polycrystalline alumina slab A , and also resonant in H_0 at the signal frequency, attenuate backward waves. A sheet of 0.025 mm Melinex M is used to adjust the transmission characteristics of the slow wave structure. Pump power (30 150 Mc/s) is transmitted by the waveguide W .

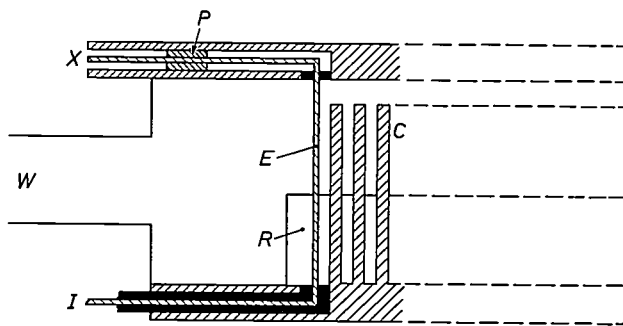


Fig. 19. Matching system from coaxial line to comb. I coaxial input line. E conductor, extension of the central conductor of both the input (I) and the terminating (X) coaxial line. P short circuiting plunger. C comb structure. R ruby slab. W pump waveguide. Matching is achieved by adjusting position of P and distance of E from comb.

justment is obtained by varying the current through two coils attached to the pole faces of the permanent magnet. Connections from the top of the cryostat to the coaxial leads on the maser comb structure are made through low thermal conductivity coaxial lines which terminate at the top of the cryostat in waveguide-coaxial transitions (fig. 21). The pump energy is introduced via a low thermal conductivity waveguide (WG 22).

To exclude air from the system (air is of course solid at liquid helium temperatures) it is necessary that all these leads should be vacuum tight. The input and output waveguides are sealed with thin terylene sheet windows and the pump waveguide with a mica window, all the seals being in the room

temperature part of the apparatus. A series of carbon resistors attached at various levels to the connecting lead structure permits monitoring of the liquid helium level in the dewar vessel.

The whole maser package is mounted on a cradle

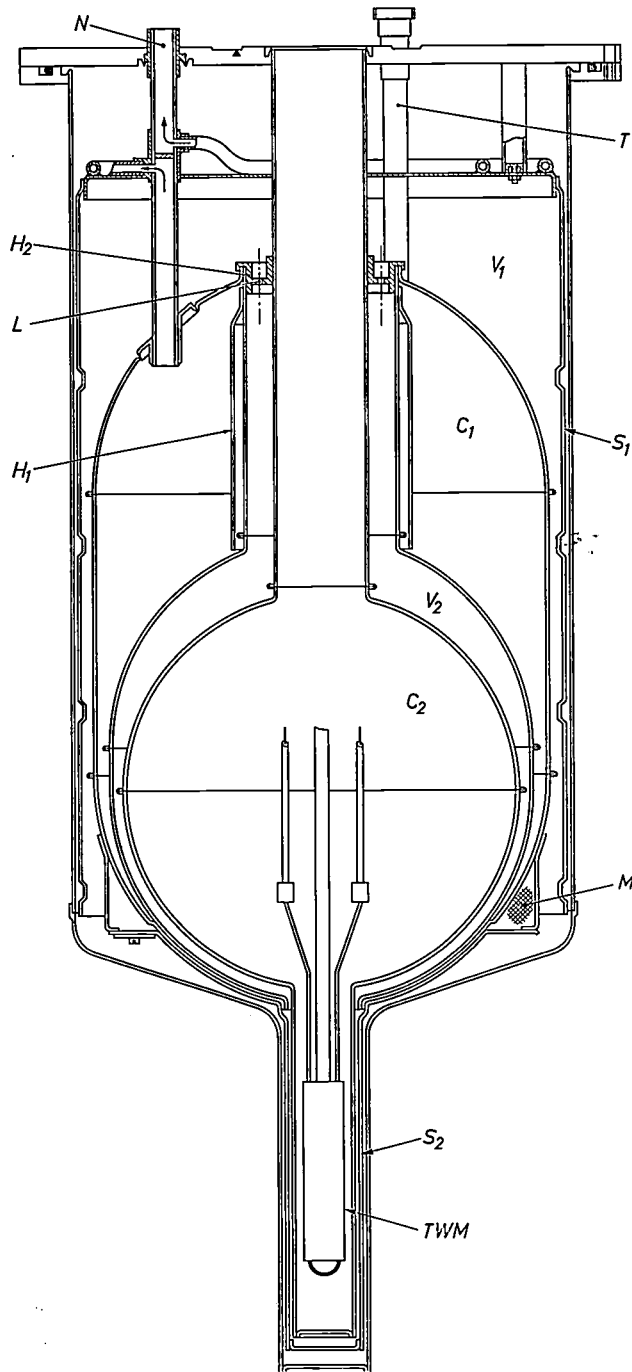


Fig. 20. Sectional drawing of double dewar vessel. Length 100 cm, max. diameter 33 cm.

C_1 liquid nitrogen container. C_2 liquid helium container. V_1, V_2 vacuum spaces. N nitrogen vapour outlet. S_1 copper radiation shield cooled at its top by nitrogen vapour. S_2 copper radiation shield cooled at its top by liquid nitrogen. H_1, H_2 , copper heat conductors keeping a fixed point on the neck of the helium container at liquid nitrogen temperature. L holes linking vacuum spaces. T filling and venting tubes. M molecular sieve (getter material to absorb residual gases). TWM travelling wave maser.

which allows it to be tipped through 45° from the vertical once it has been charged with liquid nitrogen and helium. This is its operating position when the aerial on which it is mounted is directed towards the horizon, and as the aerial moves to the zenith the maser moves through 90° to a position 45° the other side of the vertical.

The complete package is shown in figure 3 mounted on the aerial structure in its operating position, with a dewar vessel which allows an operating time per filling of liquid helium of about 8 hours. The maser is operated at a temperature of 1.5°K , the pressure over the boiling liquid being reduced by means of a pump situated lower on the aerial structure. Fig 22 shows a later version of the maser with a much larger dewar vessel which gives an operating time per filling of about 2 days.

The maser has been operated in a homogeneous magnetic field and also with a suitable stepped magnetic field to obtain greater bandwidth at the expense of gain. The performance figures of the maser under such conditions are:

Operation in a homogeneous magnetic field:

Electronic gain	52.5 dB
Bandwidth to 3 dB points	16 Mc/s
Total structure forward loss	11 dB
Total structure backward loss	70 dB
Net forward gain	41.5 dB
Noise temperature	$15 \pm 4^\circ\text{K}$

Operation in stepped magnetic field ($\Delta H \approx 5 \text{ Oe}$):

Net forward gain	30 dB
Bandwidth to 3 dB points	28 Mc/s

These performance figures are in reasonable agreement with the design predictions outlined previously.

Systems considerations and conclusions

The packaged travelling wave maser which is described above is one of the first such devices to be regularly employed in a systems application, and its operation has proved to be reliable and consistent. The principal operational difficulty is the need for repeated liquid helium transfers on site, a difficulty which is mitigated by the use of very large storage capacity maser dewar vessels, and which would be eliminated by the use of a closed cycle helium temperature refrigeration system.

A further operational difficulty encountered was a drift in the centre frequency of the maser due to changes in the field provided by the permanent magnet. These were the result of ambient temperature variations. This effect can be entirely eliminated by the employment of persistent current superconducting electromagnets housed in the dewar

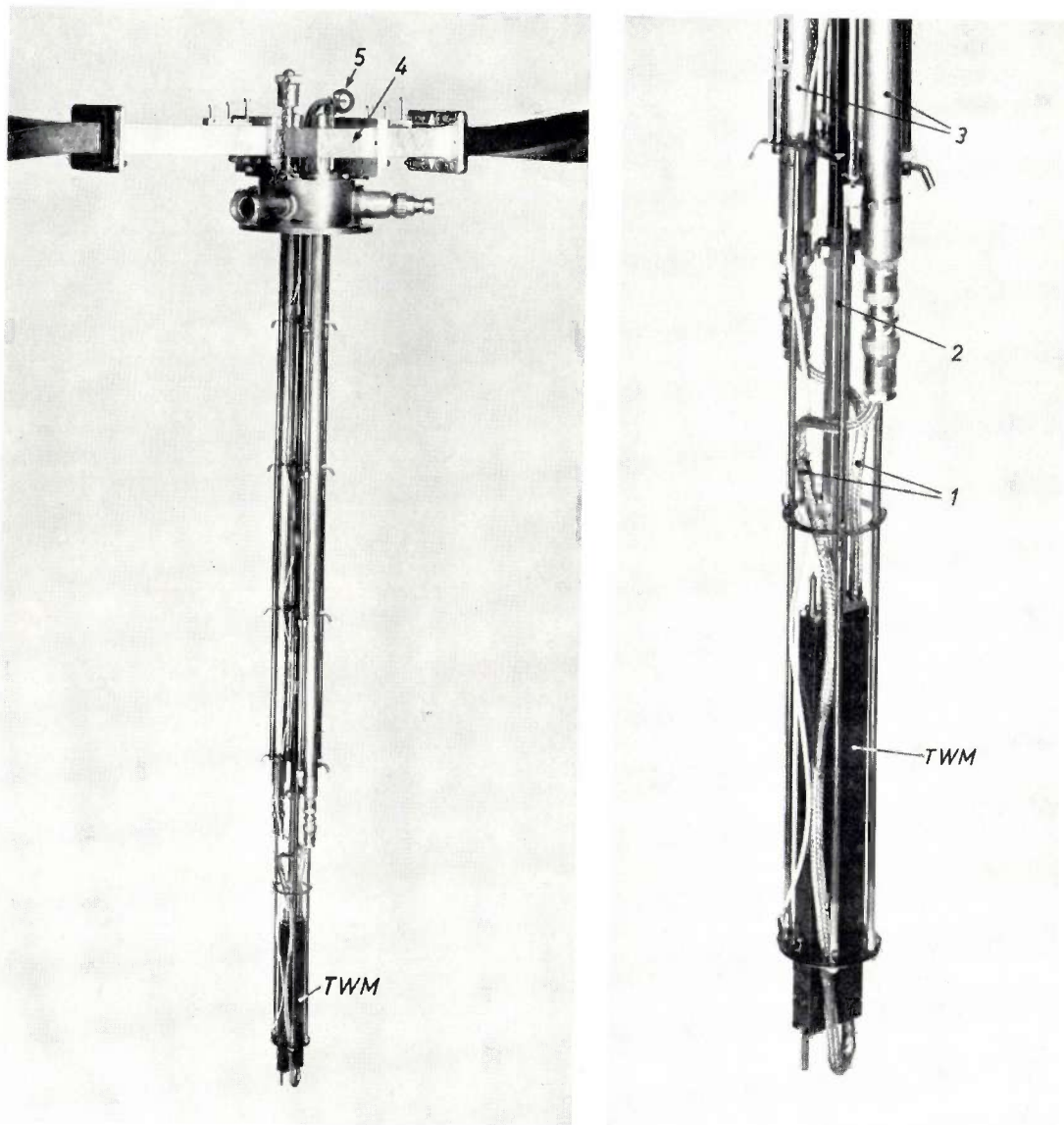


Fig. 21. Cryostat head and maser connection leads (enlarged view of lower end at right). *TWM* travelling wave maser. 1 coaxial leads (cf. fig. 19). 2 low thermal conductivity pump waveguide. 3 low thermal conductivity coaxial lines. 4 one of the two waveguide-coaxial transitions. 5 connection of pump waveguide.

vessel, such as have recently been developed at Mullard Research Laboratories, based on the work of P. P. Cioffi²³).

We may note that the noise performance of the maser described may be further improved by careful attention to the reduction of radio frequency loss in the input lead (eq. 25 and 26). This loss is the major contributor to the noise temperature of the maser amplifier, and the use of a waveguide feed down the neck of the dewar vessel would substantially reduce this. A noise temperature for the maser of 3-4 °K, as measured at its input terminals,

is entirely practical. However, the spectacular decrease in noise temperature of the first amplifier of a receiver system which is offered by the maser compared with more conventional amplifiers (a good travelling wave tube at this frequency has a noise temperature of 900 °K), may not be fully utilized at present because of the noise contributions of other parts of the system. These sources of noise arise as a result of loss in other necessary circuit components which precede the maser such as filters, diplexer, feed horns etc. The antenna itself also may make an appreciable contribution to the overall system noise temperature as it will have side lobes of its radiation pattern which accept noise

²³) P. P. Cioffi, J. appl. Phys. **33**, 875, 1962.

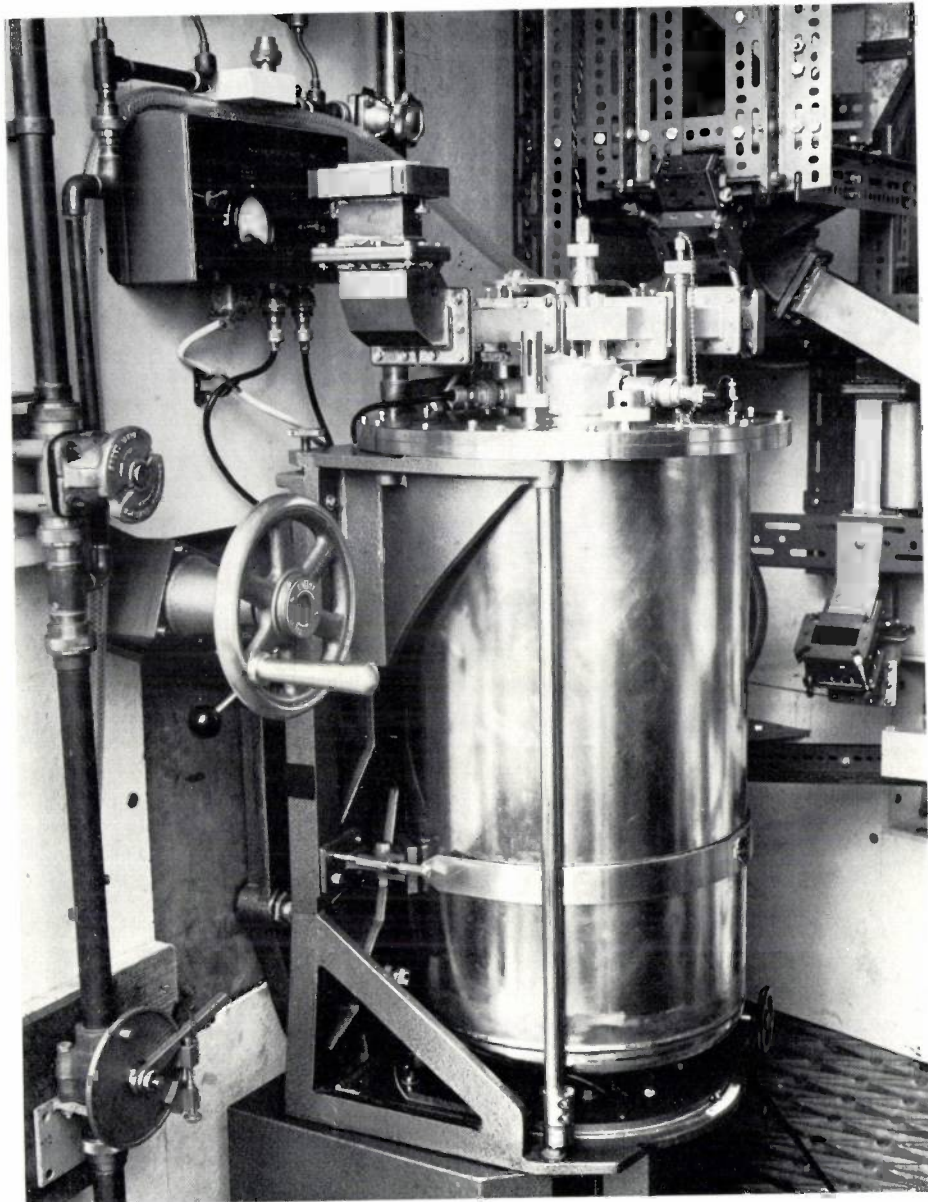


Fig. 22. Travelling wave maser with large storage capacity dewar vessel. (Photo published by permission of the British G.P.O.)

radiated from the ground. It is to be expected that these other noise contributions will be substantially reduced as further attention is directed towards their elimination, and that systems with very low overall noise temperature which can fully utilize the potentialities of the maser noise performance will soon be realized.

Appendix I

Calculation of Q_m for a TWM

The quality factor Q_m of the maser material has been defined as:

$$Q_m = \frac{2\pi f_s W_s}{P_m} \dots \dots \dots (28)$$

P_m in this equation is the power emitted per unit length of the maser material and may be written:

$$P_m = \Delta n V_c h f_s W_{ij}, \dots \dots \dots (29)$$

where Δn is the population density difference between the two levels i and j between which the signal transition takes place. W_{ij} is the transition probability defined (eq. 13) and V_c is the volume of crystal per unit length of the structure.

Δn may be written in terms of the equilibrium population difference Δn_0 and the inversion I through:

$$\Delta n = -I \Delta n_0.$$

In general the RF magnetic field amplitude and polarization will vary within the active crystal and thus if a correct value is to be obtained for P_m , the transition probability W_{ij} should be integrated over the volume of the crystal.

The power emitted from an element of material as indicated in fig. 23 is:

$$dP_m = \Delta n \, dx \, dy \, dz \, hf_s \, W_{ij}$$

$$= \Delta n \, dx \, dy \, dz \, hf_s \frac{\gamma^2}{4} \varphi(f) |(\mathbf{A} + j\mathbf{B}) \cdot (\mathbf{H} + j\mathbf{H}')|^2. \quad (30)$$

Let us now suppose that the plane of polarization of the RF magnetic field and the plane defined by the matrix element vectors \mathbf{A} and \mathbf{B} are coincident. (This is a case frequently met in practice but if this condition is not satisfied then the vectors \mathbf{A} and \mathbf{B} must be replaced, in what follows, by their projections

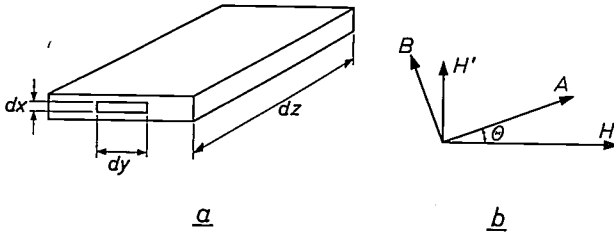


Fig. 23. a) Volume element of the maser material. b) H and H' are the magnetic field vectors. \mathbf{A} and \mathbf{B} are the matrix element vectors.

on the plane of polarization of the RF field.) If the angle between the vectors \mathbf{A} and \mathbf{H} (the larger field component) is Θ and if we resolve the elliptically polarized field into two circularly polarized components H_+ and H_- of opposite sense such that:

$$H = H_+ + H_-, \quad H' = H_+ - H_-$$

then equation (30) may be rewritten:

$$dP_m = \Delta n \, hf_s \frac{\gamma^2}{4} \varphi(f) [H_+^2(A+B)^2 + H_-^2(A-B)^2 + 2H_+H_- \cos 2\Theta (A^2 - B^2)] \, dx \, dy \, dz. \quad (31)$$

Integrating over unit length of the crystal (volume V_c):

$$P_m = \Delta n \, hf_s \frac{\gamma^2}{4} \varphi(f) [(A+B)^2 \int_{V_c} H_+^2 \, dv + (A-B)^2 \int_{V_c} H_-^2 \, dv + 2 \cos 2\Theta (A^2 - B^2) \int_{V_c} H_+H_- \, dv]. \quad (32)$$

The integrals in this expression can only be evaluated if we have an exact knowledge of the field distribution, which in most TWM's we do not have, although in the cases of uniformly loaded rectangular waveguides or strip lines eq. (32) can be integrated directly. If we define a structure reciprocity factor R as:

$$R = \frac{\int_{V_c} H_-^2 \, dv}{\int_{V_c} H_+^2 \, dv}, \quad (33)$$

then (32) may be written approximately as:

$$P_m = \Delta n \, hf_s \frac{\gamma^2}{4} \varphi(f) \int_{V_c} H_+^2 \, dv [(A+B)^2 + R(A-B)^2 + 2 \cos 2\Theta (A^2 - B^2)R]. \quad (34)$$

The mean magnetic energy stored in the maser material per unit length is (in c.g.s. units):

$$M_m = \frac{\mu}{8\pi} (1 + R) \int_{V_c} H_+^2 \, dv = \frac{\mu}{16\pi} \int_{V_c} \mathbf{H} \cdot \mathbf{H}^* \, dv,$$

whence:

$$\int_{V_c} H_+^2 \, dv = \frac{1}{2(1+R)} \int_{V_c} \mathbf{H} \cdot \mathbf{H}^* \, dv. \quad (35)$$

The mean magnetic energy stored in the whole structure per unit length is

$$\frac{W_s}{2} = \frac{\mu}{16\pi} \int_{V_c} \mathbf{H} \cdot \mathbf{H}^* \, dv. \quad (36)$$

From (34), (35) and (36) we find eq. (19):

$$\frac{1}{Q_m} = \Delta n \, h \frac{\gamma^2}{1+R} \frac{\varphi(f)}{2} \eta [(A+B)^2 + R(A-B)^2 + 2 \cos 2\Theta (A^2 - B^2)R], \quad (37)$$

in which

$$\eta = \frac{\int_{V_c} \mathbf{H} \mathbf{H}^* \, dv}{\int_{V_c} \mathbf{H} \mathbf{H}^* \, dv} \quad (38)$$

is the filling factor.

Appendix II

Calculation of the noise temperature of the TWM

The equivalent noise temperature of a maser amplifier is its most important characteristic. To calculate the noise temperature we recall a basic result of radiation theory that a body at a temperature T emits incoherent radiation (noise), the power in a single mode and in a frequency band of width Δf being:

$$P_n = \frac{a \, hf \, \Delta f}{\exp\left(\frac{hf}{kT}\right) - 1} = a \Phi(T) \Delta f \quad (39)$$

$$= a \, kT \, \Delta f \quad \text{for } \frac{hf}{kT} \ll 1. \quad (40)$$

a is the emission coefficient of the body which is equal to its absorption coefficient.

Ditchfield²⁴) has shown that this result may be applied to bodies containing energy levels the populations of which are inverted. Considering an element of the TWM and a narrow frequency band around the signal centre frequency, we may then write (cf. fig. 24) the increment of noise power as:

$$dP_n = -\alpha_L P_n \, dz + \alpha_L \Phi(T_0) \Delta f \, dz + g P_n \, dz - g \Phi(T_m) \Delta f \, dz.$$

structure loss thermal noise from structure gain thermal noise from maser material; abs. coeff. = $-g$

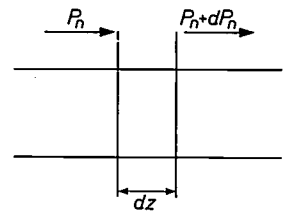


Fig. 24. Increase in noise power P_n in an element of length dz of the travelling wave maser.

Integrating this expression we find that the output noise power is given by

$$P_{n_0} = G' P_{n_i} + \frac{[\alpha_L \Phi(T_0) - g \Phi(T_m)] \Delta f}{g - \alpha_L} (G' - 1), \quad (41)$$

in which we have written

$$G' = e^{(g - \alpha_L)L} = \text{net numerical gain of the maser.}$$

The noise power at the input terminals of the active part of the maser is made up of two components, the source noise $\Phi(T_s) \Delta f$ and the thermal noise contributed by loss in the leads to the active part of the maser. Thus:

$$P_{n_i} = [(1 - a) \Phi(T_s) + a \Phi(T_a)] \Delta f, \quad (42)$$

where a is the loss factor of the input leads and T_a their mean temperature. The loss factor of the output leads can be taken

²⁴) C. R. Ditchfield, Solid State Electronics 4, 171, 1962.

into account similarly but noise due to this cause is usually negligible. Assuming $G' \gg 1$ and $|g| \gg |\alpha_L|$ and using the linear approximation for $\Phi(T)$, $\Phi(T) = kT$, we have:

$$P_{n_0} = G'(P_{n_i} + k|T_m|\Delta f) = G'[(1 - \alpha)kT_s + \alpha kT_a + k|T_m|]\Delta f.$$

The net gain of the maser including the input leads is $G'(1 - \alpha)$. Thus the noise figure (cf³) of the TWM including the input leads is:

$$F = \frac{1}{G'(1 - \alpha)} \frac{P_{n_0}}{kT_s \Delta f} = 1 + \frac{1}{T_s} \frac{\alpha T_a + |T_m|}{1 - \alpha}, \quad (43)$$

whence the equivalent noise temperature of the maser is:

$$T_n = \frac{\alpha T_a + |T_m|}{1 - \alpha}. \quad (44)$$

The spin temperature T_m can be related to the ambient temperature T_0 and the inversion I . The thermal equilibrium population difference Δn_0 is:

$$\begin{aligned} \Delta n_0 &= n_2 - n_1 = n_1 \left[\exp\left(-\frac{hf_{12}}{kT_0}\right) - 1 \right] \\ &\approx -n_1 \frac{hf_{12}}{kT_0} \text{ if } \frac{hf_{12}}{kT_0} \ll 1. \end{aligned} \quad (45)$$

The population difference during operation of the maser is, in the same way,

$$\Delta n \approx -n_1 \frac{hf_{12}}{kT_m} \text{ if } \frac{hf_{12}}{kT_m} \ll 1 \quad (46)$$

The actual population of level 1 is not appreciably altered by the pumping (i.e. $\Delta n \ll n_1$), so that we may put $n_1 \approx n_1$. Then, by definition of the inversion I and (45) and (46):

$$T = -\frac{\Delta n}{\Delta n_0} \approx -\frac{T_0}{T_m},$$

or, for $T_m < 0$:

$$|T_m| \approx \frac{T_0}{T},$$

whence from (44) we obtain eq. (25):

$$T_n = \frac{1}{(1 - \alpha)} \left[\alpha T_a + \frac{T_0}{T} \right].$$

Appendix III (Note of the editor)

In the rationalized Giorgi system the "magnetic dipole moment" and the "magnetic area moment" (electromagnetic moment) have different dimensions (Wbm and Am² respectively), which calls for special attention when using these and related concepts such as "magnetization" and "gyromagnetic ratio". Conversion to the rationalized Giorgi system and a notation in accordance with (expected) recommendations of the International Electrotechnical Committee and the International Organization for Standardization is obtained as follows:

- 1) Read everywhere "magnetic induction B" instead of "magnetic field H" and 10⁻⁴ Wb/m² instead of "1 Oe".
- 2) Drop the c in the expressions for β, γ and the resonant frequency on pages 291 and 293 (the unit for β becomes Am²; the resonance equation reads $\omega = \gamma B$).
- 3) Multiply the expressions (19), (27), the one following (27), and (37) for $1/Q_m$ by $\mu_0/4\pi$ (this results after matching the expressions for the stored energy to the Giorgi system in Appendix I). In the calculation on p. 29 substitute 1 cm⁻³ = 10⁶ m⁻³, 1 gauss = 10⁻⁴ Wb/m², 1 erg = 10⁻⁷ joule.
- 4) Read the Kittel resonance equation (p. 304) as $\omega = \gamma[B_0 - \mu_0 M_s (3N_z - 1)/2]$, in which M_s is the saturation magnetization.

Summary. The signals received from communication satellites are of the order of 10⁻¹³ watt, even with highly directional aerials at the ground stations. Signals of this level dictate the use of ground station receivers with very low noise temperatures, and thus the solid state travelling wave maser, which has the lowest available noise temperature, is used as the first amplifier in such systems.

The operation of a solid state maser depends on the resonant interaction of radiofrequency signals with paramagnetic ions occupying discrete energy levels. This interaction is discussed for the simple case of free electrons in a static magnetic field and for paramagnetic ions in crystals. To obtain amplification from such systems a population inversion is required between a pair of levels resonant at the signal frequency. The method,

proposed by Bloembergen, of obtaining a continuous population inversion ("pumping" in a three-level system) is discussed.

The factors affecting the design of travelling wave masers and the choice of suitable materials are reviewed. The method of increasing the instantaneous bandwidth of the maser, by applying a static field which varies along the length of the structure, is discussed. The design and construction at Mullard Research Laboratories of a maser operating at 4170 Mc/s for use in the Goonhilly Down satellite communication ground station of the British General Post Office is outlined. This maser, consisting of a slow wave comb structure containing as the active material a ruby single crystal at 1.5 °K in a magnetic field of 3280 Oe and pumped at a frequency of 30 150 Mc/s, has a noise temperature of less than 20 °K.

"COMPATIBLE" SINGLE-SIDEBAND MODULATION

by T. J. van KESSEL *).

621.376.24

As broadcasting transmitters are continuously increasing in power and number, it is desirable to reduce their bandwidth in the frequency channels allocated to them. One means to this end is single-sideband modulation. If signals modulated in this way can be received by sets currently in use, then the single-sideband modulation is said to be "compatible" with the conventional double-sideband system, and can therefore be introduced gradually. This article describes various methods of single-sideband modulation, with special reference to a new method, called the "squaring system".

In radio broadcasting an audio frequency signal, i.e. music or speech, is transmitted by means of a radio-frequency carrier wave. For this purpose the carrier is modulated by the audio signal, which is then recovered in the receiver by demodulation.

The most commonly used method of modulation is *amplitude modulation*, in which the amplitude of the carrier wave is varied in accordance with the waveform of the audio signal to be transmitted. Let this audio signal be a simple cosine oscillation with angular frequency p . The modulated RF signal will then have the following form as a function of time:

$$v(t) = (1 + a \cos pt) \cos \omega t, \text{ where } a \leq 1. \quad (1)$$

In this expression a is the modulation depth and ω is the angular frequency of the RF oscillation. The modulation depth a must be less than unity, since the demodulator (detector) in the receiver cannot distinguish a "negative" amplitude from a "positive" one.

The amplitude-modulated signal can be regarded as the sum of three unmodulated signals. This can be seen by writing (1) in the following form:

$$v(t) = \cos \omega t + \frac{a}{2} \cos(\omega + p)t + \frac{a}{2} \cos(\omega - p)t. \quad \dots (1a)$$

The last two terms in the right-hand side of (1a) represent signals called the upper and lower *sidebands*. They lie symmetrically at a frequency distance $\pm p$ from the unmodulated carrier. It is evident, then, that the amplitude-modulated signal takes up an unnecessary amount of space in the frequency channel available, since all the information to be transmitted is already present in one of the sidebands. In view of the overcrowding of the frequency bands, attempts have understandably been made to find a method of reducing the bandwidth of the transmitter. An early proposal was to transmit only one of the sidebands. Without taking other special measures,

however, this method is not practicable. To make this clear, we shall first consider what happens when one of the sidebands is omitted. This will make it easier to understand the methods that can in fact be used.

In the following we assume throughout that the transmitted signal can be received by a conventional receiver, in which the demodulator responds to the instantaneous amplitude of the RF signal. This implies that the receiver is also capable — without conversion — of handling the normal amplitude-modulated signal with two sidebands. The new form of modulation is then *compatible* with normal amplitude modulation, and if necessary can gradually be introduced for broadcasting transmitters now in existence or yet to be built.

In *fig. 1* the first term on the right-hand side of

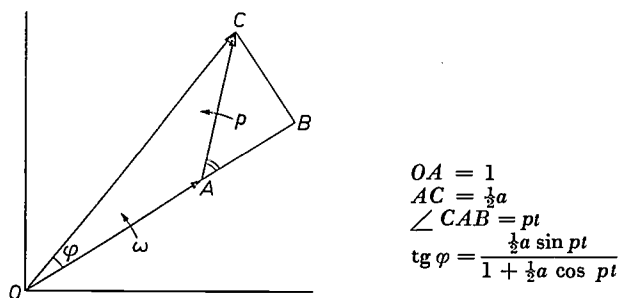


Fig. 1. Vector diagram of an amplitude-modulated RF signal with only one side component (sideband). The carrier is represented by the vector OA , rotating with angular velocity ω . With respect to OA the side component AC has the relative angular velocity p , the latter being the modulation frequency. The sum OC of both vectors represents the RF signal. This shows an amplitude modulation which is not purely sinusoidal, and also phase modulation.

(1a), i.e. the constant *carrier*, $\cos \omega t$, is represented in the conventional way by a vector OA rotating at an angular velocity ω . The second term is taken as the single sideband to be transmitted, and this is represented by the vector AC , which, with respect to OA , has the relative angular velocity p . The instantaneous value of the amplitude of the RF signal is then equal to the length of the vector OC .

*) Philips Research Laboratories, Eindhoven.

The relation

$$(OC)^2 = (OB)^2 + (BC)^2 = \left(1 + \frac{a}{2} \cos pt\right)^2 + \left(\frac{a}{2} \sin pt\right)^2,$$

reduces, after elementary mathematical treatment, to:

$$OC = \sqrt{1 + \frac{a^2}{4} + a \cos pt} \dots (2)$$

Using the binomial theorem, a square root form of this kind can be expanded to form the series:

$$\sqrt{1 + x} = 1 + \frac{x}{2} - \frac{x^2}{8} + \frac{x^3}{16} - \frac{5x^4}{128} + \dots$$

Applying this to expression (2), and taking only the first terms that interest us, we find after some manipulation:

$$OC = 1 + \frac{a^2}{16} + \frac{a}{2} \left(1 - \frac{a^2}{32}\right) \cos pt - \frac{a^2}{16} \cos 2pt + \frac{a^3}{64} \cos 3pt \dots (3)$$

We can see from this that by simply omitting one sideband the amplitude waveform, or "envelope", of the radio-frequency signal also contains higher harmonics of the desired audio frequency. After demodulation, the audio signal will therefore show harmonic distortion, particularly in the case of deep modulation. We may therefore conclude that the single-sideband method, as remarked, is not practicable without corrective measures.

From fig. 1 we can also read a second effect which occurs when only one sideband is transmitted. The vector *OC*, which corresponds to the total RF signal, then no longer rotates at a constant angular velocity ω , but periodically lags and leads with respect to *OA*, with an angle φ given by:

$$\tan \varphi = \frac{\frac{1}{2}a \sin pt}{1 + \frac{1}{2}a \cos pt} \dots (4)$$

In other words, the single-sideband signal shows *phase modulation*. In itself this is not serious, because a normal amplitude or envelope detector does not respond to phase modulation. We shall see presently that the signals that can suitably be used for single-sideband modulation also show phase modulation.

If it were possible to arrange the single-sideband modulation without giving rise to the above-mentioned distortion due to higher harmonics in the envelope of the RF signal, two advantages would be obtained. One of them, the reduction of the transmitter bandwidth, has already been mentioned.

With the constantly increasing demand for transmitters in the frequency bands available for broadcast purposes, single-sideband modulation would make it possible to use more transmitters or to reduce the interference between them.

A second advantage of a narrower frequency channel is that it reduces the noise and similar interference received. In general the interference energy received is proportional to the bandwidth of the receiver. The general introduction of single-sideband modulation could thus lead to an improvement of the signal-to-noise ratio by a factor of 2. Given the same radiant power, the transmitter could therefore cover a larger area.

We shall now consider three methods by which the distortion can be reduced in the uncorrected single-sideband signal given by expressions (2) and (3). The third method to be discussed, that of the "squaring" of this signal, will receive special attention. This method was devised and developed in Philips Research Laboratories in Eindhoven ¹⁾.

Use of negative feedback

An obvious method of reducing the distortion in the envelope of the SSB (single-sideband) signal is represented schematically in fig. 2. It is analogous

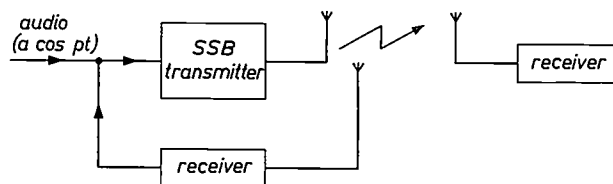


Fig. 2. Application of the negative feedback principle to single-sideband modulation. The amplitude modulation of the transmitted RF signal, not initially free from distortion, is added, after detection, in opposite phase to the modulating audio signal.

with the method of reducing distortion by means of *negative feedback* in low-frequency systems.

The audio signal is supplied to a transmitter with normal amplitude modulation, where one of the sidebands is removed by a filter. The signal which this transmitter sends out therefore shows the envelope distortion discussed above. This distorted signal is received and detected at the same location, and the audio signal thus obtained is then added in opposite phase to the original modulating signal. The result is reduced distortion in the transmitted RF signal.

We shall not discuss this method here in detail, but comment briefly on the result. Without going

¹⁾ Th. J. van Kessel, F. L. H. M. Stumpers and J. M. A. Uyen, A method for obtaining compatible single-sideband modulation, E.B.U. Review, Part A, no. 71, 12-19, 1962.

into mathematics, it can be seen that the signal sent out will extend further into the frequency spectrum on the side of the side-band transmitted. Evidently, in order to remove the second harmonic in the detected signal, the RF signal must contain a compensating side component with the frequency $\omega + 2p$, etc. The result is a broadening of the transmitted frequency spectrum on one side, which partly cancels the bandwidth limitation aimed at. It will be shown in the following, however, that this need not in practice be such a serious drawback. The main disadvantage of this method is much rather a technical problem, for it is in fact impossible to apply sufficient negative feedback. Just as with other systems employing negative feedback, phase shifts — due in particular here to the SSB filter — very soon give rise to instability. The system then goes into self-oscillation ("motor-boating"). For technical application, then, some other procedure has to be found.

Combination of phase and amplitude modulation

We have seen that the removal of a sideband causes phase modulation in the RF signal. Kahn ²⁾ has described a method of obtaining compatible single-sideband modulation which turns this phase modulation to good use. Since the envelope must not ultimately be distorted, the RF signal sent out will in principle be of the form:

$$v(t) = (1 + a \cos pt) \cos [\omega t + \Omega(pt)]. \quad \dots (5)$$

The question here is what condition the phase modulation $\Omega(pt)$ must satisfy in order for the signal to be a single sideband one. In eq. (5) ω again denotes the carrier frequency, and $a \cos pt$ is again the audio signal.

Calculations show that the required $\Omega(pt)$ can be fairly well approximated by starting from the "normal" phase modulation (4) and then increasing the phase deviation by a factor of 1.4. This is done by first multiplying the frequency by 7 and then dividing the resultant frequency by 5. Such transformations of a carrier-wave frequency, in which the modulating frequency does not change, are standard practice in radio engineering.

A block diagram of Kahn's system is given in fig. 3. A carrier with a frequency having $\frac{5}{7}$ of the desired value is modulated in amplitude with the audio signal, after which a sideband is suppressed. A limiter cuts off the amplitude modulation from the SSB signal thus obtained, leaving a carrier which is modulated purely in phase. Next, this carrier is multiplied in frequency by the factor $\frac{7}{5}$ in the man-

ner described, after which it is modulated in amplitude again with the audio signal. The signal produced in this way is a very reasonable approximation to the ideal SSB signal with an undistorted envelope. Further particulars of this system, which is already used by some broadcasting stations in the United States, will be found in the article mentioned below ²⁾.

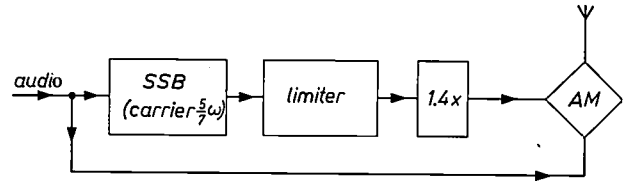


Fig. 3. Schematic diagram of a single-sideband transmitter combining phase and amplitude modulation. The amplitude modulation is removed from the original SSB signal by a limiter. The phase modulation is then increased by a factor 1.4, after which the RF signal is again modulated in amplitude.

Squaring method

At the beginning of this article we recalled that a normal amplitude-modulated signal consists of three equidistant components: the carrier in the centre, and on either side a component having a frequency difference equal to the modulating audio frequency p . The sum of these components is an amplitude-modulated radio-frequency signal without envelope distortion.

The method we shall now discuss for obtaining an SSB signal with an undistorted envelope is based on the remarkable fact that three equally spaced components can be arranged in such a way that one of the *outer* components acts as the carrier wave.

To make the new procedure clear we shall first deal separately with the conditions in which an RF signal with three components of frequencies ω , $\omega + p$ and $\omega + 2p$ has an undistorted envelope with the modulation frequency p .

In general we may write:

$$v(t) = A \cos \omega t + B \cos(\omega + p)t + C \cos(\omega + 2p)t, \quad \dots (6)$$

and we choose A , B and C so that the envelope of this signal has the form:

$$m(t) = P + Q \cos pt. \quad \dots (7)$$

If we analyse this problem, we find that the desired result can be achieved in two ways, given respectively by:

$$B = P, A = C = Q/2 \quad \dots (8)$$

and

$$B = Q, 4AC = B^2, A + C = P. \quad \dots (9)$$

The first case, given by (8) can be recognized as a normal amplitude-modulated signal with two side-

²⁾ L. R. Kahn, Compatible single sideband, Proc. Inst. Radio Engrs. 49, 1503-1527, 1961.

bands, the B component in (6) functioning as the carrier. This case, then, offers nothing new.

The second case given by (9) does, however, present an interesting new possibility. As Q denotes the depth of modulation, and because $B=Q$, we can regard the B component as a sideband. Since A and C are symmetrical in (9), we can now take one of these components as the carrier. The other then becomes a correctiveside component, at the frequency distance $2p$, which together with the B component yields an undistorted envelope. It is this possibility that underlies the third method, or squaring method, to be discussed below.

The fact that the signal postulated by (6) and (7) in fact leads to the possibilities given by (8) and (9) can be understood as follows. If, using the basic method represented in fig. 1, we calculate the square of the envelope of the signal defined by (6), we find:

$$[m(t)]^2 = (A - C)^2 + B^2 + 2B(A + C) \cos pt + 4 AC \cos^2 pt.$$

In view of (7), this must correspond to:

$$[m(t)]^2 = P^2 + 2PQ \cos pt + Q^2 \cos^2 pt.$$

We may therefore conclude:

$$\left. \begin{aligned} (A - C)^2 + B^2 &= P^2, \\ B(A + C) &= PQ, \\ 4AC &= Q^2, \end{aligned} \right\} \dots \dots (7a)$$

We may consider this as three equations containing the two unknown quantities P and Q . If they are to have a solution, then the three equations must be interdependent. It is clear that this interdependence, which provides us with a relation between A , B and C , is given by: $P^2Q^2 = (PQ)^2$. We may therefore write:

$$[B(A + C)]^2 = 4AC [(A - C)^2 + B^2].$$

This yields:

$$B^2(A - C)^2 = 4AC(A - C)^2.$$

From this it follows that $A = C$, or $B^2 = 4AC$. Together with the three equations of (7a) this gives us precisely the cases (8) and (9).

The addition of a corrective side component at twice the frequency distance from the carrier has, in principle at least, the disadvantage of cancelling the bandwidth limiting aimed at. There is one circumstance, however, which in fact removes this drawback. From eq. (3) it can be seen that the distortion of the uncorrected SSB signal is serious only when the modulation is very deep. Experience has shown that, in the transmission of music or speech, very deep modulation occurs only at low audio frequencies, lower for example than 1000 to 2000 c/s. It is therefore sufficient to add a corrective side component pertaining to these frequencies, and this remains within the frequency spectrum also transmitted with uncorrected single-sideband modulation. (Similar considerations apply to the other

methods mentioned for obtaining "compatible" single-sideband modulation.)

An advantage of the method using the corrective side component is the ease with which the required signal can be obtained. To illustrate this, taking a simple case, we write in (6): $A = 1$ and $B = 2b$. In conjunction with eq. (9) this gives: $C = b^2$, $P = 1 + b^2$ and $Q = 2b$. The required RF signal then has the form:

$$v(t) = \cos \omega t + 2b \cos(\omega + p)t + b^2 \cos(\omega + 2p)t. \dots (6a)$$

This signal is obtained by starting from a normal SSB signal with $\omega/2$ as carrier frequency, and given by:

$$v(t) = \cos \frac{\omega}{2} t + b \cos\left(\frac{\omega}{2} + p\right) t. \dots (10)$$

By *squaring* this signal and then selecting the RF component in the proximity of the frequency ω , we find the required signal (6a). The squaring process is effected by passing the signal (10) through an amplifier stage which has a non-linear, preferably square-law characteristic and which is followed by a network tuned to the frequency ω . This is a standard procedure in radio engineering.

This "squaring" method would indeed be a very simple solution for compatible single-sideband modulation — henceforth called CSSB — if it were not for the fact that modulation with two or more audio frequencies gives rise to intermodulation distortion in the envelope ¹⁾.

Let the signal before squaring have the form:

$$v_1(t) = \cos \frac{\omega}{2} t + b_1 \cos\left(\frac{\omega}{2} + p_1\right) t + b_2 \cos\left(\frac{\omega}{2} + p_2\right) t. \dots (11)$$

After squaring we then find as the envelope:

$$m_2(t) = 1 + b_1^2 + b_2^2 + 2b_1 \cos p_1 t + 2b_2 \cos p_2 t + 2b_1 b_2 \cos (p_2 - p_1) t. (12)$$

To make the squaring method really practicable for CSSB it is necessary to suppress the last term in (12), which we call the product or intermodulation term. We shall now examine the method by which this is done.

Eliminating the intermodulation from the amplitude of the squared signal

The interfering intermodulation is removed from the envelope of the squared signal by removing the amplitude modulation of the signal in an amplitude limiter and remodulating the remainder with the undistorted audio signal. We shall presently see how

this is done by considering a block diagram of the circuit. First, however, some fundamental points will be dealt with.

The operations referred to do not change the phase modulation of the RF signal, but they do change the spectral composition. Obviously, the spectral composition after squaring only fits the envelope given by eq. (12), i.e. the envelope with the intermodulation term. The disappearance of the intermodulation term is due to the addition of two new side components at the frequency distance $p_2 - p_1$ on either side of the carrier. This is represented in fig. 4b, and fig. 4a gives the uncorrected spectral composition appertaining to eq. (12). (The new side components together produce an amplitude modulation which exactly cancels out the intermodulation term.)

The removal of the intermodulation thus has the effect of broadening the radiated frequency spectrum on the side where the sideband is suppressed (not transmitted). This broadening is not, however, of the difference frequencies of the low-frequency tones p_2 and p_1 , both of which are already fairly low. For, as we have seen, it is only in their case that modulation depths occur that might lead to serious distortion.

We are now sufficiently advanced to be able to discuss the block diagram of a complete transmission system for CSSB, shown in fig. 5. On the left, the audio-frequency speech or music signal is conducted to an SSB modulator, which is also supplied with the carrier wave having the frequency $\omega/2$. The circuit of this modulator is designed so that it only delivers the sideband occurring in eq. (10). Before squaring takes place it is therefore necessary to add a carrier. This is done in the block marked “expander” with a plus sign. The purpose of the block marked “expander” will be touched upon presently.

The squaring and amplitude-limiting operations are carried out in the next two stages in the block diagram. At the output of the limiter stage, then, a signal modulated purely in phase is presented to the transmitter, where the signal is remodulated with the undistorted audio signal. The method by which this audio signal is obtained calls for some further explanation.

The simplest procedure would be to modulate the

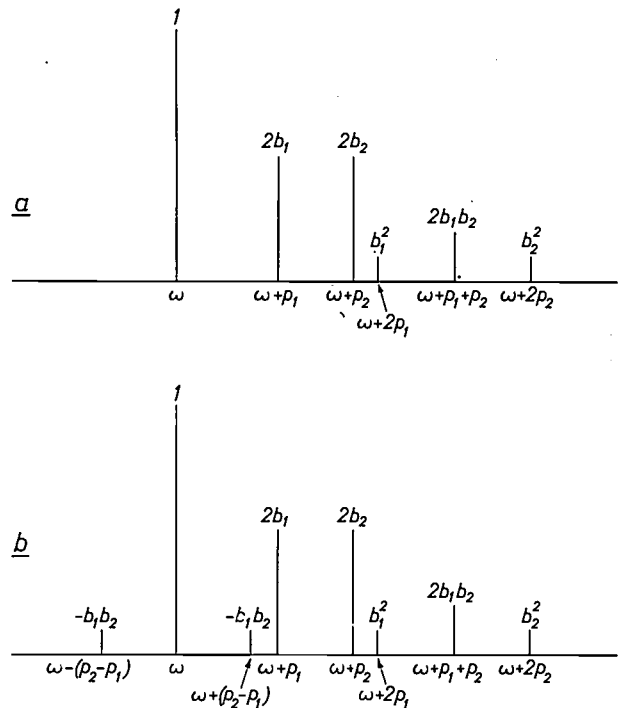


Fig. 4. a). Frequency spectrum of an SSB signal, modulated by two audio frequencies p_1 and p_2 , and obtained by the squaring method. The spectrum contains an intermodulation component $\omega + p_1 + p_2$, which coincides with the difference tone $p_2 - p_1$ occurring in the signal envelope given by eq. (12). This envelope, then, does not contain the sum frequency $p_2 + p_1$. b). When the interfering intermodulation term has been removed from the amplitude modulation by a limiter and remodulation, the frequency spectrum is seen to be somewhat wider. The two components not yet found in (a) thus cancel out the interfering difference frequency in the envelope.

transmitter with the original audio signal used in the SSB modulator. This is ruled out, however, because of the phase shift which the SSB filter in this modulator produced in the audio frequency. The original audio signal therefore no longer “matches” the SSB signal. For this reason the remodulation must be done with an audio signal which is derived from the SSB signal.

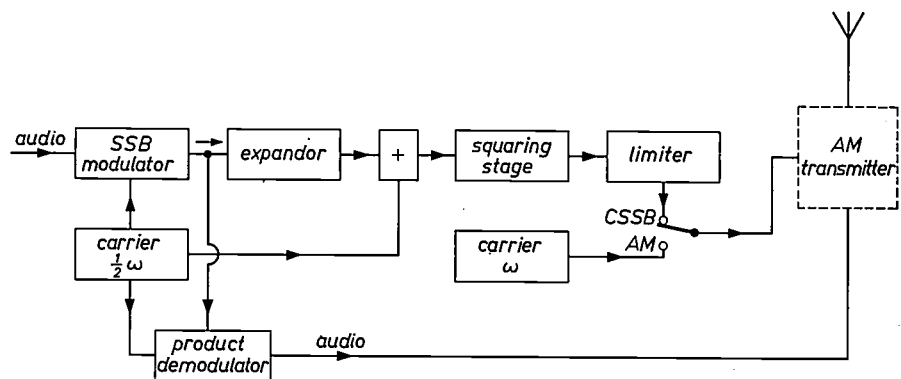


Fig. 5. Complete block diagram of a transmitter for “compatible” single-sideband modulation by the squaring method developed at Philips. The frequency of the primary SSB signal is doubled in this process. The non-linear distortion of the modulation depth in the squaring stage is removed by the preceding “expander”. The AM transmitter is supplied with a signal modulated only in phase, which is then remodulated in amplitude. This ensures that the ultimate amplitude modulation is free from distortion.

In the block marked "product demodulator" in fig. 5 the SSB signal, i.e. the sideband of the signal given by eq. (10), is mixed with the carrier having the frequency $\omega/2$. The result of this operation is a signal with audio frequency p , and it is this that is finally used for the amplitude modulation of the transmitter.

Introduction of a non-linear element

We now have to consider the network referred to in fig. 5 as "expandor". Its function is to compensate for a change which squaring causes in the depth of modulation.

We have already seen that the signal given by (6) or (6a) has the modulation depth Q/P given by (7). In view of the relations in (9) it follows that the modulation depth of the signal (6a) is:

$$\frac{Q}{P} = \frac{2b}{1 + b^2} \dots \dots \dots (13)$$

Since the modulation depth is b before squaring, we see that this operation almost doubles the modulation depth for small values of b . For large values of b this is no longer the case. Generally speaking, eq. (13) gives a non-linear relation between the modulation depth before and after squaring.

The audio signal used for modulating the transmitter is derived from the RF signal before squaring. In general, then, this audio signal is proportional to b , and therefore does not exactly fit the required modulation depth given by (13).

This drawback can be partly overcome if we approximate (13) as a function of b by a linear relation in which the modulation depth is somewhat smaller than $2b$. This method, which has previously been dealt with in detail ¹⁾, will not be discussed here. A better method is to remove the non-linearity. This is done in the block diagram shown in fig. 5 by amplifying the transmitted sideband non-linearly before squaring. In the "expandor" the large amplitudes of the SSB signal are therefore given more amplification than the low ones. In conjunction with the non-linear function (13) this then produces a modulation depth which is proportional to that of the original audio signal.

Of course, the audio signal could be subjected to non-linear attenuation or compression before being used for remodulation. The "compressor" would then have to follow behind the product demodulator. The construction of such a non-linear audio amplifier is, in view of the need to minimize distortion, more difficult than one for a radio-frequency signal.

The limiter in fig. 5, the function of which is to suppress the amplitude modulation of the SSB

signal, generally works well only up to modulation depths of about 95%, as the instantaneous value of the amplitude should not be too small. The signal delivered by the squaring stage should not therefore be modulated up to 100% in amplitude. In the AM transmitter it is of course possible to remodulate to 100%, and this is basically the procedure adopted. As the fully modulated signal no longer completely matches the phase modulation present, it will show some slight change in spectral composition, but the consequent distortion upon reception is very low compared with the distortion already present as a rule in ordinary receivers. We shall return to the latter point presently.

To complete the description of the transmitting system shown in fig. 5, a further interesting feature should be noted. Since the AM transmitter can be 100% modulated with a non-distorted audio signal, this transmitter can easily be switched over to normal amplitude modulation. To do so it is only necessary to replace the phase-modulated RF signal from the limiter by an unmodulated carrier with the frequency ω . This is indicated in the figure by the switch with two positions: CSSB and AM. On the transmitter side too, then, the method described is completely compatible with the method of amplitude modulation hitherto employed:

Fig. 6 shows a switching unit containing all the elements of fig. 5, except the normal AM transmitter. The relatively small dimensions are sufficient indication that experiments with, or the introduction of this system of CSSB need present no technical problems.

Tests on the squaring system

In cooperation with engineers of the Netherlands G.P.O., tests have been carried out on a 10 kW medium-wave transmitter, operating with signals from a CSSB modulator in accordance with the method described. The results showed that the linear, non-linear and intermodulation distortion did not differ significantly from the corresponding distortion in normal amplitude modulation of the same transmitter.

At modulation depths of 50%, 80% and 90%, sideband suppression was better than 40 dB, 35 dB and 30 dB respectively. From this it can be concluded that the aerial signal fully complies with the requirements which CSSB may be expected to meet.

With a view to the possible introduction of CSSB modulation, it is especially important to have some idea of the reception results in a standard AM receiver. A survey of these results is presented below.

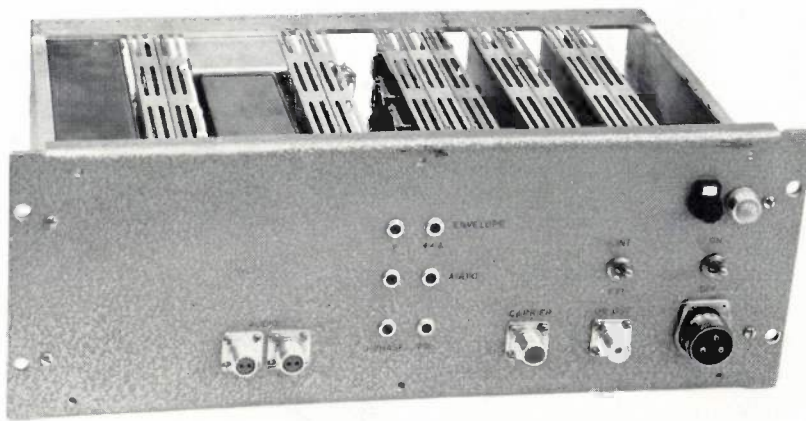


Fig. 6. Example of a switching unit containing all elements required for adapting a standard AM transmitter to CSSB based on the squaring method. Together with this transmitter the unit shown corresponds to the block diagram in fig. 5. The relatively small dimensions make it technically a simple matter to experiment with, or introduce, this system of C.S.S.B.

The quality is governed primarily by the band-pass characteristic of the IF filters in the receiver. These should be lined up so as to avoid any disturbance of the ratio between the three components of the CSSB signal. Since, as explained, the correctivesideband is of interest only at relatively low audio frequencies, this requirement is generally satisfied.

For a conventional AM receiver, fig. 7 gives a plot of the linear and non-linear distortion as a function of the audio frequency p , both for AM and CSSB, at 50% modulation depth. As the new modulation method makes it possible, because of the smaller bandwidth, to obtain better reproduction of the high audio frequencies by slight detuning, test results for CSSB are also given with the receiver detuned 1 kc/s and 2 kc/s. The result, as can be seen from the figure, is less linear distortion without any troublesome increase in non-linear distortion.

The curves for the second harmonic, $2p$, which may be taken as representative of the non-linear distortion, indicate that at audio frequencies above about 1000 c/s the non-linear distortion is greater with CSSB than with AM. At this point we repeat that a modulation depth of 50% seldom occurs at these frequencies. The increase of distortion can easily be explained by the attenuation which the corrective side component suffers in the IF filter. When the receiver is detuned, the ratio between the components of the detected signal changes. This too gives rise to increased non-linear distortion at the higher audio-frequencies.

Above about 3000 c/s, however, it can be seen that the non-linear distortion decreases again. This is bound up with the fact that at these frequencies the

main side component also suffers attenuation. From eq. (6a) it can be deduced that the corrective side component should then decrease quadratically in order to produce again an undistorted RF signal. This more or less quadratic attenuation occurs in the IF filter.

The energy distribution of speech or music in the audio frequency spectrum is such that tones above 2 kc/s seldom account for more than 15% of the total modulation. This means that, as far as these tones are concerned, the correc-

tive component is in fact unimportant, and the uncorrected SSB signal is already sufficiently free from distortion. For this reason, detuning of the receiver is quite permissible with CSSB, and in practice it results in a noticeably better reproduction of the

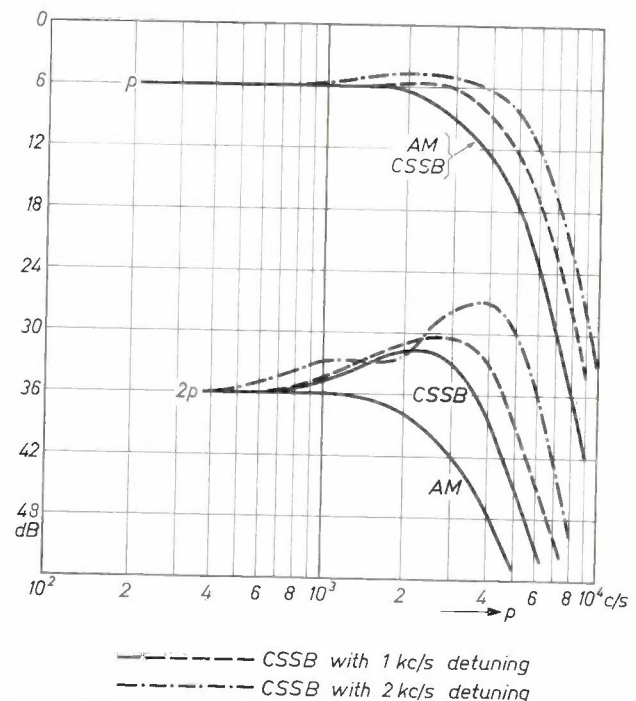


Fig. 7. Frequency response characteristic and non-linear distortion in normal AM and CSSB reception with a conventional AM receiver at 50% modulation depth. The strength of the second harmonic ($2p$) may be considered representative of the non-linear distortion. By detuning the receiver 1 to 2 kc/s for CSSB reception, the reproduction of the high audio frequencies is improved without appreciably increasing the non-linear distortion. When interpreting the curves it should be remembered that, with speech and music, a modulation depth of 50% hardly ever occurs at frequencies above 1 kc/s. At smaller depths of modulation the distortion decreases quadratically.

high tones without any significant increase of non-linear distortion. This improvement of reception quality, together with the other advantages mentioned in the foregoing, is a particularly strong argument in favour of the gradual introduction of CSSB.

Interference between transmitters

Apart from the reception quality when a conventional type of receiver is used, an important factor in the judgement of CSSB is the interference between transmitters. To determine this interference, tests have been carried out on the lines illustrated in *fig. 8*.

A standard programme, consisting of filtered noise having an energy distribution corresponding to that of music, is transmitted via the first transmitter in conjunction with a receiver tuned to it. Connected to the output of the receiver is a psophometer, which measures the strength of the programme. (A psophometer is a voltmeter preceded by a filter which simulates the sensitivity of the human ear).

Next, the programme is switched over to an interfering transmitter, which is likewise connected to the input of the receiver. When a certain difference exists between the carrier frequencies of the two transmitters, the output of the interfering transmitter is adjusted until the psophometer gives the same reading again.

The results were plotted to produce the contours shown in *fig. 9*, which represent the relative strength (interference ratio) of the transmitters as a function of the frequency difference. If the meter is adjusted in this test not to the same but to a smaller deflection for the interfering transmitter, the contours can be moved correspondingly upwards. The tests related to three different situations:

- 1) Both transmitters with normal amplitude modulation (solid curve).
- 2) Both transmitters with CSSB modulation and the sideband on the same side of the carrier (dashed curve).

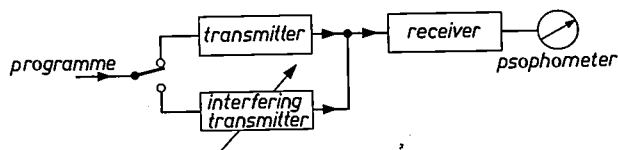


Fig. 8. Test arrangement for determining the interference between two transmitters, both for normal AM and for CSSB. The transmitter under test and the interfering transmitter are modulated in turn with a standard programme. The relative strength (interference ratio) of the transmitters is measured when the interfering transmitter is heard just as strongly as the other. A filter in the psophometer simulates for this purpose the sensitivity characteristic of the human ear.

- 3) Both transmitters with CSSB modulation and the sideband at different sides of the carrier (dot-dash curve).

Whether, in the event of CSSB being introduced, case (2) or perhaps even case (3) will be encountered depends upon the arrangements agreed upon, and cannot yet be predicted. Both cases therefore had to be studied in these tests. When CSSB was applied, the receiver was detuned 2 kc/s, since this may be considered as the normal mode of operation.

The form of the curves can best be explained by distinguishing three separate regions of frequency difference between the transmitters.

- a) If the frequency difference is so slight that the interference tone of the carrier waves falls in the

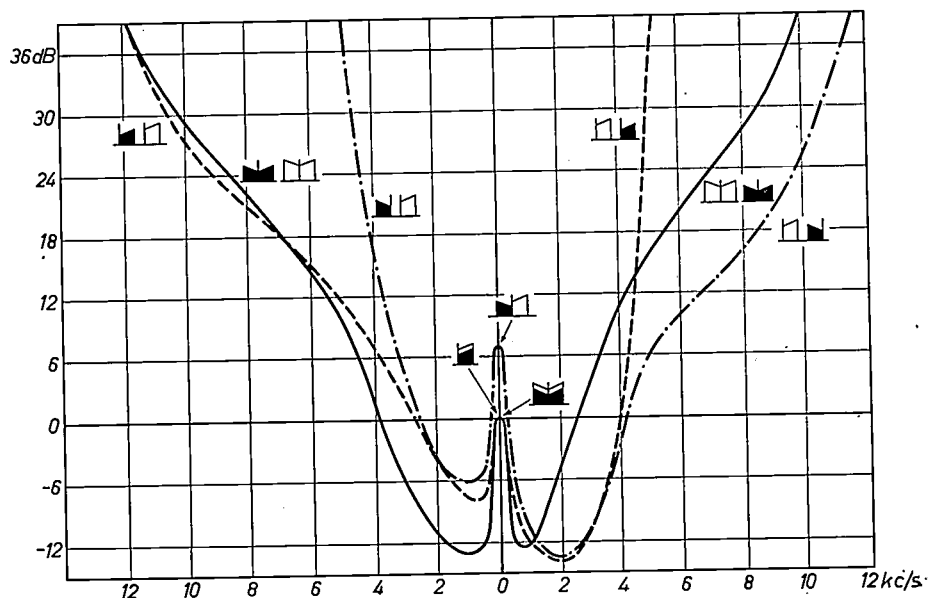


Fig. 9. Results of measurements with the set-up shown in *fig. 8*. The relative strength (interference ratio) of the interfering and the transmitter under test, for reception at equal strength, is plotted as a function of the difference in the carrier frequencies between two transmitters both with AM or both with CSSB. In the latter case, two further situations are distinguished: the transmitted sidebands are on the same side or on different sides of the carrier. The sidebands are represented by the black and white symbols (the white ones representing the transmitter under test, the black ones the interfering transmitter). In CSSB reception (sideband on the right) the receiver is detuned 2 kc/s on the right to improve the reproduction of the high audio frequencies (see *fig. 7*). This accounts for the asymmetry in the relevant contours. As compared with AM the interference with CSSB is substantially lower if the sideband transmitted by the interfering station is on the opposite side from that transmitted by the desired station.

region of low aural sensitivity, i.e. below about 100 c/s, the interference is largely caused by the modulation of the interfering transmitter. In the case of AM (case 1) both transmitters are as if they were interchangeable under these conditions, and the interfering transmitter will have to be just as powerful as that under test if the interference is to produce the same deflection on the meter as the standard programme. In case (2), i.e. CSSB with the sideband of both transmitters on the same side, the situation is still roughly the same. The situation is different in case (3), i.e. CSSB with the sideband of the transmitter under test on a different side from that of the interfering transmitter: owing to the detuning of the receiver, the interfering sideband is then amplified less than the other. As can be seen in the figure, one thus gains 7 dB.

- b) Where the frequency difference is greater, falling in the region of maximum aural sensitivity, i.e. between about 100 c/s and 4000 c/s, the interference tone of the carriers is the most troublesome effect. Since this does not depend on the method of modulation, the CSSB system will not — on the average — offer any further gain.

The difference tone decreases in strength when the interfering carrier, with increasing frequency difference, is attenuated in the IF filter in the receiver. In this region, then, the contours give a picture of the filter characteristic with that of the psophometer added to it.

- c. At frequency differences above 6 kc/s the interference is mainly due to one of the sidebands of the interfering signal penetrating into the spectrum of the desired signal. It is clear that on average CSSB now offers an improvement, due to the absence of a sideband. In evaluating the advantage gained, one should take into account that the remaining sideband is 6 dB stronger than with AM.

Concluding, it may be said that a change-over from AM to CSSB can considerably reduce interference between stations. Moreover, detuning the receivers from the carrier position can lead to an improvement of reproduction quality.

Summary. The ever-increasing power and number of broadcasting transmitters makes it desirable to reduce their bandwidth in the frequency channels allocated to them. Single-sideband modulation is one means to this end. If signals modulated in this way can be received by sets currently in use, the single-sideband modulation is said to be "compatible" with the conventional double-sideband system, and can be introduced gradually. The article deals in particular with the "squaring method" developed by Philips for obtaining the SSB signal required for this purpose. The underlying idea is that amplitude modulation sufficiently free from distortion can be achieved by adding a corrective side component, lying within the transmitted sideband, to a non-corrected SSB signal. The circuitry needed to adapt a standard AM transmitter for SSB modulation by this method can be accommodated in a simple switching unit.

Tests show that compatible SSB modulation offers better reproduction of the high audio frequencies without any troublesome increase in non-linear distortion. Greater freedom from interference is also possible, enabling the transmitter to cover a wider area.

A 5000 : 1 SCALE MODEL OF THE MAGNETIC RECORDING PROCESS

by D. L. A. TJADEN *) and J. LEYTEN *).

621.318.24.087

Although magnetic recording is widely used for all kinds of purposes, little is yet known about the actual process by which signals are recorded in the thin magnetic coating of the tape. Attempts are being made to gain a better understanding of this process with the aid of a model of the tape and recording head scaled up 5000 : 1 and in which the distribution of the magnetization over the thickness of the coating is measured.

In the past 15 to 20 years magnetic recording has developed into an indispensable tool, both for recording sound and video signals and for the registration of machine data (measuring, regulating, control and computer signals). This development was based on the improvements in the properties of the

magnetic tape and in those of the recording and playback heads. If one asks, however, to what these improvements are due, one has to admit, rather disappointedly perhaps, that they were obtained for the most part by trial and error. In our opinion the reason for this is that fundamental understanding of the factors that govern the recording process is still imperfect. This applies particularly to the

*) Philips Research Laboratories, Eindhoven.

region of low aural sensitivity, i.e. below about 100 c/s, the interference is largely caused by the modulation of the interfering transmitter. In the case of AM (case 1) both transmitters are as if they were interchangeable under these conditions, and the interfering transmitter will have to be just as powerful as that under test if the interference is to produce the same deflection on the meter as the standard programme. In case (2), i.e. CSSB with the sideband of both transmitters on the same side, the situation is still roughly the same. The situation is different in case (3), i.e. CSSB with the sideband of the transmitter under test on a different side from that of the interfering transmitter: owing to the detuning of the receiver, the interfering sideband is then amplified less than the other. As can be seen in the figure, one thus gains 7 dB.

- b) Where the frequency difference is greater, falling in the region of maximum aural sensitivity, i.e. between about 100 c/s and 4000 c/s, the interference tone of the carriers is the most troublesome effect. Since this does not depend on the method of modulation, the CSSB system will not — on the average — offer any further gain.

The difference tone decreases in strength when the interfering carrier, with increasing frequency difference, is attenuated in the IF filter in the receiver. In this region, then, the contours give a picture of the filter characteristic with that of the psophometer added to it.

- c. At frequency differences above 6 kc/s the interference is mainly due to one of the sidebands of the interfering signal penetrating into the spectrum of the desired signal. It is clear that on average CSSB now offers an improvement, due to the absence of a sideband. In evaluating the advantage gained, one should take into account that the remaining sideband is 6 dB stronger than with AM.

Concluding, it may be said that a change-over from AM to CSSB can considerably reduce interference between stations. Moreover, detuning the receivers from the carrier position can lead to an improvement of reproduction quality.

Summary. The ever-increasing power and number of broadcasting transmitters makes it desirable to reduce their bandwidth in the frequency channels allocated to them. Single-sideband modulation is one means to this end. If signals modulated in this way can be received by sets currently in use, the single-sideband modulation is said to be "compatible" with the conventional double-sideband system, and can be introduced gradually. The article deals in particular with the "squaring method" developed by Philips for obtaining the SSB signal required for this purpose. The underlying idea is that amplitude modulation sufficiently free from distortion can be achieved by adding a corrective side component, lying within the transmitted sideband, to a non-corrected SSB signal. The circuitry needed to adapt a standard AM transmitter for SSB modulation by this method can be accommodated in a simple switching unit.

Tests show that compatible SSB modulation offers better reproduction of the high audio frequencies without any troublesome increase in non-linear distortion. Greater freedom from interference is also possible, enabling the transmitter to cover a wider area.

A 5000 : 1 SCALE MODEL OF THE MAGNETIC RECORDING PROCESS

by D. L. A. TJADEN *) and J. LEYTEN *).

621.318.24.087

Although magnetic recording is widely used for all kinds of purposes, little is yet known about the actual process by which signals are recorded in the thin magnetic coating of the tape. Attempts are being made to gain a better understanding of this process with the aid of a model of the tape and recording head scaled up 5000 : 1 and in which the distribution of the magnetization over the thickness of the coating is measured.

In the past 15 to 20 years magnetic recording has developed into an indispensable tool, both for recording sound and video signals and for the registration of machine data (measuring, regulating, control and computer signals). This development was based on the improvements in the properties of the

magnetic tape and in those of the recording and playback heads. If one asks, however, to what these improvements are due, one has to admit, rather disappointedly perhaps, that they were obtained for the most part by trial and error. In our opinion the reason for this is that fundamental understanding of the factors that govern the recording process is still imperfect. This applies particularly to the

*) Philips Research Laboratories, Eindhoven.

recording process at very short wavelengths, that is to say at high signal frequencies and/or low tape speeds. But even where the recording of longer wavelengths is concerned, it is difficult to predict exactly the behaviour of a tape from its magnetic properties.

How is it that the theory is so far behind the practice? It should be possible in principle to describe the recording process by passing a piece of tape over the recording head and ascertaining how the form of the magnetization curve of the tape material — at points at varying depths in the tape — varies. The situation is complicated, however, because as the tape passes the head the magnetizing field changes not only in strength but also in direction (turning through a total of 180° , see *fig. 1*), and also by the fact that the

the signal current applied to the recording head, a recorded wavelength is obtained which is in the same ratio to gap length and layer thickness as in the normal magnetic recording process. Theoretical considerations show that, given this condition, and provided the magnetizing field-strengths have the same magnitude, the spatial variation of the magnetization vector in the layer may be expected to be a fairly faithful copy of that in the normal process. In the large model this magnetization vector can be measured directly and accurately on samples removed from the layer after a recording.

It is reasonable to assume that the magnetization pattern is not essentially affected by the other dimensions in the recording process; this is fortu-

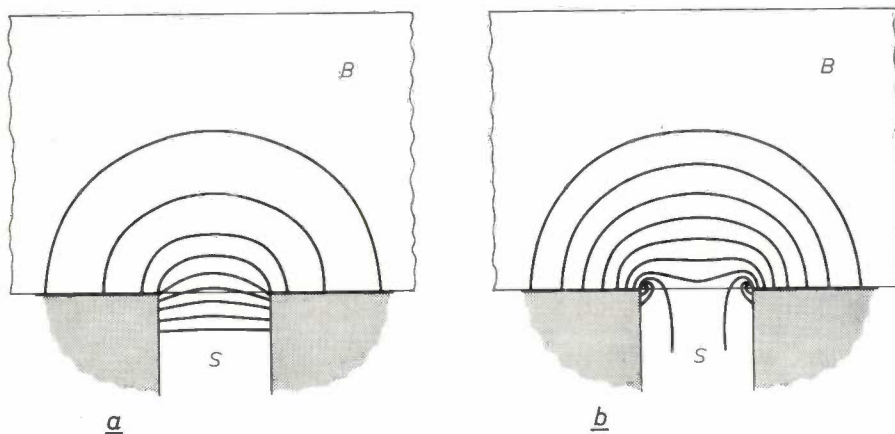


Fig. 1. Qualitative picture of the magnetic field near the gap *S* of a magnetic recording head. *B* is the coating of magnetic material on the tape.
a) Conventional pattern of lines of force.
b) Lines of equal field strength ($H = \text{constant}$).

magnetization at any given instant is determined to a considerable extent by demagnetizing fields. In view of these complications, we have in fact to rely on experimental data to improve our knowledge of the behaviour of a magnetic tape, especially data on the way in which the resultant magnetization vector changes in magnitude and direction over the thickness of the magnetic coating after the recording of a simple signal. Hitherto, such data have been almost completely lacking, and there is little hope of obtaining them from direct measurements on the 0.01 mm thick coatings of normal magnetic tapes.

To overcome this difficulty, a large-scale model of the magnetic recording process has been constructed at the Philips Research Laboratories, Eindhoven; the essential dimensions have been scaled up by a factor of 5000, the recording head being given a gap length of 2 cm and the magnetic coating of the "tape" a thickness of 5 cm. By appropriately choosing the speed at which the tape travels and the frequency of

date, for scaling up all dimensions by a factor of 5000 would have led to an impossible construction. *Fig. 2* shows the form of the recording head and tape as originally adopted. The tape is only 60 cm

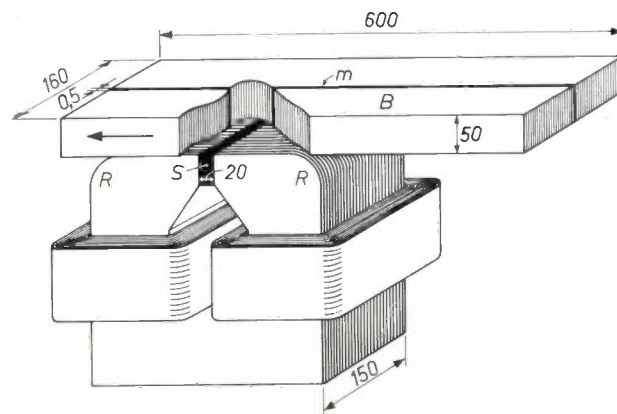


Fig. 2. Dimensional drawing of the large-scale model of recording head and tape. The tape *B* is composed of three longitudinal strips; the measurements are performed on samples taken from the middle strip *m*. Part of the tape is here cut away to disclose the gap *S* in the recording head. Dimensions in mm.

long and consists of a dispersion in a suitable material of grains of $\gamma\text{Fe}_2\text{O}_3$ — exactly the same grains as used on a normal magnetic tape. The dispersion is contained in a tray of non-ferromagnetic material and consists of three longitudinal strips. It is from the middle strip (*m* in fig. 2), which is only 0.5 mm thick, that the samples are removed for measurement, and this strip is therefore renewed for each experiment.

spread is real, that is to say it would also be ascertainable in the real tape if one were to consider an equivalently narrow strip, in practice it is averaged out by the enormous width of the track in relation to the individual grain.

Construction of the model

The complete experimental set-up in its original form is shown in fig. 3. On the table can be seen the large recording head, and above this a track with

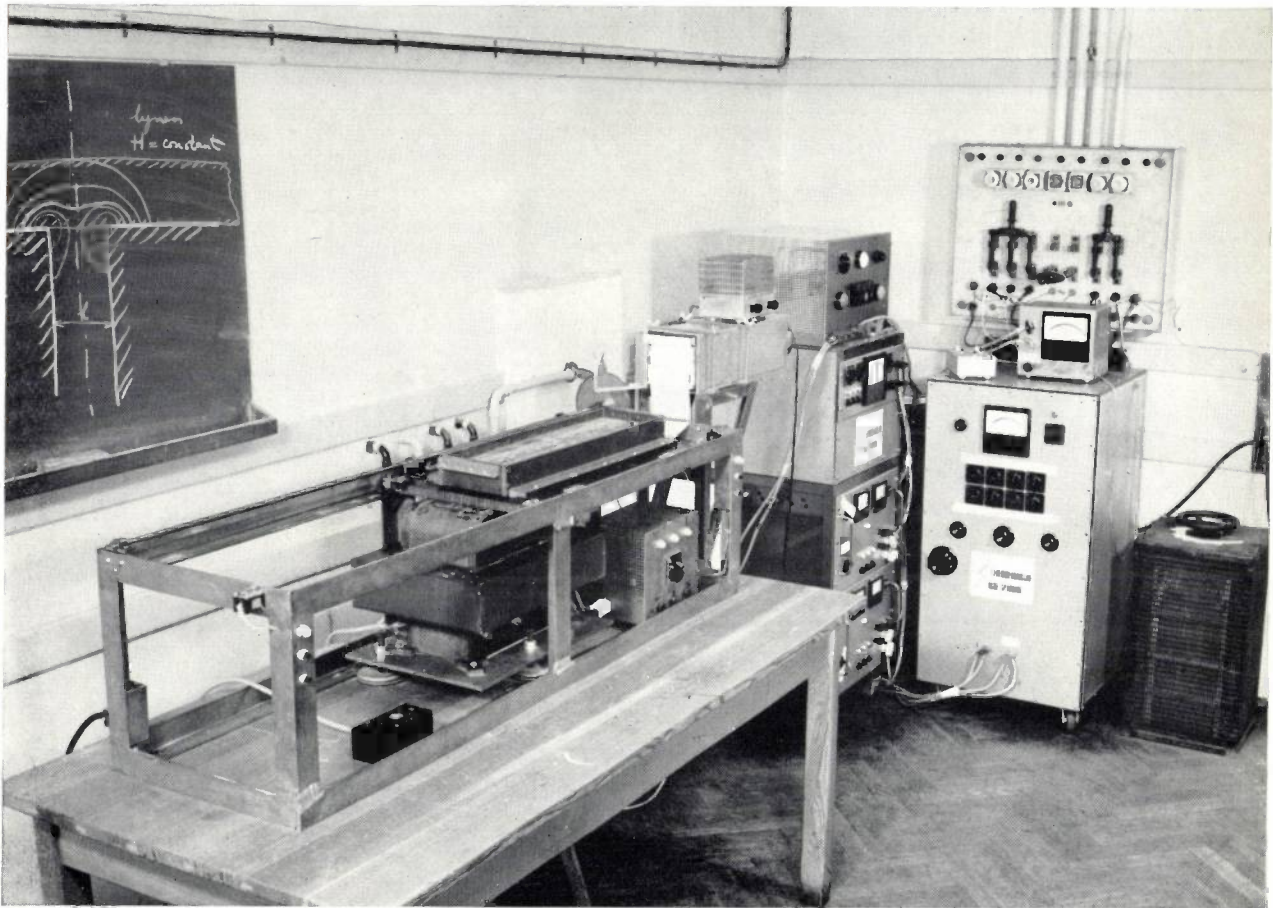


Fig. 3. Complete arrangement of the large-scale model of the magnetic recording process (first version). On the table can be seen the large recording head, and above this the tray with magnetic layer, carried on a roller track. In the background, from left to right: the generator for the signal current of 0.1 c/s (maximum 10 A), surmounted by a cabinet with relay switchgear; then the generator for the bias current of 50 c/s (maximum 60 A); and finally a rheostat for controlling a DC signal (maximum 70 A).

Although in our model the grains are a factor of 5000 too small in relation to the wavelength, this does not — provided we disregard the noise — cause any significant errors. In fact, if the grains were to be scaled up — supposing it were possible — fundamental difficulties would then really arise. In the first place a grain enlarged 5000 times would contain innumerable Weiss domains, whereas most of the real grains contain no more than one Weiss domain (i.e. no Bloch walls). The coercivity of the large grains would therefore be considerably less than that of the small ones. Secondly, the samples, which we want to be relatively small with a view to good spatial definition, would contain so few grains that the measurement results would inevitably show a very wide spread. Although this

rollers on which the tray containing the dispersion is moved over the head on a carriage. In this arrangement the carriage is moved by means of a screw shaft driven by an electric motor. The speed of travel can be varied slightly. The tape speed we normally use is 0.4 cm per second. In fig. 4 the head and the carriage (with the tray removed) are shown more clearly. It can also be seen that the carriage draws along behind it a strip of recording paper. On this strip is traced a record of the signal applied to the head.

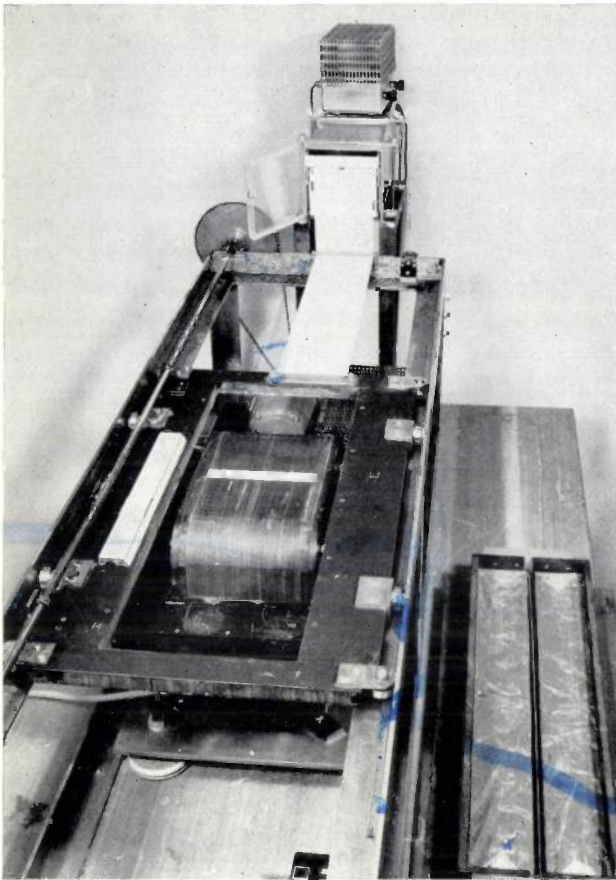


Fig. 4. Recording head and roller track with carriage. The tray containing the magnetic layer has been removed and placed on the table on the right. The recording-head gap, which, like conventional heads, is filled with a non-ferromagnetic material, has been painted white to make it show up. The carriage draws along behind it a paper strip on which a diagram of the signal current applied to the head is recorded.

The signal current has a fixed frequency of 0.1 c/s. The recorded wavelength is then 4 cm, which corresponds to a wavelength of $8 \mu\text{m}$ in normal recording. The latter wavelength is obtained, for example, at a signal frequency of 12 000 c/s and a tape speed of $9\frac{1}{2}$ cm/sec. For generating the signal current a somewhat unconventional generator is required, not because of the very low frequency (this is easily produced with an RC generator), but because of the very high current needed. In normal recording the largest magnetizing signal field-strengths ever required (approx. 10^4 A/m) can be generated at the greatest depth in the tape with about 0.3 ampere turns. In the model the distances from the material to be magnetized to the air gap of the recording head have been enlarged by a factor of 5000, which means

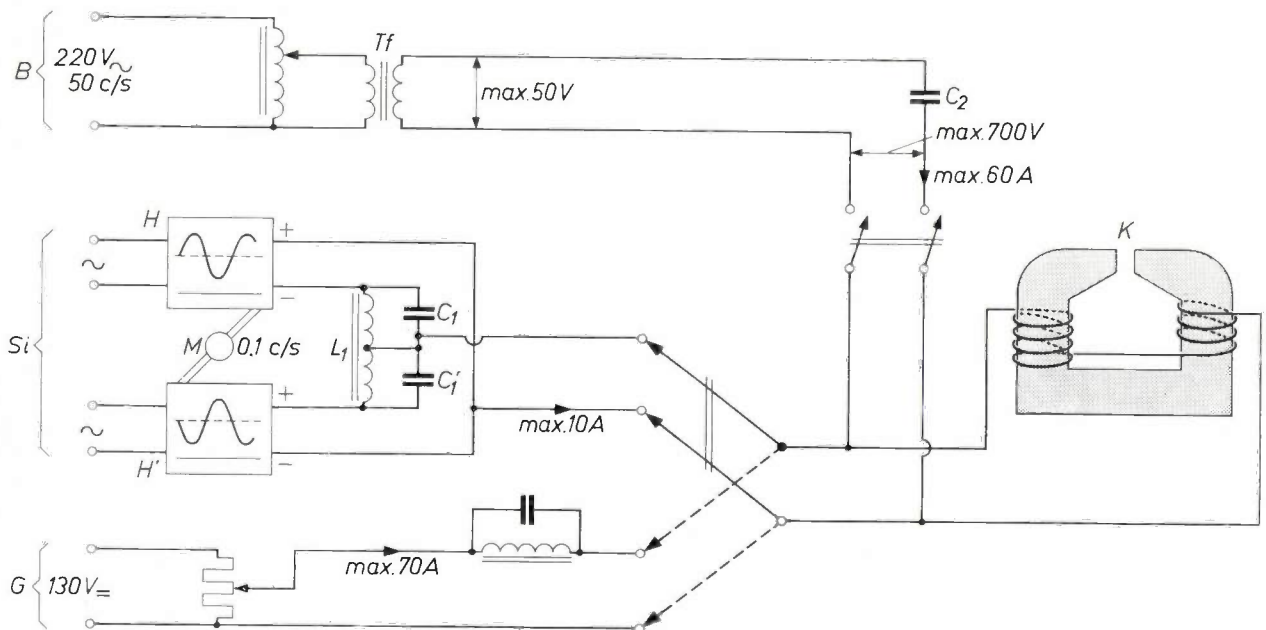


Fig. 5. Simplified diagram of the circuitry for supplying an AC signal (S_i), a DC signal (G) and a bias current (B). K recording head. The AC signal of 0.1 c/s is delivered by two stabilized power supply circuits, H and H' , connected in push-pull. The output voltage of each of these circuits is controlled, with the aid of a small electric motor M , and sinusoidally varied 6 times per minute between 5 and 15 V, while H and H' operate in anti-phase. At the moments when both are delivering the same voltage (10 V) the current through the recording head K is zero; in the interim periods the current through K is alternately positive and negative. $L_1-C_1-C_1'$ is a filter that keeps the 50 c/s bias current outside H and H' .

The bias current is supplied from the mains via a variable transformer and an isolating transformer T_2 . Since the capacitor C_2 with the coil of the recording head constitutes a circuit tuned to the mains frequency, the output voltage of T_2 need not be more than 50 V.

that for the same purpose we need roughly 2000 ampere turns. The recording head designed by us contains 175 turns, so that signal currents up to about 10 A should be possible. The principle of the generator used to produce these signal currents is illustrated in *fig. 5* and explained in the caption.

The same figure shows how we generate the "high-frequency" bias current which is always superimposed on the signal in normal recording, and which it must be possible to supply to the recording head in our case too. For convenience we chose for the bias current the frequency of the mains, 50 c/s. (In itself

The first measurements were on a "tape" consisting of randomly orientated grains dispersed in vaseline. In practice the grains in the tapes used for magnetic recording are usually needle-shaped. They have a single preferred direction of magnetization, and in the manufacturing process this is arranged to lie mainly in the long axis of the tape. We were able subsequently to devise a method of making our tape in such a way as to simulate this preferential orientation, a plastic material with dispersed grains being calendered so as to align the grains. This material is now used for the middle strip from which the sam-

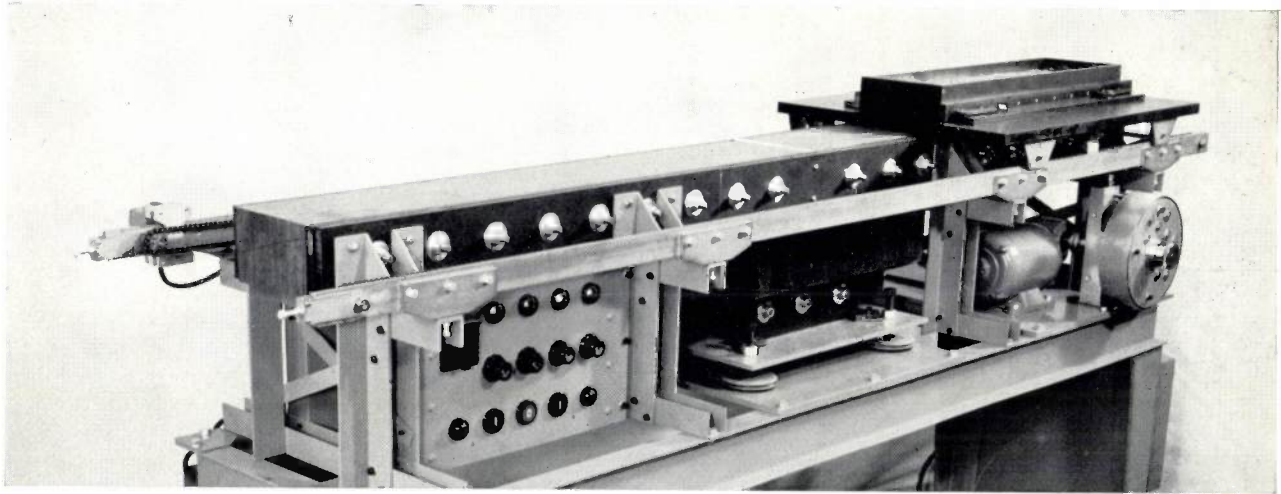


Fig. 6. Model of recording head and tape in its present form. The pole pieces of the head have been lengthened so that their ends are not passed by the tray containing the tape material. The tray in this version is drawn along the track by two chains, which proved to give a smoother motion at high speeds than a screw shaft.

a frequency of a few c/s would be high enough, even at our maximum tape speed, to make the recorded wavelength of the bias current smaller than the diameter of the samples measured.) Bias currents up to 60 A should be obtainable. The voltage on the coil around the recording head (inductance 35 mH) is then about 700 V, a value low enough to avoid insulation difficulties. The power dissipated in the recording head, due to eddy currents, etc., is about 2.5 kW.

The recording of pulses can also be studied in the model. For this purpose the recording head is supplied with a direct current of about 70 A maximum, and the steep leading edge of a pulse is simulated by switching the current on and off.

All the equipment used for generating and controlling the various currents applied to the recording head can be seen in *fig. 3* in the background.

amples are taken. The space in the tray on either side of the exchangeable middle strip is also filled with a large number of narrow, tightly packed plastic strips fabricated in the same way.

In the first experiments it was soon apparent that the pole pieces of the recording head, which were relatively far too small in length, caused interfering edge effects: the field concentration at the edges (*R* in *fig. 2*) also affected the resultant magnetization in the tape after passing the gap. It is scarcely feasible to scale up the pole pieces to 5000 : 1 (this would make them several tens of metres long); the edge effects can, however, be avoided by making the pole pieces long enough so that the piece of tape used, does not pass their ends. We were able to satisfy this condition in a subsequent version of the model in which the tape speed can also be varied between much wider limits (*fig. 6*).

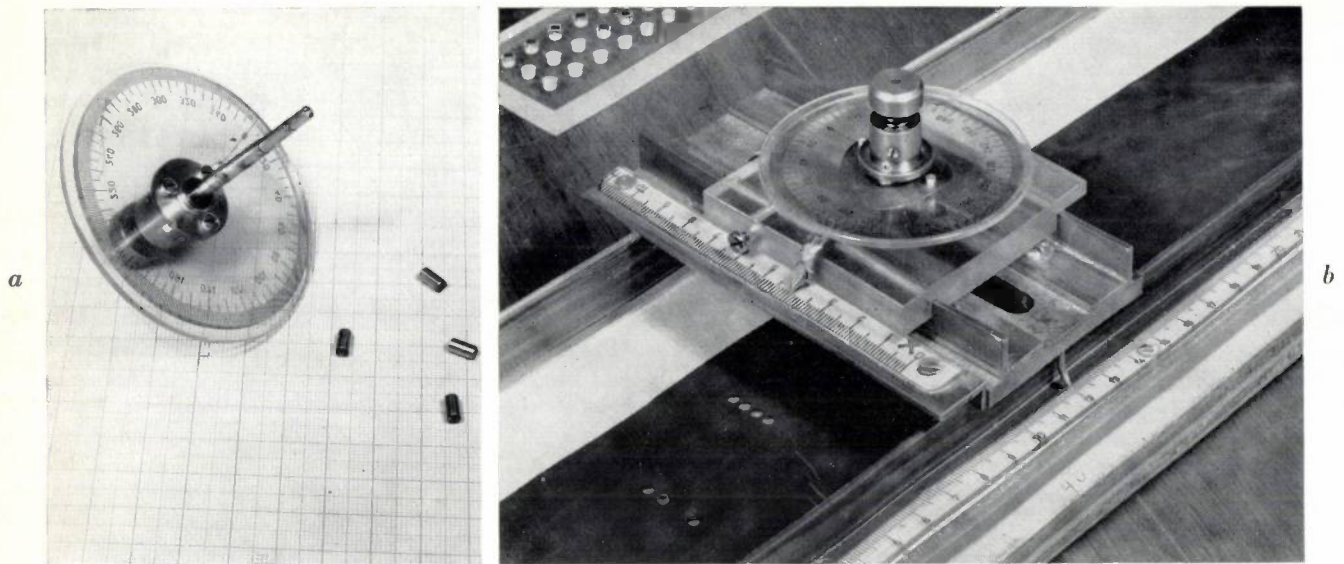


Fig. 7. Device for punching out disc-shaped samples from the 0.5 mm thick middle strip of the tape.

- a) Holder with graduated circle; over the end of the spindle is fitted an interchangeable hollow punch which collects the sample.
- b) Roller track and carriage with which the holder can be placed above any desired point of the tape. A sample can only be punched out when the zero pointer of the graduated circle on the holder is parallel to the long axis of the track (and hence of the tape). Some samples have already been punched out of the tape.

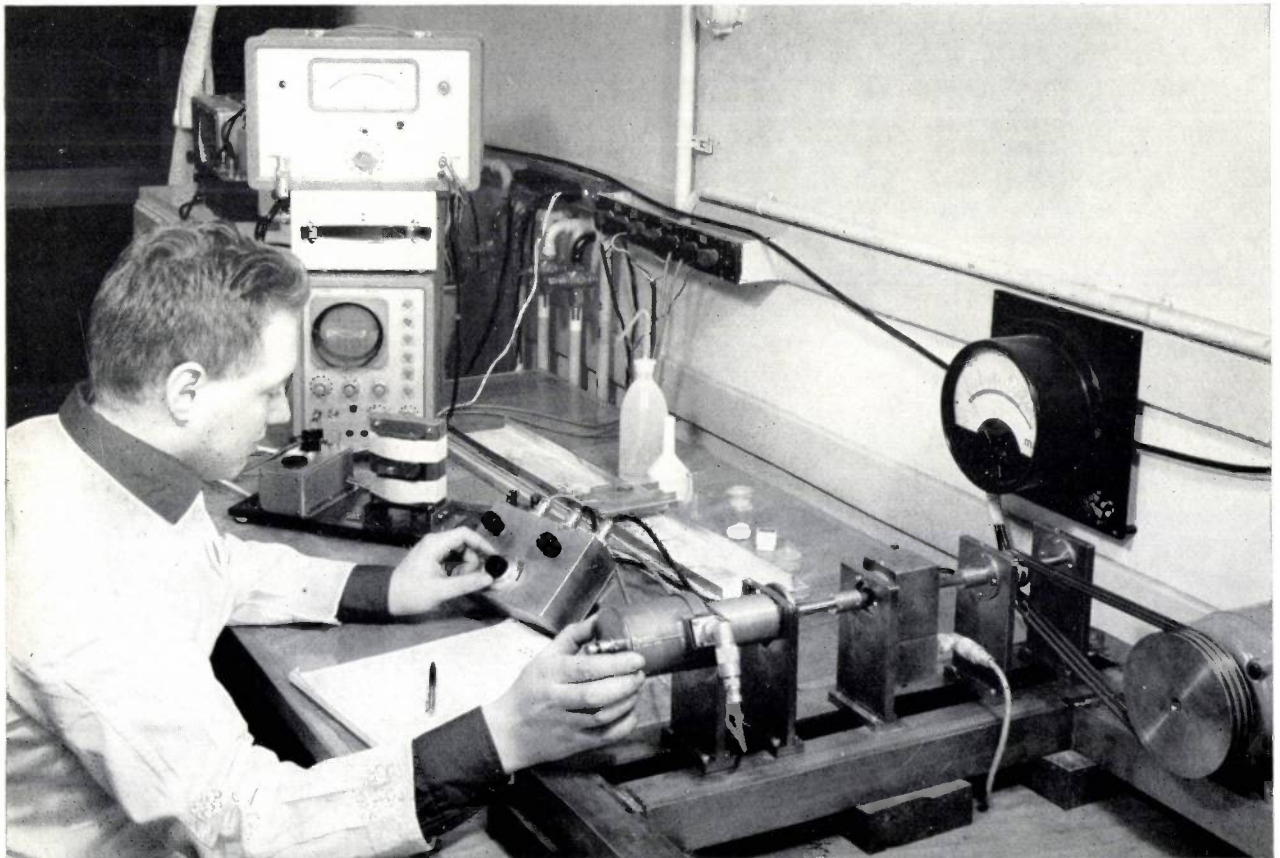


Fig. 8. Equipment for measuring the magnitude and direction of the magnetization of the individual samples. In the right foreground can be seen the magnetometer proper, in which the holder with graduated circle and sample is placed. For further particulars, see fig. 9. The alternating voltage generated by the magnetized sample is compared with a signal generated by a "reference magnet". By rotating the sample holder the phases of both alternating voltages are equalized, and their amplitudes are equalized by regulating a calibrated

attenuator.

To eliminate approximately the influence of the demagnetization factor of the sample, each sample after measurement is momentarily magnetized to saturation (this is done by the electromagnet that can be seen in front of the oscilloscope) and the magnitude of the magnetic moment of the remanence is determined in the same way with the magnetometer. This being done, the hollow punch with the sample is removed from the holder and a new measurement started.

Measurement of the samples

The samples — discs of 3 mm diameter — are punched out of the 0.5 mm thick centre strip of our "tape" by means of a device shown in *fig. 7*. The holder in which the sample is collected carries a graduated circle which, in the punching operation, is kept with its zero angle always exactly in the long axis of the tape by means of two guide pins. The location of each sample can be measured on the centimetre scales to within an accuracy of $\frac{1}{2}$ mm. The magnitude and direction of the magnetic moment of each sample are then measured by means of an instrument which is illustrated in *figs. 8 and 9*. It is based on the same principle as the rotating sample magnetometer. The phase and magnitude of the alternating voltage induced in the coil give the direction and magnitude of the magnetic moment of the sample. In our arrangement the roles have merely been reversed: the sample, introduced together with the holder into the instrument, remains stationary, while the two pole pieces rotate around it at 175 r.p.s. For convenience, the coil and the other part of the magnetic circuit are also kept stationary. The small air gap that we have to leave between this part and the pole pieces (*l* in *fig. 9a*) does practically no harm. The advantage of this arrangement is that it takes very little time and trouble to change from one sample to the next — an important consideration in view of the large series of measurements needed for each experiment.

The actual measurement is done by a null method. The magnitude and phase of the induced e.m.f. are compared on an oscilloscope with those of a reference signal, generated in a small coil by a magnet on the shaft of the rotating pole pieces (*fig. 9b*). By turning the holder with the sample through a given angle, the phases of both signals can be equalized, while at the same time the amplitudes are equalized with a variable attenuator. The direction of the magnetic moment of the sample can then be read from the scale around the holder with an accuracy of about $\frac{1}{2}^\circ$, and the magnitude of the magnetic moment can be read from the attenuator.

A drawback of the measuring arrangement described is its sensitivity to constant stray fields. Good mu-metal screening is fitted to counteract such interference.

The magnetic moments of the samples punched from the tape do not give directly the magnetization in situ in which we are interested. After the sample is punched out its magnetic state is subject to a demagnetizing field different from that in the tape. Experiments have shown that the effects of this field can for all practical purposes be eliminated

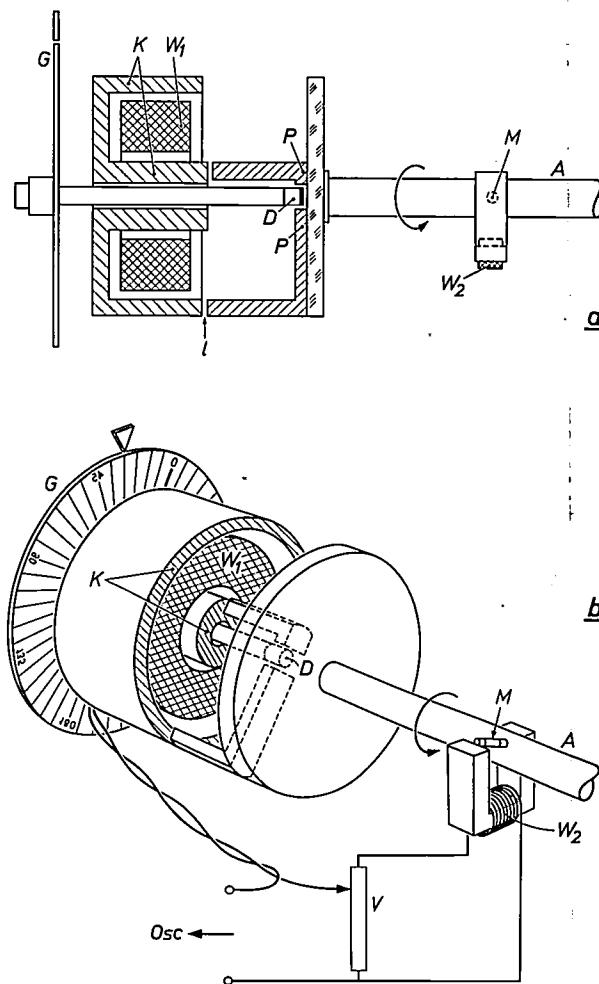


Fig. 9. a) Principle of the magnetometer for measuring the samples. *D* hollow punch with magnetized sample, at the end of the holder with graduated circle *G*. The holder remains stationary, but can be turned by hand to any required position. The ferrite core *K* with coil *W*₁ is also stationary, but the pole pieces *P* of this magnetic circuit, which are separated from the core *K* by a narrow air gap *l*, are fixed to the shaft *A* and rotate at 175 r.p.s. around the sample. In the perspective drawing (b) it can be seen that the shaft also carries a small magnet *M* which induces in the coil *W*₂ an alternating voltage, which serves as a reference signal. The alternating voltage induced by the sample in *W*₁ is compared with that induced in *W*₂, both in phase and amplitude, by rotating the holder and regulating the attenuator *V*; this can be monitored on an oscilloscope (*Osc*).

— together with the effect of any inhomogeneity in the dispersion — by determining in addition the magnetic moment of the remanence of each sample after saturation, and by dividing the measured moment of the recorded magnetization by the value so found.

Some results of measurements

Finally, we shall mention some of the results of measurements carried out in the first experiments on our model.

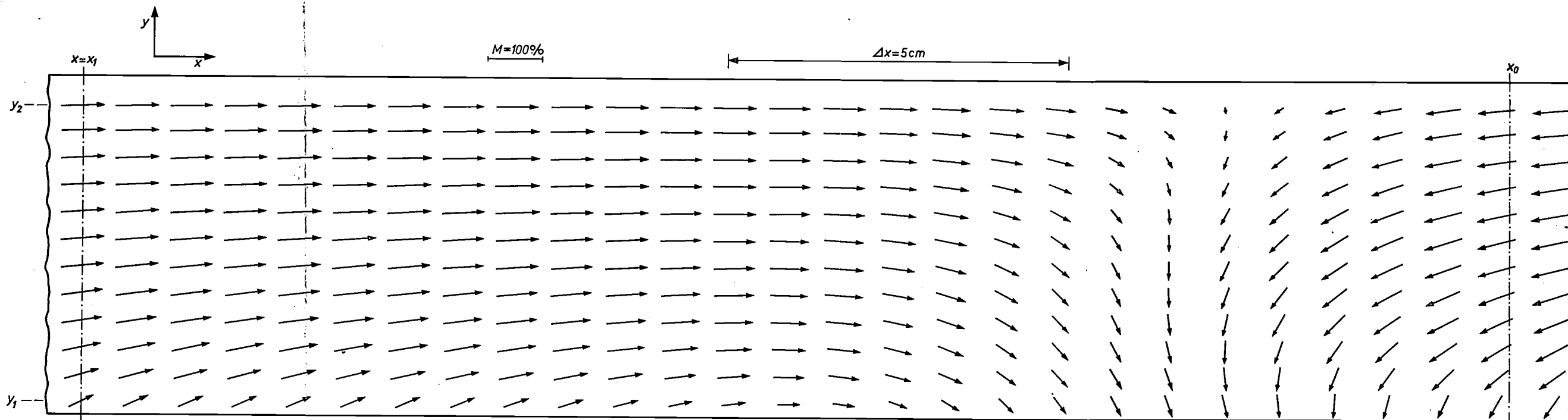


Fig. 10. a) State of magnetization of the tape after recording the *step function* signal represented in (b). The drawing shows the vertical plane of symmetry of the tape (elevation sketch of the middle strip, m in fig. 2), with the magnetization drawn at numerous points in magnitude and direction. The recording-head gap is drawn at the location (x_0) where it happened to be in relation to the tape at the moment of the discontinuity. Its relative direction of travel is indicated by the arrow (the fact that a value of the signal (b) can be seen here opposite each position x of (a) does *not* mean that this value was recorded at the location x , but simply that the signal had that value when the recording head was at the position x).

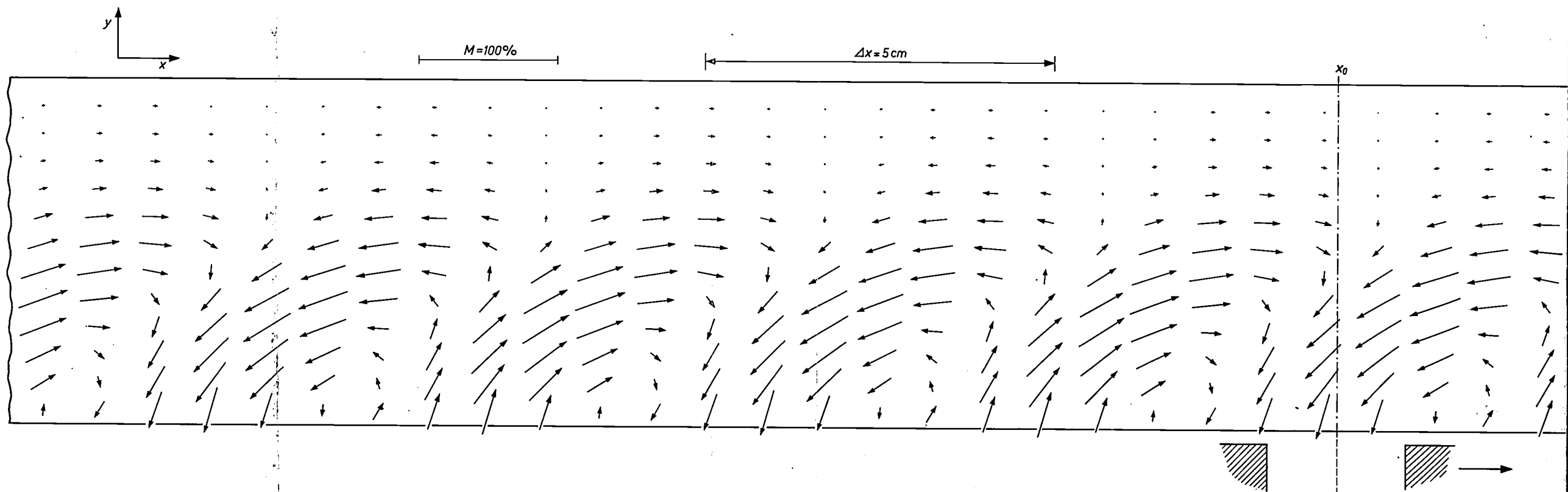
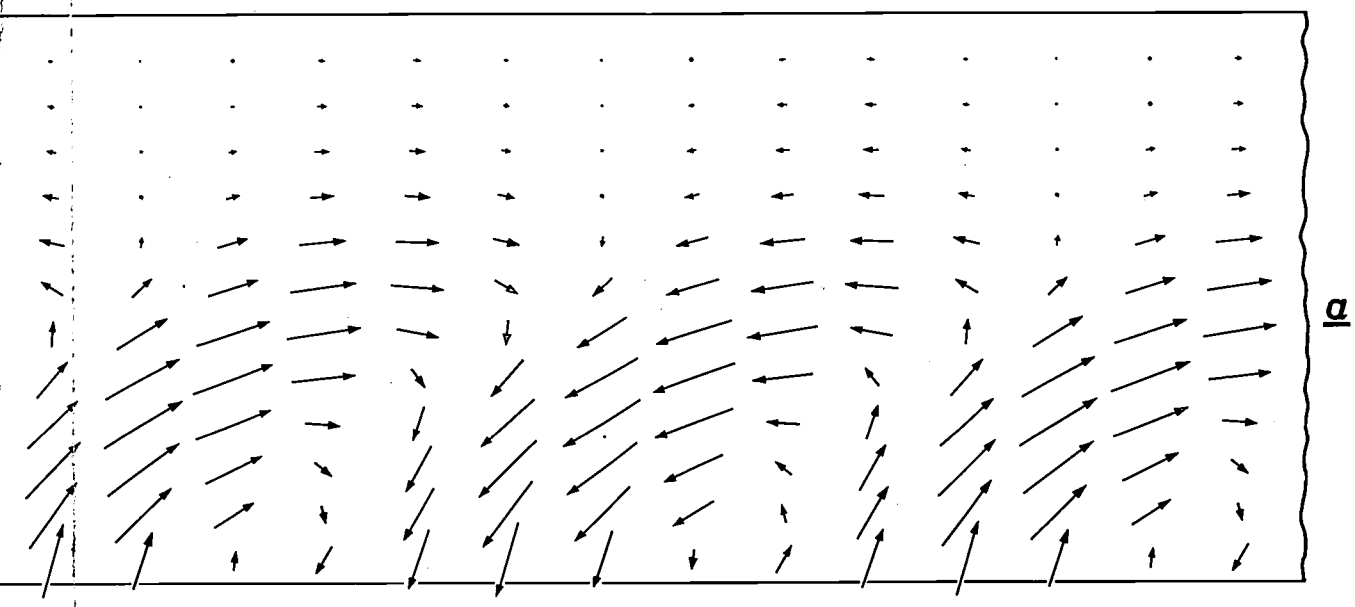
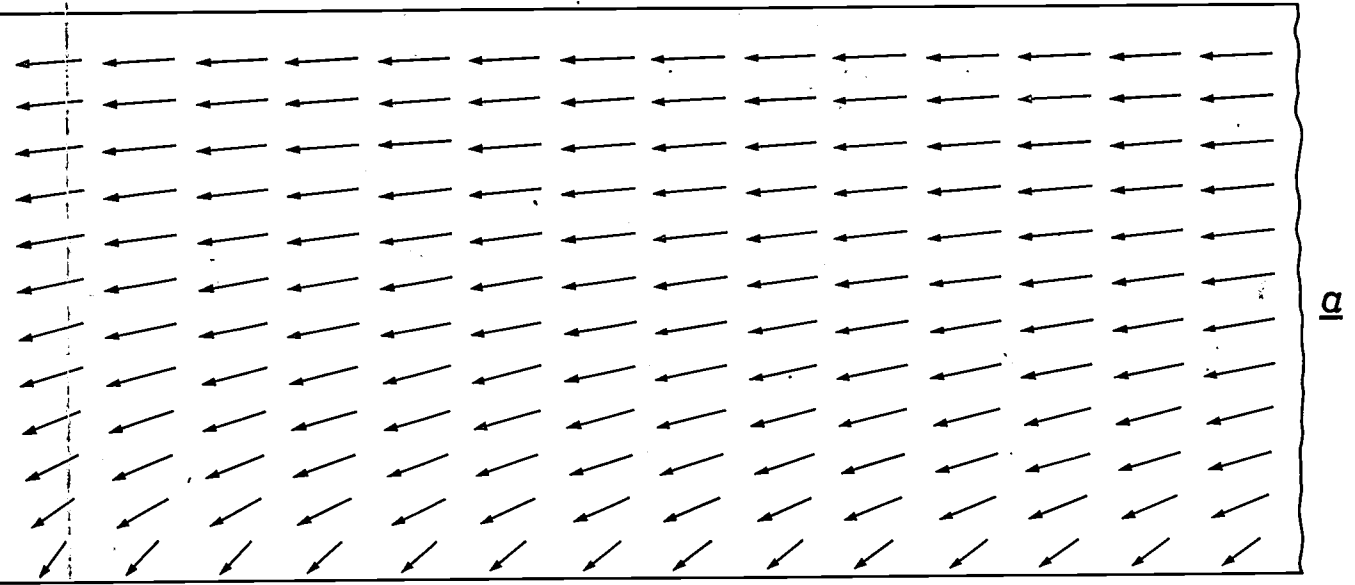


Fig. 13. Representation as in fig. 10 of the state of magnetization of the tape (a) but now after the recording of a *sinusoidal* signal (b). The scale for the magnetization is here more than $3 \times$ larger than in fig. 10. The recording-head gap is drawn at the location (x_0) where it happened to be at one of the moments at which the signal current passed through zero. (For the relation between (a) and (b), see the caption to fig. 10.)



The strip shown in *fig. 10a* represents a section of the vertical plane of symmetry of the magnetic layer. The magnetization, produced by recording a particular signal, has been indicated in this cross-section by drawing to scale at numerous points the magnetization vector with the measured orientation. In this case the signal was a *step function*, obtained by switching a direct current at a certain moment from positive to negative (*fig. 10b*). The recording was made without bias current.

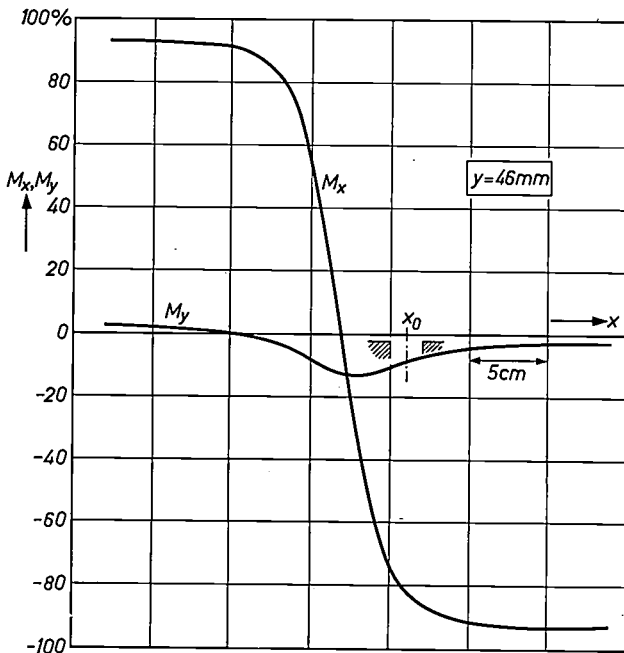
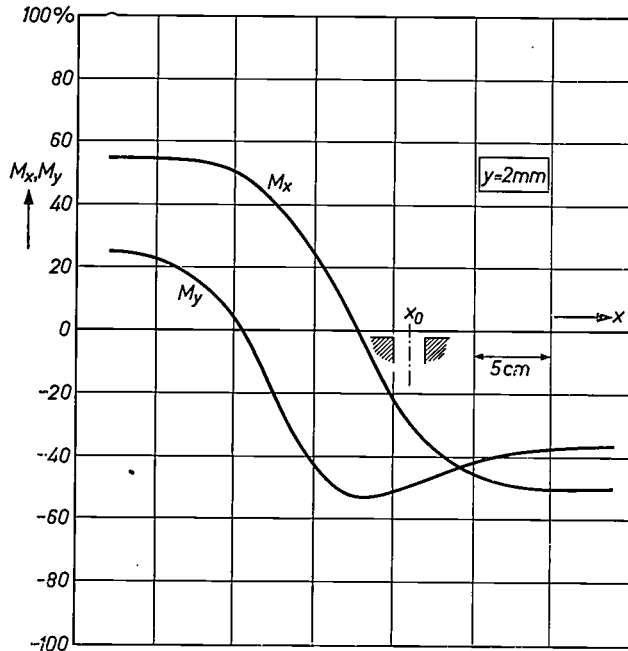


Fig. 11. The components M_x and M_y of the magnetization, measured in the recording represented in *fig. 10*, are plotted here versus the location x at a given depth y in the tape: in *a*) at a depth $y_1 = 2$ mm, and *b*) at a depth $y_2 = 46$ mm. These depths are indicated in *fig. 10a*.

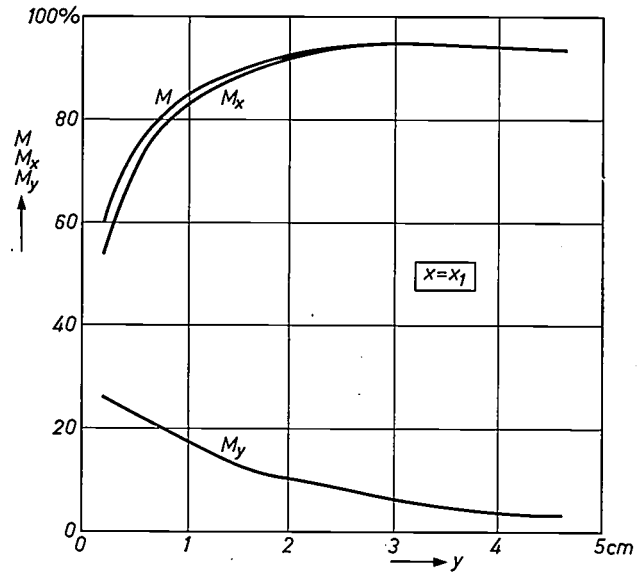


Fig. 12. Magnitude M of the magnetization, and components M_x and M_y , measured in the recording represented in *fig. 10*, plotted as a function of the depth y in the tape at a given location x_1 . The cross-section x_1 is indicated in *fig. 10a*.

Owing to the finite diameter of the samples, the curves begin at $y = 2$ mm.

To obtain a more quantitative presentation of the measuring results, the longitudinal and vertical components of the magnetization, M_x and M_y , can be plotted as a function of location x at a given depth y in the tape, and also as a function of the depth y at a given location x in the tape. A plot of the former kind is given in *fig. 11* for the results in *fig. 10*, in respect of two different depths, $y_1 = 2$ mm and $y_2 = 46$ mm. Upon reversal of the direction of the current, the component M_x at the depth y_2 is seen to change direction much more abruptly than at the depth y_1 ; in other words the step function is recorded more sharply deep inside the tape than near the surface. The behaviour of the component M_y contributes to this effect. Remarkably enough, M_y does not reverse simultaneously with M_x but quite a bit "earlier", i.e. at a greater distance x behind the gap, which is moving relative to the tape. As a consequence of this, the step function is less sharply defined at the surface, but deep inside the tape the definition is not affected because there M_y is very small.

In *fig. 12* the values M_x and M_y are plotted in the other manner mentioned, i.e. as a function of the depth y at a given location x on the tape. The location chosen here is $x_1 = 21$ cm in front of the cross-section (x_0) that was just passing the gap when the current was reversed. The tape material at x_1 knows nothing of the discontinuity about to occur, and has thus "seen" a pure direct current. It follows from the curves — as is also apparent in *fig. 10* — that the magnetization near the surface of the tape then makes a fairly large angle with the long axis of the

tape. The absolute value M of the magnetization, which is also plotted in fig. 12, is everywhere lower than the remanence that would follow from the given field strength. This is presumably a consequence of the rotation of the field during the recording process. A similar result has recently been found by other investigators working along entirely different lines¹⁾.

Fig. 13a presents in the same manner as in fig. 10 the magnetic state of the layer after the recording of a sinusoidal signal. The wave-form of this signal is shown in fig. 13b. The reasons for the much more complicated picture obtained in this case will not be dealt with here.

In order, however, to make clearer the kind of theoretical problems we hope to bring nearer to a solution with the model described, we shall discuss as a final example the result of recording a simple direct current, this time however together with a bias current. For this purpose the non-oriented tape material was used. In fig. 14 the magnetization M together with the longitudinal and vertical components M_x and M_y are again plotted as a function of depth y in the layer, for a bias current with an amplitude of 20 A and a direct current of 1 A. The result differs considerably from that found without bias current: up to a certain depth y the longitudinal component M_x now increases more or less proportionately with y . The total magnetization is substantially lower nearer the surface than somewhat deeper in the layer.

From the point of view of playback a state of magnetization of this nature is far more unfavourable than homogeneous magnetization of the whole magnetic layer. It can be calculated that in the latter

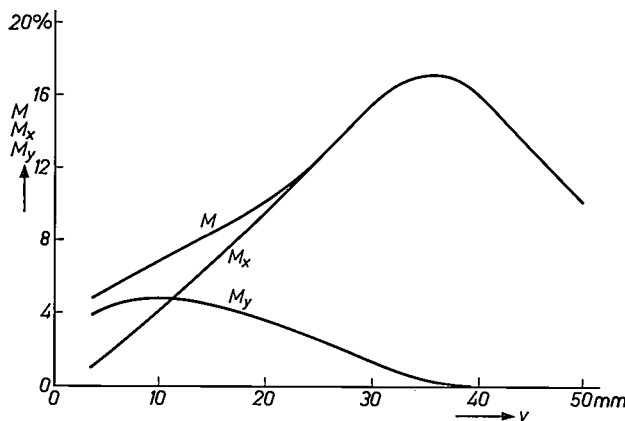


Fig. 14. Measured magnetization M and components M_x and M_y , as a function of the depth y , for a signal consisting of a direct current (1 A) with a superimposed bias current (20 A).

case the output signal obtained in a long-wave recording would be about 3 dB stronger (assuming that the current used in both recordings is such as to result in the same non-linear distortion from the curved $B-H$ line); at short waves the difference would be even more marked.

The occurrence of a magnetization state as shown in fig. 14 can to some extent be understood as follows²⁾. According to the present theory³⁾, the actual recording takes place in a ring-shaped zone situated just beyond the centre of the air gap in the recording head; the amplitude of the bias field in this zone is roughly equal to the coercivity of the tape material (see fig. 15). This means that every

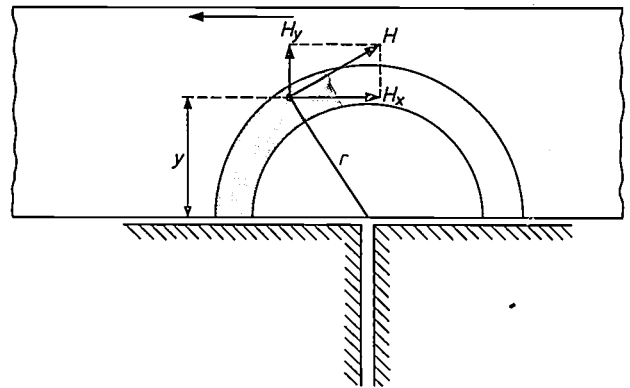


Fig. 15. The actual recording process takes place in a zone around the gap (the "recording zone", shown shaded), where the amplitude of the field H generated by the bias current is roughly equal to the coercivity of the tape material.

part of the tape emerges from the process with a magnetization M proportional to the signal field-strength to which it was subjected at the instant of passing the "recording zone". If there were no tape present, the field strengths H_x and H_y in this zone would be given to a first approximation by

$$H_x = \frac{niy}{\pi r^2},$$

$$H_y = -\frac{ni \sqrt{r^2 - y^2}}{\pi r^2},$$

where n is the number of turns, i the signal current and r the radius (partly determined by the bias current) of the recording zone. This field distribution would then cause M_x and M_y to vary as a function of y in the manner shown in fig. 16. It can be seen that the curves in fig. 14 agree very nicely with this

¹⁾ H. S. Templeton and G. Bate, Proc. Intermag. Conf. Washington 1963, p. 7-4.

²⁾ D. L. A. Tjaden, Proc. 3rd Int. Congress on Acoustics, Stuttgart 1959, Part II, page 758.

³⁾ W. K. Westmijze, Philips Res. Repts. 8, 250, 1953.

picture up to a certain extent (or rather to a certain depth), except that the vertical component M_y is substantially reduced. This effect, which is responsible for the above-mentioned loss in reproduction, is attributable to the demagnetizing effect of the part of the tape which, with a certain magnetization, has already left the recording zone.

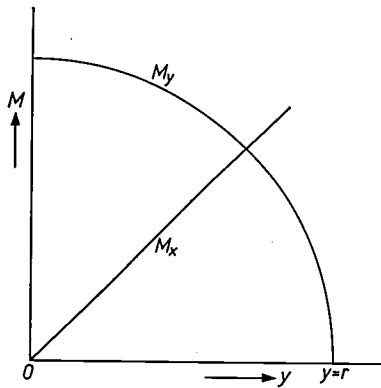


Fig. 16. Theoretical curve of M_x and M_y , derived from fig. 15, as a function of y , for a recording of the same signal as used for fig. 14.

This demagnetizing influence is one of the effects that will be extensively investigated. The considerable size of the model makes it possible to apply other techniques than simply the measurement of samples after a recording. It is intended, for example, to carry out measurements in which, during the

recording, the middle strip will carry a number of Hall generators, which will make it possible to observe and record on an oscilloscope the local fields and their fluctuations, during the recording of both DC and AC signals. A report on these investigations will be published in due course.

In conclusion, it should be mentioned that the equipment was devised in cooperation with G. W. van Oosterhout of this laboratory. The construction was largely the work of J. R. P. N. Crüts. For the oriented tape material at present in use we are indebted to M. L. van Splunder of Philips Plastics Laboratory and to the cooperation of the Plastics Research Institute (T.N.O.) of Delft.

Summary. In magnetic recording the magnetic coating of the tape is magnetized over its entire thickness as it passes the recording head. Little is yet known about the manner in which the magnitude and direction of this magnetization vary as a function of depth in the tape. To obtain data on this subject, a model of the tape and recording head has been built in Philips Laboratories at Eindhoven in which all essential dimensions (air gap, tape thickness, recorded wavelength) are scaled up by a factor of 5000. Provided the number of ampere turns of the recording head is scaled up by the same factor — which makes it necessary to build a somewhat unconventional generator — the state of the magnetization produced in the tape (disregarding fluctuation effects) is a true copy of that in normal recording. The "tape" contains an interchangeable middle strip, 5 cm wide and $\frac{1}{2}$ mm thick, from which numerous small samples are punched out after a signal has been recorded. The magnitude and direction of the magnetization of these samples are measured by means of a special magnetometer.

Some results of the measurements hitherto carried out are discussed and their theoretical significance commented upon.

ERRATUM

In the article "New forms of bearing: the gas and the spiral groove bearing", Philips tech. Rev. 25, 1963/64 (No. 10), a sentence from a proof has erroneously remained, viz, the sentence on p. 266, right-hand column, lines 11-8 from the bottom: "This pump effect . . . on the grooves". This sentence should be deleted.

SOME SIMPLE ACTIVE FILTERS FOR LOW FREQUENCIES

by G. KLEIN *) and J. J. ZAALBERG van ZELST *).

621.372.542.2

The growing interest shown during recent years in electrical measurements at very low frequencies has led to a demand for special low-frequency filters. Coils, which are commonly used in filters for higher frequencies, have certain disadvantages at low frequencies. In this article the authors describe some circuits in which the use of coils is avoided.

Introduction

In radio engineering and in other branches of electrotechnology it is the practice to give circuits specified frequency-dependent characteristics by using capacitors and coils. These two circuit elements have properties that are to a certain extent opposed to one another. When an alternating voltage is applied, the current flowing in a capacitor leads the voltage in phase, whereas in a coil the current lags in phase. Again, in a capacitor the reactance decreases with rising frequency, whereas in a coil it increases.

Among the passive electric networks composed of combinations of capacitors and coils, the electric filters, which are used for separating signals with certain frequencies from signals with other frequencies, form an important subgroup. For this purpose the use of capacitors *and* coils is not strictly necessary. A filter can be built using only one of these elements in combination with resistors. By combining coils and capacitors, however, it is easy to produce a much sharper separation between wanted and unwanted signals.

One of the simplest and most familiar passive filter networks is the parallel resonant circuit (here referred to as an LC circuit) which can be considered as formed from the parallel arrangement of a capacitor, a coil (both loss-free) and a resistor (see fig. 1). In such a circuit the modulus of the impedance is maximum at the resonant frequency

$$\omega_0 = 1/\sqrt{LC} \dots \dots \dots (1)$$

For any given value ω of the frequency, the impedance can be written in the form:

$$Z(\omega) = \frac{R}{1 + j\beta Q}, \dots \dots \dots (2)$$

where β is an abbreviated notation for $\omega/\omega_0 - \omega_0/\omega$.

*) Philips Research Laboratories, Eindhoven.

If $|\omega - \omega_0|$ is small compared with ω_0 , we can write β in the form:

$$\beta = \frac{2(\omega - \omega_0)}{\omega_0}$$

In this case, then, β is twice the "relative detuning".

In equation (2) Q is the figure of merit, here given by:

$$Q = \frac{R}{\omega_0 L} = \omega_0 CR \dots \dots \dots (3)$$

The modulus of the impedance Z , plotted as a function of frequency, has the form of the familiar resonance curve (fig. 1). The curve is narrower, i.e. the LC circuit more selective, the higher the value of Q . The difference between the two frequencies at which $|Z|$ is a factor of $\sqrt{2}$ smaller than the maximum value is normally referred to as the bandwidth.

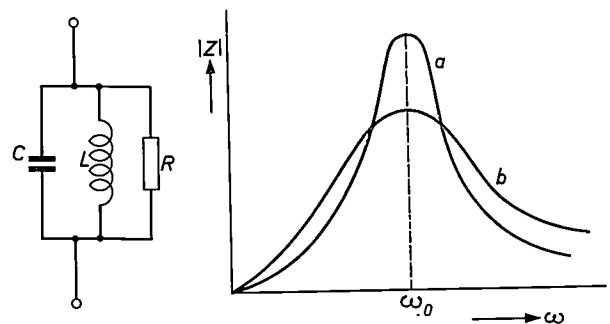


Fig. 1. Left: resonant circuit consisting of a coil, an inductance, a capacitance and a resistance in parallel LC circuit. Right: frequency characteristic (resonance curve) for two LC circuits. The resonant frequency is ω_0 . The network to which curve a relates has a higher figure of merit Q .

Filters for very low frequencies

In recent years a growing interest has been shown in electrical measurements at very low frequencies. In the fields of physics and chemistry, for instance,

measurements are frequently carried out with intermittent light; examples are measurements of photoconductivity and of light adsorption in liquids and crystals. The periodic interruption of the light makes it possible to use AC amplifiers for this purpose, which are easier to build and to operate than DC amplifiers. Measurements at very low frequencies are also important in various electro-medical applications, particularly in cardiography, encephalography and myography.

In some of these cases, filters are required which reduce interference to the minimum at the low frequencies involved. Sometimes, too, filters are needed for separating signals of different very low frequencies. This is notably the case in encephalography, where it is occasionally necessary to perform a harmonic analysis of the cerebral voltages, the presence or absence of voltages of certain frequencies having a bearing on the diagnosis of epilepsy. To give some idea of the resolving power required in such a case, it may be mentioned that filters are sometimes needed which have a bandwidth of 1 c/s at a centre frequency of some tens of cycles per second.

To build filters for lower frequencies it is necessary, as can be deduced from eq. (1), to use capacitors of higher capacitance and/or coils of higher inductance. As regards the capacitors, this does not as a rule present insuperable difficulties; the capacitance of a capacitor contained in a given volume can be increased by enlarging the surface area of the plates and by making the dielectric thinner. The construction of coils having a very high inductance involves considerable, and often intractable problems. Coils of this kind always contain a core, which may consist of iron alloy lamellae or of ferroxcube. This makes high-inductance coils relatively bulky and heavy, as also does the larger number of turns required to produce a higher inductance.

Apart from the drawbacks of large bulk and/or weight, there are various other disadvantages attached to the use of high-inductance coils. As a rule they are expensive, because of the large amount of material used, and it takes much more time to produce them. Such a coil, once made, is not very "flexible", that is to say its properties are difficult to modify. In most cases, indeed, it is not practicable to change the inductance value. This, together with the unavoidable variation during manufacture, can make it difficult to produce a coil with an accurately specified inductance. Another drawback is that the properties of coils of this kind tend to vary more markedly with temperature than those of most

other circuit elements. Finally, problems can also arise from the necessity of screening the coils against stray magnetic fields. At low frequencies ferromagnetic cans have to be used for this purpose, possibly combined with one or more cans made of a material possessing good electrical conductivity. This again puts up the weight and the price.

The above-mentioned objections to the use of large coils have resulted in the development of circuits which contain no coils, but have the same properties as circuits that do. A familiar example is the feedback amplifier incorporating in the feedback loop a twin-T filter composed of capacitors and resistors¹⁾. The characteristics of a network of this kind correspond to those of an *LC* circuit. Alignment, however, is somewhat laborious, particularly where several amplifiers tuned to different frequencies are to be connected in cascade.

The object of this article is to draw attention to a type of filter with which the same or even better results can often be achieved, and which is simpler to align than the above-mentioned feedback amplifier. This type of filter has in fact long been known; here, however, after giving a brief outline of its principles, we shall consider some of the less familiar aspects. In particular it will be shown that various measures can be taken to achieve considerable precision with filters of this type and some lesser known applications will be touched upon²⁾.

Principle of the circuit

Our starting point is a resistance-coupled amplifier stage, as represented by the diagram in *fig. 2*.

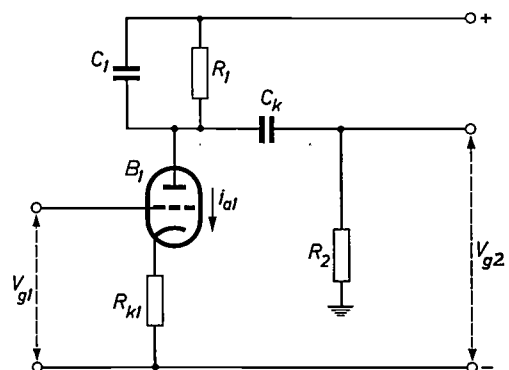


Fig. 2. Amplifying stage with resistance coupling.

¹⁾ A filter of this kind is described by G. Klein and J.J. Zaalberg van Zelst in: A low-frequency oscillator with very low distortion under non-linear loading, Philips tech. Rev. 25, 22-30, 1963/64 (No. 1), p. 27.

²⁾ A special application is described by K. Teer, Audibility of phase errors, Philips tech. Rev. 25, 176-178, 1963/64 (No. 6/7).

Connected in parallel with the resistor R_1 in the anode circuit of the triode B_1 is a capacitor C_1 , and the output voltage V_{g2} ³⁾ of the anode is taken off via a capacitance-resistance coupling C_k-R_2 . It can readily be shown that the relation between the anode alternating current i_{a1} of B_1 and the voltage V_{g2} is:

$$\frac{V_{g2}}{i_{a1}} = \frac{-j\omega R_1 R_2 C_k}{1 + j\omega(R_1 C_1 + R_1 C_k + R_2 C_k) - \omega^2 R_1 R_2 C_1 C_k} \dots (4)$$

The same relation between V_{g2} and i_{a1} would have been found if we had incorporated in the anode network of B_1 an LC circuit consisting of a parallel arrangement of a resistance R' , an inductance L' and a capacitance C' (see fig. 3). These three elements

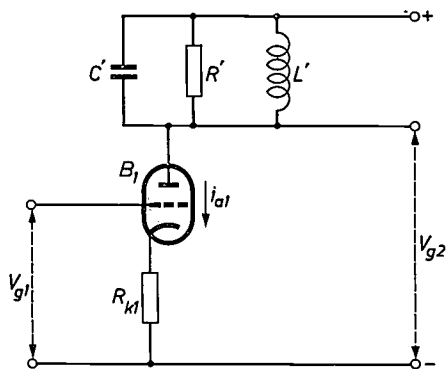


Fig. 3. With appropriate values of L' , C' and R' this circuit is equivalent to fig. 2. The figure of merit is in that case very low.

would then have to have the following magnitudes:

$$R' = \frac{R_1 R_2 C_k}{R_1 C_1 + R_1 C_k + R_2 C_k}, \dots (5)$$

$$L' = R_1 R_2 C_k, \dots (6)$$

$$C' = C_1. \dots (7)$$

The resonant frequency of this equivalent circuit would thus be:

$$\omega_0 = \frac{1}{\sqrt{L' C'}} = \frac{1}{\sqrt{R_1 R_2 C_1 C_k}}, \dots (8)$$

and the figure of merit:

$$Q = \frac{R'}{\omega_0 L'} = \frac{\sqrt{R_1 R_2 C_1 C_k}}{R_1 C_1 + R_1 C_k + R_2 C_k}. \dots (9)$$

The quotient of V_{g2} and i_{a1} can then be written in the form:

³⁾ The notation V_{g2} is used here because later in the article this voltage will be applied to the grid of another valve (see e.g. fig. 4).

$$\frac{V_{g2}}{i_{a1}} = \frac{-R'}{1 + j\beta Q} \dots (10)$$

If the resistance R_{k1} in the cathode lead of B_1 is large compared with the reciprocal of the transconductance, and if, moreover, the amplification factor of B_1 is very high, then $i_{a1} = V_{g1}/R_{k1}$, and eq. (10) becomes:

$$V_{g2} = \frac{-R'}{R_{k1}(1 + j\beta Q)} V_{g1} \dots (11)$$

This analogy with LC circuits is also found with normal amplifying stages. As a rule C_1 is then made up of the anode capacitance of the valve and the wiring capacitance. By way of illustration it will be useful here to insert some conventional values in the expressions (5) to (9), i.e.

$$R_1 = 10 \text{ k}\Omega, R_2 = 1 \text{ M}\Omega, C_1 = 10 \text{ pF} \text{ and } C_k = 0.1 \mu\text{F}.$$

We then find:

$$R' = 9.99 \text{ k}\Omega, L' = 10^3 \text{ H}, C' = 10 \text{ pF}, \omega_0 = 10^4 \text{ rad/s} \text{ and } Q = 10^{-3}.$$

The value of Q found here is exceptionally small compared with that of conventional resonant circuits (10 to 100). Further, it is already apparent that the circuit in fig. 2 behaves like an LC circuit containing a coil with a very high value of L . Because of the low value of C_1 , however, ω_0 is not particularly small. If we make C_1 and C_k much larger, e.g. both $1 \mu\text{F}$, then we find from (5) to (9):

$$R' = 9.98 \text{ k}\Omega, L' = 10^4 \text{ H}, C' = 1 \mu\text{F}, \omega_0 = 10 \text{ rad/s} \text{ and } Q = 9.8 \times 10^{-2}.$$

The resonant frequency is now extremely low, but Q is still very small.

We may now ask whether a higher Q might be obtained by choosing different resistance and capacitance values. This is indeed found to be the case; for Q it is possible to achieve a maximum value of $\frac{1}{2}$, although usually a somewhat lower value is accepted, the reason being that the signals are more strongly attenuated the nearer Q approaches the value $\frac{1}{2}$.

To demonstrate the latter point, we combine (5) and (9) to form the following equation:

$$Q^2 + \frac{R'^2}{R_1 R_2} = \frac{\frac{R_1(C_1 + C_k)}{R_2 C_k}}{\left\{ \frac{R_1(C_1 + C_k)}{R_2 C_k} + 1 \right\}^2} \dots (12)$$

The right-hand side has an absolute maximum of $\frac{1}{4}$ for

$$\frac{R_1(C_1 + C_k)}{R_2 C_k} = 1. \dots (13)$$

At a very low value of R' , or at very high values of R_1 and/or R_2 , Q can therefore approach $\frac{1}{2}$. Now R_1 and R_2 cannot be given unlimitedly high values without affecting the operation of the two valves, these resistances being included in the anode and grid circuits respectively. If Q is to approach $\frac{1}{2}$, therefore, R' will have to be small, which means that the signal transmission by the filter will be poor.

Since, moreover, a Q of $\frac{1}{2}$ is still very low, it would not be possible in this way to design a filter that satisfied practical selectivity requirements, if it were not for the fact that the figure of merit can be considerably increased by the use of feedback. This resembles the effect of feedback in an oscillator. Here too, the effective Q of a circuit is increased by feedback until, at an almost infinitely high Q , oscillation occurs.

Circuit using feedback

Feedback can be obtained by applying to the input of the filter a current which is proportional to the output voltage. A suitable circuit for this purpose is shown in *fig. 4*. The output voltage here is obtained by applying the voltage V_{g2} to the grid of a triode B_2 connected as a cathode follower. The feedback occurs through the resistance R_t shunted between the cathodes. The way the circuit works can be understood in simple terms by assuming that the two triodes function as ideal cathode followers. (To approximate to this ideal, the resistances R_{k1} and R_{k2} should be extremely high, and so too should the amplification factors of the valves.) In this case the cathodes carry alternating voltages V_{k1} and V_{k2} which are equal to the respective alternating grid-voltages V_{g1} and V_{g2} . Calculating V_{g2} ($= V_{k2}$) as a function of V_{g1} ($= V_{k1}$), we then find:

$$V_{g2} = -V_{g1} \frac{R_t + R_{k1}}{R_{k1}(R_t - R')} \frac{R'}{1 + j\beta \frac{R_t}{R_t - R'} Q} \dots (14)$$

The anode current of B_1 equals the sum of the currents in R_{k1} and R_t , hence:

$$i_{a1} = \frac{V_{k1}}{R_{k1}} + \frac{V_{k1} - V_{k2}}{R_t}$$

Using (10) we write:

$$V_{g2} = \frac{-R'}{1 + j\beta Q} \left(\frac{V_{k1}}{R_{k1}} + \frac{V_{k1} - V_{k2}}{R_t} \right),$$

which leads, after some manipulation, to equation (14).

Since the situation is entirely analogous to that in *fig. 2*, except that eq. (14) now applies instead of eq. (11), we see that the characteristics of the cir-

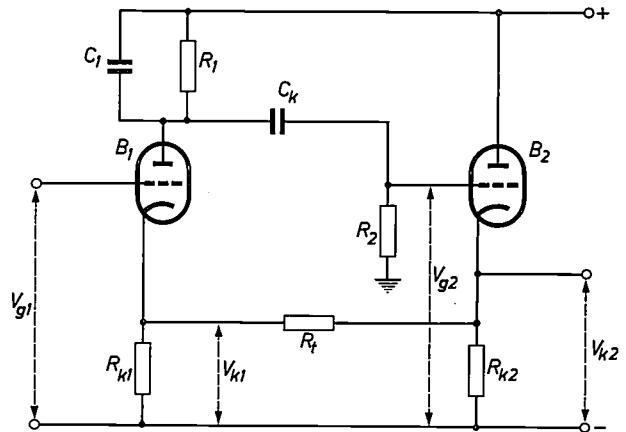


Fig. 4. The figure of merit can be increased by using feedback. In the circuit shown here this is done by introducing the triode B_2 as a cathode follower and a resistance R_t between the cathodes of the two valves.

cuit again correspond to those of an LC circuit, but now with a figure of merit

$$Q' = \frac{R_t}{R_t - R'} Q.$$

Thus, by the use of feedback, the figure of merit is increased by a factor $R_t/(R_t - R')$. Raising this factor to 100 or more results in values of Q' comparable with those of LC circuits designed for higher frequencies.

The resonant frequency is not altered by the application of the feedback; the inductance L' , however, is increased by a factor $(R_t + R_{k1})/R_t$ and the capacitance C' reduced by the same factor. Instead of the resistance R' from (11) we now have in (14) the resistance $R'(R_t + R_{k1})/(R_t - R')$. The use of feedback thus increases the signal transmission by a factor $(R_t + R_{k1})/(R_t - R')$.

Circuit design; stability

Deciding on the optimum circuit values for a filter under given conditions is usually a complicated problem owing to the large number of variables involved. Moreover the choice of the values of resistances and capacitances is restricted by various practical considerations.

We have seen that the high value of Q required for good selectivity can be achieved by means of feedback. The extent to which this can be done, however, is limited by the fact that a filter is always required to possess a certain *stability*, that is to say its characteristics are required to have a certain constancy under variations that may occur in the components used. In this respect the valves are the greatest danger. If a highly stable circuit is required, they set a limit to the extent to which feedback can be employed.

This can be understood by considering that equation (14), applicable to fig. 4, represents only an approximation since it takes no account of the fact that a cathode follower has an internal resistance which can be said to be roughly equivalent to the reciprocal of the transconductance of the relevant valve. If we take this into account, we find that instead of the resistance R_t shunted between the cathodes of the two valves, we should introduce in the equations a resistance $R_t' = R_t + 1/S_1 + 1/S_2$, where S_1 and S_2 are the transconductances of B_1 and B_2 respectively. Now, for a stable circuit with strong feedback it is most important that the value of R_t' should be highly constant. For if the factor $R_t'/(R_t' - R')$, by which the figure of merit is multiplied, is to be made sufficiently large, R_t' should not differ significantly from R' . A small percentage change in R_t' therefore has a considerable influence on the factor in question, and therefore also on the figure of merit ultimately obtained. Slight variations in the transconductance of the valves can thus cause substantial variations in the Q of the filter.

To minimize this effect it is necessary to use for R_t a highly stable resistance which is large compared with $1/S_1 + 1/S_2$. This means that the circuit should be designed so as to give R' a high value also, and this, according to (5), can only be done by using large values for R_1 and R_2 . We have already noted that there are limits to the values we can give to these resistances, and this in fact means a limitation of the degree of feedback that can be adopted when rigorous stability requirements are imposed. In most cases the circuit will therefore be so designed as to obtain the highest possible figure of merit even without feedback, i.e. a Q as close to $\frac{1}{2}$ as a reasonable signal transmission permits. If we choose R_1, R_2, C_1 and C_k so as to satisfy (13), then in accordance with (9) and (5) we have:

$$Q = \frac{1}{2} \sqrt{\frac{C_1}{C_1 + C_k}} \text{ and } R' = \frac{1}{2}R_1.$$

If, for example, we now take $C_k = \frac{1}{4}C_1$ (to satisfy (13)) we must then make $R_2 = 5R_1$, then $Q = 1/\sqrt{5} \approx 0.45$. Since the maximum value of R' is equal to R_1 — i.e. when R_2C_k is large compared with $R_1(C_1 + C_k)$ — the signal transmission at $C_k = \frac{1}{4}C_1$ and $R_2 = 5R_1$ is still 50% of that of the maximum that can be achieved at a given value of R_1 . This can be regarded as a reasonable compromise.

In some cases, to ensure that the filter is satisfactorily stable in operation, R_1 and R_2 will have to be higher than is desirable from the point of view of the valves. When the relevant requirements are not too divergent, both can sometimes be met by connecting the anode of B_1 and/or the grid of B_2 to tappings on R_1 and R_2 respectively (see fig. 5). It can easily be seen that

the filter action is now governed by the total values of R_1 and R_2 , while only parts of these resistances are incorporated in the anode circuit of B_1 and the grid circuit of B_2 .

Two other limitations of the magnitude of the resistances may be mentioned, the first being the fact that very high resistances possessing high stability (metal film types) are difficult to produce. The other point is that parallel with R_2 is the input capacitance of the valve B_2 . If R_2 is high or the frequency for which the relevant filter was designed is not very low (e.g. a few hundred c/s) it may well be that the impedance of the input capacitance of B_2 is not to be disregarded, and since a capacitance of this kind is always a rather unstable quantity, it can have an adverse effect on the stability of the filter. The effect is more pronounced the higher the value of R_2 , and

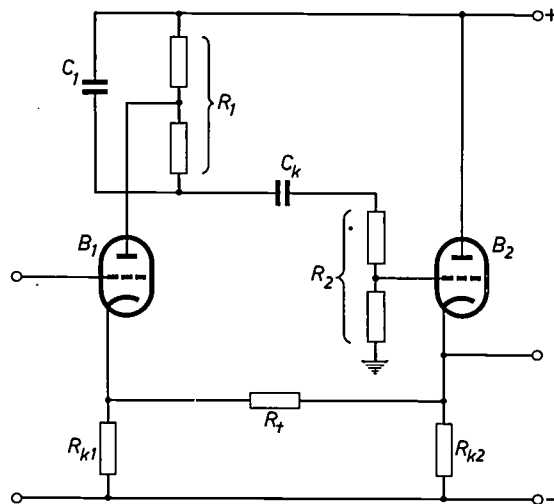


Fig. 5. The resistances in the anode circuit of B_1 and in the grid circuit of B_2 should sometimes be lower than the resistances R_1 and R_2 that govern the filter action. It may then be an improvement to connect the anode of B_1 and the grid of B_2 to tappings on R_1 and R_2 .

this too sets a limit to the permissible value of R_2 . A means of reducing the influence of the unstable input capacitance of B_2 is to connect a sufficiently large and stable capacitor in parallel with R_2 .

In this case the filter proper is formed by two resistors and three capacitors (fig. 6). From the equation giving the relation between V_{g2} and i_{a1} we find that for this circuit also we can draw an equivalent circuit as represented in fig. 3. Without going any further into this subject, it will be useful to give the equations which then take the place of (5) to (9):

$$R' = \frac{R_1 R_2 C_k}{R_1(C_1 + C_k) + R_2(C_2 + C_k)}, \dots (5')$$

$$L' = R_1 R_2 C_k, \dots (6')$$

$$C' = \frac{1}{C_k} (C_1 C_2 + C_1 C_k + C_2 C_k), \dots (7')$$

$$\omega_0 = \frac{1}{\sqrt{R_1 R_2 (C_1 C_2 + C_1 C_k + C_2 C_k)}}, \dots (8')$$

$$Q = \frac{\sqrt{R_1 R_2 (C_1 C_2 + C_1 C_k + C_2 C_k)}}{R_1(C_1 + C_k) + R_2(C_2 + C_k)}, \dots (9')$$

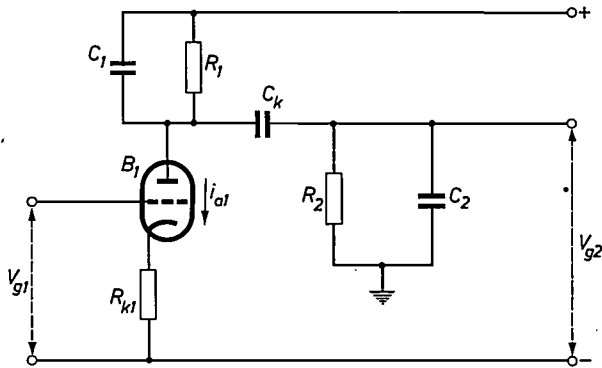


Fig. 6. When the frequency of the signals is not very low and /o the resistance R_2 is very high, the capacitance C_2 may have to be taken into account.

In this case too, as may be deduced from these equations, the maximum value of Q is equal to $\frac{1}{2}$. In this respect, then, the introduction of C_2 makes no difference.

Circuits of high stability

As has been shown, the principal objection to high stability of a filter designed along the lines described above, arises from the variations that may occur in the transconductance of the valves. Substantial improvements can be achieved in this respect by employing circuits in which the feedback is brought about in a different manner. For example, a marked improvement can be obtained by using for the feedback a separate valve, on the principle illustrated in the diagram in fig. 7. Valves B_1 and B_2 have the same functions here as in fig. 4. The anode circuit of B_2 now contains a resistance R_{a2} . The alternating anode voltage of B_2 is applied to the grid of B_3 , whose anode is connected to the anode of B_1 . (The DC biasing of the valves will not be dealt with here.) When the resistances R_{k2} and R_{k3} are very large compared with the reciprocal of the transconductance of the relevant valves, the alternating anode current of B_3 is:

$$i_{a3} = -V_{g2} \frac{R_{a2}}{R_{k2} R_{k3}}$$

This current, together with the alternating current from the anode of B_1 , is fed to the input of the actual filter. Here again, then, the strength of the feedback is determined primarily by a number of resistances, i.e. R_{a2} , R_{k2} and R_{k3} . The smaller the recip-

rocal values of the transconductances of B_2 and B_3 compared with R_{k2} and R_{k3} , the more accurately is this approximation satisfied, and since the latter resistances can readily be made higher than R_t in fig. 4, variations in the transconductance of the valves can easily be made to have less effect on the strength of the feedback in the circuit of fig. 7 than in that of fig. 4; the Q of the circuit in fig. 7 can therefore be more stable.

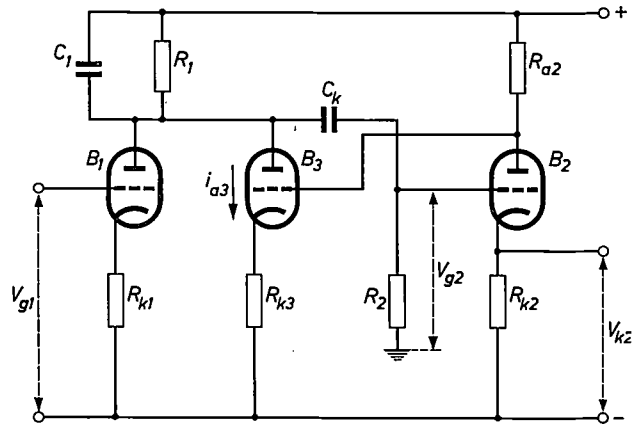


Fig. 7. The stability of the filter can be improved by using a separate valve B_3 for the feedback.

An even greater improvement can be made by using yet another valve, denoted B_4 in fig. 8. The operation of this circuit can again be understood by assuming that B_2 functions as an ideal cathode follower, and B_3 likewise. The alternating voltages on both the grid and cathode of B_3 are then equal to $-V_{g2} R_{a2} / R_{k2}$. If we now choose the values of R_2 and R_3 such that $R_2 : R_3 = R_{k2} : R_{a2}$, then the point

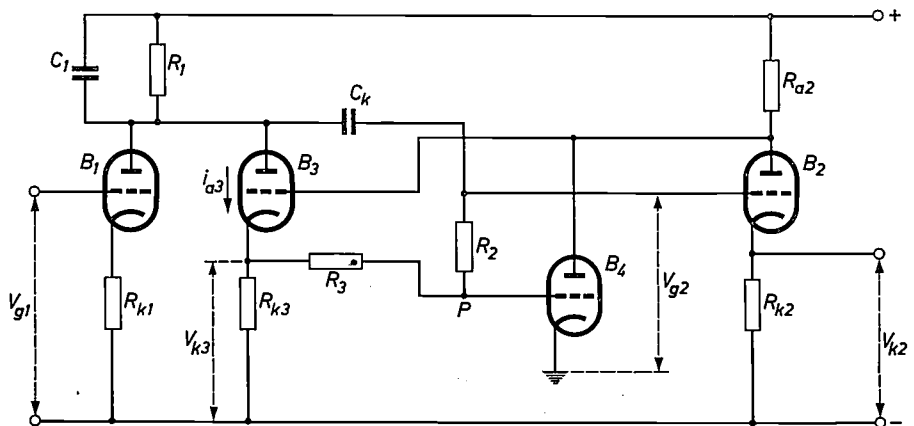


Fig. 8. Higher stability can be obtained by using a fourth valve B_4 , which makes the amount of feedback less dependent on variations in the transconductances of B_2 and B_3 .

P will carry no alternating voltage with respect to earth, and therefore no alternating anode-current will flow in B_4 . The operation of the circuit in fig. 8 is then identical with that in fig. 7. (The only difference is that fig. 7 contains the resistor R_{k3} for alternating current in the cathode lead of B_3 , whereas fig. 8 contains R_{k3} and R_3 in parallel.) Any change in this situation produces an alternating voltage at point P . This gives rise in B_4 to an alternating current which has a corrective effect, owing to the anode of B_4 being connected with that of B_2 . In this way, then, the voltages and currents always adjust themselves so that there is virtually no alternating voltage at point P , and it can easily be seen that in this case the ratio of the alternating current i_{a3} and the alternating voltage V_{g2} is governed solely by the resistances R_2 , R_3 and R_{k3} . Owing to

flat and broad top can be obtained by this method, using three tuned circuits, the figure of merit of one of them being half that of the two others, and the latter two being tuned to specific frequencies which are higher and lower than the resonant frequency of the first one. This principle can also be applied by using, instead of LC circuits, active filters on the principle described above; the alignment of the networks, however, is rather laborious as it is with passive filters.

Another method of obtaining a flat frequency characteristic with passive LC circuits is to couple circuits which are all tuned to the same frequency. This principle can also be applied to the active filters described here, the "coupling" being achieved by introducing negative feedback between pairs of filters.

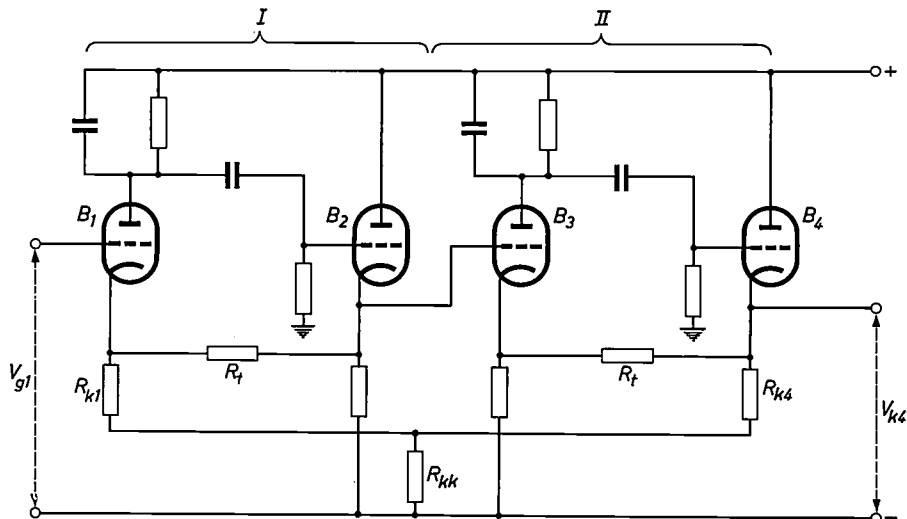


Fig. 9. Combination of two active filters, I and II, with negative feedback obtained by means of R_{kk} . The frequency characteristic achieved with this circuit corresponds to that of two coupled LC circuits.

the corrective effect of B_4 , variations in the transconductance of the valves have no effect on this ratio, and therefore the feedback is extremely stable, making it possible to give the figure of merit of the filter an exceptionally high and stable value.

Obtaining a flatter frequency characteristic

As we have shown, the frequency characteristic of a filter as drawn in figs. 4 to 8 corresponds to that of an LC circuit. In many cases a characteristic will be required that is flatter at the top and has steeper sides, as can be obtained for example with the aid of two or more non-coupled LC circuits whose resonant frequencies do not coincide (staggered tuning). A frequency characteristic having an exceptionally

An example of such a circuit is shown in fig. 9. The two filters are denoted by I and II. The negative feedback takes place via a common resistance R_{kk} introduced in the cathode lead of the first valve (B_1) in the first filter and of the second valve (B_4) in the second filter⁴⁾.

Making some simplifying assumptions, i.e. by treating B_2 and B_4 as ideal cathode followers and assuming that R_{kk} is small compared with R_{k1} and R_{k4} , it is

⁴⁾ Instead of the resistances R_{k1} , R_{k4} and R_{kk} , a delta connection of resistances might have been used. A drawback, however, is the very high value that would then be needed for the feedback resistor, which would be difficult to make with sufficient stability. In this respect the small resistance R_{kk} presents no difficulties.

easily computed that the relation between the output voltage V_{k4} and the input voltage V_{g1} is given by the expression:

$$V_{k4} = \frac{AV_{g1}}{(1+j\beta Q') + Ap} \quad \dots (15)$$

Here A is the gain of the circuit without negative feedback at the resonant frequency, i.e. at $R_{kk} = 0$, and $\beta = 0$, while

$$p = \frac{R_{kk}}{R_{k4}} \frac{R_t}{R_{k1} + R_t}$$

This quantity is thus a measure of the strength of the feedback. If we now take $Ap = 1$, say, then (15) becomes:

$$V_{k4} = \frac{AV_{g1}}{(1 + j\beta Q')^2 + 1} \quad \dots (16)$$

and the relation between the moduli of V_{k4} and V_{g1} is then given by

$$|V_{k4}| = \frac{A}{\sqrt{4 + \beta^4 Q'^4}} |V_{g1}| \quad \dots (17)$$

The behaviour of $|V_{k4}|/|V_{g1}|$ as a function of β is in this case identical with that in a band-pass filter consisting of two critically coupled LC circuits. The characteristic is flatter and has steeper sides than that belonging to a single LC circuit.

By using combinations of such filters with different "couplings" (Ap) it is possible to meet widely varying requirements with regard to the frequency characteristic. A filter as in fig. 4 can, for example, be connected in cascade with a filter as in fig. 9; with suitable dimensioning, a frequency characteristic can then be obtained corresponding to that of three LC circuits with staggered tuning. The conformity of the equations makes it possible to treat the design of such configurations mathematically in the same way as the design of filters using LC circuits.

Filters I and II in fig. 9 are circuited on the principle represented in fig. 4. Obviously, to achieve greater stability one can also use the circuits of fig. 7 or fig. 8 as "building bricks".

Low-pass filters

The filters described above are of the band-pass type, that is to say the frequency band which is transmitted by the filter is limited on both the low and high frequency sides. For certain experiments, however, *low-pass* filters are wanted, i.e. filters which pass all signals components with frequencies below a certain critical frequency. A filter of this type is approximated in the first instance by a single resistor and a single capacitor (see fig. 10). One can think of

a low-pass filter as being derived from the band-pass type by making the capacitance C_k infinitely large, i.e. by short-circuiting it, thus making the resonant frequency zero. (The resistors R_1 and R_2 in fig. 2 are now in parallel for alternating current and in fig. 10 are replaced by a single resistance R .)

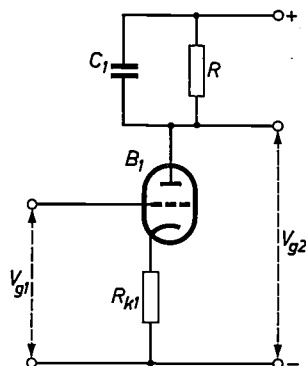


Fig. 10. AC circuit for a low-pass filter.

Introducing feedback here in the same way as represented in fig. 4, we obtain the diagram shown in fig. 11. The relation between input and output signal is now:

$$V_{k2} = V_{g2} = -V_{g1} \frac{R_t + R_{k1}}{R_t - R} \frac{R}{R_{k1} \left(1 + j\omega \frac{R_t}{R_t - R} C_1 R \right)} \quad \dots (18)$$

It can be seen from this that the feedback has the same effect on the frequency characteristic as increasing C_1 by a factor $R_t/(R_t - R)$. For limiting the pass-band to very low frequencies it will be easier to use a high value of C_1 than to introduce feedback, and the latter will therefore seldom be used for a simple low-pass filter.

The situation is different, however, if here too use is made of the possibility of connecting two stages in cascade and introducing negative feedback. An

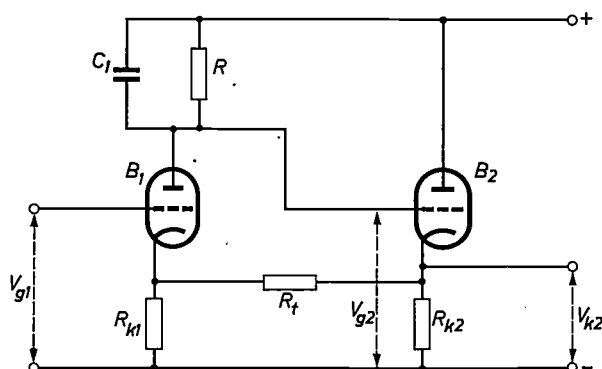


Fig. 11. Low-pass filter with feedback. The effect of the feedback on the frequency characteristic is the same as that of an increase in the capacitance C_1 .

arrangement of this kind is shown in *fig. 12*, using two identical filters and negative feedback via the resistor R_{tk} ⁵⁾. Assuming again that the resistances in the cathode leads are very high, we can derive the following expression for the relation between the output voltage V_{k3} and the input voltage V_{g1} :

$$V_{k3} = \frac{A(1+p)V_{g1}}{(1+j\omega C_1 R)^2 + Ap} \dots (19)$$

Here $A = R^2/(R_{k1}R_{k2})$ and $p = R_{k1}/R_{tk}$. Since we have assumed that R_{k1} , R_{k2} and R_{k3} are very large,

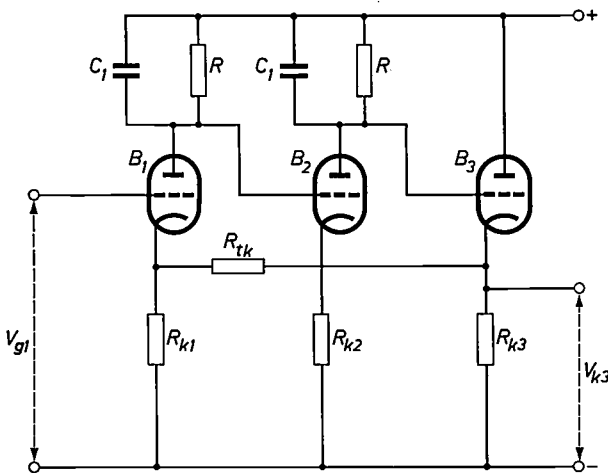


Fig. 12. Low-pass filter consisting of the cascade arrangement of two identical filters as in *fig. 10*, negative feedback being introduced by means of the resistance R_{tk} .

A is the gain of the circuit at zero frequency and with the negative feedback out of operation (i.e. at $R_{tk} = \infty$). Further, p is a measure of the strength of the negative feedback.

From (19) it follows that for $\omega = 0$ the output voltage is:

$$V_{k3.0} = \frac{A(1+p)V_{g1}}{1+Ap} \dots (20)$$

In *fig. 13* the ratio

$$\left| \frac{V_{k3}}{V_{k3.0}} \right| = \left| \frac{1+Ap}{(1+j\omega C_1 R)^2 + Ap} \right| \dots (21)$$

is plotted as a function of ω for various values of Ap ,

⁵⁾ Since neither of the two individual filters is provided with feedback, this circuit can be designed with only three valves, whereas in *fig. 9* four valves were needed. Furthermore, unlike *fig. 9*, the negative feedback here is obtained with a delta connection of the resistances R_{k1} , R_{k3} and R_{tk} . The reason for this is that, owing to the absence of feedback in the individual filters, the total gain in *fig. 12* is much smaller than in *fig. 9*. To obtain sufficient effect from the feedback, a common resistance in series with R_{k1} and R_{k3} would therefore have to be much larger than R_{kk} in *fig. 9*. In this case the introduction of a resistance between the cathodes of B_1 and B_3 is a better solution, because such a resistance has less influence on the DC biasing of the two valves.

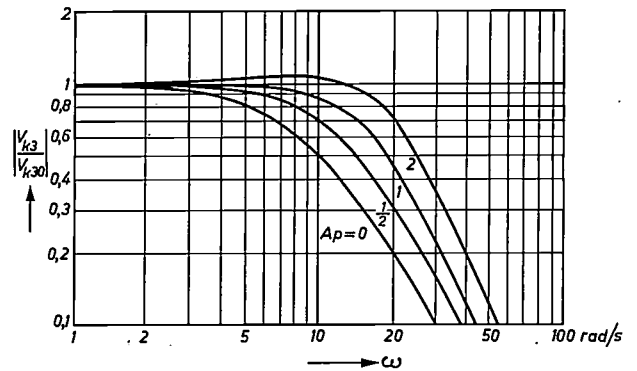


Fig. 13. Frequency characteristics for a low-pass filter as in *fig. 12*.

keeping the product $C_1 R$ constant for all curves (0.1 s). The curve drawn for $Ap = 0$ applies to the case without negative feedback. Comparison with the other curves shows that the use of feedback can lead to a much flatter frequency characteristic, which cannot be obtained with passive RC circuits.

With low-pass filters too, it is possible to build more extensive networks by combining filters having different $C_1 R$ values. By suitable dimensioning, curves can be obtained which are even flatter at the top and have a steeper descending portion.

Application as a delay network

The analogy existing between LC circuits and the active filters described above makes it possible to use these active filters in cases where it is required to delay signals of extremely low frequency without causing any distortion. This can be useful, for example, when building an electrical analogue of a control system involving transmission lags. An electrical analogue of this type can be used for analyzing the stability conditions of the control system.

Where a network is required to transmit each signal undistorted but with a certain retardation, the phase delay must be independent of the frequency, and consequently the phase shift suffered by the various components must be proportional to their frequencies. Furthermore, the amplitude ratio between input and output must be independent of the frequency.

A familiar circuit with which this can be realized in a limited phase-shift region is shown in *fig. 14a*. A less familiar circuit with which the same results can be achieved, and which offers advantages in connection with the following considerations, is given in *fig. 14b*. Assuming for simplicity that R_1 and R_2 are large with respect to R and R_k , and choosing the resistances so as to satisfy the equation:

$$\frac{R_1}{R_2} = \frac{2R_k}{R}, \dots (22)$$

then the relation between V_g and V_u is given by:

$$\frac{V_g}{V_u} = \frac{R_1 + R_2}{R_2} \frac{1 + j\omega C_1 R}{-1 + j\omega C_1 R} \quad (23)$$

The modulus of this expression is indeed independent of ω , and the argument is $2 \tan^{-1} \omega C_1 R \pm 180^\circ$. The voltage V_u thus lags in phase behind V_g by an angle $2 \tan^{-1} \omega C_1 R \pm 180^\circ$. We shall henceforth consider only the frequency-dependent term $\varphi = 2 \tan^{-1} \omega C_1 R$ of this phase shift, since the constant quantity $\pm 180^\circ$ can be compensated, e.g. by

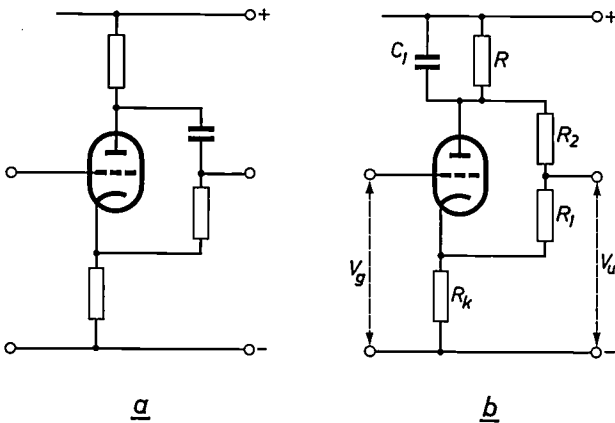


Fig. 14. Circuits in which the signals have a constant phase lag within a limited frequency range, and a constant ratio between the amplitudes of input and output signal.

using two stages in cascade. In fig. 15 curve *a* gives the variation of φ as a function of ω . At small values of $\omega C_1 R$, then, $\tan^{-1} \omega C_1 R \approx \omega C_1 R$, and therefore φ is approximately proportional to ω . This applies, however, only up to a limited value of φ (e.g. 60°). The proportionality region can be extended by con-

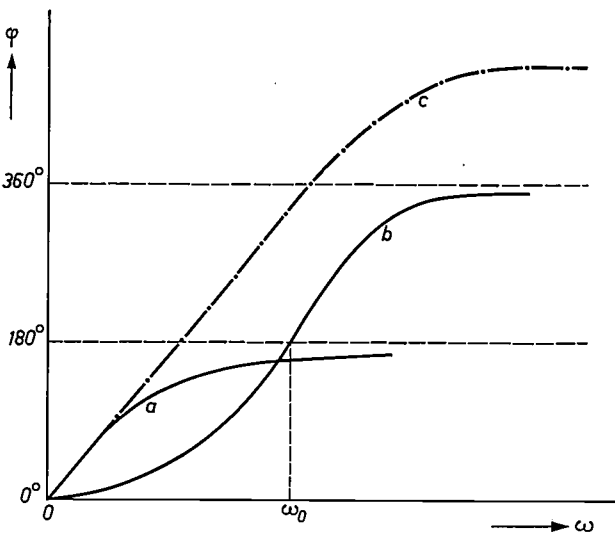


Fig. 15. Phase characteristic of the circuits in fig. 14 (a) and of the circuits in figs. 16 and 17 (b). Connected in cascade and suitably dimensioned, these circuits give the phase characteristic *c*.

necting in cascade with a circuit as in fig. 14 one or more elements whose phase characteristics have linear portions at frequency values differing from zero. This can be done with a circuit as shown in fig. 16, for example, which differs from that in fig. 14b in that the anode circuit of the valve contains an LC circuit instead of the CR combination. In this configuration the following relation exists between V_g and V_u :

$$\frac{V_g}{V_u} = \frac{R_1 + R_2}{R_2} \frac{1 + j\beta Q}{-1 + j\beta Q} \quad (24)$$

(Here β again represents $\omega/\omega_0 - \omega_0/\omega$.) The voltage V_u now lags in phase behind V_g by an angle $2 \tan^{-1} \beta Q \pm 180^\circ$. Fig. 15 gives a plot of $\varphi = 2 \tan^{-1} \beta Q + 180^\circ$ as a function of ω (curve *b*). Using circuits as in fig. 14 and fig. 16 connected in cascade, a phase shift is obtained between input and output voltage which can be found by adding the ordinates of curves *a* and *b* (curve *c*). Choosing suitable circuit values we can now obtain a linear variation over a much wider region than is possible using a circuit as in fig. 14 alone.

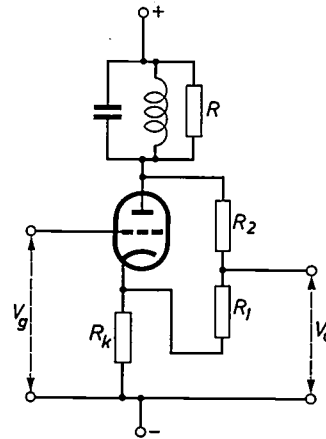


Fig. 16. Circuit giving a phase characteristic that has a linear portion round a frequency differing from the value zero.

The principle described can also be applied at very low frequencies when a filter as in fig. 4 is to be used instead of an LC circuit. The voltage divider between input and output can be produced by using two resistors R_{t1} and R_{t2} instead of the feedback resistor R_t in the circuit shown in fig. 17. The ratio of these resistances should now satisfy the expression:

$$\frac{R_{t1}}{R_{t2}} = \frac{2R_{k1}}{R'} \quad (25)$$

where R' is given by (5). By means of a cascade arrangement of the circuits of fig. 14 and fig. 17, we can thus obtain a phase characteristic of the form represented by curve *c* in fig. 15.

The "proportionality region" can be still further extended by adding to the circuit one or more filters as in fig. 17, having different resonant frequencies. If these resonant frequencies and the figures of merit are properly chosen, a phase characteristic can be obtained which is almost linear in a wide range of frequencies from zero upwards. This

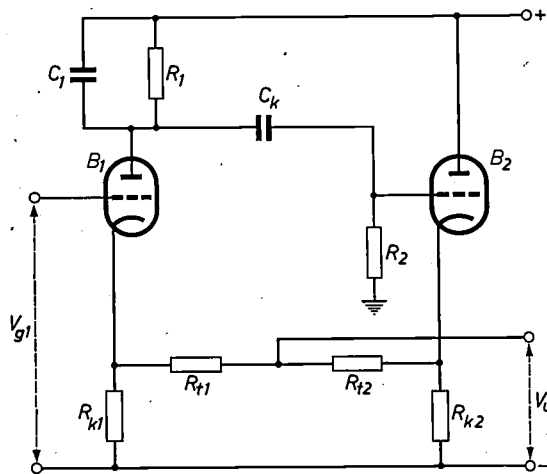


Fig. 17. Circuit which, suitably dimensioned, can be made identical at low frequencies with a circuit as shown in fig. 16.

means that signals that possess components lying only in this region have a constant phase delay and therefore undergo a certain delay without any distortion. The figures of merit of the various circuits connected in cascade should, to a good approximation, be virtually proportional to the resonant frequencies. This implies that some of these filters require a fairly high Q , which, within certain limits, can be achieved by means of feedback.

Final considerations

In the foregoing we have referred to the analogy existing between certain filters composed of resistances and capacitances, and filters using one or more LC circuits. In conclusion we should point to a *difference* between these two circuits that can be of importance in practical applications, namely the fact that the feedback employed to achieve a reasonably high figure of merit causes an increase in the *noise level*. Because of this fact, filters based on the principle described in this article can only be used when the signal level is sufficiently high, higher than that at which filters with LC circuits can be employed.

Finally, it may be mentioned that circuits on the principles described here can also be designed with transistors. In this case, however, the input resistance is much smaller than with valves, which restricts the choice of the circuit elements that can be used.

Summary. Certain active electric networks composed of amplifying valves, resistors and capacitors have characteristics that correspond to those of passive networks containing inductors. At very low frequencies, where coils have certain disadvantages, good use can be made of active networks of this kind. The authors discuss the design of band-pass and low-pass filters, using feedback to achieve a reasonably high figure of merit. They also deal with various circuits for giving these filters exceptionally high stability.

By connecting two filters in cascade and using negative feedback, a frequency characteristic corresponding to that of two coupled LC circuits can be achieved. Finally, reference is made to the possibility of designing networks in this way whose amplitude characteristic is flat within a given frequency range and whose phase characteristic is practically linear, so that signals only containing components in this frequency range can pass through these networks with a certain delay without suffering distortion.

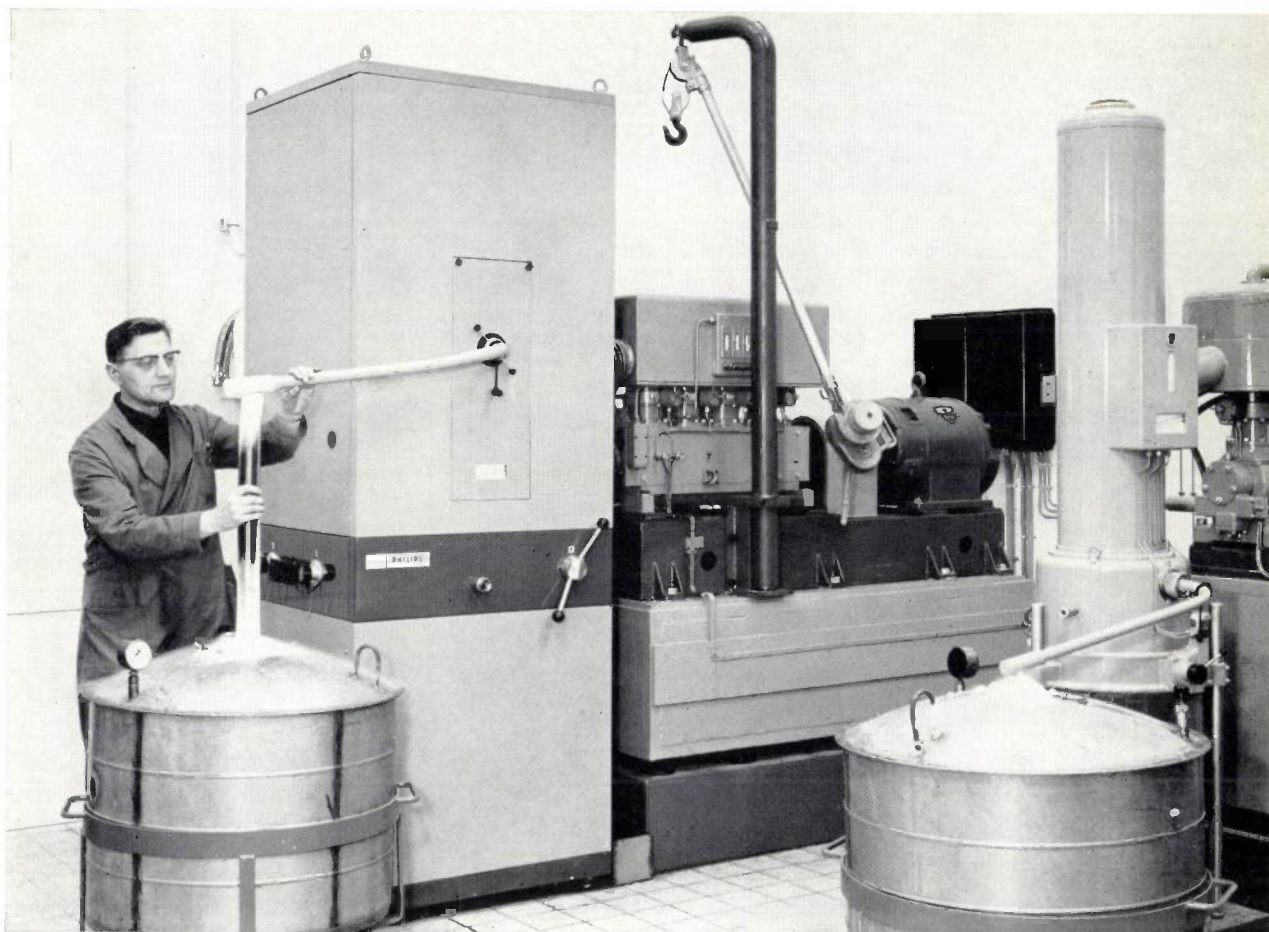
PRODUCTION CENTRE FOR LIQUID NITROGEN

In the last ten years many laboratories have been equipped with a Philips gas refrigerating machine, enabling them to supply their own liquid air requirements. Since in many cases there is a preference for pure liquid nitrogen, many of these machines are used in combination with an air fractionating column, also developed by Philips, which is adapted to the gas refrigerating machine. In our own laboratories — as elsewhere — it is found that the ease with which the liquid air or nitrogen can be obtained greatly stimulates its use. The small installation earlier described ¹⁾ ²⁾, which in its present form delivers 6.5 litres of liquid nitrogen an hour, often

turns out after some time to be too small. With this in mind, a gas refrigerating machine has been developed which combines four of the original single-cylinder machines. A larger air fractionating column adapted to the large machine is also available.

The photograph on p. 341 was taken in the liquid air

- 1) J. W. L. Köhler and C. O. Jonkers, Fundamentals of the gas refrigerating machine, and Construction of a gas refrigerating machine, Philips tech. Rev. 16, 69-78 and 105-115, 1954/55.
- 2) J. van der Ster and J. W. L. Köhler, A small air fractionating column used with a gas refrigerating machine for producing liquid nitrogen, Philips tech. Rev. 20, 177-187, 1958/59.



production centre in the new research building recently opened by Philips³⁾. Partly visible on the far right is a gas refrigerating machine of the single-cylinder type; beside it is the air fractionating column in which the liquid nitrogen is separated. In the centre is the four-cylinder version, with the large air fractionating column in the tall cabinet on the left. This installation delivers liquid nitrogen with a purity better than 99.5%. Production can be regulated to between 15 and 30 litres per hour. The liquid nitrogen is collected in the round vessels in the foreground.

A special feature of the methods of separation and condensation employed is that the air, and the nitrogen to be separated from it and condensed, is nowhere subjected to compression. Apart from the spaces in the gas refrigerating machine where the low-temperature generating Stirling process takes place, the pressure remains atmospheric in all parts of the equipment.

The large installation can operate continuously until it has produced about 7000 litres of liquid nitrogen. The quantity limit is governed by the process of removing the water vapour and carbon

dioxide from the air to be condensed. This is done by a "snow separator"⁴⁾. The snow separator is filled to maximum capacity after the production of some 7000 litres of liquid nitrogen. After defrosting — which takes about 5 hours and for which warm air is used — a running-up period of about 1.5 hours is needed before the installation is ready for use again. The warm air is supplied by auxiliary apparatus (not visible in the photograph) which can be connected to the installation. The crank-handle with the two black knobs, which can be seen on the front of the cabinet containing the large air fractionating column, therefore has three positions: running up, operation, defrosting. The small knob to the left of the handle is used for controlling the flow of exhausted oxygen, so as to give the nitrogen the required purity. The panel immediately above this knob contains two liquid pressure gauges, which give readings of the air intake and the oxygen exhaust.

The hoisting tackle on the gas refrigerating machine serves for lifting the head of the machine for periodic maintenance.

³⁾ Philips tech. Rev. 24, 339, 1962/63 (No. 11/12).

⁴⁾ C. J. M. van der Laan and K. Roozendaal, A snow separator for liquid-air installations, Philips tech. Rev. 23, 48-54, 1961/62.

SUBJECT INDEX, VOLUMES 16-25

Figures in bold type indicate the volume number, and those in ordinary type the page number. For subjects dealt with in volumes 1-15 the reader should refer to the respective decennial indexes at the end of volumes 10, 15 and 20.

- Absorption wedges, circular optical — 22,402
 Acaricides, see "Tedion V 18"
- Accelerators for elementary particles:
 generator for fast neutrons 17,109
 sealed neutron tube 23,325
 practical importance of — (inaugural address Oosterkamp) 24, 1
 see further Cyclotron and Linear electron accelerators
- Acoustics, see Sound
- Aerials:
 for radar (Luneburg lens) 22, 29
 see further Radio receivers, aerials
- Agrobiological research:
 laboratory for — 16,353
 control of animal pests 17,146
 fungicides 17,222
 growth substances in plants 17,294
 formulation of pesticides 19,165
 "Tedion V 18", experiments with radioactive isotope 21,276
 balance of nature 23,101
- Aircraft and lightning 16,296
- Air engine, new construction with rhombic drive mechanism 20,245
- Airfield beaconing:
 design and light sources 16,273
 supply units 17, 10
- Air fractionating } see Refrigerating technique
 Air liquefier }
 Alkali halides, lattice imperfections studied on — 20, 69
- Alloy-diffusion technique for manufacturing HF transistors 24,231
- Ambiophony, see Sound, modern acoustical techniques
- Amplifiers:
 for carrier telephony 16,287
 pre-amplifier for pick-up (AG 9005) 18,238
 with single-ended push-pull output 19, 41
 wide-band — with 7 cm disc-seal triode 19,145
 10 W wide-band — with 7 cm disc-seal triode 21, 41
 75 cm — for radio-astronomy (with EC 157) 21,317
 see also Difference amplifiers and Noise
- Amplifying valves:
 noise in —, see Noise
 professional — 18,181
 disc-seal triodes for cm waves:
 EC 57 18,317
 EC 59 20,225
 with metal-ceramic wall (OZ 92) 21,104
 experimental 5 cm triode various applications 22, 16
 see also Amplifiers
- sub-miniature valves:
 construction 18,217
 tungsten wire for — 18,222
- Ampliscope ("harmonizing" X-ray images) 24,285
- Analogue computers:
 for determining colour point of light source 23,118
 plotting of electron trajectories with resistance network and — 23,352
- Analysis:
 gas —, see Omegatron
 spectrochemical — with X-rays 17,269
- Antennae, see Aerials
- Arc welding, see Welding
- Atmosphere, exploration with radio waves 22, 61
- Automation:
 of filament-coiling machine 21,309
 automatic digital photometer for testing incandescent lamps 23,244
 see further Mechanization and Numerical control
- Balance of nature (inaugural address Van der Veen) 23,101
- Ballasts for gas-discharge lamps:
 noise emission of — 18,110
 • small — (in polyester resin) 18,279
 life of transformers and chokes 20, 59
 life of capacitors 20,162
- Barium getter films 19,290
- Barium titanate for capacitors 17,129
- Beacons:
 microwave — with multi-reflex klystron 24,184
 airfield beaconing } 16,273
 } 17, 10
- Beam extraction, see Cyclotron
- Beam transmitters:
 with double FM 17,317
 frequency stabilization for — 17,334
 wide-band amplifier using 7 cm disc-seal triode 19,145
 10 W wide-band amplifier using 7 cm disc-seal triode 21, 41
 relay stations for — using disc-seal triodes 22, 16
 transmitting valves for —:
 multi-reflex klystron 17,328
 disc-seal triodes } 18,317
 } 20,225
- Beamed light sources, automatic recording of isocandela diagrams } 20,288
 } 23,278
- Bearings:
 magnetic journal bearing 22,232
- contactless —, principle 25,253
 gas — 25,259
 spiral-groove — 25,265
- Bend tests, machine for — 17,246
- Beta radiation, measurement of weak — 20,170
- Binaural hearing, see Stereophony
- Bitter patterns for investigation of magnetization reversal process 24,244
- Brussels World Fair (Expo) 1958:
 Philips pavilion (4 articles) 20, 1
 "Electronic Poem" 20, 37
- Bulb-blowing machines 22,320
- Cadmium sulphide:
 photoresistors using — 20,277
 etch pits on — 22,266
- Calculating machine of Blaise Pascal 24,102
- Camera tubes for TV, see Television camera tubes
- Capacitors:
 materials with high ϵ 17,129
 life in ballasts 20,162
 precision variable — 20,234
- Car headlamps:
 with an asymmetric dipped beam 16,351
 bulbs, inspection of filament (photograph) 24,180
 with iodine lamps 23,242
- Car radio 24, 27
- Carbon-arc image furnace for zone melting of oxides 23,161
- Cardboard, reduction of trim-losses with computer 24,121
- Cardiography, vector-electro— 21, 24
- Cardiotachometer for continuous measurements 21,304
- Carrier telephony, feedback amplifier for — 16,287
- Cascade generator, see High-tension generator
- Cathodes:
 dispenser —, q.v.
 oxide —, q.v.
 thoriated-tungsten — in } 19,118
 transmitting valves } 20,301
- Cathode-ray tubes:
 secondary emission from the screen 16, 26
 sedimentation of screens 16,232
 rectangular — of high aspect ratio 18,298
 low-voltage — 19,159
 oxide cathode with half-watt heater for — 23, 22
 measurement of intensity distribution in spot 25,152
 see also Television picture tubes
- Cheater circuits for testing of thyatrons 16, 43

- Chladni's figures on vibrating capacitor 19, 84
 Chokes, life in ballasts 20, 59
 Cinefluorography, see X-ray image intensifier
 Cinema projection, see Film projection
 Cleating, improved method of — 19,268
 Clinical thermometer 17,255
 CO₂ welding 24, 20
 Coil winding, orthocyclic — 23,365
 Coiling machine, see Filament-coiling machine
 Coiless filters for low frequencies 25,330
 Cold-cathode tubes Z 800 U, Z 801 U 18,128
 Colour point, analogue computer for — of light source 23,118
 Colour rendering of "TL" lamps 18,249
 Colour television, see Television, colour —
 Complex quantities at varying frequencies, cathode-ray display 18,380
 Computers, analogue —, see Analogue computers
 Computer, count-rate — 17,249
Computers, digital electronic:
 random-access magnetic-core memories for — 20,193
 the PASCAL 23, 1
 listening in to the PASCAL 24,164
 applications:
 magnetic field of isochronous cyclotron 24,106
 reduction of trim-losses of corrugated cardboard 24,121
 potential fields, electron trajectories 24,130
 vacuum deposition of resistors 24,144
 design of loudspeaker magnets 24,150
 solving a chessboard puzzle 24,157
 Condensers, see Capacitors
 Contact microradiography } 17, 45
 } 19,221
 Contactless bearing, principle 25,253
Control engineering and theory:
 electronic control of industrial processes 17, 21
 control of operating parameters in suspension reactor of KEMA 21,121
 automatic control in glass manufacture 22,311
 theory of linear control systems 23,109
 loop gain and stability 23,151
 non-linear recording instrument in control system 23,167
 Converters, see DC/AC converters
 Corrugated cardboard, reduction of trim-losses with computer 24,121
Counters:
 monitor for radioactive contamination 16,201
 with decade scaler tubes (E 1 T) 16,360
 transistorized monitor 21,201
 indicator tube for transistorized decade — 21,267
 scintillation counter, q.v.
 see also Counter tubes
 Counter, particle — 21,253
 Counter, preset, for automatic control of filament-coiling machine 21,309
Counter tubes:
 Geiger-Müller —:
 ring of — for thyroid examination 18, 87
 for X-ray analysis 18,262
 guard counter for weak beta radiation 20,170
 scintillation counter, q.v.
 X-ray intensity measurement with —:
 diffractometer 16,123
 methods 17,206
 count-rate computer 17,249
 X-ray spectrochemical analysis 17,269
 design and properties of counter tubes 18,262
 proportional counter tube for X-rays 18,264
 see also Counters
 Crackle-free potentiometer 20,283
Crystals:
 structure determination with X-rays 22,126
 structure determination with neutrons 23, 69
 lattice imperfections in ionic — 22,362
 see also Germanium and Silicon
Cyclotron:
 CERN 600 MeV synchro—:
 design 22,142
 radio-frequency system 22,149
 tuning-fork modulator 22,162
 Chladni's figures on vibrating capacitor 19, 84
 Orsay 160 MeV synchro— with beam-extraction system 23,381
 investigation of magnetic field of isochronous — 24,106
DC/AC converters:
 vibrator — 16,118
 centrifugal (mercury jet) — 18, 13
 transistor — 20,362
 using Si controlled rectifiers 23,272
 Deaf-mute children, musical instrument for — 18,276
 Deformation of metals 16,341
 Delay lines, ultrasonic 25,234
 Delta modulation 24,355
 Delta Project Netherlands, study of littoral drift 21,157
 Deposition of circular absorption wedge 22,402
 Deposition of resistors 24,144
 Dew-point hygrometer using Peltier cooling 21,196
Diamond:
 — dies 16, 91
 styli for gramophone pick-ups 19,324
 orientation of — for tools 21,178
 Dichroic mirrors } 19, 59
 } 24,263
 Dielectric constant, materials with high — 17,129
Difference amplifiers:
 general considerations 22,345
 circuits for — } 23,142
 } 23,173
 with rejection factor > 10⁶ 24,275
 application in cardiology 21, 24
 Diffusion studies with tracers, grinding machine 25,191
 Digital electronic computers, see Computers, digital electronic
 Directional hearing, see Stereophony
Directional isolators:
 application of ferroxcube for — 18,158
 for 8 mm and 4 mm waves 22, 11
 Discharge flash lamps, see Flash lamps, electronic
 Discharge tubes, see Gas-discharge tubes
 Disc-seal triodes, see Amplifying valves
Dislocations:
 generation of — by thermal stresses 19,357
 Ge crystals free of — 21,340
 influence in metals, semiconductors and ionic crystals 22,362
 projection topographs of — 23, 82
Dispenser cathodes:
 introduction 19,177
 pressed cathode 19,179
 impregnated cathode 19,186
 machining of tungsten for impregnated cathodes 17, 97
 L cathode, application in disc-seal triode EC 57 18,317
 in magnetrons } 21, 1
 } 23,316
 } 25,217
 Displacement measurements, determining magnetic quantities by — 25,207
 Displacement pick-up 17, 63
 Donders, F.C., reaction-time research by — 25, 75
 DONDERS, electronic system for measuring human reactions 25, 64
Doping:
 preparative methods of Ge and Si 21,185
 inhomogeneities in Ge and Si 25,195
 see further Solid-state research
Dosimetry:
 pocket dosimeter for X-radiation and gamma radiation 16,134
 of very weak X-radiation 19,264
 dosimeters for therapy and diagnostics 23, 55
 "Duvadilan" (vasodilating pharmaceutical) 24, 69
 Electret with photoconductor 23,310
 Electroluminescence 19, 1
Electrolytic tank:
 study of thermal-conductivity problems 18, 52
 automatic plotting of electron trajectories 22,245
 Electrometer, vibrating capacitor for — 25, 95
 Electron emission, secondary, see Secondary emission
 Electron gun for picture tubes 18, 73
Electron microscope:
 of simplified construction (EM 75 kV) 17, 47

- emission —:
 demonstration austenite-pearlite transformation 16,337
 construction 18, 1
 ultramicrotome for — specimens 17,178
 investigation of SiC whiskers 24,181
 — photographs:
 ferroxdure 18,237
 "Ticonal" } 19, 11
 } 24,380
- Electron trajectories:**
 focusing in X-ray tubes . . . 20,291
 plotting — with electrolytic tank 22,245
 plotting — with resistance network and analogue computer 23,352
 calculation of — with digital computer 24,130
- Electron tubes:**
 microphony in — 22, 71
 cold-cathode tubes Z 800 U, Z 801 U 18,128
 see further:
 Amplifying valves
 Cathode-ray tubes
 Television camera tubes
 Television picture tubes
 Thyratrons
 Transmitting valves
- Electronic control of industrial processes 17, 21
 Electronic games 17,362
 Electronic music, see Music
 "Electronic Poem" at Brussels World Fair 1958 20, 37
 Electronics in the wood industry 23, 29
 Electroscope 16,134
 Enamelled wire, manufacture and testing 23,342
- Entropy:**
 concept of — 16,258
 examples and applications } 16,298
 } 16,321
 — and information 18,201
- Etch pits:**
 study of dislocations based on — 21,342
 on CdS 22,266
 on ZnS 24, 61
- Experiments, science of — (statistical series design; inaugural address Hamaker) 22,105
 Expo, see Brussels World Fair (Expo) 1958
- Faraday cage 23,155
- Faraday effect:**
 application in unidirectional waveguides 18,158
 observation of Weiss domains by means of — 19,286
- Feedback amplifiers for carrier telephony 16,287
- Ferrites, see:
 Ferroxcube
 Ferroxdure
 Ferroxplana
 Gyromagnetic resonance
- Ferroceptor 16,186
 Ferro-electricity, application in capacitors 17,129
- Ferromagnetic resonance (gyromagnetic resonance) { 18, 82
 } 18,158
 } 19,304
- Ferroxcube:**
 with rectangular hysteresis loop:
 theory and properties . . . 16, 49
 switching time 18,336
 application for magnetic-core memories 20,193
 magnetization reversal process 24,242
- various applications:
 inductive aerial 16,186
 inductive aerial for FM amplitude modulation of centimetre waves 18, 82
 in unidirectional waveguides 18,158
 piezomagnetic vibrators 18,285
 pulse transformer 19, 28
 magnetic-core memories 20,193
- Ferroxdure:**
 crystal-oriented — (ferroxdure II and III) 16,141
 electron-microscope photograph 18,237
 comparison with other materials 18,358
 topotaxy with — 20,354
- applications:
 magnetodynamic gramophone pick-up 18,101
 pulse transformer 19, 28
 loudspeaker magnets . . . 24,150
- Ferroxplana:**
 development and properties 18,145
 crystal-oriented — 19,209
 topotactically oriented — . . . 20,354
 analysis of crystal structure 22,135
- Filament-coiling machine:**
 automatic control 21,309
 visual inspection 22,239
- Filament lamps, see Incandescent lamps
- Film projection:**
 professional 16 mm projector 16,158
 projector for 70 mm and 35 mm film ("Todd-A.O.") 17,299
 mirror-condenser lamp for 8 mm — 19,233
 with pulsed light source (FP 20 S with SPP 800 W) 21, 73
 projector of simplified design (FP 20) 21, 83
- Filters, active (coilless), for low frequencies 25,330
- Fingerprinting via total internal reflection 24,271
- Fittings, temperatures in — for incandescent lamps 21,300
- Fizeau fringes, intersecting, observed with interference mirror 23,380
- Flash bulbs (type "Photoflux"):**
 with simplified cap 16, 88
 ignition with capacitor . . . 16,333
- Flash lamps, electronic-:**
 design and properties . . . 16, 13
 recent developments 22,377
- Fluctuations, see Noise
- Fluorescent lamps:**
 with directional light distribution ("TL" F) 17,198
- in a starterless circuit } 17,288
 ("TL" M) } 18, 17
 with natural colour rendering ("TL" de luxe) 18,249
 double-flux "TL" lamp 19,333
 with increased luminous efficiency 25,114
 radio interference from — . . . 20,135
 supply of — in vehicles:
 with direct current ("TL" C) 18, 11
 with centrifugal converter 18, 13
 with resistor converter 20,362
 with converter using Si controlled rectifier . . . 23,272
 ballasts, q.v.
 see also Lighting
- Fluorescent screen for colour TV 23,133
- Flying-spot scanner, see Television, flying-spot scanner
- Focusing of X-ray tubes 20,291
- Foucault pendulum in United Nations building 19,236
- Fracturing of steel resulting from hydrogen 24,252
 "Frena" and "Frenac" 19, 73
- Frequency modulation:**
 FM reception with strong interference 22,352
 multipath-transmission effects 22,393
 beam transmitter with double FM } 17,317
 } 17,334
 see further Radio receivers
- Fungicides, see Agrobiological research
- Gallium phosphide, P-N luminescence } 22,360
 } 25, 20
- Gamma radiation:**
 pocket dosimeter 16,134
 monitor for nuclear reactor 19,278
 reduction of — background 20,170
 scintillation counter } 20,209
 } 20,263
- Gas analysis, see Omegatron
- Gas bearings 25,259
 Gas binder, barium film 19,290
- Gas-discharge lamps:**
 ballasts for —, q.v.
 see further:
 Flash lamps, electronic-
 Fluorescent lamps
 Mercury lamps
 Sodium lamps
- Gas-discharge tubes:**
 cold-cathode tubes Z 800 U, Z 801 U 18,128
 indicator tube for counter . . . 21,267
 see also Thyratrons
- Gas laser, small stable — 24, 95
- Gas refrigerating machine, see Refrigerating technique
- Gas spectroscopy, microwave — 22,187
- Geiger-Müller tubes, see Counter tubes
- Germanium:**
 — diodes:
 theory and construction 16,213
 application of point-contact Ge diodes 16,225
 dislocations in — 19,357

- preparative methods (zone melting, floating crucible) . . . 21,185
 dislocation-free — crystals . . . 21,340
 inhomogeneities in doped — crystals . . . 25,195
 — transistors, see Transistors
 Getter films, barium — . . . 19,290
 Getter ion-pump . . . 22,260
- Glass:**
 sealing of window and cone of picture tubes . . . 19,318
 demountable seals for — . . . 22, 53
 — throughout the Ages . . . 22,282
 structure (e.g. invert glasses) . . . 22,300
 automatic control in — manufacture . . . 22,311
 bulb-blowing machines . . . 22,320
 testing of materials for glass-to-metal seals . . . 22,337
 Glazes, gloss point . . . 17,153
- Gramophones:**
 fabrication of records . . . 17,101
 fabrication of sapphire and diamond styli for pick-ups . . . 19,324
 high notes, reproduction . . . 18, 89
 magnetodynamic pick-up . . . 18,101
 recorded velocities on stereophonic test records . . . 23, 89
 Grid emission of various materials . . . 19,123
 Grinding machine for tracer diffusion studies . . . 25,191
 Growth substances in plants . . . 17,294
 Guard counter . . . 20,170
- Gyrator:**
 a new network element . . . 18,120
 realization for microwaves . . . 18,158
- Gyromagnetic resonance (ferromagnetic resonance)** . . . 18, 82
 . . . 18,158
 . . . 19,304
-
- Hall coefficient, measurement . . . 20,220
 Harbour radar of Rotterdam . . . 20,349
- Hearing:**
 — aids . . . 17,315
 . . . 19,130
 see also Perception
- Heart rate, continuous measurement of — . . . 21,304
- Heat conduction, study with electrolytic tank . . . 18, 52
- Herbicides, see Agrobiological research
- High-frequency heating:**
 inductive —, with hydrogen thyratrons . . . 20,101
 transmitting valves for — . . . 20,299
 application in wood industry . . . 23, 30
- High-tension generator:**
 compact 100 kV generator for neutron tube . . . 23,338
 1 MV — for fast neutrons . . . 17,109
- History:**
 50 years of high-pressure mercury lamp . . . 18,167
 glass throughout the Ages . . . 22,282
 radiation furnaces . . . 23,182
 birth of Philips' lamp factory . . . 23,222
 calculating machine of Blaise Pascal . . . 24,102
- 50 years of Philips research in physics . . . 24,341
 40 years of Philips research in solid-state chemistry . . . 24,364
 50 years of gas-filled lamp . . . 25, 2
 Wolfgang von Kempelen's speaking machine . . . 25, 48
 reaction-time measurements . . . 25, 75
- Hot-gas engine, new construction with rhombic drive mechanism . . . 20,245
 Hydraulic servomotor . . . 24,320
- Hydrogen in iron and steel . . . 24,221
 . . . 24,252
- Hypar (hyperbolic paraboloid) shells for Philips pavilion on Brussels World Fair (Expo) 1958 . . . 20, 2
 . . . 20, 9
 . . . 20, 17
 . . . 20, 27
- Hysteresis loop:**
 automatic recording . . . 16, 79
 ferrites with rectangular —, see Ferroxcube
-
- Illumination, see Lighting
- Image iconoscope . . . 17,189
- Image intensifier:**
 X-ray —, see X-ray image intensifier
 based on electroluminescence with electrostatic "zoom" optics . . . 19, 1
 . . . 25, 88
- Impedance measurements, see Lecher lines
- Implosion-proof picture tube . . . 25, 81
- Impurities in metals:**
 effects of — (inaugural address Fast) . . . 16,341
 in tungsten . . . 19,109
 hydrogen in iron and steel . . . 24,221
 . . . 24,252
- Incandescent lamps:**
 for airfield beaconing . . . 16,280
 additives in tungsten for filaments . . . 19,109
 mirror-condenser lamp for 8 mm projectors . . . 19,233
 automatic control of filament-coiling machine . . . 21,309
 bulb-blowing machines for — birth of a lamp factory, 1891 . . . 22,320
 . . . 23,222
 iodine — . . . 23,237
 . . . 23,242
 automatic digital photometer shock testing of — . . . 23,244
 . . . 24,199
 50 years of gas-filled — . . . 25, 2
 see further Car headlamps
- Indicator tube for transistorized decade counting circuits . . . 21,267
- Indium antimonide, properties and applications . . . 22,217
- Information theory and entropy . . . 18,201
- Inhomogeneities in doped Ge and Si crystals . . . 25,195
- Insecticides, see Agrobiological research
- Intensification of X-ray images, see X-ray image intensifier
- Interference of light in thin films . . . 19, 59
- Interference mirrors for colour separation . . . 24,263
- Interpolation with electronic computing unit . . . 24,106
 . . . 24,308
- Iodine incandescent lamps . . . 23,237
 . . . 23,242
- Ion burn in TV picture tubes . . . 16, 27
- Ionization manometer:**
 simple — . . . 17,121
 used as a pump . . . 20,145
- IPOVOX . . . 25, 46
- Iron, see Steel
- Isocandela diagrams, automatic recording of — . . . 20,288
 . . . 23,278
- Isotopes, see Radio-isotopes
- Isosuprine ("Duvadilan") . . . 24, 69
-
- Junction transistors, see Transistors
-
- Klystrons:**
 multi-reflex — . . . 17,328
 multi-reflex — for microwave beacons . . . 24,184
 . . . 18, 51
 reflex — for 4 mm waves . . . 21,221
 reflex — for 2.5 mm waves . . . 21, 221
 low-noise high-power — . . . 18,361
-
- Laboratories, see Research Laboratories
- Lamps:**
 of constant intensity, simple circuit . . . 21,229
 see further:
 Flash bulbs
 Flash lamps, electronic-
 Fluorescent lamps
 Incandescent lamps
 Lighting
 Mercury lamps
 Sodium lamps
- Laser, small stable gas — . . . 24, 95
- Lathe headstock, high-precision . . . 19, 68
- Lattice imperfections:**
 in connection with foreign atoms (inaugural address Fast) . . . 16,341
 studied on alkali halides . . . 20, 69
 chemical — and dielectric losses . . . 22,274
 influence in metals, semiconductors and ionic crystals . . . 22,362
 see also Germanium and Silicon
- L cathode, see Dispenser cathodes
- Lecher lines:**
 for reflection and impedance measurements . . . 16,309
 for VHF impedance measurements on balanced objects . . . 21, 88
- Levitation by magnetic fields . . . 18,125
- Light, units . . . 17, 77
- Light amplifier . . . 19, 1
- Light sources, see Lamps
- Lighting:**
 in vehicles . . . 18, 11
 . . . 20,362
 of Dutch National War Memorial, Amsterdam . . . 18,300
 open-air laboratory for road lighting . . . 19,202
 automatic recording of isocandela diagrams . . . 20,288
 . . . 23,278
 of traffic routes . . . 23,258

- Lightning and aircraft 16,296
 Line converters with ultrasonic delay lines 25,249
- Linear electron accelerators:**
 application for X-ray therapy in industrial radiography installation 23,197
 Linear programming 24,123
 Liquid-air installations, see Refrigerating technique
- Littoral drift, study with radio-isotopes (Netherlands Delta Project) 21,157
- Loudspeakers:**
 twin-cone — 16,241
 — installation for high-fidelity reproduction in the home 18,304
 high-resistance — 19, 42
 public-address — 20,318
 performance tests on — 21,362
 design of ferroxdure — magnets with computer 24,150
- Low temperatures, research at —, see Solid-state research
- Machine tools, numerical control } 24,171
 of — } 24,299
- Magic-eye indicator tube (E 82 M) 18,243
 Magnets, dimensions of permanent — of various materials 18,358
 Magnetic-core memories 20,193
- Magnetic fields, static:**
 levitation by — 18,125
 generation of strong — with superconducting dynamo 25, 16
- Magnetic materials:**
 automatic recording of hysteresis loops 16, 79
 comparison of — 18,358
 determining magnetic quantities by displacement measurements 25,207
 fast and accurate measurements on small samples (vibration method) 25,227
 see further:
 Ferroxcube
 Ferroxdure
 Ferroxplana
 "Ticonal"
- Magnetic recording:**
 for programme control 20, 45
 wheel store for TV signals 22, 1
 tape for TV (studio quality) 24, 81
 5000:1 scale model of — process 25,319
- Magnetic resonance:**
 gyro— (ferro—), q.v.
 para— 19,301
 nuclear — 21,286
 double — 24,206
- Magnetodynamic pick-up 18,173
- Magnetostrictive vibrators, see Piezomagnetic vibrators
 Magnetron cooker 22, 89
- Magnetrons:**
 range of pulsed — for 3 cm to 4 mm waves 21, 1
 for microwave cooker 22, 91
- with dispenser cathode 23,316
 pulsed — for 2½ mm waves 25,217
- Mains-voltage stabilizers 17, 1
 Masers, solid-state — 25,289
 Match boxes, inspection of veneer 23, 33
- Materials research:**
 bend tests 17,246
 with X-ray image intensifier 17, 93
 X-ray inspection of steel during rolling 21,281
 4 MeV radiography installation for — 23,197
 Mechanical stresses in glass 22,337
 Mechanical tests: bend test apparatus 17,246
- Mechanization:**
 bulb-blowing machines 22,320
 mechanized mounting of TV sets 24, 41
 vibratory feeders 24, 84
- Memories, magnetic-core — 20,193
- Mercury lamps:**
 low-pressure fluorescent —, see Fluorescent lamps
 high-pressure —:
 review of development 18,167
 application of HPK lamp for floodlighting 18,300
 pulsed super-high-pressure mercury lamp (SPP 800 W) 21, 73
- Metals:**
 impurities, influence (inaugural address Fast) 16,341
 iron and steel, see Steel
 tungsten, q.v.
- Meteorology:**
 radio sonde 16,148
 radar sonde 19,258
- Microphones, placing of —, see Sound, modern acoustical techniques
 Microphony in electron tubes 22, 71
 Microradiography } 17, 45
 } 19,221
 Microtome, ultra— 17,178
 Microwave cooker 22, 89
- Microwaves:**
 wide-band amplifier using 7 cm disc-seal triode 19,145
 10 W wide-band amplifier using 7 cm disc-seal triode 21, 41
 directional isolators } 18,158
 } 22, 11
 applications of — triodes 22, 16
 waveguide equipment for } 22,113
 2 mm waves } 22,181
 screened room for — experiments 23,155
 beacons with multi-reflex klystron 24,184
 see also:
 Amplifying valves
 Klystrons
 Magnetrons
 Noise
 Radar
- Milling machine, see Numerical control
 Millivoltmeter, electronic DC — (GM 6010) 16,117
 19, 59
 Mirrors, dichroic } 24,263
 }
 Mirror cameras, see Schmidt optical system
- Mirror-condenser lamp for 8 mm projectors 19,233
- Modulation methods:**
 survey (symposium paper) 24,353
 amplitude modulation of cm waves by means of ferroxcube 18, 82
 "Frena" and "Frenac" 19, 73
 "compatible" single-sideband modulation 25,311
 frequency modulation, q.v.
- Molecular weight, determination with thermistor 20,357
- Monitoring, see Radiation monitoring
- Motion-picture projection, see Film projection
- Mounting on printed-wiring panels 24, 41
- Multiplier tubes, see Photomultipliers
 Multi-reflex tubes, see Klystrons
- Music:**
 electronic:
 technical aids; composition (Badings) 19,191
 Philips pavilion Brussels (Varèse) 20, 43
 various instruments 17,363
 instrument for deaf-mute children 18,276
 comparison between reproduced and "live" — 17,171
 ambiophony, see Sound, modern acoustical techniques
- Negative feedback in telephone cable repeaters 16,287
- Neon installations, stray capacitances in — 21,207
- Neutrons:**
 — diffraction 23, 69
 monitoring of — flux in { swimming-pool-type reactor 19,249
 } 19,273
 monitoring of — flux in { suspension reactor 21,134
 } 21,144
 sealed — tube 23,325
 generator for fast — 17,109
- Nitrogen, production of liquid } 20,177
 — from air } 25,340
- Noematachograph 25, 75
- Noise:**
 general survey (inaugural address Knol) 20, 50
 receiver with very low — level (radio-astronomy) 17,351
 — figure, automatic indicator 18,141
 — measurement on klystron diode as — standard for decimetre waves 20,108
 standard — sources (microwaves) 23,293
 — generator for mm waves 22,391
 speech transmission at high — levels ("Frena", "Frenac") 19, 73
 in X-ray image intensifier 17, 72
 } 20,216
 in scintillation counter } 20,263
- NTC resistors, see Thermistor applications
 Nuclear magnetic resonance 21,286
 Nuclear reactions for production of radio-isotopes 16, 1

- Nuclear reactors:**
 swimming-pool type, monitoring equipment . . . } 19,245
 suspension — of KEMA: } 19,273
 reasons behind choice . . . 21,109
 measurement and control of operating parameters . . . 21,121
 monitoring of low neutron flux 21,134
 monitoring of high neutron flux 21,144
 safety circuits 21,148
- Nuclear research, technical applications (inaugural address Oosterkamp) 24, 1**
- Nuclides, radioactive, see Radioisotopes**
- Numerical control:**
 of machine tools in general (public lecture Viersma) . . . 24,171
 of contour milling machine { 24,299
 { 24,308
 { 24,320
- Omegatron:**
 for qualitative gas analysis . . . 19,218
 for quantitative gas analysis . . . 22,195
 analysis of residual gases in TV picture tubes 23,122
- Operations Research 25,105**
- Opto-electronics (inaugural address Diemer) 23,189**
- Orthocyclic coil winding 23,365**
- Oscillator, LF — with low distortion under non-linear loading . . . 25,22**
- Oscilloscope tubes, see Cathode-ray tubes**
- Oxides, zone melting of — 23,161**
- Oxide cathodes:**
 for loads of 1 to 2 A/cm² . . . 23, 19
 with half-watt heater 23, 22
- Paramagnetic resonance 19,301**
- Parametric amplification, simple experiments 21, 47**
- Particle counter and sizer 21,253**
- Pascal, calculating machine of Blaise — 24,102**
- PASCAL, digital electronic computer 23, 1**
 { 24,164
- Pavilion at Expo, see Brussels World Fair (Expo) 1958**
- Peltier cooling, application in dew-point hygrometer 21,196**
- Peltier effect in resistance welding 20,188**
- Pendulum, Foucault — in United Nations building 19,236**
- Perception:**
 Institute for — Research . . . 25, 33
 — of pitch 25, 37
 phonetic research 25, 43
 investigation of visual sensory system 25, 50
 measure of perceptual work 25, 56
 electronic system for measuring human reactions . . . 25, 64
 history of reaction-time measurements 25, 75
 audibility of phase errors . . . 25,176
 see also **Vision**
- Pest control } see Agrobiological
 Pesticides } research**
- Phase errors, audibility of — . . . 25,176**
- Phonetic research 25, 43**
- Photocells:**
 photomultipliers, q.v.
 photoresistors, q.v.
 phototransistor in pyrometer . . . 20, 89
 phototransistor in relay . . . 19,280
- Photoconductivity:**
 principles (concepts; contacts on semiconductors) 25,120
 photoresistors, q.v.
 opto-electronics (inaugural address Diemer) 23,189
 photorectifying layer for reading matrix 23,310
 TV camera tube with lead-oxide layer 16, 23
 TV camera tube "Plumbicon" 24, 57
 "Photoflux" lamp, see **Flash bulbs**
- Photography, see Flash bulbs and Flash lamps, electronic-**
- Photometer, automatic digital, for testing incandescent lamps . . . 23,244**
- Photomultipliers:**
 construction and problems . . . 16,250
 stroboscopic operation of — . . . 19, 50
 use for flying-spot scanning (50 AVP) 21,237
 see also **Scintillation counter**
- Photoresistors:**
 using CdS 20,277
 using InSb 22,217
 application for stabilized light source 21,229
- Phytopharmaceutical research, see Agrobiological research**
- Pick-up, displacement — 17, 63**
- Pick-up, magnetodynamic . . . } 18,101
 { 18,173**
- Pick-up, vibration — 17, 61**
- Picture tubes, see Television picture tubes**
- Piezomagnetic vibrators:**
 ferrocube for — 18,285
 application } 18,325
 { 18,368
- Pitch perception 25, 37**
- "Plumbicon", TV camera tube . . . } 24, 57
 { 25,133**
- P-N luminescence in GaP 22,360**
- Pol, Balth. van der, scientific work "Posyn", "Potermo" and "Povin" wire 22, 36**
- Potential distribution:**
 determination with resistance network 21, 10
 calculation with electronic computer 24,130
- Potentiometer, crackle-free 20,283**
- Precision grinding machine for tracer diffusion studies 25,191**
- Precision lathe headstock 19, 68**
- Precision variable capacitors 20,234**
- Prime numbers from computer 24,164**
- Printed wiring:**
 in radio sets 20,113
 in car radio 24, 27
 mechanized mounting on — panels (TV set) 24, 41
- Prism for colour separation in colour TV 24,263**
- Process control, see Control engineering and theory**
- Projection of films, see Film projection**
- Projection television } 19,338
 { 20,327**
- Proportional counter 18,264**
- Pulling of crystals } 21,185
 { 21,340
 { 25,195**
- Pulse transformer for radar transmitter 19, 28**
- Pulsed magnetron, see Magnetrons**
- Pupillary reflex 25, 50**
- Puzzle, solving with PASCAL 24,157**
- Pyrometer using phototransistor 20, 89**
- Radar:**
 pulse transformer for radar transmitter 19, 28
 — sonde 19,258
 — system for Rotterdam 20,349
 8 mm — installation 21, 92
 high-speed scanning — antenna (Lunenburg lens) 22, 29
 4 mm — installation 25,274
- Radiation heating:**
 zone-melting furnace 23,161
 ancient radiation furnaces 23,182
- Radiation monitoring:**
 with pocket dosimeter 16,134
 of hands, feet and clothing . . . 16,201
 transistorized monitor 21,201
 see further **Counter tubes and Dosimetry**
- Radio-astronomy:**
 radiation from interstellar hydrogen (21 cm) 17,305
 design of receiver for hydrogen radiation 17,351
 75 cm receiver for — 21,317
- Radio interference from fluorescent lamps 20,135**
- Radio-isotopes:**
 production methods 16, 1
 monitor for radioactive contamination 16,201
 radioactive iodine in thyroid gland 18, 87
 as X-ray sources 18,229
 measurement of weak beta activity 20,170
 study of littoral drift in Netherlands Delta Project experiments with "Tedion V 18" 21,157
 grinding machine for diffusion studies 25,191
- Radio receivers:**
 aerials:
 inductive — 16,181
 FM — 17,348
 small ferrocube FM — 24,332
 FM section of — 17,342
 ratio detector for FM 17,345
 transistor — powered by a thermopile 18,155
 printed wiring in — 20,113
 transistor car radio with push-button tuning 24, 27
 see also:
**Amplifying valves
 Loudspeakers
 Noise**

- Radio sonde 16,148
 Radio valves, see **Amplifying valves**
 Radio waves, exploring the atmosphere with — (inaugural address Bremmer) 22, 61
 Reaction times, human —, see **Perception**
 Reading matrix, photorectifying layer for — 23,310
 Receiver valves, see **Amplifying valves**
- Rectifiers:**
 Si controlled — in converters 23,272
 see further:
 Germanium diodes
 Thyratrons
 Voltage stabilization
- Reflection measurements using transmission line 16,309
 Reflex klystrons, see **Klystrons**
- Refrigerating technique:**
 gas refrigerating machine, fundamentals 16, 69
 gas refrigerating machine, construction 16,105
 air fractionating column 20,177
 snow separator for liquid-air installations 23, 48
 production centre for liquid nitrogen 25,340
- Relay satellite, solid-state maser in — 25,289
 Relay tubes, see **Cold-cathode tubes and Thyratrons**
 Remote control: wireless-powered toys 24, 59
 Repeaters for carrier telephony . 16,287
- Research Laboratories:**
 40th anniversary (Science goes to the Fair) 17,362
 new complex of buildings in the Netherlands 24,385
 Symposium Eindhoven 1963 24,339-414
- Research: science and industry (address Casimir) 20, 85
 Residue effect 25, 37
- Resistance network:**
 description 21, 10
 application for plotting of electron trajectories 23,352
- Resistance welding, influence of Peltier effect in — 20,188
 Resistivity of semiconductors, measurement 20,220
 Resistors, vacuum deposition of — 24,144
 Resonance isolators, see **Directional isolators**
 Road lighting, see **Lighting**
 Rolling of steel, X-ray inspection during — 21,281
- Sapphire styli for gramophone pick-ups 19,324
 Satellite communication systems, solid-state masers in — 25,289
 Sawmill, electronics in — 23, 29
 Scalers, see **Counters**
 "Scenioscope", TV camera tube 17,189
- Schmidt optical system:**
 for general X-ray diagnostics 16, 58
 for projection TV 19,338
 for X-ray cinefluorography . 20,331
- Science and industry (address Casimir) 20, 85
- Scintillation counter:**
 fundamentals 20,209
 signal-to-noise ratio and dead time 20,263
 X-ray intensity measurement 18,266
- Screened room for microwave experiments 23,155
- Secondary emission:**
 from fluorescent screens . . . 16, 26
 in television camera tubes . . 17,189
 in photomultiplier 21,237
- Semiconductors:**
 measurement of resistivity and Hall coefficient 20,220
 gallium phosphide, P-N luminescence 25, 20
 see further:
 Germanium
 Photoconductivity
 Silicon
 Solid-state research
 Thermistor applications
 Transistors
- Series connection of lamps (air-field beaconing) 17, 10
 Servomotor, hydraulic, for milling machine 24,320
 Shock testing of incandescent lamps 24,199
- Silicon:**
 preparation by floating-zone technique 21,185
 — controlled rectifiers in converters 23,272
 — carbide whiskers 24,181
 inhomogeneities in doped — crystals 25,195
- Single-ended push-pull circuit . . 19, 41
 Single-sideband modulation, "compatible" 25,311
 Snow separator for liquid-air installations 23, 48
- Sodium lamps:**
 recent improvements in — . 23,246
 for traffic routes 23,258
- Solderability of wire 20,158
 Solid-state chemistry, survey of Philips contributions (symposium paper) 24,364
 Solid-state masers 25,289
- Solid-state research:**
 survey (inaugural address Polder) 21,334
 at low temperatures:
 introduction 22,190
 electron conduction 22,226
 thermal conduction in insulators; paramagnetism; dielectric losses . . 22,268
 heating in vapour with pressure and temperature adjustment 24,240
 see also **Lattice imperfections and Semiconductors**
- Sonde, radar 19,258
 Sonde, radio 16,148
- Sound:**
 modern acoustical techniques (acoustics control) { 17,258
 20,309
 21, 52
 hearing aids } 17,315
 19,130
- acoustic spectrum analyser with electronic scanning . . 21,349
 see further:
 Gramophones
 Loudspeakers
 Music
- Speaking machine of v. Kempelen 25, 48
 Spectrochemical analysis with X-rays 17,269
 Spectroscopy, microwave gas — 22,187
 Spectroscopy, time-resolved . . 19, 50
 Speech synthesis 25, 46
 Spiral-groove bearings 25,265
 Stabilization of frequency in beam transmitter 17,334
 Stabilization of voltage, see **Voltage stabilization**
 Stabilized light source, simple circuit 21,229
 Stars, variable: discovery with TV technique 19,140
 Statistics, applied (inaugural address Hamaker) 22,105
- Steel:**
 X-ray inspection during rolling 21,281
 arc-welding — 24, 14
 hydrogen in iron and — } 24,221
 24,252
- Stereophony:**
 comparison between reproduced and "live" music . . 17,171
 application in theatres . . } 20,309
 21, 52
- Stereophonic test records, recorded velocities 23, 89
 Stereophoto of dislocations . . . 23, 86
 Stereo-reverberation (ambiophony), see **Sound, modern acoustical techniques**
- Strain gauges, application in model tests of Brussels World Fair pavilion 20, 19
 Stresses in glass, investigation . . 22,337
 Structure analysis, see **Crystals**
 Stud welding 17, 37
 Subminiature valves, see **Amplifying valves**
 Superconducting circuit, dynamo for — 25, 16
 Suspension reactor of KEMA, see **Nuclear reactors**
 "Symmetrix" X-ray diagnostic table 17,112
 Symposium Philips Research Laboratories, Eindhoven 1963 } 24,339-414
- Synchrocyclotron, see **Cyclotron**
 Systems conversion in television with ultrasonic delay lines . . . 25,249
- Tap, high-vacuum — with short outgassing time 17,184
 Tape recorders, see **Magnetic recording**
- "Tedion V 18" { 17,152
 19,165
 21,276
- Telephony:**
 feedback amplifiers for carrier — 16,287
 private branch exchange UB 49 18, 19
 uniselector U 45a } 18, 19
 18,349
 at high noise levels ("Frena", "Frenac") 19, 73

- Television, application of ultrasonic delay lines to 25,234
- Television camera tubes:
 image iconoscope with glass target ("Scenioscope") . . . 17,189
 photoconductive — 16, 23
 "Plumbicon" } 24, 57
 } 25,133
- Television, colour —:
 fundamentals 19, 86
 dichroic mirrors 19, 59
 colour-separating prisms . . . 24,263
 projection (e.g. on 2.25 × 3 m) 19,338
 for medical teaching 20,327
 flying-spot scanner for — . . . 21,234
 fluorescent screen for picture tube 23,133
- Television, flying-spot scanner:
 for 35 mm film 18,193
 for colour television 21,234
 application for the discovery of variable stars 19,140
- Television picture tubes:
 secondary emission from the screen 16, 26
 sedimentation of screens . . . 16,232
 pentode gun 18, 73
 photographs of implosion . . . 18,260
 sealing of window and cone . . 19,318
 analysis of residual gases . . . 23,122
 fluorescent screen for colour — 23,133
 implosion-proof — 25, 81
- Television receivers:
 visual acuity 16,172
 for four standards 17,161
 phase linearity of — 18, 33
 luminous frame around screen . 19,156
 dosimetry of weak X-radiation in — 19,264
- Television recording:
 magnetic wheel store for — . . . 22, 1
 on magnetic tape (studio quality). 24, 81
- Television standards:
 considerations on the different — 16,195
 receiver for four standards . . . 17,161
 systems conversion with ultrasonic delay lines 25,249
- Telstar, solid-state maser in — . . 25,289
- Temperature measurement:
 clinical thermometer 17,255
 pyrometer using phototransistor 20, 89
 of solutions, to determine molecular weights 20,357
- Theatres, see **Sound**, modern acoustical techniques
- Therapy, X-ray —, see **X-ray therapy**
- Thermal conductivity, electrolytic tank for study of — . . . 18, 52
- Thermal conductivity of solids, measuring method 21,357
- Thermistor applications:
 voltage stabilizer 17, 1
 clinical thermometer 17,255
 in transistor circuits } 18,240
 } 20,132
 determination of molecular weights 20,357
- Thermopile-powered transistor radio receiver 18,155
 "Thermoplac" wire 23,371
 Thoriated-tungsten cathodes in } 19,118
 transmitting valves } 20,301
- Thyratrons:
 testing by measurement of grid current 16, 43
 life testing (MT 5544 and MT 5545) 16, 98
 hydrogen — for induction heating 20,101
- Thyroid gland, measurement of radioactive iodine in — 18, 87
- "Ticonal":
 electron-microscope photographs } 19, 11
 } 24,380
 comparison of magnetic materials (e.g. — XX) 18,358
- Titanates for capacitors 17,129
- "TL" lamps, see **Fluorescent lamps**
- "Todd-A.O." film projector 17,299
- Topotaxy 20,354
- Total-reflection fingerprinting . . 24,271
- Toys, wireless-powered 24, 59
- Tracers, see **Radio-isotopes**
- Transducers } 17, 61
 } 17, 63
- Transformers, life in ballasts . . . 20, 59
- Transistors:
 simple theory 17,233
 at high current densities 18, 61
 as network element at low } 19, 15
 frequencies } 19, 98
 } 20,122
 production of stable — 22,204
 manufacturing HF — with alloy-diffusion technique . . 24,231
 behaviour with increasing frequency 25,156
- applications:
 hearing aids } 17,315
 } 19,130
 radio receiver powered by thermopile 18,155
 pre-amplifier for magnetodynamic pick-up . . . 18,238
 light relay 19,280
 pyrometer using phototransistor 20, 89
 DC/AC converter for "TL" lamp supply . . . 20,362
 car radio 24, 27
 stabilized 2000 V power supply with valves and transistors 25,181
- Transmitting valves:
 UHF triode up to 900 Mc/s (TBL 2/300) 19,118
 grid emission of various } 19,123
 materials } 20,269
 for HF heating and generation of ultrasonic energy . . 20,299
 see further:
 Amplifying valves
 Klystrons
 Magnetrons
- Triodes, see **Amplifying valves and Transmitting valves**
- Tubes, see **Electron tubes**
- Tungsten:
 machining technique 17, 97
 — wire for small radio valves . . 18,222
 function of additives in — . . . 19,109
- Tuning-fork modulator for } 19, 84
 CERN synchrocyclotron . . . } 22,162
- Tuning indicator tube (E 82 M) . . 18,243
- Turbines, continuous monitoring of — 17, 59
- Ultra-high frequencies:
 transmitting triode TBL2/300 . . 19,118
 75 cm receiver for radio-astronomy 21,317
 see further:
 Amplifying valves
 Frequency modulation
 Lecher lines
 Noise
- Ultramicrotome 17,178
- Ultrasonics:
 ferroxcube for piezomagnetic vibrators 18,285
 machining with — (50 W and 2 kW drills) . . . } 18,325
 } 18,368
 transmitting valves for — . . . 20,299
 delay lines, application to TV . . 25,234
- Unilines, see **Directional isolators**
- Uniselector for telephone exchanges (U 45a) 18,349
- Vacuum deposition of resistors . . 24,144
- Vacuum technique:
 tap with short outgassing time 17,184
 ionization gauge } 17,121
 } 20,153
 ultra-high vacua 20,145
 metal vacuum equipment 21,173
 demountable glass seals 22, 53
 getter ion-pump 22,260
 see further **Omegatron**
- Valves, see **Electron tubes**
- Vapour, heating in — with pressure and temperature adjustment . 24,240
- Vapour deposition of circular absorption wedge 22,402
- Variable capacitors, precision — . 20,234
- Vasodilator "Duvadilan" 24, 69
- Vector-electrocardiography 21, 24
- Velocity modulation, see **Klystrons**
- Vibrating capacitor, for electrometer 25, 95
- Vibration pick-up, electrodynamic (PR 9260) 17, 61
- Vibrator, DC/AC converter 16,118
- Vibratory feeders 24, 84
- Vision:
 visual acuity in connection with TV 16,172
 luminous frame around TV screen 19,156
 investigation of visual sensory system 25, 50
 at low light levels 25, 88
- Voltage ratio, cathode-ray display of complex — 18,380
- Voltage stabilization:
 mains — 17, 1
 for emission electron microscope (45 kV) 18, 1
 2000 V power supply with valves and transistors 25,181
- Voltmeter, electronic DC milli— (GM 6010) 16,117

- Waveguide equipment for 2 mm waves } 22,113
 waves } 22,181
- Weed control, see Agrobiological research
- Weiss domains, observation of —:
 with Faraday effect 19,286
 with Bitter patterns 24,244
- Welding:
 stud — 17, 37
 enclosed — 20, 94
 influence of Peltier effect in resistance — 20,188
 arc — of steel (zircon-basic electrode; CO₂ welding) 24, 14
 Whiskers, SiC — 24,181
 Winding, orthocyclic 23,365
- Wire:
 thin tungsten — 18,222
 solderability 20,158
 manufacture and testing of enamelled — 23,342
 orthocyclic coil winding 23,365
 "Thermoplac" — 23,371
 Wireless-powered toys 24, 59
 Wood industry, electronics in — 23, 29
- Work physiology:
 cardiometer 21,304
 measure of perceptual work 25, 56
- X-ray diagnostics:
 fluorography for general — 16, 58
 with image intensifier 17, 88
 "Symmetrix" table 17,112
- "Müller" UGX unit 17,138
 dosimeters for — 23, 55
 "harmonizing" X-ray images 24,285
- X-ray diffraction:
 counter-tube diffractometer 16,123
 determination of crystal structures 22,126
 see further Counter tubes, X-ray intensity measurement with —
- X-ray image intensifier:
 design of 5" (12.5 cm) tube 17, 69
 perception of object detail 17, 71
 optical aids for — 17, 77
 — fitted with periscope optical system 17, 84
 medical aspects 17, 88
 industrial radiology with — 17, 93
 cinefluorography with 5" (12.5 cm) tube 17, 89
 cinefluorography with 11" (28 cm) tube 20,331
 application for orientation of diamonds 21,178
 inspection of hot steel billets with — 21,281
- X-rays, industrial radiology:
 with image intensifier 17, 93
 of hot steel billets 21,281
 linear accelerator for —, 4 MeV 23,197
- X-ray therapy:
 with moving tube (TU 1) 16, 33
 linear electron accelerators for — 17, 31
 dosimeters for — 23, 55
- X-ray tubes:
 for microradiography } 17, 45
 } 19,224
 investigation of heat conduction in anode 18, 52
 diffraction tube for 10 kW 19,314
 distant-focus — 20,291
- X-rays, miscellaneous:
 cinefluorography, see X-ray image intensifier
 dosimetry of very weak radiation 19,264
 fluorescence analysis 17,269
 "harmonizing" X-ray images 24,285
 intensity measurement with counter tubes, see Counter tubes, X-ray intensity measurement with —
 microradiography } 17, 45
 } 19,221
 pocket dosimeter 16,134
 projection topographs of dislocations 23, 82
 radioactive nuclides as X-ray sources 18,229
 spectrochemical analysis 17,269
- Zinc sulphide, etch pits 24, 61
- Zone melting:
 of Ge and Si, various methods (e.g. floating-zone technique) 21,185
 of oxides in carbon-arc image furnace 23,161
 "Zoom" optics, image intensifier with electrostatic — 25, 88

AUTHOR INDEX, VOLUMES 16-25

Figures in bold type indicate the volume number, and those in ordinary type the page number. Articles marked with an asterisk * are short communications. For articles published in volumes 1-15 the reader should refer to the respective decennial indexes at the end of volumes 10, 15 and 20.

- Addink, C. C. J.
 * An electrical clinical thermometer 17,255
- Admiraal, D. J. H.
 An acoustic spectrum analyser with electronic scanning 21,349
- Alink, R. J. H., H. J. Pel and B. W. Speekman
 Manufacture and testing of enamelled wire 23,342
- Allaries, H.
 A 4 mm radar installation 25,274
- Almer, F. H. R. and A. Kuiper
 New developments in oxide-coated cathodes,
 II. An oxide-coated cathode with a half-watt heater
 for cathode-ray tubes 23, 22
 — and P. G. van Zanten
- * An experimental pyrometer using a phototransistor
 and designed for radio-tube inspection 20, 89
- Alphen, P. M. van
 The application of the X-ray image intensifier,
 III. Optical aids for the image intensifier 17, 77
 Applications of the interference of light in thin films
 — and M. Bierman 19, 59
- * A mirror-condenser lamp for 8 mm projectors 19,233
- Andrieux, G., see Gieles, J. P. M.
- Arlman, J. J., J. N. Svašek and B. Verkerk
 The use of radioactive isotopes for the study of litto-
 ral drift 21,157
- Aten, A. H. W. and J. Halberstadt
 The production of radio-isotopes 16, 1
- Baas, G.
 * Demonstration of the austenite-pearlite transforma-
 tion by means of the emission electron microscope 16,337
 — and G. W. Rathenau
 An emission electron microscope for research at high
 temperatures 18, 1
- Backers, F. T.
 A magnetic journal bearing 22,232
 — and J. H. Wessels
- * An experimental apparatus for recording television
 signals on magnetic tape 24, 81
- Badings, H. and J. W. de Bruyn
 Electronic music 19,191
- Bähler, W.
 * Automatic recording of luminous intensity diagrams
 An instrument for automatically recording isocan-
 dela diagrams of beamed light sources 23,278
- Bakker, W., see Oort, J. F. van
- Balder, J. J.
 * A luminous frame around the television screen 19,156
 Iodine incandescent lamps,
 II. Possible applications 23,242
 — and M. H. A. van de Weijer
 The "TL" F lamp, a tubular fluorescent lamp with a
 directional light distribution 17,198
- Balder, T. C.
 * Influence of the Peltier effect in resistance welding 20,188
- Bandringa, M., see Venema, A.
- Barneveld, E. J. van
 Fast counter circuits with decade scaler tubes 16,360
- Bartlett, B. E., see King, R. E. J.
- Basel, C. von, H. J. Lindenhovius and G. W. van
 Santen
 Electronic equipment for the continuous monitoring
 of turbines 17, 59
- Bastiaans, C. R. and J. van der Steen
 Optical measurement of recorded velocities on stereo-
 phonic test records 23, 89
- Bathelt, R. R. and G. A. W. Vermeulen
 An experimental fluorescent screen in direct-viewing
 tubes for colour television 23,133
- Bayfield, W. A., see Nemet, A.
- Beek, R. van and W. W. Boelens
 Printed wiring in radio sets 20,113
 — and A. J. Halbmeyer
 Mechanized mounting of components on printed-
 wiring panels 24, 41
- Beekman, W. J. H., A. Verhoeff and H. W. van der
 Voorn
 * An X-ray diffraction tube with rotating anode for
 10 kW continuous loading 19,314
- Beer, A. J. F. de
 * An electrically screened room for microwave experi-
 ments 23,155
 —, H. Groendijk and J. L. Verster
 The plotting of electron trajectories with the aid of
 a resistance network and an analogue computer 23,352
- Beijersbergen, J. P., M. Beun and J. te Winkel
 The junction transistor as a network element at low
 frequencies,
 I. Characteristics and *h* parameters 19, 15
 II. Equivalent circuits and dependence of the *h*
 parameters on operating point 19, 98
 III. Stabilization of the operating point, in partic-
 ular with regard to temperature changes 20,122
- Beljers, H. G.
 Amplitude modulation of centimetre waves by
 means of ferroxcube 18, 82
 The application of ferroxcube in unidirectional wave-
 guides and its bearing on the principle of reciprocity
 Resonance isolators for millimetre waves 18,158
 22, 11
- Berkhout, H. L.
 A television receiver suitable for four standards 17,161
- Beun, M. and L. J. Tummers
 The behaviour of transistors with increasing fre-
 quency 25,156
 —, see Beijersbergen, J. P.
- Bierman, M., see Alphen, P. M. van
- Biermasz, A. L. and A. J. Michels
 An electronic D.C. millivoltmeter 16,117
- Blackler, F. G.
 * Rectangular cathode-ray tubes of high aspect ratio 18,298
- Bleekma, G. J. and J. J. Schurink
 A loudspeaker installation for high-fidelity reproduc-
 tion in the home 18,304
- Blink, W. P. van den, E. H. Eetema and P. C. van der
 Willigen
 Stud welding with welding cartridges 17, 37
- Blok, H. and J. J. Rietveld
 Inductive aerials in modern broadcast receivers,
 I. Brief history and general description 16,181
 II. Technical aspects of inductive aerials 16,188
- Blom, P.
 * A transistor hearing aid 17,315
 — and P. Boxman
 A transistor hearing aid 19,130
- Boelens, W. W., see Beek, R. van
- Boer, F. de, P. Cirkel, W. F. Nienhuis and C. J. W. Panis
 An implosion-proof picture tube for television 25, 81
 — and H. Emmens
 Sedimentation of fluorescent screens in cathode-ray
 tubes 16,232
 — and W. F. Nienhuis
 Low-voltage oscilloscope tubes 19,159
- Boer, J. B. de
 Light-beacons to aid landing aircraft 16,273
 * The "Duplo" car headlamp bulb with an asymmetric
 dipped beam 16,351
 Lighting of traffic routes 23,258
 —, see Rutgers van der Loeff, M.
- Boerdijk, A. H.
 * Levitation by static magnetic fields 18,125

- Boerman, J. R., see Schagen, P.
- Bollée, B.
- * Chladni's figures on the vibrating capacitor of a synchrocyclotron 19, 84
- and F. Krienen
- The CERN 600 MeV synchrocyclotron at Geneva, III. The tuning-fork modulator 22,162
- and G. de Vries
- * Experiments in the field of parametric amplification 21, 47
- Bommel, A. J. van, see Braun, P. B.
- Boort, H. J. J. van
- A tubular fluorescent lamp with increased luminous efficiency 25,114
- , M. Klerk and A. A. Kruithof
- Radio interference from fluorescent lamps 20,135
- and D. Kolkman
- The double-flux "TL" lamp, a fluorescent lamp of high output per unit length 19,333
- Borgman, J.
- * An application of television for the discovery of variable stars 19,140
- Botden, T. P. J.
- A gas-discharge indicator tube for transistorized decade counting circuits 21,267
- Bouma, A. L. and F. K. Ligtenberg
- The Philips pavilion at the 1958 Brussels World Fair, III. Model tests for proving the construction of the pavilion 20, 17
- Bouma, H., H. W. Horeman and J. A. J. Roufs
- Some investigations of the visual sensory system 25, 50
- Bouwhuis, G., see Lang, H. de
- Bouwmeester, E. and N. Warmoltz
- A simple and reliable ionization manometer 17,121
- , see Warmoltz, N.
- Boxman, P., see Blom, P.
- Braun, P. B. and A. J. van Bommel
- X-ray determination of crystal structures 22,126
- , see Jonker, G. H.
- Bregman, F., see Tol, M. van
- Brekoo, H. P. J. and A. Verhoeff
- * An experimental high-tension generator of very small dimensions 23,338
- Brenner, H.
- The scientific work of Balthasar van der Pol 22, 36
- Exploring the atmosphere with radio waves 22, 61
- Brockelsby, C. F. and J. S. Palfreman
- Ultrasonic delay lines and their applications to television 25,234
- Brockman, F. G. and W. G. Steneck
- A new automatic hysteresis-curve recorder 16, 79
- Brooker, M. W. and D. G. Ware
- Cheater circuits for the testing of thyratrons, I. Measurement of grid current 16, 43
- II. Life testing at high commutation factors 16, 98
- Brown, W. B., see Hendee, C. F.
- Bruijning, H. G. and A. Rademakers
- Pre-magnetization of the core of a pulse transformer by means of ferroxdure 19, 28
- , see Heide, H. van der
- Bruin, S. L. de
- The "Electronic Poem" performed in the Philips pavilion at the 1958 Brussels World Fair, C. The electronic control system 20, 45
- Bruining, H., see Heijne, L.
- Bruyn, J. W. de, see Badings, H.
- Bueren, H. G. van
- Lattice imperfections in metals, semiconductors and ionic crystals 22,362
- Burger, G. C. E. and G. Klein
- Vector-electrocardiography 21, 24
- Burgt, C. M. van der
- Ferroxcube material for piezomagnetic vibrators 18,285
- Cant, B. A.
- Problems in the construction of small radio valves 18,217
- Casimir, H. B. G.
- Science and industry 20, 85
- General introduction to the Symposium at the Philips Research Laboratories, Eindhoven, Sept. 26/27, 1963 24,340
- Some main lines of 50 years of Philips Research in physics 24,341
- Cayzac, J.
- Automatic frequency stabilization for a beam transmitter working on centimetric waves 17,334
- Champeix, R., H. Dormont and E. Morilleau
- A photomultiplier tube for scintillation counting 16,250
- Chippendale, T. R.
- * Linear electron accelerators for deep X-ray therapy 17, 31
- A 4 MeV industrial radiography installation 23,197
- Cirkel, P., see Boer, F. de
- Cock, H. G. de
- Vibratory feeders 24, 84
- Coetier, F.
- The multi-reflex klystron as a transmitting valve in beam transmitters 17,328
- Cohen, A.
- Phonetic research 25, 43
- Combée, B.
- * An X-ray tube for microradiography 17, 45
- and A. Recourt
- A simple apparatus for contact microradiography between 1.5 and 5 kV 19,221
- Coppola, P. P., see Hughes, R. C.
- Couwenberg, H. J. M., see Kooy, C.
- Cupido, P. M.
- Automatic control in glass manufacture 22,311
- Custers, J. F. H. and A. J. van der Wagt
- * The orientation of diamonds for tools by means of an X-ray image intensifier 21,178
- Dagnunar, S. S., E. G. Meerburg and A. Stecker
- Microphony in electron tubes 22, 71
- Dam, L. P. M. ten and D. Kolkman
- Lighting in trains and other transport vehicles with fluorescent lamps 18, 11
- Deelman, H. E.
- * An improved method of cleating 19,268
- Dekkers, A. J. and A. J. W. Duijvestijn
- Solving a chessboard puzzle with the PASCAL 24,157
- Dekkers, J. R. M., see Knippenberg, W. F.
- Dell, H. A., D. S. Hobbs and M. S. Richards
- An automatic particle counter and sizer 21,253
- , see Goddard, N. E.
- Diemer, G.
- Opto-electronics 23,189
- , H. A. Klasens and P. Zalm
- Electroluminescence and image intensification 19, 1
- , K. Rodenhuis and J. G. van Wijngaarden
- The EC 57, a disc-seal microwave triode with L cathode 18,317
- , see Santen, J. G. van
- Dikhoff, J. A. M.
- Inhomogeneities in doped germanium and silicon crystals 25,195
- Does de Bye, J. A. W. van der
- The scintillation counter 20,209
- Signal-to-noise ratio and dead time of a scintillation counter 20,263
- Doesschate, G. ten
- Notes on the history of reaction-time measurements 25, 75
- Domburg, J., see Schouten, J. F.
- Doorn, C. Z. van
- * Heating a solid in vapour with independent pressure and temperature adjustment 24,240
- Dorgelo, E. G.
- Transmitting valves for use in industry 20,299
- Dormont, H., see Champeix, R.
- Dorsten, A. C. van
- * Lightning and aircraft 16,296
- * A generator for fast neutrons 17,109
- and J. B. Le Poole
- The EM 75 kV, an electron microscope of simplified construction 17, 47
- Dowling, P. H., C. F. Hendee, T. R. Kohler and W. Parrish
- Counters for X-ray analysis 18,262
- Drift, A. van der, see Haan, E. F. de
- Ducot, C.
- Beam transmitters with double frequency modulation 17,317
- Duijvestijn, A. J. W., see Dekkers, A. J.
- Duis, J. A. ten
- * An apparatus for testing the solderability of wire 20,158
- Dumbrill, H. W., see Hardenberg, J. J. C.

- Duuren, K. van**
* A simple and compact arrangement for measuring the β -activity of weak radioactive samples . . . 20,170
- Duyfjes, W.**
The formulation of pesticides 19,165
- Duyster, H. C.**
The Philips pavilion at the 1958 Brussels World Fair, IV. Construction of the pavilion in prestressed concrete 20, 27
- Edens, A. H.**
A method of sealing the window and cone of television picture-tubes 19,318
- Einramhof, F.**
Visual inspection of moving lamp filaments on a coiling machine 22,239
- and P. Havas
Automatic control of a filament-coiling machine with the aid of preset counters 21,309
- Eland, A. J.**
* Etch pits on cadmium-sulphide crystals 22,266
* Etch pits on a zinc-sulphide crystal 24, 61
- Elenbaas, W.**
Fifty years of the high-pressure mercury-vapour lamp 18,167
- and T. Hehenkamp
A new fluorescent lamp in a starterless circuit . . . 17,288
- Emmens, H.**, see Boer, F. de
- Enz, U. and H. Zijlstra**
Determining magnetic quantities by displacement measurements 25,207
- Ernrich, W.**, see Klopfer, A.
- Es, C. W. van, M. Gevers and F. C. de Ronde**
Waveguide equipment for 2 mm microwaves,
I. Components 22,113
II. Measuring set-ups 22,181
- Espersen, G. A.**
Dispenser cathodes for magnetrons 23,316
- and J. W. Rogers
Electron emission of materials for electron tubes . . 20,269
- , see Plante, R. A. La
- Esvelde, C. J.**, see Wijn, H. P. J.
- Ettema, E. H.**, see Blink, W. P. van den
- Exalto, L. J. H.**
Temperatures in fittings for incandescent lamps . . 21,300
- Fast, J. D.**
Entropy in science and technology,
I. The concept of entropy 16,258
II. Examples and applications 16,298
III. Examples and applications (continued) . . . 16,321
Foreign atoms in metals 16,341
- and D. J. van Ooijen
Hydrogen in iron and steel,
I. Solution and precipitation 24,221
II. Fracturing 24,252
- and F. L. H. M. Stumpers
Entropy in science and technology,
IV. Entropy and information 18,201
- Feddema, J.**
The application of the X-ray image intensifier,
V. Medical aspects of the image intensifier . . . 17, 88
- Fine, S. and C. F. Hendee**
Nuclear X-ray sources 18,229
- Forbes, R. J.**
Glass throughout the Ages 22,282
- Fortuin, G. J.**
Visual acuity in connection with television . . . 16,172
- Foskett, R. D.**, see Neppiras, E. A.
- Francken, J. C.**
The resistance network, a simple and accurate aid to the solution of potential problems 21, 10
- , J. de Gier and W. F. Nienhuis
A pentode gun for television picture tubes 18, 73
- , see Waal, J. van der
- Fransen, J. J. B. and H. J. R. Perdijk**
Barium getter films 19,290
- Geels, B. H.**
A private automatic branch exchange using high-speed uniselectors 18, 19
- Geenen, M. J. W.**
* A machine for bend tests 17,246
- Geldermans, P.**, see Wijn, H. P. J.
- Gentner, W.**
The CERN 600 MeV synchrocyclotron at Geneva,
I. Object and design 22,142
- Gerthsen, P., J. A. A. Gilsing and M. van Tol**
An automatic dew-point hygrometer using Peltier cooling 21,196
- Gevers, M.**, see Es, C. W. van
- Gieles, J. P. M.**
A 4000 Mc/s wide-band amplifier using a disc-seal triode 19,145
Applications of microwave triodes 22, 16
- and G. Andrieux
A wide-band triode amplifier with an output of 10 W at 4000 Mc/s 21, 41
- Gier, J. de, A. C. Kleisma and J. Peper**
Secondary emission from the screen of a picture tube . 16, 26
- , see Francken, J. C.
- Gier, N. A. de, W. van Gool and J. G. van Santen**
Photo-resistors made of compressed and sintered cadmium sulphide 20,277
- Gilsing, J. A. A.**, see Gerthsen, P.
- Ginkel, H. van**
Flying-spot scanners for colour television 21,234
- Glässer, W., H. C. Grimmeiss and H. Scholz**
* Luminescent P-N junctions in gallium phosphide . . 25, 20
- Goddard, N. E. and H. A. Dell**
* A radar sonde system for upper-air measurements . 19,258
- Goedkoop, J. A.**
Neutron diffraction 23, 69
- Gool, W. van**, see Gier, N. A. de
- Goorissen, J.**
Segregation and distribution of impurities in the preparation of germanium and silicon 21,185
- Gorter, E. W.**, see Wijn, H. P. J.
- Gradstein, S.**
* Radiation furnaces of past centuries 23,182
* The calculating machine of Blaise Pascal 24,102
- Greefkes, J. A.**, see Jager, F. de
- Grimmeiss, H. G. and H. Koelmans**
* P-N luminescence in gallium phosphide 22,360
- , see Glässer, W.
- Groendijk, H.**
* A noise diode for ultra-high frequencies 20,108
- , see Beer, A. J. F. de
- Gude, H. te and E. Schaaff**
* A new kind of tuning indicator tube 18,243
- Haaf, F. E. L. ten, G. Klein and F. J. Schijff**
Monitoring, control and safety equipment for a nuclear reactor of the swimming-pool type,
II. Further description of certain component units . 19,273
- Haan, E. F. de**
* The "Plumbicon", a new television camera tube . . 24, 57
- , A. van der Drift and P. P. M. Schampers
The "Plumbicon", a new television camera tube . . 25,133
- Haanstra, H. B.**
A simple ultramicrotome 17,178
- , J. J. de Jong and J. M. G. Smeets
* The sub-microscopic structure of "Ticonal" G magnet steel 19, 11
- , see Knippenberg, W. F.
- Hagedoorn, H. L.**, see Verster, N. F.
- Haisma, J., S. J. van Hoppe, H. de Lang and J. van der Wal**
* A small, stable gas laser 24, 95
- Haitjema, M. T., W. Kopinga and S. J. Porte**
Performance tests on loudspeakers 21,362
- Halberstadt, J.**
Experiments with radioactive preparations of the acaricide "Tedion V 18" 21,276
- , see Aten, A. H. W.
- Halbertsma, N. A.**
The birth of a lamp factory in 1891 23,222
- Halbmeyer, A. J.**, see Beek, R. van
- Hamacher, E. A. and K. Lowitzsch**
The "Norelco" counting-rate computer 17,249
- , see Parrish, W.
- Hamaker, H. C.**
Applied statistics, an important phase in the development of experimental science 22,105
- Hammar, M., A. Rydahl and B. Westerlund**
Electronics in the wood industry 23, 29

- Hamming, I. and J. F. T. van Heemskerck Veeckens
* An open-air laboratory for road lighting 19,202
- Hardeman, G. E. G.
Double magnetic resonance 24,206
- Hardenberg, J. J. C.
An apparatus for cinefluorography with an 11 inch
X-ray image intensifier 20,331
- and H. W. Dumbrill
The "Symmetrix", a universal table and stand for
X-ray diagnosis 17,112
- Haringx, J. A.
A numerically controlled contour milling machine,
I. General description 24,299
- and H. van Suchtelen
The Foucault pendulum in the United Nations build-
ing in New York 19,236
- Harrick, N. J.
Fingerprinting via total internal reflection 24,271
- Hart, P. A. H.
Standard noise sources 23,293
- and G. H. Plantinga
* An experimental noise generator for millimetre waves 22,391
- Harten, G. A. and A. K. Koroncai
A transistor cardi tachometer for continuous meas-
urements on working persons 21,304
- Hauer, A. and M. van Tol
A radio sonde for meteorological observations . . . 16,148
- Havas, P., see Einramhof, F.
- Haven, Y.
Lattice imperfections in crystals, studied on alkali
halides 20, 69
- Heemskerck Veeckens, J. F. T. van, see Hamming, I.
- Hehenkamp, T.
Supply units for airfield light beaconing systems . . 17, 10
- * Small ballasts for fluorescent lamps 18,279
- The life of ballasts for gas-discharge lamps,
I. Transformers and chokes 20, 59
- II. Capacitors 20,162
- and J. J. Wilting
Transistor D.C. converters for fluorescent-lamp
power supplies 20,362
- , see Elenbaas, W.
- Heide, H. van der, H. G. Bruijning and H. P. J. Wijn
Switching time of ferrites with rectangular hysteresis
loop 18,336
- Heijn, H. J. and N. C. de Troye
A fast method of reading magnetic-core memories . . 20,193
- Heijne, L.
Physical principles of photoconductivity,
I. Basic concepts; contacts on semiconductors . . 25,120
- , P. Schagen and H. Bruining
An experimental photoconductive camera tube for
television 16, 23
- Hendee, C. F. and W. B. Brown
Stroboscopic operation of photomultiplier tubes . . 19, 50
- , see Dowling, P. H.
- , see Fine, S.
- Hengel, J. van and J. Volger
* A transistor radio receiver powered by a thermopile 18,155
- Hesselink, J. and K. Reinsma
Dosimeters for X-radiation 23, 55
- Heuven, E. W. van
The noise emission of ballasts for fluorescent lamps 18,110
- Shock testing of incandescent lamps 24,199
- Hobbs, D. S., see Dell, H. A.
- Hoekstra, P. and C. Meyer
Motion-picture projection with a pulsed light source 21, 73
- Holm, W. A. and F. H. J. van der Poel
* Colour television in medical teaching 20,327
- Hondius Boldingh, W.
Mirror cameras for general X-ray diagnostics . . . 16, 58
- Hoogenband, J. C. van den and J. Stolk
Reflection and impedance measurements by means
of a long transmission line 16,309
- Hoppe, S. J. van, see Haisma, J.
- Horeman, H. W., see Bouma, H.
- Horseling, J.
* A high-vacuum tap with short outgassing time . . 17,184
- Horst, H. L. van der and P. H. G. van Vlodrop
An experimental induction-heating generator using
hydrogen thyratrons 20,101
- Huber, C. and J. Rodrigues de Miranda
A transistor pre-amplifier for the magnetodynamic
pick-up 18,238
- Hughes, R. C. and P. P. Coppola
Dispenser cathodes,
II. The pressed cathode 19,179
- Huijjer, P., W. T. Langendam and J. A. Lely
Vacuum deposition of resistors 24,144
- Huissoon, M.
The F.M. section of modern broadcast receivers,
II. The built-in F.M. aerial 17,348
- Hurck, N. van, see Seeger, C. L.
- , see Stumpers, F. L. H. M.
- Iperen, B. B. van
* A reflex klystron for 4 mm waves 18, 51
- Reflex klystrons for wavelengths of 4 and 2.5 mm . . 21,221
- and J. L. van Lidth de Jeude
A multi-reflex klystron for use in microwave beacons 24,184
- Jager, F. de
Modulation, yesterday and tomorrow 24,353
- and J. A. Greefkes
"Frena", a system of speech transmission at high
noise levels 19, 73
- Jager, J.
The application of point-contact germanium diodes 16,225
- Jansen Gration, M. J.
The planning of the new complex of buildings for
Philips Research Laboratories in the Netherlands 24,385
- Jaspers, A. M. J.
* The measurement of radioactive iodine in the thy-
roid gland 18, 87
- Jenkinson, A. E.
Projection topographs of dislocations 23, 82
- Jensen, H., see Verse, H.
- Jochems, P. J. W.
The alloy-diffusion technique for manufacturing
high-frequency transistors 24,231
- Jonas, B. and G. Seitz
Demountable seals for glass high-vacuum equipment 22, 53
- Jong, J. J. de, see Haanstra, H. B.
- Jonker, G. H.
Capacitor materials with high dielectric constant . . 17,129
- , H. P. J. Wijn and P. B. Braun
Ferroxplana, hexagonal ferromagnetic iron-oxide
compounds for very high frequencies 18,145
- Jonkers, C. O., see Köhler, J. W. L.
- Kalff, L. C.
The "Electronic Poem" performed in the Philips
pavilion at the 1958 Brussels World Fair,
A. The light effects 20, 37
- Kerstens, J. B. S. M.
Mechanical phenomena in gramophone pick-ups at
high audio frequencies 18, 89
- Kessel, T. J. van
"Compatible" single-sideband modulation 25,311
- King, R. E. J. and B. E. Bartlett
Properties and applications of indium antimonide . . 22,217
- Klasens, H. A., see Diemer, G.
- Klein, G. and J. J. Zaalberg van Zelst
General considerations on difference amplifiers . . . 22,345
- 23,142
- Circuits for difference amplifiers, I, II } 23,173
- Difference amplifiers with a rejection factor greater
than one million 24,275
- A low-frequency oscillator with very low distortion
under non-linear loading 25, 22
- Combinations of valves and transistors in a stabilized
2000 V power supply 25,181
- Some simple active filters for low frequencies . . . 25,330
- , see Burger, G. C. E.
- , see Haaf, F. E. L. ten
- Kleis, D.
Modern acoustical engineering,
I. General principles 20,309
- II. Electro-acoustical installations in large theatres 21, 52
- Kleisma, A. C., see Gier, J. de
- Klerk, M., see Boort, H. J. J. van
- Klopper, A. and W. Ermrich
A small getter ion-pump 22,260
- and W. Schmidt
An omegatron for the quantitative analysis of gases 22,195

- Knippenberg, W.F., H.B. Haanstra and J.R.M. Dekkers**
 * Crystal growth of silicon carbide 24,181
- Knol, K. S.**
 Noise. A general survey 20, 50
- Knowles, J. E.**
 The magnetization reversal process in square-loop ferrites 24,242
- Koelmans, H., see Grimmeiss, H. G.**
- Köhler, J. W. L. and C. O. Jonkers**
 Fundamentals of the gas refrigerating machine . . . 16, 69
 Construction of a gas refrigerating machine 16,105
- , see Ster, J. van der
- Kohler, T. R., see Dowling, P. H.**
- Kolkman, D., see Boort, H. J. J. van**
- , see Dam, L. P. M. ten
- Koopmans, M. J.**
 Fungicide research 17,222
- Kooy, C.**
 * Direct observation of Weiss domains by means of the Faraday effect 19,286
 — and H. J. M. Couwenberg
 Zone melting of oxides in a carbon-arc image furnace 23,161
- Kopinga, W., see Haitjema, M. T.**
- Koroncai, A. K., see Harten, G. A.**
- Kortleven, S., see Schmitter, K. H.**
- Koster, J.**
 Multipath transmission effects in FM reception and their simulation in the laboratory 22,393
- Kotte, J. J.**
 A professional cine projector for 16 mm film . . . 16,158
 * A cinema projector for 70 mm and 35 mm films . . 17,299
 A motion-picture projector of simplified design . . 21, 83
- Krienen, F., see Bollée, B.**
- Kroon, D. J.**
 Nuclear magnetic resonance. 21,286
- Kruijf, G. T. de and N. F. Verster**
 The Orsay 160 MeV synchrocyclotron with beam-extraction system 23,381
- Kruithof, A. A. and J. L. Ouweltjes**
 Colour and colour rendering of tubular fluorescent lamps 18,249
- , see Boort, H. J. J. van
- Kuiper, A., see Almer, F. H. R.**
- Kuntke, A. H. G.**
 Distant-focus X-ray tubes 20,291
- Laan, C. J. M. van der and K. Roozendaal**
 A snow separator for liquid-air installations . . . 23, 48
- Lang, G. and R. O. Schumacher**
 The application of the X-ray image intensifier, VI. Industrial radiology with the image intensifier 17, 93
- Lang, H. de and G. Bouwhuis**
 Colour separation in colour-television cameras . . . 24,263
- , see Haisma, J.
- Langendam, W. T., see Huijer, P.**
- , see Reynst, M. F.
- Leblans, L. M. L. J.**
 * A high-precision lathe headstock 19, 68
 — and M. L. Verheijke
 * A precision grinding machine for tracer diffusion studies 25,191
- Lely, J. A., see Huijer, P.**
- Lemmens, H. J. and P. Zalm**
 New developments in oxide-coated cathodes,
 I. Oxide-coated cathodes for loads of 1 to 2 A/cm² 23, 19
- Lenders, W. L. L.**
 The orthocyclic method of coil winding 23,365
- Levi, R.**
 A technique for machining tungsten 17, 97
 Dispenser cathodes,
 III. The impregnated cathode 19,186
- Leyten, J., see Tjaden, D. L. A.**
- Lidth de Jeude, J. L. van, see Iperen, B. B. van**
- Ligtenberg, F. K., see Bouma, A. L.**
- Lindhovius, H. J., see Basel, C. von**
- Lokker, J. C.**
 Fifty years of the gas-filled lamp 25, 2
- Loos, C. H.**
 Influence of the non-linear behaviour of a recording instrument on the properties of a control system . 23,167
- Lopes Cardozo, B., see Ritsma, R. J.**
- Lotgering, F. K.**
 * Topotactically crystal-oriented ferromagnetics . . . 20,354
- Lowitzsch, K., see Hamacher, E. A.**
- , see Parrish, W.
- Maartens, J. H. J., see Schagen, P.**
- Meerburg, E. G., see Dagpunar, S. S.**
- Meerendonk, H. W. van den and J. H. Schouten**
 Trim-losses in the manufacture of corrugated cardboard 24,121
- Meerkamp van Embden, H. J.**
 * The evolution of the permanent magnet: a brief review 18,358
- Meijer, R. J.**
 The Philips hot-gas engine with rhombic drive mechanism 20,245
- Meijering, J. L. and G. D. Rieck**
 The function of additives in tungsten for filaments . 19,109
- Meltzer, J.**
 Research on the control of animal pests 17,146
- Mentzel, E. and H. Stietzel**
 A metal-ceramic disc-seal triode for frequencies up to 6000 Mc/s 21,104
- Meyer, C.**
 Recent developments in electronic-flash lamps . . . 22,377
- , see Hoekstra, P.
- Michels, A. J., see Biermasz, A. L.**
- Miranda, J. Rodrigues de, see Rodrigues de Miranda, J.**
- Moed, H. D.**
 A new vasodilating pharmaceutical 24, 69
- Morilleau, E., see Champeix, R.**
- Muijderman, E. A.**
 New forms of bearing: the gas and the spiral groove bearing 25,253
- Muller, C. A.**
 A receiver for the radio waves from interstellar hydrogen,
 I. The investigation of the hydrogen radiation . . . 17,305
 II. Design of the receiver 17,351
- Nemet, A., R. B. Stephens and W. A. Bayfield**
 A radioactive-contamination monitor for the hands, feet and clothing 16,201
- Neppiras, E. A. and R. D. Foskett**
 Ultrasonic machining,
 I. Technique and equipment 18,325
 II. Operating conditions and performance of ultrasonic drills 18,368
- Nie, A. G. van and J. J. Zaalberg van Zelst**
 A vibrating capacitor driven by a high-frequency electric field 25, 95
- Nienhuis, K., see Reifenschweiler, O.**
- Nienhuis, W. F., see Boer., F. de**
- , see Francken, J. C.
- Nijenhuis, W.**
 The PASCAL, a fast digital electronic computer for the Philips Computing Centre 23, 1
 Listening in to the PASCAL 24,164
- Noordermeer, L. J., see Oosterhout, G. W. van**
- Okkerse, B.**
 A method of growing dislocation-free germanium crystals 21,340
- Ommering, R. C. van and G. C. M. Schoenaker**
 A numerically controlled contour milling machine,
 II. The computing unit 24,308
- Ooijen, D. J. van, see Fast, J. D.**
- Ooms, J. L.**
 The recording and production of gramophone records 17,101
- Oort, J. F. van and W. Bakker**
 Wireless-powered toys 24, 59
- Oosterhout, G. W. van and L. J. Noordermeer**
 Fast and accurate magnetic measurements on samples weighing a few milligrammes 25,227
- Oosterkamp, W. J.**
 Technical fruits of nuclear research 24, 1
- , J. Proper and M. C. Teves
 X-ray inspection of hot steel billets during rolling . 21,281
- , J. Proper and J. J. F. de Wijk
 * Dosimetry of the very weak X-radiation generated in television receivers and X-ray diffraction apparatus 19,264
- , see Tol, T.
- Ouweltjes, J. L., see Kruithof, A. A.**
- Palfreeman, J. S., see Brockelsby, C. F.**

- Panis, C. J. W., see Boer, F. de
 Papenhuijzen, P. J.
 A transmitting triode for frequencies up to 900 Mc/s 19,118
 Parrish, W.
 X-ray intensity measurements with counter tubes 17,206
 X-ray spectrochemical analysis 17,269
 —, E. A. Hamacher and K. Lowitzsch
 The "Norelco" X-ray diffractometer 16,123
 —, see Dowling, P. H.
 Pasma, D. and G. Spakman
 A transistor car radio with push-button tuning 24, 27
 Pauw, L. J. van der
 * A method of measuring the resistivity and Hall coefficient on lamellae of arbitrary shape 20,220
 Pel, H. J., see Alink, R. J. H.,
 Pelt, J. G. van
 * The use of thermistors in the ebullioscopic determination of molecular weights 20,357
 Penning, P.
 The generation of dislocations by thermal stresses 19,357
 Peper, J.
 * Analysis of the gaseous contents of sealed cathode-ray tubes with the aid of the omegatron 19,218
 —, see Gier, J. de
 Perdijk, H. J. R., see Fransen, J. J. B.
 Plante, R. A. La and G. A. Espersen
 A low-noise klystron with high power output 18,361
 Plantinga, G. H.
 A pulsed magnetron for 2½ mm waves 25,217
 —, see Hart, P. A. H.
 —, see Verweel, J.
 Ploegsma, A. W.
 * Fabrication of sapphire and diamond styli for gramophone pick-ups 19,324
 Ploos van Amstel, J. J. A.
 Methods of producing stable transistors 22,204
 Poel, F. H. J. van der
 A flying-spot scanner for televising 35 mm film 18,193
 —, see Holm, W. A.
 Polder, D.
 The fruits and foundations of solid-state research 21,334
 Poole, J. B. Le, see Dorsten, A. C. van
 Poorter, T. and F. W. de Vrijer
 The projection of colour-television pictures 19,338
 Porte, S. J., see Haijema, M. T.
 Prins, B. H. G. and J. M. G. Seppen
 * The port of Rotterdam radar system 20,349
 Proper, J., see Oosterkamp, W. J.
 Quant, H. de and P. Zijp
 The F.M. section of modern broadcast receivers,
 I. Circuitry and structural design 17,342
 Rademakers, A., see Bruijning, H. G.
 Rathenau, G. W., see Baas, G.
 —, see Stuijts, A. L.
 Recourt, A., see Combée, B.
 Reifenschweiler, O. and K. Nienhuis
 The neutron tube, a simple and compact neutron source 23,325
 Reiniger, F.
 The study of thermal conductivity problems by means of the electrolytic tank 18, 52
 Reinsma, K., see Hesselink, J.
 Remedi, G.
 Science goes to the Fair 17,362
 Reynst, M. F. and W. T. Langendam
 Design of ferroxdure loudspeaker magnets 24,150
 Richards, M. S., see Dell, H. A.
 Rieck, G. D., see Meijering, J. L.
 Rietveld, J. J., see Blok, H.
 Rijssel, T. W. van, see Schagen, P.
 Ritsma, R. J. and B. Lopes Cardozo
 The perception of pitch 25, 37
 Robinson, N. W.
 Electronic flash-tubes 16, 13
 Rodenhuis, K., H. Santing and H. J. M. van Tol
 The life and reliability of valves 18,181
 —, see Diemer, G.
 Rodrigues de Miranda, J.
 Audio amplifiers with single-ended push-pull output 19, 41
 —, see Huber, C.
 Rogers, J. W., see Espersen, G. A.
 Ronde, F. C. de, see Es, C. W. van
 Roosdorp, H. J.
 Electronic control of industrial processes 17, 21
 Roozendaal, K., see Laan, C. J. M. van der
 Roufs, J. A. J., see Bouma, H.
 Rutgers van der Loeff, M. and J. B. de Boer
 * Floodlighting of the Dutch National War Memorial in Amsterdam 18,300
 Rydahl, A., see Hammar, M.
 Santen, G. W. van, see Basel, C. von
 Santen, J. G. van and G. Diemer
 A photorectifying layer for a reading matrix 23,310
 —, see Gier, N. A. de
 Santing, H., see Rodenhuis, K.
 Schaaff, E., see Gude, H. te
 Schagen, M. J. van
 * Cathode-ray display of complex quantities at varying frequencies 18,380
 Schagen, P., J. R. Boerman, J. H. J. Maartens and T. W. van Rijssel
 The "Scenioscope", a new television camera tube 17,189
 —, see Heijne, L.
 —, see Woodhead, A. W.
 Schalkwijk, W. F.
 Operations Research 25,105
 Schampers, P. P. M., see Haan, E. F. de
 —, see Warmoltz, N.
 Schee, B. L. A. van der and M. van Tol
 Instrumentation for a subcritical homogeneous suspension reactor,
 II. Measurement and control of operating parameters 21,121
 Schiefer, G.
 A slotted lecher line for impedance measurements in the metric and decimetric wave bands 21, 88
 A small ferrocube aerial for VHF reception 24,332
 Schijff, F. J.
 Instrumentation for a subcritical homogeneous suspension reactor,
 IV. The safety circuits 21,148
 —, see Haaf, F. E. L. ten
 Schmidt, W.
 The heating of food in a microwave cooker 22, 89
 Schmidt, W., see Klopfer, A.
 Schmitter, K. H. and S. Kortleven
 The CERN 600 MeV synchrocyclotron at Geneva,
 II. The radio-frequency system 22,149
 Schoenaker, G. C. M., see Ommering, R. C. van
 Scholz, H., see Glässer, W.
 Schouten, J. F.
 The Institute for Perception Research 25, 33
 — and J. Domburg
 The DONDERS, an electronic system for measuring human reactions 25, 64
 Schouten, J. H., see Meerendonk, H. W. van den
 Schröder, J.
 A simple method of determining the thermal conductivity of solids 21,357
 Schultink, L., H. L. Spier and A. J. van der Wagt
 The wear of diamond dies 16, 91
 — and P. G. van Zanten
 Thin tungsten wire for small radio valves 18,222
 Schumacher, R. O., see Lang, G.
 Schurink, J. J.
 The twin-cone moving-coil loudspeaker 16,241
 —, see Bleeksma, G. J.
 Schwab, V. V. and J. G. van Wijngaarden
 The EC 59, a transmitting triode with 10 W output at 4000 Mc/s 20,225
 Seeger, C. L., F. L. H. M. Stumpers and N. van Hurck
 A 75 cm receiver for radio astronomy and some observational results 21,317
 Seitz, G., see Jonas, B.
 Seppen, J. M. G. and J. Verstraten
 An 8 mm high-resolution radar installation 21, 92
 —, see Prins, B. H. G.
 Slooten, J. van
 FM reception under conditions of strong interference 22,352
 Smeets, J. M. G., see Haanstra, H. B.
 Smith, F. W., see Walling, J. C.
 Spakman, G., see Pasma, D.

- Speekman, B. W., see Alink, R. J. H.
 Spier, H. L., see Schultink, L.
 Stecker, A., see Dagpunar, S. S.
 Steen, J. van der, see Bastiaans, C. R.
 Steneck, W. G., see Brockman, F. G.
 Stephens, R. B.
 Mains-voltage stabilizers 17, 1
 —, see Nemet, A.
 Ster, J. van der and J. W. L. Köhler
 A small air fractionating column used with a gas re-
 frigerating machine for producing liquid nitrogen 20,177
 Stevels, J. M.
 New light on the structure of glass 22,300
 Stieltjes, F. H. and L. J. Tummers
 Simple theory of the junction transistor 17,233
 Behaviour of the transistor at high current densities 18, 61
 Stietzel, H., see Mentzel, E.
 Stolk, J., see Hoogenband, J. C. van den
 Stuijts, A. L., G. W. Rathenau and G. H. Weber
 Ferroxdure II and III, anisotropic permanent-mag-
 net materials 16,141
 — and H. P. J. Wijn
 Crystal-oriented ferroplana 19,209
 Stumpers, F. L. H. M. and N. van Hurck
 * An automatic noise-figure indicator 18,141
 —, see Fast, J. D.
 —, see Seeger, C. L.
 Suchtelen, H. van
 A simple circuit for a light source of constant inten-
 sity 21,229
 —, see Haringx, J. A.
 Svašek, J. N., see Arlman, J. J.
 Tak, W.
 The "Electronic Poem" performed in the Philips
 pavilion at the 1958 Brussels World Fair,
 B. The sound effects 20, 43
 Taylor, D. G., see Woodhead, A. W.
 Teer, K.
 * The audibility of phase errors 25,176
 Tellegen, B. D. H.
 The gyrator, an electric network element 18,120
 Teves, M. C.
 The application of the X-ray image intensifier,
 I. General survey 17, 69
 —, see Oosterkamp, W. J.
 Tijen, J. W. van
 Iodine incandescent lamps,
 I. Principle 23,237
 Tjaden, D. L. A. and J. Leyten
 A 5000 : 1 scale model of the magnetic recording
 process 25,319
 Tol, H. J. M. van, see Rodenhuis, K.
 Tol, M. van
 Monitoring, control and safety equipment for a nu-
 clear reactor of the swimming-pool type,
 I. General description 19,245
 Instrumentation for a subcritical homogeneous sus-
 pension reactor,
 IIIB. The monitoring of high neutron flux with the
 aid of an electrometer 21,144
 The application of control theory to linear control
 systems 23,109
 Loop gain and stability of simple control systems 23,151
 — and F. Bregman
 A transistorized radiation monitor 21,201
 —, see Gerthsen, P.
 —, see Hauer, A.
 —, see Schee, B. L. A. van der
 Tol, T. and W. J. Oosterkamp
 The application of the X-ray image intensifier,
 II. The perception of small object-detail 17, 71
 Tosswill, C. H.
 Cold-cathode trigger tubes 18,128
 Troye, N. C. de, see Heijn, H. J.
 Tummers, L. J., see Beun, M.
 —, see Stieltjes, F. H.
 Turnbull, A. A.
 Precision variable capacitors 20,234
 Unk, J. M.
 A high-speed uniselector for automatic telephone ex-
 changes 18,349
 Valster, F.
 A high-speed scanning radar antenna 22, 29
 Veen, R. van der
 "Boekesteijn", the agrobiological laboratory of N.V.
 Philips-Roxane 16,353
 Growth substances in plants 17,294
 The balance of nature 23,101
 Venema, A.
 Dispenser cathodes,
 I. Introduction 19,177
 — and M. Bandringa
 The production and measurement of ultra-high vacua 20,145
 Verheijke, M. L., see Leblans, L. M. L. J.
 Verhoeff, A., see Beekman, W. J. H.
 —, see Brekoo, H. P. J.
 Verkerk, B., see Arlman, J. J.
 Vermeulen, G. A. W., see Bathelt, R. R.
 Vermeulen, R.
 A comparison between reproduced and "live" music 17,171
 Stereo-reverberation 17,258
 * A musical instrument for deaf-mute children 18,276
 Verse, H.
 A universal apparatus for X-ray therapy with mov-
 ing field irradiation 16, 33
 — and H. Jensen
 The application of the X-ray image intensifier,
 IV. Equipment for spot film radiography incorpo-
 rating an image intensifier fitted with a periscope
 optical system 17, 84
 — and K. Weigel
 A novel type of diagnostic X-ray unit 17,138
 Verster, J. L.
 An apparatus for automatically plotting electron
 trajectories 22,245
 —, see Beer, A. J. F. de
 Verster, N. F. and H. L. Hagedoorn
 Investigation of the magnetic field of an isochronous
 cyclotron 24,106
 —, see Kruiff, G. T. de
 Verstraten, J., see Seppen, J. M. G.
 Verweel, J. and G. H. Plantinga
 A range of pulsed magnetrons for centimetre and
 millimetre waves 21, 1
 Vessem, J. C. van
 The theory and construction of germanium diodes 16,213
 Viersma, T. J.
 Some considerations on the numerical control of
 machine tools 24,171
 A numerically controlled contour milling machine,
 III. The hydraulic servomotor 24,320
 Vink, H. J.
 Contributions of the Philips Research Laboratories
 to solid-state chemistry 24,364
 Vlaardingebroek, M. T.
 * An experimental disc-seal triode for 6000 Mc/s 21,167
 Vlodrop, P. H. G. van, see Horst, H. L. van der
 Volger, J.
 Solid-state research at low temperatures,
 I. Introduction 22,190
 II. Electron conduction in metals and semicon-
 ductors 22,226
 III. Thermal conduction in insulators; paramagnet-
 ism; dielectric losses related to chemical lattice
 imperfections 22,268
 A dynamo for generating a persistent current in a
 superconducting circuit 25, 16
 —, see Hengel, J. van
 Voorn, H. W. van der, see Beekman, W. J. H.
 Vreedenburgh, C. G. J.
 The Philips pavilion at the 1958 Brussels World Fair,
 II. The hyperbolic-paraboloidal shell and its me-
 chanical properties 20, 9
 Vriend, J. A. de
 Ignition of "Photoflux" flash-bulbs with the aid of a
 capacitor 16,333
 Vries, G. de, see Bollée, B.
 Vries, J. de
 Testing of materials for glass-to-metal seals by means
 of stress birefringence 22,337
 Vries, R. W. P. de
 The gloss point of glazes 17,153

- Vrijer, F. W. de
Fundamentals of colour television 19, 86
—, see Poorter, T.
- Waal, B. van der
A simple analogue computer for determining the colour point of a light source 23,118
- Waal, J. van der and J. C. Francken
Analysis of residual gases in television picture tubes with the aid of the omegatron 23,122
- Wagt, A. J. van der, see Custers, J. F. H.
—, see Schultink, L.
- Wal, J. van der
* Circular optical absorption wedges 22,402
—, see Haisma, J.
- Walling, J. C. and F. W. Smith
Solid state masers and their use in satellite communication systems 25,289
- Ware, D. G., see Brooker, M. W.
- Warmoltz, N. and E. Bouwmeester
Metal vacuum equipment 21,173
— and P. P. M. Schampers
A pocket dosimeter, with built-in charger, for X-radiation and gamma radiation 16,134
—, see Bouwmeester, E.
- Weber, C.
Calculation of potential fields and electron trajectories using an electronic computer 24,130
* Measuring the light-intensity distribution in the spot on a cathode-ray-tube screen 25,152
- Weber, G. H., see Stuijts, A. L.
- Weel, A. van
Phase linearity of television receivers 18, 33
- Weigel, K., see Verse, H.
- Weijer, M. H. A. van de
Recent improvements in sodium lamps 23,246
—, see Balder, J. J.
- Went, J. J.
Instrumentation for a subcritical homogeneous suspension reactor,
I. Reasons behind the choice of a homogeneous suspension reactor 21,109
- Werner, W.
The different television standards considered from the point of view of receiver design 16,195
- Wessels, J. H.
A magnetic wheel store for recording television signals 22, 1
—, see Backers, F. T.
- Westerkowsky, K., see Zieler, E.
- Westerlund, B., see Hammar, M.
- Westhoff, J. M.
In search of a measure of perceptual work 25, 56
- Westra, R.
A "Photoflux" flash-bulb with simplified cap 16, 88
- Wieringen, J. S. van
Paramagnetic resonance 19,301
- Wijk, J. J. F. de, see Oosterkamp, W. J.
- Wijn, H. P. J., E. W. Gorter, C. J. Esveldt and P. Geldermans
Conditions for square hysteresis loops in ferrites 16, 49
—, see Heide, H. van der
—, see Jonker, G. H.
—, see Stuijts, A. L.
- Wijngaarden, J. G. van, see Diemer, G.
—, see Schwab, V. V.
- Willigen, P. C. van der
Some modern methods of arc-welding steel 24, 14
—, see Blink, W. P. van den
- Wiltig, J. J.
Stray capacitances in neon installations 21,207
DC/AC converters using silicon controlled rectifiers for fluorescent lighting 23,272
—, see Hehenkamp, T.
- Winkel, J. te
Feedback amplifiers for carrier telephone systems 16,287
—, see Beijersbergen, J. P.
- Wittenberg, N.
A magnetodynamic gramophone pick-up,
I. Construction 18,101
II. Frequency characteristics 18,173
- Woodhead, A. W., D. G. Taylor and P. Schagen
An experimental image-intensifier tube with electrostatic "zoom" optics 25, 88
- Xenakis, Y.
The Philips pavilion at the 1958 Brussels World Fair,
I. The architectural design of Le Corbusier and Xenakis 20, 2
- Zaalberg van Zelst, J. J., see Klein, G.
—, see Nie, A. G. van
- Zalm, P., see Diemer, G.
—, see Lemmens, H. J.
- Zanten, P. G. van, see Almer, F. H. R.
—, see Schultink, L.
- Zieler, E. and K. Westerkowsky
The Ampliscope, an experimental apparatus for "harmonizing" X-ray images 24,285
- Zijlstra, H., see Enz, U.
- Zijp, P., see Quant, H. de
- Zoethout, G.
* Enclosed welding of rail sections 20, 94
- Zolingen, J. J. van
Instrumentation for a subcritical homogeneous suspension reactor,
IIIA. The monitoring of low neutron flux by means of fast pulse-counting channels 21,134
- Zonneveld, P. van
Mechanical production of bulbs for electric lamps and radio valves 22,320